INFORMATION TO USERS

This manuscript has been reproduced from the microfilm master. UMI films the text directly from the original or copy submitted. Thus, some thesis and dissertation copies are in typewriter face, while others may be from any type of computer printer.

The quality of this reproduction is dependent upon the quality of the copy submitted. Broken or indistinct print, colored or poor quality illustrations and photographs, print bleedthrough, substandard margins, and improper alignment can adversely affect reproduction.

In the unlikely event that the author did not send UMI a complete manuscript and there are missing pages, these will be noted. Also, if unauthorized copyright material had to be removed, a note will indicate the deletion.

Oversize materials (e.g., maps, drawings, charts) are reproduced by sectioning the original, beginning at the upper left-hand corner and continuing from left to right in equal sections with small overlaps. Each original is also photographed in one exposure and is included in reduced form at the back of the book.

Photographs included in the original manuscript have been reproduced xerographically in this copy. Higher quality 6" x 9" black and white photographic prints are available for any photographs or illustrations appearing in this copy for an additional charge. Contact UMI directly to order.

UMI®

Bell & Howell Information and Learning
300 North Zeeb Road, Ann Arbor, MI 48106-1346 USA
800-521-0600

The Application of Cone Penetration Test Data to Facies Analysis of the Fraser River Delta, British Columbia

by

Patrick Alistair Monahan
B.Sc., University of British Columbia, 1974

A Dissertation Submitted in Partial Fulfillment of the
Requirements for the Degree of

DOCTOR OF PHILOSOPHY

in the School of Earth and Ocean Sciences

We accept this dissertation as conforming
to the required standard

Dr. J.V. Barrie, Co-supervisor (School of Earth and Ocean Sciences)

Dr. C.R. Barnes, Co-supervisor (School of Earth and Ocean Sciences)

Dr. M. J. Whiticar, Departmental Member (School of Earth and Ocean Sciences)

Dr. O. Niemann, Outside member (Department of Geography)

Mr. D. VanDine, Additional member

Dr. P.K. Robertson, External Examiner (Department of Civil Engineering, University of Alberta)

Co-supervisors: Dr. J.V Barrie and Dr. C.R. Barnes

ABSTRACT

Cone penetration tests (CPTs) have been developed for engineering investigations of sands and finer sediments. CPTs produce high resolution, repeatable and continuous records to depths of several tens of metres, and resemble wireline logs used in the petroleum industry. It is the objective of this dissertation to demonstrate that they can be used for facies analysis in a similar manner, by using these data to develop a facies model for the modern Fraser River delta, British Columbia, Canada. CPT data provide reliable estimates of sediment type and grain size, so that bed thicknesses, sharp and gradational contacts, coarsening and fining upward sequences, bed continuity and dips can be readily identified.

The facies model of the Fraser delta is based on a database of over 800 CPTs and 20 continuously cored boreholes. These data demonstrate that the topset is dominated by a nearly continuous sharp-based sand unit that is 8 to 30 m thick, fines upward and is interpreted to represent a complex of distributary channel deposits. The widespread distribution of this sand unit is the result of distributary channel migration in a tidal flat setting and avulsion or channel switching in the upper delta plain. The sand unit is gradationally overlain by a thinner sequence of interbedded sands and silts deposited in tidal flat, abandoned channel and floodplain environments. Deposits of the upper foreset (<60 m) dip up to 7° seaward and are dominated by silts, interbedded and interlaminated with sands. Several intergradational facies, ranging from dominantly silt to dominantly sand, occur and represent increasing proximity to active distributary mouths. These sediments are organized into metre-scale sandy and silty coarsening-upward sequences that are interpreted to represent annual deposits, and sharp-based sand units that represent sedimentary gravity flow deposits. Deeper foreset deposits are dominated by bioturbated silts. The distribution of facies on both the topset and the foreset has been controlled by the interaction of tidal and fluvial processes.

CPT data played a key role in developing this facies model of the Fraser River delta. Most facies have distinct CPT signatures. For example, the topset sand unit and overlying deposits have a CPT signature comparable to the "bell-shaped" gamma ray log signature typical of channel deposits. In the foreset, the seaward dips, the coarsening upward sequences and the sharp-based sands are readily observable on CPT data. Although cores were essential to confirm the facies significance of these signatures, the large volume of CPT data permitted recognition of facies distributions and relationships "at a glance" throughout the delta, rather than at the relatively few site where continuous cores were available. Furthermore, CPTs can be acquired for a fraction of the cost of continuous cores, so that CPT data are potentially an invaluable tool for stratigraphic investigations of other modern sedimentary environments dominated by sands and finer sediments.

Examiners:

Dr. J.V. Barrie, Co-supervisor (School of Earth and Ocean Sciences)

Dr. C.R. Barnes, Co-supervisor (School of Earth and Ocean Sciences)

Dr. M. J. Whiticar, Departmental Member (School of Earth and Ocean Sciences)

Dr. O. Niemann, Outside member (Department of Geography)

Mr. D. VanDine, Additional member

Dr. P.K. Robertson, External Examiner (Department of Civil Engineering, University of Alberta)

TABLE OF CONTENTS

LIST OF TABLES

LIST OF FIGURES

ACKNOWLEDGMENTS

A project of this magnitude could only have been achieved with the help of a large number of people. A particular debt of gratitude is owed to Vaughn Barrie and John Luternauer of the GSC, who provided the resources and funding for this research, in particular for drilling, grain size analysis and radiocarbon dating. The author is grateful for the assistance of many other individuals at the GSC, in particular, John Clague for providing many radiocarbon dates; Jim Hunter for providing gamma ray logs and SCPT data; Harold Christian, Scott Dallimore and Kimberly Edwardson for the opportunity to participate in their drilling programs; Trudie Forbes and Kim Conway for assistance in the laboratory and with the preparation for field operations; Marji Johns for assistance in the field and providing data foraminiferal faunas in cores; and Dave Mosher and Bruce Hart for assistance in the field and lab. The grain size analyzes done at the Pacific Geoscience Centre were conducted by Rod Smith, Caleen Kilby, Trudie Forbes and Kim Conway.

In addition to the CPT data provided by the GSC, CPT and other geotechnical data were obtained from the British Columbia Ministry of Transportation and Highways (MOTH), British Columbia Hydro and Power Corporation, the British Columbia Geological Survey, British Columbia Rail Company, B.C. Gas Corporation, the Civil Engineering Department of the University of British Columbia (UBC), the City of Richmond, Richmond School District, the District of Delta, Delta School District, Richmond Hospital, Delta Christian School, Vancouver International Airport Authority, Vancouver Port Corporation, Public Works Canada, ConeTec Investigations Ltd., Klohn-Crippen Engineering, GeoPacific Consultants, AGRA Earth and Environmental Ltd., Macleod Geotechnical Ltd., Cook, Pickering and Doyle Ltd., Golder Associates. Thurber Engineering Ltd., Triton Consultants Ltd., the Dominion Company, PBK Engineering Ltd., and Delcan Consultants Ltd. In particular, the author thanks the following individuals at these agencies for their enthusiastic

assistance in the search for data: Kirby Reimer, Don Gillespie, Don Lister, Blain Good, Kay Ahlfield, John Psutka, Ray Stewart, Anne Barker, Dick Campanella, David Woeller, Ilmar Weemees, Jim Greig, Sonny Singha, Dave Berriman, Matt Kokan, Bryan Watts, Alex Sy, Steve Ahlfield, Les Banas, Susan Hollingshead, Paul Henederson, David Siu, Ed Harrington, Jim Masden, Blair Gohl, Martin Lawrence, Ernie Naesgaard, Doug Wallis, Richard Butler, Upul Atukorala and Michael Tarbotton. The author also acknowledges the assistance of Peter Robertson and Barb Hoffman of the Civil Engineering Department of the University of Alberta for providing the opportunity to participate in the CANLEX project. The CPT data used for this study was generated by ConeTec Investigations Ltd., UBC, MOTH, Foundex Exploration Ltd, and Hughes InSitu Ltd. The author is exceedingly grateful for the assistance of the following in learning the intricacies of cone penetration testing; Dick Campanella, Peter Robertson, David Woeller, Ilmar Weemees, Jim Greig, Don Gillespie, Alex Sy, Ed Harrington, Jim Masden and John Hughes.

The boreholes for this project were drilled by Sonic Drilling Ltd., Foundex Explorations Ltd, and Mud Bay Drilling Ltd. The author gratefully acknowledges the enthusiastic support of these companies' personnel in the field, notably Ray Roussy, Adrian Wilson and Gordon Gibbons. The author also acknowledges the assistance of the following agencies in providing access to drill sites: the City of Richmond, the Richmond School District, Richmond Hospital, the District of Delta, B.C. Hydro, MOTH, Westshore Terminals, B.C. Rail, Transport Canada, Coast Guard Canada, and the Nottingham family. Thanks are due also to Domtar for permitting use of samples from a site in Coquitlam, and to Jodi Everard for providing CPT data at this site.

The author gratefully acknowledges the support and encouragement of his committee: Vaughn Barrie; Chris Barnes, Michael Whiticar and Olaf Niemann of the University of Victoria; and Doug VanDine of VanDine Geological Engineering, who gave freely of his time to improve this product. The author also appreciates the diligence of Brian Sawyer and Richard Franklin, who drafted many of the figures. A note of thanks is also due to Vic

Levson of the B.C. Geological Survey and Roy Hyndman and Chris Yorath of the Geological Survey of Canada for support and encouragement. Financial support for this research was provided by the University of Victoria, the National Sciences and Engineering Research Council and the American Association of Petroleum Geologists.

Figure 3-1 is reproduced here with permission of its author, Dr. P.K. Robertson of the University of Alberta. The following figures are reproduced here with permission of their publishers: Figure 1-1 (Geological Society, London); Figures 2-3 and 3-3b (National Research Council of Canada); Figure 3-3a (American Society of Civil Engineers); and Figures 2-1 and 2-6 (Geological Survey of Canada). The core photographs were all taken by me. However, some appear in Clague et al. (1998; Figures 6-29, 6-31 and 6-47b) and are also reproduced here with permission of the Geological Survey of Canada.

In conclusion, this project could not have been completed without the love and understanding of Cathie, Adam, Sarah and Erin.

To

Cathie

CHAPTER 1

INTRODUCTION

Cone penetration tests (CPTs) are now widely used in geotechnical investigations of sands and finer sediments, but to date have had limited application to geological investigations. CPTs produce continuous records of subsurface conditions, from which estimates of the types of sediments penetrated and their properties can be made (Campanella et al., 1983; Robertson and Campanella, 1983a, b, 1986; Lunne et al., 1997). These records resemble wireline (i.e. geophysical) logs used in the petroleum industry, which are a primary tool for subsurface geological investigations. Furthermore, the patterns of log curves can be used as indicators of depositional environment, or sedimentary facies (Figure 1-1; e.g. Reading, 1986). The principal objective of this dissertation is to demonstrate that CPT data can be used for facies analysis in a similar manner, by using these data to develop a facies model for the modern Fraser River delta, British Columbia. This dissertation is relevant to geologists interested in facies analysis of modern sediments, as well as geotechnical engineers knowledgeable about CPTs and who could apply facies analysis to their investigations.

CPTs provide continuous and repeatable measurements of sands and finer sediments to depths of tens of metres at a fraction of the cost of boreholes cored to comparable depths. Furthermore, CPTs are commonly available from engineering investigations, so that CPT data can provide a vastly larger database for stratigraphic investigations of modern sedimentary environments than would be provided by conventional coring programs alone. The Fraser delta is ideally suited for this purpose because thousands of CPTs have been conducted in the course of engineering investigations since 1980. Over 800 have been obtained for this study.

The use of wireline logs for facies identification was first described in the literature by Visher (1969), and since then has become standard practice in subsurface investigations

(Serra, 1986; Reading, 1986; Cant, 1992). Facies attributes provided by wireline logs are generally limited to gross lithology, grain size trends and the nature of geological contacts (sharp or gradational). In sands and sandstones, two of the most commonly described natural gamma ray (gamma ray) or spontaneous potential (SP) log signatures are the fining-upward "bell" shape typical of channel deposits and the coarsening-upward "funnel" shape typical of beach and barrier bar deposits (Figure 1-1). Many authors have cautioned against uncritical use of log shape for facies interpretation (e.g. Reading, 1986; Rider, 1990; Cant, 1992). Similar log shapes may be generated in different facies and other factors can cause a log shape to vary from the norm for that environment. For example, the presence of a shale-clast conglomerate at the base of a channel sand can obscure the sharp base and fining-upward appearance of the log signature. However, log shape can be a valuable first approximation of facies in order to direct future investigations. Furthermore, the repetition of distinct log signatures throughout a particular area has geological significance; and if core data are available to determine the facies of those signatures, then log shape can be a powerful tool in facies mapping and analysis.

Accordingly, in this study a suite of continuously cored boreholes located adjacent to CPTs provides the basis for facies identification of the CPT log signatures. These signatures are then be applied to other CPTs to determine facies distributions and relationships beyond the limits of borehole control.

This dissertation begins with a discussion of pertinent background information. The Fraser delta is discussed in Chapter 2: its geographic, fluvial and oceanographic setting, the previous subsurface investigations conducted there and its stratigraphic framework. In Chapter 3 a summary of cone penetration testing is presented.

The field and laboratory procedures used in this project are described in Chapter 4. This chapter discusses: the CPT database; the procedures for CPT data analysis; the coring methods and associated drilling-induced errors; the field and laboratory core logging

procedures; the selection of samples for grain size analysis to compare with CPT measurements; the use of gamma ray logs to depth correct core depths in order to correlate grain size samples with adjacent CPTs; the procedures used to correct ^{14}C dates for reservoir age; and the terminology used.

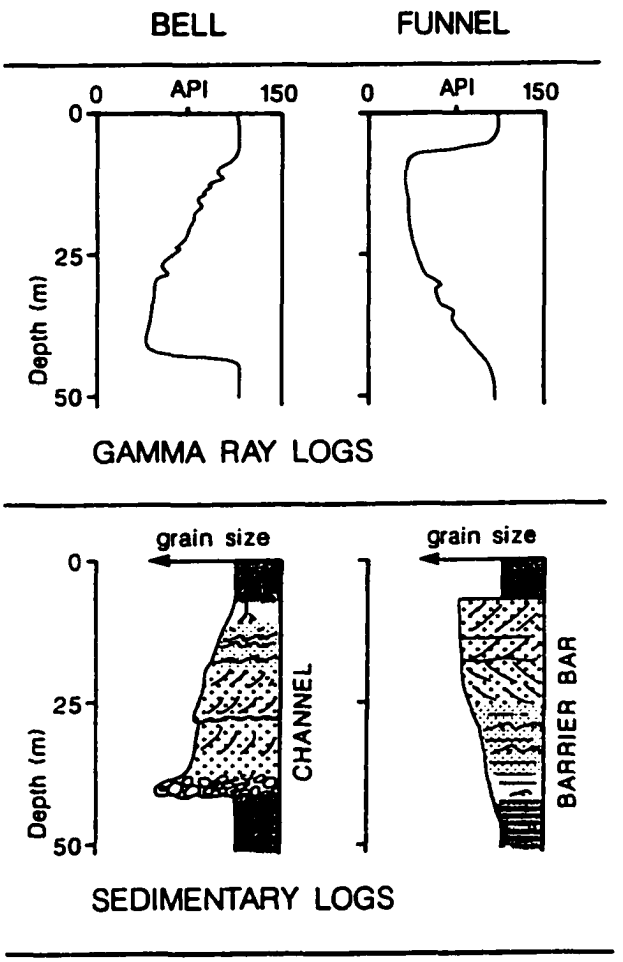

Figure 1-1. Typical grain size profiles and gamma ray log signatures for channel and barrier bar sands (from Serra and Sulpice, 1975, and Rider, 1990).

The results of investigations into the relationship of grain size to CPT measurements in the Fraser delta are presented in Chapter 5. This subject is discussed in detail because grain size

is an important control over CPT measurements, as indicated by the CPT soil classification charts (e.g. Olsen and Malone, 1988; Robertson, 1990). Furthermore, in the Fraser delta grain size also correlates with cone bearing in sand deposits (e.g. Monahan et al., 1995b), although in most industrial applications variations in cone bearing measurements in sands are generally interpreted to represent variations in density. The grain size to CPT correlations established here provide the basis for the recognition of grain size trends in the deposits of the Fraser delta. Grain size trends are among the facies attributes best represented in CPTs, as they are in wireline logs.

In Chapter 6, the sedimentary facies of the Fraser delta are defined, the CPT signatures of each facies are described and the facies are interpreted on the basis of these data and integrated into a facies model for the delta. Because CPTs in the delta have penetrated to a maximum depth of 100 metres and deposits of the modern Fraser delta extend to much greater depths, this discussion focusses on facies occurring above that depth.

The contribution made by CPT data to this analysis and the applicability of using CPT data for facies analysis in general are discussed in Chapter 7, followed by the conclusions in Chapter 8. The analysis presented in this dissertation is intended to provide a model for the application of CPT data to facies analysis in other modern sedimentary environments.

Early results of this study have been presented in a series of papers, conference proceedings and abstracts (Monahan, 1993; Monahan et al., 1993a, b, c, 1994, 1995a, b, 1996, 1997; Luternauer et al., 1993, 1994; Christian et al., 1994; Clague et al., 1998). These papers are referenced in this dissertation to show where data and conclusions have been published, but are not used to support the interpretations made here. All data and interpretations that appear in these sources and are relevant to this dissertation are also presented here.

CHAPTER 2

THE FRASER RIVER DELTA: SETTING AND GEOLOGICAL SUMMARY

SETTING OF THE FRASER RIVER DELTA

Geographic Setting

The modern Fraser River delta has a subaerial and subaqueous area of 975 km^2 and is the largest on the west coast of Canada (Milliman, 1980). It is located at the west end of the Fraser Lowland, a triangular-shaped lowland that separates the Coast Mountains on the north from the Cascade Mountains to the south; and at the southeastern end of the Strait of Georgia, a semi-enclosed marine basin separated from the Pacific Ocean by Vancouver Island (Holland, 1976; Figure 2-1).

The Fraser delta underlies the southern parts of Greater Vancouver and is experiencing rapid urban and industrial growth. It includes all of the City of Richmond, most of the District of Delta, and parts of the Cities of Vancouver, Burnaby, and New Westminster. This area is situated in one of the most seismically active regions in Canada (Rogers, 1994), and the deltaic sands are susceptible to earthquake-induced liquefaction (Byrne, 1978; Clague et al., 1992, 1997; Watts et al., 1992). Consequently, a large volume of CPT data has been generated in the area for both foundation design and liquefaction assessment (Finn et al., 1989; Finn et al., 1990).

Fluvial Regime

The Fraser River is the largest river to reach Canada's west coast. It flows 1360 km to the sea from its source in the Rocky Mountains and drains an area of 250,000 km^2 in central and

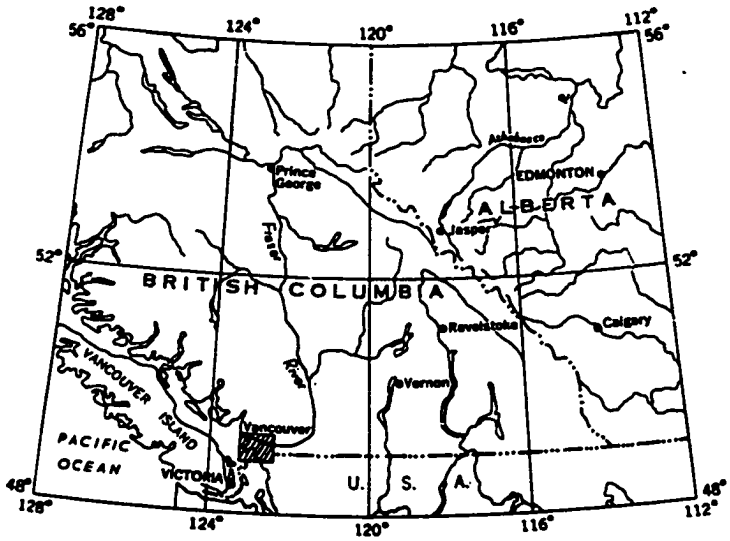

Inset

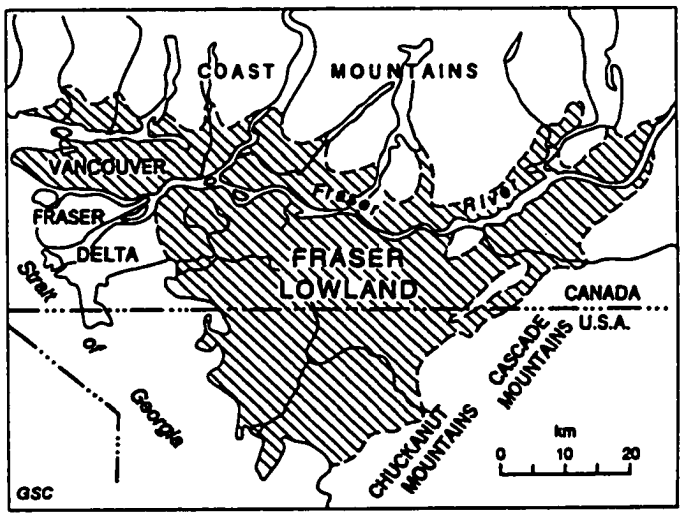

Figure 2-1. Map showing location of the Fraser Lowland and Fraser delta. From Armstrong (1984).

southern British Columbia. The mean discharge at Mission, 75 km upstream from the river mouth, is 3400 m^3s^{-1} (Church et al., 1990; Wolman et al., 1990). River flows show marked seasonal variations. Peak flows during the spring freshet are generally between 5000 and 15000 m^3s^{-1}, whereas minimum flow during the winter is less than 1000 m^3s^{-1} (Milliman, 1980; Church et al., 1990; McLean and Tassone, 1991). In terms of mean flow, the Fraser is the 30th largest of the world's rivers to reach tidewater, larger than the Nile and the Rhine (Nace, 1970; in Leopold, 1994).

The mean annual sediment load is 17.3 million tonnes, of which 35% is sand, 50% is silt and 15% is clay (McLean and Tassone, 1991). Of this sediment load, 80% is transported during the spring freshet (Milliman, 1980). However, the peak in sediment load precedes the peak in river flow by a month or more (Kostaschuk et al., 1989, 1992b; Kostaschuk and Luternauer, 1989; Church et al., 1990; Wolman et al., 1990).

Oceanographic Regime

The Fraser River flows into the Strait of Georgia, a northwest-trending, glacially-scoured marine trough that is 220 km long and 30 km wide (Figures 2-1and 2-2; Holland, 1976). Water depths in the Strait of Georgia exceed 400 m, and at the base of the delta slope, water depth varies from 100 to 300 m.

Wave energy in the Strait of Georgia is low. Significant wave heights exceed 0.8 m only 10% of the time off the Fraser delta, and they generally do not exceed 2.7 m. Winds from the northwest have the longest fetch, so that waves generated by these winds are the largest to affect the delta front (Thomson, undated; 1981).

Tides in the Strait of Georgia are mixed semi-diurnal. At the river mouth at Sand Heads the mean tidal range is 3.1 m and the spring (i.e. large) tidal range is 4.8 m (Thomson, 1981).

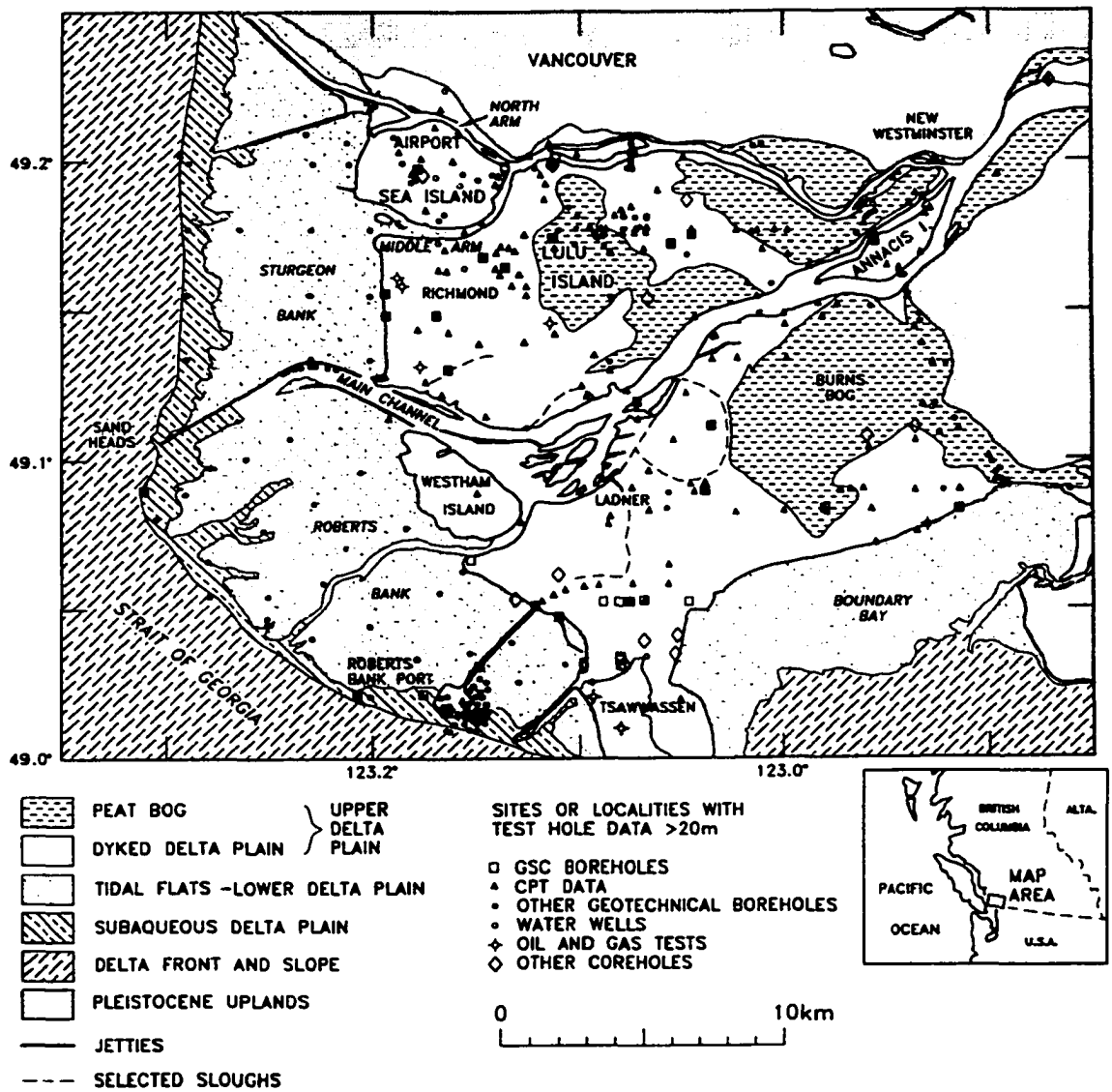

Figure 2-2. Map showing modern sedimentary environments of the Fraser River delta and the distribution of CPT (shown by triangles) and other testhole data. Surficial geology from Armstrong and Hicock (1976a, b), Luternauer and Murray (1973), and Williams and Roberts (1989). Figure modified from Monahan et al. (1993c, 1997).

Tidal influence extends 120 km upstream when river flow is low, and 75 km upstream when it is high (Thomson, 1981). On a rising tide, a wedge of salt water from the Strait of Georgia intrudes beneath the fresh river water in the river channel, and subsequently flows back to sea on the falling tide. This salt wedge can extend 30 km upstream as far as the head of the delta during periods of low flow, but during peak flow it is restricted in the Main Channel to the reach crossing the tidal flats (Figure 2-2; Thomson, 1981; Church et al., 1990; Kostaschuk et al., 1989, 1992b; Kostaschuk and Luternauer, 1989). As the salt wedge lifts the river water off its bed, sand in suspension is deposited in the river channel. The sand is resuspended as the salt wedge withdraws on a falling tide, so that transport of sand in suspension past the river mouth occurs only during low tide (Kostaschuk et al., 1989, 1992b; Kostaschuk and Luternauer, 1989).

At the river mouth at Sand Heads, the river discharges a plume of sediment-laden fresh to brackish water that drifts preferentially to the north, primarily as a result of Coriolis force, tidal currents and possibly internal gravity waves in the Strait of Georgia (Thomson, undated, 1975,1981; Luternauer, 1980).

Along the delta slope off the southern part of Roberts Bank, northwest-flowing flood tidal currents are stronger than ebb tidal currents, and are strong enough to transport sand size material at depths of up to 100 m (Luternauer, 1977, 1980; Kostaschuk et al., 1995; Hart et al., 1998).

MODERN SEDIMENTARY ENVIRONMENTS (Figure 2-2)

The delta is flanked by Pleistocene uplands that are up to 120 m in elevation and underlie the municipalities of Vancouver, Burnaby and New Westminster to the north and Surrey and parts of Delta to the east .

An upper delta plain extends 23 km west from a gap in the Pleistocene uplands at New Westminster (Armstrong and Hicock, 1976a, b; Clague et al., 1983, 1991; Williams and Roberts, 1989). The upper delta plain is mantled by silt deposited in fresh to brackish floodplain marshes and, in its eastern parts, by domed peat deposits up to 8 m thick. Most of it is between mean sea level and the level of the highest tides, although the parts of the peat bogs are higher in elevation. The upper delta plain is now dyked to protect it from flooding, and a system of drainage ditches and pumping stations maintain the water table below the ground surface. The upper delta plain forms the inhabited part of the delta.

At its southern end, the upper delta plain adjoins the Tsawwassen upland, a Pleistocene upland that was a former island in the Strait of Georgia before being connected with the mainland by growth of the delta (Mathews and Shepard, 1963; Clague et al., 1983, 1991). The Tsawwassen upland separates the marine parts of the delta (i.e. seaward from the upper delta plain) into a western, active part that is prograding into the Strait of Georgia and a southern, abandoned part that faces onto Boundary Bay. Prior to construction of the dykes that stabilized it, the Boundary Bay shoreline was undergoing a marine transgression (Armstrong and Hicock, 1976a, b; Hutchinson et al., 1995).

A lower delta plain consisting of dominantly sandy tidal flats up to 9 km wide extends seaward from the upper delta plain to the lowest limit of tides. Large-scale (50-100 m) sandy bedforms are developed on the tidal flats north of the Main Channel, which are most exposed to winds with the longest fetch in the Strait of Georgia (Luternauer, 1980). Tidal flat sediments grade landward from fine sand to silt. The tidal flats are primarily unvegetated, but a strip of tidal marshes underlain by silt occurs along the landward margin of this zone (Luternauer and Murray, 1973; Luternauer, 1980; Clague et al., 1983, 1991; Williams and Roberts, 1989). A subaqueous delta plain mantled by sand extends up to 2 km from the low tide line to a break in slope at a depth of up to 9 m below low tide (Luternauer and Murray, 1973; Williams and Roberts, 1989).

The river divides into four distributaries where it crosses the upper delta plain. However, 75-80% of the flow and of the sedimentary load is carried by the Main Channel (Milliman, 1980; Thomson, 1981). Distributary channels have a maximum depth of 22 m and are floored by fine to coarse sand, locally including gravel (Johnston, 1921; Mathews and Shepard, 1962). Historical records show that the Main Channel has migrated extensively across the tidal flats prior to construction of jetties that now fix its position (Figure 2-3; Johnston, 1921; Clague et al., 1983; Luternauer and Finn, 1983). Although distributary channels in the modern upper delta plain have been more stable, some channel migration has occurred in historical times (Figure 2-4; Johnston, 1921; North et al., 1979; Monahan, et al., 1993c, 1995). The linear gap in the peat bogs in eastern Lulu Island, which has been interpreted to represent a former distributary crossing the floodplain, indicates that major avulsive events have also occurred (Johnston, 1921; Clague et al., 1983; Monahan et al., 1993c; Hutchinson et al., 1995).

Beyond the subaqueous platform, the western delta slope descends at an average of 1.5° to depths of up to 300 m in the Strait of Georgia. The upper part of this slope is commonly inclined 7° or more. The southern delta slope facing onto Boundary Bay is less well defined and terminates in water depths of approximately 30 m (Clague et al., 1983, 1991).

The western delta slope is dominantly silty to the north and sandy to the south of the mouth of the Main Channel (Clague et al., 1983, 1991; McLaren and Ren, 1995). Delta slope silts were deposited from suspension from the plume of sediment-laden fresh to brackish water discharged from the river mouth (Hart et al., 1992; Evoy et al., 1994). Some of the delta slope sands have been deposited from sediment gravity flows that originated at the top of the slope and were transported downslope in a series of large gulleys, or "sea-valleys", bypassing the upper slope (Kostaschuk et al., 1992a; Hart et al., 1992, 1998; Evoy et al., 1994). Failures at the river mouth involving up to 10^6 m^3 of sediment have occurred and provide a likely source for these gravity flow deposits (McKenna et al., 1992). A sand-wave field that occurs on the delta slope off the southern part of Roberts Bank and extends to depths greater

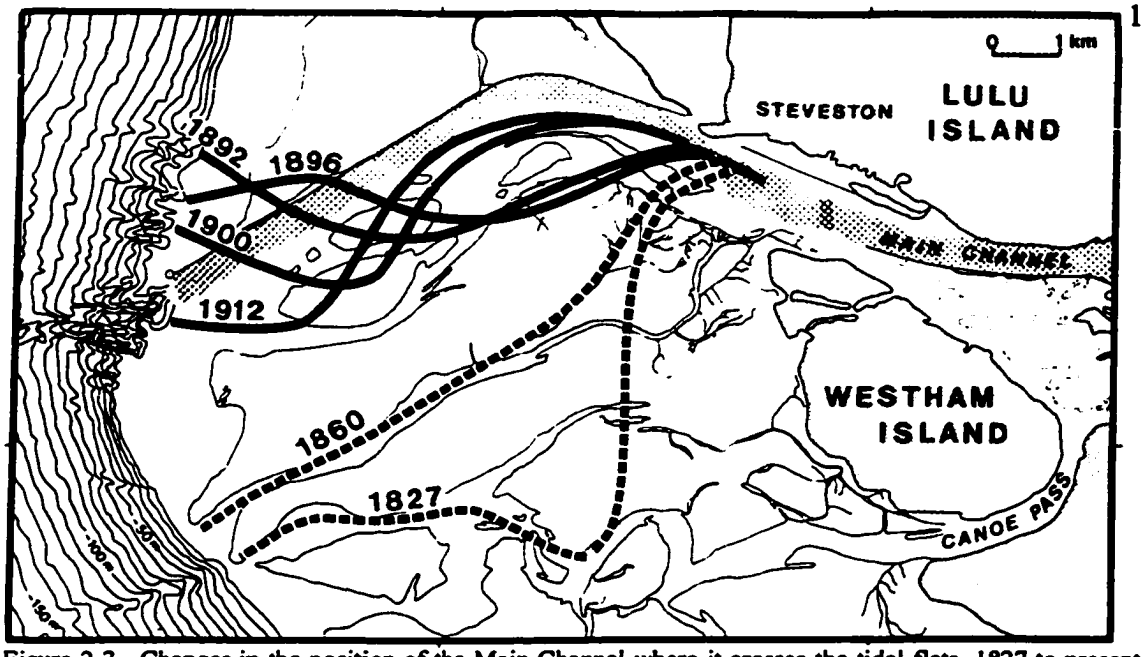

Figure 2-3. Changes in the position of the Main Channel where it crosses the tidal flats, 1827 to present. Former channel positions were obtained from old charts and maps. The present channel position is marked by a cross hatch pattern, and is bounded on the north by a jetty. From Clague et al. (1983) and Luternauer and Finn (1983). Note that between 1896 and 1912 a series of downstream migrating meanders reworked 10km^2 of the tidal flats.

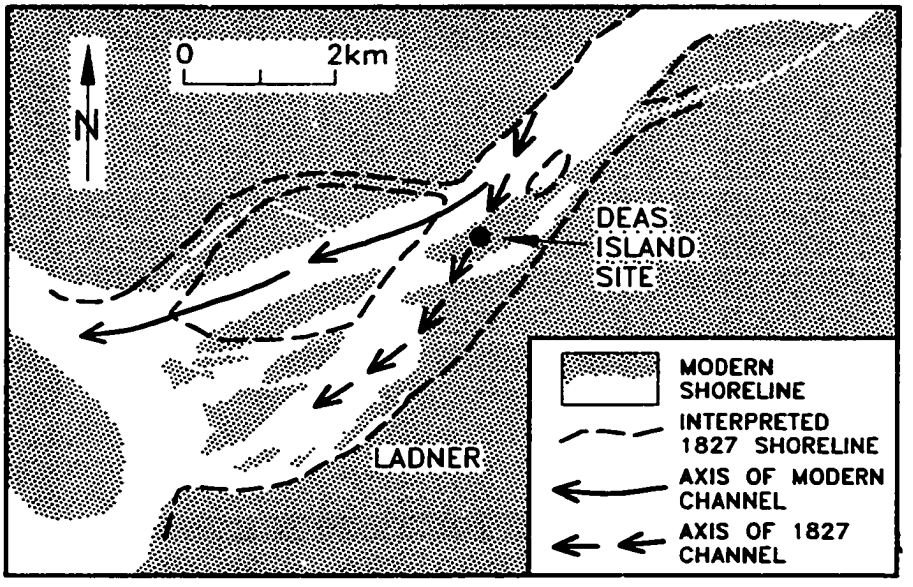

Figure 2-4. Positions of the Main Channel where it crosses the upper delta plain, 1827 and present. Former channel position taken from 1827 Admiralty Survey. Note position of small island that has migrated downstream to its present position (Deas Island). This is the site of Borehole FD94-1. Modified from Monahan et al. (1995).

than 100 m is being developed under the influence of the dominant northwest-flowing flood tidal currents described above (Luternauer, 1977, 1980; Kostaschuk et al., 1995; Barrie and Currie, in press). The sand-wave field is sourced from a complex of sandy river mouth failure deposits that underlies this part of the slope (Hart et al., 1995, 1998; Currie and Mosher, 1996; Barrie and Currie, in press). Consequently, this part of the delta slope is erosional under present conditions - sand is not supplied from fluvial or other sources southeast of Roberts Bank. In addition to the river-mouth failures described above, evidence of delta slope instability is provided by a series of shallow rotational slides on the delta slope immediately south of the Main Channel, and a series of ridges of disturbed sediment near the base of the slope called the "foreslope hills" (Tiffin et al.,1971; Hart et al., 1992, 1995; Hart, 1993; Christian et al., 1997b).

Northwest of the delta slope, the Strait of Georgia is floored with silt and clay derived from the Fraser River, and can be considered the delta bottomset (Pharo and Barnes, 1976). Northwest fining of these sediments indicates that net sediment transport is in that direction.

PREVIOUS INVESTIGATIONS OF THE STRATIGRAPHY OF THE DELTA

The initial investigations of the Fraser delta by Johnston (1921) and Mathews and Shepard (1962) concentrated on the surficial deposits, supplemented by data from some deep geotechnical testholes and petroleum exploratory wells. The first systematic subsurface investigation of the stratigraphy of the delta was by Clague et al. (1983) who established the basic chronology of the growth of the delta. They incorporated data from the logs of over 1500 geotechnical testholes into their interpretations and on the basis of these data, representative vertical stratigraphic sections for several parts of the delta were prepared. However, the borehole logs were primarily descriptive with standard penetration test (SPT) data and did not lend themselves to more detailed correlations and stratigraphic interpretations.

Scientific drilling and geophysical investigations with the intent of documenting the stratigraphy of the delta commenced in the mid 1980's, primarily under the leadership of the Geological Survey of Canada (GSC) and Simon Fraser University (SFU). Roberts et al. (1985) reported on a shallow coring program that focussed on the southern part of the delta and identified the presence of both fluvial and littoral sediments. Williams (1988) and Williams and Roberts (1989, 1990) investigated the uppermost topset deposits on Lulu Island in detail in a series of shallow boreholes and documented the chronology of the mid to late Holocene sea level rise from the depth and thickness of floodplain silts. Luternauer et al. (1986, 1991), Jol (1988), Jol and Roberts (1988, 1992), Pullan et al. (1989, 1998), and Clague et al. (1991) discussed the results of reflection seismic and drilling programs in the southernmost part of the delta. They documented the chronology of delta progradation in that area, the closure of the channel that separated Point Roberts from the delta, and the presence of a thick sequence of sandy foreset beds below topset silts and sands. Patterson and Cameron (1991) and Patterson and Luternauer (1993) described the foraminiferal faunas recovered from the GSC drillholes. Preliminary results of wireline logging have been presented by Hunter et al. (1994, 1998) and Mwenifumbo et al. (1994).

In the early phases of this study, Monahan (1993) and Monahan et al. (1993a, b, c, 1994, 1995a, b, 1997) documented the presence of a complex of distributary channel sand deposits underlying most of the delta plain and described the upper part of the foreset, on the basis of the GSC drillhole data and a large database of geotechnical testholes, (Figure 2-5). CPT data were critical to these studies for the widespread recognition of sharp and gradational lithological boundaries, coarsening and fining upward sequences and dips in foreset beds.

Concurrently with this study, Williams and Luternauer (1991) and Hutchinson et al. (1995) documented the presence of a former distributary channel that flowed into Mud Bay on the southern margin of the delta. This investigation is discussed in more detail in Appendix I.

Some of the GSC drilling programs in which the author participated and which provided data

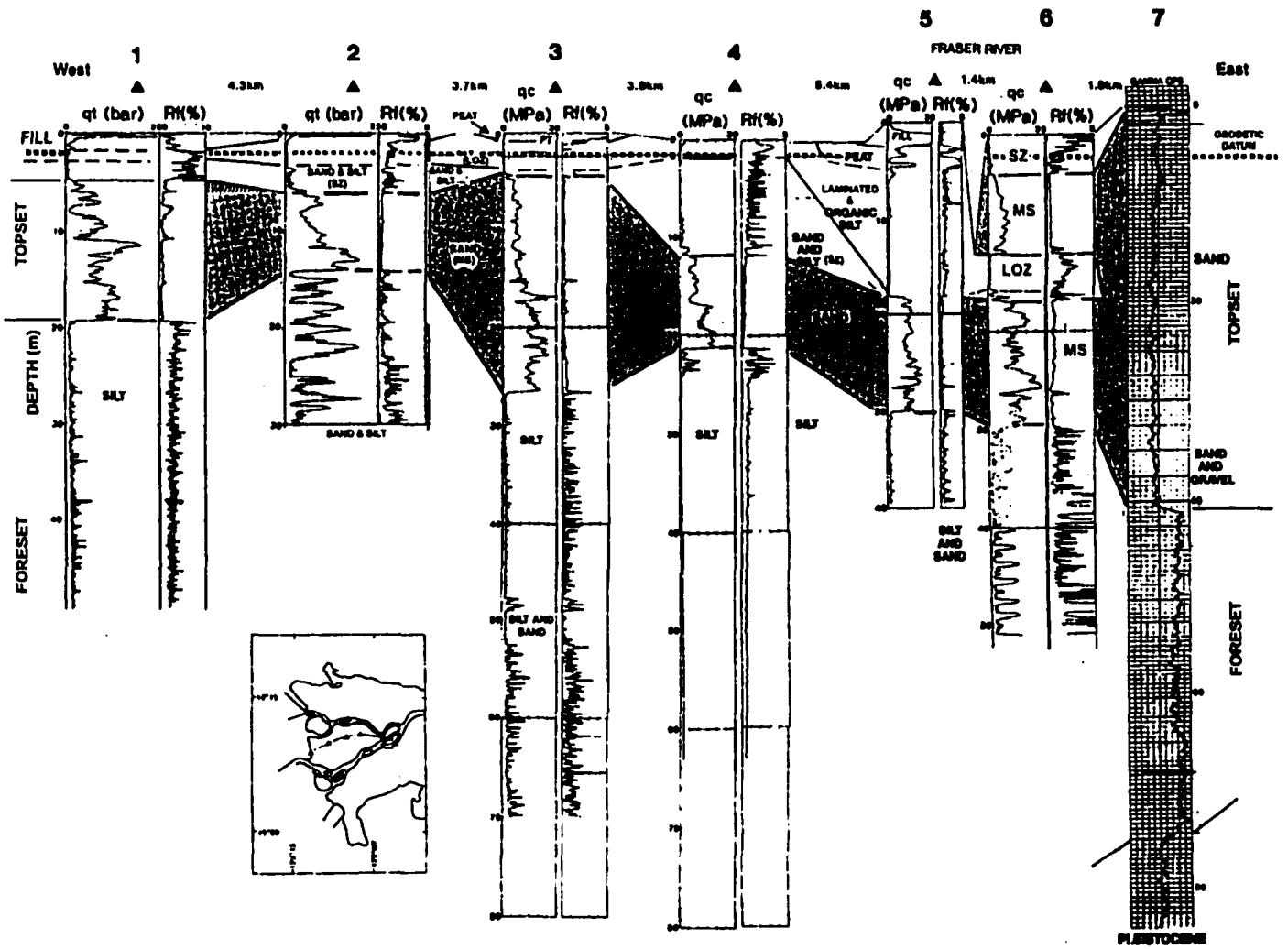

Figure 2-5. East-west CPT cross section across the upper delta plain, showing the continuity of the sand unit (stippled) in the lower part of the topset. The underlying sediments are foreset deposits. The easternmost log is a gamma ray log. For facies symbols see Table 6-1. Figure modified from Monahan et al., 1993a, b, c, and 1997.

for this dissertation have been described in part by other authors. Christian et al. (1994a, 1994b, 1995, 1997a) published preliminary results of recent onshore and offshore GSC drilling and CPT programs in the Roberts Bank and Sand Heads areas. Dallimore et al. (1995, 1996) described the preliminary results of three 300 m holes in 1994 and 1996.

Many geotechnical studies have been conducted in the delta (e.g. Luternauer and Finn, 1983, Campanella et al., 1983). Notable among those that pertain to the stratigraphy of the delta are those by Terzhagi (1962), who commented on the stratigraphic conclusions drawn by Mathews and Shepard (1962); Wallis (1979), who prepared representative vertical stratigraphic sections for several parts of the delta; and Watts et al. (1992) who used CPT data to correlate the stratigraphic unit defined by Williams and Roberts (1989).

STRATIGRAPHIC SUMMARY OF THE FRASER DELTA

The Fraser River delta is entirely Holocene in age (Clague et al., 1993, 1991). Deposits of the delta have a maximum known thickness of 305 m (Dallimore et al., 1996) and overlie Pleistocene glaciogenic sediments (Hamilton, 1991; Hart et al., 1995; Luternauer et al., 1994; Clague et al., 1998). Relative sea level has risen approximately 13 m as the Fraser delta has prograded into the Strait of Georgia, although most of this rise occurred between 8000 and 4500 ^{14}C years B.P. (Clague et al., 1983; Williams and Roberts, 1989, 1991). The deltaic section can be subdivided into topset, foreset and bottomset units (Monahan et al., 1993c, 1997; Luternauer et al., 1993, 1994; Clague et al., 1998).

The topset thins from a maximum of 40 m at the apex of the delta to 20 m or less at the western margin of the upper delta plain as a result of the mid Holocene rise in relative sea level (Figure 2-5; Clague et al., 1983; Williams, 1988; Williams and Roberts, 1989, 1991; Monahan et al., 1993a, b, c, 1995b, 1997; Hutchinson et al., 1995). The topset forms an overall fining-upward sequence that grades up from a lower sand unit, that forms a distinct

stratigraphic marker, to an overlying package of sands and silts. The topset is dominated by the lower sand unit, which is generally 8 to 30 m thick, has a sharp base with several metres of local relief and has a gradational top (Monahan et al., 1993a, b, c, 1995, 1997). The sand unit is overlain by a thin unit of interbedded sands and silts. On the upper delta plain, these are in turn overlain by floodplain silts, which are locally capped by peat.

Deposits of the topset sand unit sharply overlie sediments in which seaward dips up to 7° can commonly be recognized on reflection seismic profiles and CPT correlations, and represent foreset deposits (Pullan et al., 1989, 1998; Clague et al., 1991, 1998; Monahan, 1993; Monahan et al., 1993c, 1995, 1997). Foreset deposits are up to 165 m thick.

Foreset deposits include both silts and sands interlaminated and interbedded on a variety of scales. Silts of the upper foreset (<60 m) are laminated and commonly include thin very fine sand interbeds. Silts of the lower foreset are commonly bioturbated and are progressively finer with depth (Christian et al., 1994; Dallimore et al., 1995, 1996). Sand is most common in the upper foreset. In the southernmost part of the delta, sand-dominated units up to 30 m thick occur interbedded with thinner silt-dominated units and extend to depths as great as 130 m (Clague et al., 1991; Luternauer et al., 1991). Further to the north, where the foreset as a whole is dominated by silt, sand-dominated units up to 30 m thick occur locally at the top of the foreset (Monahan, 1993; Monahan et al., 1997; Luternauer et al., 1994; Clague et al., 1998).

In deeper deltaic sections, the foreset deposits overlie up to 120 m of clayey silt with minor sand that accumulated more slowly than the overlying foreset (Figure 2-6; from Luternauer et al., 1994; Figure 7). These form the bottomset of the delta and are analogous to the sediments of the modern Strait of Georgia (Clague et al., 1983, 1991; Luternauer, et al., 1993, 1994; Clague et al., 1998).

Deltaic deposits conformably overlie glaciomarine pebbly silts deposited at the close of the

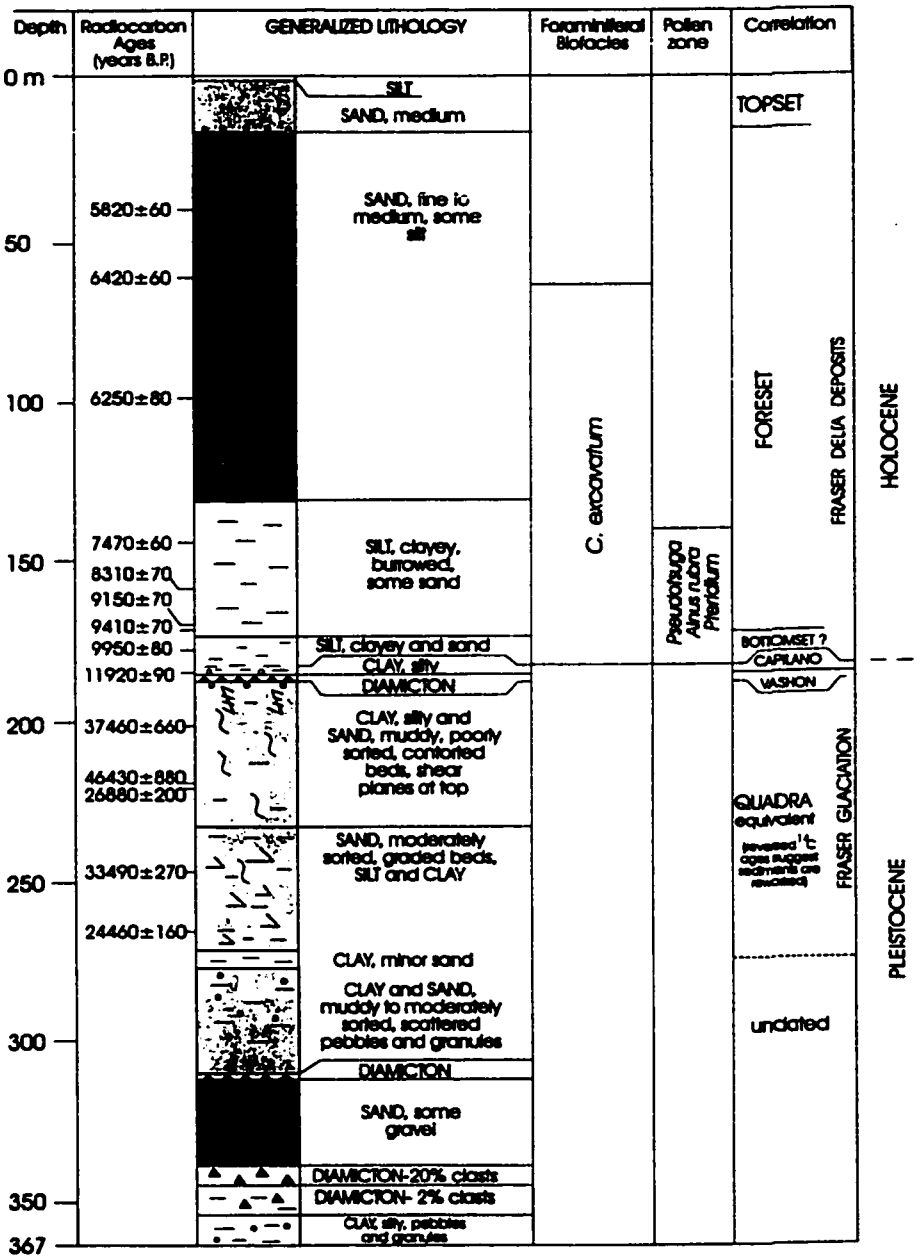

Figure 2-6. Holocene and Pleistocene stratigraphy in GSC borehole FD87-1, from Luternauer et al., 1994, Figure 7. Note the identification of bottomset deposits based on the slower sedimentation rate than foreset deposits and presence of sandy interbeds; and the identification of Capilano glaciomarine deposits based on the presence of pebbly silts and radiocarbon dates (Armstrong, 1981). Note that ^{14}C dates are uncorrected for reservoir effects. See Appendix F for corrected depths.

Late Wisconsinan Fraser Glaciation 11,000 to 13,000 years B.P. (Figure 2-4; Armstrong, 1981; Hamilton, 1991; Hart et al., 1995; Luternauer et al., 1994; Clague et al., 1998). The glaciomarine sediments, which are a facies of the Capilano sediments (Armstrong, 1981), are generally a few metres thick in boreholes on the modern upper delta plain, but are locally as thick as 20 m (Luternauer et al., 1991, 1994; Dallimore 1995, 1996; Clague et al., 1998). They overlie dense diamicton of the Vashon Till of the Fraser Glaciation, which in turn overlies older overconsolidated[1] glacial and non-glacial deposits. At sites where Capilano glaciomarine deposits have not been identified on the margins of the delta, the base of the deltaic section is marked by the presence of dense sand and gravel deposits and refusal in standard penetration tests (SPTs) and CPTs (e.g. Figure 6-21; Monahan et al., 1995). These coarser sediments may include shallower facies of the Capilano sediments, as well as the Vashon Till and earlier Pleistocene deposits.

---

[1]For definition, see Appendix A.

CHAPTER 3

CONE PENETRATION TESTING

BASIC PRINCIPLES AND OPERATION

Excellent descriptions of cone penetration testing are provided by Campanella et al. (1983), Campanella and Robertson (1988), Robertson and Campanella (1983a, b, 1986), Robertson et al. (1986), Robertson (1990) and Lunne et al. (1997). Much of this chapter is derived from these sources. The summary presented here is not intended to be exhaustive, but to focus on those factors critical to the *geological* interpretation of cone penetration test (CPT) data.

Cone penetration testing originated in the Netherlands in the 1930's with the use of mechanical devices (Broms and Flodin, 1988; Lunne et al., 1997). Electrical cone penetrometers, which permitted continuous recording and the use of load cells capable of much more sensitive measurements than mechanical devices, were first introduced in Germany in 1944. Much of the subsequent development of these devices occurred in the Netherlands (Broms and Flodin, 1988). In the last 20 years, cone penetration testing has been greatly advanced by Campanella and his students at the University of British Columbia (Campanella et al., 1983; Robertson and Campanella, 1983a, b, 1986; Robertson et al., 1986), and as a results of their efforts, a large volume of CPT data has been generated in the Fraser delta.

A CPT is performed by pushing an instrumented cone-tipped rod into unlithified sediment at 2 cm/sec, usually with a purpose-built drilling rig using a hydraulic jacking system. The equipment and operating procedures conform to internationally defined standards (e.g. ISSMFE Technical Committee on Penetration Testing, 1988; ISSMFE, 1989). A sketch

of a cone penetrometer is shown in Figure 3-1 and a typical CPT plot is shown in Figure 3-2. The cone has a 60° apical angle and most cones used have a 10 cm^2 projection area, although 15 cm^2 cones are also available. A load cell in the tip records the resistance to penetration at the cone tip - the *cone bearing* or *tip resistance*. In general, cone bearing in sands is higher than in finer sediments. A friction sleeve is located immediately above the cone tip and records the frictional resistance of the sediments penetrated - the *sleeve friction* in Figure 3-2. The friction sleeve has an area of 150 cm^2 in a 10 cm^2 cone, and 225 cm^2 in a 15 cm^2 cone. The absolute values of friction are greater in sands than finer sediments. However, the *friction ratio*, the ratio of sleeve friction to the cone bearing, is *lower* in sands than in finer sediments, and the friction ratio curve resembles a gamma ray log used in the petroleum industry. The cone bearing and friction ratio curves can be cross plotted to provide a more reliable *estimate* of sediment type on "soil classification charts"[1] developed by several workers (Figure 3-3a; e.g. Robertson and Campanella, 1986).

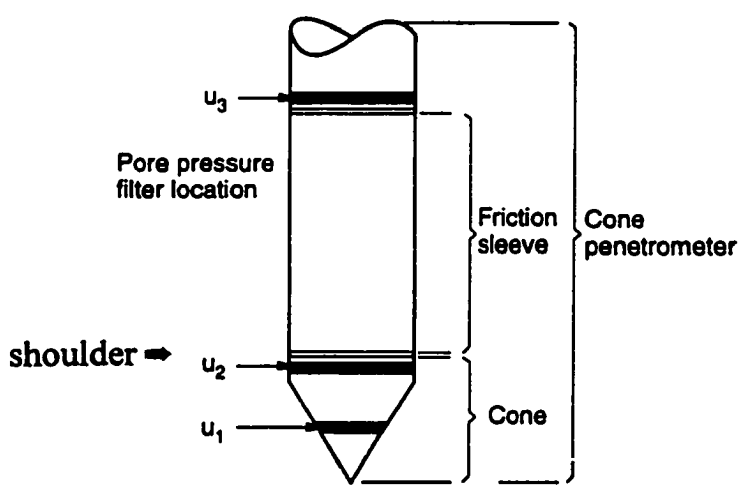

Figure 3-1. Terminology for cone penetrometers. 10 cm^2 cone penetrometers have a diameter of 3.56 cm, and 15 cm^2 cone penetrometers have a diameter of 4.37 cm. From Lunne at al. (1997).

---

[1] The term "soil classification chart" appears throughout the industry and is used here as well. However, it provides an estimate of the sediment type based on CPT responses. Strictly speaking, soil classification requires samples.

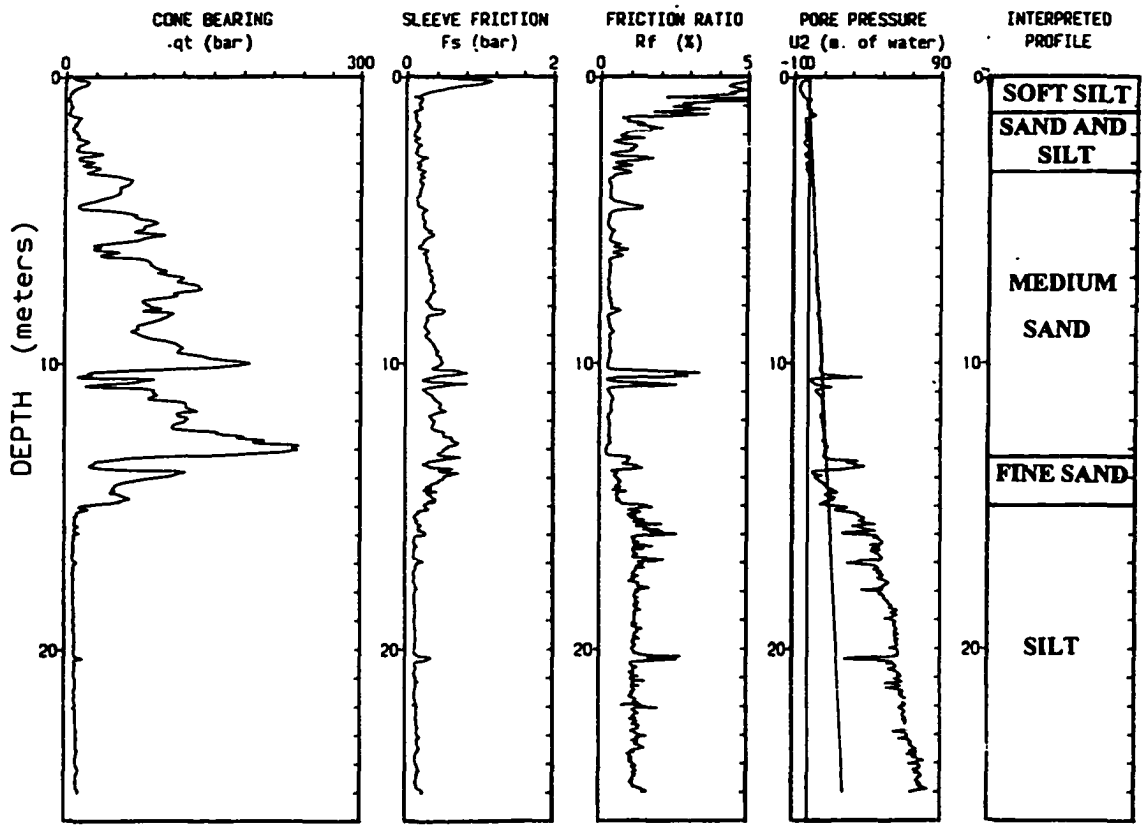

Figure 3-2. Cone penetration test plot from the UBC test site at McDonald's Farm on the north side of Sea Island, Fraser River delta. Data courtesy of R.C. Campanella. From left to right: cone bearing, is a measure of the resistance to penetration at the cone tip; sleeve friction, is a measure of the frictional resistance recorded immediately above the tip; friction ratio is the ratio of sleeve friction to cone bearing; pore pressure is the dynamic pore pressure induced by the cone, and is referenced to hydrostatic pressure shown by the straight line; and interpreted profile is the lithology (modified from Campanella et al., 1983; and Robertson et al., 1983). Cone bearing and sleeve friction are recorded in bars, and pore pressure is recorded in metres of water (1 m of water = 0.0981 bars). Note that cone bearing is high in sand and low in finer sediments, and that friction ratio is low in sands and higher in finer sediments. Pore pressures are greater than hydrostatic in silts and below hydrostatic in fine sands. Pore pressures in medium and coarser sands generally fall on the hydrostatic gradient.

A pore pressure transducer records the dynamic pore pressure induced by penetration of the cone. CPTs with pore pressure data are also called "CPTUs" or "piezocones", and most modern CPTs are CPTUs. Pore pressure measurements are referenced to the hydrostatic water pressure, shown by the straight line on the pore pressure curve in Figure 3-2. Silts and clays generally have pore pressures greater than hydrostatic. Conversely, fine and/or dense sands have pore pressures less than hydrostatic, because they dilate as they fail under cone penetration, causing a volume increase and corresponding pore pressure decrease. In coarser and/or looser sands, in which the permeability is sufficient to overcome any induced pore pressure changes, the pore pressures plot on the hydrostatic pressure gradient. Pore pressure data can also be cross-plotted with cone bearing to provide an estimate of sediment type (Figure 3-3a; Robertson and Campanella, 1986). Pore pressure on the soil classification chart is represented by B_q, the pore pressure parameter ratio, which is defined below in the section on normalization of CPT data. Pore pressure can be measured at several positions on the cone: on the cone tip itself - U_1; immediately above the cone tip - U_2; and above the friction sleeve - U_3 (Figure 3-1). In most commercial cones, the pore pressure is measured at the U_2 position, because it is less susceptible to damage than the U_1 position, yet it is close enough to the tip where the maximum pore pressure changes occur. Furthermore, the U_2 position is the best to measure pore pressure for corrections to cone bearing (Robertson and Campanella, 1986). This will be discussed further below.

Additional sensors can be added. A resistivity module located above the friction sleeve can be added to provide a continuous record of resistivity (RCPT, i.e. resistivity cone penetration test; van der Graaf and Zuidberg, 1985; Campanella and Weemees, 1990). A geophone can be added above the friction sleeve to record a shear-wave velocity profile (SCPT, i.e. seismic cone penetration test; Robertson et al., 1992a). Shear wave arrivals are generally recorded every meter during rod breaks, and interval velocities are computed from the difference in arrival times. Both RCPTs and SCPTs are routinely, if not commonly, recorded in the Fraser delta. Other sensors, that are currently being introduced in CPTs conducted in the Fraser delta include a natural gamma ray module that measures natural radioactivity and is

Figure 3-3. Soil classification charts based on CPT data. These charts are used to cross plot CPT data to provide an *estimate* of the sediment type (i.e. soil behaviour type).

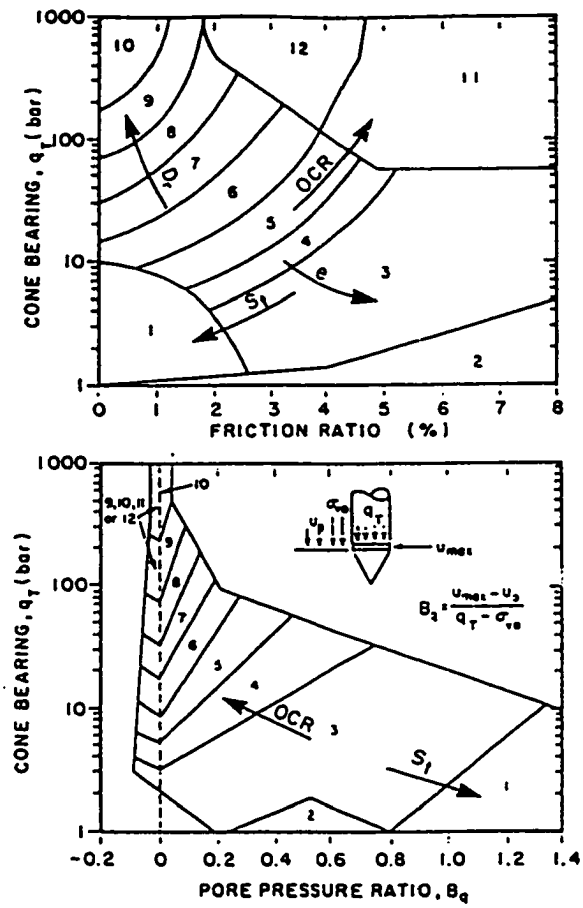

Zone	Soil Behaviour Type
1	sensitive fine grained
2	organic material
3	clay
4	silty clay to clay
5	clayey silt to silty clay
6	sandy silt to clayey silt
7	silty sand to sandy silt
8	sand to silty sand
9	sand
10	gravelly sand to sand
11	very stiff fine grained*
12	sand to clayey sand*

* overconsolidated or cemented.

Figure 3-3a. Soil classification charts using CPT data uncorrected for overburden stress: cone bearing and friction ratio above and cone bearing and pore pressure parameter ratio (B_q: see text for definition) below. Dr = relative density or density index; OCR = overconsolidation ratio; e = void ratio; St = sensitivity. From Robertson et al. (1986). For definitions of terms see Appendix A.

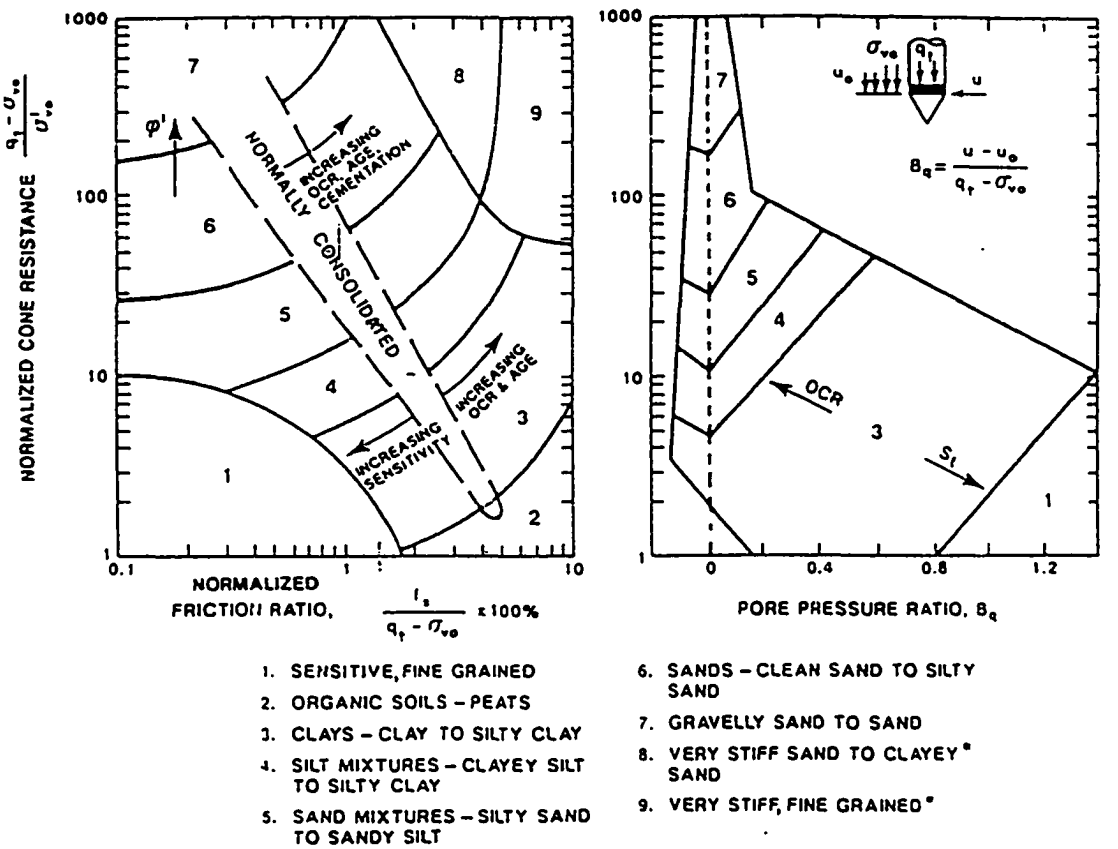

Figure 3-3b. Soil classification charts using CPT data normalized for overburden stress: normalized cone bearing (Q_t) and normalized friction ratio (F_R) on the right, and normalized cone bearing (Q_t) and pore pressure parameter ratio (B_q) on the right. See text for definitions. Abbreviations as in Figure 3-3a. From Robertson (1990).

comparable to a gamma ray log used in the petroleum industry (Singha et al., 1997); a gamma-gamma module that measures density and is comparable to a density log used in the petroleum industry (van der Graaf, 1985; Sully and Echezuria, 1988; Singha et al., 1997); and a ultra-violet induced fluorescence moduie to identify hydrocarbon contaminants (Woeller and Robertson, 1997). This dissertation deals with the standard CPT measurements and parameters derived from them, that is cone bearing, sleeve friction and pore pressure.

Data are recorded by the cone penetrometer are transmitted to the surface, usually by means of a cable threaded through the push rods. However, in some cases data is transmitted to the surface acoustically (e.g. Sy et al., 1987; Moran et al., 1989). Data are recorded digitally, usually every 2.5 or 5 cm. Push rods are 1 m in length.

Because measurements are measured at or near the cone tip, they are unaffected by friction of the push rods in the sediment. However, rod friction limits the depth of penetration, which is usually 30 to 70 m. Deeper penetration requires pushing the cone from the base of a drilled hole. CPT's cannot usually penetrate thick gravel beds, till, or overconsolidated[2] sand.

Several methods have been developed to acquire CPT data offshore (e.g. van der Graaf, 1985; Lunne et al., 1997). One of the simplest for shallow water depths, and that used for offshore operations in the Fraser delta, is using a land-based rig mounted on a spud barge with a moon pool[2].

---

[2]For definition see Appendix A.

CPT MEASUREMENTS AND CORRECTIONS

With appropriate calibration and maintenance, load cells and pressure transducers can have an accuracy and precision of 0.2% of full scale output, but under field conditions, repeatability is usually less (Lunne et al., 1997). The most significant source of error in cone bearing measurements is a zero shift due to temperature, although in the Fraser delta this is estimated to be generally less than 1 bar (I. Weemees (ConeTec), pers. comm. 1998; see also Schaap and Zuidberg, 1982; Lunne et al., 1986). The effect of this zero shift is proportionately greater in soft fine grained sediments in which cone bearing is low. Field tests of a variety of cones have shown that the variation in cone bearing in a uniform sediment independent of temperature is usually less than 1 bar (Lunne et al., 1986).

Cone bearing values in all cone penetrometers must be corrected for the effect of pore pressure acting on the shoulder area immediately above the cone. Cone bearing corrected for pore pressure, "q_t", is defined as:

$$q_t = q_c + (1-a)\,u \qquad 1)$$

where: q_c = measured cone bearing,

u = measured pore pressure, and

a = cone bearing net area ratio, which is approximately the ratio of the load cell cross sectional area to the projected area of the cone.

The value of "a" may be estimated from the cone geometry, but in practice should be determined in a calibration vessel (Campanella and Robertson, 1988; Robertson, 1990). In data used for this project, "a" varies from 0.57 to 0.85 (Table 4-1). As can be seen from equation 1 and Figure 3-2, this correction is significant principally in fine grained soils, where q_c is small and u may be large. The U_2 position provides the best measure of pore pressure ("u") for this correction.

Where pore pressure data are available, the friction ratio, R_f is usually expressed as:

$$R_f = f_s / q_t \qquad 2)$$

where: f_s = measured sleeve friction.

A correction for water pressure similar to that for cone bearing can theoretically be applied to the friction sleeve measurements, because the dynamic water pressure varies from one end of the friction sleeve to the other (Robertson, 1990; Lunne at al., 1997). This correction is greatly reduced if a cone penetrometer with an equal end area friction sleeve is used[3]. However, pore pressure data are required at *both* ends of the friction sleeve (i.e. U_2 and U_3 positions) to make reliable corrections, and CPTs with such measurements are rare.

Friction sleeve measurements, and consequently the derived friction ratio values, are commonly less accurate and repeatable than cone bearing measurements (Lunne et al., 1986; Robertson, 1990). Reasons for this include the inability to apply the water pressure correction on friction sleeve measurements, as described above, and design difference between cones, such as the end area ratio of the friction sleeve, can cause differences in sleeve friction measurements (Lunne et al., 1997; Robertson and Wride, 1997). In addition, wear on the friction sleeve after prolonged use reduces friction measurements, in some cases up to 45% (Schaap and Zuidberg, 1982; Lunne et al., 1986; Jekel, 1988). Conversely, a new friction sleeve placed behind a worn cone may record *higher* friction if the diameter difference between the sleeve and cone exceeds established specifications (D. Gillespie, pers. comm. 1998). Furthermore, many cones are *subtraction* cones, in which two load cells in series record the cone bearing and the cone bearing plus sleeve friction respectively and the sleeve friction is derived by subtraction. This arrangement provides a robust design, but friction sleeve measurements are much lower than cone bearing measurements and the total

---

3 i.e. the ends of the friction sleeve exposed to water pressure have the same area.

capacity of the load cells, so that errors in friction sleeve measurements are proportionately larger. Finally, errors in cone bearing can have a significant effect on the friction ratio in fine sediments, where cone bearing is typically low and friction ratio high. As a result of these errors, friction ratio measurements are generally consistent within a particular CPT, but may not be repeatable between tests.

Pore pressure data are commonly expressed as the *excess pore pressure*, "dU", the difference between the measured pore pressure and hydrostatic pressure;

$$dU = u - u_0 \qquad 3)$$

where: u_0 = hydrostatic pore pressure.

CPT DATA INTERPRETATION

Cone bearing measurements increase with relative density, shear strength, grain size, age[4], cementation, overconsolidation[5] and in situ stress (Figure 3-3; Robertson and Campanella, 1986; Robertson et al., 1986). Gravelly intervals can cause sharp increases in cone bearing. Mineralogy affects the compressibility of the sediment, and as compressibility increases, cone bearing decreases. Friction ratio increases with overconsolidation and decreases with increasing sensitivity[5] in fine sediments.

Cone bearing measurements are also affected by strata above and below the cone tip, so that

---

4

Sediment ageing includes several processes that increase shear strength with time. These appear to be primarily due to particle rearrangement on a microscopic scale rather than cementation (Schmertmann, 1992). See also Chapter 5.

5

For definition, see Appendix A.

abrupt stratigraphic changes are reflected as a more gradual change on cone bearing measurements, and cone bearing values in thin beds are different from those in thicker beds of exactly the same material (Robertson and Campanella, 1986; Robertson and Fear, 1996; Lunne et al., 1997). The sphere of influence of cone bearing measurements increases with sediment stiffness. Consequently, thin beds with low cone bearing are better resolved (i.e. mechanical properties correctly measured) than thin beds with higher cone bearing. Based on a theoretical approach, Vreugenhill et al. (1994) have proposed correction factors for thin beds of sand encased in finer sediments. Because the correction factors are large, Robertson and Fear (1996) and Lunne et al. (1997) have recommended conservative application of these correction factors.

As noted above, pore pressure measurements provide an estimate of the permeability of the sediment, and consequently, its grain size and/or density. During pauses in cone penetration, that usually occur during rod breaks, pore pressures dissipate, and the rate of dissipation can be measured and provide additional information on the permeability and coefficient of consolidation (Robertson et al., 1992b). Pore pressure measurements also provide information as to whether penetration is taking place under drained or undrained conditions[6]. As penetration in fine grained soils changes from undrained to drained conditions, cone bearing increases slightly, but sleeve friction, and consequently friction ratio increases several fold (Campanella et al., 1983). Changes in drainage conditions in a uniform sediment can occur due to dissipation of pore pressures during rod breaks, particularly the prolonged rod breaks that occur in SCPTs. Consequently, rod breaks can be expressed in a uniform sediment as pronounced friction ratio peaks and pore pressure minima (in fine sediments) with sharp tops and gradational bases 1 m apart (see Chapter 5).

---

6 For definition, see Appendix A.

NORMALIZATION OF CPT DATA FOR OVERBURDEN STRESS

In situ stress conditions are an important control over CPT measurements. A uniform sediment appears to change from one sediment type to another with depth on sediment classification charts that do not take in situ stresses into consideration. Consequently, Robertson (1990) developed a soil classification chart based on CPT data normalized for overburden stress (Figure 3-3b), using the following equations:

Normalized cone bearing: $Q_t = (q_t - \sigma_{vo})/\sigma'_{vo}$ 4)

Normalized friction ratio: $F_R = f_s/(q_t - \sigma_{vo}) \times 100\%$ 5)

Pore pressure parameter ratio: $B_q = dU/(q_t - \sigma_{vo})$ 6)

where: σ_{vo} = vertical overburden stress (i.e. average unit weight times depth; unit weight is density times gravitational acceleration), and

σ'_{vo}= effective vertical overburden stress (i.e. σ_{vo} less hydrostatic pressure).

Robertson and Fear (1996) and Lunne et al. (1997) have defined a normalized soil behaviour type index, I_C, based on the observation that normally consolidated sediments fall on a straight line on the normalized soil classification chart, and that with increasing overconsolidation, age and cementation would follow an arcuate path normal to this line (Figure 3-3b). I_C is defined as follows:

$$I_C = [(3.47 - \log Q_t)^2 + (\log F_R + 1.22)^2]^{0.5} \quad 7)$$

The boundaries of soil behaviour type are listed in the Table 3-1.

TABLE 3-1: Boundaries of Soil Behaviour Types (Robertson and Fear, 1996)

Soil Behaviour Type Index, I_C	Soil Behaviour Type
$I_C < 1.31$	gravelly sand
$1.31 < I_C < 2.05$	sands: clean sand to silty sand
$2.05 < I_C < 2.60$	sand mixtures: silty sand to sandy silt
$2.60 < I_C < 2.95$	silt mixtures: clayey silt to silty clay
$2.95 < I_C < 3.60$	clays
$I_C > 3.60$	organic soils: peats

In addition, Robertson and Fear (1996) and Lunne et al. (1997) proposed a general relationship between I_C and fines content (FC):

$$FC = 1.75\ I_C^3 - 3.7. \qquad 8)$$

In this context, "fines content" is that of the engineering literature, the fraction finer than 0.074 mm or 3.75 ϕ (see Chapter 4).

However, several other procedures are used for normalizing cone bearing for overburden stress in sand in the assessment of liquefaction susceptibility, and normalization of cone bearing in sand is still a matter of debate. For example, Robertson and colleagues (Robertson and Campanella, 1985; Robertson et al., 1992a; Robertson and Fear, 1996; and Lunne et al., 1997) use the following equation:

Normalized cone bearing: $$q_{c1} = (q_c/Pa)(Pa/\sigma'_{vo})^{0.5} \qquad 9)$$

where: Pa = atmospheric pressure.

Equation 9 uses the same correction factor, $(Pa/\sigma'_{vo})^{0.5}$, as that generally used to normalize

standard penetration test blowcount data for overburden stress (Liao and Whitman, 1986). In this equation, measured cone bearing (q_c) is divided by Pa to make q_{c1} dimensionless, as are Q_t, F_R, and B_q. However, others (Kayen et al., 1992; Stark and Olson 1995; Olson and Stark, 1998) use the following equation:

$$q_{c1(Kayen)} = q_c(1.8/(0.8+(\sigma'_{vo}/Pa)) \quad 10)$$

Olsen and Malone (1988) and Olsen (1994) have proposed normalization of cone bearing data according to the general equation:

$$q_{c1(Olsen)} = (q_c - \sigma_{vo})\,(Pa/\sigma'_{vo})^c \quad 11)$$

where c, the cone stress exponent, varies from approximately 0.5 in sands to 1.0 in normally consolidated silts and clays. This equation links equations 4 and 9, where the stress exponents are 1 and 0.5 respectively[7]. This approach appears to be conceptually sound. In normally consolidated silts and clays, cone bearing generally increases *linearly* with depth (i.e. c =1.0), justifying the use of Q_t in these sediments (Robertson, 1990; Lunne et al., 1997). In sand, Konrad (1997) has derived a cone stress exponent of 0.627 from laboratory data. However, application of equation 11 requires a cumbersome iterative process (Robertson, pers. comm. 1995; Lunne et al., 1997).

More recently, Robertson and Wride (1997, 1998) have proposed a simple iterative procedure based on I_C to normalize cone bearing data using a variable cone stress exponent. Most silts and clays are normalized using c=1, sands are normalized using c=0.5, and intermediate soil types are normalized with a somewhat arbitrarily defined value of c=0.75.

7

In sands, $q_c \sim q_t$, and $q_c >> \sigma_{vo}$, so that $q_c \sim (q_t - \sigma_{vo})$. Furthermore, $q_{c1(Olsen)}$ can be made dimensionless by dividing $(q_c - \sigma_{vo})$ by Pa.

In this procedure the parameter herein referred to as Q is substituted for Q_t in equation 7 and is defined as:

$$Q = (q_t - \sigma_{vo})(Pa/\sigma'_{vo})^c \qquad 12)$$

I_C is calculated initially using c=1 (ie $Q=Q_t$). Where I_C is greater than 2.6, no further adjustment is required. Where I_C is less than 2.6, Q and I_C are recalculated using c=0.5. If the recalculated I_C is greater than 2.6, then Q and I_C are recalculated again using c=0.75. The final value of I_C, based on the appropriate values of c and hence of Q, is herein referred to as I_F.

In investigations where σ'_{vo} is between 0.5 and 1.5 atmospheres (0.5 to 1.5 bar, or ~5 to ~15 m depth in most Fraser delta deposits), the different normalization procedures produce similar results (Robertson and Fear, 1997; Olson and Stark, 1998). However, appropriate normalization is required for investigations that span greater depth ranges, such as this study. The choice of normalization procedures used for this research is discussed and justified in Chapters 4 and 5.

GEOLOGICAL USE OF CPT DATA

CPTs have been used extensively for geologic mapping in the Netherlands (de Mulder, 1990, pers. comm. 1993), but published results elsewhere are limited. De Mulder (1979) and de Mulder and Bakker (1989) presented cross sections from sites in the Netherlands based on penetration resistance values, with representative CPT's. De Mulder and Westerhoff (1985) briefly described CPT characteristics of three coastal sand depositional environments and related those characteristics to depositional processes.

In North America, Schoustra (1975) recognized that CPT data could be used for stratigraphic

correlation in a manner similar to wireline logs, and showed a representative cross section from a site in California. Moran et al. (1989) showed that sedimentologically distinct units in the Late Wisconsin Mackenzie delta could be distinguished in a CPT profile at a site in the Beaufort Sea, and could be correlated with borehole and seismic data. Taylor et al. (1993) integrated CPT, seismic and borehole data in their investigation of Hibernia on the Grand Banks of Newfoundland.

Several studies have used CPT data for geological investigations in the Fraser River delta. Watts et al. (1992) showed a CPT cross section correlating the stratigraphic units defined by Williams and Roberts (1989). Both Monahan et al., (1993a, c) and Mwenifumbo et al. (written communication, 1992; 1994) have commented on the similarity of the friction ratio curve to gamma ray logs. As noted in the previous chapter, CPT data were critical to the identification and interpretation of the topset sand and foreset deposits by Monahan (1993) and Monahan et al. (1993a, b, c, 1994, 1995a, b, 1997) in the early phases of this study. On the basis of CPT data, sharp and gradational lithological boundaries, coarsening and fining upward sequences and dips in foreset beds could be recognized beyond the limits of borehole control. In their documentation of a distributary channel system flowing into Boundary Bay, Hutchinson et al. (1995) used CPT data in part to define some of the facies in the topset. Most recently, Christian et al. (1997a) discussed the stratigraphy of foreset deposits at the river mouth at Sand Heads, based in part on CPT data. The stratigraphic conclusions reached by the last two studies differ from those reached by this author, based on a regional interpretation of the CPT data, and are discussed in Appendix I.

CHAPTER 4

DATA COLLECTION AND ANALYSIS

INTRODUCTION

In order to apply CPT data to facies analysis in the Fraser delta, a CPT database was developed throughout the delta, and a suite of continuously cored boreholes was drilled adjacent to selected CPTs in order to determine the facies significance of shapes of the CPT curves and the CPT expression of each facies. The cores were logged in the field and in the laboratory. Based on the visual examination of the cores, grain size trends appeared to be reflected in CPT measurements. Consequently, a suite of grain size samples was analyzed to determine the correlations of grain size with CPT measurements. The cores were depth-corrected to remove the effects of core disturbance, primarily by the use of borehole gamma ray logs, and correlated with the adjacent CPTs in order to compare the grain size measurements with normalized CPT data. In addition, several samples were submitted for radiocarbon dating. This chapter describes the procedures and methods used in these steps, including an analysis of the repeatability of CPT data, and concludes with a description of the terminolgy, grain size parameters and units of measurement used in this dissertation.

CPT DATABASE

A database of 863 CPTs from 175 sites in the Fraser delta was collected for this study (Figure 2-2). Most are located on the upper delta plain, and are concentrated on Sea Island (Vancouver International Airport), western Lulu Island (Richmond Centre), and along the highway network. However, 81 are located on the lower delta plain, subaqueous platform and the uppermost part of the slope, particularly in the vicinity of Roberts Bank Port, the artificial island on the outer tidal flats and subaqueous platform at the southern end of

Roberts Bank. The deepest CPT reached a depth of 100.25 m, but most reached depths between 20 and 40 m (Figure 4-1). In addition to the CPTs, 785 geotechnical borehole logs, generally with standard penetration test data were also obtained to provide lithological data.

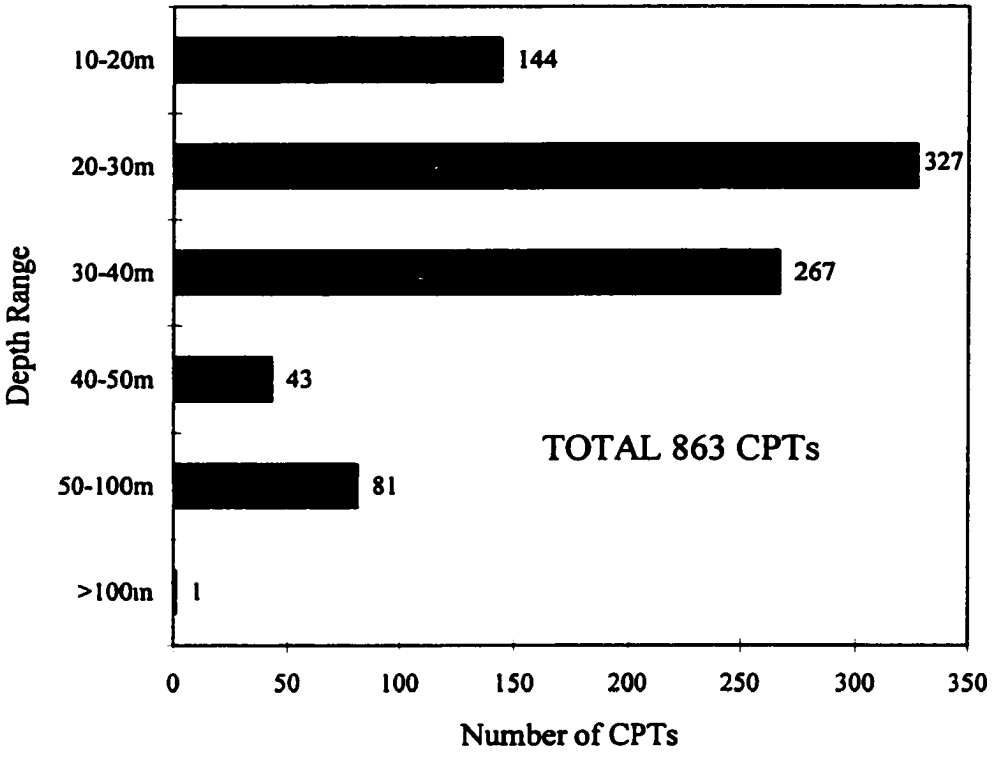

Figure 4-1. Bar graph showing the depth range of CPT data obtained for this study.

Of the CPT database, 91 CPTs were generated by the GSC as part of a regional investigation of the delta and 55 were generated by the Civil Engineering Department at the University of British Columbia for research. The remainder were generated in the course of engineering investigations and were obtained from a variety of public and private agencies. Data collection focussed on public agencies, because they have an interest in supporting research, they tend to own more buildings with a broader geographical distribution than individual

private owners, and public projects have included more CPTs than private ones. In most cases, the building or property owners were approached for the data, and they instructed geotechnical consultants to release the data for this project. However, the public agencies that have their own geotechnical departments were able to provide the data directly. Further discussion of data collection procedures in the Fraser delta is provided by Monahan and Luternauer (1994)

Most CPT data were obtained in the form of paper records. However, digital data were obtained for 342 CPTs. These were performed by five operators: ConeTec Investigations Ltd. (ConeTec), the Civil Engineering Department of the University of British Columbia (UBC), the British Columbia Ministry of Transportation and Highways (MOTH), Foundex Exploration Ltd. (Foundex), and Hughes InSitu Ltd. (Hughes). ConeTec, UBC, and Hughes manufactured their own penetrometers. Some of the cones used by UBC, and all of the cones used by MOTH were manufactured by Hogentogler & Co., Inc. The cone used by Foundex was manufactured by Geotech AB. Specifications of the equipment (Table 4-1) were provided by the operators, except for the Foundex equipment, which was calibrated by Sy et al. (1987).

Table 4-1: Summary of Digital Cpt Database, by Operator

operator	number of CPTs	cone size	"a"	Friction end area	data recording interval	Pore Pressure location
ConeTec	180	10 cm^2	0.85	equal	5 cm	U_2
	3	15 cm^2	0.85	equal	5 cm	U_2
UBC	27	10 cm^2	0.80-0.85	equal	2.5 cm	U_1,U_2,U_3
MOTH	102	10 cm^2	0.85	equal	5 cm	U_2
Foundex	4	10 cm^2	0.65	unequal	5 cm	U_2
Hughes	19	10 cm^2	0.57-0.65	unequal	5 cm	U_2
	7	15 cm^2	0.59	unequal	5 cm	U_2

CPT DATA ANALYSIS

Where digital data were available, cone bearing measurements were corrected for pore pressure effects using equation 1 in Chapter 3, and the values for "a" are summarized in Table 4-1. In order to compare data from different depths, CPT data were normalized for effective overburden stress.

In normalizing cone bearing, Q_t (equation 4, Chapter 3), q_{c1} (equation 9, Chapter 3), and Q (equation 12 and the iterative process outlined in Chapter 3) were computed. Q is used here to compare suites of samples or intervals that include both sands and silts. As described in Chapter 3, Q is based on a cone stress exponent (c) that is 0.5 in sands and 1.0 in most silts and clays. However, in suites of samples consisting only of sand or silt, q_{c1} (c=0.5) and Q_t (c=1.0)[1] are both shown and compared in Chapter 5 to demonstrate that the c does change with sediment type, and to justify the use of Q.

Furthermore, q_{c1} and Q_t are shown with Q on plots of normalized CPT data, because Q is based in part on friction ratio values, which are less repeatable than cone bearing, and because q_{c1} and Q_t retain the form of the original data over depth intervals of a few metres, whereas Q reduces or exaggerates differences between sand and silt. Normalization of cone bearing can be visualized as a clockwise rotation of cone bearing around a depth where effective overburden stress (σ'_{vo}) equals 1 atmoshere (1 bar, or ~10 m). Normalized cone bearing is less than measured cone bearing (q_t) below this depth and greater above. The normalizing correction (i.e. amount of rotation) increases as c increases (i.e. is greater in silt than in sand). However, q_t is less in silts than in sands, so that the differences between sand and silt are exaggerated using a variable stress exponent below 10 m and reduced above.

Normalized friction ratios (F_R) and normalized pore pressure parameter ratios (B_q) were

---

[1]In sands $q_{c1} \sim Q$, and in most silts and clays , $Q=Q_t$.

derived using equations 5 and 6 from Chapter 3, respectively. As can seen by comparing equations 2 and 5 in Chapter 3, the effect of normalizing friction ratio is significant in silts where q_t is low, but not in sands, where q_t is high. Soil behaviour type index, I_F, has also been calculated as described in Chapter 3.

CPT data were normalized for effective overburden stress assuming an average unit weight of 19 kN/m^3 (equivalent to a density of 1939 kg/m^3). Although unit weights are provided in the CPT interpretation program CPTINT 5.0 (Campanella, 1993), these were not used because they are based on a correlation between cone bearing and unit weight. The correlations in Chapter 3 are intended to demonstrate the relationships between grain size and cone bearing without the effect of an assumed density correction. Furthermore, the computed values of normalized cone bearing are relatively insensitive to variations in unit weight for the types of sediments represented in these cores.

Both normalized and non-normalized characteristics of CPT data of each facies are discussed in Chapter 6. Although normalized data are required for quantitative facies definitions, non-normalized data require less processing and generally have the same form as normalized data over intervals 10 m or less, showing cone bearing increasing and decreasing upward sequences in a similar way. The use of non-normalized data also permits comparison of CPT data that were obtained in digital form with the CPT data that were obtained in the form of paper records and are not readily normalized. Furthermore, normalizing corrections are large near the surface, and in near surface deposits with low cone bearing, normalizing can magnify apparent differences that may reflect the limits of accuracy between different CPTs ($\pm$ 1 or 2 bars).

Correction factors proposed by Vreugdenhil et al.(1994) for thin units of sand interbedded in finer sediments have not been applied to these data. Many thin beds in this dataset are in the 5 to 10 cm range, and the ratio of cone bearing in the sand beds to surrounding silts is less than 2. These parameters are at or below the limits where their corrections apply.

Furthermore, where these corrections can be applied, the correction factors are large, so that Robertson and Fear (1996) and Lunne et al. (1997) have recommended conservative application of these correction factors.

REPEATABILITY OF CPT DATA

In order to test the repeatability of CPT data collected in the Fraser delta, comparisons of 4 operators' data (ConeTec, UBC, MOTH, Hughes) were made at 5 sites where uniform deposits were interpreted to be present. These comparisons are presented in more detail in Appendix E. Cone bearing measurements were generally repeatable within ± 1 to 1.5 bar, slightly greater than reported by Lunne et al. (1986). This repeatabilty is best demonstrated where uniform silt deposits occur. Slightly greater variation occurs in CPTs in sands, but this probably reflects the natural variability of the sand deposits (Figure 4-2). No variation between operators was evident.

Friction ratio values were far less repeatable. In particular, Hughes' data consistently generated higher and more variable friction ratios than the other operators'. No consistent distinctions could be made between the other operator's data. However, there were commonly greater differences in friction ratios *between* adjacent CPTs than there were *within* a particular CPT. In a uniform silt layer at one site (Kidd2, borehole K2V2), average friction ratio varied by a factor of 5 in a suite of 5 CPTs (excluding the Hughes CPTs), although within each CPT the variation was low, between 7 and 30% (Figure 4-2). Variations in friction ratios between CPTs in uniform deposits were generated by variation in sleeve friction measurements, but in shallow deposits where cone bearing was low, variation in friction ratios up to a factor of 1.5 were generated by variation in cone bearing. Consequently, friction ratio measurements appear to be consistent within a particular CPT, but may not be repeatable between tests, so that the friction ratio curve is less useful for quantitative analysis.

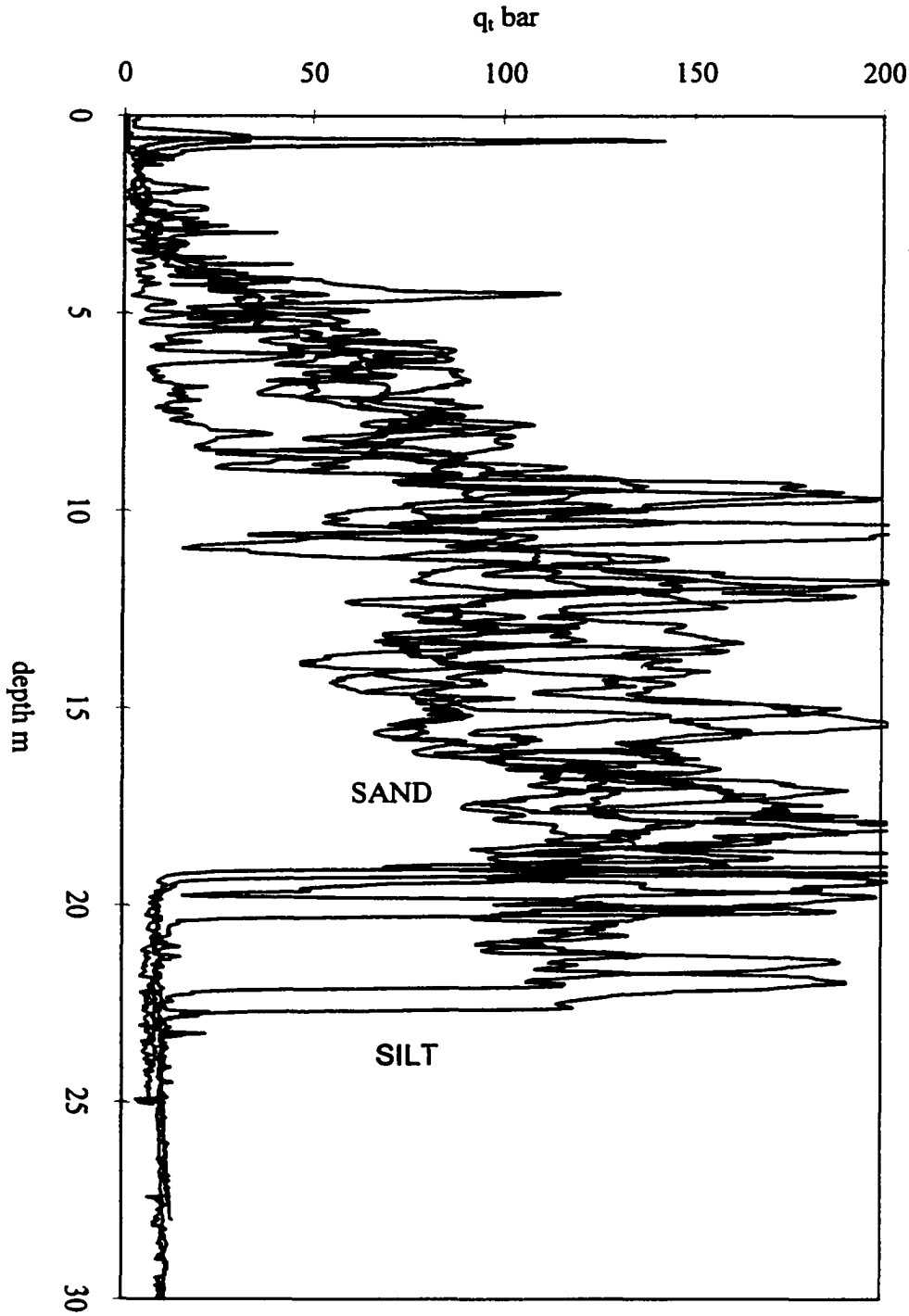

Figure 4-2a. Superimposed cone bearing curves (q_t) for 5 CPTs at Kidd2, performed by UBC and ConeTec. Note the contact between the sand and silt unit occurs where q_t increases sharply upward between 19 and 23 m. Note also that q_t in the silts varies by $\pm$ 1.5 bar. In the sands, variation in q_t is much greater but is primarily due to natural variation of the deposit.

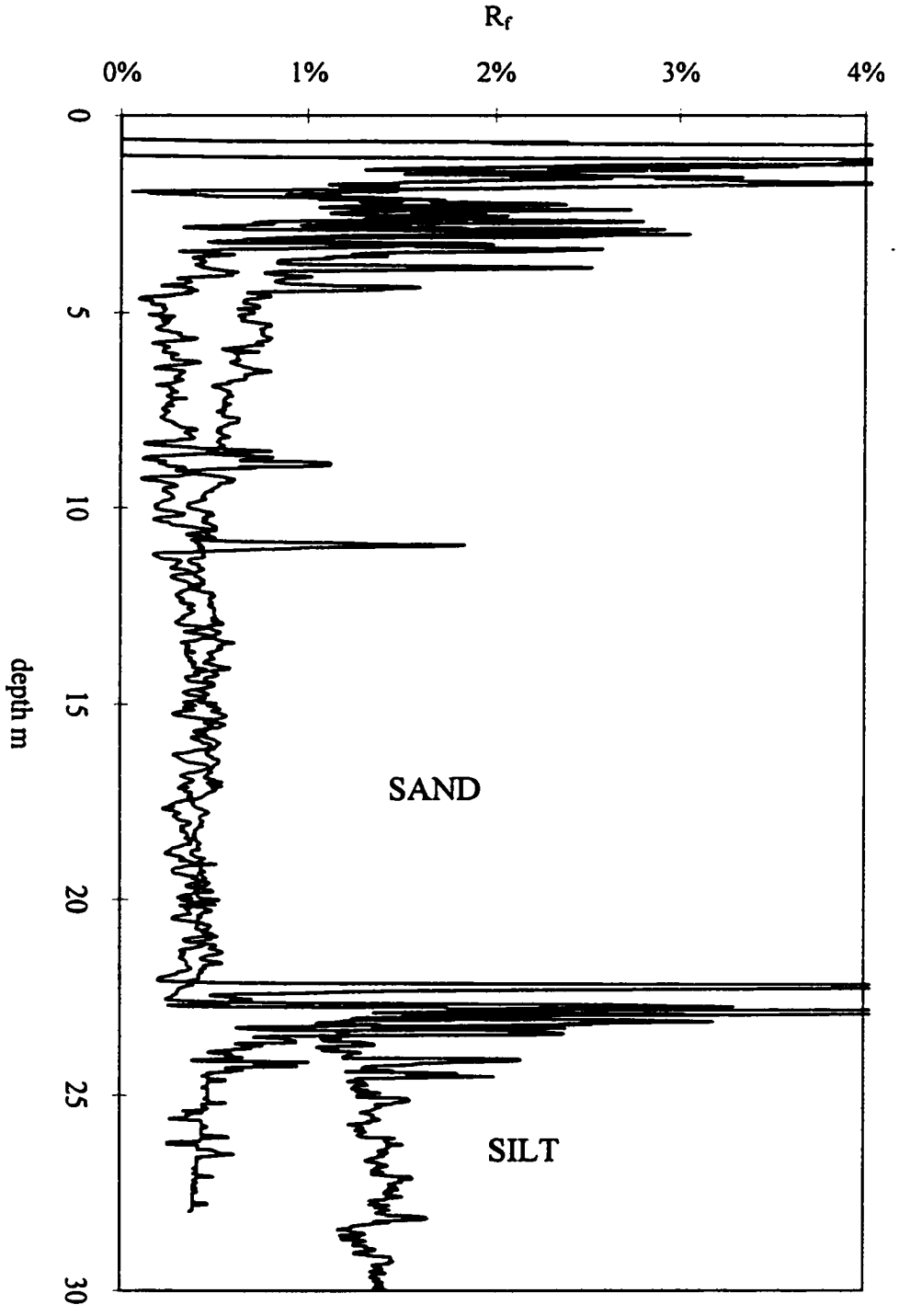

Figure 4-2b. Superimposed friction ratio (R_f) curves for 2 CPTs at Kidd2, 2 m apart. The contact between the sand and the underlying silt unit in these CPTs is marked by a R_f peak at 22 m. Note R_f varies by a factor of 3 in the silts in these CPTs (factor of 5 in 5 CPTs in Figure 4-2a), but that the variation within each CPT is low. The CPTs were both performed by UBC.

Pore pressure measurements were generally repeatable within 1 m, excluding Hughes' data which was not consistent with that of the other operators.

Data provided by Foundex could not be evaluated in a similar manner, because the CPT occurred greater than 50 m from the nearest CPT by another operator, and stratigraphic variation is indicated. However, it is interpreted to be comparable to the other operator's data because cone bearing values are generally comparable between the different operators, and the cone bearing, friction ratio, and pore pressure curves have the same character as those curves as on data provided by ConeTec, UBC and MOTH.

On the basis of these comparisons, all operators' cone bearing data could be compared quantitatively in Chapters 5 and 6, and data provided by ConeTec, UBC and Foundex could be used in the quantitative comparisons of grain size and other CPT data in Chapter 5.

DRILLING PROGRAM

Cores from 22 boreholes drilled adjacent to CPTs between 1992 and 1995 were logged by the author (Figure 4-3; Table 4-2). Most were drilled by the GSC, and of those, FD92-11, FD95S-1 and the three offshore boreholes were drilled in partnership with B.C. Hydro. FD94-1 and K2V2 were drilled as part of the CANLEX Project (Canadian Liquefaction Experiment; List and Robertson, 1995; Robertson et al., in prep.) and DT13 was drilled as part of a private contaminated site investigation. Details of each site are presented in Appendix B.

Cores from 13 of these boreholes were located within a few metres of the adjacent CPTs, were logged in the field and relogged in detail in the laboratory (Table 4-2a). These boreholes were drilled by Sonic Drilling Ltd. using a rotary-vibratory ("sonic") system and

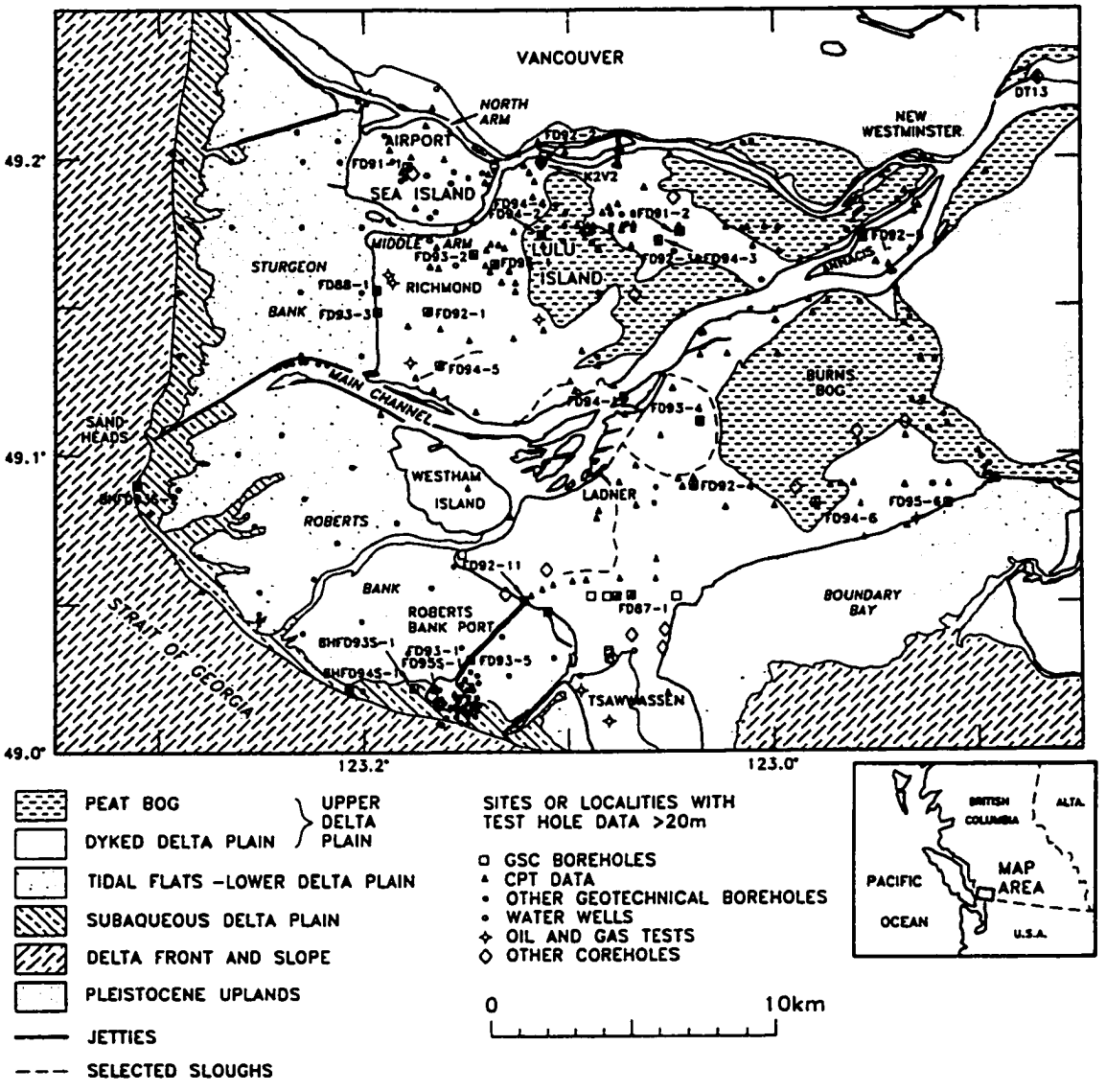

Figure 4-3. Map of the Fraser delta showing the boreholes used in this study.

by Foundex Exploration Ltd., using a mud rotary drilling system with a modified triple tube retractor core barrel ("triple tube retractor"). The coring methods are discussed below. Most of these boreholes are located on the upper delta plain. However, three are located at Roberts Bank Port and on the causeway leading across the tidal flats.

Of these 13 boreholes, 6 were drilled adjacent to existing CPTs in order to examine specific shapes of CPT curves: FD93-2, FD93-3, FD93-4, FD93-5, FD94-5 and FD94-6. The CPTs were located to within a couple of metres using site plans from the original CPT investigations, although in the case of FD93-5, a new CPT was conducted after drilling and was located 2 metres from the borehole. The other 7 boreholes were drilled as part of detailed site investigations that included acquisition of the adjacent CPT data, so that the locations of the CPTs relative to the boreholes are known. The latter investigations include Canoe Pass in the Municipality of Delta (FD92-11; Christian et al., 1994), Roberts Bank Port (FD93-1 and FD95S-1; Christian et al., 1995), the deep GSC borehole at No. 4 Road and Alderbridge Way in Richmond (FD94-2 and FD94-4; Dallimore et al., 1995; Monahan et al., 1997), and the CANLEX sites (FD94-1 and K2V2; List and Robertson, 1995; Monahan et al., 1995). At two sites, both a sonic and triple tube retractor borehole were drilled. With the exception of FD95S-1, these boreholes were continuously cored. Many of the CPTs adjacent to these boreholes are SCPTs, in which pore pressures can change significantly during rod breaks (see Chapters 3 and 5). Several of the SCPTs are included in reports by Woeller et al. (1993a, 1994).

Five additional sonic boreholes (Table 4-2b) located on the upper delta plain and one located on the Fraser River floodplain upstream of the delta were logged in the field. Only a few intervals in these boreholes were relogged in detail in the laboratory. Those drilled in 1992 (FD92-2, FD92-3, FD92-4 and FD92-5) were located at distances of tens of metres from the nearest CPTs, so that detailed correlations could not be confidently made with the CPTs.

Three boreholes were drilled on the subaqueous platform by Mud Bay Drilling Ltd. using a

mobile rotary drilling system mounted on a spud barge with a moon pool[2] (Table 4-2c). Shelby tube samples were taken at selected intervals. These cores were logged in the field and relogged in detail in the laboratory. Due to positioning difficulties with the spud barge, the boreholes were located 55 to 120 m from the nearest CPTs, so that in these cases too, detailed correlations could not be confidently made.

Data from these boreholes are supplemented by published logs and unpublished field notes on 8 additional GSC boreholes drilled adjacent to CPTs between 1987 and 1996 (Table 4-2d). Most of these are an indeterminate distance from the adjacent CPT. In boreholes FD87-1 and FD88-1 cores were taken discontinuously, every 3 to 8 metres, with a Standard Penetration Test split spoon sampler (Luternauer et al., 1991).

All of the sonic and triple tube retractor boreholes, with the exception of FD90-2 and DT13, were cased with PVC and logged using Geonics EM-39 conductivity and natural gamma ray (gamma ray) tools. These logs were provided by J.A. Hunter of the GSC. Most of the logs are included in Hunter et al. (1994, 1998) and those for FD94-2 and FD94-4 are shown in Dallimore et al. (1995) and Monahan et al. (1997). Gamma ray logs respond to the natural radioactivity of sediments, which is generally low in sands and is high in finer sediments (e.g. Schlumberger, 1989). Consequently, gamma ray logs were used in this project to identify stratigraphic contacts and to depth-correct cores, as described below (Figure 4-4). Because the gamma ray signal is dependent upon the decay of individual atomic nuclei, it fluctuates within a uniform deposit. For example, when the tool was pushed into a pile of sand on the ground surface before a logging run, the signal varied by 10 counts per second. Because of this natural fluctuation, bedding in thinly interbedded sand and silt could not be resolved (e.g. Figure 4-5).

---

2 For definitions, see Appendix A.

TABLE 4-2: SUMMARY OF BOREHOLES AND ADJACENT CPTS

4-2a: BOREHOLES LOGGED IN DETAIL

Location		Borehole				CPT						References and Comments
site	setting	#	depth m	type	distance to CPT	#	depth m	operator	type	"a"	U	
Canoe Pass Terminal, Delta	upper delta plain	FD92-11	101	triple tube	7.7 m	CPT 92-1	100	Foundex	10 cm^2	0.65	U_2	Christian et al., 1994a; Hunter et al., 1994
Roberts Bank Deltaport,Delta	subaqueous platform	FD93-1	54	sonic	5 m	SCPT 1 95-109	90	ConeTec	15 cm^2	0.85	U_2	Christian et al., 1995; Hunter et al., 1994. FD95S-1 logged to 115m.
		FD95S-1	150	triple tube	3.7 m							
Richmond Hospital	upper delta plain	FD93-2	52	sonic	< 3 m	CPT-1 93-109	25	ConeTec	10 cm^2	0.85	U_2	Hunter et al., 1994
Richmond sea dykes at Francis Road	upper delta plain	FD93-3	48	sonic	< 3 m	SCPT-1 89-140	49	ConeTec	10 cm^2	0.85	U_2	Finn et al., 1990; Hunter et al., 1994; Monahan et al., 1997
60th Ave. & 68th St., Delta	upper delta plain	FD93-4	51	sonic	< 3 m	SCPT 13 93-102	35	ConeTec	10 cm^2	0.85		Woeller et. al., 1993a; Hunter et al., 1994
Roberts Bank Deltaport Causeway, Delta	lower delta plain	FD93-5	48	sonic	2 m	SCPT 13 94-112	36	ConeTec	10 cm^2	0.85	U_2	Hunter et al., 1994; Woeller et al., 1994
Deas Island, Delta	upper delta plain	FD94-1	48	sonic	1.5 m	SCPT 1 94-112	41	ConeTec	10 cm^2	0.85	U_2	Woeller et al., 1994; Monahan, et al., 1995
Coast Guard Radio Tower, No. 4 Road & Alderbridge Rd., Richmond	upper delta plain	FD94-2	53	sonic	1.5 m	SCPT 14 94-112	58	ConeTec	10 cm^2	0.85	U_2	Woeller et al., 1994; Dallimore et al., 1995; Monahan et al., 1997. FD94-4 logged to 60m
		FD94-4	301	triple tube								
Phoenix Slough, Richmond	upper delta plain	FD94-5	24	sonic	< 3 m	CPT 2 91-101	35	ConeTec	10 cm^2	0.85	U_2	
BC Rail& 88th St., Delta	upper delta plain	FD94-6	23	sonic	< 3 m	SCPT 7 94-112	36	ConeTec	10 cm^2	0.85	U_2	Woeller et al., 1994
Kidd 2 Substation, Richmond	upper delta plain	K2V2	20	sonic	4.5 m	CPT KD9302	49	UBC	10 cm^2	0.80	U_3	Monahan, et al., 1995, 1997; UBC, 1995

TABLE 4-2: SUMMARY OF BOREHOLES AND ADJACENT CPTS

4-2b: ADDITIONAL SONIC BOREHOLES

Location		Borehole				CPT						References and Comments
site	setting	#	depth m	type	distance to CPT	#	depth m	operator	type	"a"	U	
River Road & No.4 Road, Richmond (Kidd 2 Substation)	upper delta plain	FD92-2	35	sonic	~60 m	CPT9305	30	Hughes	10 cm^2	0.6	U_2	Hunter et al., 1994; Monahan et al., 1995
						CPT 4F 92-180	25	ConeTec	10 cm^2	0.9	U_2	
MOT Radio Tower, Westminster Highway between #6 & #7 Rd, Richmond	upper delta plain	FD92-3	41	sonic	?	RCPT 3 92-103	19	ConeTec	10 cm^2	0.9	U_2	Hunter et al., 1994; Woeller et al., 1993b. Paper copy of CPT only.
Arnott Substation, Delta	upper delta plain	FD92-4	48	sonic	~65 m	CPT 9309	51	Hughes	10 cm^2	0.6	U_2	Hunter et al., 1994
Westbridge, Annacis Is, Delta	upper delta plain	FD92-5	63	sonic	~10 m	SCPT 91-3	39	MOTH	10 cm^2	0.9	U_2	Hunter et al., 1994; also paper record of CPT 87-C1A
South end 112th St., Delta	upper delta plain	FD95-6	101	sonic	~3 m	SCPT 10 94-112	31	ConeTec	10 cm^2	0.9	U_2	Woeller et al., 1994; core to 57 m; drilled to 101.
Domtar Site, Coquitlam	Fraser River floodplain	DT13	33	sonic	3 m	CPT DOM9306	28	UBC	10 cm^2	0.80	U_2	Everard, 1995. No gamma ray log.

4-2c: OFFSHORE BOREHOLES

Roberts Bank, site 1	subaqeous platform	BHFD93S-1	24	shelby	~65 m	SCPT 6 93-175	29	ConeTec	10 cm^2	0.9	U_2	Christian; 1994b
Sand Heads	subaqeous platform	BHFD93S-2	16	shelby	~55 m	SCPT 4 93-175	25	ConeTec	10 cm^2	0.9	U_2	Christian; 1997a
Roberts Bank, site 2	subaqeous platform	BHFD94S-1	20	shelby	~120 m	SCPT 2 94-180	44	ConeTec	10 cm^2	0.9	U_2	Christian; 1994b

TABLE 4-2: SUMMARY OF BOREHOLES AND ADJACENT CPTS
4-2d: SUPPLEMENTAL GSC BOREHOLES, NOT LOGGED BY AUTHOR

Location		Borehole				CPT						References and Comments
site	setting	#	depth m	type	distance to CPT	#	depth m	operator	type	"a"	U	
28th Ave & 56th St., Delta	upper delta plain	FD87-1	367	split spoon 3-137 m	6 m	SCPT 1 87-110	45	ConeTec	10 cm^2	0.85	U_2	ConeTec, 1987; Luternauer et al., 1991; Hunter et al., 1994; Mwenifumbo et al., 1994. Paper copy of CPT only.
Richmond sea dykes at Blundel Road	upper delta plain	FD88-1	122	split spoon	14 m	SCPT 1 88-123	30	ConeTec	10 cm^2	0.85	U_2	Finn, 1988; Finn et al., 1989; Hunter et al., 1994; Mwenifumbo et al., 1994. Paper copy of CPT only.
Arthur Laing Bridge, Sea Island	upper delta plain	FD90-1	43	sonic		SCPT 1 96-110	35	ConeTec	10 cm^2	0.85	U_2	Hunter et al., 1994
Francis Rd. & Railway Ave., Richmond	upper delta plain	FD90-2	55	sonic	?	RCPT 1 92-103	25	ConeTec	10 cm^2	0.85	U_2	Woeller et al., 1993b. No gamma ray log. Paper copy of CPT only
Vancouver Airport Terminal; Sea Island	upper delta plain	FD91-1	55	sonic	?	RCPT 1	19	ConeTec	10 cm^2	0.85	U_2	Patterson and Luternauer, 1993; Woeller et al., 1993b;Hunter et al., 1994; Luternauer et al., in press. Paper copy of CPT only
#7 Rd. & Mayfair Golf Course, Richmond.	upper delta plain	FD91-2	45	sonic	?	RCPT 2 92-103	30	ConeTec	10 cm^2	0.85	U_2	Woeller et al., 1993b; Hunter et al., 1994. Paper copy of CPT only.
MOT Radio Tower, Westminster Highway between #6 & #7 Rd, Richmond	upper delta plain	FD94-3	305	triple tube retractor		SCPT17 94-112	21	ConeTec	10 cm^2	0.85	U_2	Woeller et al., 1994; Dallimore et al., 1995. Same site as FD92-3.
Richmond City Hall	upper delta plain	FD96-1	328	triple tube retractor	23 m	CPT 3 93-190	31	ConeTec	10 cm^2	0.85	U_2	Dallimore et al., 1996

CORING METHODS AND DEPTH CORRECTIONS

Sonic Cores

Sonic drilling, or rotary-vibratory drilling, uses a vibrating system that liquefies sediment along the cutting edge of the drill bit, but has rotary capability so that it can also drill through rock (Swanson, 1994). Cores are cut continuously in 3 or 6 m (10 or 20 ft) increments. After each core is cut, steel casing is advanced to the same depth as the base of the core and the entire drill string is tripped to the surface. The core is extruded by vibrating the retrieved core barrel and letting the core slide into a soft plastic sleeve slipped on to the outside of the core barrel. The core has a diameter of 10.8 cm and the diameter of the plastic sleeve is 12.7 cm when fully opened. After the final total depth of the borehole is reached and the final core is retrieved, the steel casing is retrieved. In the Sonic boreholes drilled for this study, permanent PVC casing was run inside the steel casing so that wireline logs could subsequently be run.

The sonic system produces excellent cores, particularly in sands, where fine textural details such as cross-bedding (e.g. Figure 6-28) are commonly preserved, and core recovery is generally above 75%. Lithological contacts and facies sequences are readily observed in the long cores recovered by this system. However, this system has a number of sources of error that affect core interpretation.

In sand intervals, excess sand can occur at the *top* of a core. This is commonly sand that flowed or "heaved" into the borehole when the previous core was brought to the surface, but it may include losses from the previous core. It is generally very loose, wet and has a tendency to flow, and may contain drilling grease. The sand generally appears massive, but may have a disturbed appearance, with irregular patches of sand of one grain size range encased in sand of another. However, excess sand is best recognized where distinct silt interbeds or sand-silt contacts are present in the undisturbed part of the core and the core can

be depth-corrected by correlating these markers with the gamma ray log (Figure 4-4). The amount of excess sand is generally less than 1 m, but can be as much as 1.4 m. In most cases, excess sand must be disregarded, although occasionally losses from the previous core may be recognized if distinct silt interbeds that can be recognized on the gamma ray log or firm sand are present. Rarely, sand interpreted to be "heaved" and derived from uphole sandy strata was recovered at the tops of cores within the foreset silt. This sand was interpreted to be out of place because of the absence of a typical sand response at the depth of the core on the gamma ray log.

Sand can expand laterally in the plastic bag as it is being extruded from the core barrel and the recovered core will shorten. Based on the ratio of the cross sectional areas of the plastic bag and the core barrel, the interval thickness can be corrected by a factor 1.38. However, where distinct silt beds or contact occur, depth correction is best done with the gamma ray log.

Core deformation can occur in silty intervals, particularly in the laminated sandy to clayey silts of the foreset. Differential deformation of these sediments during the coring and extrusion process can generate lobes of sandy silt 10 to 20 cm long protruding along the axis of the core into finer sediments. Although the thickness of individual laminae cannot be resolved due to this deformation, the thicknesses of larger intervals (e.g. metre-scale coarsening-upward sequences described in Chapter 5 and 6) relative to one another in the same core are interpreted to be correct. Core expansion can also occur in the foreset silts, in part as a result of expansion of gas contained in the sediment, and can produce apparent core recoveries that are up to 27% thicker than the cored intervals. These cores were depth-corrected by assuming that the expansion factor was uniform throughout a specific core.

In interbedded sand and silt sections, the core can penetrate silts without coring (i.e. displacement) so that missing core can occur within a silt interval in the middle or top of a core. These displaced core intervals can also be identified by correlation of the core with the

gamma ray log.

Triple Tube Retractor Cores

The triple tube retractor coring system operated by Foundex uses a wireline retrievable core barrel, so that the entire drill string does not have to be tripped out to recover each core. Cores are cut in 1.5 or 3 m increments (5 or 10 feet) and have a diameter of 8.3 cm. The cores are extruded hydraulically from the core barrel still encased in a split metal liner, which is then opened to expose the core. This drilling system is capable of drilling greater depths than the Sonic drilling rig available at the time in the Vancouver area, and consequently has been used for all the deep GSC boreholes (Christian et al., 1994a, 1995; Dallimore et al., 1995, 1996).

Core recovery was generally less than 50% in the sands of the topset, but in sands deeper in the foreset recovery approached 100%. In silts, core recovery was high and cores did not have the differential deformation features that were commonly present in the sonic system. However, the top parts of cores in silts in the upper part of the foreset were commonly highly disturbed, being converted into a soft mud with gas bubbles and lacking the fine laminations that characterize the undisturbed silts. The disturbed intervals were 20 to 50 cm thick in FD92-11, which was cored in 1.5 m increments, and over a metre in FD94-4, which was cored in 3 m increments. This form of core disturbance was probably generated by suction as the previous core was recovered. It was not encountered in cores deeper in the foreset where stiffer silts occur. Cores were correlated to gamma ray logs, but less depth correction was generally required than for the sonic cores. An exception is FD95S-1, in which a correction of approximately 1 to 1.5 m was required for all cores. Because the gamma ray log appeared to be on depth with the offsetting CPT, the depth correction was probably required because of an extra length of drill pipe in the drill string.

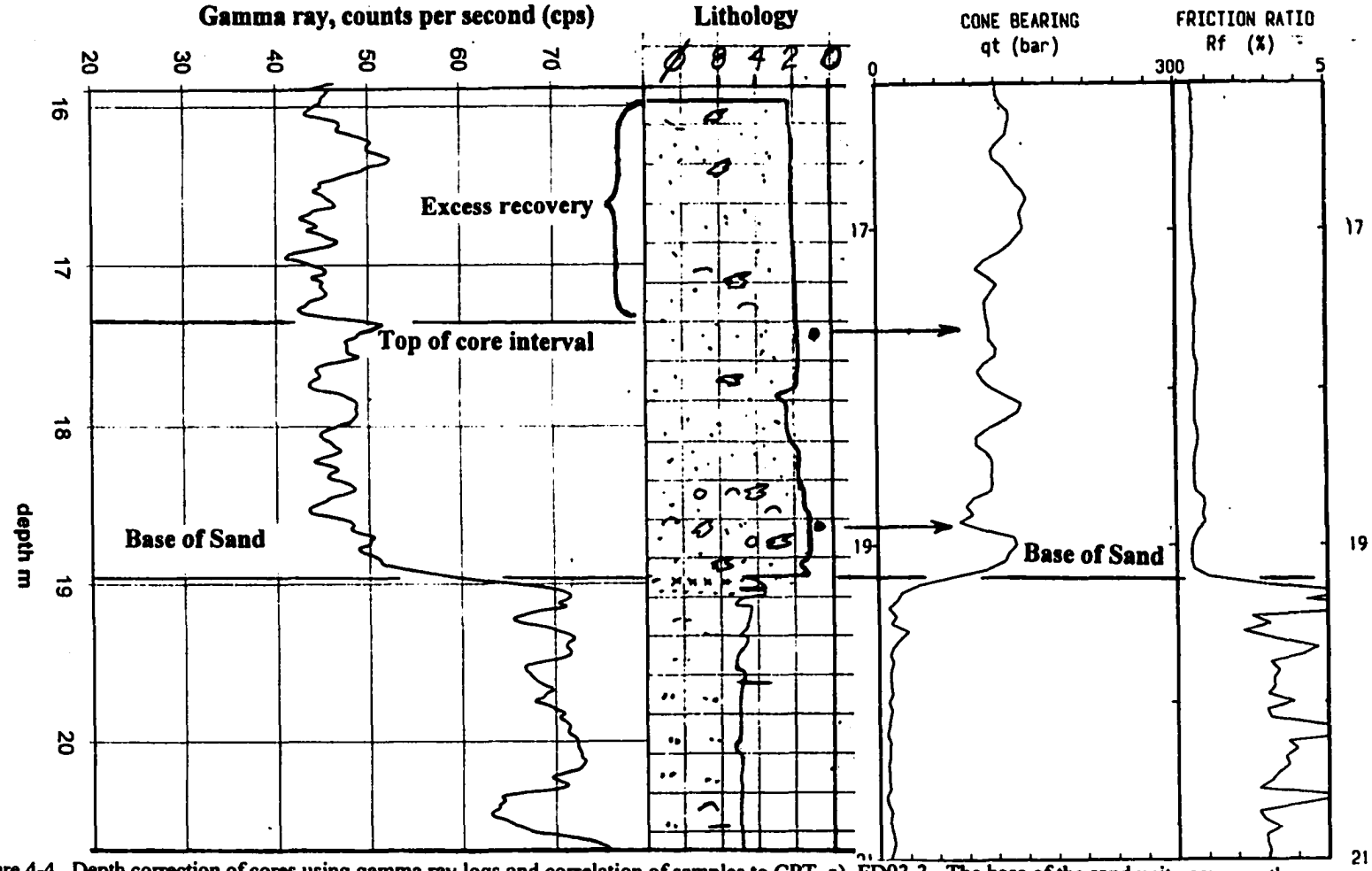

Figure 4-4. Depth correction of cores using gamma ray logs and correlation of samples to CPT. a) FD93-3. The base of the sand unit occurs on the gamma ray log at 19 m. The core was depth corrected by adjusting it upward so that this contact is at the same depth in core as on the log: By doing this, 1.4 m of sand at the top of the core can be seen to come from above the top of the core interval at 17.37 m, and is excess recovery. The core can correlated to the CPT by lining up the base of the sand in the core with the base on the CPT, where it is shown by a sharp change in cone bearing and increase in friction ratio at ~19.2 m. On the basis of this correlation, the grain size samples (dots) can be correlated to a specific CPT readings (arrows). Although the core could be correlated directly with the CPT, the gamma ray log provides the confidence to make such a large depth correction to correlate grain size samples with CPT readings.

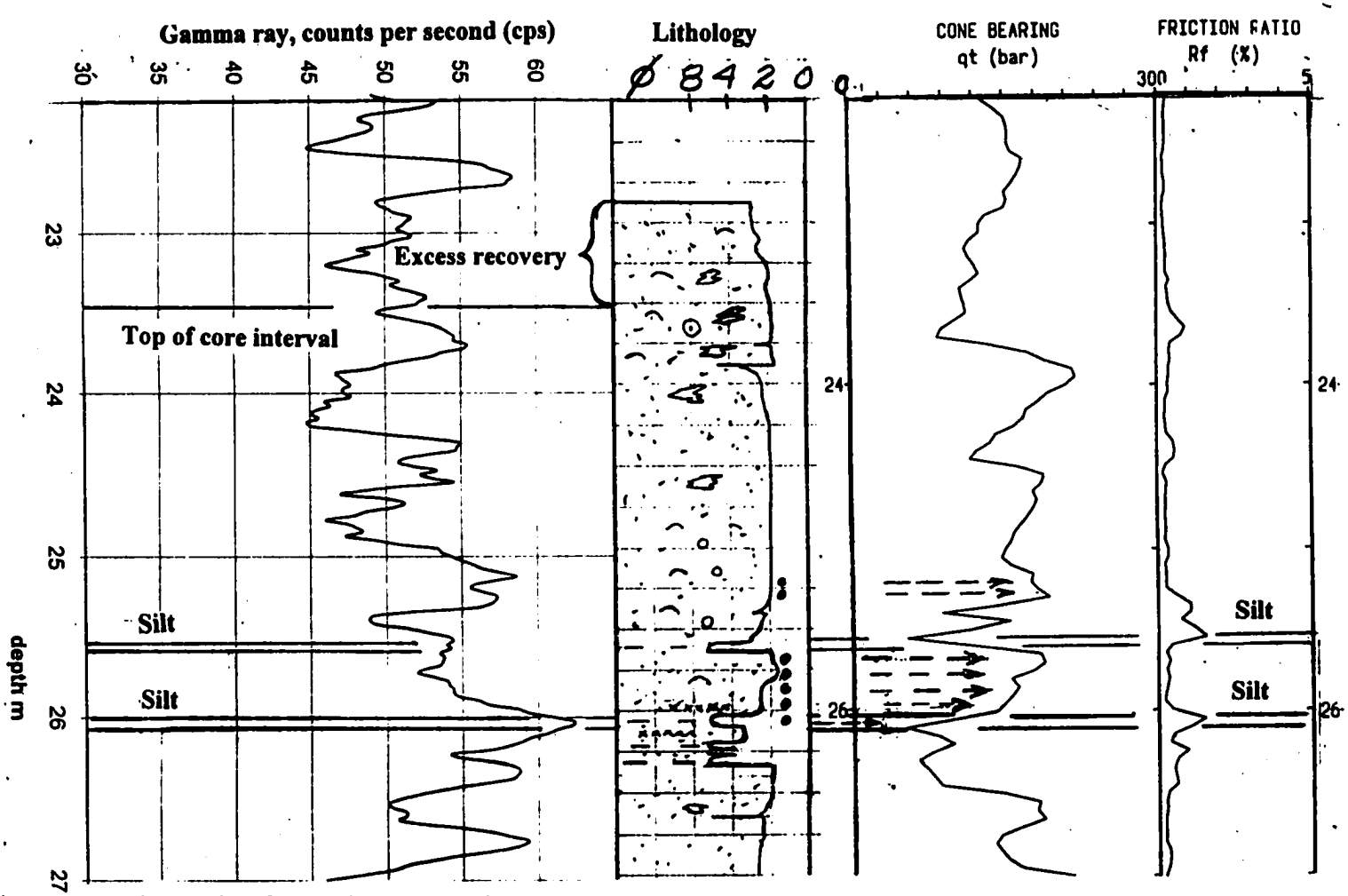

Figure 4-4. Depth correction of cores using gamma ray logs and correlation of samples to CPT. b) FD94-1. The thickest silt bed in the core can be correlated with the gamma ray peak at 26 m. By adjusting the core upward in depth, 0.6 m of sand comes from above the top of the core interval at 23.47, and is excess sand. The core can be then correlated with the CPT by lining up the two silt peaks, which are represented on the CPT by friction ratio peaks and cone bearing minima and which occur on depth with the depth corrected core. On the basis of this correlation, the grain size samples (dots) can be correlated to a specific CPT readings (arrows). Although here, too, the core can be correlated directly with the CPT, the gamma ray log provides the confidence to make a depth adjustment of 0.6 m from the core to the CPT.

Shelby Tubes Samples in Offshore Boreholes

The offshore boreholes were drilled using a mobile rotary drilling rig. The drill string was tripped out of the hole in order to core. Cores were cut intermittently using a hydraulic Shelby piston sampler, 60 cm long and 8 cm in diameter, and cores were extruded from the Shelby tubes hydraulically. Recovery was generally 60 to 80%. Except for some disturbance in the upper few centimetres, core quality was generally good. Nonetheless, the utility of these cores for this project was limited by the short sample interval, intermittent sampling and the distance from the nearest CPTs.

CORE LOGGING IN THE FIELD AND LABORATORY

As each core was recovered, it was placed into one or more 1.5 m lengths of split PVC pipe 10 cm in diameter to keep the core intact and then split. In the case of the sonic system, each core was placed on the ground while still in the plastic bag and rolled into the split pipe; and with the pipe beneath the core, the plastic bag was cut open and the core split. The cores were described and photographed in the field, and placed into "D-tubes" for transportation to the laboratory, where they were relogged in detail and rephotographed. When the cores were reexamined in the laboratory, they had dried slightly, bringing out some subtle features not evident in the wet core.

GRAIN SIZE SAMPLING PROCEDURES

In order to quantitatively assess the grain size significance of CPT measurements, 383 grain size samples were analyzed from boreholes located within a few metres of the adjacent CPTs. Two basic sampling strategies were followed. Widely spaced samples were taken at irregular intervals to determine the grain size changes on scales of several metres to tens of

metres. To determine grain size changes of smaller scale sequences, regularly spaced samples were taken every 5 to 50 cm over intervals of 0.5 to 5 metres. Because of the distortion of the foreset silts in the sonic boreholes, most samples in these intervals were taken from the triple tube retractor cores. The grain size samples are summarized by borehole in Table 5-1 and are tabulated in Appendix C.

Most samples were taken in the laboratory by cutting a rectangular block representing a stratigraphic interval of 5 cm out of the core. In these cases, each sample represents all parts of the 5 cm interval equally, including all coarser and finer laminae. Samples had an initial wet weight of 40 to 80 grams. However, those samples with a high gravel component (e.g. in FD94-5) incorporated the entire retained core in the 5 cm interval to reduce the effect that individual large particles would have on the grain size distribution. Exceptions to these procedures are the widely spaced samples from FD92-11, which were taken in the field and represent intervals of 3 to 14 cm; and three samples in the foreset in FD93-2 which were also taken in the field and represent 5 cm intervals.

GRAIN SIZE SAMPLE ANALYSIS PROCEDURES

Of the grain size samples, 353 were analyzed by the staff of the sediment laboratory at the Pacific Geoscience Centre (PGC) of the GSC, where the grain size samples were analyzed according to the following procedures. Grain size is reported in the ϕ scale, where ϕ is equal to the negative log to the base 2 of grain size in millimetres.

Samples were dried, weighed and wet sieved to separate the gravel (>2 mm or <-1ϕ; retained by #10 sieve), sand (0.0625 to 2 mm or 4 to -1ϕ) and mud (<0.0625 mm or >4ϕ; passing through # 230 sieve) fractions. The gravel and sand fractions were then dried and weighed and the mud fraction weights were determined by subtraction of the sand and gravel from the initial dry weights.

Aqueous suspensions containing the mud fractions were concentrated using a centrifuge, and 50 mL subsamples were taken for determination of the grain size distributions using a SediGraph 5100 Particle Size Analyzer. The SediGraph uses a finely collimated horizontal beam of X-rays to determine the sediment concentration in the subsample. It measures the changes in sediment concentration with time and with depth in the suspension, by slowly moving the cell containing the sediment suspension downwards across the horizontal beam of X-rays (McCave and Syvitski, 1991). From these changes in sediment concentration, settling velocity distributions were generated. The SediGraph is interfaced with a MasterTech 51 Automated Sampler and a Compaq PC so that up to 18 samples can be run unattended.

Grain size distributions for the sand fractions are measured in a 2 metre settling tube filled with distilled water. A pan at the base of the tube is weighed continuously by a Mettler AE 160 balance interfaced with an IBM PC to provide a settling velocity distribution for each sample (Conway, pers. comm. 1996).

From the settling velocity distributions, particle size distributions of the mud and sand fractions were determined by Stoke's Law. However, the particle sizes reported are those of spherical equivalents with a density of 2.65 g/cm^3 rather than true particle sizes. Grain size distributions are reported in 0.25 ϕ intervals. Sand and mud fraction less than 5% of the total weight are not analyzed.

Grain size distributions of the gravel fractions were determined by sieve in 0.5 ϕ intervals.

The grain size distributions of the sand, mud and gravel fractions were merged using software designed at the PGC to give continuous grain size distributions. The software also computed the median (ϕ_{50} and D_{50}), and moment mean and standard deviation (Friedman and Sanders, 1978). Grain size systems of this type produce results that are repeatable within 5% (Barrie, pers. comm. 1997). However, a far greater source of variability in the grain size data

is due to sample selection, particularly in samples of laminated sediments, where moving the sampled interval slightly would change the grain size parameters significantly.

The remaining 30 grain size samples, all from FD95S-1, were analyzed by staff at the sediment laboratory of the Atlantic Geoscience Centre (AGC) of the GSC using similar procedures and equipment. However, there sand and mud fractions less than 5% were analyzed and grain size distributions were reported in 0.2 ϕ intervals. The results of the grain size analyses are tabulated in Appendix C.

CORRELATION OF CORES TO CPTS

In order to compare the grain size measurements with specific CPT measurements, as well as larger-scale sequences observed in cores and the CPTs, the cores were correlated with the adjacent CPTs using the following procedures. As described above, the individual cores were initially depth-corrected to remove the effects of core compression, expansion and excess sand, generally by correlation of distinct beds or contacts in the core with gamma ray logs (Figure 4-4). The cores were then correlated to CPTs by stratigraphic correlation of beds with a distinct CPT response, such as silt interbeds within a sand sequence.

Distinct beds or contacts could not be identified on the gamma ray logs in some intervals, such as in thick sequences of sand or in thinly interbedded sequences of silt and sand where beds were not resolved by the gamma ray logs. There, the cores were directly correlated with CPTs on the basis of distinct marker beds in the core and CPT, such as thin silty intervals within a thick sand unit. Cone bearing peaks were interpreted to represent sand beds within a silt sequence or gravelly beds in sand units. In the case of continuous 5 cm grain size samples in silt sequences in the triple tube retractor cores, adjustment for core expansion and compression were required.

Based on these correlations, the midpoint of each grain size sample was correlated with the nearest CPT reading. The grain size to CPT correlations developed have a certain degree of subjectivity, particularly where gamma ray logs could not be used. In addition, real stratigraphic changes may occur between the borehole and CPT. Consequently, the correlations developed should be taken to indicate the extent to which CPT readings *can* be explained by grain size variations. The grain size data and corresponding CPT data and calculations are tabulated in Appendix D.

For each borehole, a composite log was prepared, showing the depth-corrected lithology and correlations to the adjacent CPT. An example is shown in Figure 4-5. Composite logs for the all boreholes examined for this study are presented in Appendix B.

COLLECTION AND RESERVOIR CORRECTION OF RADIOCARBON SAMPLES

Thirty-five samples for radiocarbon dating were taken from the cores examined for this study and are summarized in Appendix G. These samples were taken by the author, J.J. Clague and J.L. Luternauer. Where possible, twigs, small shells, or shells from a monospecific assemblage indicating a minimum of reworking and transport were selected. Most of the samples were submitted to the Isotrace Laboratory at the University of Toronto, where they were analyzed by Accelerator Mass Spectrometry. The remainder were analyzed at the GSC laboratory in Ottawa by proportional gas counting. The measured dates were reported corrected to a base of $\delta^{13}C$ + -25 ‰.

Work by Robinson and Thompson (1980) and Southon et al. (1990) suggests that a ^{14}C reservoir age of approximately 800 years has prevailed in the marine waters of coastal British Columbia for most of the Holocene. Consequently, a correction of this amount has been applied to the dates on shell material.

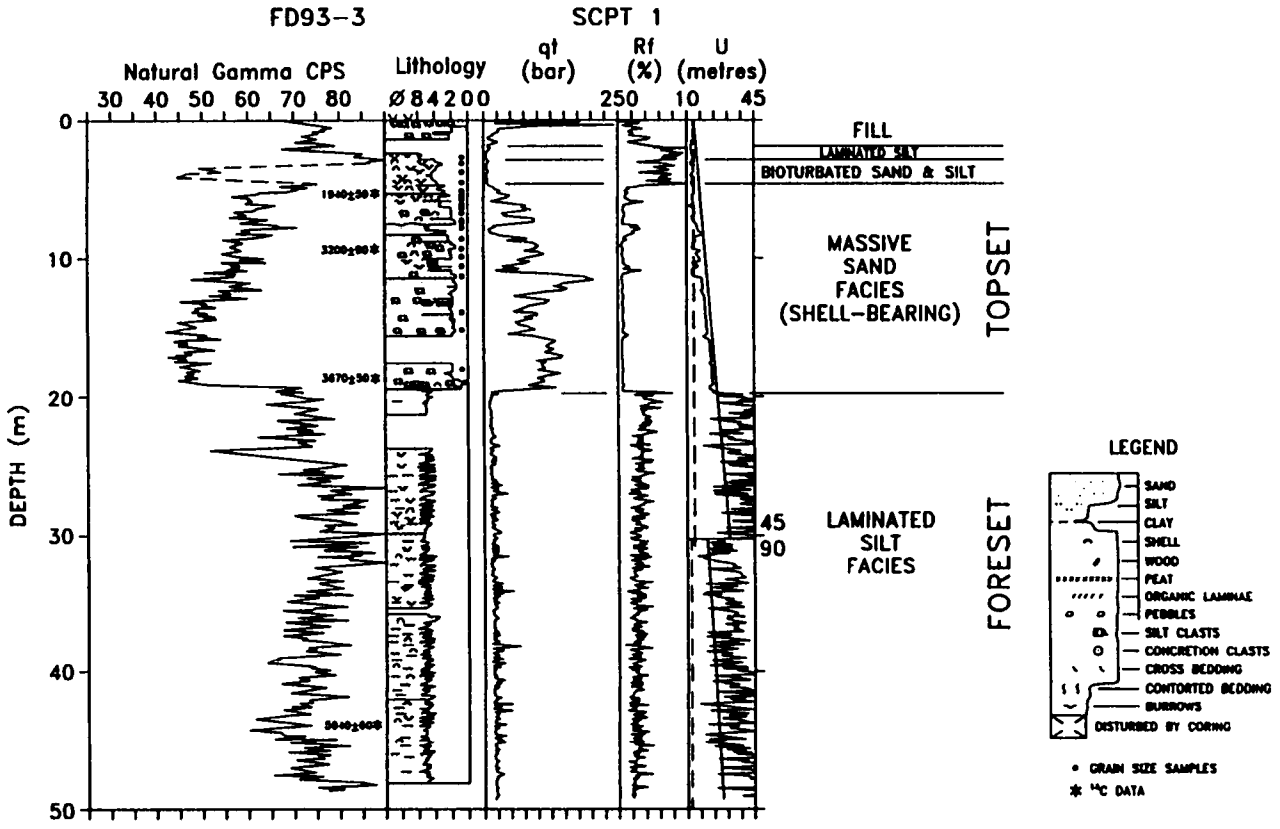

Figure 4-5. Composite log of FD93-3, showing gamma ray log, depth-corrected lithology and the adjacent CPT and division into topset and foreset deposits (from Monahan et al., 1997).

TERMINOLOGY, GRAIN SIZE PARAMETERS AND UNITS

The Wentworth (1922) grain size scale is used here and is summarized in Table 4-3. In the silt range, where grain size is more difficult to estimate visually than in the sand range, the terms clayey and sandy silt are used in core descriptions where grain size analyses are not available, and correspond approximately with very fine to fine and medium to coarse silts of the Wentworth scale, respectively.

Table 4-3: Wentworth Grain Size Scale

Grain Size Range	Wentworth Size Class
$-2 > \phi > -6$ (4 - 64 mm)	pebble
$-1 > \phi > -2$ (2 - 4 mm)	granule
$0 > \phi > -1$ (1 - 2 mm)	very coarse sand
$1 > \phi > 0$ (0.5 - 1 mm)	coarse sand
$2 > \phi > 1$ (0.25 - 0.5 mm)	medium sand
$3 > \phi > 2$ (0.125 - 0.25 mm)	fine sand
$4 > \phi > 3$ (0.063 - 0.125 mm)	very fine sand
$5 > \phi > 4$ (0.031- 0.063 mm)	coarse silt
$6 > \phi > 5$ (0.016 - 0.031mm)	medium silt
$7 > \phi > 6$ (0.008 - 0.016 mm)	fine silt
$8 > \phi > 7$ (0.004 - 0.008 mm)	very fine silt
$\phi > 8$ (< 0.004 mm)	clay

The mean and standard deviation reported here are moment measures, as defined by Friedman and Sanders (1978). The ranges of sorting classes are also provided by Friedman and Sanders, and summarized in Table 4-4.

Table 4-4: Range of Sorting Classes

Range of Standard Deviation ϕ	Sorting Class
<0.35	very well sorted
0.35 - 0.50	well sorted
0.50 - 0.80	moderately well sorted
0.80 - 1.40	moderately sorted
1.40 - 2.00	poorly sorted
2.00 - 2.60	very poorly sorted
>2.60	extremely poorly sorted

ϕ_{50} is used here as a measure of average grain size rather than the mean. ϕ_{50} is also a more robust measurement less subject to error. For example, at the PGC laboratory, the silt and clay fractions were not analyzed in samples where these fractions were less than 5%, potentially underestimating the standard deviation and overestimating the mean. Furthermore, most engineering studies comparing CPT and grain size report D_{50}, the median in millimetres, rather than the mean. Most importantly, however, the mean grain sizes of most very fine sands analyzed here are greater than 4ϕ and overlap with those of the coarse silts (see Figure 5-1a). They are corrrectly distinguished from silts on the basis of ϕ_{50}. Although the mean is a better representation of all the grain sizes present in a sample than ϕ_{50}, it does not generally yield significantly different correlations with CPT data here.

" Mud content", or "silt and clay content" is the fraction finer than 4ϕ (0.063 mm). This contrasts with the "fines content" (FC) of geotechnical engineering usage, which is defined as the fraction finer than 3.75 ϕ (0.074 mm, passing the #200 seive; Terzaghi et al., 1996). Although it is inconsistent with the Wentworth scale, FC is used in the comparisons of CPT and grain size data in Chapter 5 because it is the parameter used in the CPT and related

literature (e.g. Stark and Olson, 1995; Robertson et al., in prep.)[3].

The terms for the scale of beds and laminae are those defined by Reineck and Singh (1975), and are summarized in Table 4-5. The definitions of laminae overlap with those of thin and very thin beds.

Table 4-5: Scale Definitions for Beds and Laminae

BEDS	
> 100cm	very thick bed
30 - 100cm	thick bed
10 - 30 cm	medium bed
1 - 10 cm	thin bed
< 1 cm	very thin bed

LAMINAE	
> 30 mm	very thick lamina
10 - 30 mm	thick lamina
3 - 10 mm	medium lamina
1 - 3 mm	thin lamina
< 1 mm	very thin lamina

CPT data are reported in the following units: cone bearing and sleeve friction in bars (=100 kPa or 0.1 MPa), and pore pressure in metres of water (m H_20 = 9.81 kPa, 0.0981 bars, 0.00981 MPa). This usage is consistent with that of the principal CPT operators in the Fraser delta.

All depths in cores correlated with CPTs are reported as depths on the CPTs rather than cores. The depths of all samples in both core as well as the CPT correlation points are tabulated in Appendix D.

Following the usage of Devore (1991), statistical correlations are said to be strong if R^2 is

---

3

In Canada, FC is defined as the fraction finer than 0.075mm (Canadian Foundation Engineering Manual, 1992). However, this usage is not followed in the CPT and related literature and is not followed here.

greater than 0.64, moderate if R^2 is between 0.25 and 0.64, and weak if R^2 is less than 0.25.

CHAPTER 5

THE CORRELATION OF CONE PENETRATION TEST MEASUREMENTS WITH GRAIN SIZE AND OTHER GEOLOGICAL FACTORS

INTRODUCTION

Grain size exerts a fundamental control over CPT measurements, as reflected by the CPT soil classification charts (Fig. 3-3; Olsen and Malone, 1988; Robertson et al., 1986; Robertson, 1990). However, variations in cone bearing values in sand deposits are commonly interpreted to represent variations in density rather than grain size. It is the objective of this chapter to demonstrate that CPT measurements, including cone bearing in sands, can be correlated with grain size and other geological factors in sediments of the Fraser delta. Recognition of coarsening and fining upward sequences is fundamental to facies analysis. Consequently, the extent to which these are reflected in CPT data is a key element of this chapter and provides the basis for understanding the textural significance of CPT measurements in the facies analysis presented in Chapter 6.

CPT measurements are controlled by several variables in addition to grain size, including density (and dependent shear strength characteristics), overburden stress, stress history (i.e. overconsolidation[1]), cementation, age, mineralogy, and stratigraphic factors, such as thin beds in which CPT measurements are not fully resolved (i.e. mechanical properties not correctly measured; Robertson and Campanella, 1986; Robertson et al., 1986; Lunne et al., 1997). Several of these variables are not significant in the deposits of the Fraser delta. These sediments were deposited during a period of gradual sea level rise since the last glaciation. Consequently, the current overburden stresses are the maximum to which they have been

---

[1] For definition, see Appendix A.

subjected and they are generally not overconsolidated. These sediments are all derived from the same source, the drainage basin of the Fraser River, so that mineralogical variations are minimal. With the exception of some calcareous concretions (see also Johnston, 1921; Garrison et al., 1969; Nelson and Lawrence, 1984), no cementation was observed in the sediments of the Fraser delta examined in this study. This conclusion was also reached by Eslaamizaad and Robertson (1996) based on a comparison of cone bearing and shear-wave velocity data at the CANLEX sites in the Fraser delta, where boreholes FD94-1 and K2V2 of this study are located (Monahan et al., 1995).

With appropriate normalization for overburden stress, the principal variables controlling CPT data in the Fraser delta can be reduced to density, grain size, age and stratigraphic factors. The effects of age can be assessed by stratigraphic position and radiocarbon dates (Appendix D), and stratigraphic factors can be assessed from observations of the cores.

METHODOLOGY

In order to quantitatively assess the grain size significance of CPT measurements, 383 grain size samples from 11 boreholes were analyzed and compared with measurements in adjacent CPTs. The strategies and procedures for taking grain size samples, analyzing them, correlating them with CPT measurements and analyzing CPT data are described in Chapter 4. A summary of the boreholes from which grain size samples were taken and the specifications of the adjacent CPTs is presented in Table 5-1, and details of correlation procedures at each site and detailed results of the grain size to CPT correlations are presented in Appendix A. The grain size data and the corresponding CPT measurements and calculations are tabulated in Appendix B.

The grain size samples span a depth range of 0.9 to 99.6 m, although most are shallower than 30 m, and range in age from historic to over 8000 ^{14}C years. 10 cm^2 cones were used for the

CPTs, with one exception (FD95S-1), where a 15 cm^2 cone was used. CPT data from the 10 cm^2 cones were compared with grain size data separately from those from the 15 cm^2 cone (32 samples). Pore pressure was measured in the U_2 position in all CPTs other than the one adjacent to borehole K2V2, where it was measured in the U_3 position (27 samples; see Figure 3-1).

Cone bearing measurements for groups of samples including both sands and silts were normalized for effective overburden stress using Q, in which the cone stress exponent (c) varies from 0.5 in sand to 1.0 in silt and clay (equation 12, Chapter 3). Because several other procedures have been proposed to normalize cone bearing, this chapter also includes comparisons of two of the most commonly used, q_{c1} (c=0.5) and Q_t (c=1.0; equations 9 and 4, Chapter 3, respectively), in sands and finer sediments. These analyses demonstrate that the c does change with sediment type and justify the use of Q.

SOURCES OF ERROR

As described earlier, errors in grain size measurements, CPT measurements, and calculation of normalized CPT parameters are generally in the order of a few percent or less. Greater sources of error are due to uncertainties in correlations between cores and CPTs, including real stratigraphic changes that may occur between them, and sampling procedures. Although many sand samples were taken from sands that appeared uniform over tens of centimetres, samples from laminated silts included variable proportions of coarser and finer sediment. Moving the sampled interval slightly in many cases would have altered the mix of coarser and finer laminae.

TABLE 5-1: Summary of Boreholes with Grain Size Analyses and CPTs Used for Comparison

Borehole				grain size samples					CPT					
#	location	type	distance to CPT	#	thick cm	spacing	lab-oratory	depth range (CPT depths)	#	depth m	operator	type	"a"	U
FD92-11	Canoe Pass Terminal, Delta	triple tube retractor	7.7 m	57	3-14	irregular	PGC	2.05-99.6 m	CPT 92-1	100	Foundex	10 cm^2	0.65	U_2
				21	5	regular	PGC	23.4-24.4 m						
FD93-2	Richmond Hospital	Sonic	< 3 m	32	5	regular	PGC	0.9-5.2 m	CPT-1 93-109	25	ConeTec	10 cm^2	0.85	U_2
				3	5	irregular	PGC	22.6-24.45 m						
FD93-3	Richmond dykes at Francis Road	Sonic	< 3 m	21	5	irregular	PGC	2.45-18.85 m	SCPT-1 89-140	49	ConeTec	10 cm^2	0.85	U_2
FD93-5	Roberts Bank Deltaport Causeway, Delta	Sonic	2 m	34	5	regular	PGC	20.5-22.9 m	SCPT 13 94-112	36	ConeTec	10 cm^2	0.85	U_2
FD94-1	Deas Island, Delta	Sonic	1.5 m	27	5	regular/ irregular	PGC	3.95-31.65 m	SCPT 1 94 112	41	ConeTec	10 cm^2	0.85	U_2
FD94-4	Coast Guard Radio Tower, No. 4 Road and Alderbridge Rd., Richmond	triple tube retractor		51	5	regular	PGC	23.85-42.1 m	SCPT 14 94-112	58	ConeTec	10 cm^2	0.85	U_2
FD94-5	Phoenix Slough, Richmond	Sonic	< 3 m	26	5	regular	PGC	12.3-16.45 m	CPT 2 91-101	35	ConeTec	10 cm^2	0.85	U_2
FD94-6	BC Rail and 88th St., Delta	Sonic	< 3 m	43	5	regular	PGC	2.45-21.45 m	SCPT 7 94 112	36	ConeTec	10 cm^2	0.85	U_2
FD95S-1	Roberts Bank Deltaport, Delta	triple tube retractor	3.7 m	30	5	regular	AGC	40.75-90.35 m	SCPT 1 95-109	90	ConeTec	15 cm^2	0.85	U_2
				2	5		PGC	66.95-67.3 m						
K2V2	Kidd 2 Substation, Richmond	Sonic	4.5 m	27	5	regular	PGC	8.85-20.38 m	CPT KD9302	49	UBC	10 cm^2	0.80	U_3
DT13	Domtar Site, Coquitlam	Sonic	3 m	9	5	regular	PGC	21.08-22.73 m	CPT DOM9306	28	UBC	10 cm^2	0.80	U_2

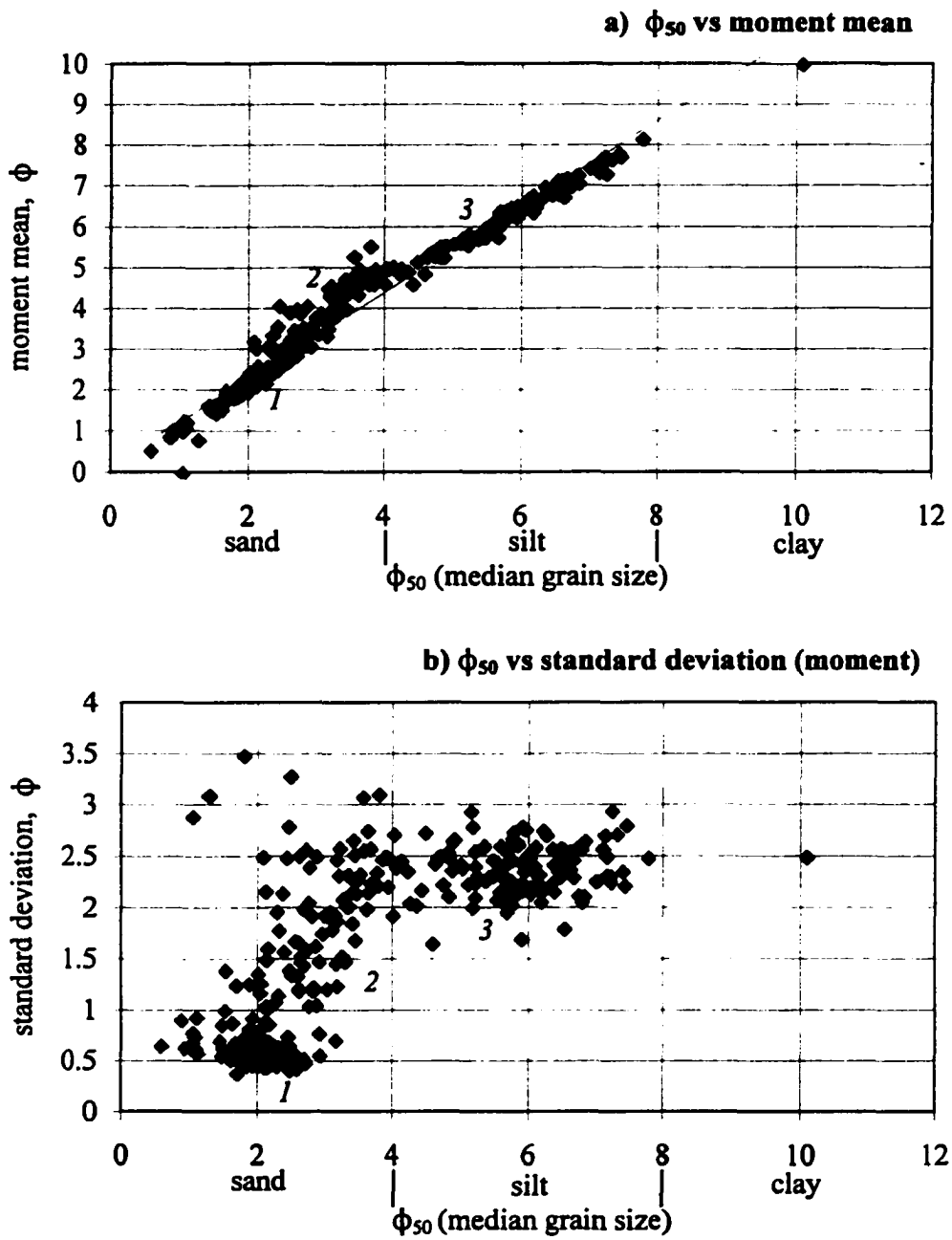

Figure 5-1. ϕ_{50} (median grain size) vs (a) mean and (b) standard deviation, samples analyzed at PGC (n=353). Note 3 groups: 1) moderately well sorted sands (mean close to the median), 2) moderately to very poorly sorted fine to very fine sand (mean finer than the median), and 3) very pooly sorted silts.

GRAIN SIZE CHARACTERISTICS

The grain size samples include 253 of sand, 129 of silt, and 1 of clay. Cross plots of median grain size (ϕ_{50}), mean grain size and standard deviation (moment) demonstrate that these samples generally fall into 3 distinct groups (Figure 5-1a and b). A group of moderately well sorted fine and medium sands (0.4<standard deviation<0.8, and $1<\phi_{50}<3$) forms a distinct cluster on the ϕ_{50} vs standard deviation plot and coincides with those sands where ϕ_{50} is close to mean grain size. A second group consists of fine and very fine sands ($2<\phi_{50}<4$) that are moderately to very poorly sorted (0.8<standard deviation<2.6). As grain size decreases in this group, standard deviation increases and the mean becomes progressively finer than ϕ_{50}, reflecting increasing proportions of silt and clay. The distinction between the first two groups may not be as sharp as it appears on these plots, because of the PGC laboratory procedures, which potentially underestimate the standard deviation and overestimate the mean in clean sands, as described in Chapter 4. The third group consists of poorly and very poorly sorted silt and clay, in which the mean grain size is generally finer than ϕ_{50}.

GRAIN SIZE TO CPT CORRELATIONS

CPT parameters for the grain size samples correlated with 10 cm^2 cones are plotted on the normalized soil classification chart, sorted by ϕ_{50} range in Figure 5-2 Sand samples from one borehole (FD94-6) are excluded from Figure 5-2a and other comparisons for sands with 10 cm^2 cones, because the cone bearing values are anomalously high and represent a different population of grain size to CPT correlations (Figure 5-3).

Excluding the sand samples from this borehole, a dataset of 317 samples remains for 10 cm^2 cones. Although grain size sampling was selective and not all geological environments and depth ranges are proportionately represented, some general correlations can be made. In the

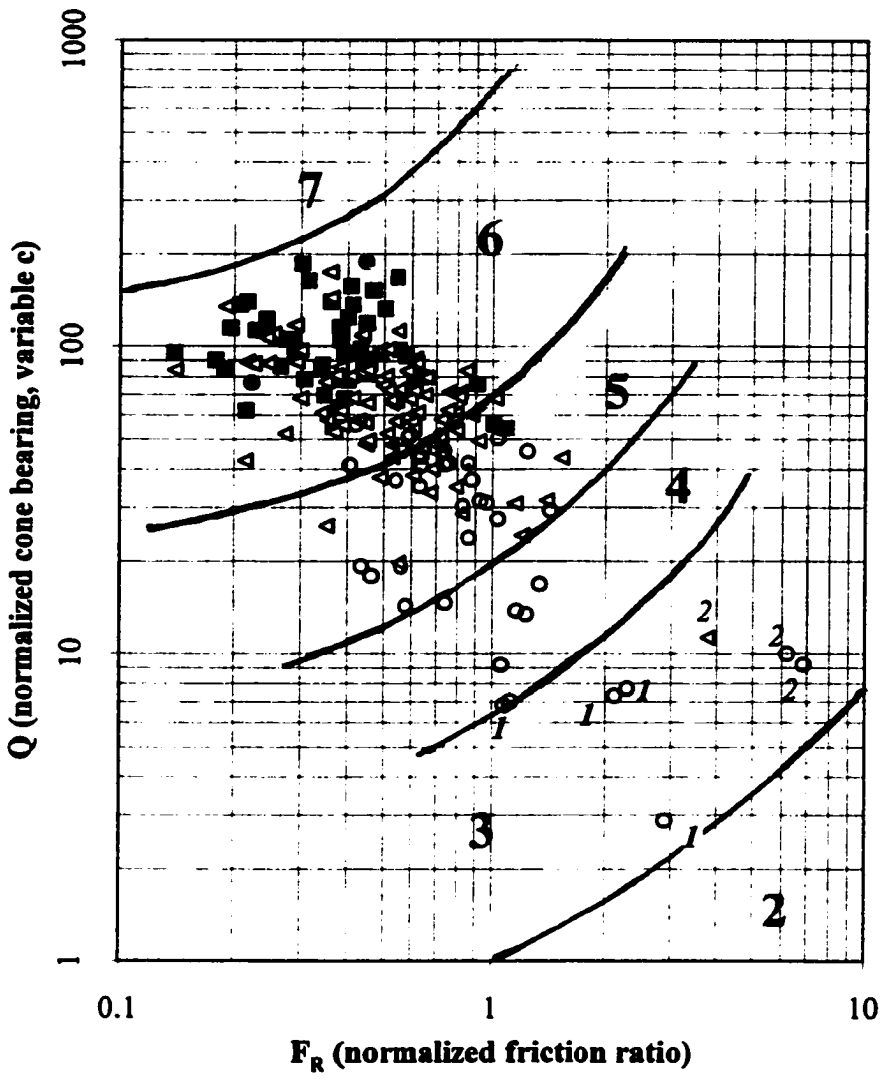

GRAIN SIZE SYMBOLS

- ● $0 < \phi_{50} < 1$
- ■ $1 < \phi_{50} < 2$
- ◁ $2 < \phi_{50} < 3$
- O $3 < \phi_{50} < 4$

SOIL BEHAVIOUR TYPES

2: organic soils - peats
3: clays - clay to silty clay
4: silt mixtures - clayey silt to silty clay
5: sand mixtures - silty sand to sandy silt
6: sands - clean sand to silty sand
7: gravelly sand to sand

Figure 5-2a. Grain size to CPT correlations for sand samples plotted by grain size range on the normalized soil classification chart (see Figure 3-3b). In general coarser sands plot with higher cone bearing and lower fiction ratio. Note 1) thin sands interbedded in silt,in which low cone bearing values are primarily thin bed effects; and 2) anomalously high friction ratio values in fine and very fine sands in CPT adjacent to borehole FD93-3.

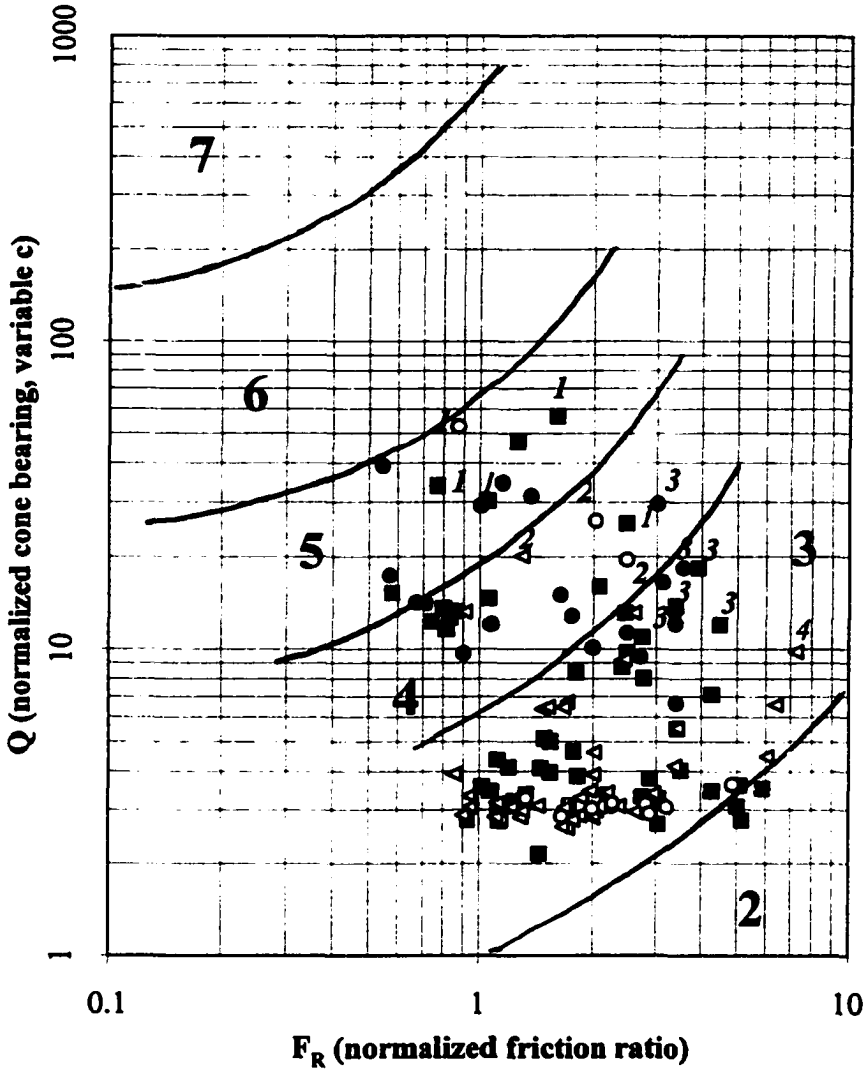

GRAIN SIZE SYMBOLS

- ● $4 < \phi_{50} < 5$
- ■ $5 < \phi_{50} < 6$
- < $6 < \phi_{50} < 7$
- O $7 < \phi_{50} < 8$

SOIL BEHAVIOUR TYPES

2: organic soils - peats
3: clays - clay to silty clay
4: silt mixtures - clayey silt to silty clay
5: sand mixtures - silty sand to sandy silt
6: sands - clean sand to silty sand
7: gravelly sand to sand

Figure 5-2b. Grain size to CPT correlations for silt samples plotted by grain size range on the normalized soil classification chart (see Figure 3-3b). Note 1) thin beds of silt in sand in which cone bearing is not resolved; 2) desiccated silts; 3) disturbed silts; and 4) anomalously high friction ratio in silt in CPT adjacent to borehole FD93-3.

sand range, most samples plot on the normalized soil classification chart with higher cone bearing and lower friction ratio as grain size increases (Figure 5-2a). In the silt range (Figure 5-2b), the increase in cone bearing with grain size is less clear, although the coarser silts generally have higher cone bearing, and friction ratio values are more variable. These factors are examined in more detail below.

Cone bearing and pore pressure

The interpretation of cone bearing data is interrelated to that of pore pressure. Consequently, these parameters are discussed together.

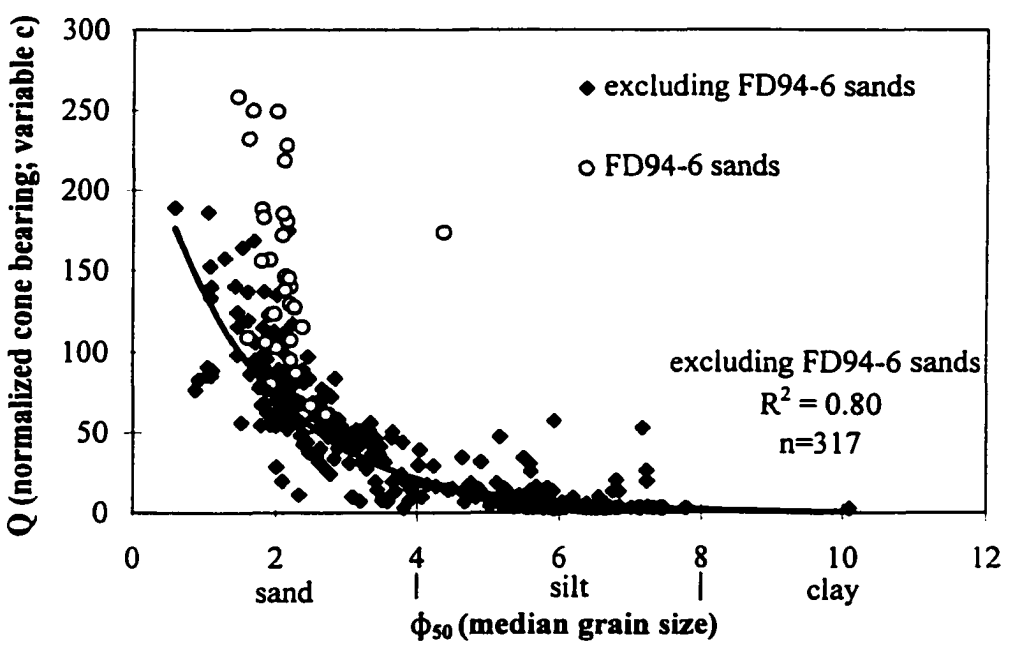

Figure 5-3. ϕ_{50} (median grain size) vs Q (normalized cone bearing; variable cone stress exponent, c). Data from 10cm² cones only (n=351). Samples from borehole FD94-6 are high compared to these from the other boreholes. The trendline and R^2 are for samples excluding those from borehole FD94-6 (n=317).

ϕ_{50} correlates well with normalized cone bearing Q (exponential R^2= 0.80; n=317; Figure 5-3)[2]. Cone bearing is relatively insensitive to grain size finer than $5\phi_{50}$, increases gradually with grain size through the coarse silt range, and increases more sharply with grain size through the sand range. Plots of fines content (FC) to Q show that cone bearing is insensitive to FC where FC is less than 10%, but that it correlates moderately with FC where FC is greater than 10% (R^2=0.62; n=203; Figure 5-4)

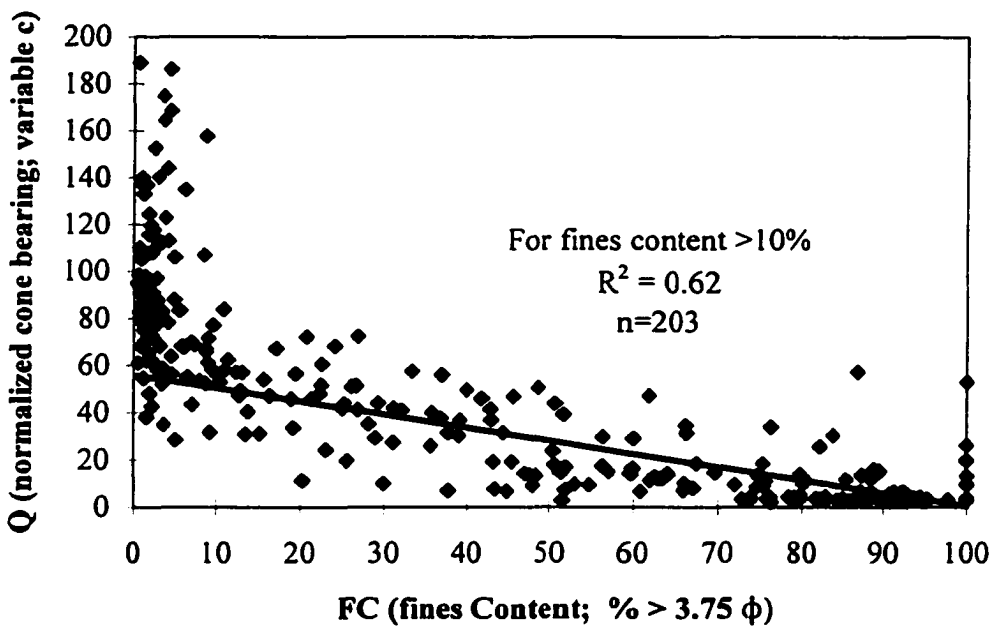

Figure 5-4. Fines content (FC) vs Q (normalized cone bearing using variable cone stress exponent, c). Trendline and correlation coefficient apply to samples with FC greater than 10% (n=203).

Due to the relative insensitivity of cone bearing to grain size in the silt range, an abrupt change in cone bearing from typical silt values to increasing values may not represent the start of a coarsening sequence, but where a grain size threshold is crossed within such a sequence. An example is provided by a 4.3 m sampled interval in the upper part of the topset that fines upward from fine sand to very fine silt (Figure 5-5). In the fine sand below 4

2

$Q = 250\exp(-0.62\phi_{50}) \pm 21$ ($\pm$ 1 standard error).

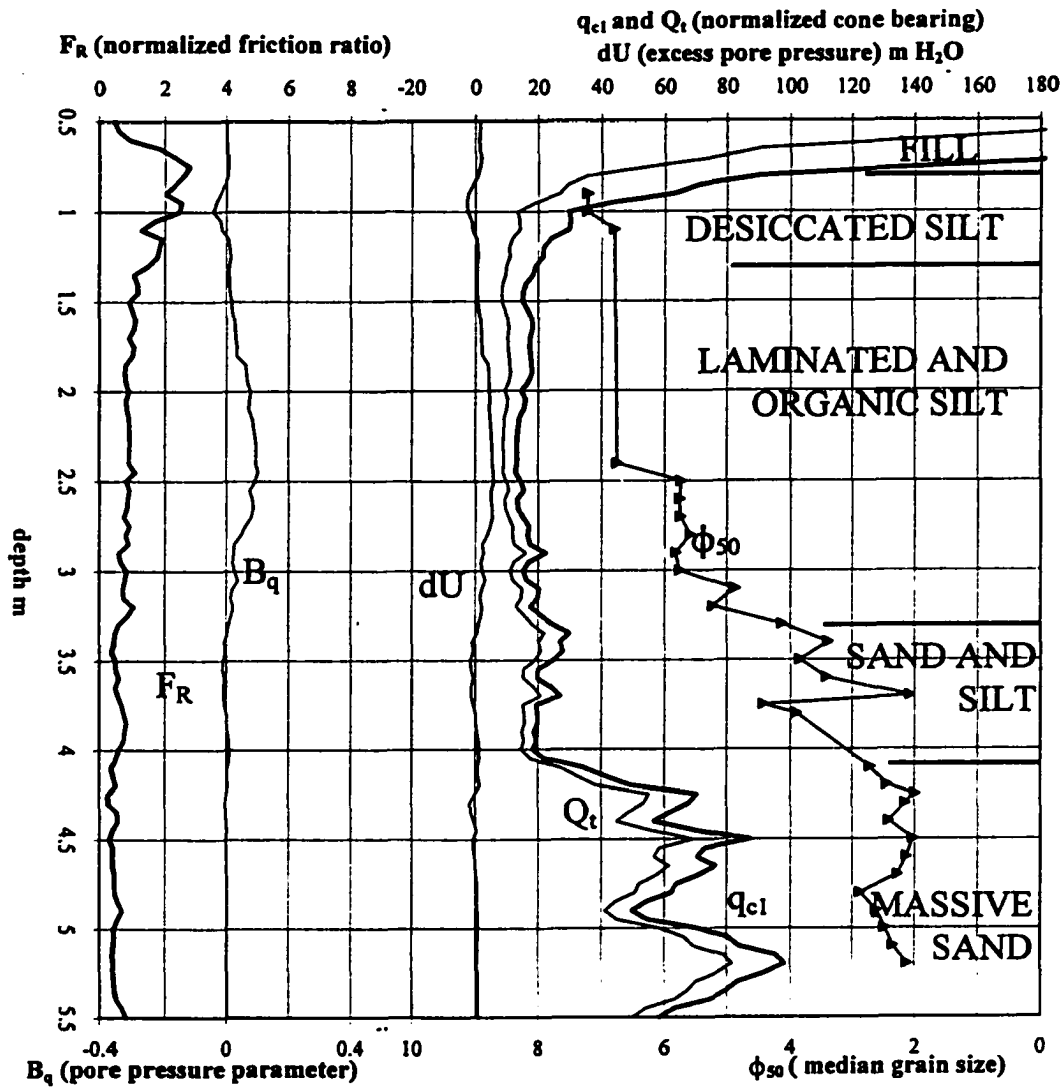

Figure 5-5. FD93-2; grain size and CPT data in upper part of topset. Note cone bearing decreasing upward sequence correspnds to fining upward sequence.

metres, cone bearing correlates moderately with grain size and decreases upward. At 4 m cone bearing changes sharply, and decreases only gradually upward through the interval of very fine sand and silt from 4 to 2.4 m. Minor cone bearing peaks in this interval correspond to coarser silt and very fine sand interbeds.

B_q is near zero in medium and coarse sands and slightly negative (B_q >-0.05) in fine to very fine sands (Figure 5-6). B_q is generally negative in coarse silts. Where ϕ_{50} is greater than 5, B_q is generally positive, although some negative values occur. These trends are shown in the fining upward sequence in the upper topset described above (Figure 5-5). B_q is near zero in the sands below 4 m, negative in the very fine sands between 4 and 3.4 m and positive in the mainly medium silts above.

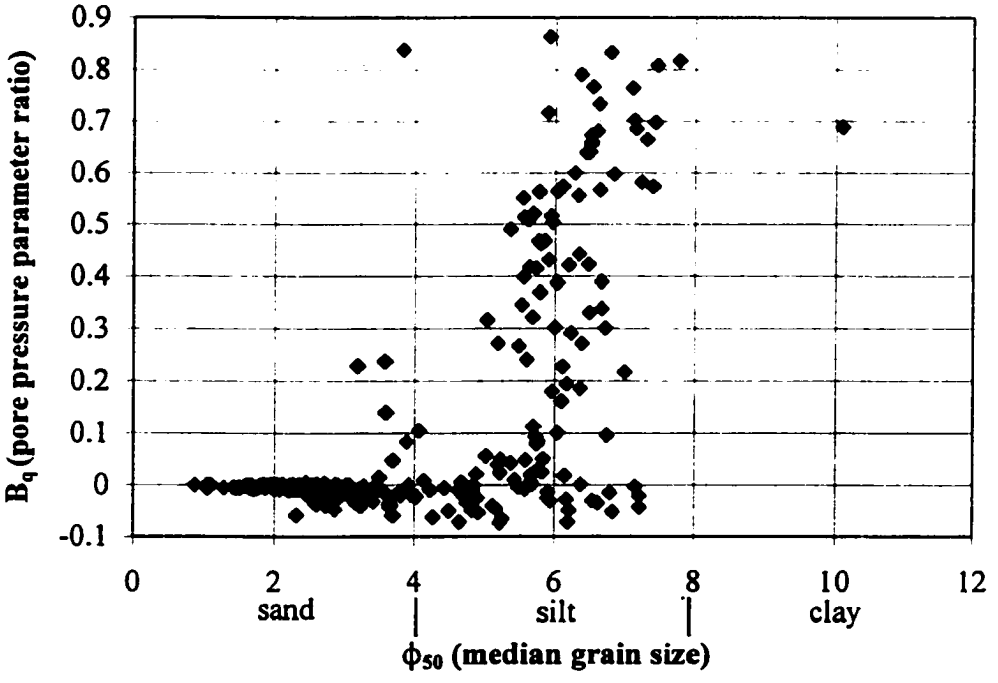

Figure 5-6. ϕ_{50} (median grain size) vs B_q (pore pressure parameter ratio). This plot includes data where pore pressure was measured in the U_2 position only (n=290).

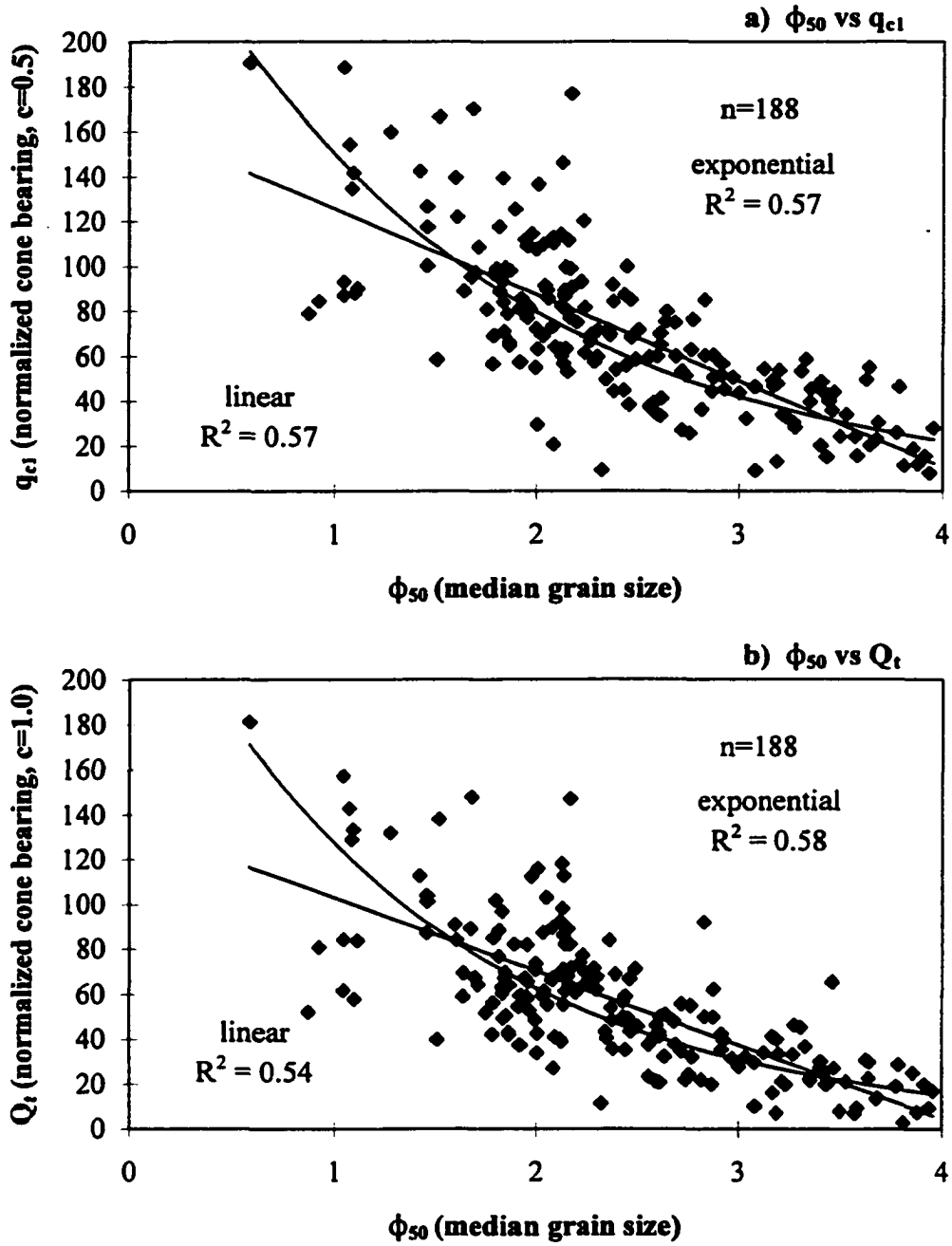

Figure 5-7. ϕ_{50} (median grain size) vs cone bearing in sands: a) ϕ_{50} vs q_{c1}, and b) ϕ_{50} vs Q_t.

Because sands and finer sediments have different CPT responses, they are discussed separately below.

Sands

Within the sand range, ϕ_{50} correlates moderately with both q_{c1} and Q_t (Figure 5-7a and b), and the differences between the two normalizing procedures are not statistically significant (linear correlations R^2= 0.57 and 0.54; and exponential correlations R^2= 0.57 and 0.58 respectively; n=188)[3]. Thus, approximately 50% of the variation in normalized cone bearing in the sands analyzed here can be explained by variation in ϕ_{50}, and this correlation provides a framework to interpret subsequent observations.

Normalization of sands for overburden stress. Sand samples from borehole FD92-11 span a depth range of 97.4 m and provide a unique opportunity to compare parameters for normalizing cone bearing in sand. For the purposes of this comparison, sand samples were grouped into three depth intervals (Figure 5-8):

1) 0-14.55 m; topset; interbedded sand and silt to 5 m and massive sand below (n=9);

2) 14.55-54.9 m; upper foreset; laminated silt with very fine sand interbeds grading down to interbedded sands and silts (n=17); and

3) 54.9-99.6 m; lower foreset; uniform bioturbated silt, with graded sandy intervals at 72 m and at the base (n=4).

The ϕ_{50} to q_{c1} trendlines for each depth interval are similar to each other (Figure 5-9a) and to the general ϕ_{50} to q_{c1} trendline for sands (Figure 5-7a). Conversely, the ϕ_{50} to Q_t

---

3

z=0.44 (linear) and z=0.15 (exponential). z<1.96 in both cases, so that the differences between q_{c1} and Q_t are not significant at the 95% confidence level (Spiegel, 1996).

$q_{c1} = -38\phi_{50}+164 \pm 24$ (linear), and $q_{c1} = 284\exp(-0.64\phi_{50}) \pm 25$ (exponential);
$Q_t = -33\phi_{50}+136 \pm 22$ (linear), and $Q_t = 259\exp(-0.71\phi_{50}) \pm 23$ (exponential).

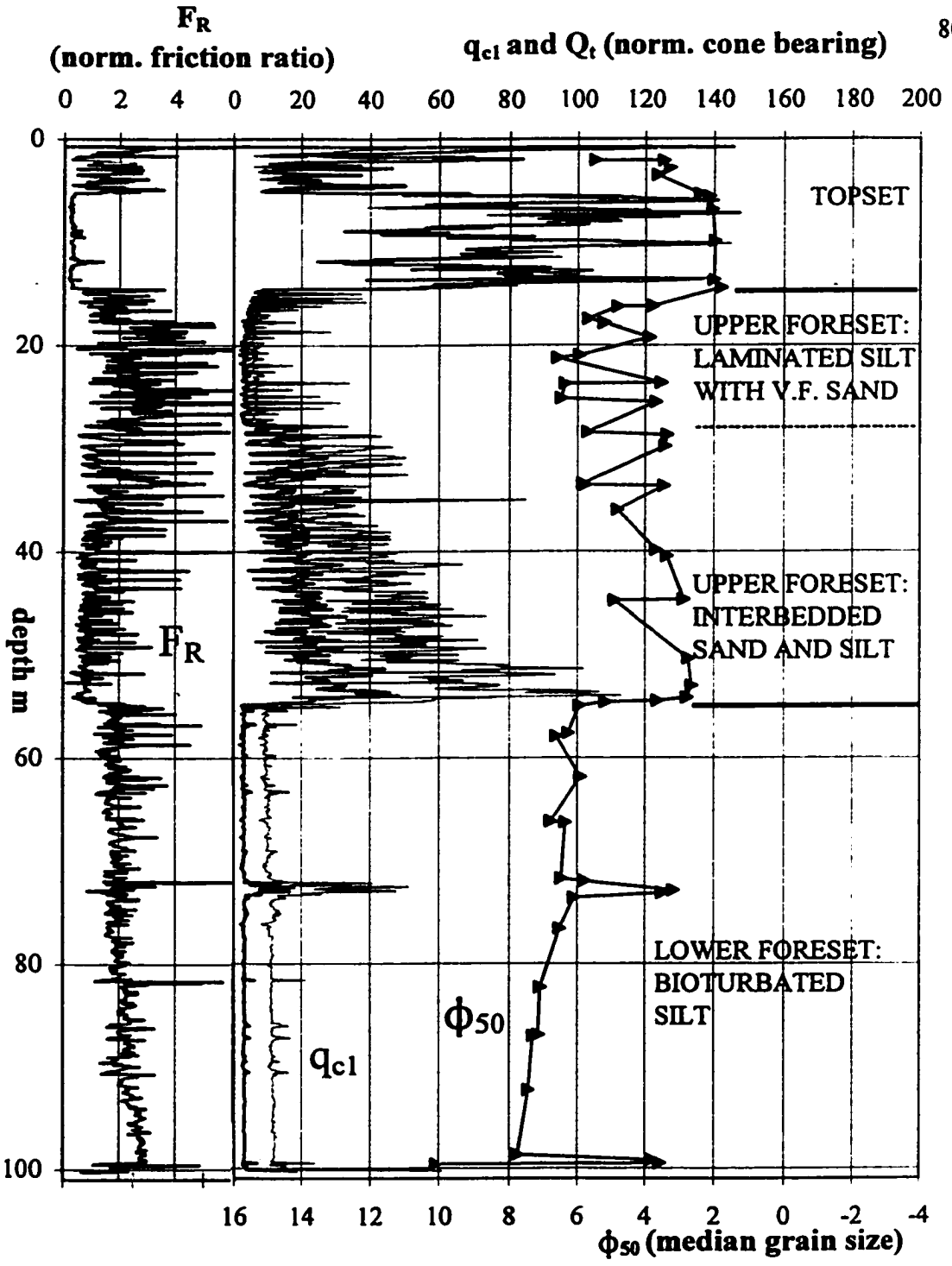

Figure 5-8. FD92-11 grain size and CPT data. Note low Q_t in foreset sands at 45-54 m; in lower foreset silts, Q is uniform but q_{c1} increases downward; F_R more variable and higher in upper than lower foreset.

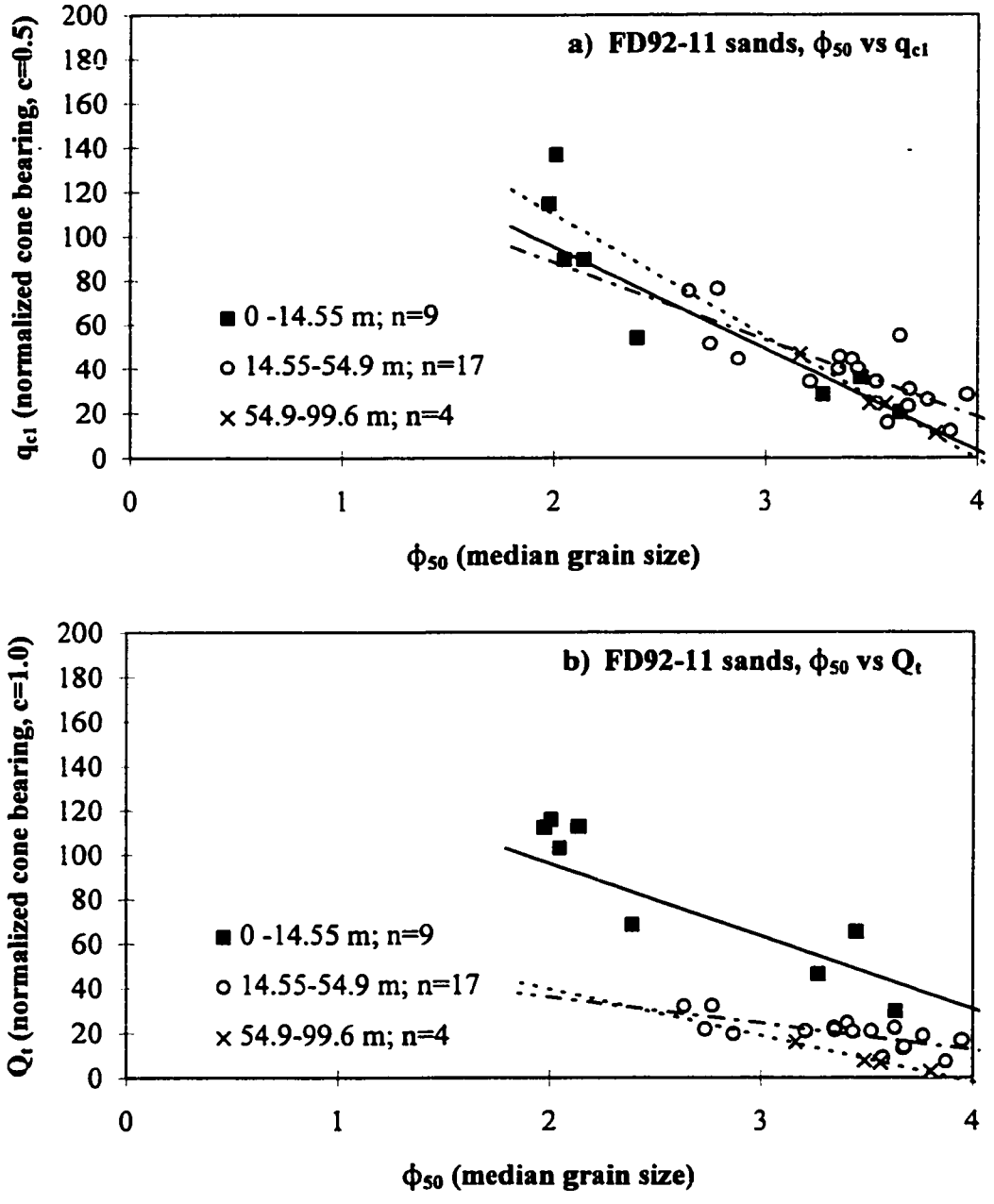

Figure 5-9. ϕ_{50} vs cone bearing, sand samples in FD92-11, a) ϕ_{50} vs q_{c1}, and b) ϕ_{50} vs Q_t. Note linear ϕ_{50} vs q_{c1} trendlines are similar for each depth interval and similar to the linear ϕ_{50} vs q_{c1} trendline for sands (Figure 5-7a). Linear ϕ_{50} to Q_t trendlines for each interval are lower for successively lower depth intervals. See Figure 5-8 for stratigraphy at this site.

trendlines for each interval have lower cone bearing for successively deeper intervals (Figure 5-9b). The samples and trendline for the shallowest interval plot above the general ϕ_{50} to Q_t trendline for sands (Figure 5-7b), whereas those for the deeper intervals plot below it.

Similarly, sands from 40 to 90 m depth in FD95S-1(n=32), where a 15 cm^2 cone was used, have a similar distribution on the grain size to cone bearing plot normalized with q_{c1} as the samples from boreholes where 10 cm^2 cones were used (Figure 5-10a). Conversely, samples from FD95S-1 have lower values of Q_t for samples of comparable grain size than those in the other boreholes (Figure 5-10b). Most of the sand samples from the other boreholes are from shallower depths than those in FD95S-1 (179 out of 188).

In both examples, normalizing sands with q_{c1} produces more consistent results than Q_t, which generates lower values in deeper sands than in shallower ones. In the following correlations, q_{c1} is used to represent normalized cone bearing in sand.

Influence of fines, gravel and thin beds on ϕ_{50} to q_{c1} correlations. The correlation between normalized cone bearing and ϕ_{50} is related in part to the correlation of cone bearing with FC, where FC exceeds 10% (Figure 5-4). Sands with FC greater than 10% generally have lower cone bearing than clean sands with similar ϕ_{50} (Figure 5-11).

However, ϕ_{50} correlates moderately with q_{c1} in sands with FC less than 10% ($R^2 = 0.31$; n=114; Figure 5-11), and the trendline for this correlation is similar to the general ϕ_{50} to q_{c1} trendline for sands (Figure 5-7a). The ϕ_{50} to q_{c1} correlation in these sands is not a function of sorting; the sands with FC less than 10% are moderately well sorted (standard deviation=0.73$\pm$0.4), and sorting in this group has no correlation with q_{c1} (standard deviation vs q_{c1}, $R^2 = 0.07$)[4].

---

[4] Sands with FC<10% correspond the moderately well sorted fine and medium sands shown as group 1 in Figure 5-1.

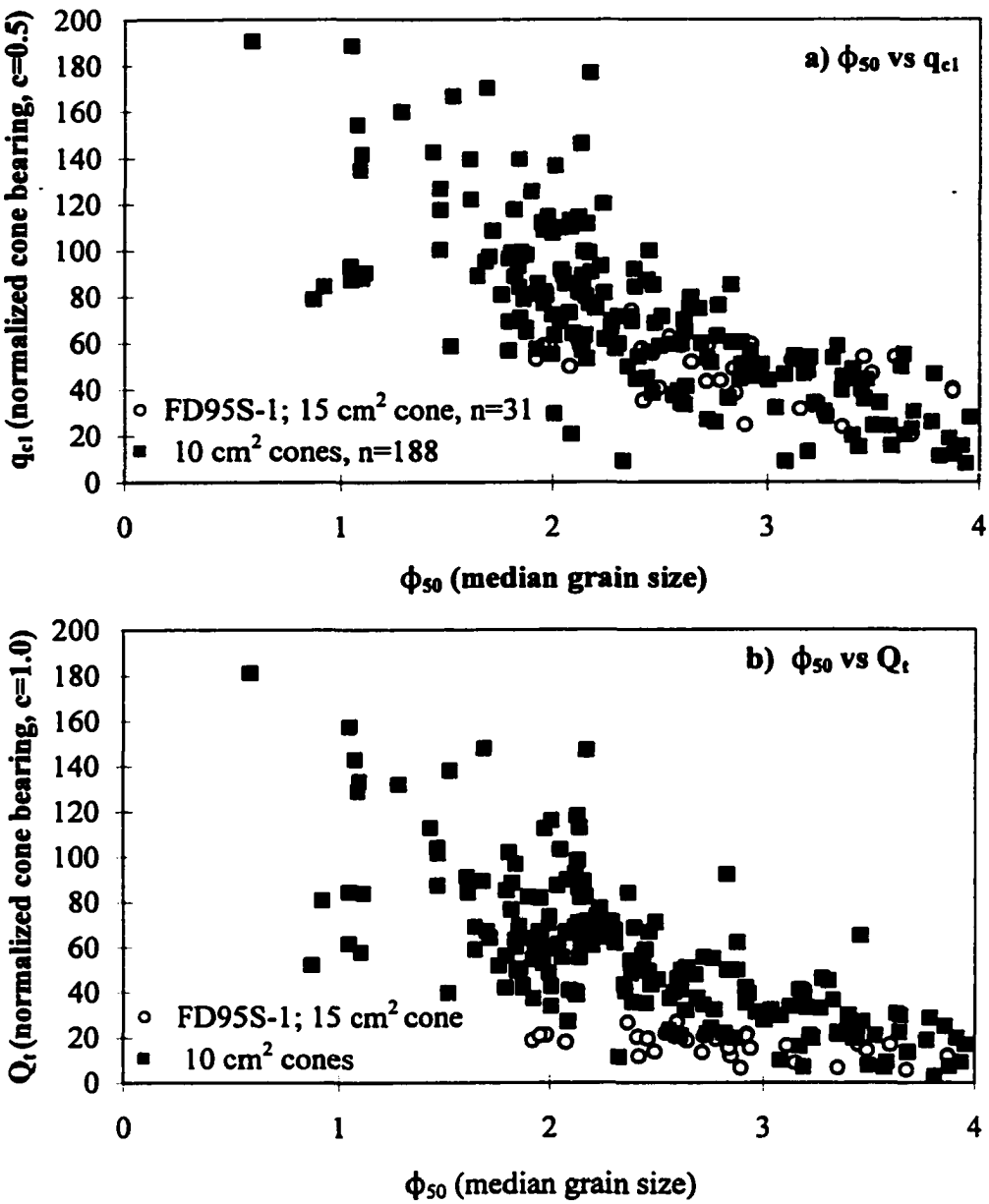

Figure 5-10. ϕ_{50} vs cone bearing, sand samples in FD95S-1, where a 15cm^2 cone was used (n=31) compared to data from 10cm^2 cones (n=188); a) ϕ_{50} vs q_{c1}, and b) ϕ_{50} vs Q_t. Note that data from 15cm^2 cone has a similar distribution to the data from the 10cm^2 cones on the ϕ_{50} vs q_{c1}plot but plot low on the ϕ_{50} vs Q_t plot.

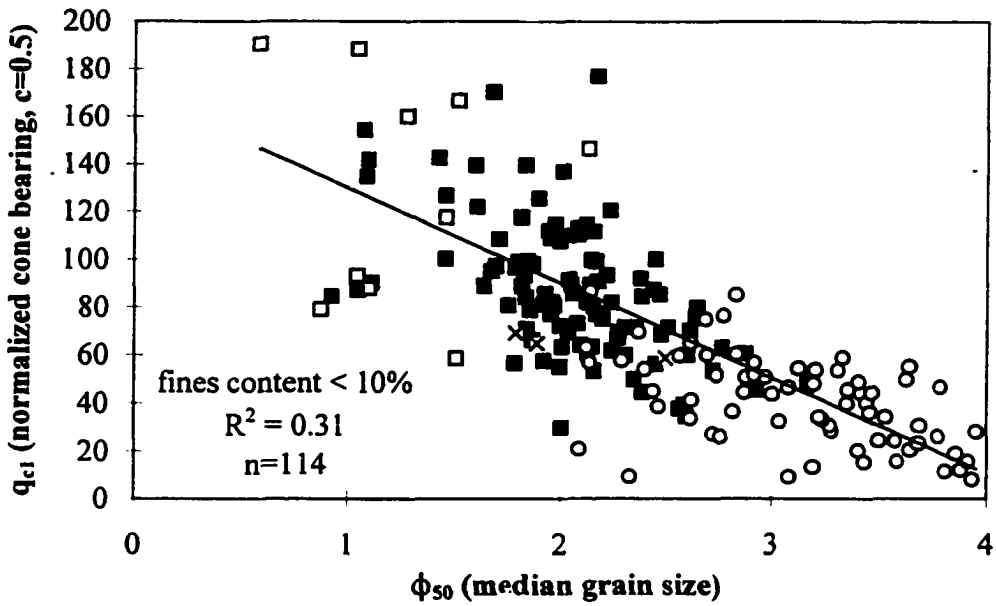

Figure 5-11. ϕ_{50} vs q_{c1} for sands sorted by fines and gravel content. Trendline is for samples with fines content less than 10% (with gravel both greater and less than 2%), and is similar to that for all sands (Figure 5-7a). Note that among the samples with greater than 2% gravel, those with less than 10% fines generally plot above this trendline, but that samples with more than 10% fines plot below it.

Only 13 samples have greater than 2% gravel. Of those with less than 10% fines (n=10), most have q_{c1} values higher than the general ϕ_{50} to q_{c1} trendline for sands, whereas those with greater than 10% fines (n=3) have lower q_{c1} values (Figure 5-11).

The general ϕ_{50} to q_{c1} correlation for sands (Figure 5-7) includes fine and very fine sands thinly interbedded with silts in the foreset. However, this correlation is not created by thin bed effects as a result of including these samples, because the ϕ_{50} to q_{c1} trendline for samples from the topset sand only, which generally occur in thick to massive beds (massive sand facies, see Chapter 6; R^2=0.42; n= 130; Figure 5-12), is close to the general ϕ_{50} to q_{c1}

trendline for sands (Figure 5-7a)

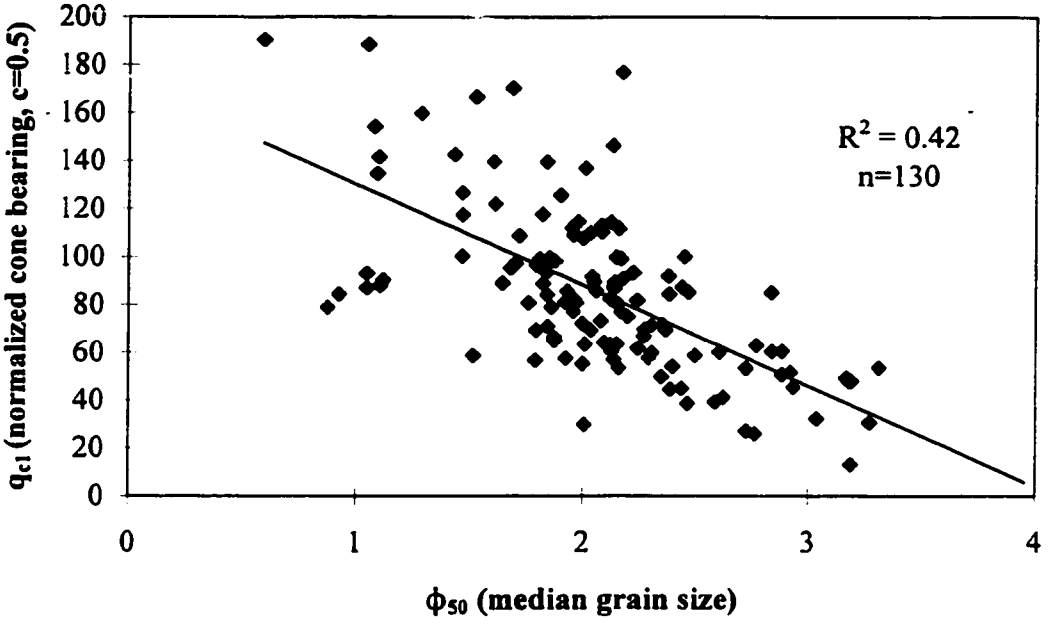

Figure 5-12. ϕ_{50} vs q_{c1} for topset sand (massive sand facies; n=130). Note that the trendline is similar to the general ϕ_{50} to q_{c1} for sands (Figure 5-7a).

These correlations demonstrate that normalized cone bearing correlates with FC, gravel, content and ϕ_{50}. Silty and gravelly sands generally have lower and higher cone bearing, respectively. However, cone bearing also correlates moderately with ϕ_{50} in clean moderately well sorted sands.

An example in which cone bearing can be seen to correlate well with grain size in the sand range is shown in Figure 5-13 (FD94-5; R^2= 0.76; n=22). The sampled interval includes a generally coarsening upward sequence, from fine to medium sand at the base to medium to coarse gravelly sand at the top, capped by a very fine sand interval. The highest cone bearing occurs in gravelly sand.

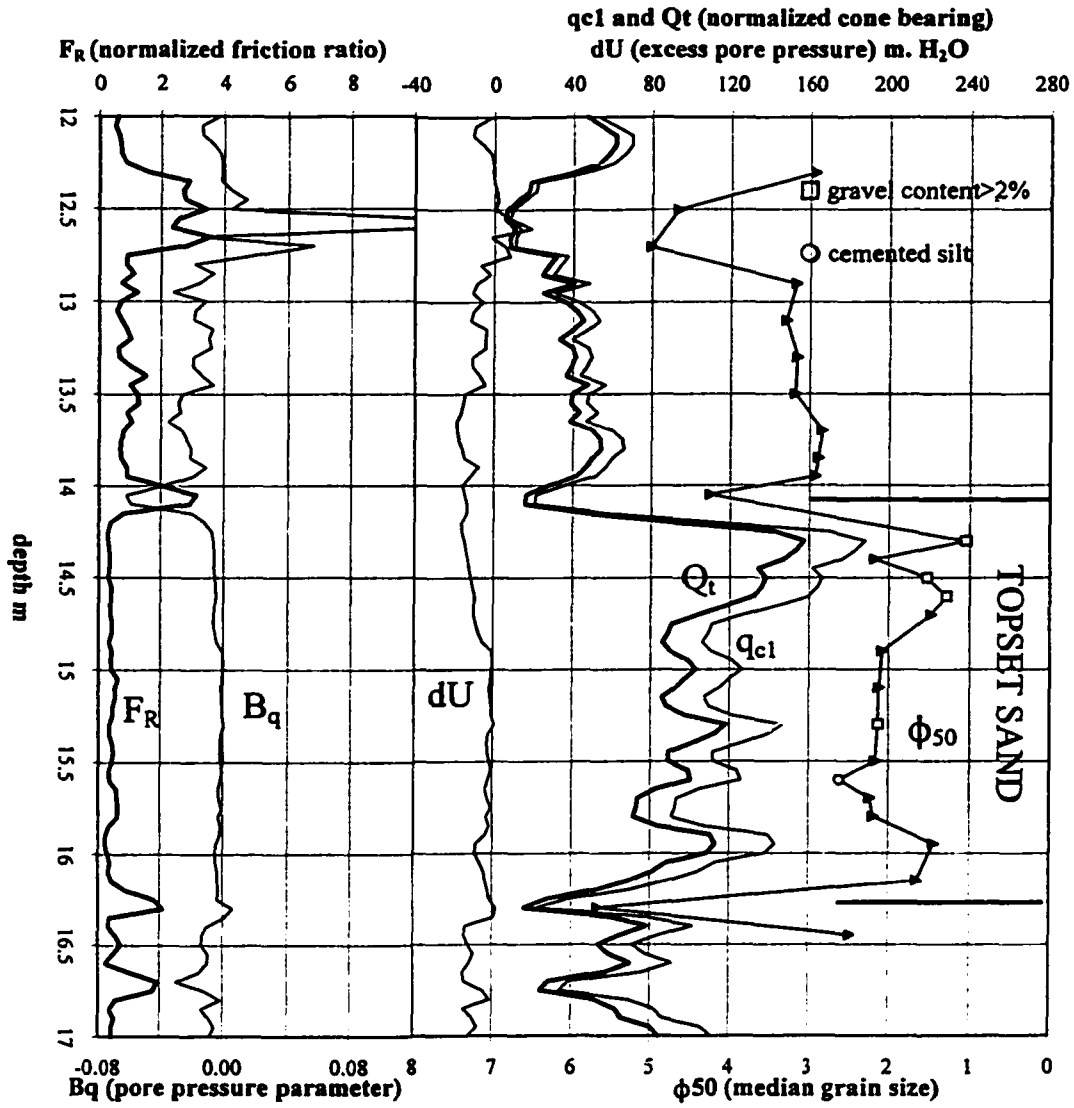

Figure 5-13. FD94-5; grain size and CPT data through a cone bearing increasing upward sequence in the topset sand (distal subfacies of the massive sands) and overlying deposits.

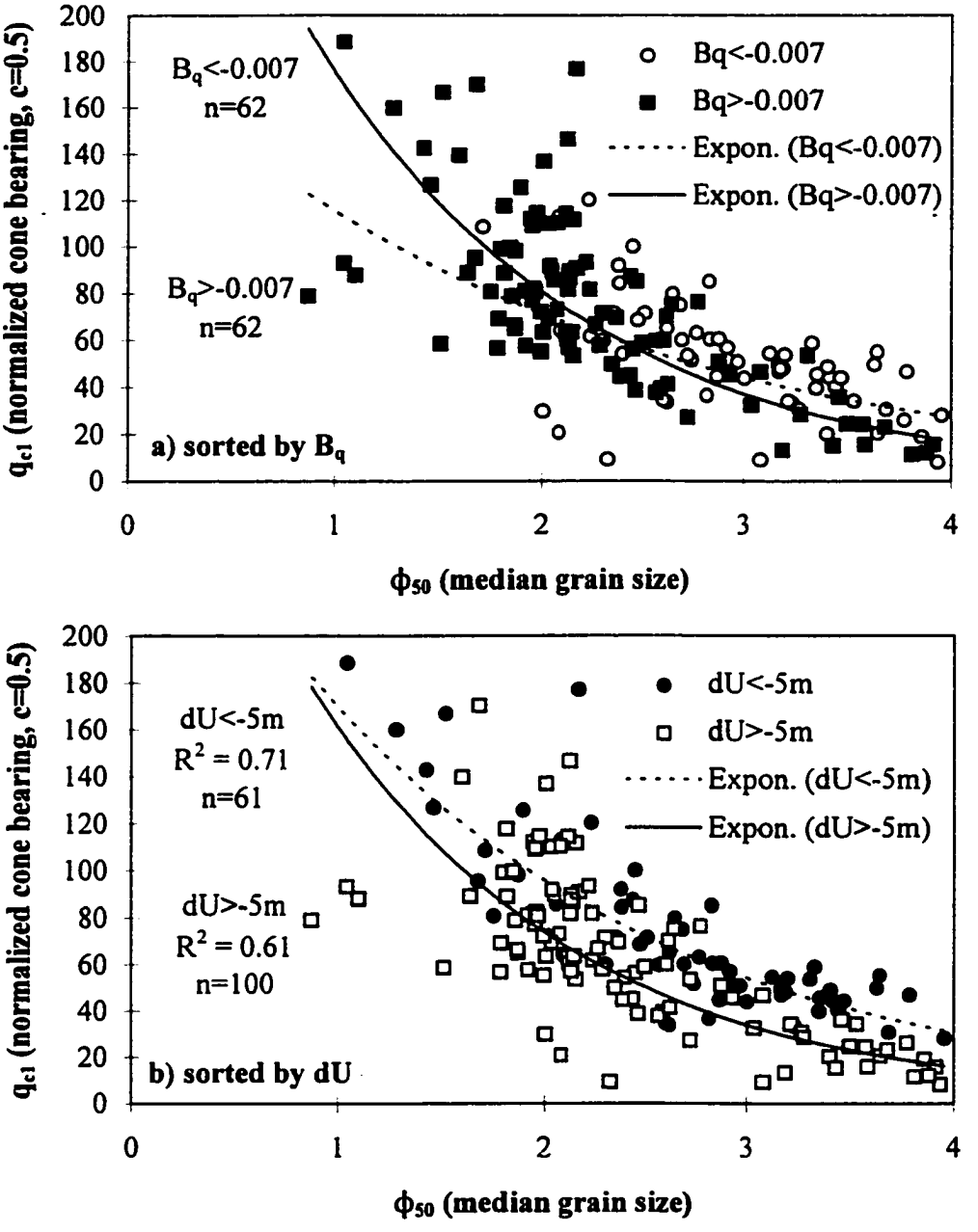

Figure 5-14. ϕ_{50} to q_{c1} a) sorted by B_q < -0.007 (n=62) and > -0.007 (n=99); and b) sorted by dU <-5m (n=61) and >-5m (n=100). Pore pressure measured in U2 position only. B_q is low in finer sands (note overlapping trendlines in 5-14a), but dU is low in sands with higher cone bearing and finer grain size (note parallel trendlines in 5-14b).

Interrelationship of cone bearing to pore pressure. B_q tends to be more negative in finer than coarser sands (Figures 5-6 and 5-14a). However, in some coarser sands strongly negative dU values occur, but B_q is not strongly negative because of the high cone bearing[5]. A plot of ϕ_{50} to q_{c1} separated into two dU ranges (>-5 m, n=100; and <-5 m, n=61) defines two subsets of data that extend from medium to very fine sand and have nearly parallel trendlines (Figure 5-14b). Sands with lower (i.e. more negative) dU plot with higher cone bearing (q_{c1} 20 higher on the trendline) and finer grain size (0.5ϕ finer on the trendline). Consequently, increasing cone bearing associated with decreasing dU does not generally represent sediment coarsening, and is interpreted instead to represent increasing density. Negative dU reflects increased dilatancy and dense sands are more dilatant than loose sands (Terzaghi et al., 1996). Examples from two boreholes illustrate this point.

A cone bearing increasing upward sand sequence in the upper foreset between 21.35 and 23 m in borehole FD93-5 corresponds to a coarsening upward sand sequence in that it has a gradational base with underlying silts and a sharp top (Figure 5-15). In the lower part of this sequence (below 22.1 m), the upward increase in cone bearing parallels a general upward increase in grain size. Three finer scale cone bearing increasing upward sequences occur within this interval and correspond with finer scale coarsening upward sequences. However, in the upper part of this sequence, q_{c1} increases upward from 60 to 80, but grain size does not, remaining in the mid-fine sand range with an average fines content of 10%. B_q and dU are negative throughout the sequence, but are least negative at the base of the upper part of the sequence, where grain size reaches the maximum, and decrease upward through the interval where grain size does not change (dU as low as -20 m). Cone bearing in the upper part of the sequence is in the same range as in the overlying topset sands, which are coarser but have dU near zero.

Another example is provided by FD94-6 (Figure 5-16). At the base of the topset sand, an

---

5

$B_q = dU/(q_t-\sigma_{vo})$, and in sands $q_t >> \sigma_{vo}$ (equation 7, Chapter 3).

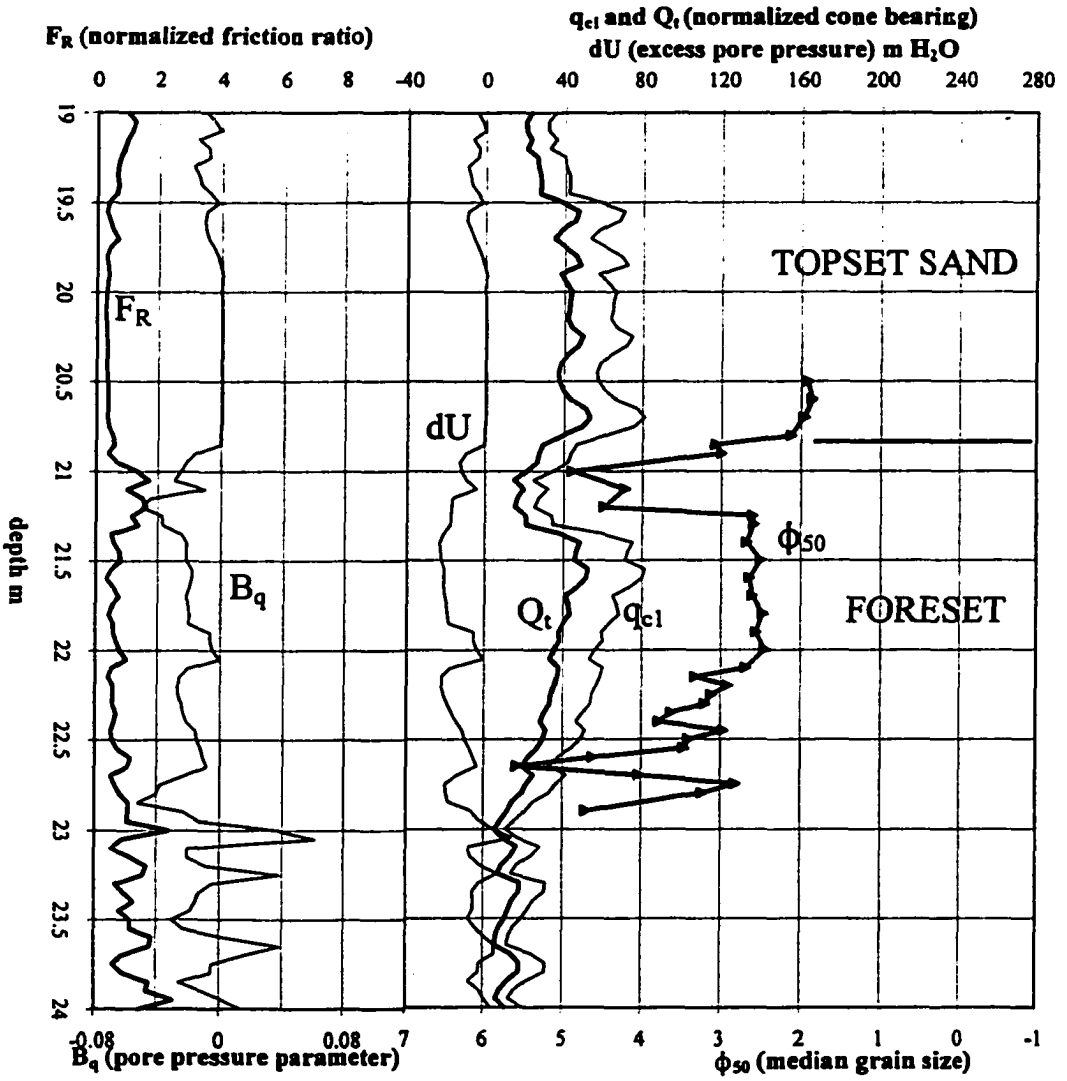

Figure 5-15. FD93-5; grain size and CPT data in upper foreset and lower topset. Cone bearing increasing upward sequence (21.25 to 23m) reflects in part upward coarsening; in upper part (with negative dU), increasing q_{c1} is not associated with coarsening but is interpreted to represent increasing density.

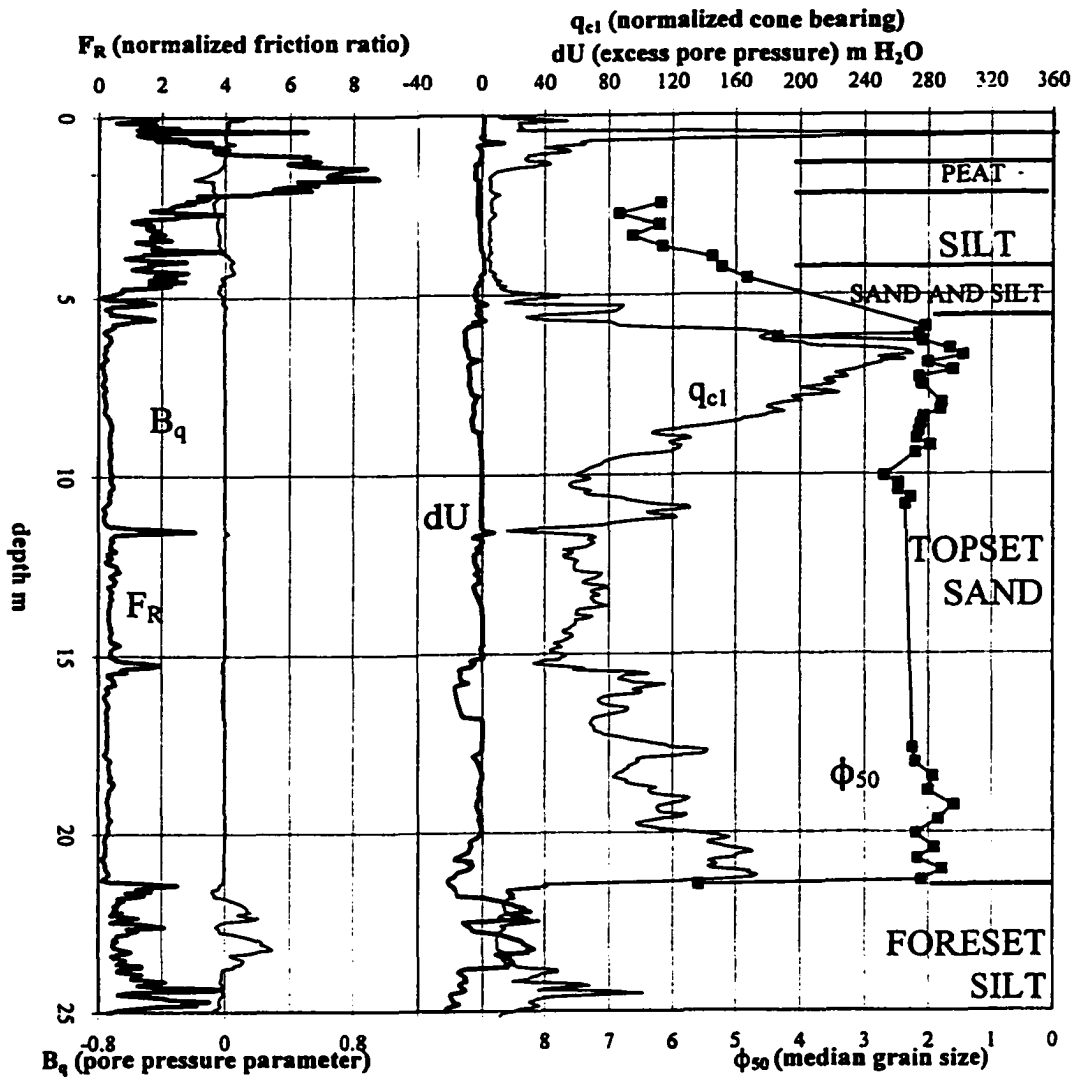

Figure 5-16. FD94-6; grain size and CPT data in the topset and upper part of foreset. Note negative excess pore pressures associated with high cone bearing at top and base of topset sand. The high cone bearing reflects denser rather than coarser sands.

interval of higher cone bearing below 20 m with strongly negative dU (as low as -22 m) does not correspond an interval of coarser sand. In contrast, dU is near zero in sampled intervals between 18 and 20 m and 10 and 12 m, where cone bearing generally follows grain size and cone bearing decreasing upward sequences correspond generally to fining upward sequences. The cone bearing increasing upward sequence between 6 and 10 m is anomalous, having significantly higher cone bearing than sands with similar grain size in other boreholes (commonly, $q_{cl} > 200$; Figure 5-3). Here too, the elevated cone bearing values are associated with negative dU (-5 to -10 m), and is interpreted to represent increased density. However, this cone bearing increasing upward sequence also corresponds to a coarsening upward sequence. This site is located adjacent to the B.C. Rail tracks, and the elevated cone bearing values are interpreted to reflect densification due to the vibrations from passing trains.

Gravel and other coarse particles also appear to correlate with high cone bearing and negative dU in sands. In the coarsening upward sequence in FD94-5 described above (Figure 5-13), dU decreases to between -7 and -16 m in the coarsest intervals at the top of the sequence, where the gravelly sand interbeds are concentrated. The gravel component in these samples varies from 6 to 23 %, and consists of pebbles and granules as well as centimetre-scale clasts of cemented silt and sand[6]. Similarly, in a sharp-based fine to medium sand unit in the foreset between 63.35 to 67.35 m in FD95S-1, the highest cone bearing and most negative dU occurs in a shell- and silt clast-rich interval (Figure 5-17). dU is less negative in most of this sand unit. Negative dU in gravelly and shell-rich sands may result from extensive rearrangement of sediment particles as the large sediment particles are displaced during cone penetration.

Relationships to age. In the previous examples, cone bearing increases associated with negative dU are unrelated to age. However, similar increases in cone bearing and decreases

---

6

The cemented clasts are interpreted to represent transported concretions. Such concretions have been reported within the distributary channels of the modern Fraser River (Johnston, 1921; Garrison et al., 1969; Nelson and Lawrence, 1984).

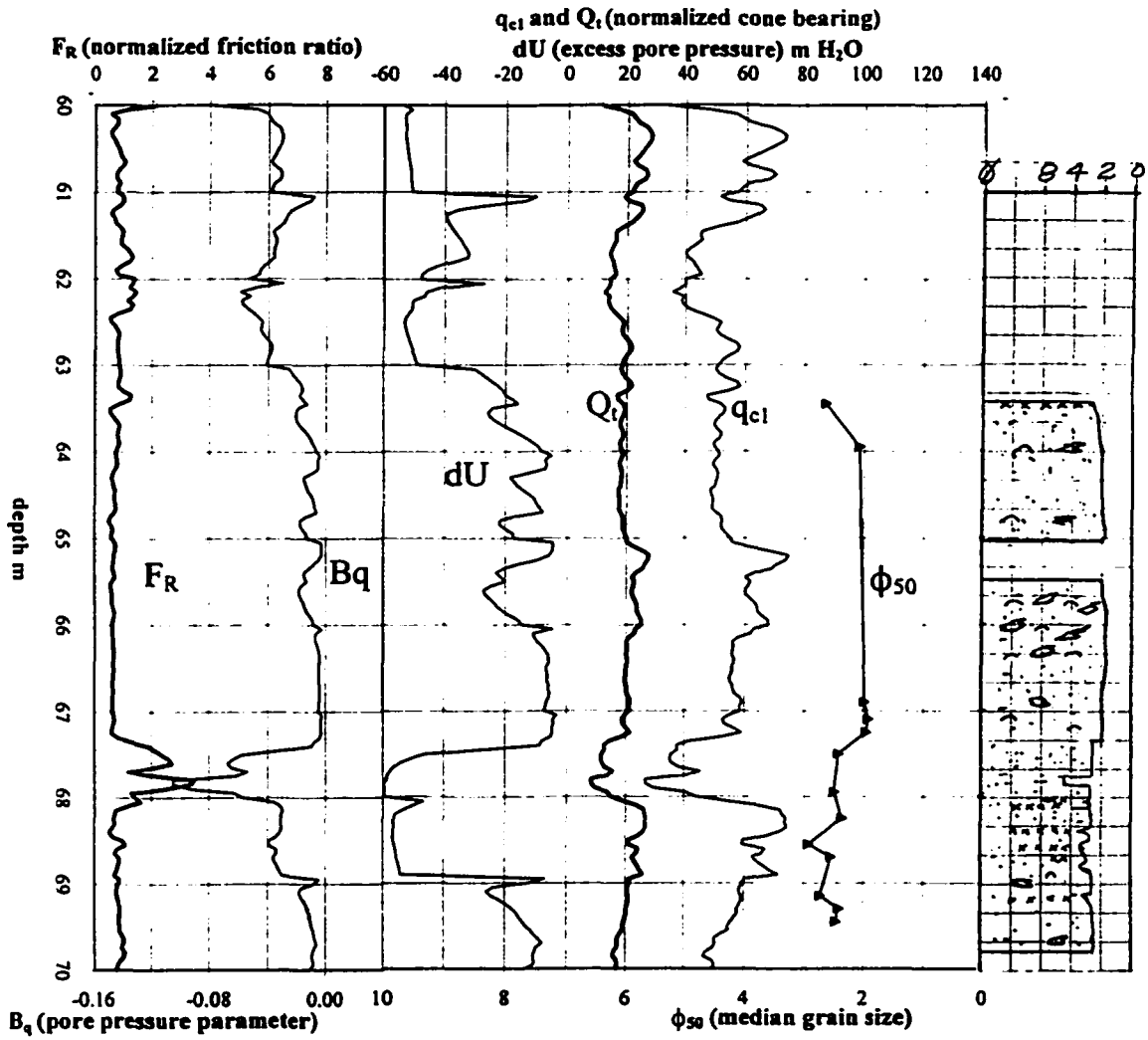

Figure 5-17. FD95S-1; grain size data, CPT data and core log between 60 and 70 m. Note sharp-based sand unit between 63.45 and 67.35 m.

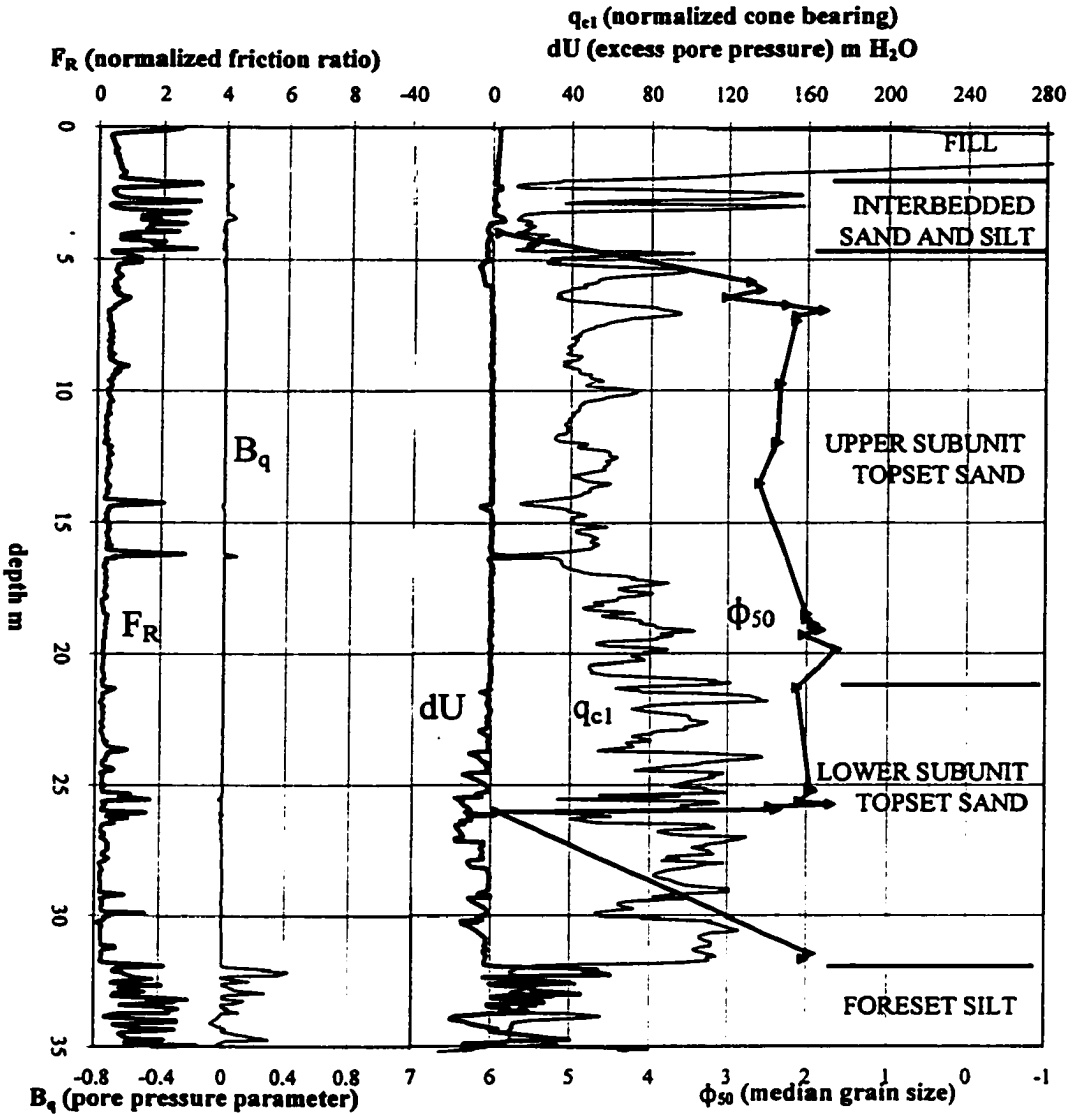

Figure 5-18. FD94-1; grain size and CPT data, topset. Upper subunit of topset sand is shell-free and historic in age. The lower subunit is shell-bearing and ~8000 ^{14}C years in age.

in dU occur with age. In one example the topset sand unit can be subdivided into 2 subunits (FD94-1; Figure 5-18). The upper subunit occurs between 4.9 to 21.4 m, lacks shell material, and was deposited at least in part during the historic period - a twig from 10 m depth was radiocarbon dated at 10±60 years (TO-4374; Appendix F; Monahan et al., 1995). The lower subunit occurs between 21.4 to 31.7 m, is shell-bearing, and is significantly older - a whole shell was radiocarbon dated at 8260±80 years (TO-4595).

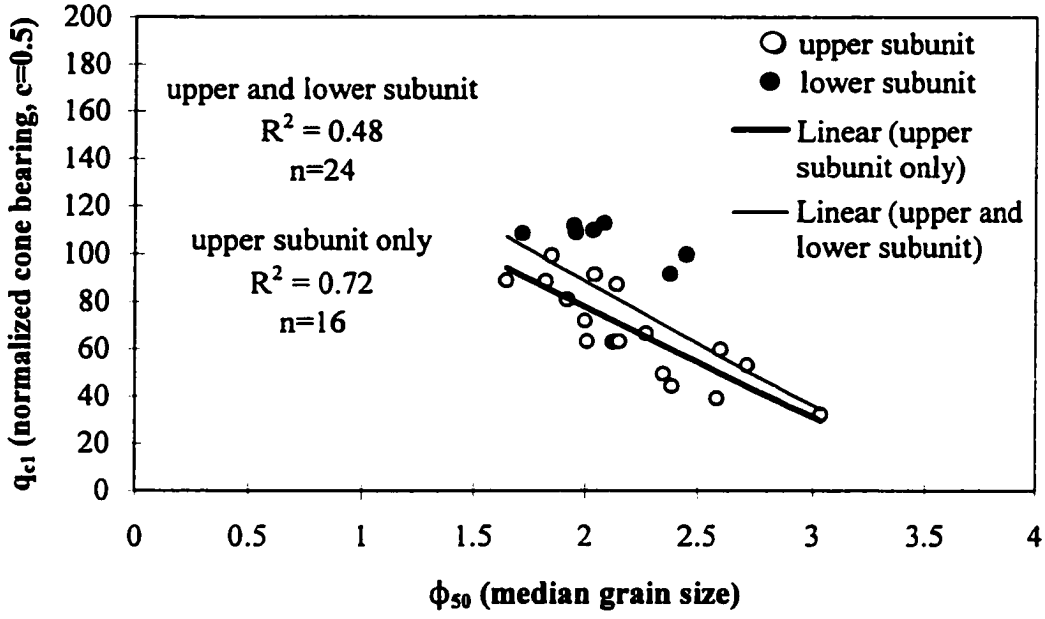

Figure 5-19. ϕ_{50} vs q_{c1} for the topset sand in FD94-1. Note that in the upper shell-free subunit (historic in age), q_{c1} is generally lower than in the lower shell-bearing subunit (~8000 ^{14}C years in age). The sample from the lower subunit with low q_{c1} is a silty sand (FC=23%). Modified from Monahan et al. (1995).

The two subunits correspond to the shell-free and shell-bearing subfacies on the massive sand facies of the topset, defined in the following chapter. In the upper subunit q_{c1} is generally lower than in the lower subunit for equivalent ϕ_{50}[7]. Furthermore, dU is generally

---

7

Comparing samples from both subunits together, ϕ_{50} correlates moderately with q_{c1} (R^2= 0.48; n=24), but in the upper subunit ϕ_{50} and has a better correlation with q_{c1} (R^2= 0.72; n= 16). However, the difference in R^2 is significant at only the 70% confidence level (z=1.12).

near zero in the upper subunit but commonly negative (dU=-3 to -18 m) in the lower subunit. In another example from the floodplain upstream of the delta (DT13), the topset sand also consists of two subunits (Figure 5-20a). The upper is between 4 to 21.7 m and consists primarily of medium and coarse sand with up to 5% gravel. The lower extends to a depth of 32 m and consists of fine to medium sand. Although these deposits are undated, they are interpreted to be significantly different in age. As will be discussed in the next chapter, the depth of the base of the lower subunit suggests that it was deposited when sea level was lower in the early Holocene, whereas the elevation of the top of the upper subunit indicates that it was deposited after sea level reached its current position 2500 years ago, and it includes coarse sands typical of fluvial channels of the floodplain. Nine samples were analyzed in at the top of the lower subunit and across the contact into the upper subunit (Figure 5-20b). The sands from the upper subunit have lower cone bearing than most of those in the lower unit, which are finer. However, in a general way, a cone bearing decreasing upward sequence in the lower subunit corresponds to a fining upward sequence. dU is generally near zero in the upper sand unit, whereas it tends to be negative in the older sand unit.

In both examples, older sands have higher cone bearing and more negative dU than younger sands. This subject will be discussed more fully in Chapter 6.

Recognition of coarsening and fining upward sequences. The correlation of grain size with cone bearing, qualified by dU, permits recognition of coarsening upward and fining upward sequences in sands on a variety of scales.

For example, in borehole FD94-1 (Figure 5-18), the visual core observation and the grain size analyses demonstrate that the overall upward decrease in cone bearing in the upper subunit reflects a general decametre-scale upward fining sequence. dU is near zero in most

---

The relationship of cone bearing to age is discussed further in Chapter 6.

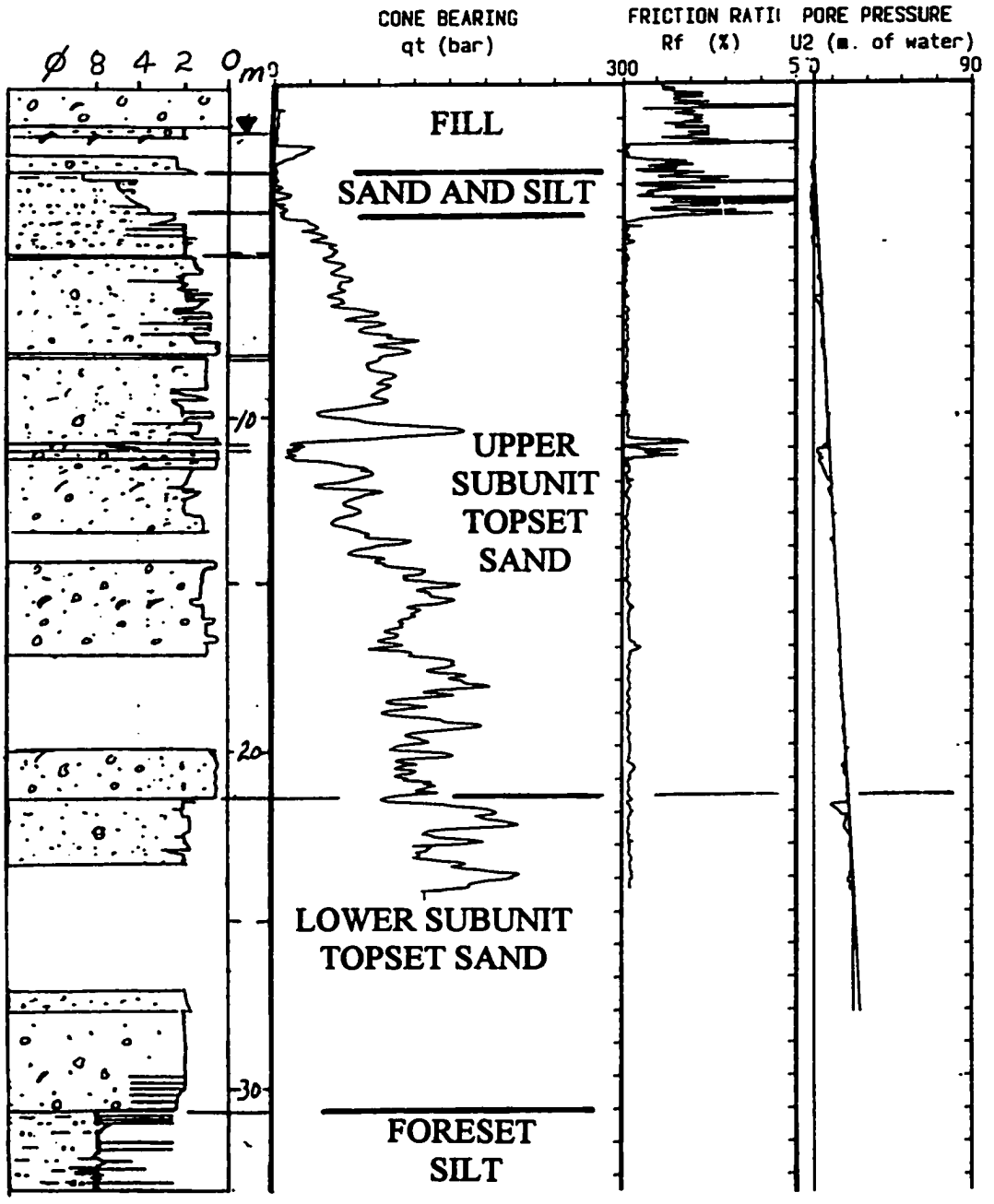

Figure 5-20a. DT13, composite log (non-normalized CPT data and core log). Note that the upper subunit of the topset sand is coarser but has lower cone bearing than the lower subunit. The contact between the two subunits is shown in more detail in Figure 5-20b.

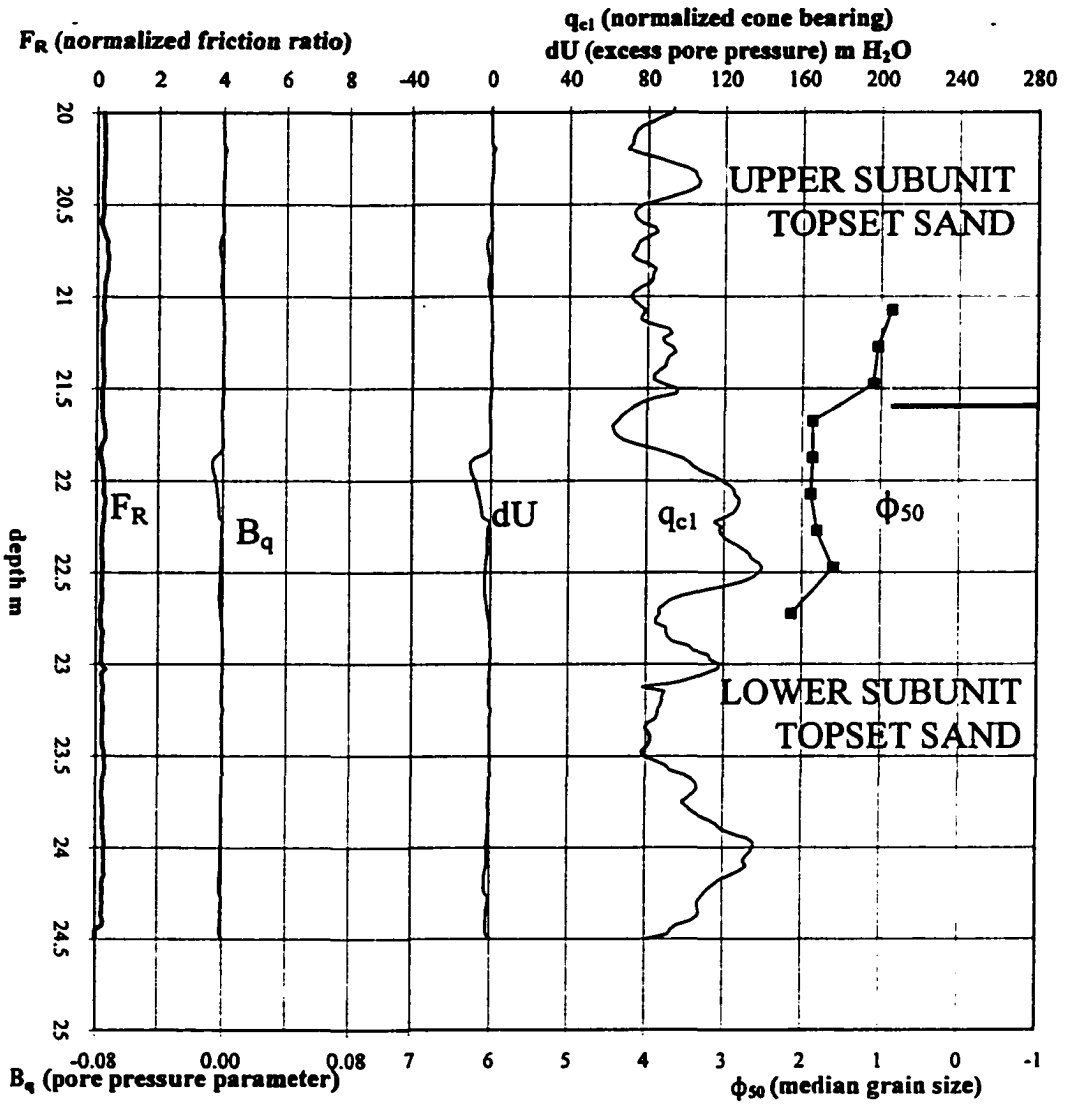

Figure 5-20b: DT13; grain size and CPT data across boundary of lower and upper subunits of topset sand. Note higher cone bearing in older subunit.

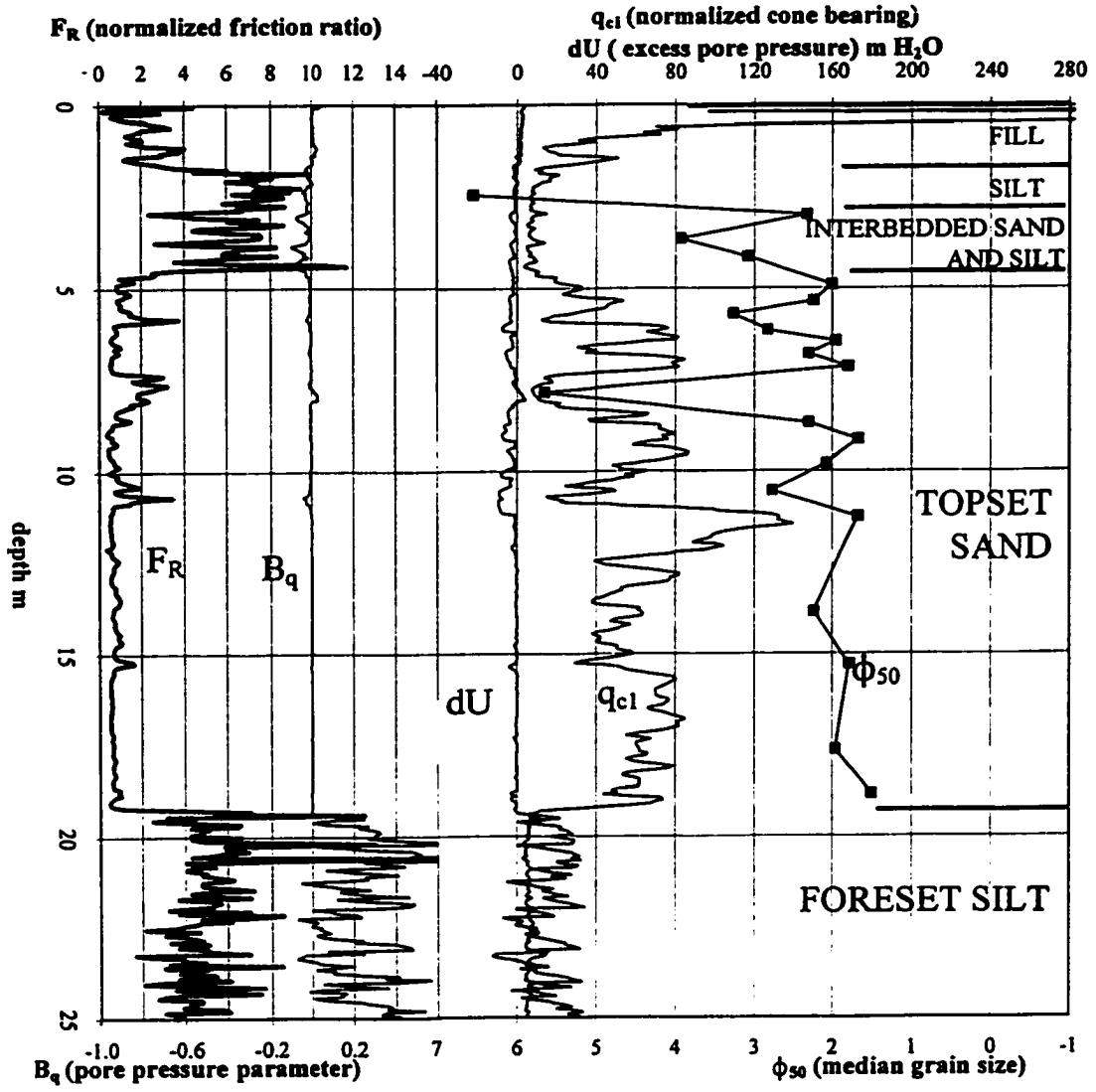

Figure 5-21. FD93-3; grain size and CPT data, topset. Note upward fining in topset sand expressed as an upward increase in silt interbeds, and decrease in dU.

of this subunit. Two metre-scale cone bearing increasing upward sequences occur at the top of the sand - the lower reflects upward coarsening, but the upper, in which dU is negative, does not and represents upward increasing density.

In another example in the topset sand (FD93-3), grain size analyses define a generally upward fining upward sequence that continues into the overlying silt and sand (Figure 5-21). Sands in the fine to medium sand range occur throughout the topset sand, but the coarsest sand is at the base and interbeds of finer sand and silt occur toward the top. Although exceptions occur, ϕ_{50} correlates moderately with q_{cl} in sands (R^2= 0.35; n=19). dU is near zero in the lower half of the sand, but is generally negative (dU<- 3m) in the upper part. In this case, the upward decrease in dU corresponds to an upward decrease in cone bearing, and reflects upward fining.

Similarly, between 63 and 68 m in borehole FD95S-1 described above (Figure 5-17), decreasing dU is associated with decreasing cone bearing and reflects sediment fining. This interval includes fine sand, overlain by a sharp-based sand unit that consists of fine to medium sand (ϕ_{50}~2) and fines upward in the top 50 cm. In a general way, cone bearing correlates with grain size, and dU inversely correlates with grain size and cone bearing in this interval (Figure 5-10a and 5-17). dU is strongly negative (dU= -50 to -60 m) in the fine sand at the base of the interval, low negative in the lower part of the sharp-based sand unit, and decreases upward in the finer sands at the top. As discussed above, dU diverges from this inverse correlation with grain size and cone bearing in the shell and class-rich interval, where it is more negative. The high cone bearing in fine sands below 68 m is associated with strongly negative dU, and reflects denser sand.

Silts and Clay

In silts and clay, cone bearing is generally insensitive to grain size finer than $5\phi_{50}$, but increases gradually as grain size increases in coarse silts (Figure 5-22; for 10cm^2 cones, n=129; 128 silt and 1 clay sample). Samples with anomalously high cone bearing on the on

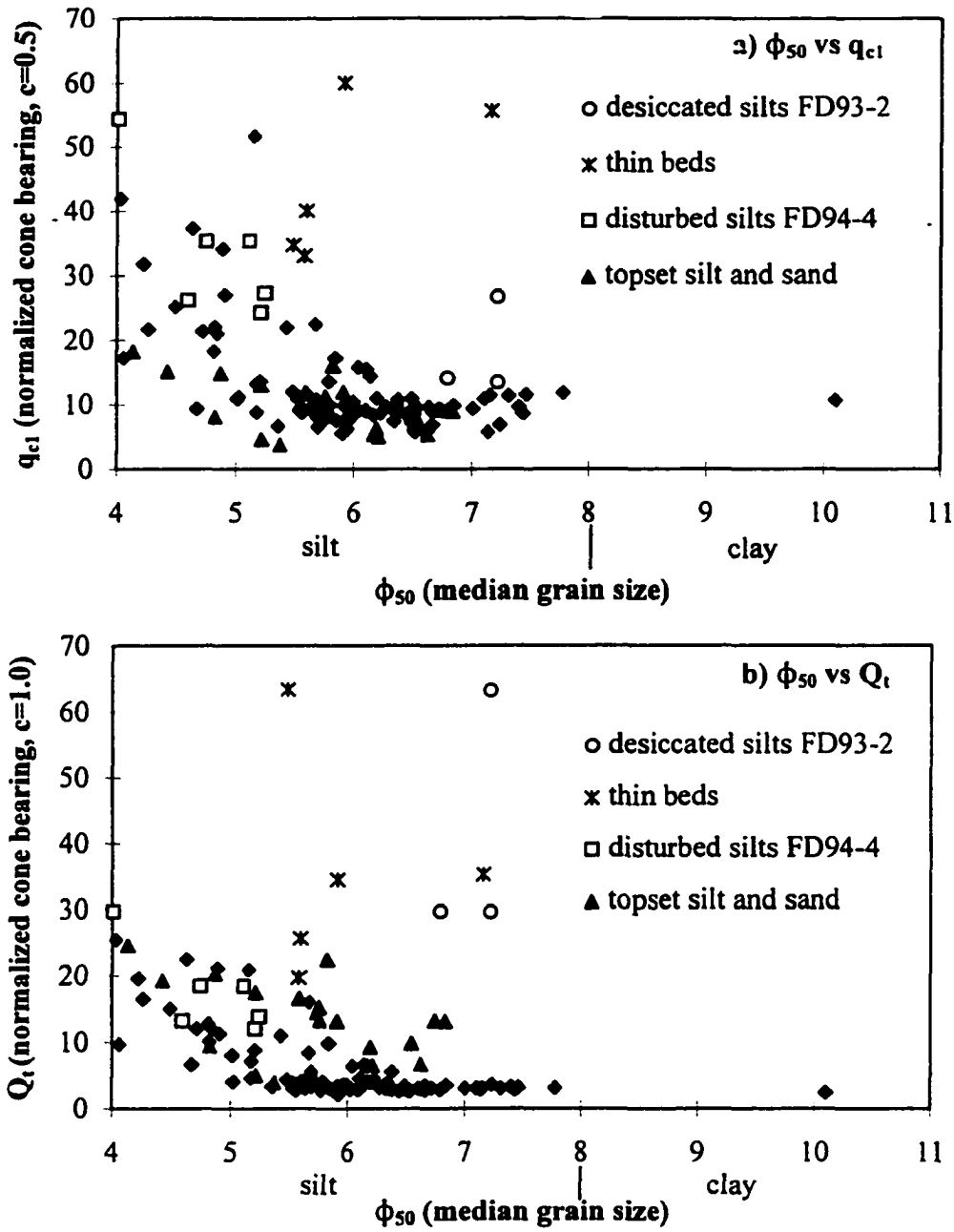

Figure 5-22. ϕ_{50} vs cone bearing in silts; a) ϕ_{50} vs q_{c1}, and b) ϕ_{50} vs Q_t; n=129. Excluding points with anomalously high cone bearing (the thin beds and desiccated silts), ϕ_{50} correlates better with Q_t than q_{c1} in siltsand clays (exponential R^2=0.40 and 0.28 respectively).

the plots of ϕ_{50} to q_{c1} and Q_t are desiccated silts from the top of the topset and thin silt interbeds (<15 cm) in sand, in which cone bearing is not resolved (Figure 5-2b). Excluding these samples, ϕ_{50} correlates better with Q_t than q_{c1} in the silt and clay range (exponential R^2 = 0.41 and 0.29 respectively, n=121)[8].

Interrelationship of cone bearing to pore pressure. B_q is negative in silt coarser than $5\phi_{50}$, but both positive and negative values occur in finer silt and clay (Figure 5-6). Plotting cone bearing against B_q separates the samples of silt and clay into two groups (Figure 5-23; Figure 5-23b is a modification of the normalized soil classification chart shown in Figure 3-3b). In the first (n=67), B_q is between 0.15 and 0.90 and cone bearing is low (the samples plot as clays on the normalized soil classification chart). In the other group (n=62), B_q is between -0.1 to 0.15 and cone bearing has a much greater range (the samples plot as silts to sands). The separation of the two groups is more pronounced using Q_t than q_{c1}: there is less overlap of Q_t values between the two groups (only 4 samples) than there is for q_{c1} values. These two groups are interpreted to represent cone penetration under undrained conditions and drained conditions[9] respectively. In silts where B_q exceeds 0.15, ϕ_{50} correlates weakly with B_q (R^2 = 0.23; n=66; Figure 5-6)

Normalization of silts for overburden stress. As shown above, ϕ_{50} correlates better with Q_t than with q_{c1} in the silt and clay samples. Furthermore, where B_q exceeds 0.15, normalizing silts with Q_t produces more consistent results than using q_{c1}. Samples in which B_q exceeds 0.15 span a 81 m depth range in the delta foreset (n=67). Shallower than 50 m, they are from laminated silts in which grain size varies from 5 to $7.5\phi_{50}$ (Figure 5-24a). Below 57 m, they are from bioturbated silts in FD92-11, and become finer with depth (Figure 5-8). In these samples, Q_t values occupy a narrow range, between 2 and 5, and are generally insensitive to

---

8

The difference in R^2 is significant only at the 77% confidence level; z=1.20

9

In undrained penetration, the force of penetration is transferred to the liquid rather than the solid phase and results in a pore pressure increase.

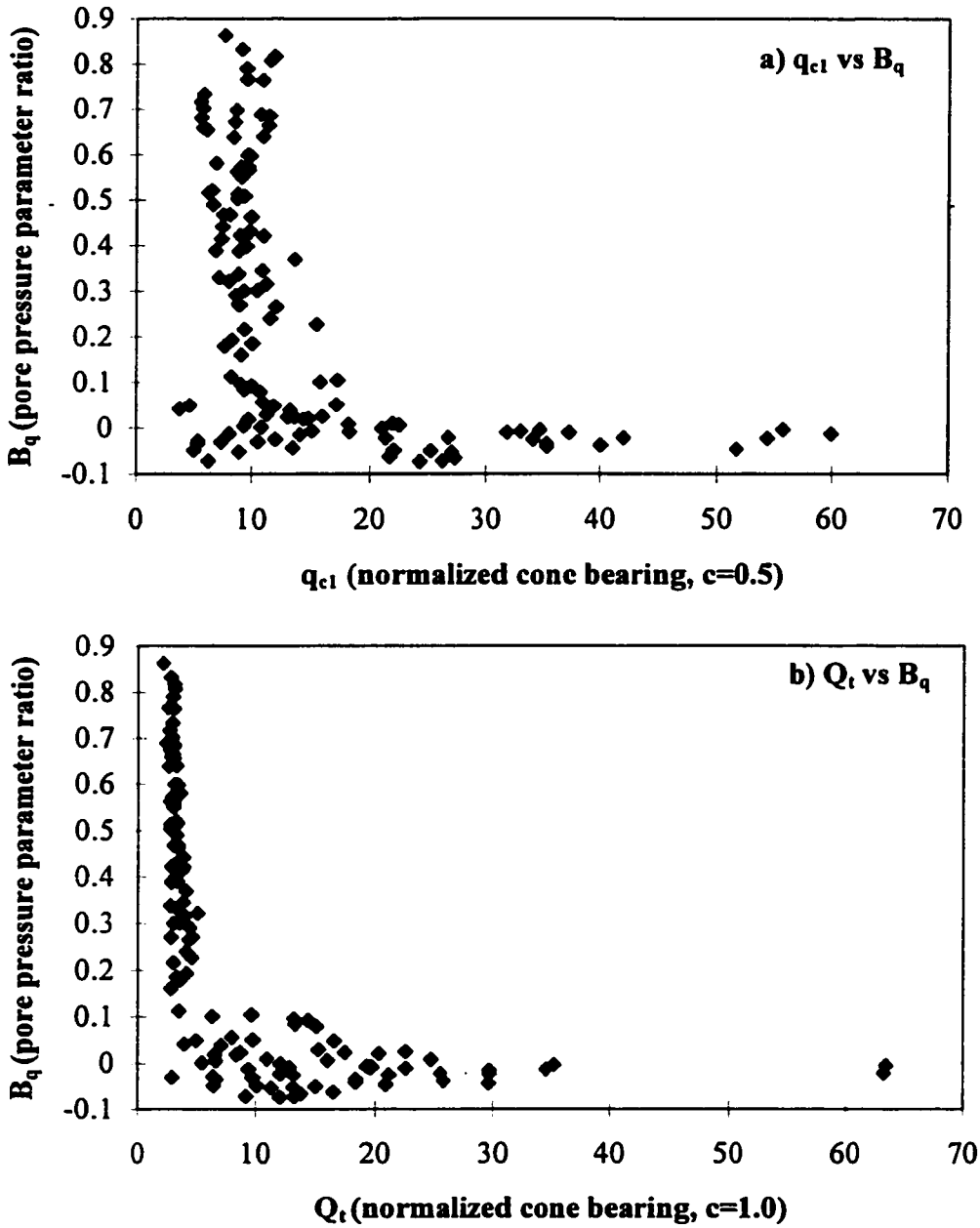

Figure 5-23. Cone bearing vs B_q in silts and clay; a) q_{c1} vs B_q and b) Q_t vs B_q. Note that samples form two groups: one with B_q>0.15 (n=67), which consists of normally consolidated silts penetrated under undrained conditions, and the other with B_q<0.15 (n=62), which consists of coarse and overconsolidated silts penetrated under drained conditions. Separation of the two groups is more pronounced using Q_t than q_{c1}. Note that the plot of Q_t vs B_q is a modified form of the normalized soil classification chart shown in Figure 3-3b.

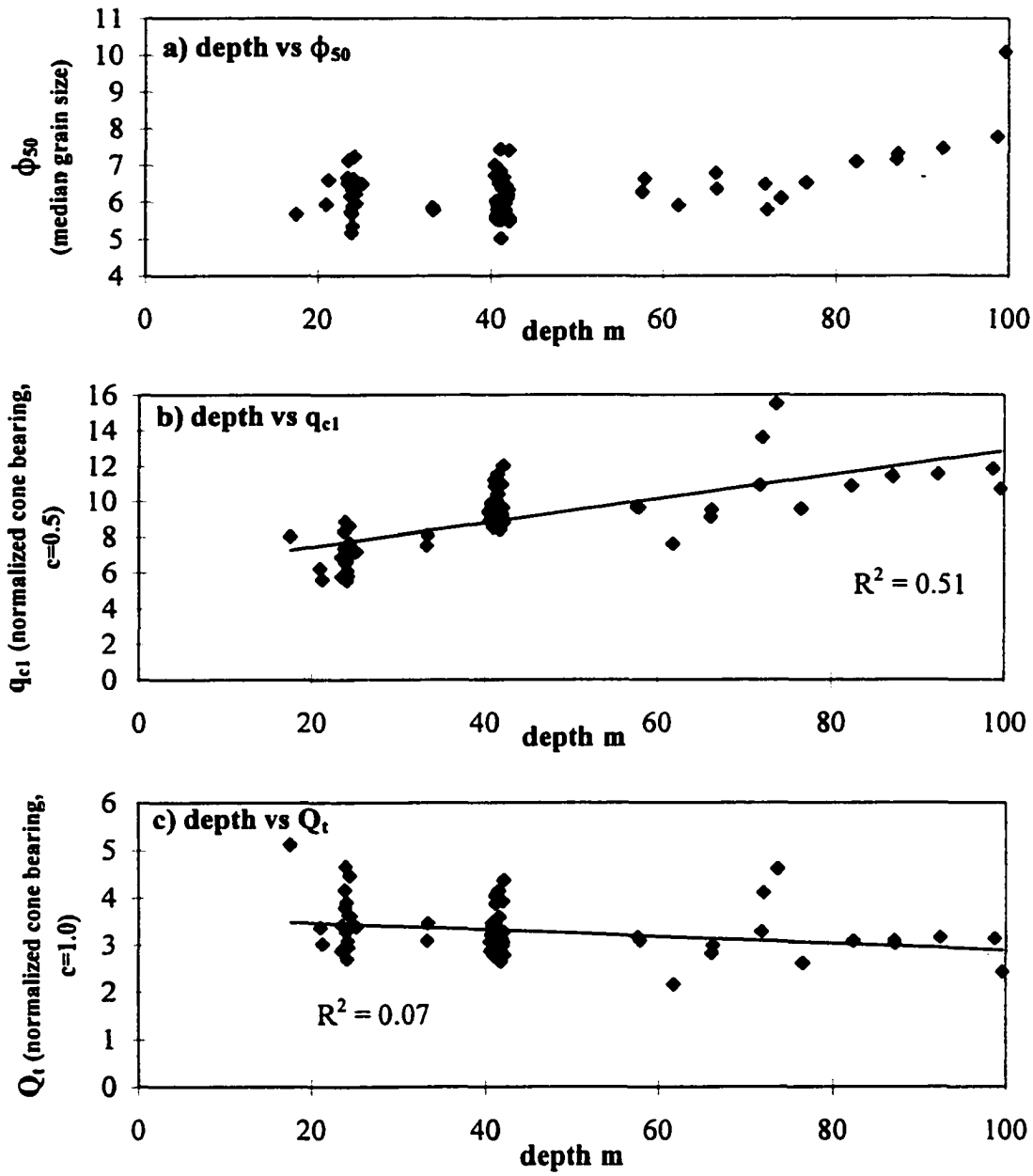

Figure 5-24. Silt (n=66) and clay (n=1) with B_q>0.15; a) depth vs ϕ_{50}, b) depth vs q_{c1}, and c) depth vs Q_t. Note that silts become finer with depth. q_{c1} increases with depth and undercorrects for overburden stress. Q_t shows little variation with depth, effectively normalizing silt and clay for efective overburden stress.

depth (R^2=0.07; Figure 5-24c). However, q_{c1} increases with depth (R^2=0.51; Figure 5-24b), and thus does not remove the effects of increasing overburden stress.

Cone bearing and pore pressure in silts and clays finer than $5\phi_{50}$. In the silts and clay samples in which B_q exceeds 0.15, Q_t is between 2 and 5, typical of normally consolidated deposits (Lunne et al., 1997), and changes little with grain size (Figure 5-22). Silts with a comparable range in grain size ($>5\phi_{50}$) and in which B_q is less than 0.15 have higher Q_t values. Most of these occur in the silt unit in the upper part of the topset beneath the desiccated silts, and may be slightly overconsolidated (Figures 5-5 and 5-16).

Correlation of grain size with cone bearing and pore pressure in laminated silts. Much of the upper foreset consists of laminated silts, which are commonly organized into decimeter to metre-scale sequences that coarsen upward from clayey silt to sandy silt and very fine sand. The upward coarsening in these sequences is not steady, and smaller-scale coarsening upward sequences occur within the larger sequences. On CPT data, these sequences are represented by sharply bounded, metre-scale pore pressure decreasing upward sequences, that change from high positive to low negative values. As noted above, ϕ_{50} has a weak correlation with B_q where it exceeds 0.15. Continuous grain size samples were analyzed across such sequences in two boreholes.

The sampled interval in borehole FD92-11 crosses one of a series of half metre to metre-scale sequences marked by upward decreasing pore pressures and cyclic cone bearing peaks (Figure 5-25a). This pore pressure sequence corresponds to a sedimentary sequence that coarsens upwards from a very fine silt to a very fine sand and is in turn sharply overlain by a very fine silt[10]. In this sequence, ϕ_{50} correlates moderately with B_q (R^2= 0.46; n=21; Figure

---

[10] The sediments are laminated on a scale finer than the interval thickness of the grain size samples (5 cm) masking some textural details. For example, the laminated sandy interval at the top of the underlying sequence is 5 cm thick and is split between 2 grain size samples, so that it appears as a silt rather than a sand peak (Figure 6-50).

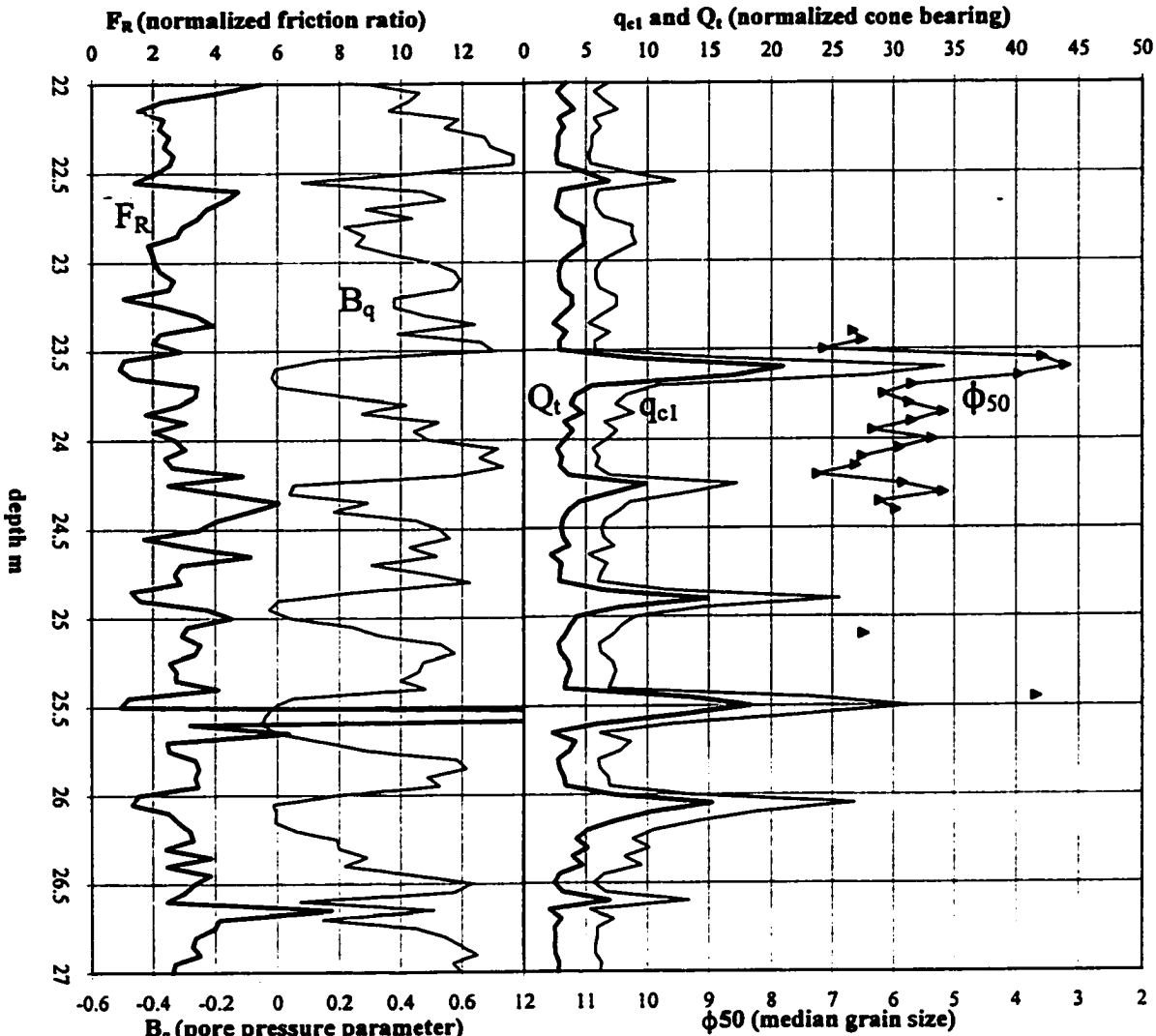

Figure 5-25a. FD92-11; grain size and CPT data through a coarsening upward sequence between 23.5 and 24.4 m in laminated silts of upper foreset. Note that this sequence corresponds a sequence marked by upward decreasing B_q and upward increasing Q_t. See Figure 5-8 for site stratigraphy.

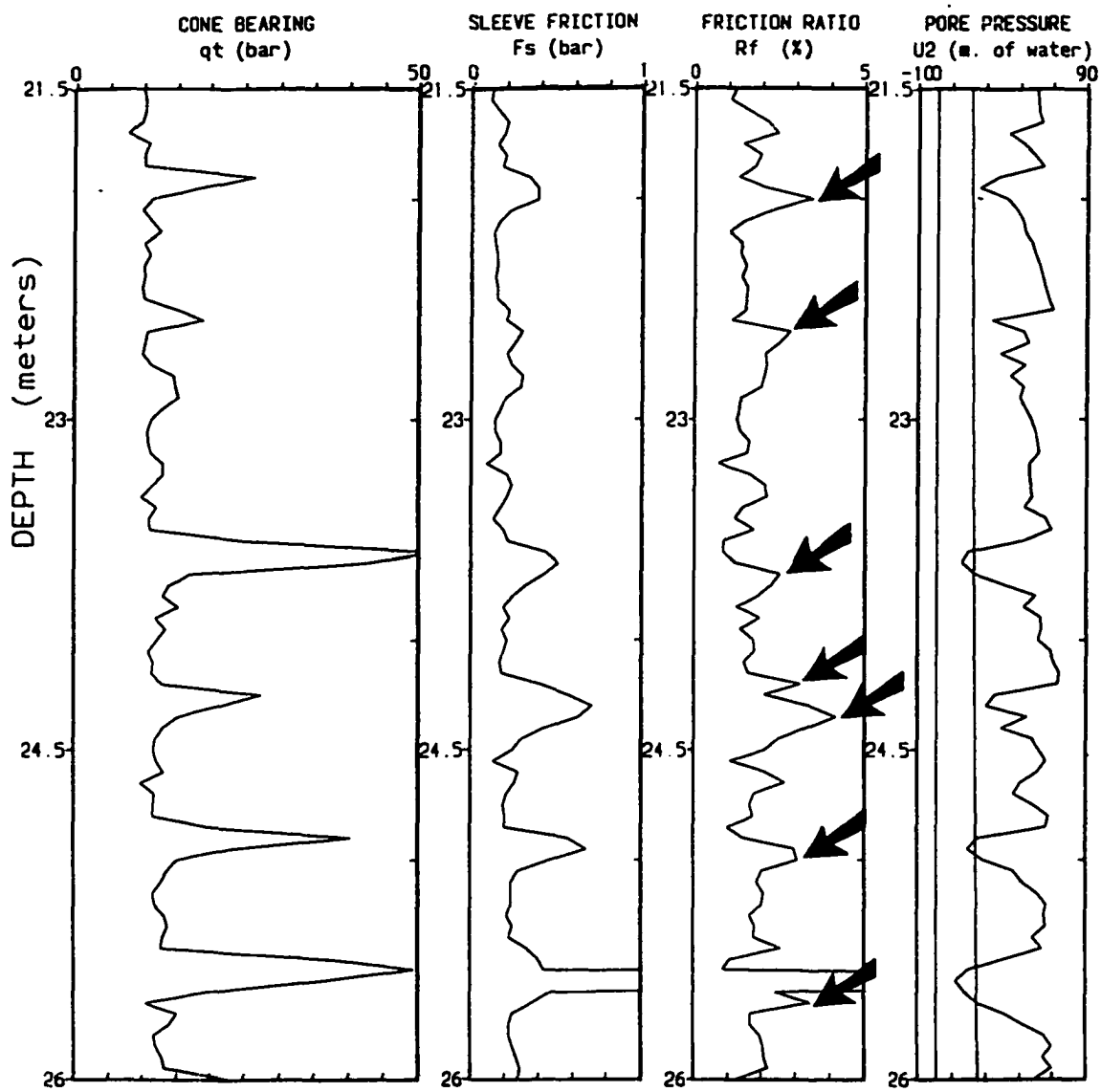

Figure 5-25b. FD92-11; non-normalized CPT data through coarsening upward sequences in laminated silts of upper foreset. Same interval as shown in Figure 5-25a, showing grain size data through analyzed interval between 23.4 and 24.4 m. Note that sleeve friction peaks associated with sand beds(cone bearing peaks) appear to be thicker (are represented by more readings). Consequently, friction ratio peaks commonly occur immediately above and below sand beds (arrows). Negative excess pore pressures (dU; pore pressure less than hydrostatic) beneath sand beds also contribute to friction ratio peaks there.

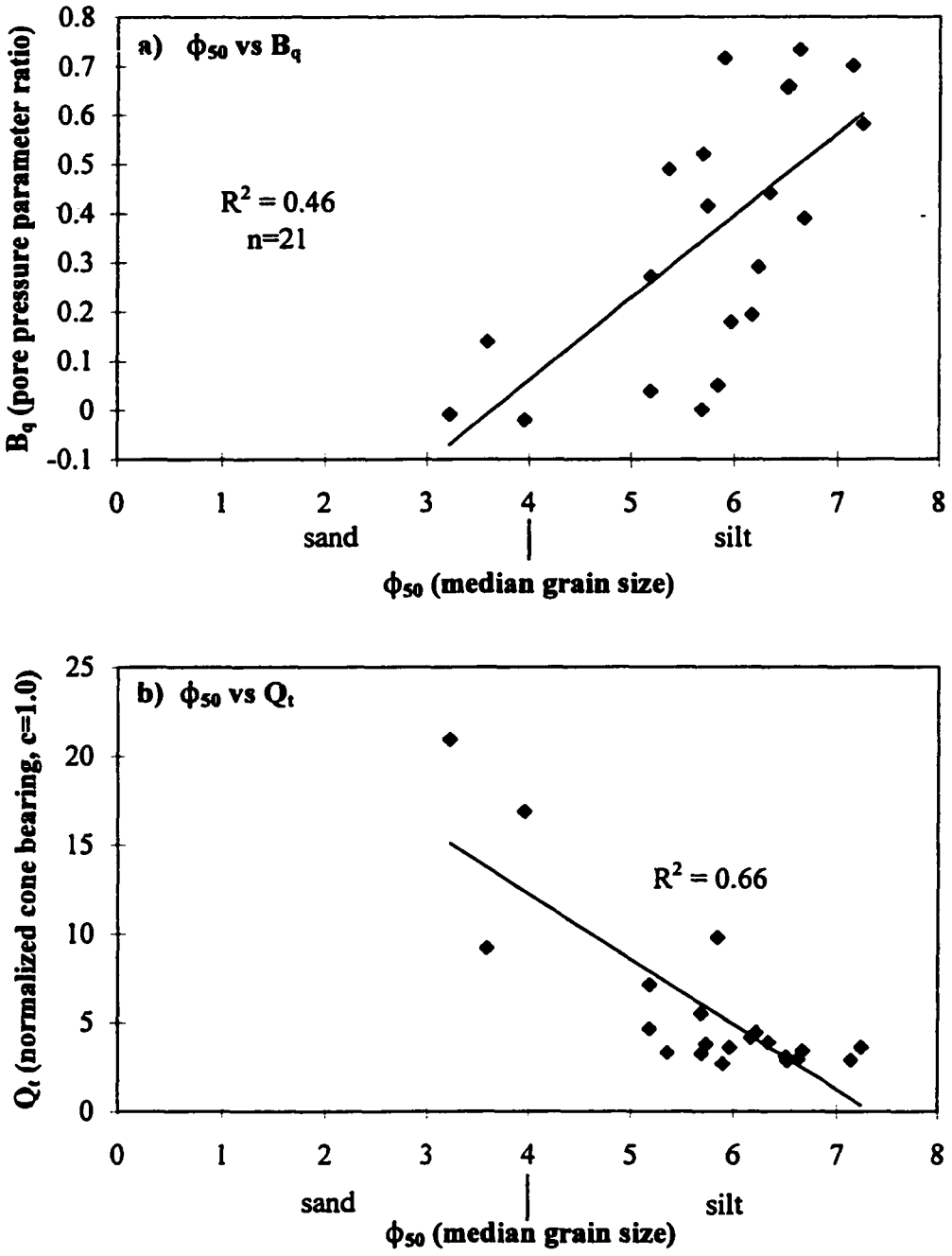

Figure 5-26. ϕ_{50} to CPT parameters, through coarsening upward sequence in laminated silts of upper foreset between 23.4 and 24.4m in borehole FD92-11; a) ϕ_{50} vs B_q ; b) ϕ_{50} vs Q_t.

5-26a). The correlation of ϕ_{50} with Q_t is good (R^2= 0.68; n=21; Figure 5-26b), although this correlation is primarily driven by the sand bed at the top of the sequence and the correlation of ϕ_{50} with Q_t in the silt samples is poor (R^2= 0.18; n=18).

In borehole FD94-4, samples were analyzed across one a series of half metre to metre-scale sharply bounded coarsening upward sequences (Figure 5-27a). The sequence in the sampled interval is defined by the presence of clayey silt at the base, where it abruptly overlies sandy silt of the preceding sequence, and sandy silt at the top, where it is abruptly overlain by clayey silt of the following sequence. A series of half metre to metre-scale sequences marked by upward decreasing pore pressures occur on the adjacent CPT, and in some cases pore pressure minima are associated with small cone bearing peaks. However, this is a SCPT, in which shear wave velocities were recorded every metre at rod breaks (Chapter 3). The time taken to record shear wave velocity (2 and 4 minutes) was sufficient for dU to dissipate from greater 50 to less than 10 m in this facies, so that pore pressure minima occur immediately below rod breaks. Following rod breaks, pore pressures increased rapidly, and stabilized after pore pressures in equilibrium with the sediment had been reestablished. Within the sampled interval a rod break occurred at 41.15, where B_q dissipated from 0.35 to less than 0.06. The pore pressure is interpreted to have recovered by a depth of 41.70 m. However, metre-scale pore pressure variations independent of rod breaks can also be recognized on the SCPT on the basis of sharp downward decreases in pore pressure that do not coincide with rod breaks: B_q decreases from 0.60 to 0.32 between 41.05 and 41.10 m, and from 0.57 to 0.26 between 42.00 and 42.05 m. These changes indicate sharp downward changes from finer to coarser silt (see soil classification chart; Figure 3-3; Robertson, 1990), and correlate with the boundaries of the coarsening upward sequence in the sampled interval.

Corrected pore pressure were estimated between 40 and 45 metres depth based on the amount of the pore pressure dissipation during rod breaks, a linear pore pressure recovery[11],

---

[11] Nearly linear pore pressure recoveries occur in the bioturbated silts of the lower foreset in

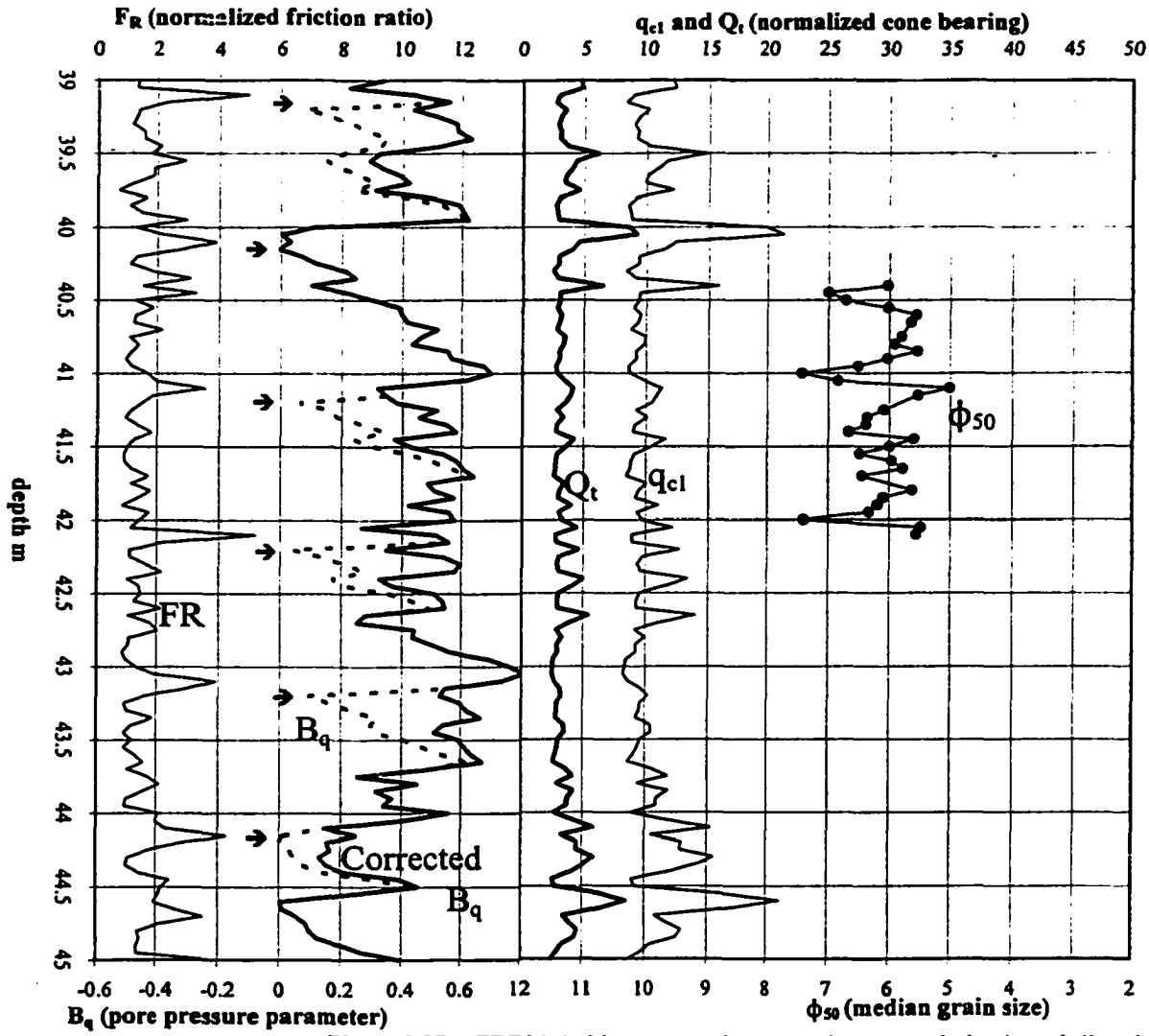

Figure 5-27a. FDF94-4. Note coarsening upward sequence in laminated silts of upper foreset (41.05 and 42.0m), reflected by upward decreasing corrected B_q →First reading below a rod break; note that F_R peak due to rod break occurs 10 cm higher than B_q minimum.

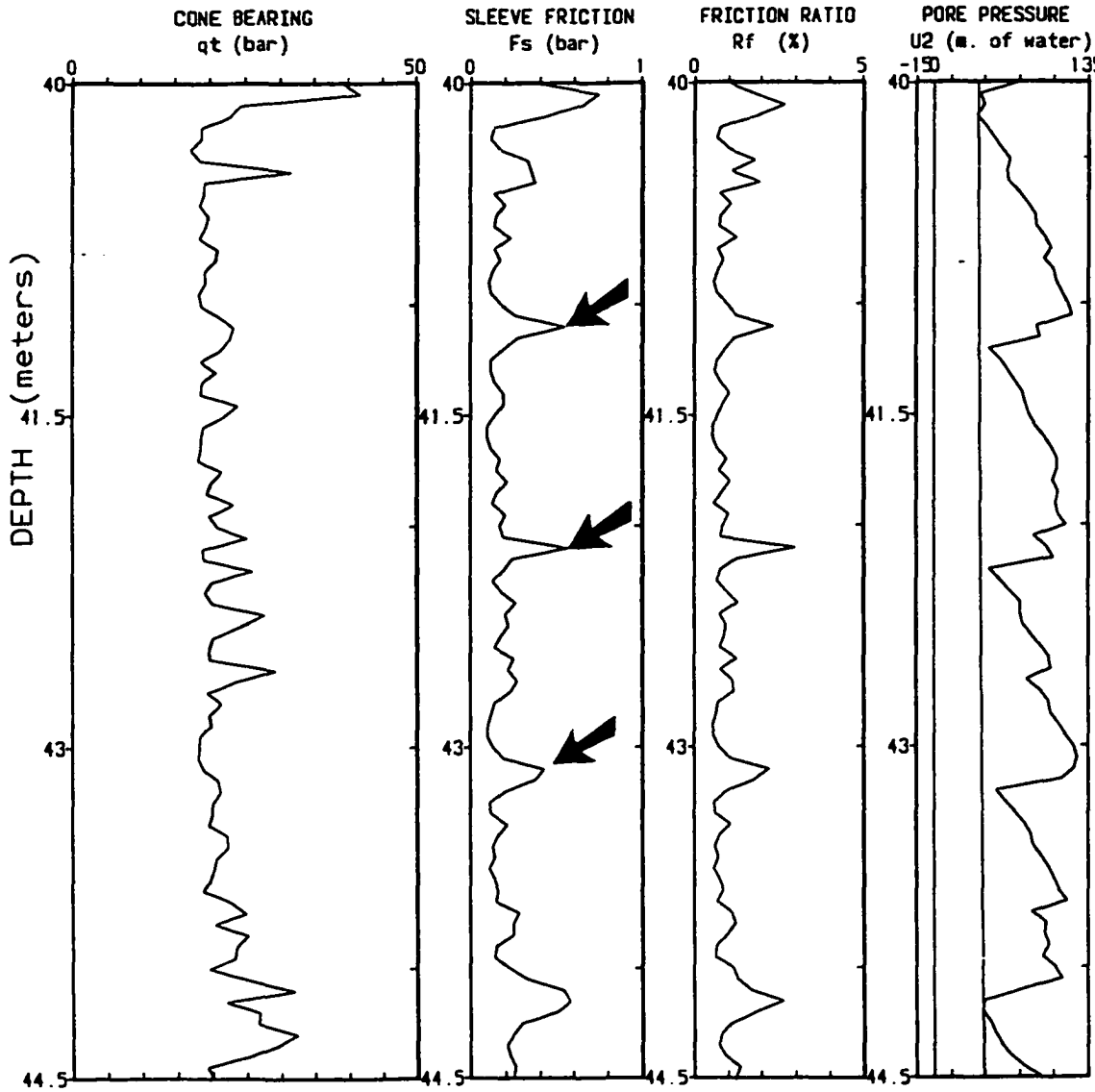

Figure 5-27b. FD94-4; non-normalized CPT data through coarsening upward sequences in laminated silts of upper foreset. Same interval as shown in Figure 5-27a, showing grain size data through analyzed interval between 40.4 and 42.1 m. Note sleeve friction and friction ratio peaks 1 metre apart due to rod breaks (arrows). The pore pressure minima associated with rod breaks are 2 readings (10 cm) below the friction ratio peaks, because the centre of the friction sleeve, where sleeve friction values are assigned, is 10 cm above the cone tip.

and the estimated point of pore pressure recovery on the CPT, although this latter point is subjective. The corrected pore pressures in this interval in FD94-4 define a series of sharply bounded sequences with upward decreasing pore pressures consistent with upward coarsening sequences observed in core (Figure 5-27a).

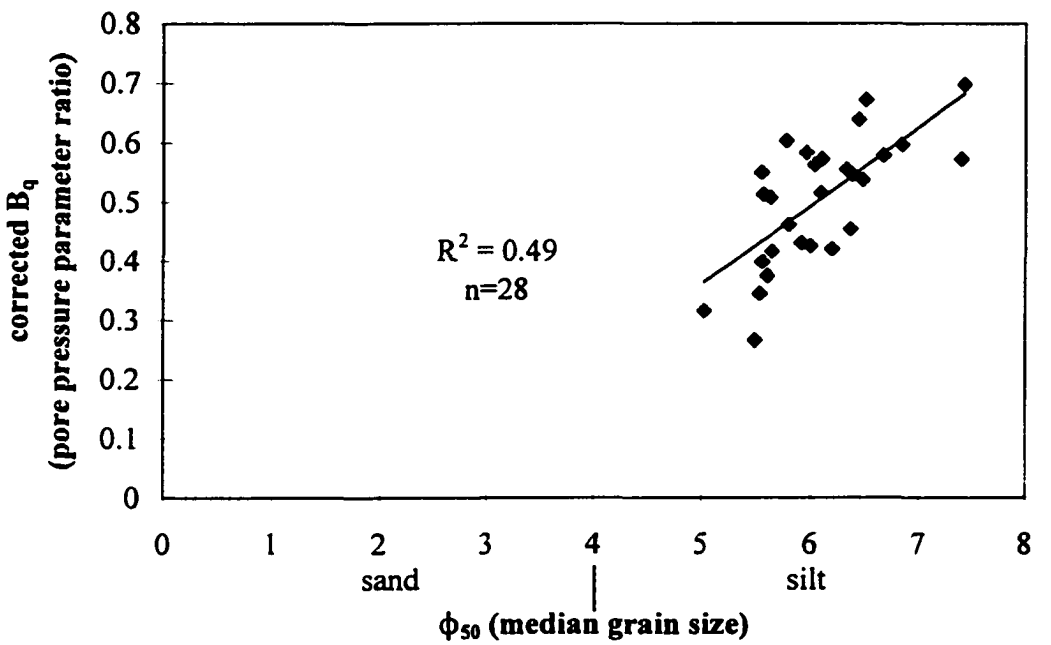

Figure 5-28. ϕ_{50} vs corrected B_q through coarsening upward sequence in laminated silts of upper foreset between 41.6 and 42.1m in borehole FD94-4.

Within the sampled interval, ϕ_{50} correlates in a general way with the corrected B_q. Some of the secondary grain size maxima in the coarsening upward sequence are reflected in the pore pressure curves. The correlation is poor above 40.6 metres, where B_q and dU are low and are interpreted to be within the interval of pore pressure recovery below a sand bed at 40 m (see section below on resolution of thin beds). Excluding the points above 40.6 m, ϕ_{50} correlates moderately with corrected B_q (R^2= 0.49; n=28; Figure 5-28). Q_t varies between

---

the CPT adjacent to FD92-11, where little stratification is present to obscure pore pressure recovery patterns.

3 and 4 in the sampled interval. Grain size peaks generally correlate with minor cone bearing peaks.

These observations show that B_q correlates in a general way with ϕ_{50} in the silt range, and coarsening upward sequences are reflected on adjacent CPTs by sharply bounded pore pressure decreasing upward sequences. However, pore pressure dissipation during rod breaks, particularly in a SCPT, can also generate metre-scale sharply bounded pore pressure decreasing upward sequences that can mimic and mask the pore pressures generated by coarsening upward sequences.

Resolution of thin beds

Cone bearing appears to be fully resolved in very fine sand interbeds in silt as thin as 10 cm. For example, in the sampled interval in FD92-11 described above (Figure 5-25), the very fine sand bed at the top of the sampled interval is 13 cm thick and the peak q_{c1} is comparable to that in other sands of similar grain size (q_{c1}=34; ϕ_{50}=3.2; compare with Figure 5-7). Sand beds as thin as 5 cm are represented by cone bearing peaks in which q_{c1} values are less than in other sands of comparable grain size (Figure 5-2a). Examples are the very fine sand bed at the base of the sampled interval in FD92-11 (Figure 5-25), and a fine sand bed in the topset silt and sand interval in FD93-2 (Figures 5-5 and 6-20), which are both 5 cm thick.

Resolution of thin sand beds appears to be different on the cone bearing and pore pressure curves. For example, the sand bed in the sampled interval in FD92-11 is approximately 13 cm thick (equivalent to 3 CPT readings), approximately the same thickness as the cone bearing peak (3 readings). However, the equivalent pore pressure minimum is 25 cm thick (5 CPT readings), and extends below the cone bearing peak. Pore pressure takes time to recover to equilibrium in silts after generating negative B_q in sand interbeds.

Cone bearing may not be resolved in thin sand interbeds in coarser sand. For example, in a 12 cm thick bed of fine sand occurring between two gravelly sand beds at the top of the

coarsening upward sequence in FD94-5 (Figure 5-13), cone bearing is higher than in sands with comparable grain size (ϕ_{50}=2.17, q_{c1}= 177; Figure 5-7).

Similarly, cone bearing in silt interbeds thinner than 15 cm in sand is higher than in silts of comparable grain size (Figures 5-2b and 5-22) and is not resolved. Examples are an 8 to 15 cm thick silt bed in the lower part of the topset sand (Figure 5-29a; ϕ_{50}=7.2, Q_t = 35); and a 5 cm thick medium silt between two coarse silt beds at the base of a coarsening upward sequence in the foreset (Figure 5-15; FD93-5; ϕ_{50}=5.6, Q_t=20).

Sharp contacts of sand and silt beds

Sharp contacts between the thick sand beds and underlying silt beds are generally resolved within 10 cm on the cone bearing curve over a fourfold decrease in cone bearing. An example is provided by the base of the topset sand in FD94-4, where fine to medium sands sharply overlie silt and very fine sand of the foreset (Figure 5-29). On the cone bearing curve the contact is resolved within 10 cm (q_t changes downward from 120 to 30 bars over 3 CPT readings).

Sharp sand to silt contacts are also evident on the pore pressure curve. They are marked by a downward decrease in dU, where fine to medium sands in which dU is near zero overlie coarse silts and/or fine sands (Figure 5-15); or by an increase in dU from negative or near zero to positive (Figure 5-29). However, the pore pressure change is commonly offset up to 20 cm downward relative to the cone bearing change. In the example in Figure 5-29, dU is negative 2 readings below the transitional cone bearing value between sand and silt.

Friction Ratio

ϕ_{50} and FC correlate in a general way with normalized friction ratio, F_R (R^2= 0.38 and 0.37 respectively; Figure 5-30). Several anomalously high values occur in the sand range, and

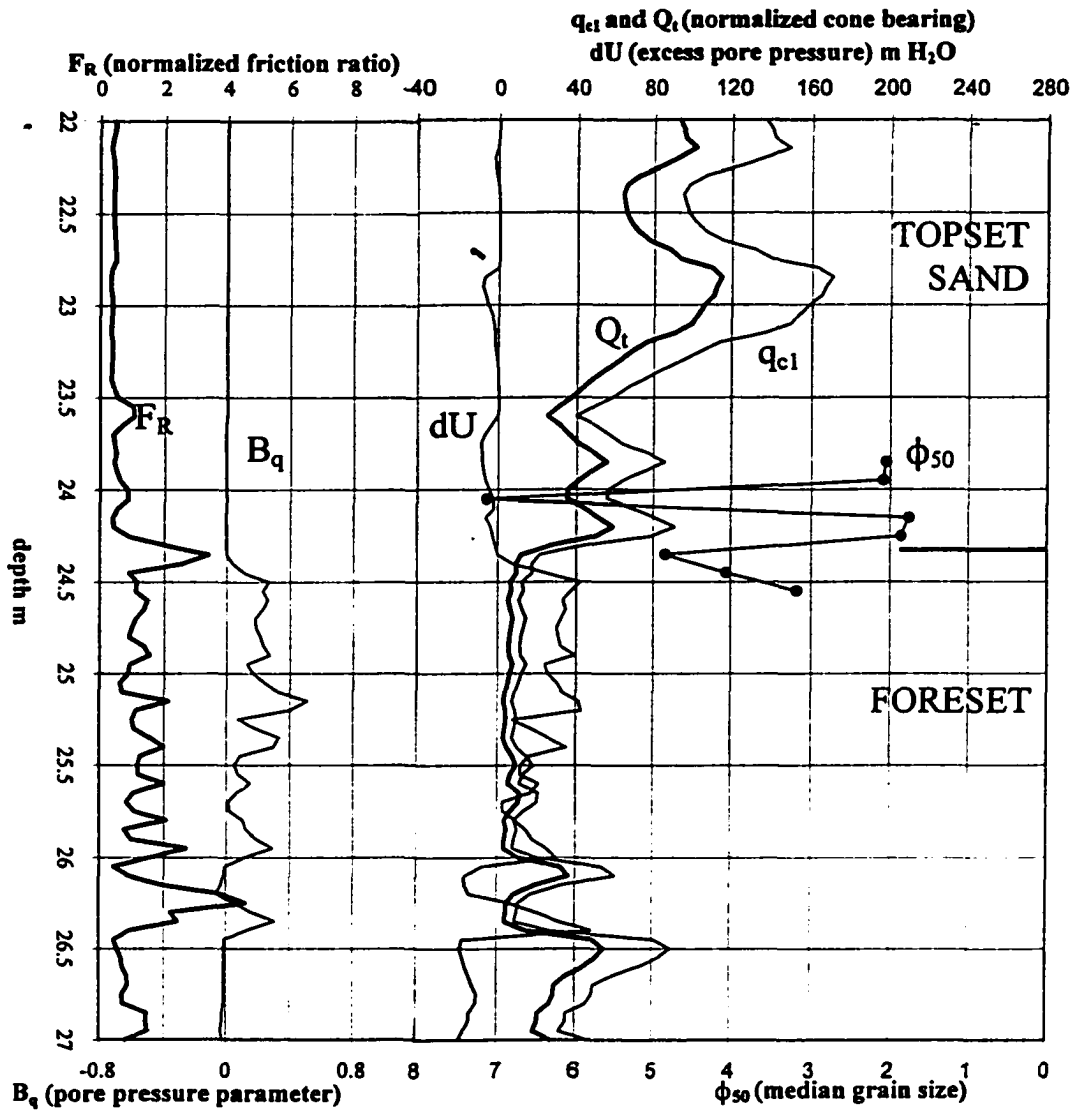

Figure 5-29a. FD94-4; grain size and CPT data across the lower part of the topset sand and the upper part of the foreset. Note F_R peak at base of sand.

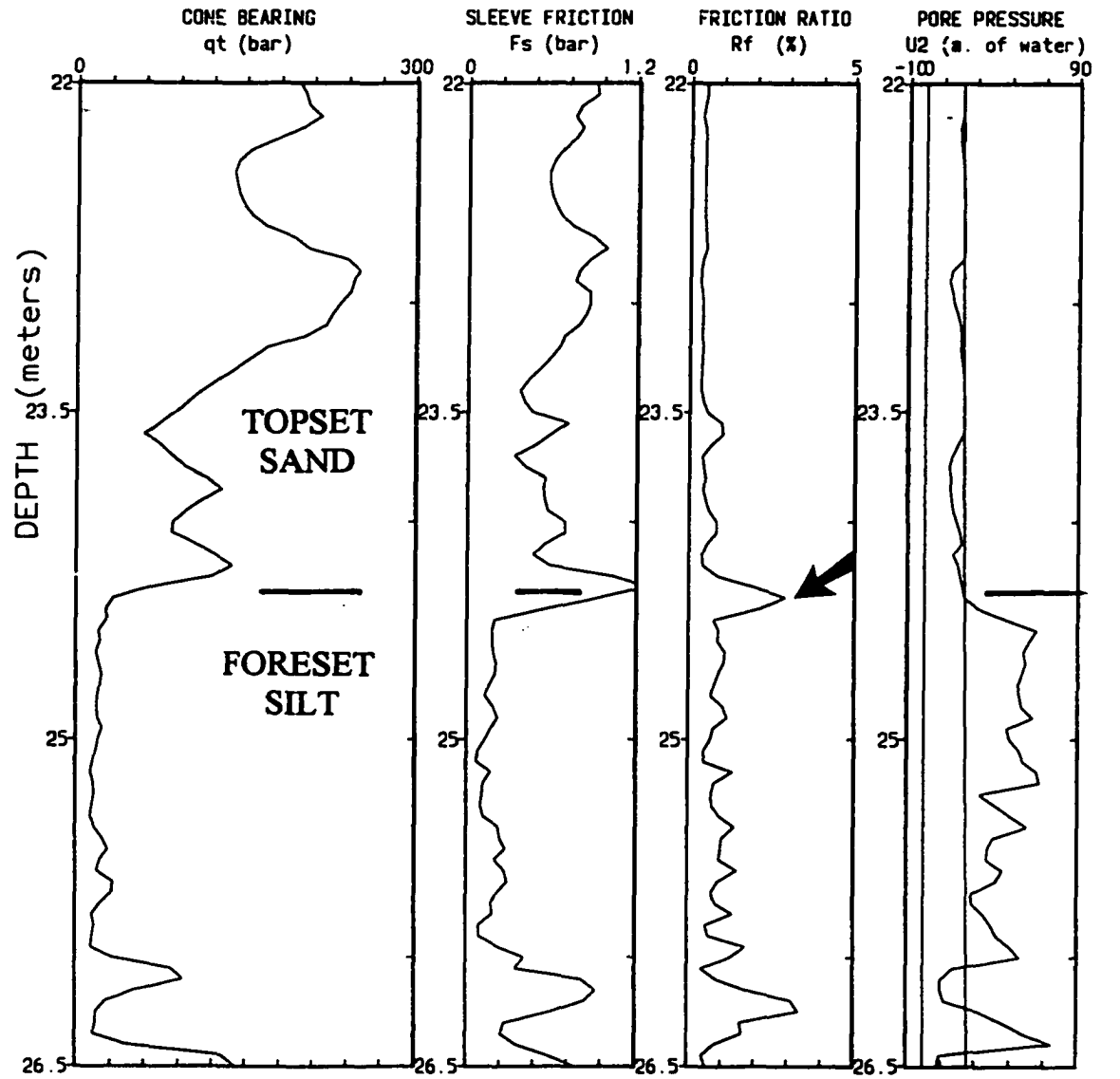

Figure 5-29b. FD94-4; non-normalized CPT data across contact of the topset sand with underlying foreset silt. Same interval as Figure 5-29a. Note the friction ratio peak immediately below the topset sand. This peak is associated with sleeve friction higher than in the overlying sand and low B_q (recorded pore pressure is close to hydrostatic pressure), and is interpreted to result from undrained penetration in the uppermost foreset silts.

these are all from one CPT (Figure 5-2a and b). As described in Chapters 3 and 4, sleeve friction measurements are less repeatable than cone bearing.

Two general trends can be observed on the ϕ_{50} to F_R plot (Figure 5-30a). In the sand range, F_R values are generally low. In the silt range, a broad range of values for F_R occurs and F_R correlates poorly with grain size.

High F_R values commonly occur in silts interbedded with sand. This is well illustrated by the samples from FD92-11, where F_R values are much higher and more variable in silts interbedded and interlaminated with sands in the upper foreset (14.55 and 54.6 m; F_R = 1 to 6) than in the bioturbated silts of the lower foreset, which generally lack sand interbeds (54.6 and 99.6 m; F_R = 1 to 3; Figure 5-8, 5-31). The F_R peaks occur immediately above and below sand beds (Figures 5-25). Similarly, a pronounced friction ratio peak commonly occurs immediately below the base of the topset sand where it overlies silts with positive B_q and dU (Figure 5-29).

The friction ratio peaks at sand bed boundaries appear to be controlled primarily by two factors: the geometry of the cone penetrometer and drainage conditions during cone penetration. Because the friction sleeve is 13 cm long, a thin sand bed represented by a single cone bearing reading would be in contact with and exert friction on the friction sleeve for 2 or 3 readings (at 5 cm intervals). Sleeve friction is generally higher in sands than silts (although the reverse is true of friction ratio), so that the interval of higher sleeve friction generated by the sand is thicker than the interval of higher cone bearing, and friction ratio peaks occur above and below sand beds (Figure 5-25a). In silt and clay, sleeve friction is higher when cone penetration occurs under drained than under undrained conditions, and because cone bearing is less affected by drainage conditions, friction ratio is also greater (Campanella et al., 1983). The friction ratio peaks below the base of the topset sand are

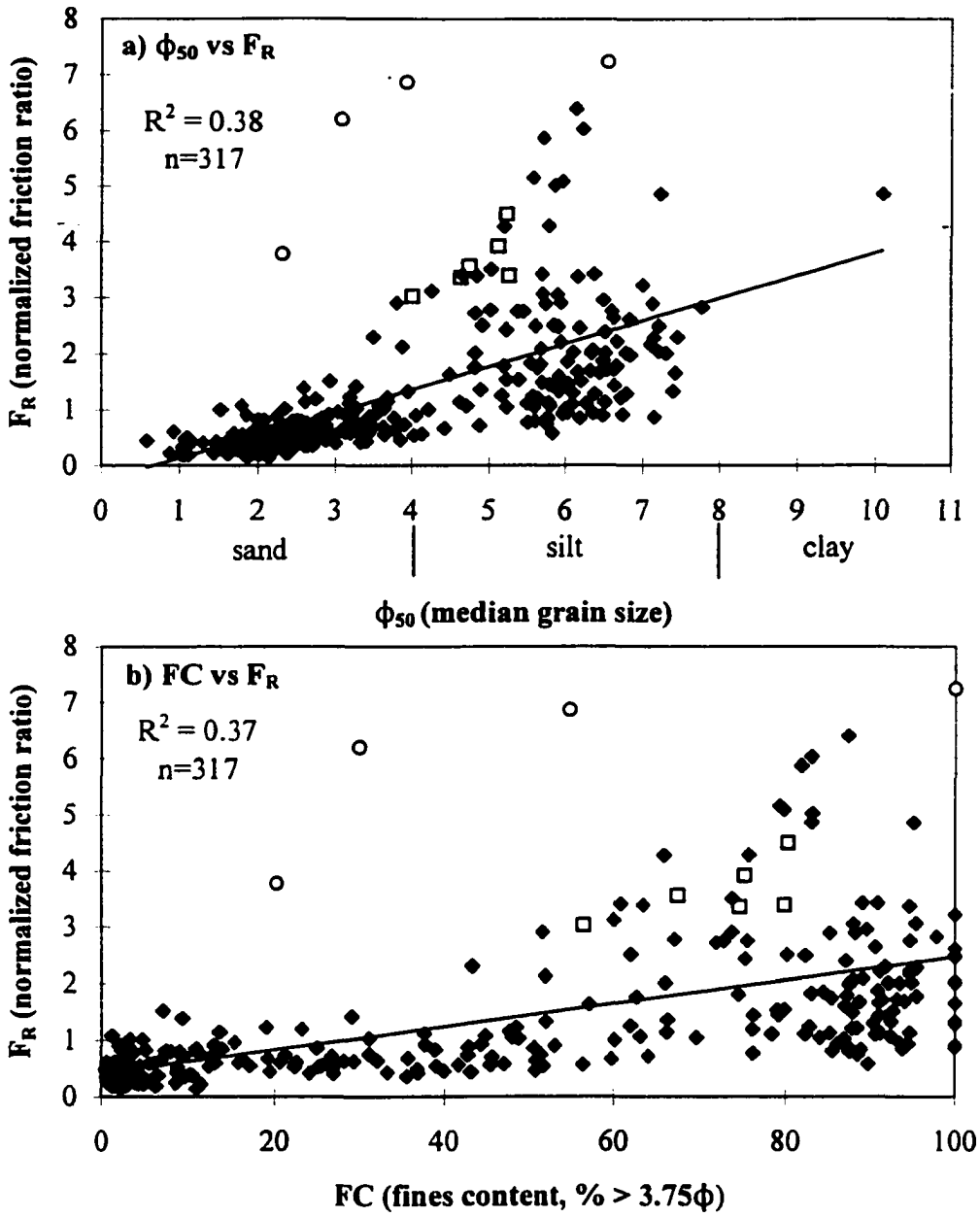

o topset interbedded sand and silt from FD93-3; anomalously high F_R

□ disturbed silt in FD94-4

Figure 5-30. Grain size vs F_R; a) ϕ_{50} vs F_R and b) FC vs F_R.

associated with sleeve friction *higher* than in the overlying sand[12] and with negative or low positive B_q (<0.15; Figure 5-29b). Consequently, they are interpreted to be a result of drained cone penetration in the uppermost silt of the foreset. Similarly, in intervals of pore pressure recovery below thin sand interbeds in silt, penetration may occur under drained conditions, contributing to friction ratio peaks there (Figure 5-25a). Drained penetration in silts below sand beds may be due to dissipation of excess pore pressure into the overlying sand. [13]

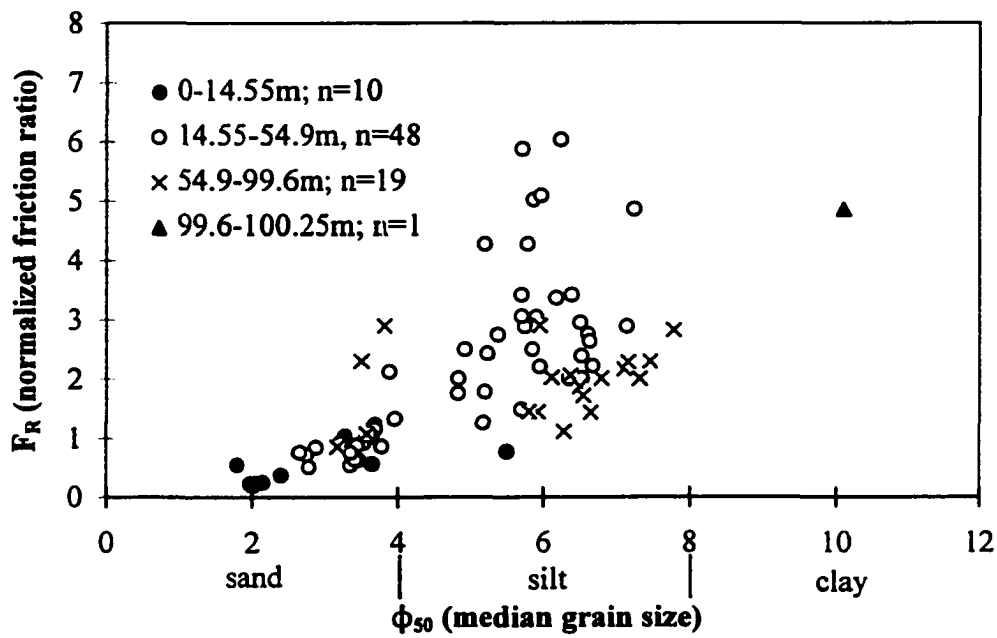

Figure 5-31. ϕ_{50} vs F_R in borehole FD92-11. Note that in silts F_R is more variable and includes higher values in the interval of interbedded silts and sands between 14.55 and 54.9 (upper foreset) than in the interval of bioturbated silts in between 54.9 and 99.6 (lower foreset). See Figure 5-8 for stratigraphy at this site.

12

Because of length of the friction sleeve, the shallowest elevated sleeve friction value occurs in the lowest reading in sand.

13

The lack of resolution in cone bearing data may also contribute to the friction ratio peaks above and below sand beds. However, where fiction ratio peaks occur at the tops of sand beds, cone bearing is in the silt range, indicating that this effect is less important than cone geometry in interbedded sand and silt (Figures 5-25b 24.2 m and 5-27b, 40.4 m).

In silts, friction ratio peaks associated with elevated sleeve friction values also occur at rod breaks in SCPTs (Figure 5-27b). Excess pore pressures dissipate at rod breaks in SCPTs, so that cone penetration is commonly resumed under drained conditions. Friction ratio peaks associated with rod breaks occur 10 cm above than the corresponding pore pressure minima because the centre of the friction sleeve, where sleeve friction values are assigned, is 10 cm above the cone tip.

Overconsolidated silts

Overconsolidated silts have been identified in two settings. The first is in a distinct interval of disturbed silts in the foreset, which is generally massive but locally includes large clasts and reoriented decimetre-scale blocks of laminated silt and sand (Figure 6-59; Monahan et al., 1997). Within this interval, ϕ_{50} correlates well with cone bearing, and cone bearing and friction ratio are generally higher than in other silts of with an equivalent grain size (Q_t=10 to 30; F_R = 2 to 4; Figures 5-2b, 5-22, 5-30 and 5-32). Excess pore pressures are anomalously low (B_q = -0.04 to -0.07; dU = -20 to -30 m). The combination of high cone bearing and friction ratio and negative excess pore pressures indicates that these sediments are overconsolidated (Robertson, 1990).

Desiccated silts at the top of the topset are also overconsolidated, as indicated by the high cone bearing and friction ratio values (Q_t= 30-70; F_R = 2 to 2.5) and negative B_q (Figure 5-2b, 5-5, and 5-22b; Robertson, 1990). Silts in the interval between the desiccated surficial silts and the topset sand may also be slightly overconsolidated. As noted above, they have higher Q_t than normally consolidated deposits (Lunne et al., 1997), and have negative to low positive B_q (<0.15) indicative of drained penetration.

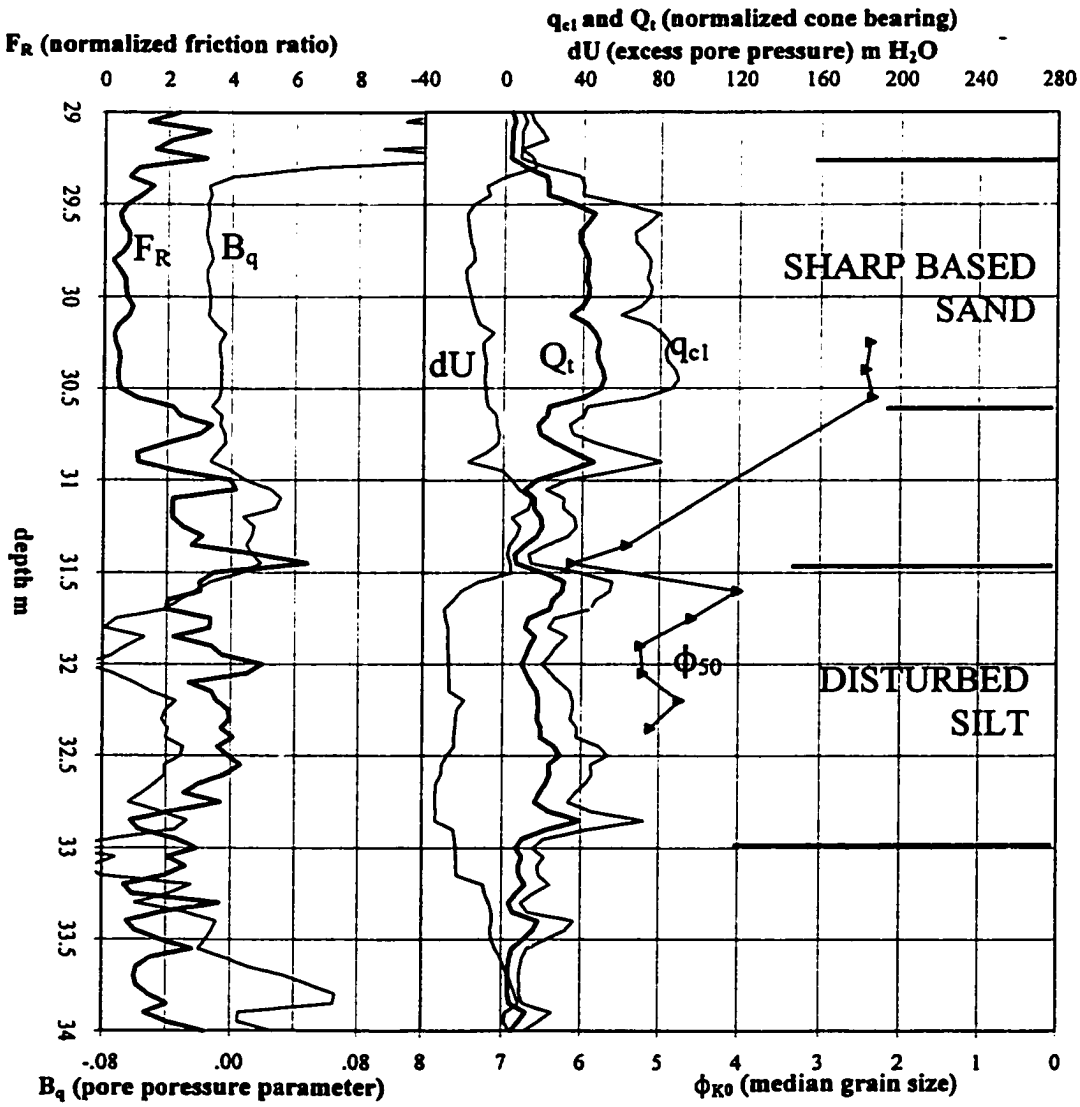

Figure 5-32. FD94-4; grain size and CPT data in sharp based sand unit and disturbed silt unit in upper part of foreset. Note high cone bearing, high friction ratio and strongly negative excess pore pressure in disturbed silt.

Soil behaviour type index, I_F

ϕ_{50} correlates well with I_F (R^2= 0.81; n=317; Figure 5-33a), which is dependent upon both Q and F_R (equations, 7 and 12, Chapter 3). The correlation of ϕ_{50} with I_F is comparable to that of ϕ_{50} with Q (R^2= 0.81; Figure 5-3), but significantly better than the correlation of ϕ_{50} with F_R (R^2= 0.38; Figure 5-30; z=10.7).

The boundaries of the Wentworth sediment classes can be computed from the linear correlation of ϕ_{50} and I_F, where:

$$I_F = 0.31\phi_{50} + 1.2 \pm 0.3$$ (Figure 5-33a).

The calculated I_F boundaries of the Wentworth sediment classes are comparable to those of the soil behaviour types of Robertson and Fear (1996) and Lunne et al. (1997; see Chapter 3) in the sand and coarse silt range, but diverge at the silt-clay boundary (Table 5-2).

FC also correlates well with I_F (R^2= 0.81; Figure 5-33b). Although scatter exists in these data, there is a linear relationship between FC and I_F, such that:

$$FC = 63\ (I_F - 1.74) \pm 20.$$

The general relationship of FC with I_F proposed by Robertson and Fear (1996) and Lunne et al. (1997; equation 8, Chapter 3) underpredicts FC for these samples. In general, most Fraser delta fines are low to medium plasticity silts (Christian et al., 1995; Dallimore et al., 1995, 1996).

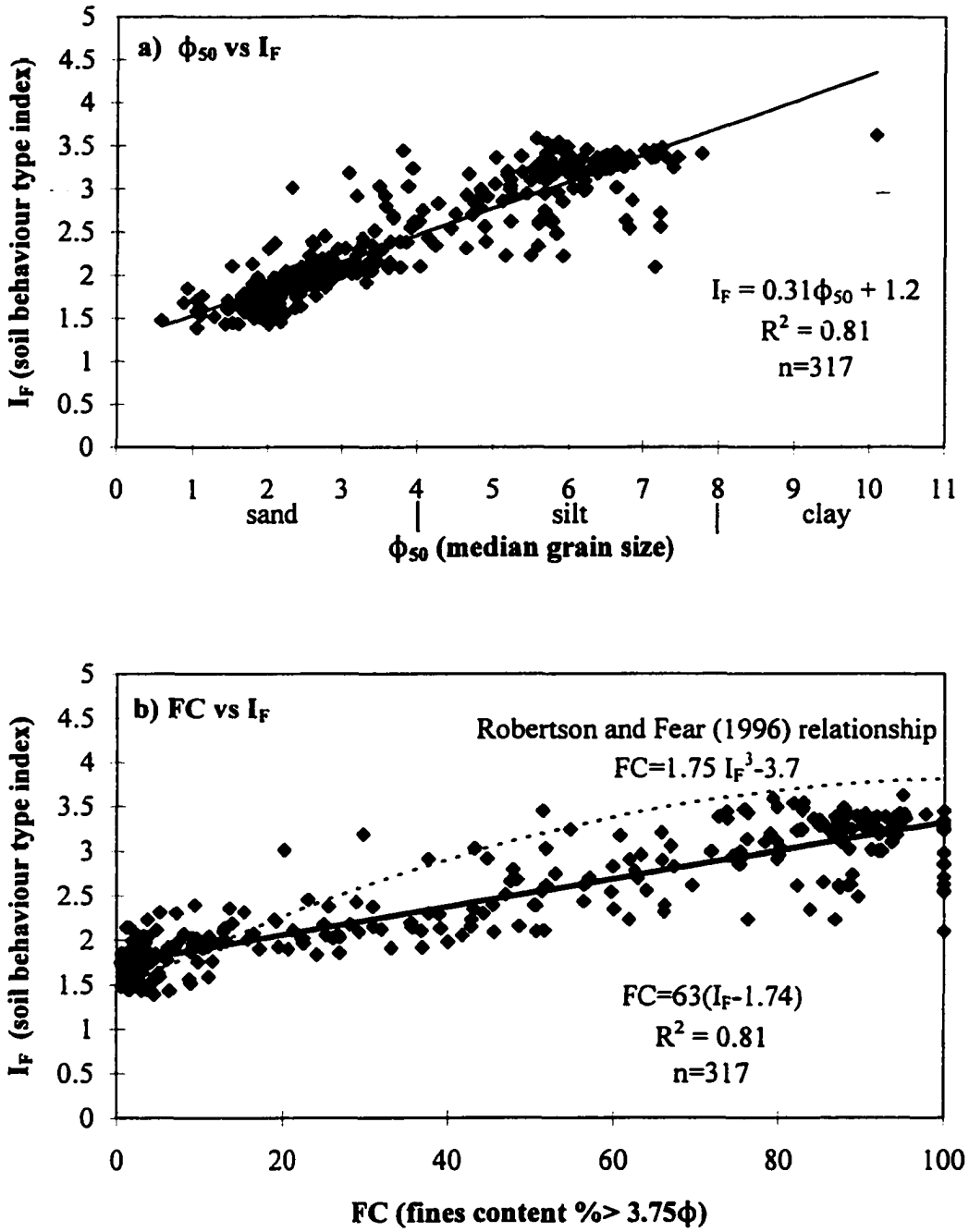

Figure 5-33. Grain size vs I_F; a) ϕ_{50} vs I_F; b) FC vs I_F. Note that the general FC to I_F relationship proposed by Robertson and Fear (1996; dashed line) underpredicts FC for these samples.

TABLE 5-2: I_F Boundaries of Wentworth (1922) sediment classes and Soil Behaviour Types (SBT, Robertson and Fear, 1996; Lunne et al., 1997)

Wentworth (1922) Sediment Class	I_F Range Fraser Delta samples	I_F Range SBT	Soil Behaviour Type –
		$I_F < 1.31$	gravelly sand
fine and medium sand $1<\phi_{50}<3$	$1.5 < I_F < 2.2$	$1.31 < I_F < 2.05$	sands: clean sand to silty sand
very fine sand $3<\phi_{50}<4$	$2.2 < I_F < 2.5$	$2.05 < I_F < 2.60$	sand mixtures: silty sand to sandy silt
silt $4<\phi_{50}<8$	$2.5 < I_F < 3.7$	$2.60 < I_F < 2.95$	silt mixtures: clayey silt to silty clay
clay $\phi_{50} > 8$	$I_F > 3.7$	$2.95 < I_F < 3.60$	clays
		$I_F > 3.60$	organic soils: peats

SUMMARY AND DISCUSSION

The results presented here demonstrate that grain size correlates with CPT measurements in the sediments of the Fraser River delta. Cone bearing is insensitive to grain size in sediments in medium and finer silt, increases gradually with grain size in the coarse silt range, and increases more sharply with grain size in the sand range. B_q is near zero in the medium sand range and becomes negative in the fine sands to medium silt range. B_q is generally positive in sediments finer than medium silt and correlates weakly with grain size where it exceeds 0.15. Friction ratio is higher in silts and clays than in sands. The control of grain size over CPT measurements described here is well known, and is reflected in the soil classification charts (Figure 3-3; Robertson, 1990).

Variations in cone bearing in sands are commonly interpreted as variations in density in industrial applications of CPT data. However, in the Fraser delta samples analyzed here, approximately 50% of the variation in cone bearing can be explained by variations in ϕ_{50}. The remaining 50% includes all other variables, including the effects of thin beds in which cone bearing values could not be fully resolved, real stratigraphic changes between the borehole and CPT, age and density. Thus a relatively low range of density variations appears to occur in these sands. Other grain size parameters also correlate with grain cone bearing: cone bearing increases with gravel content, and decreases with fines content, where greater than 10%. However, the correlation of ϕ_{50} with cone bearing is not simply a matter of sorting or fines content, because the same trend occurs in clean moderately well sorted sands as in all the sand samples taken together.

The correlation of grain size with cone bearing in sands has been implicitly recognized in other contexts. For example, Robertson et al. (1983) and Kulhawy and Mayne (1990) have shown that the ratio of cone bearing (q_c) to the standard penetration test blowcount (N) increases with increasing grain size, and their curves are shown superimposed on the ϕ_{50} to q_{c1} plot for sand samples of this study (Figure 5-34a). Although the q_c/N ratio does not increase with grain size as steeply as cone bearing, any increase in N with grain size would steepen grain size to cone bearing relationship implicit in their curves. Similarly, the cone bearing required for sand to resist liquefaction at a given level of seismic loading increases with grain size, at least for sands finer than $2\phi_{50}$ (Robertson and Campanella, 1985; Seed and deAlba, 1986; Shibata and Teparaska, 1988; Stark and Olson, 1995). Lines from the Robertson and Campanella, Seed and deAlba, and Stark and Olson relationships are shown superimposed on the ϕ_{50} to q_{c1} for sand samples of this study (Figure 5-34b). Significantly, the line generated by the points given in the Robertson and Campanella relationship is parallel to the grain size to cone bearing trendline developed here.

Consequently, cone bearing decreasing and increasing upward sequences in this setting

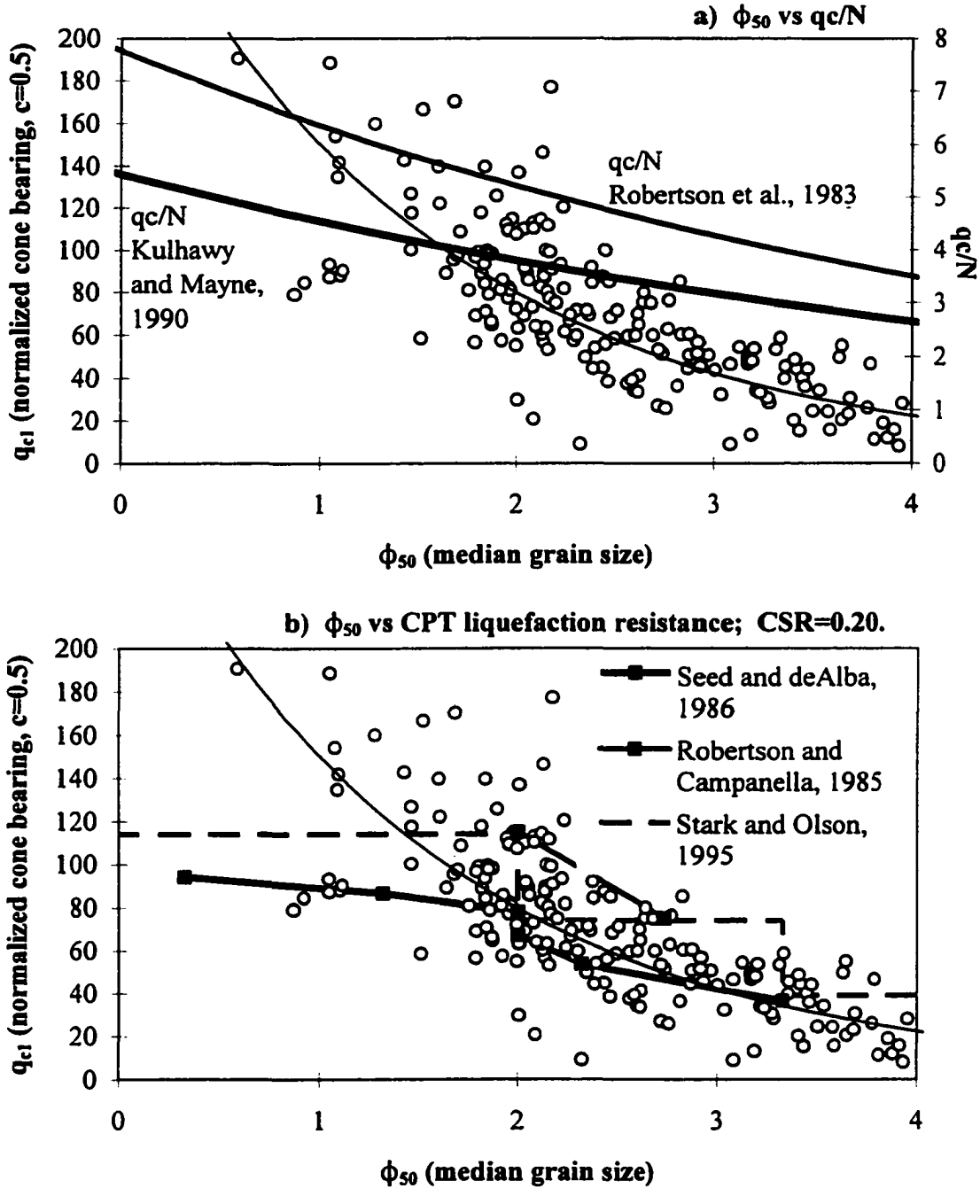

Figure 5-34. Published ϕ_{50} to cone bearing correlations superimposed on the ϕ_{50} vs q_{c1} plot for sands with exponential trendline from this study; a) ϕ_{50} vs q_c to SPT blowcount (qc/N) ratio; b) ϕ_{50} vs q_{c1} required to resist liquefaction at cyclic stress ratio (seismic loading)= 0.20.

commonly reflect fining and coarsening upward sequences respectively, particularly where the sequences include both sands and silts. Because cone bearing is relatively insensitive to grain size in the silt range, an abrupt start of a cone bearing increasing sequence above typical silt values may not represent the beginning of a coarsening sequence, but where a grain size threshold is exceeded within it.

However, cone bearing increasing sequences associated with decreasing dU represent increasing density and may not represent coarsening. Conversely, sequences in which both cone bearing and dU and B_q decrease represent sediment fining. In sands of the Fraser delta, dU is a better measure of negative excess pore pressures than B_q, because B_q can mask the effect of a pore pressure drop below hydrostatic in coarser sands where cone bearing is high. Negative dU is also associated with high cone bearing in gravelly and shell-rich sands.

The effects of ageing resemble those of increased density. Older sands in the topset sand unit have higher cone bearing and more negative dU than younger sands. These observations provide a means for identifying sand units of different ages in a sequence of stacked sand deposits of similar facies, such as sand units of different ages in the topset sand unit. The increase in cone bearing and other strength indicators in sediments with age is well known, and has been interpreted to result from grain rearrangement on a microscopic scale rather than cementation (Schmertmann, 1991). The effect of age on cone bearing in these sands will be examined further in Chapter 6.

In silts and clays, cone bearing generally correlate with factors other than grain size. In sediments finer than $5\phi_{50}$ and where undrained cone penetration occurs (i.e. B_q>0.15), Q_t ~ 2 - 5 across a range of grain sizes and is typical of normally consolidated sediments (Lunne et al., 1997). Higher cone bearing occurs in coarse and overconsolidated silts and is associated with negative or low positive B_q (<0.15). Overconsolidated silts include desiccated silts at the top of the topset, and the disturbed silts in the foreset.

In silts and clays, grain size correlates in a general way with B_q. Consequently, decimetre to metre-scale coarsening upward sequences in the laminated silts of the foreset are reflected by sharply bounded pore pressure decreasing upward sequences, in which B_q varies from >0.6 to negative. However, pore pressure dissipation during extended rod breaks, particularly in SCPTs, can also produce a series of sharply bounded pore pressure decreasing upward sequences that can mimic and mask the pore pressure response generated by coarsening upward sequences. Pore pressure minima due to rod breaks are exactly 1 m apart. Furthermore, pore pressures take a few readings to recover to equilibrium values below a sand bed, and intervals of pore pressure recovery also appear as pore pressure decreasing upward sequences. Consequently, sharp upward increases in pore pressure unrelated to rod breaks are the most diagnostic criteria for identifying coarsening upward sequences on the pore pressure curves.

Cone bearing is generally resolved in very fine sand beds as thin as 10 cm. Similarly, the sharp contacts at the bases of the topset sand and the sharp-based sands in the foreset can be resolved within 10 cm over a fourfold change in cone bearing.

Cone bearing measurements in the 15 cm^2 cone appear to be comparable to those from 10 cm^2 cones, because the ϕ_{50} to q_{c1} trends for sands are similar.

Normalization of cone bearing in sands of the Fraser delta using q_{c1} (cone stress exponent, c = 0.5) produces more consistent results than Q_t (c = 1.0). Although different normalization procedures generate similar results between depths of 5 to 15 m, using Q_t at greater depths overcorrects for effective overburden stress and can lead to the misidentification of sands as silts. Conversely, normalizing cone bearing in silts and clays of the Fraser delta using Q_t produces more consistent results than q_{c1}. In sediments finer than $5\phi_{50}$ and where cone penetration occurs under undrained conditions (B_q> 0.15), Q_t is nearly uniform over a 81 m depth range in these samples, whereas q_{c1} undercorrects for overburden stress. Q_t is probably more reliable for normalizing silts where B_q is less than 0.15 as well,

particularly those finer than $5\phi_{50}$, because changes in drainage conditions during cone penetration have a minor effect on cone bearing (Campanella et al., 1983) and the plot ϕ_{50} to cone bearing has a better correlation with Q_t than with q_{c1}. These results support the normalization method proposed by Robertson and Wride (1997, 1998) in which c = 0.5 in sands, 1.0 in most silts and 0.75 in some coarse silts. Furthermore, the soil behaviour type index, I_F, which is based on this method, correlates well with grain size.

Normally consolidated sands and silts require different cone stress exponents, because these sediment types respond differently to increasing effective overburden stress. The volume and density changes in sands due to overburden stresses in the shallow subsurface are minor (Atkins and McBride, 1992). In contrast, silts and clays compact and develop increased undrained shear strength with increasing overburden stress. Thus increasing overburden stress results in significant changes in physical properties in silts and clays, whereas in sands it does not, so that a greater correction for overburden stresses (i.e. higher cone stress exponent) should be applied to normalize silts and clays for soil classification purposes.

This discussion raises the issue of what needs to be determined by normalizing for effective overburden stress. Normalizing cone bearing for soil classification purposes should use different cone stress exponents for silts and sands. However, normalizing cone bearing in silts using a cone stress exponent of 1.0 removes the effects of real changes in physical properties. To determine the properties of a silt following removal of a load would probably require the use of a cone stress exponent of less than 1.0, because the changes in physical properties during consolidation are not reversible. Similarly, the cone stress exponent for overconsolidated fine grained sediments may be less than 1.0.

Although ϕ_{50} correlates in a general way with friction ratio, several other factors, both geological and operational, contribute to it. Friction ratio peaks occur at sand to silt contacts, so that friction ratios in silts interbedded and interlaminated with sand are more variable and include higher values than silts in which no sand interbeds occur, and friction ratio peaks

occur in silts immediately underlying the topset sand. The friction ratio peaks at sand bed boundaries are generated by the geometry of the cone penetrometer, and by undrained penetration in silts beneath the sands. Friction ratio peaks can also occur and at rod breaks in silts, particularly in SCPTs. Elevated friction ratios occur in overconsolidated sediments, such as the desiccated and disturbed silts. Furthermore, friction ratio values are the least repeatable of CPT measurements.

Because I_F is dependent upon the friction ratio, it may underestimate grain size in interbedded sands and silts. This will be discussed further in Chapter 6.

Finally, the example of FD94-6, where anomalously high cone bearing occurs and likely represents densification due to the vibrations from passing trains, demonstrates that anthropogenic alterations to the natural sediments do occur, and must be considered in any regional analysis of CPT data. Not only will grain size to CPT correlations differ from those of unaltered deposits, but data from such sites may not be representative of the surrounding area.

CHAPTER 6

FACIES OF THE MODERN FRASER RIVER DELTA

Sediments of the modern Fraser delta can be divided into topset, foreset, and bottomset deposits. The topset varies from 40 m thick at the head of the delta to a few metres on the outer margin of the tidal flats and subaqueous platform (Figures 2-5, 4-5, 6-1 to 6-6; Clague et al., 1983; Williams and Roberts, 1989; Monahan et al., 1993c, 1995, 1997). Topset deposits form a broadly fining upward sequence. The lower part consists of a massive sand facies that is generally 8 to 30 m thick and forms a distinctive stratigraphic marker. This sand is overlain gradationally by a thin interbedded sand and silt facies, that is in turn gradationally overlain by a laminated and organic silt facies in most of the upper delta plain. The silt facies is locally overlain by peat.

The topset sharply overlies foreset deposits, which are up to 165 m thick. Seaward dips, commonly up to 7°, can be recognized in foreset deposits on reflection seismic profiles and CPT correlations (Figures 6-4 to 6-6; Jol, 1988; Jol and Roberts, 1988, 1992; Pullan et al, 1989, 1998; Clague et al., 1991; Monahan et al., 1993c, 1995, 1997). The foreset is dominated by silt, complexly interlaminated and interbedded with sand on a variety of scales. Sand is most common in the upper parts of the foreset. In the southernmost part of the delta, sand-dominated intervals up to 30 m thick occur interbedded with thinner silt-dominated intervals and extend to depths as great as 130 m (Figure 2-6; Clague et al., 1991; Luternauer et al.,1991). Further to the north, highly localized sand-dominated intervals up to 30 m thick occur in the upper foreset (i.e. above ~60m; Figure 6-7; Monahan, 1993; Monahan et al., 1997; Luternauer et al., 1994; Clague et al., 1998).

Bottomset deposits have been penetrated in only a few deep boreholes and consist primarily of silt with some sand. They are up to 80 m thick and are distinguished from the overlying foreset deposits by slower sedimentation rates, estimated from multiple ^{14}C dates, and the

presence of thin sand interbeds (Figure 2-6; Luternauer et al., 1994; Clague et al., 1998; see also Luternauer et al., 1991; Dallimore et al.,1995, 1996). However, few boreholes and only one CPT reach depths greater than 100 m, so that the following discussions focus on the shallower parts of the foreset and the topset.

The sediments of the Fraser delta were deposited during a period of rising sea level during the Holocene. Sea level was 12 m below its current elevation 8000 ^{14}C years B.P. and rose to 2 m below its current elevation 4500 ^{14}C years B.P. Since then, the rate of sea level rise has slowed, and appears to have reached its present position by 2250 ^{14}C years B.P. (Williams and Roberts, 1989).

In this chapter, the facies of the Fraser delta are defined on the basis of both lithology and CPT data (summarized in Tables 6-1 and 6-2). CPT data provide estimates of gross lithology, sharp and gradational contacts, coarsening and fining upward sequences, and sediment dips. Grain size sequences are most confidently recognized from CPT data where they include both sand and silt and 80% of the variation in cone bearing can be explained by variation in grain size (Chapter 5). Although the facies of the topset are gradational, they form a distinct and repeatable facies sequence and so can be readily identified in both boreholes and CPTs. However, the much of the upper foreset consists of intergradational sandy and silty facies that are complexly interbedded. Consequently, CPT data are used provide a quantitative means to define facies on the foreset by providing estimates of the relative proportions of silt and sand and of the average grain size, in addition to the qualitative means defined above.

I_F and Q are used here to provide estimates of the proportions of silt and sand and of the average grain size of the foreset deposits. Based on the correlations shown in the preceding chapter, I_F is greater than 2.5 in silts and less in sands in the Fraser delta. Consequently the relative proportion of sand in a specific interval could be determined by the proportion with I_F less than 2.5. However, cone bearing in thin interbeds of sand and silt and are commonly

not resolved, so that using I_F underestimates relatively low proportions of both sand and silt. In order to better estimate the proportion of sand where thin sands beds occur in silt, a boundary of Q=6 (or Q_t=6)[1] is used to distinguish between sand and silt, for the following reasons.

1) Q_t is between 2.5 and 5 in most foreset silts, similar to normally consolidated silts globally (Lunne et al., 1997).

2) Q_t>6 in most sand peaks in the sampled and visually logged intervals, including thin beds that are not fully resolved (Figures 5-25a and 27a).

3) q_{c1} generally exceeds 20 in sands, so that for a unit weight of 19 kN/m^3 and water table at surface, non-normalized cone bearing (q_t or q_c) values equivalent to q_{c1}=20 are greater than Q_t=6 down to a depth of 66 m, the depth range of most CPTs used for this study[2].

Using these approaches, average sand contents for 2 m intervals were calculated continuously for each CPT depth point (2 m rolling average; Figure 6-8). A 2 m interval thickness was chosen because it is thicker than most coarsening upward sequences that occur in the foreset (described below). The proportion of sand in the thinly interbedded sands and silts is reasonably estimated using the Q>6 where less than 50%. However, where sand content exceeds 50%, or coarse or overconsolidated silts occur, using Q>6 overestimates sand content.

Average values Q, F_R, B_q and I_F were calculated to define each facies quantitatively and to provide estimates of average grain size (Table 6-2). However, I_F is greater than 2.5 in some sand-dominated facies, because I_F is dependent upon F_R, which is high where sands and silts are interbedded (Chapter 5). Consequently, I_F may underestimate average grain size, and Q

---

1 Where Q=6, Q=Q_t (equations 7 and 12 in Chapter 3).

2 For constant Q_t, non-normalized cone bearing (q_t or q_c) increases linearly with depth, whereas for constant q_{c1}, q_t increases with the square root of depth (equations 4 and 7, Chapter 3).

provides a better measure of average grain size, because it is less influenced by friction ratio measurements (Table 6-2)[3].

Two metre rolling averages were also computed for Q and F_R (Figure 6-43). Q varies between Q_t (c=1.0) in silt dominated intervals and q_{c1} (c=0.5) in sand-dominated ones. Intervals where calculated sand content is less than 50%, assuming Q>6, generally coincide with intervals where the average Q 2 m rolling average is less than 12. The rolling averages of Q, F_R, and the proportions of silt and sand were used with qualitative means to define facies boundaries in the foreset on CPT data.

FACIES OF THE TOPSET

ANTHROPOGENIC FILL

Most sites investigated for this study are capped by anthropogenic fill. On the upper delta plain, fills are generally less than 1 metre thick, although on the dykes and road embankments they are as thick as 3 m. These materials include gravel, sand, woody debris (locally known as hogfuel), silt, and mixtures of these materials. Clean sand fill is common and has high cone bearing (q_t>100 bars) and low friction ratio (R_f<1%). Hogfuel is characterized by q_t between 30 and 60 bars and friction ratio (R_f) greater than 3% (Figure 6-9; Gillespie, in Lunne et al., 1997).

On the tidal flats and subaqueous platform, fill used to build the artificial island and causeway at the Roberts Bank Port consists primarily of hydraulically emplaced sand capped by sand and gravel (Figures 6-3 and 6-6). These materials are up to 10 m thick. They

---

3

I_F is used to select the cone stress exponent (c) in the calculation of Q, but does not control the measurement of cone bearing .

include laminae of silt and organic debris and can resemble natural deposits. The fill thicknesses on these facilities were determined from the elevation of boreholes drilled prior to construction and by reference to bathymetric charts prepared in 1980, prior to the expansion of this facility. On the causeway, which was built prior to 1980, natural elevation was estimated by projection of the 1980 bathymetry across the causeway. Rip-rap composed of granitic boulders was placed long the margins of the island and causeway and was encountered in some boreholes

PEAT FACIES

Peat deposits up to 8 m thick occur at the surface on the eastern parts of the upper delta plain (Figure 2-2; Armstrong and Hicock, 1976a, b; Clague et al., 1983; Williams and Roberts, 1989). This facies generally consists of peat with little other material. However, peats up to 4 m thick on the eastern part of Lulu Island change laterally southward to interbedded peat and silt on the shore of Annacis Channel (Figure 6-10). The peat facies gradationally overlies the organic and laminated silt facies. The base of the peat facies is diachronous, and the maximum age is 5000 ^{14}C years (Clague et al., 1983; Williams and Roberts, 1983; Hutchinson, 1992; Hutchinson et al., 1995).

Peat is characterized on CPT data by higher friction ratios than any other sediment type observed in the delta: F_R generally exceeds 5, and R_f generally exceeds 4% (Figure 6-8). Cone bearing is generally low and uniform to slightly serrate: q_t is less than 10 bars, although higher cone bearing occurs locally at very shallow depths, where the peat includes woody debris and resembles hogfuel; Q and and Q_t are high because of the very shallow depth of burial. B_q varies from near zero to positive.

Figure 6-1. Caption on following page.

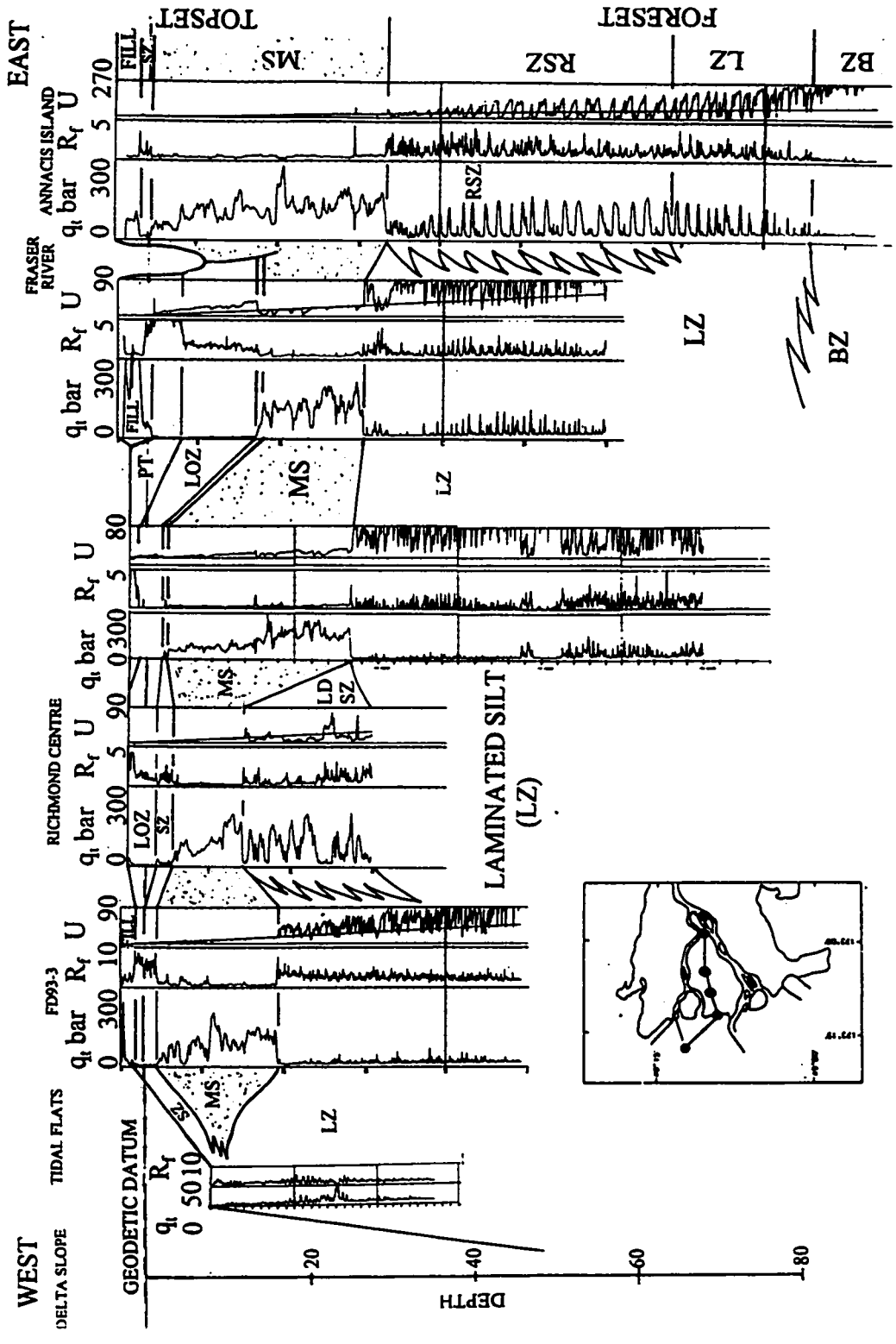

Figure 6-1. (see previous page) East-west CPT cross section across the Fraser delta, from Annacis Island to the western margin of the subaqeous platform. Note the continuity of the massive sand facies (MS; stippled) of the topset across the upper delta plain, but that it does not extend to the subaqeous platform. The low dipping interbedded sand and silt facies (LDSZ) laterally replaces the lower part of MS to the west in the central part of the upper delta plain. FD93-3 is on the dykes between the tidal flats and the upper delta plain. See also Figure 2-5. For facies symbols, see Table 6-1. R_f in % and U in metres of water.

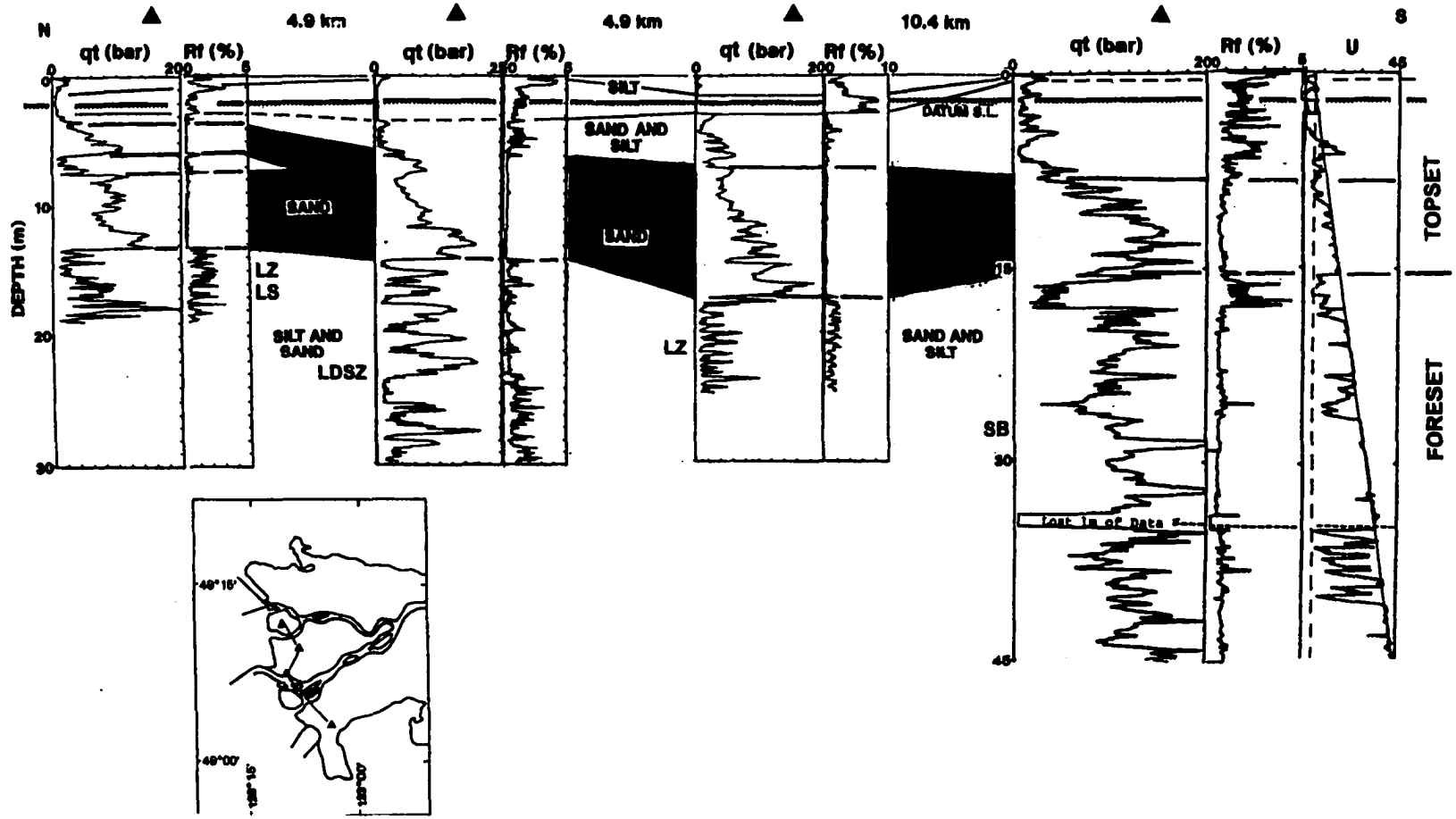

Figure 6-2. North-south CPT cross section along the western margin of the upper delta plain showing the continuity of the massive sand facies (MS; stippled). Figure modified from Monahan et al. (1993 a, b, c). For facies symbols, see Table 6-1. R_f in % and U in metres of water.

Figure 6-3. Caption on following page.

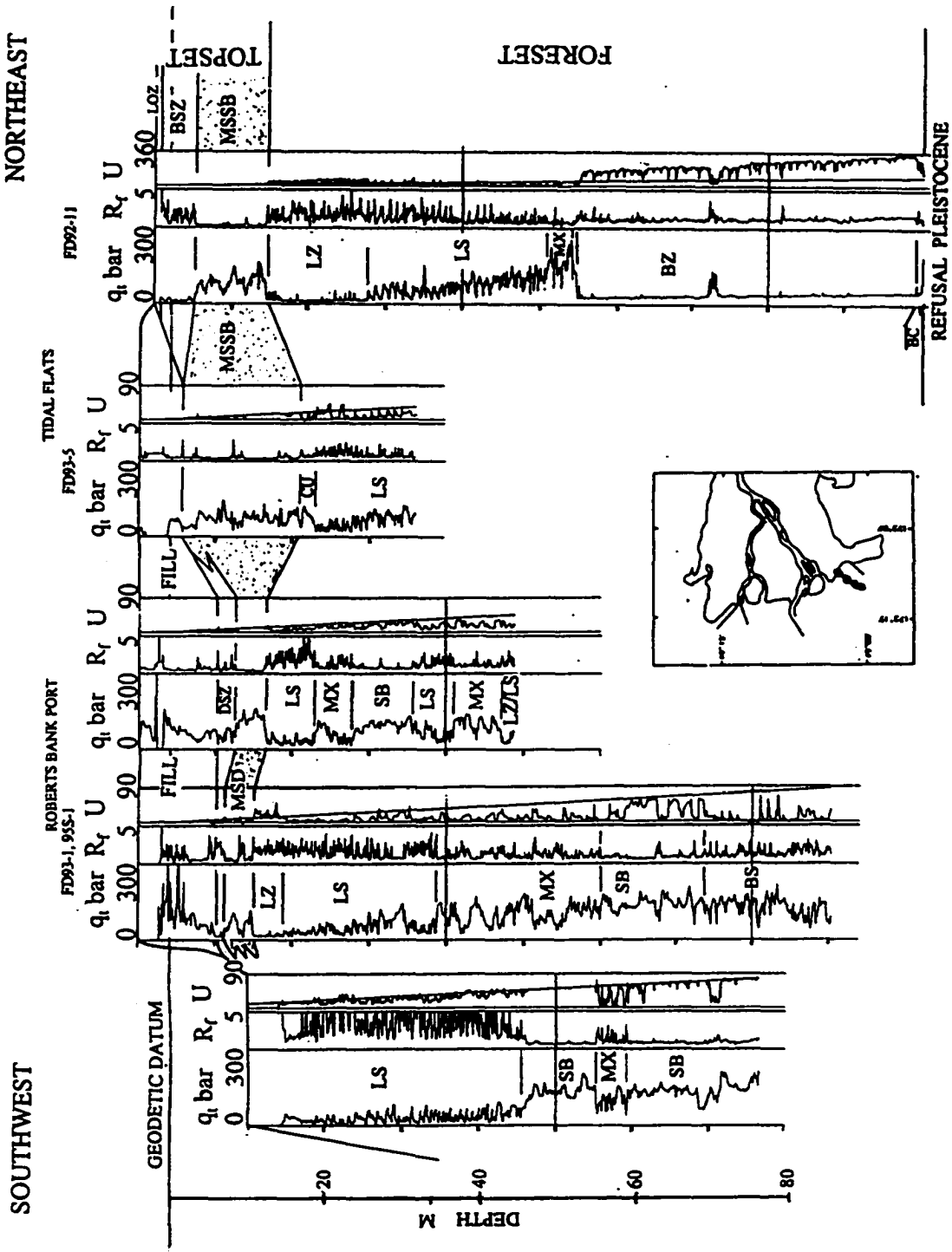

Figure 6-3 (see previous page). Northeast-southwest cross section along the causeway crossing the tidal flats to Roberts Bank Port. Note continuity of the massive sand facies of the topset crossing the tidal flats and that it thins at its distal margin (stippled; MSSB - shell bearing subfacies and MSD - distal subfacies). Facies are identified in each borehole in the foreset, but they cannot be correlated between CPTs because of the high dips (See Figure 6-6). For facies symbols, see Table 6-1. R_f in % and U in metres of water.

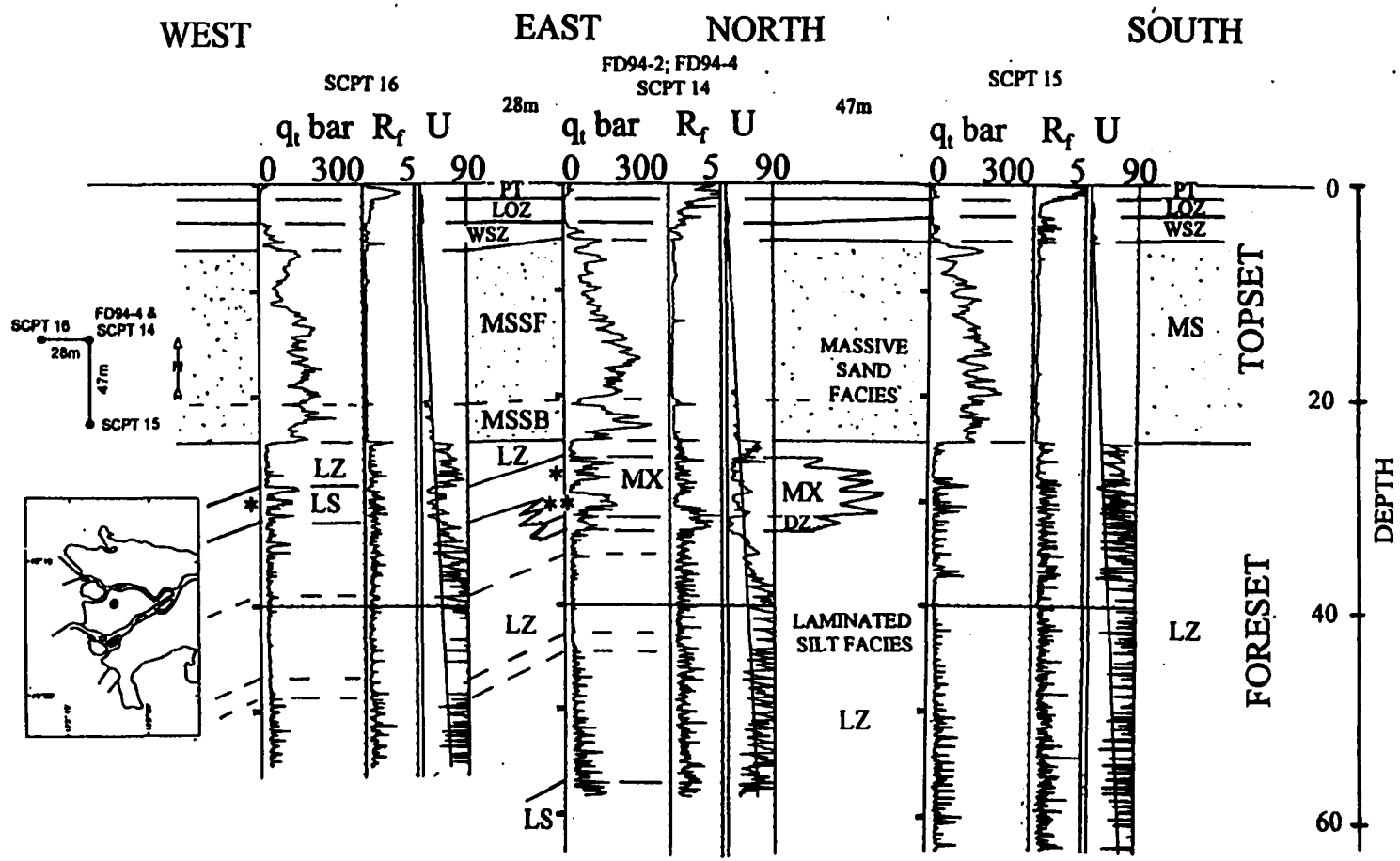

Figure 6-4. CPT cross section through FD94-4; section includes a dip component, oriented east-west, and a strike component, oriented north-south. Note the dips (7°) in the laminated silt facies foreset. Note that the mixed sand facies (MX) in SCPT 14 includes coarsening upward sand sequences (*) and sharp based sands (**), and passes laterally into laminated sand facies (LS) in SCPT 16. The coarsening upward sequences can be correlated from the (MX) in SCPT 14 to LS in SCPT 16. The middle CPT si also shown in Figure 6-34. For facies symbols, see Table 6-1. R_f in % and U in metres of water. Figure modified from Monahan et al. (1997).

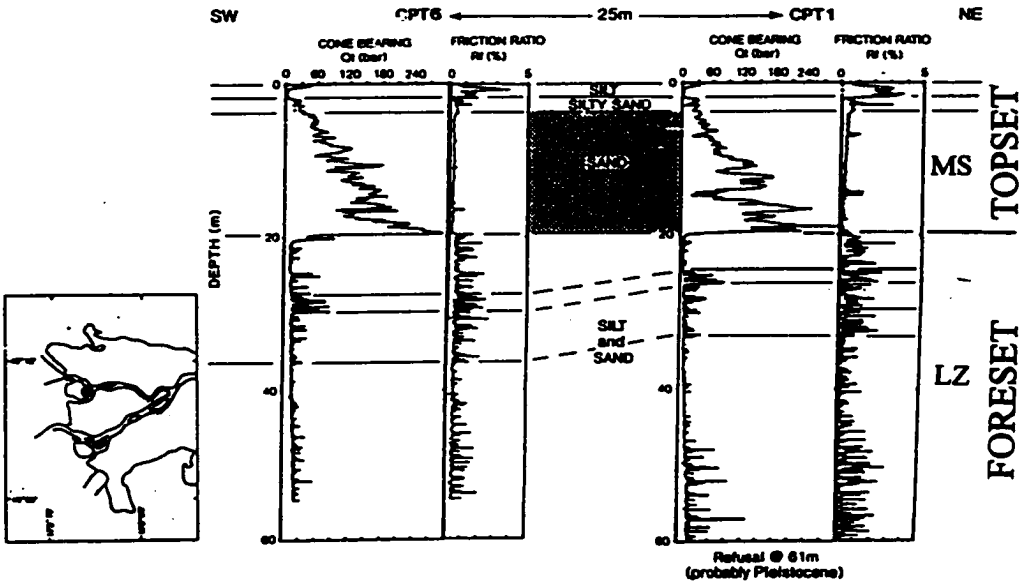

Figure 6-5. CPT cross section at a site on Sea Island, showing sharp base of massive sand facies of the topset (MS), apparent dips of 7° in the laminated silt facies (LZ) of the foreset. CPT data are not normalized (i.e. "Qt" in Figure is "q_t" as used in this dissertation). For facies symbols, see Table 6-1. CPT data from LeClair (1988), and Figure modified from Monahan et al. (1993c).

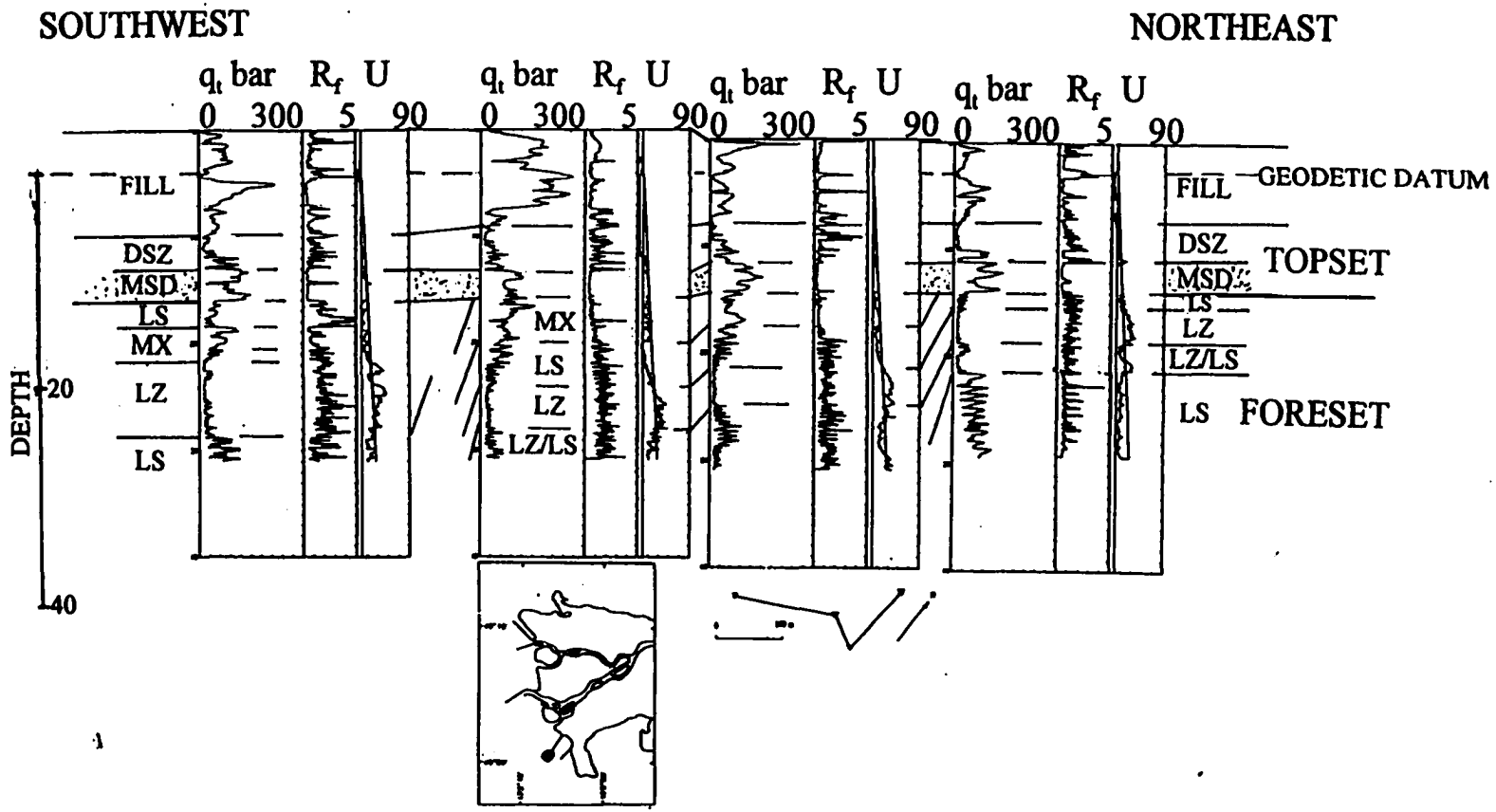

Figure 6-6a. CPT cross section at Roberts Bank Port, showing continuity of thin distal subfacies of the massive sand facies of the topset (MSD), truncating foreset strata. Note apparent dips of 3° in the foreset. For facies symbols, see Table 6-1. R_f in % and U in metres of water.

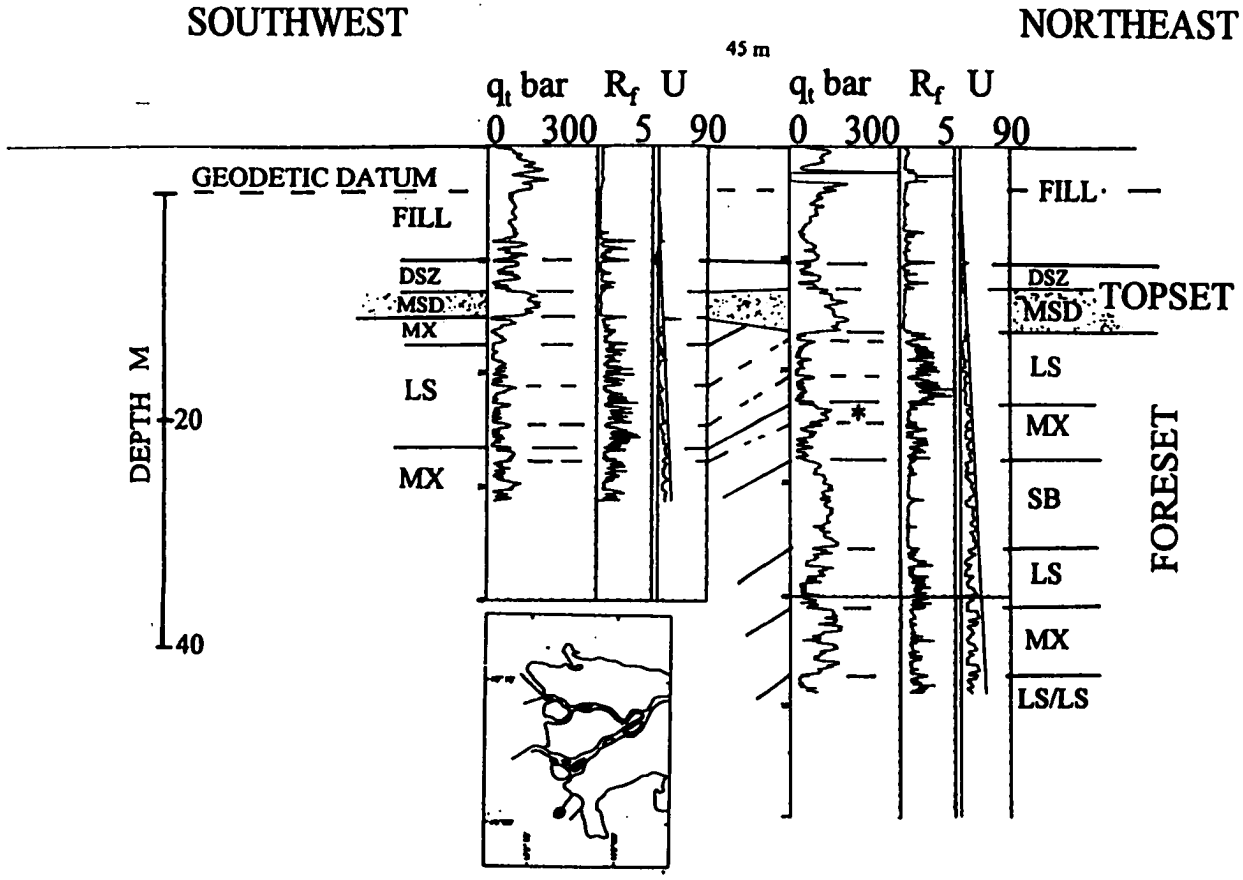

Figure 6-6b. CPT cross section at Roberts Bank Port, showing continuity of thin distal subfacies of the massive sand facies of the topset (MSD), truncating foreset strata. Note apparent dips of 5^0 in the foreset. Note sharp-based sand unit (*) in mixed sand facies of foreset. CPT on right is also shown in Figure 6-3. For facies symbols, see Table 6-1. R_f in % and U in metres of water.

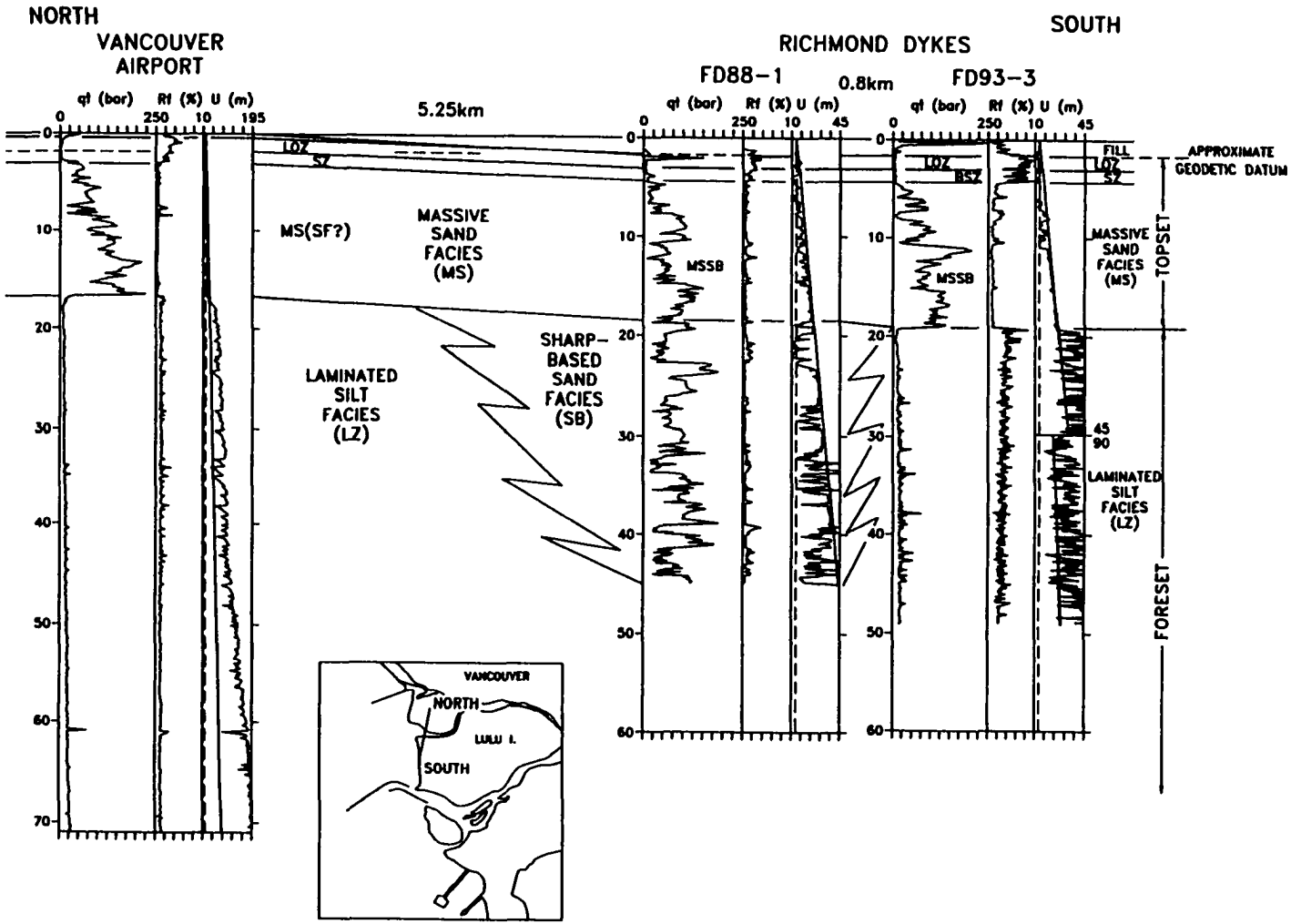

Figure 6-7. North-south CPT cross section on the western margin of the upper delta plain, showing localized occurrence of the sharp-based sand facies of the foreset. The sharp-based sands are replaced by the laminated silts typical of the upper foreset in this part of the delta within 0.8 km. The CPT at FD93-3 is also shown in Figures 2-5 and 6-1. For facies symbols, see Table 6-1. R_f in % and U in metres of water.

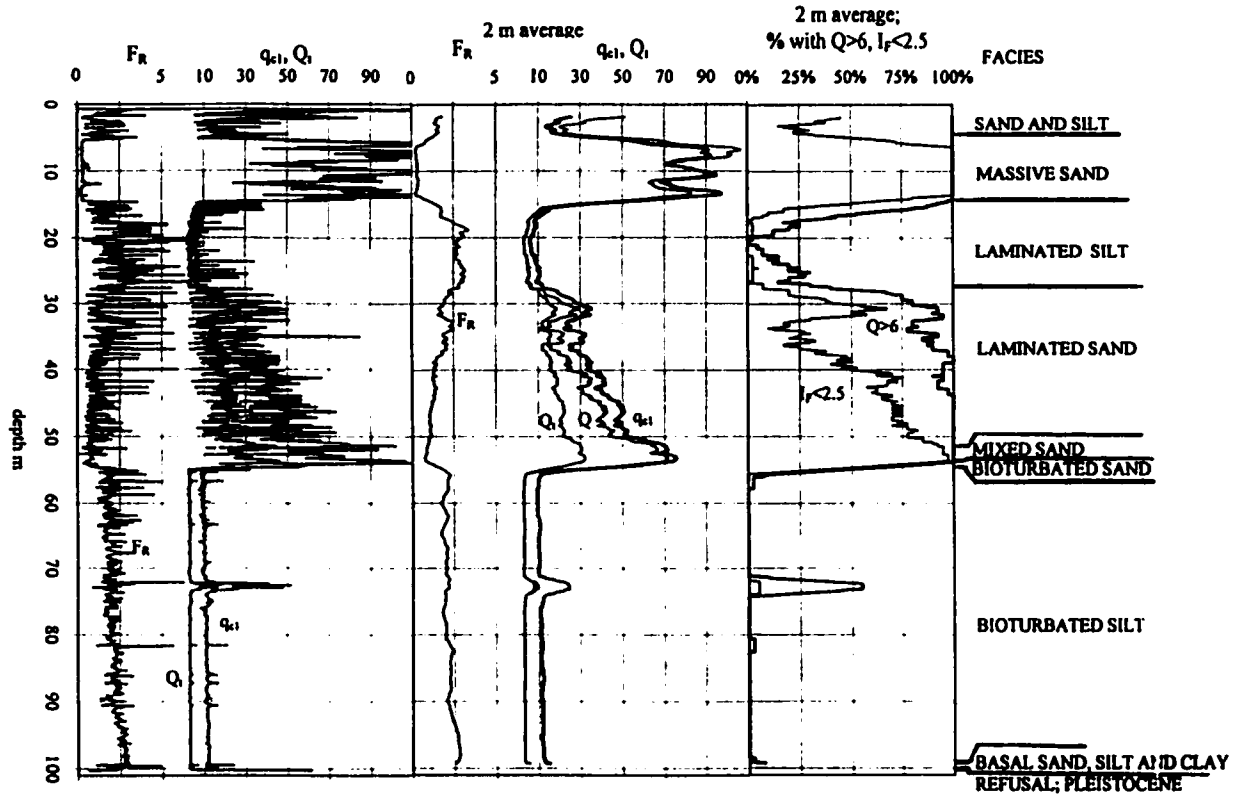

Figure 6-8. Normalized CPT data at borehole FD92-11. From left to right: normalized data (F_R, Q_t and q_{c1}); normalized data averaged over 2 m (F_R, Q_t, Q and q_{c1}); and estimates of sand content averaged over 2 m based on Q>6 and I_F<2.5. Q>6 is a better indicator of sand content where thin sands are interbedded with silt. See also Figures 5-8, 6-45 and 6-48. This CPT is also shown in Figure 6-3.

Table 6-1. Facies Summary ; Part 1; Topset

Facies (and abbreviation)	Description	Depositional Environment
Peat Facies (PT)	peat, up to 8 m thick, occurs at surface on eastern parts of upper delta plain.	raised peat bog
Laminated and Organic Silt Facies (LOZ)	organic-rich silt, 1 to 12 m thick on the upper delta plain.	floodplain (fresh water marsh) and upper tidal marsh
Interbedded Sand and Silt Facies (SZ)	interbedded sand and silt transitional between LOZ above and MS below.	
Bioturbated sand and silt subfacies **(BSZ)**	bioturbated fine to very fine sand and silt, 1 to 5 m thick; includes bivalve and intertidal foraminiferal fauna.	tidal flat
Well bedded sand and silt subfacies **(WSZ)**	laminated to medium bedded fine and very fine sand and silt, generally less than 3 m thick.	shallow partially abandoned distributary channels and bar tops in upper delta plain environment
Thick sand and silt subfacies **(TSZ)**	laminated to medium bedded medium to very fine sand and silt, generally 5 to 10 m thick. Laterally replaces the massive sand facies. Shell-free and shell-bearing variants occur.	partially abandoned distributary channels
Distal sand and silt subfacies **(DSZ)**	thin to thickly bedded very fine to medium sands and silts, locally metre-scale coarsening upward sequences occur. Occurs on outer margin of tidal flats and subaqueous platform.	partially abandoned distributary channels near the river mouth
Massive Sand Facies (MS)	fine to medium sand, 8 to 30 m thick; erosional base and gradational top, 1 or more coarsening upward sequences, locally with high angle planar cross bedding, silt clasts and pebbles.	fill of active distributary channels
Shell-free subfacies **(MSSF)**	no shell debris, overlain by the WSZ	fill of active distributary channels in upper delta plain environment
Shell-bearing subfacies **(MSSB)**	includes bivalve shells, overlain by either the MSSF or the BSZ.	fill of active distributary channels in a tidal flat environment
Distal Subfacies **(MSD)**	thin occurrences (<6m) of massive sands at outer of tidal flats and subaqueous platform, where overlain by the DSZ; at outermost occurrences, silts interbeds occur in lower part, obscuring sharp base. Locally recognized beneath MSSF in central and eastern parts of upper delta plain, includes interbedded sand and silt intervals similar to DSZ **(DSZeq)**	fill of active distributary channels near the river mouth, grading into river mouth bars.

Table 6-1. Facies Summary ; Part 1(continued); Topset

Facies (and abbreviation)	Description	Depositional Environment
Coarsening Upward Sand Facies of the Topset (CT)	interbedded sand and silt coarsening upward, based on CPT interpretation	prograding beach marginal to the delta

Part 2; Foreset

Basal Sand, Silt and Clay Facies (BC)	pink oxidizing clay, locally fractured, silt and sharp-based sands; bioturbated.,	clay and some sands may be late stage glaciomarine deposits. sharp based sands overlying the clay are bottomset gravity flow deposits that bypassed the slope.
Bioturbated Silt Facies (BZ)	bioturbated silt to clayey silt, weakly bedded, some distinct burrows preserved; some thin graded beds and laminae of very fine sand.	bottomset, lower foreset and locally upper foreset; distal suspension deposits from the plume, graded sands are sediment gravity flow deposits.
Laminated Silt Facies (LZ)	laminated clayey to sandy silt, locally with thin very fine sand beds; metre-scale coarsening upward sequences, rare burrows; apparent dips up to 7^{o}.	upper foreset; suspension deposits from the plume deposited at intermediate distances (between LS and BZ) from the river mouth.
Laminated Sand Facies (LS)	laminated fine to very fine sand and silt, commonly in metre-scale coarsening upward sequences; some sharp based sands; apparent dips up to 7^{o}.	upper foreset; primarily suspension deposits from the plume deposited at intermediate distances (between LZ and MX) from the river mouth, some sediment gravity flow deposits.
Mixed Sand facies (MX)	thin to medium beds of fine sand interbedded with laminated very fine sand and silt; fine sand occurs as metre-scale coarsening upward sequences and sharp based sands; apparent dips up to 7^{o}.	upper foreset, mixture of suspension deposits from plume and sediment gravity flow deposits, deposited close to river mouth
Sharp Based Sand Facies (SB)	>50% thick sharp based fine to medium sand units (1 to 5 m), interbedded with laminated fine to very fine sands.	upper foreset , primarily sediment gravity flow with subordinate suspension deposits formed close to river mouth

Table 6-1. Facies Summary ; Part 2 (continued); Foreset

Facies (and abbreviation)	Description	Depositional Environment
Bioturbated Sand Facies (BS)	bioturbated fine to very fine sand and silt, generally weakly bedded, some distinct burrows occur, and locally mud draped ripples occur	lower foreset, southern part of delta, where north flowing tidal currents rework delta slope deposits.
Thick Coarsening Upward Sand Facies (CU)	1 or more coarsening upward sequences, 1+ m thick and dominated by fine sand; laminated silt and very fine sand in lower part; seaward dips.	suspension deposits at river mouth
Rhythmically Interbedded Sand and Silt Facies (RSZ)	medium beds of very fine sand rhythmically interbedded with similar thicknesses of laminated very fine sand and silt, in coarsening upward sequences up to 2 m thick	suspension deposits at river mouth during initial phase of foreset deposition (at the head of the delta) when delta was building into a protected embayment.
Low Dipping Interbedded Sand and Silt Facies (LDSZ)	interbedded fine sands and laminated silts; fine sands include coarsening upward sequences 0.5 to 4 m thick and sharp based sands; laminated silt interbeds up to 3 m thick; characterized by low dips (0 to 3^{o}).	subaqueous platform ,when this environment was more extensive than today because of the rapid rate of sea level rise between 5000 and 8000 years ago.
Disturbed Silt Facies (DZ)	silt, massive, locally with clasts, reoriented blocks of laminated silt and sand, and deformed laminae	upper foreset, slump deposit near river mouth

LAMINATED AND ORGANIC SILT FACIES

The laminated and organic silt facies underlies the peat facies, where present, and occurs at the surface across most of the upper delta plain and the inshore parts of the tidal flats (Figures 6-1, 6-2, 6-4 and 6-10; Williams and Roberts, 1989). This facies consists of silts with finely disseminated organic particles. Larger (centimetre-scale) organic fragments occur are oriented vertically as well as horizontally. The organic content of this unit is variable, and appears to be greatest where this facies is thickest in the eastern part of Lulu Island, where organic content reported in British Columbia Ministry of Transportation and Highways (MOTH) boreholes varies from 5% to 40%. Thin interbeds of peat occur locally where the facies is overlain by the peat facies (Figure 6-4; Williams and Roberts, 1989). Thin to medium laminae that vary from clayey silt to sandy silt and more rarely, very fine sand are variably preserved (Figures 6-11). Where this facies occurs at the surface, a desiccated and oxidized interval less than 1 m thick is present at the surface. Rhizoconcretions consisting of red oxidized tubes a few millimetres in diameter occur in this oxidized interval and extend into the underlying silts.

This facies is up to 12 m thick at the head of the delta in the eastern part of Lulu Island, where it extends to a maximum depth of 14 m below current sea level, and thins to the west across the delta (Figure 6-1, 6-9 and 6-10; Williams and Roberts 1989). It is 2-3 m thick in boreholes in the central part of the upper delta plain (Figures 6-2, 6-4 and 6-12) and 1 m or less on the sea dykes that separate the upper and lower delta plain (Figures 4-5, 6-1 and 6-3). This facies was not observed in boreholes on margins of modern distributary channels (Figures 6-10 and 6-13).

On CPT data, this facies is characterized by low uniform to slightly serrate cone bearing (q_t >10 bars), although cone bearing is less uniform where this facies occurs at the surface (Figures 6-8, 6-9, 6-10 and 6-11). Where the facies is more than 5 m thick in the eastern part of the delta, Q_t is generally between 2 and 5 and B_q exceeds 0.15, indicating that these

deposits are normally consolidated (Lunne et al., 1997). However, where the facies is thin, average Q_t below the desiccated interval exceeds 10 and B_q is positive or low negative (<0.15), indicating slight overconsolidation in those sediments (Figure 5-5; see Chapter 5). Friction ratio values are generally high (R_f = 1 to 3 and F_R = 2 to 4) and the curve serrate. Thin friction ratio peaks indicate the presence of peat interbeds (Figure 6-4), and in some sections, the friction ratio increases upward, reflecting an upward increase in organic content (Figures 6-9 and 6-10). In the surficial desiccated interval, cone bearing increases upward, B_q is negative, and friction ratio is higher than in the underlying silts, reflecting overconsolidation due to desiccation (Figures 5-5, 6-12 and 6-16).

This facies gradationally overlies the interbedded sand and silt facies. However, locally at the head of the delta, this facies is sharply laterally replaced by the massive sand facies, which locally overlies the laminated and organic silts (Figures 6-10, 6-14 and 6-15).

In the eastern part of Lulu Island near the head of the delta, the base of this facies has been dated at 7960±140 ^{14}C years (GSC4255), and the Mazama Tephra has been identified (ca. 6800 ^{14}C years B.P.; Williams and Roberts, 1989)

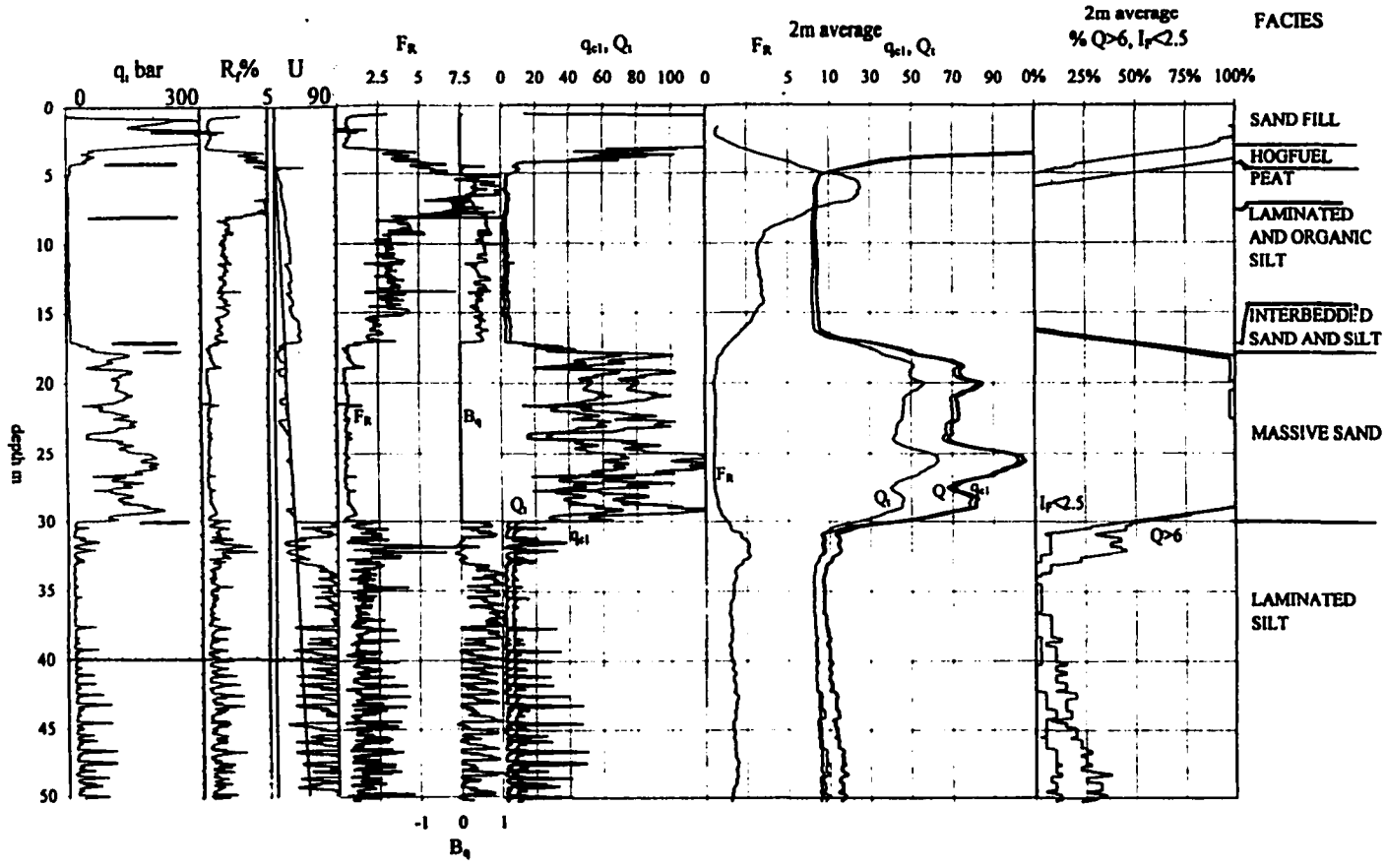

Figure 6-9. Non-normalized and normalized CPT data from a site in eastern Lulu Island showing the peat and laminated and organic silt facies. From left to right: non-normalized data (q_t, R_f and U); normalized data (F_R, B_q, Q_t and q_{c1}); normalized data averaged over 2 m (F_R, Q_t, Q and q_{c1}); and estimates of sand content averaged over 2 m based on Q>6 and I_F<2.5. Note the high friction ratio (R_f and F_R) in the peat facies and the low uniform cone bearing in the laminated and organic silt facies. This CPT is also shown in Figures 6-1 and 6-10.

Figuere 6-10. Caption on following page.

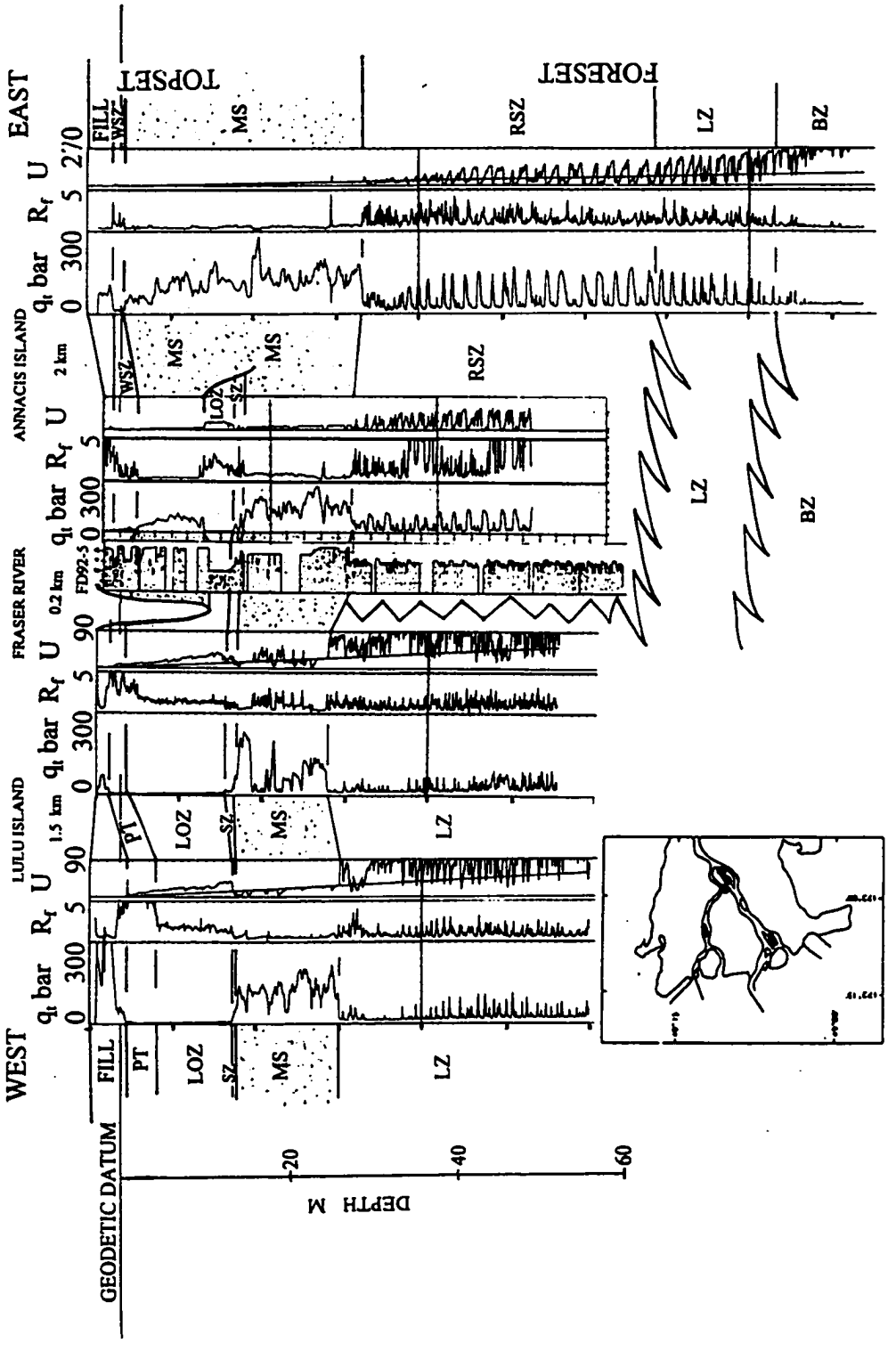

Figure 6-10 (see previous page). East-west CPT cross section in eastern part of delta, showing lateral replacement of thick laminated organic silt facies (LOZ) on Lulu Island by massive sand facies (MS) on Annacis Island. Note unit of MS overlies LOZ in FD92-5. Note silty variant of MS in 2nd CPT from left that includes several fining upward and coarsening upward sequences characteristics of MSD, DSZeq, as well as TSZ. Note rhythmically interbedded sand and silt facies (RSZ) on Annacis Island CPTs laterally equivalent to and overlying laminated and organic silt facies (LZ). For facies symbols, see Table 6-1. R_f in % and U in metres of water.

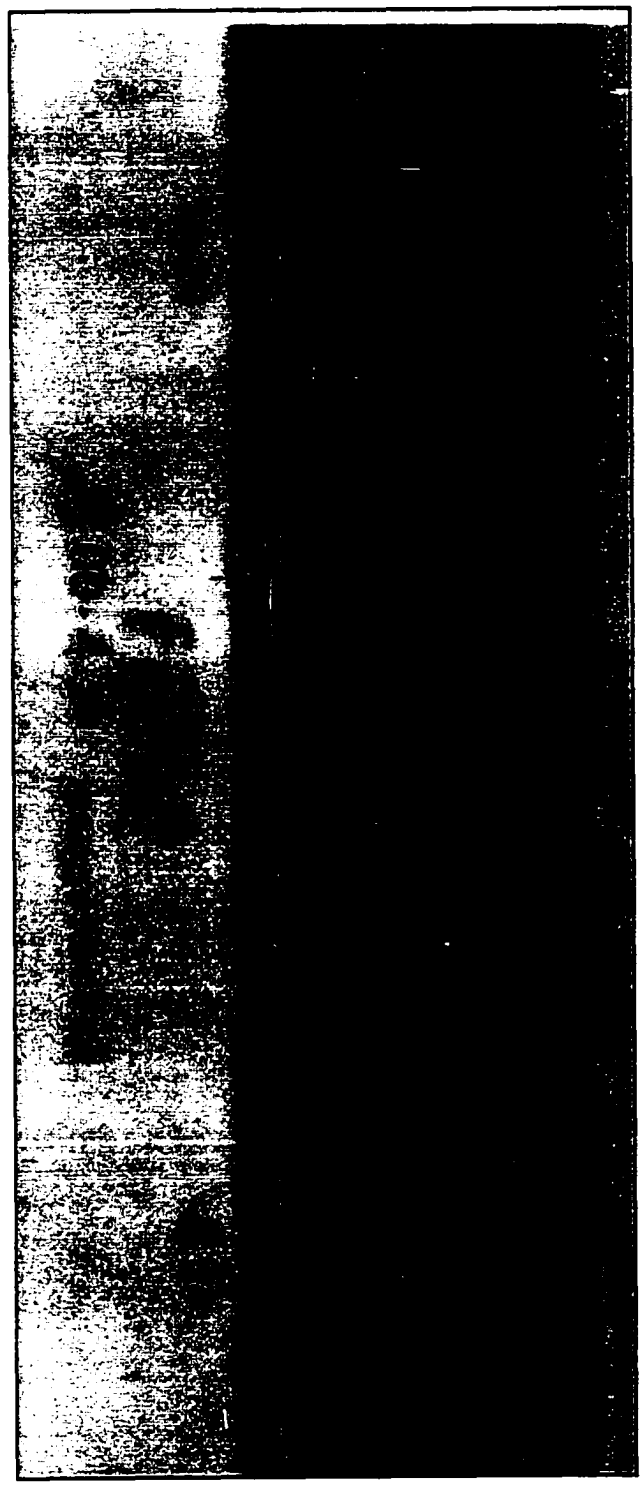

Figure 6-11. Core photograph of the laminated and organic silt facies. Note laminae in silt and organic flecks and laminae. FD94-4, CPT depth 3.30-3.60 m. See Figure 6-4. From Monahan et al. (1997).

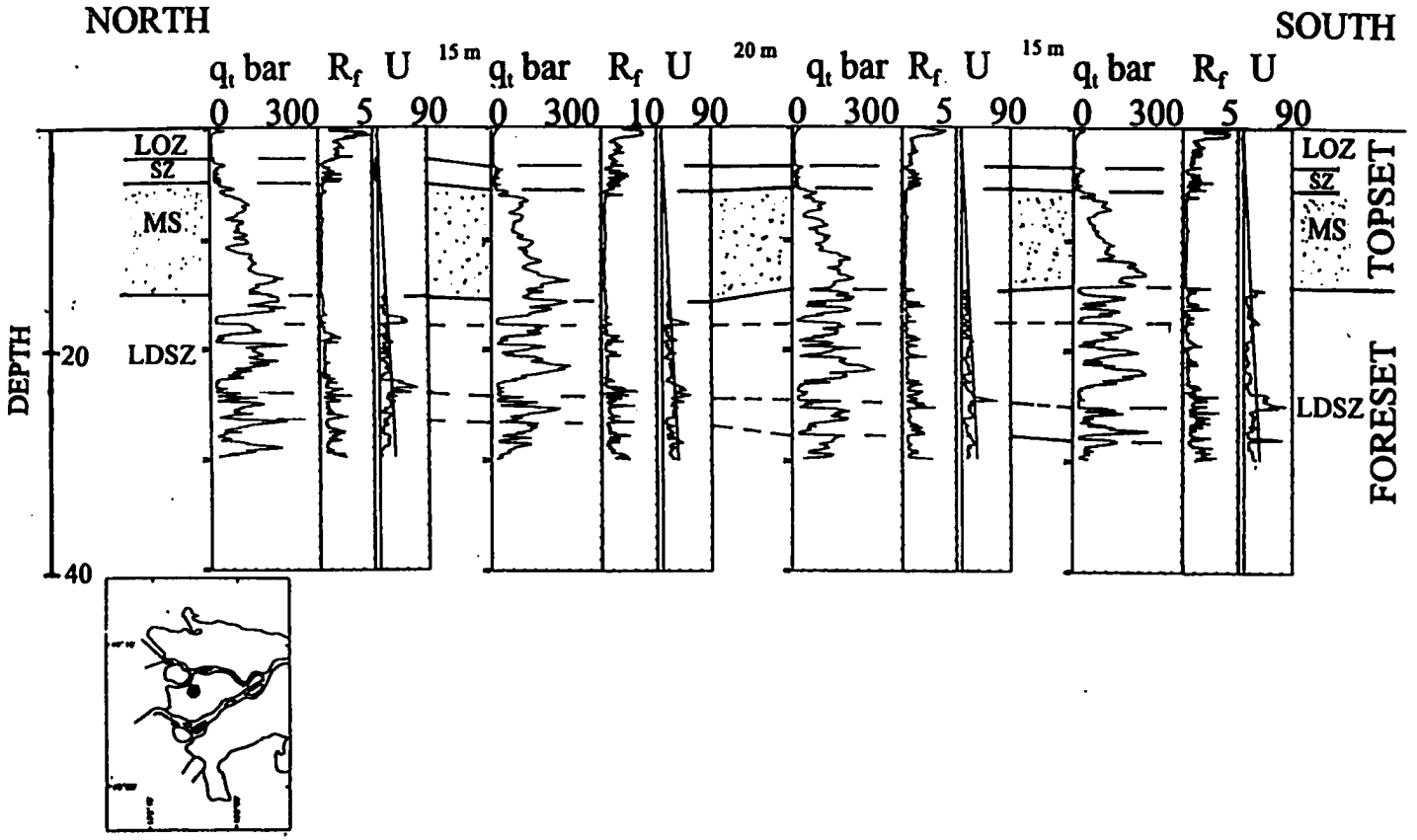

Figure 6-12. CPT cross section at a site in Richmond Centre. The basal contact of the massive sand facies (MS) in the 3 northern CPTs is picked where the low uniform friction ratio and dU near zero of this facies are replaced downward by higher and more serrate friction ratio, negative dU, and high cone bearing sandy coarsening upward sequences of the low dipping interbedded sand and silt facies (LDSZ) of the foreset. Note low apparent dips in the LDSZ, varying from negligible to ~ 1.5°. The CPT on the right is also shown in Figures 6-1 and 6-32. For facies symbols, see Table 6-1. R_f in % and U in metres of water.

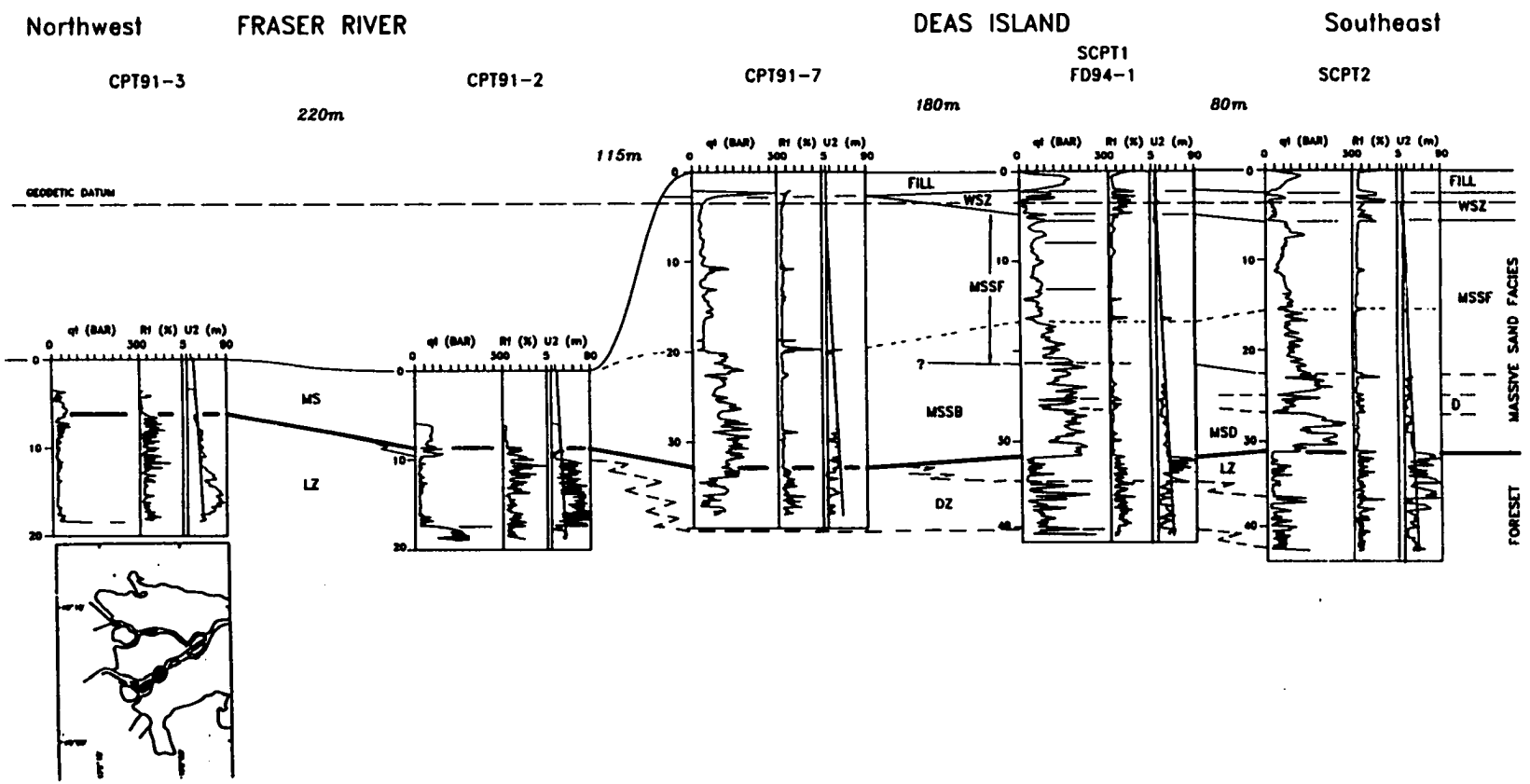

Figure 6-13. Northwest-southeast CPT cross section from the Main Channel of the Fraser River to Deas Island and borehole FD94-1 (Figures 2-4 and 4-3). Note that the base of the shell-free subfacies of the massive sand facies (MSSF) is at approximately the same depth as the depth of the river channel, and the stacking of the shell-free subfacies over the shell-bearing subfacies (MSSF). In FD94-1, enclosed organic material in MSSF and MSSB yielded dates of 10±60 (TO- 4374) and 8260±80 (TO-4595) ^{14}C years, respectively (Appendix F). Note the localized presence of the distal subfacies (MSD) and distal sand and silt equivalent (DSZeq), that grade laterally into MSSB. In the massive sand facies, cone bearing correlates with age, and the low cone bearing in MSSF is related to the very young age of the deposit (Figure 6-39). Note also thin cone bearing increasing upward sequences at the top of MSSF (for details see Figure 5-18). For facies symbols, see Table 6-1. R_f in % and U in metres of water.

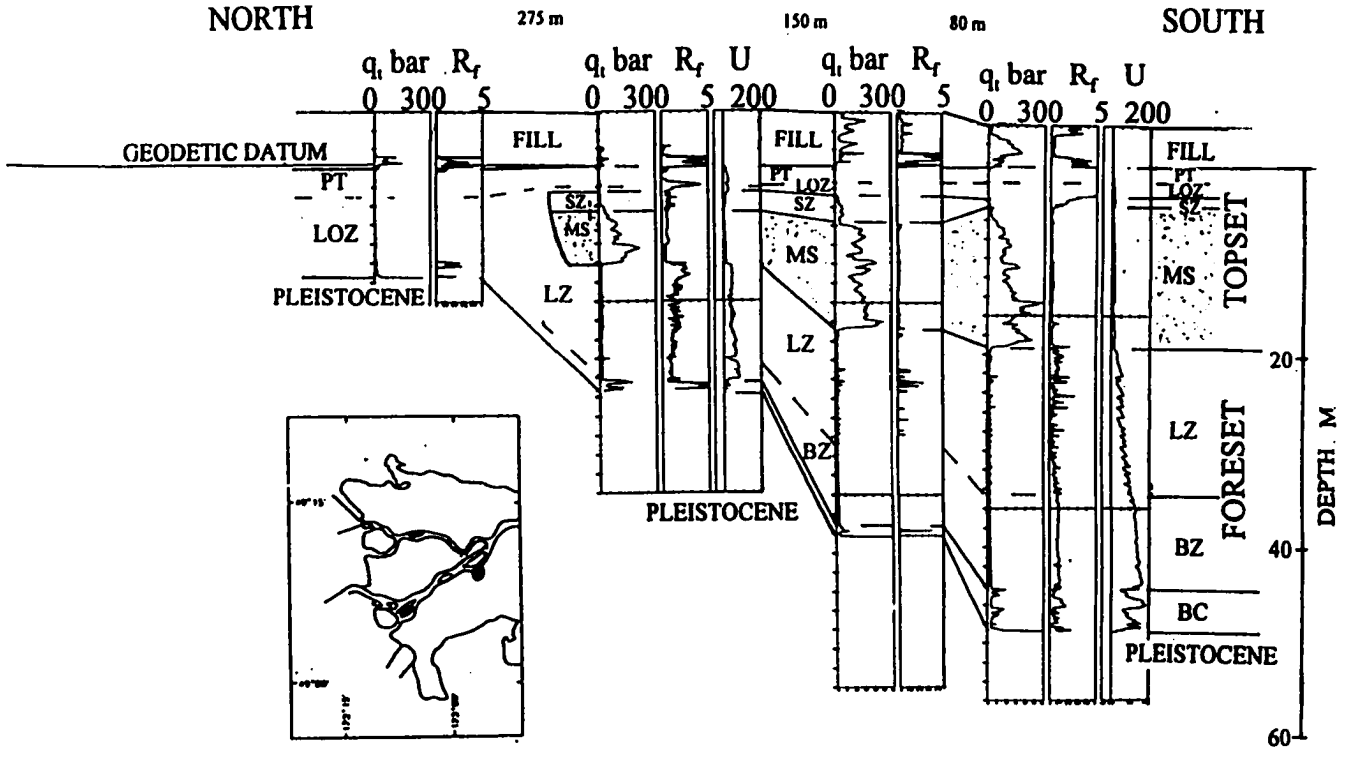

Figure 6-14. North-south CPT cross section on eastern margin of delta, showing the massive sand facies (MS) laterally replacing the laminated and organic silt facies (LOZ). Peat facies (PT) and LOZ distinguished on the basis of nearby boreholes. For facies symbols, see Table 6-1. R_f in % and U in metres of water.

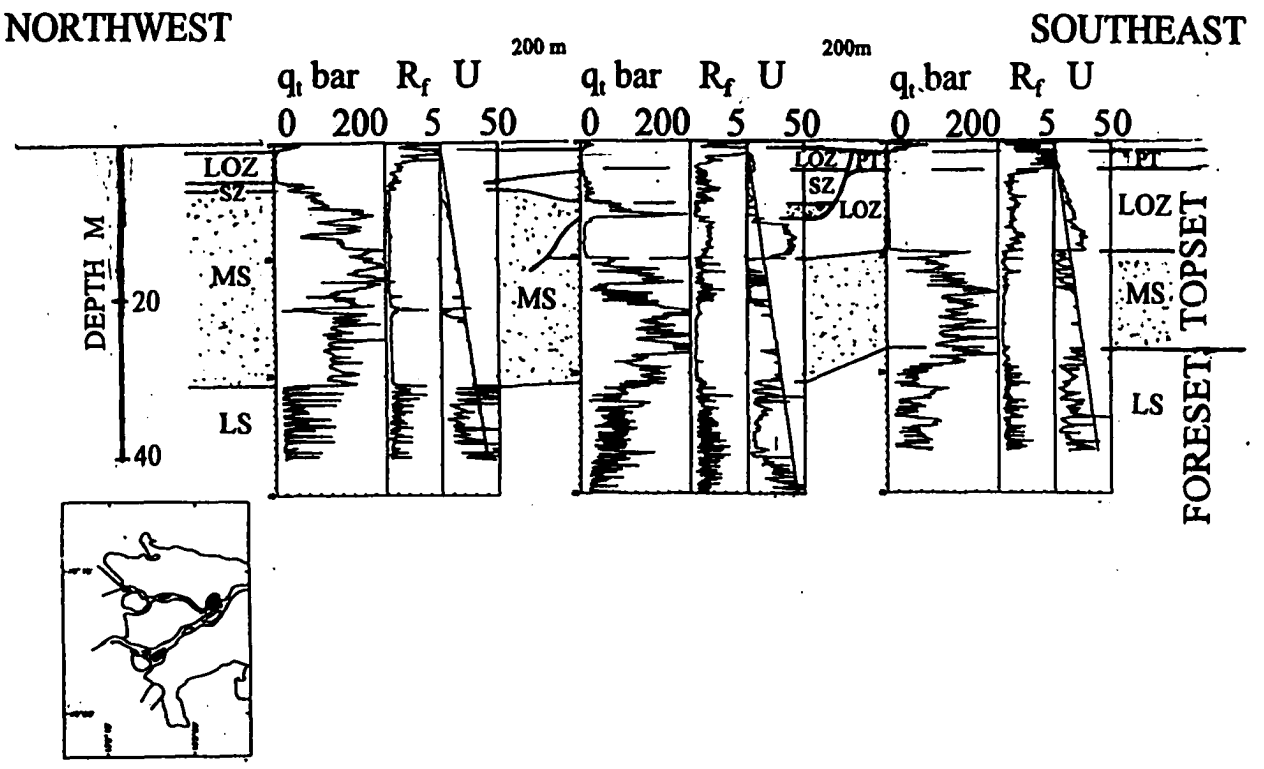

Figure 6-15. Northwest-southeast CPT cross section on northeasternmost Lulu Island. Note thick laminated and organic silt (LOZ) and peat facies (PT) in upper part of topset in southeast part of section, being replaced to northwest by massive sand facies (MS). Note thin upper lens of MS overlying LOZ in middle CPT. Northwest CPT is near the north arm of the Fraser River. For facies symbols, see Table 6-1. R_f in % and U in metres of water.

INTERBEDDED SAND AND SILT FACIES

The organic and laminated silt facies is transitional between the massive sand facies below and the laminated and organic silt facies above, and varies from laminated to medium bedded, very fine to fine sand and silt. Consequently, the expression of this facies on CPT data varies from low, variable cone bearing (q_t<15 bars; q_{cl}<25), indicative of thinly interbedded silts and very fine sands, to medium to thick sand beds with cone bearing exceeding 30 bars (q_{cl}<50) interbedded with low cone bearing silts (Figures 6-4, 6-12, 6-16 and 6-17). Friction ratio values are high and highly variable, reflecting interbedding of sands and silts, but in general increase upwards, indicating upward fining. dU is generally negative, although in thicker silts intervals positive dU occurs.

Four distinct subfacies have been observed in cores: the bioturbated sands and silts, well bedded sands and silts, thick (>4 m) sands and silts that laterally replace the massive sand facies, and distal sands and silts that overlie the distal subfacies of the massive sand facies in the modern subaqueous platform. The bioturbated and the well bedded subfacies cannot be differentiated based on CPT data alone. The thick sand and silt subfacies can distinguished by its thickness and the distal subfacies by its stratigraphic position and CPT character.

Bioturbated Sand and Silt Subfacies

This subfacies consists of burrowed interbedded sands and silts and varies from less than 1 to 5 m thick. Sands are generally very fine although fine sand with high (18%) silt and clay content also occurs . This subfacies is medium to thick bedded and bed boundaries are poorly defined. It has a burrow mottled texture (Figure 6-18), although some centimetre-scale circular horizonal burrows can be discerned (*Thalassinoides*? or *Ophiomorpha*?; see Swinbanks and Luternauer, 1987). This subfacies includes bivalve shell debris. In addition,

an intertidal foraminiferal fauna has been recovered from one borehole examined for study by M. Johns (pers. comm. 1993) and from nearby boreholes by Williams (1988).

Cone bearing in this subfacies is low and variable (Figures 4-5 and 5-21). Low decimetre-scale cone bearing peaks (q_t = 10 to 20; q_{cl} = 10 to 40) representing silty very fine sand beds rise above a silt background (q_t<5; Q_t~10). Friction ratio values are correspondingly high and variable. At one site east of Ladner, a 1 m thick fine to very fine sand bed (peak q_t = 40 and q_{cl} = 60) that occurs at the top of this subfacies can be correlated on CPT data over a distance unit of at least 600 m (Figure 6-19; 2 km using other borehole data). The sand has an abrupt to gradual base and fines upward.

This subfacies occurs in boreholes from the centre of the upper delta plain to the subaqueous platform. It underlies the laminated and organic silt facies in the upper delta plain and the uppermost tidal marshes, and probably occurs at the surface over most of the tidal flats and subaqueous platform. It generally overlies the shell-bearing subfacies of the massive sand facies, although in a borehole on the subaqueous platform, it overlies the distal sand and silt subfacies.

Well Bedded Sand and Silt Subfacies

This subfacies consists of non-bioturbated, laminated to medium bedded sands and silts and is generally less than 3 m thick (Figures 5-5, 6-12, 6-16 and 6-17). Sands are generally very fine to fine. Silt beds or laminae are internally laminated with sandy silt and very fine sand (Figure 6-20). In some beds, silt laminae occur as couplets, enclosing a thin sandy lamina and surrounded by thicker sandy laminae. Organic laminae also occur. The expression of this facies on CPT data is as described above in the introductory paragraph on the interbedded sand and silt facies.

This subfacies occurs only in the upper delta plain. Generally, it underlies the laminated and organic silts, although on the margins of modern channels it occurs at the surface (Figures 6-10 and 6-13). It overlies the shell-free subfacies of the massive sand facies.

Thick Sand and Silt Subfacies

Locally the interbedded sand and silt facies thickens downward at the expense of the underlying massive sand facies to form the thick sands and silt subfacies (Figure 6-21). It is generally 5 to 10 m thick, and the thickest occurrence is over 20 m, where the massive sand facies has been reduced to less than less than 4 m from 20 m in nearby CPTs (Figure 6-22).

This subfacies consists of thin to very thick beds of fine to medium sand interbedded with laminated silt and sand. In the fine to medium sands, some sand and silt laminae are arranged in couplets, mud-draped ripples occur, silt laminae are locally eroded and silt clasts are present, particularly at the base of sand beds (Figure 6-23). Some sand beds fine upward. Organic laminae and wood fragments are also present.

The CPT expression of this facies is variable, but in all cases reflects the interbedding of sands and silts, as described above in the introductory section on this facies, and contrasts with the laterally equivalent massive sand facies in which friction ratio is low and uniform and cone bearing is high. Decimetre- to metre-scale beds with peak q_t and q_c up to 90 bars and friction ratio between 0.5 and 2% separate thin low cone bearing minima (q_t =10 bars) and friction ratio maxima (R_f =4 to 5%; Figure 6-24). dU is negative. In the thicker sand beds, fiction ratio is low and uniform. Upward fining in sand beds is indicated by upward decreasing cone bearing and increasing friction ratio.

The subfacies commonly fines upward, represented on CPT data by an upward decrease in

cone bearing and increase in friction ratio (Figures 6-24 and 6-25). The upper beds commonly have very low serrate cone bearing (qt peaks~10). Fine-grained end members of this subfacies can be distinguished from thick occurrences of the laminated and organic silt facies, by having a more serrate cone bearing curve, and negative dU.

Locally, a 2 to 4 m thick sharp-based upward fining sand unit can be traced laterally from this subfacies into the adjacent massive sand facies using CPT data (Figures 6-25 and 6-26). These sand units are characterized by low friction ratios that increases and become more variable toward the top, and high cone bearing (q_t~ q_{c1}~ 90) that decreases upward.

Most examples of this subfacies overlie and laterally replace the shell-free subfacies of the massive sand facies. However, this subfacies also overlies and replaces the shell-bearing subfacies and distal subfacies of the massive sands. Where this occurs, this subfacies is locally bioturbated, and includes clayey silts, finer than those associated with the shell-free subfacies, and shell fragments in the sand beds (Figure 6-24).

This subfacies is not widespread. Most occurrences are situated on the courses of historically mapped arcuate or meandering sloughs on the upper delta plain, both adjacent to the Main Channel and in linear the gap in the peat bogs (Figure 2-2; North, 1979; Township of Richmond, undated). Consequently, sediment bodies of this subfacies are interpreted to form narrow curvilinear trends following these sloughs. At one site where there is sufficient CPT and other borehole data to map its distribution, this facies has a maximum thickness of 9 m and forms a narrow curvilinear trend 50 to 100 m wide (Figure 6-27).

Distal Sand and Silt Subfacies

This subfacies occurs in the outer tidal flats and subaqueous platform, where it overlies the distal subfacies of the massive sand facies. It has been observed in cores and numerous

CPTs in the vicinity of the Roberts Bank port.

The subfacies consists of thinly to thickly interbedded very fine to medium sands and laminated silts, and the CPT expression is similar to other subfacies of the interbedded sand and silt facies (Figure 6-6). Sands are generally fine to very fine and are represented by variable cone bearing peaks (q_t and q_{cl} up 90). Locally in this subfacies, decimetre- to metre-scale coarsening upward sand beds with gradational contacts with underlying silt beds occur, and can be inferred from cone bearing increasing upward sequences. Other sand beds are sharp-based and include mud-draped ripples and silt clasts. This subfacies is not bioturbated, but in one core it underlies a thin interval of the bioturbated sand and silt subfacies.

These deposits occur at elevations of -4 to -8 m (below mean sea level; 1 to 5 m below tide datum). Because the underlying deposits are less than 2000 ^{14}C years old[4], the current depth of this subfacies is similar to the water depths in which they were deposited.

4

^{14}C dates in the underlying foreset deposits range from 2460±50 years in borehole FD93-5 on the causeway east of Roberts Bank Port (TO-4281), to 1060+80 years in borehole FD93-1 on the southwest margin of Roberts Bank Port (TO-3977; see Appendix F).

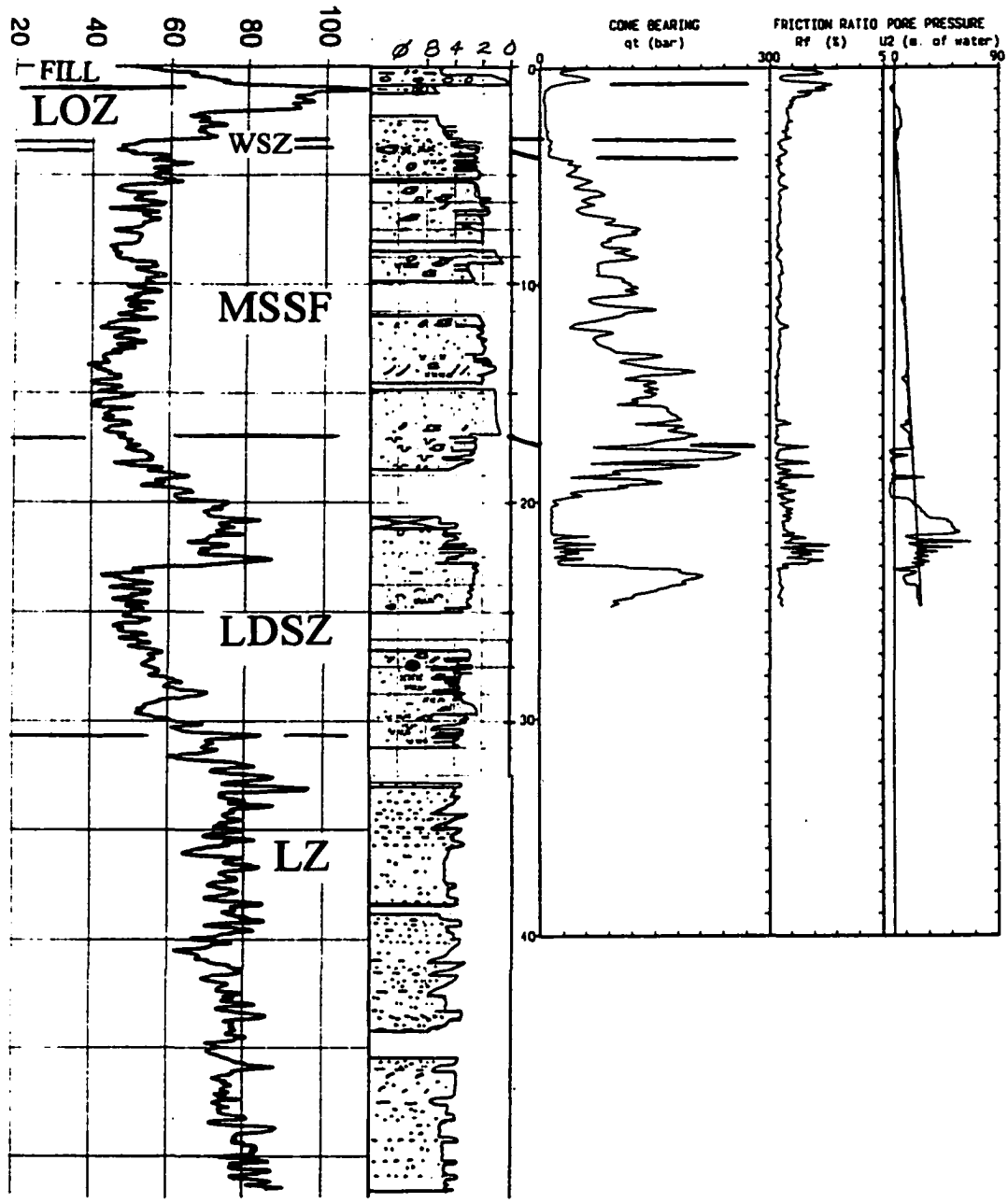

Figure 6-16. Composite log of FD93-2. From left to right; gamma ray log, in counts per second (cps), lithology log; and CPT data (q_t, R_f and U). Note the high friction ratio in the desiccated silts at the top of the laminated and organic silt facies (LOZ). Note also that the sharp base of the massive sand facies (shell-free subfacies; MSSF) is marked by an abrupt change in excess pore pressure, from strongly negative (pore pressure less than hydrostatic) in the low dipping interbedded sand and silt facies (LDSZ) to near zero (pore pressure near hydrostatic) in MSSF. Furthermore, the friction ratio curve is serrate in the LDSZ and low and uniform in the MSSF. Cone bearing is very high in the sandy coarsening upward sequences in LDSZ. See also Figure 6-58. For facies symbols, see Table 6-1.

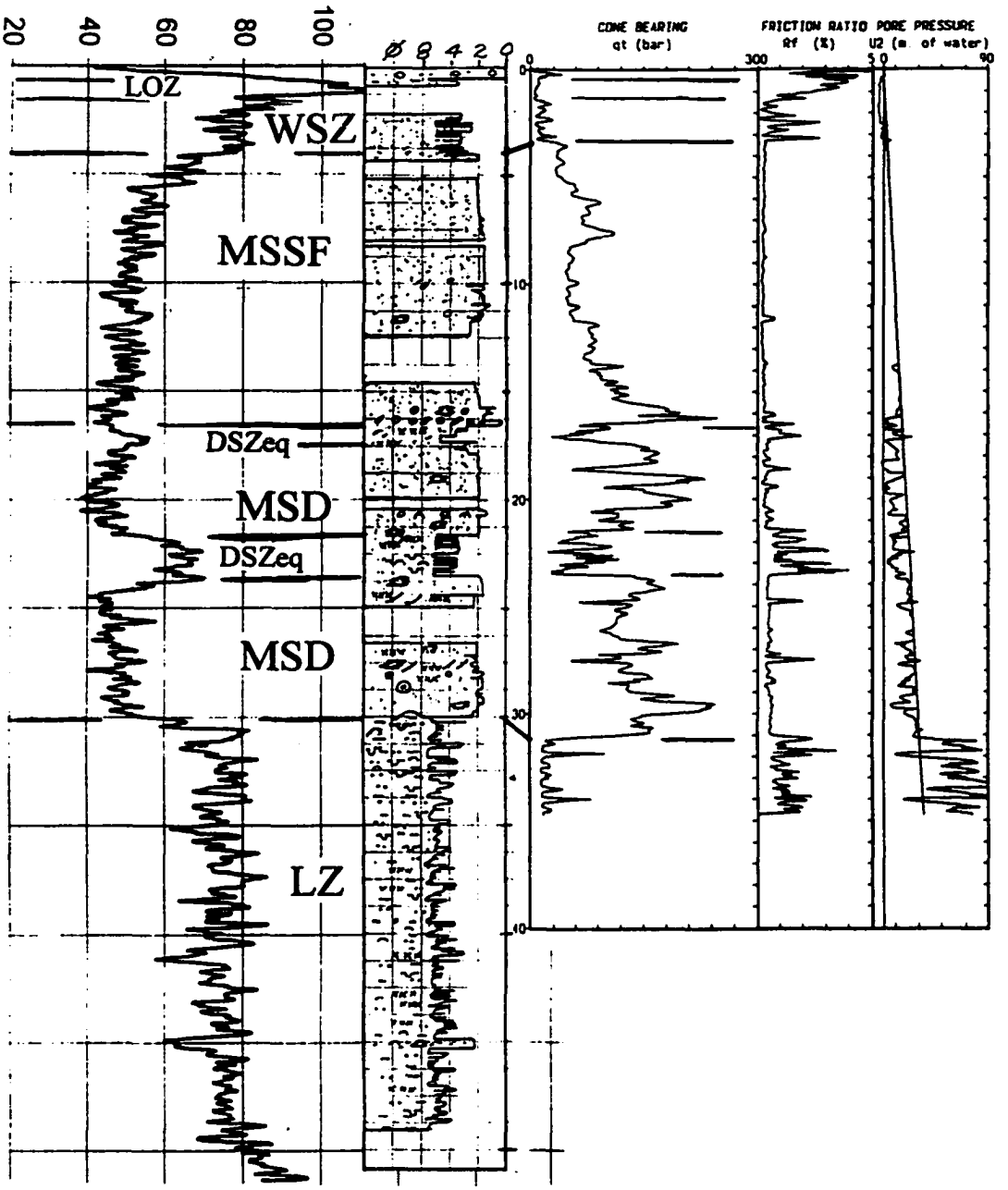

Figure 6-17. Composite log of FD93-4. From left to right; gamma ray log, in counts per second (cps), lithology log; and CPT data (q_t, R_f and U). At this site the massive sand facies consists of the shell-free subfacies (MSSF) overlying stacked distal sands of the distal subfacies (MSD) and the distal sand and silt equivalent (DSZeq). Note the blocky shape of the friction ratio in the MSD. The base of the MSD is contorted (see Figure 6-38) and is ~1 m shallower in FD93-4 than in the CPT, 2 m away (compare the CPT and the gamma ray log). This CPT is also shown in Figure 6-37. For facies symbols, see Table 6-1.

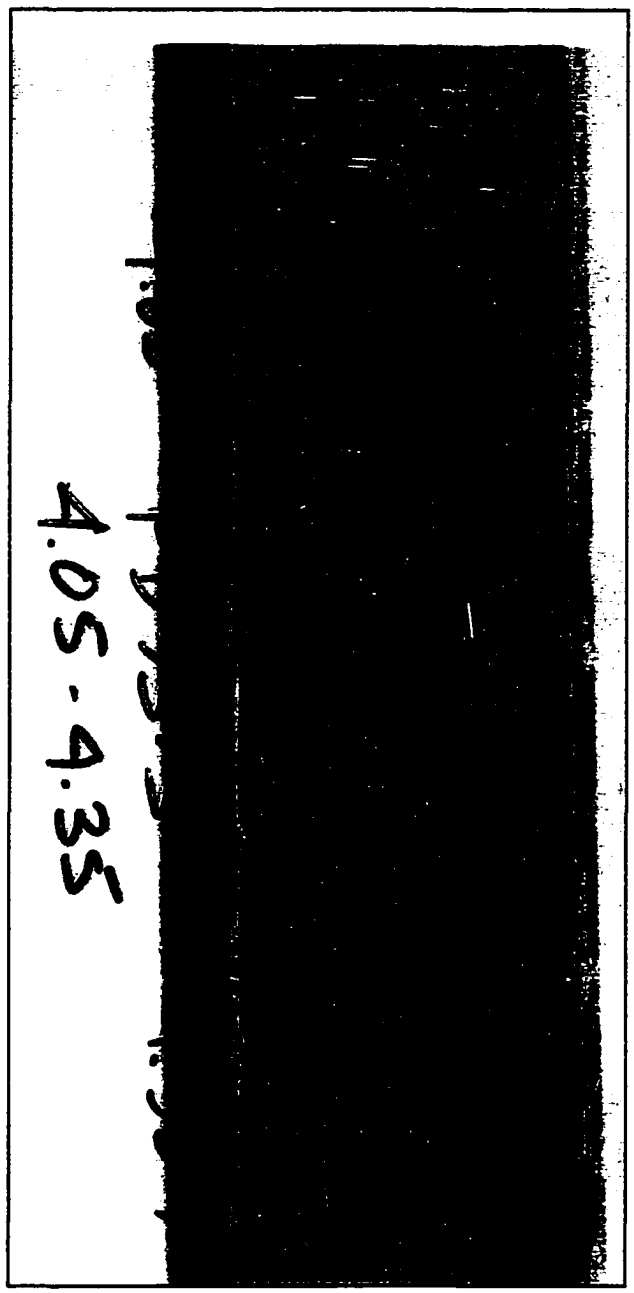

Figure 6-18. Core photograph of the interbedded sand and silt facies, bioturbated subfacies. Note mottled texture and circular to oval burrows. FD93-3, CPT depth 3.63 to 3.93 m. See Figure 4-5. From Monahan et al. (1997).

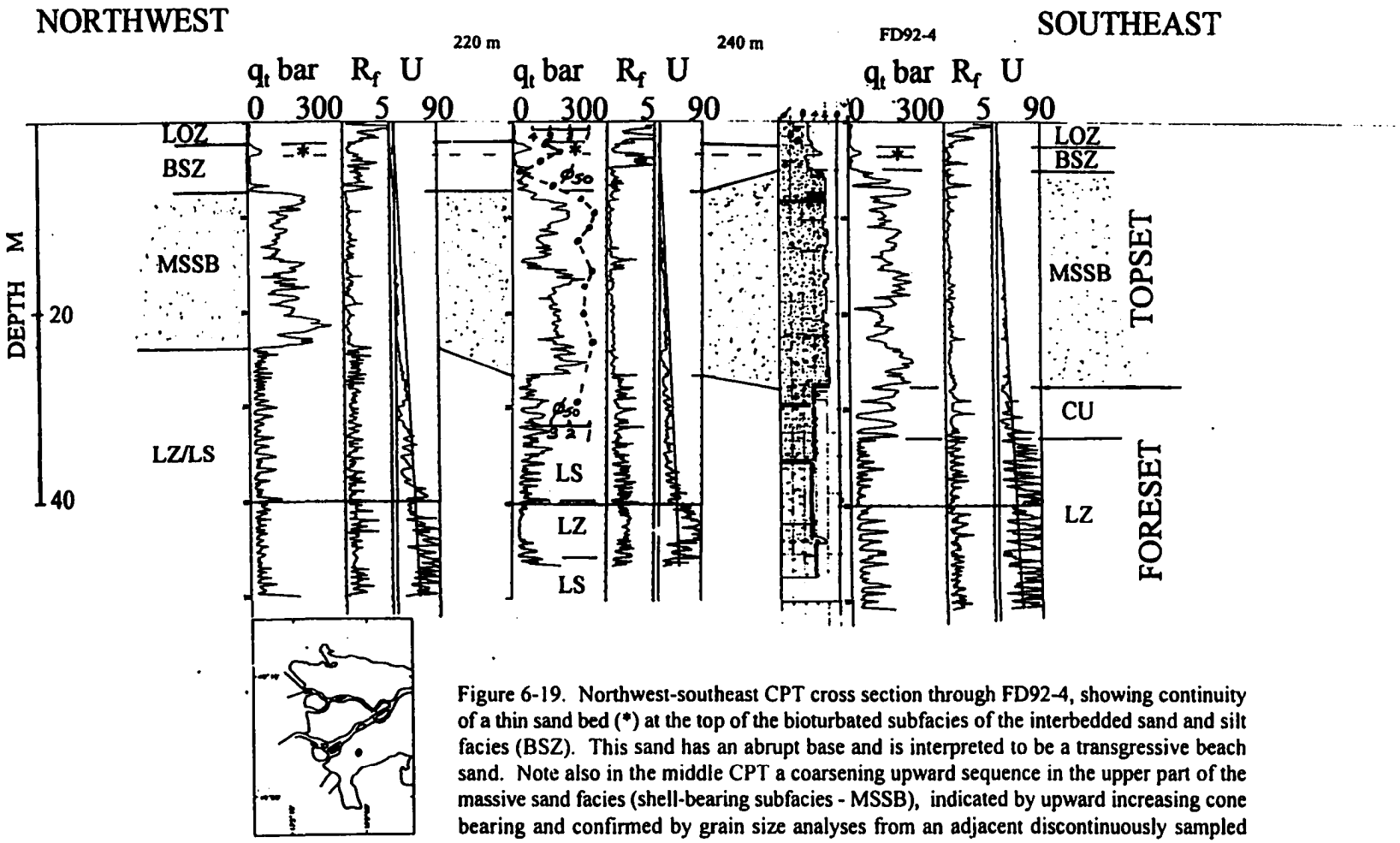

Figure 6-19. Northwest-southeast CPT cross section through FD92-4, showing continuity of a thin sand bed (*) at the top of the bioturbated subfacies of the interbedded sand and silt facies (BSZ). This sand has an abrupt base and is interpreted to be a transgressive beach sand. Note also in the middle CPT a coarsening upward sequence in the upper part of the massive sand facies (shell-bearing subfacies - MSSB), indicated by upward increasing cone bearing and confirmed by grain size analyses from an adjacent discontinuously sampled standard penetration test (SPT) borehole. Grain size samples analyzed by sieve at the PGC. Note foreset is a mixture of the laminated silt (LZ) and laminated sand facies (LS) at this site. For facies symbols, see Table 6-1. R_f in % and U in metres of water.

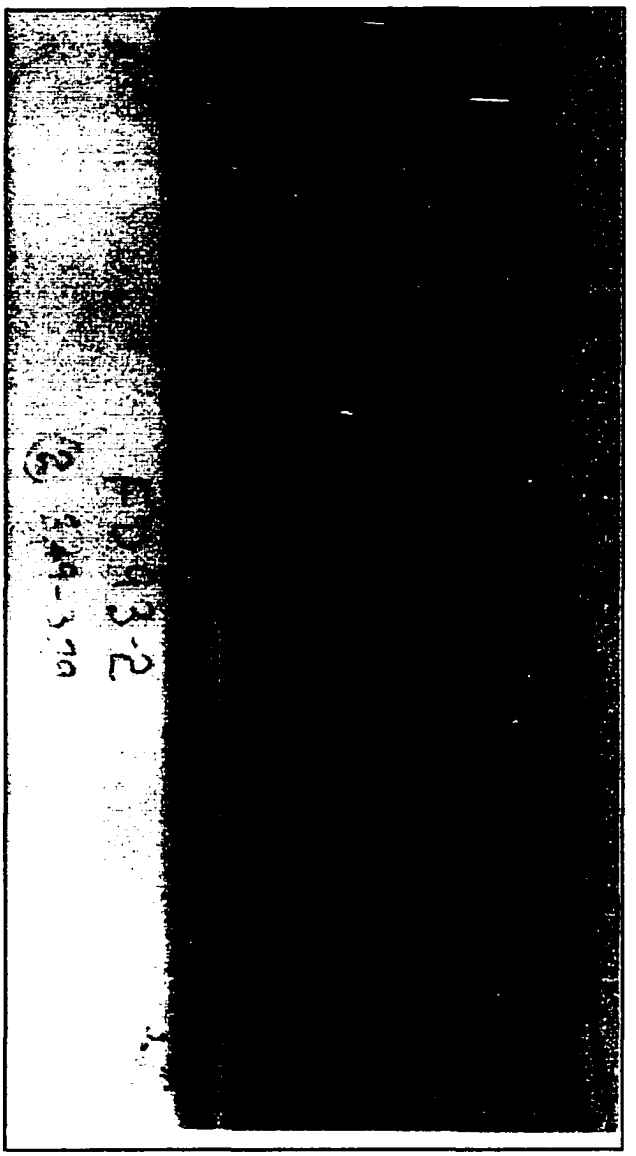

Figure 6-20. Core photograph of interbedded sand and silt facies, well bedded subfacies. FD93-2; CPT depth 3.56 to 3.86 m. See Figures 5-5 and 6-16. Cone bearing is not fully resolved in thin sand bed in centre of photograph.

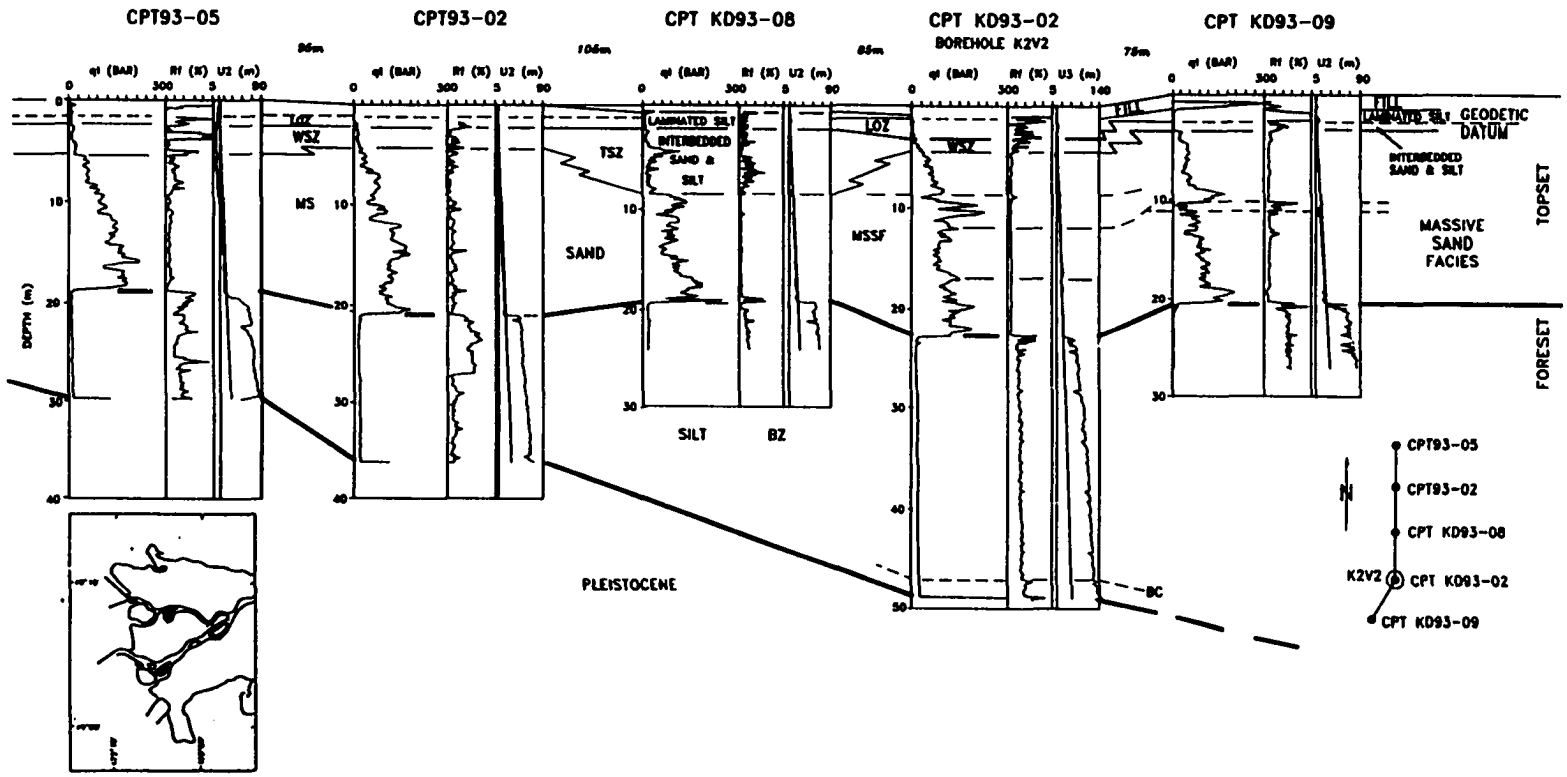

Figure 6-21. North-south CPT cross section through K2V2, on the northern margin of the delta (Kidd 2). The top of the Pleistocene is marked by refusal on the CPTs (shown by an abrupt increase in cone bearing), and dips to the south. The basal sand, silt and clay facies (BC) of the foreset was observed above the Pleistocene at borehole FD96-2, immediately adjacent to K2V2. Note the sharp base of the massive sand facies (shell-free subfacies - MSSF), which has several metres of relief. Note also the presence of the thick subfacies of the interbedded sand and silt facies (TSZ) in the middle CPT. The distribution of TSZ at this site is shown in Figure 6-27. The CPT at K2V2 is also shown in Figure 6-34. Figure modified from Monahan et al. (1995, 1997). For facies symbols, see Table 6-1. R_f in % and U in metres of water.

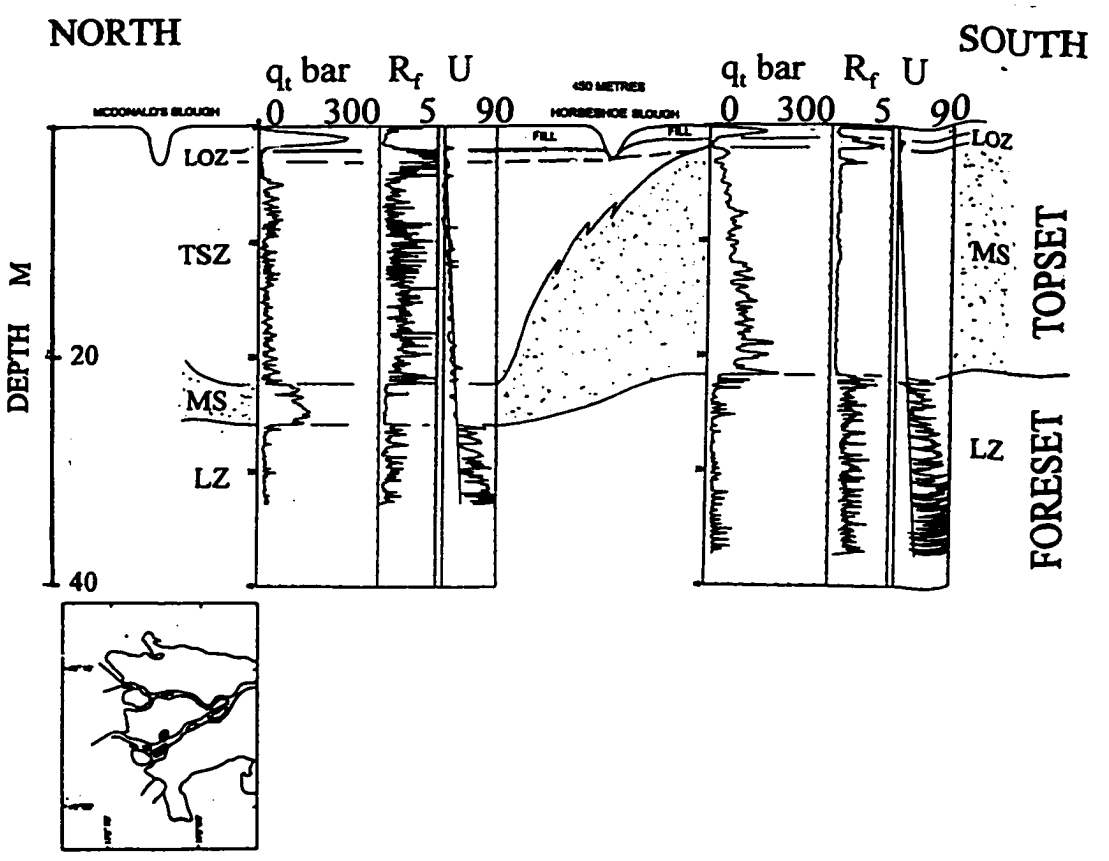

Figure 6-22. CPT cross section showing the thick subfacies of the interbedded sand and silt facies (TSZ) laterally replacing the upper part of the massive sand facies (MS). TSZ is associated with a complex of a modern sloughs (McDonald's, Horseshoe and Woodword's Sloughs; see Township of Richmond, undated), and represents partially abandoned channel fill. An active channel was mapped at this site in the 1827 Admiralty survey (Figure 2-4). For facies symbols, see Table 6-1. R_f in % and U in metres of water.

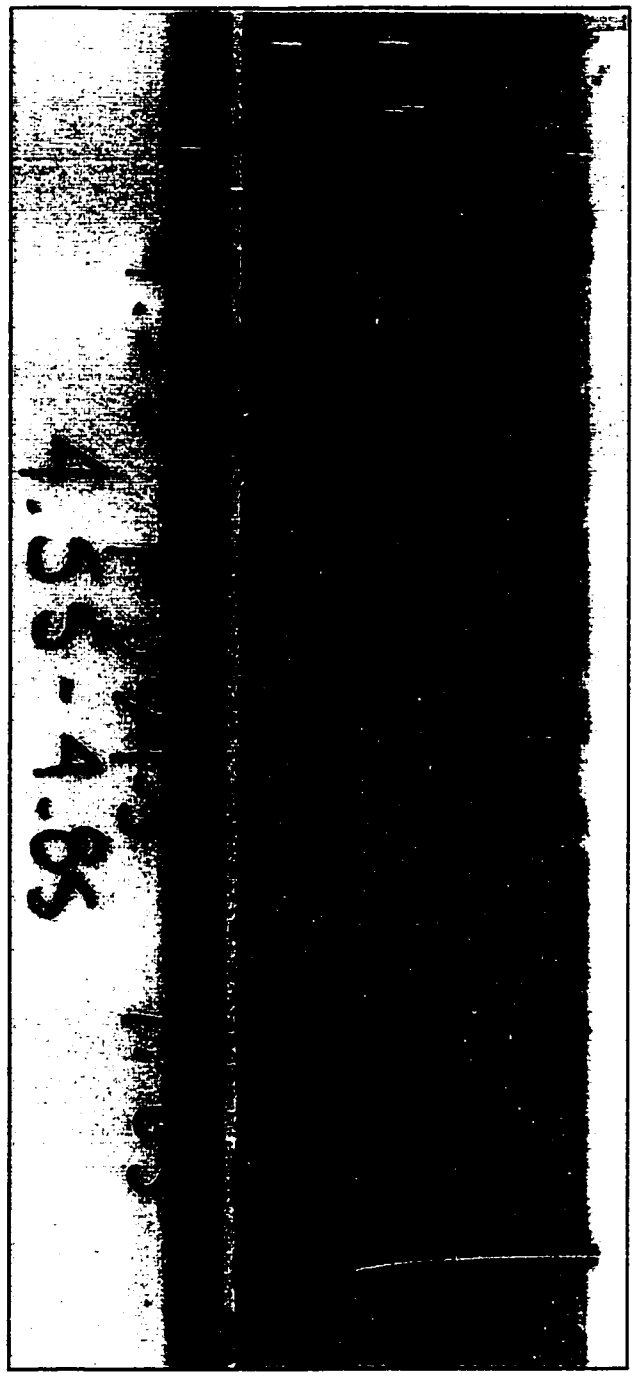

Figure 6-23. Core photograph of of the interbedded sand and silt facies, thick subfacies. Note truncated silt laminae, silt clasts, and mud-draped ripples. FD94-5, CPT depth 4.55 to 4.85m. See Figure 6-24.

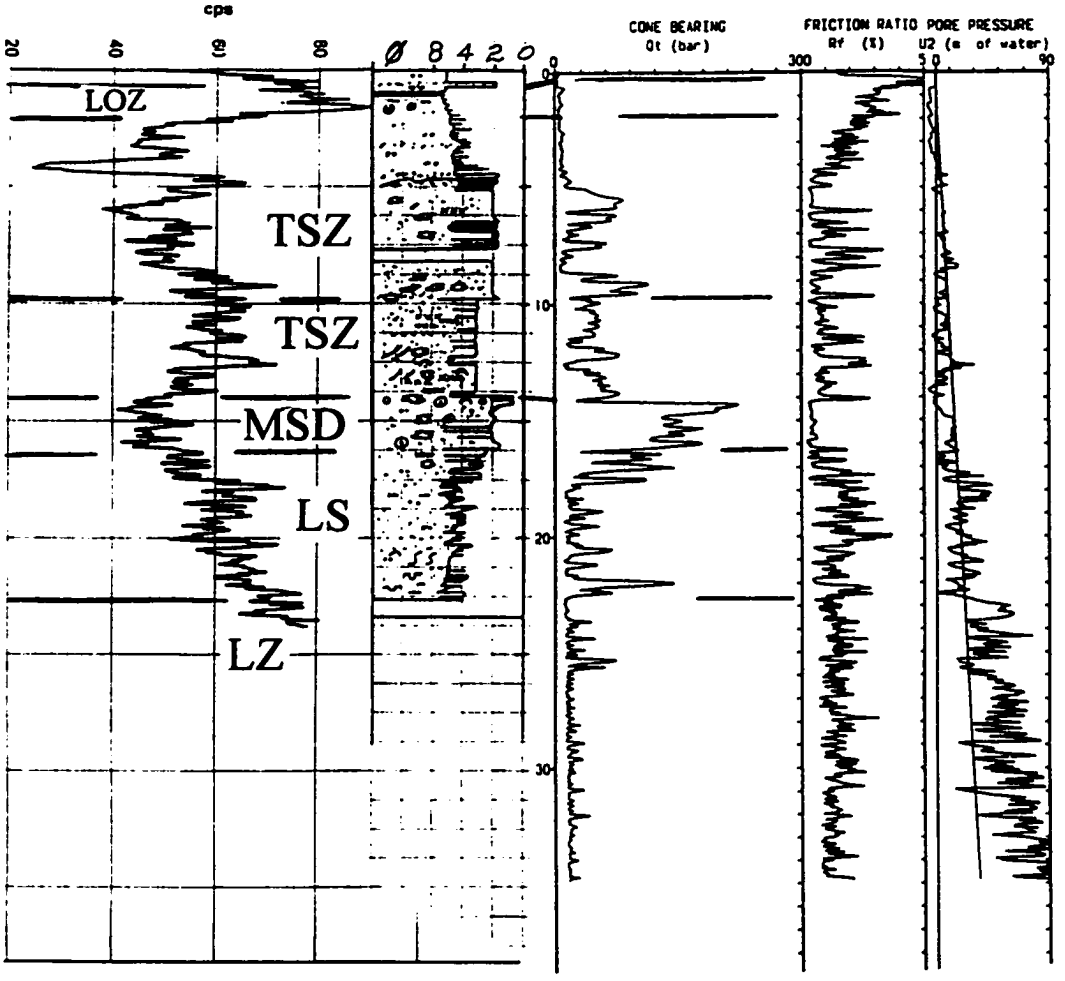

Figure 6-24. Composite log of borehole FD94-5, showing the thick subfacies of the interbedded sand and silt facies (TSZ). From left to right; gamma ray log, in counts per second (cps), lithology log; and CPT data (q_t, R_f and U). The TSZ has two subunits here; the part between 5 and 10 m is shell-free, and the part below is shell bearing. Note the distal subfacies of the massive sand facies (MSD); at this site, the lower part has a serrate friction ratio, and the sand coarsens upward to a coarse sand with clasts of silt and cemented sand (Figure 5-13). For facies symbols, see Table 6-1.

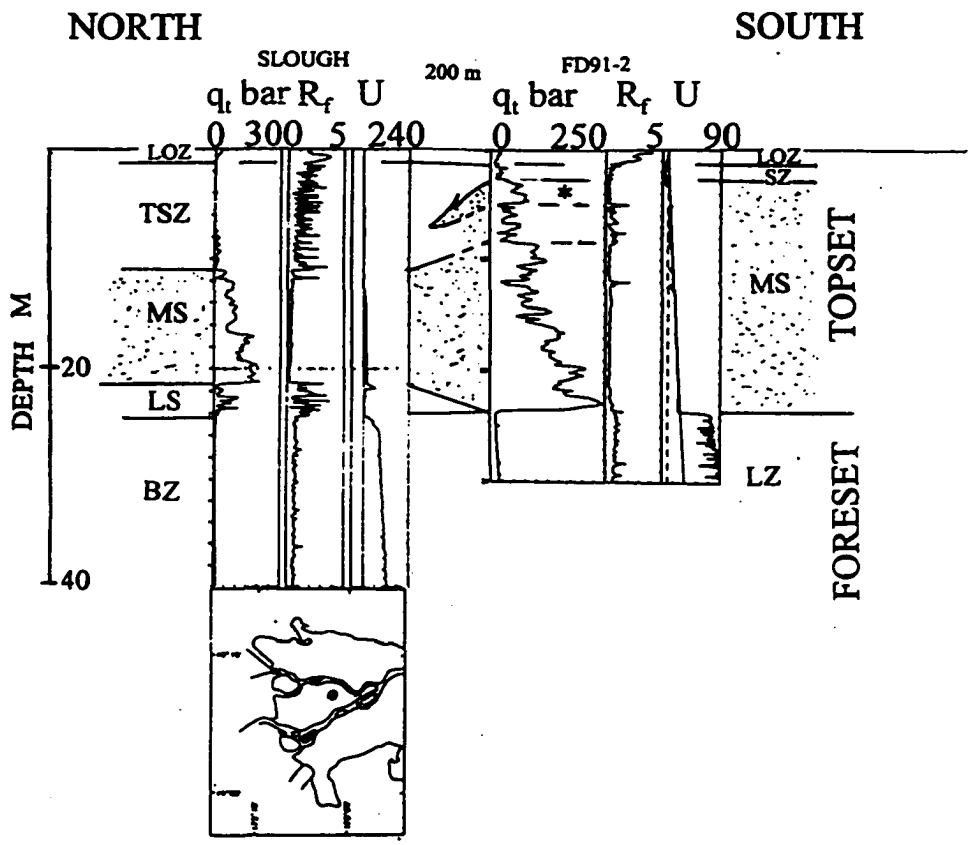

Figure 6-25. North-south CPT cross section at a site in the gap in the peat bogs in Lulu Island (#7 Rd. and Highway 91), showing the thick subfacies of the interbedded sand and silt facies (TSZ) laterally replacing the upper part of the massive sand facies (MS), which is mainly in the shell-free subfacies here (from field notes by J. Luternauer). TSZ underlies the course of a modern slough (an un-named branch of Bath Slough; see Township of Richmond, undated), and represents partially abandoned channel fill. Note the sharp-based sand in the upper part of MS (*) that is equivalent to the upper part of TSZ, and represents the last stages of active channel fill in the channel associated with the slough. These CPTs demonstrate that the gap in the peat bogs, that has been interpreted as a former upper delta plain distributary (Johnston, 1921; Clague et al., 1983), is underlain by both active and abandoned channel fill deposits. Note also erosional base of MS and that foreset is in transition between the laminated silt (LZ) and the bioturbated silt facies (BZ). For facies symbols, see Table 6-1. R_f in % and U in metres of water.

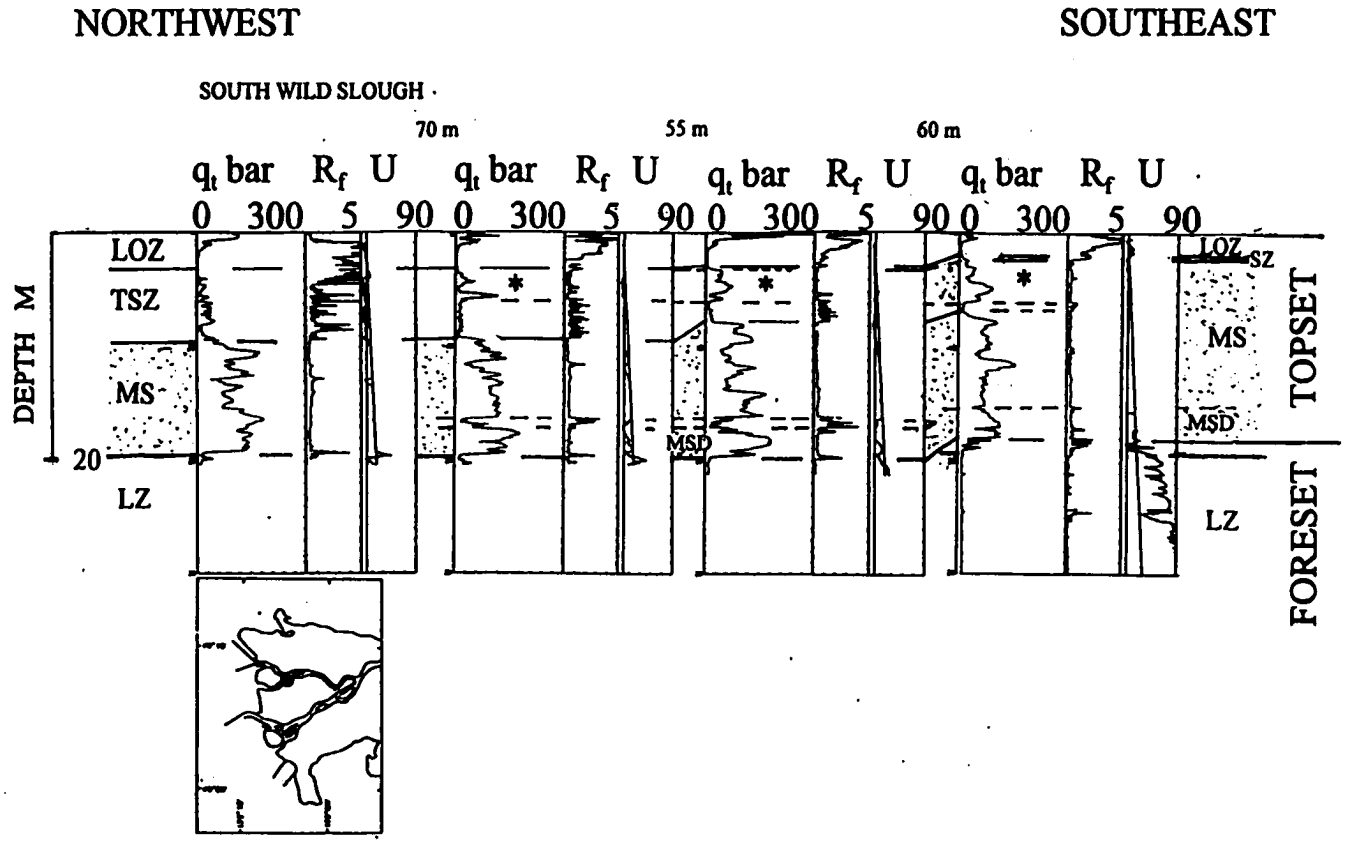

Figure 6-26. Northwest-southeast CPT cross section showing the thick subfacies of the interbedded sand and silt facies (TSZ) laterally replacing the upper part of the massive sand facies (MS). Note that TSZ underlies the course of a modern slough (South Wild Slough; see Township of Richmond, undated), and represents partially abandoned channel fill. Note the sharp-based sand (*) that can be traces from the upper part of MS into TSZ, and represents the last stages of active channel fill in the channel associated with the slough. Note the local presence of the distal subfacies (MSD) at the base of MS. For facies symbols, see Table 6-1. R_f in % and U in metres of water.

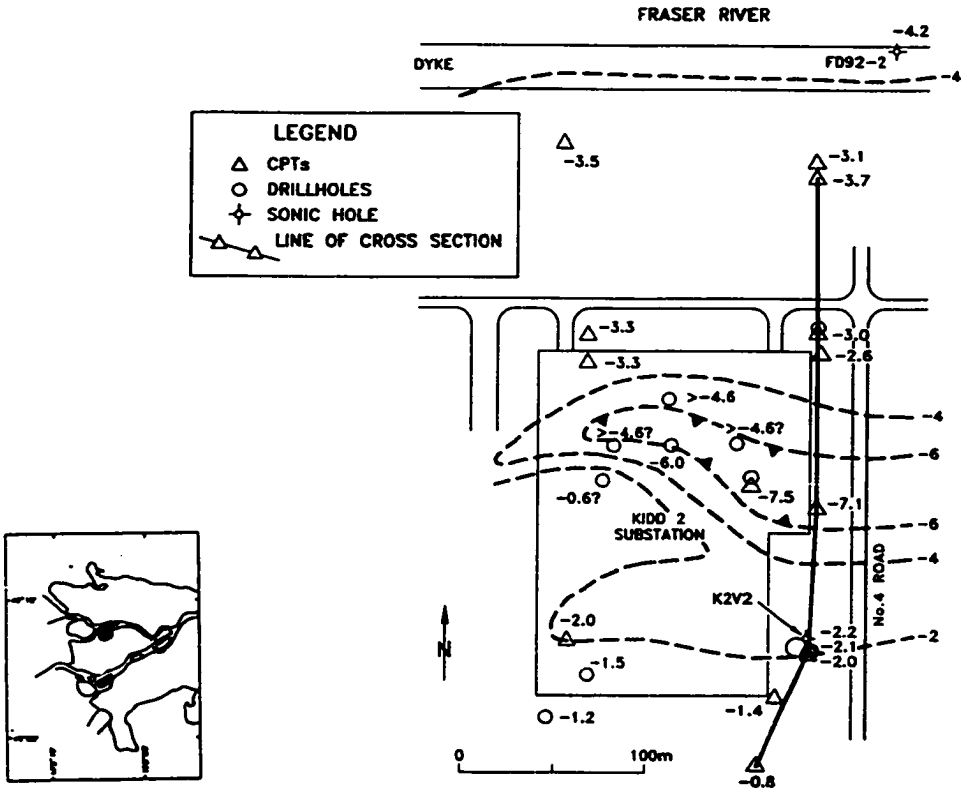

Figure 6-27. Structure contour map on the base of the interbedded sand and silt facies in the vicinity of K2V2, on the northern margin on the delta.. Where this contact is deeper than -5m, the interbedded sand and silt facies is in the tick subfacies. The line of cross section shown in Figure 6-21 is shown on the map.

MASSIVE SAND FACIES

General Description

The massive sand facies dominates the topset. It is generally 8 to 30 metres thick, has a sharp base and gradational top (Figures 6-1 to 6-5), and consists of fine to medium sands that are moderately well sorted and contain less than 5% fines. This facies appears massive in core, but high angle planar cross bedded intervals occur (Figure 6-28). Silt laminae and thin to medium beds of laminated silt and sand occur rarely. This facies is commonly organized into one or more decametre-scale sharp-based fining upward sequences (Figures 4-5, 5-18, 5-21, 6-16 and 17; Monahan et al., 1993a, b, c, 1995; 1997). Although grain size varies on a metre scale, the coarsest sands are generally at the bases and silt interbeds occur most commonly towards the tops of the fining upward sequences. Silt and clay rip-up clasts occur commonly, and a fine gravel component also occurs, particularly near the base of fining-upward sequences (Figure 6-29). Organic laminae occur singly or in laminated beds with both sands and silts.

On CPT data this facies is characterized by low uniform friction ratio (<1%), high cone bearing (q_t 30 to 250 bar, q_{c1} 30 to 200) and dU either near zero or negative (Figures 4-5, 5-18, 5-21, 6-16, 6-17 and 30). Where this facies overlies silt in the foreset, the sharp base can be readily observed on CPT data by abrupt upward increase in cone bearing, decrease in dU from positive to near zero or negative, and decrease in friction ratio (Figures 4-5, 5-18, 5-21, 6-1, 6-21). Commonly, a friction ratio peak occurs at the contact, as discussed in the previous chapter (Figures 5-29a, b and 6-4). Where this facies overlies sands of the foreset, the sharp base can usually be identified on the pore pressure and friction ratio curves by an abrupt upward change from strongly negative dU and a serrate friction ratio in foreset sands, to dU near zero and a uniform friction ratio in the massive sand facies (Figures 5-15, 6-2, 6-16 and 6-30). However, some clean sands in the foreset can also have low uniform friction ratios and dU near zero (Figure 6-7), and negative dU occurs locally at the base of the

massive sand in some CPTs (e.g. Figure 5-16), so that identification of the base of the massive sand facies is in a few cases interpretive.

The sharp base of this facies is erosional. This contact has several metres of local relief across some sites (Figure 6-21), and truncates bedding of the foreset (Figures 6-6 and 6-31).

Grain size variations in sands in this facies generally correspond to cone bearing variations, and the silt interbeds are represented by cone bearing minima, friction ratio peaks and either negative or positive dU depending on whether they are sandy or finer silt. Consequently, the decametre-scale fining upward sequences are reflected by a general upward decrease in cone bearing (Figures 5-18, 5-21, 6-4, 6-13, 6-16, 6-17 and 6-21), and may be gradationally overlain by thin intervals with high friction ratios where the sequences are capped by silt or interbedded silt and sand. Similarly, cone bearing decreases and friction ratio increases upward into the gradationally overlying interbedded sand and silt facies. In some cases upward fining in the massive sand facies is also reflected in an upward increase in the number of silt interbeds, indicated by high friction ratios and a change from dU near zero to negative dU (Figure 5-21).

Meter-scale fining and coarsening upward sand sequences also occur, and are represented by cone bearing decreasing and increasing upward sequences respectively. The coarsening upward sequences in this facies commonly occur near the top (Figures 5-16, 5-18, 6-13 and 6-19). Other cone bearing increasing upward sequences associated with increasingly negative dU occur and are related to upward increases in density rather than grain size (Figures 5-18 and 6-13).

CPT cross sections indicate that this facies varies considerably across a site. Individual beds can rarely be correlated more than a few metres, and even the decametre-scale fining upward sequences cannot be correlated more than a few tens of metres (Figure 6-21). In some cases, silt laminae occur at different depths in the cores and the offsetting CPTs, indicating that

these horizons are dipping (Figure 6-30).

Thickness, Distribution, Relationships to Other Facies and Age

The massive sand facies underlies almost all of the upper delta plain and extends beneath parts of the tidal flats and subaqueous platform (Figures 6-1 to 6-3). In a general way, the base of the massive sand facies climbs westward across the upper delta plain (Figures 2-5 and 6-1).

The facies has a maximum thickness of 40 m at the head of the delta on Annacis Island, where it comprises most of the topset (Figures 2-3 and 6-1; Monahan et al., 1993a, b, c). There, the upper part laterally replaces the thick accumulations of the laminated and organic silt facies nearby on eastern Lulu Island. Locally in this area, a unit of the massive sands overlies the laminated and organic silts and thickens downward to merge with deeper massive sands to form the very thick accumulations of the massive sand facies on Annacis Island (Figure 6-10). Similar relationships occur on the north shore of Lulu Island (Figure 6-15).

The massive sand facies exceeds 20 m in thickness at several sites along the south shore of the Main Channel east of Ladner and in the central part of the upper delta plain (Figure 6-1). Elsewhere on the upper delta plain, it is 8 to 20 m thick. Where the base of the sand facies rises sharply to the west in the central part of the upper delta plain, the lower part is laterally replaced by the low dipping interbedded sand and silt facies of the foreset (Figures 6-1 and 6-32).

The massive sand facies extends approximately halfway across Sturgeon Bank (Figures 6-1 and 6-33), and to the western edge of the tidal flats at Roberts Bank port at the southern end of Roberts Bank (Figures 6-3 and 6-6). It is not present along much of the outer margin of

the tidal flats. At its distal margins, the thickness of the massive sand facies is generally less than 6 m.

On the delta margins, where the entire deltaic section is less than 20 m thick, the massive sand is locally absent and the entire deltaic section consists of silt: laminated and organic silt at the head of the delta (Figure 6-14), and possibly the thick interbedded sands and silt at sites along the North Arm (Figure 6-34).

The massive sand facies is diachronous. Near the head of the delta on eastern Lulu Island, where it underlies thick accumulations of the laminated and organic silt facies and occurs between elevations of -13 and -30 m, the massive sand facies is older than 7960±140 ^{14}C years B.P.[5] (Figures 6-1 and 6-10; Appendix F; Williams and Roberts, 1989). At the western margin of the upper delta plain, where it occurs between depths of -3 and -20 m, it includes material dated at 1940±50 (TO-4148) to 3670±50 (TO-4149) ^{14}C years B.P. (Figures 4-5 and 6-1, FD93-3; Appendix F). Younger dates occur in sands elsewhere on the upper and lower delta plain (Figure 6-35).

5

^{14}C date on organic detritus in overlying laminated and organic silt facies (GSC4255; Williams and Roberts, 1989).

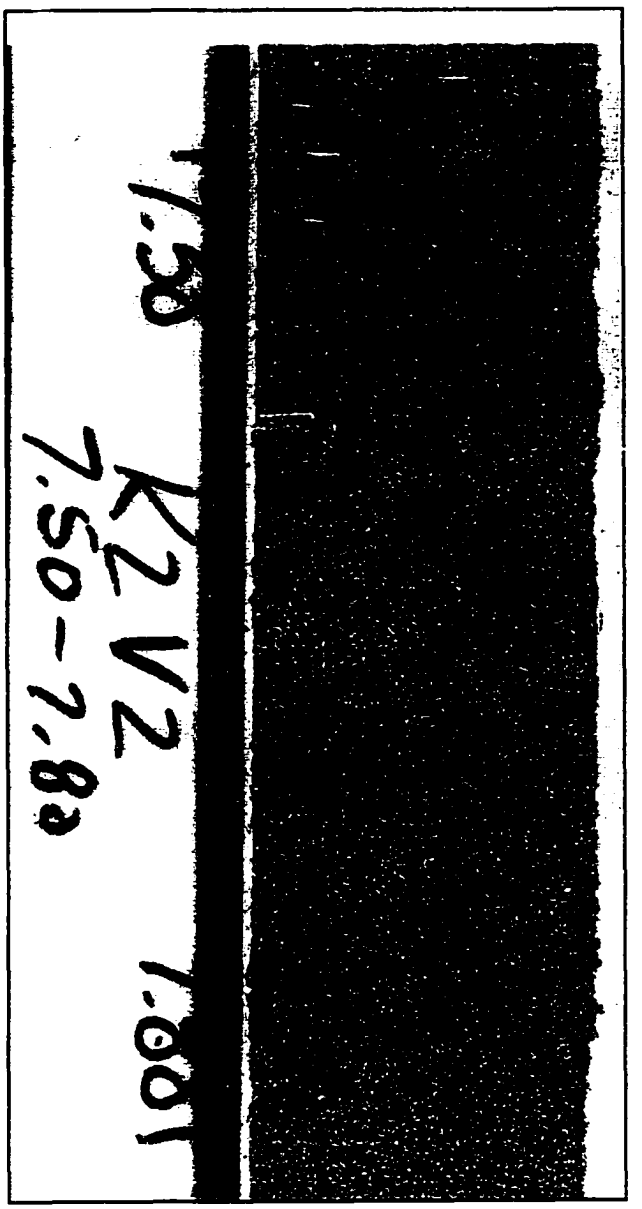

Figure 6-28. Core photograph of massive sand facies, shell-free subfacies. Note cross bedding. Borehole K2V2, CPT depth 7.50 to 7.80 m. See Figure 6-21. From Monahan et al. (1997).

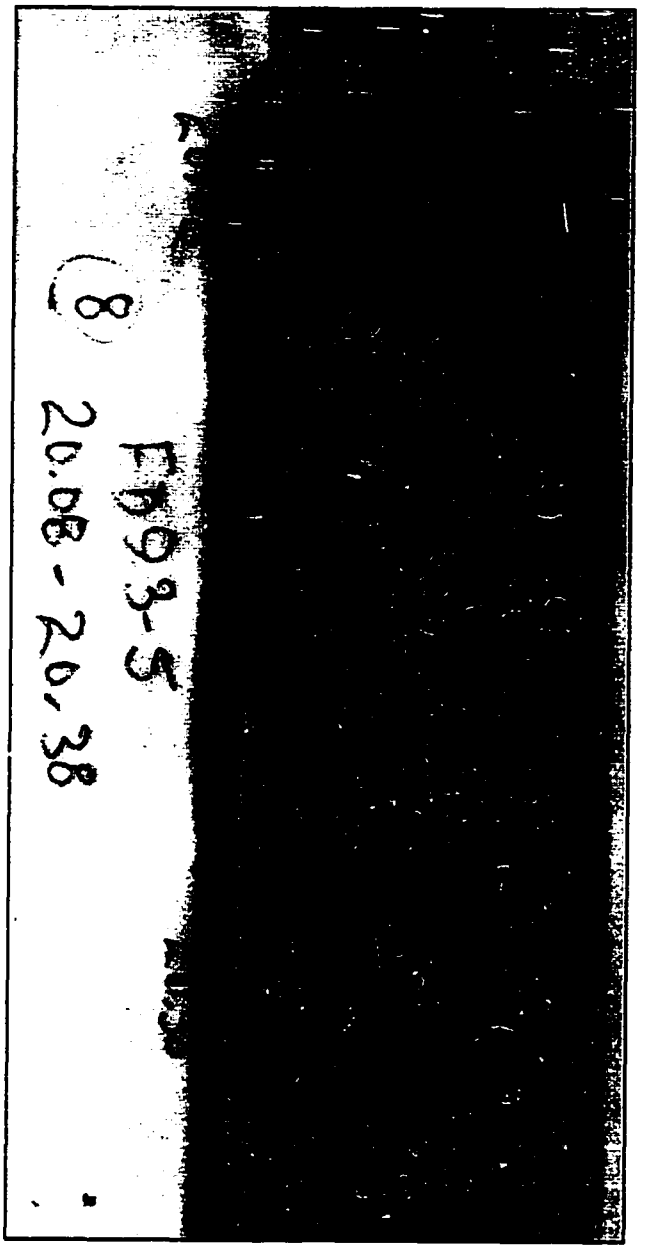

Figure 6-29. Core photograph of the massive sand facies, shell-bearing subfacies, shell- and clast-rich interval. FD93-5, CPT depth 20.15 to 20.45. See Figures 5-15, 6-3 and 6-30. Note similarity to shell- and clast-rich interval in sharp-based sand of foreset in Figure 6-47b. Also reproduced in Clague et al. (1998).

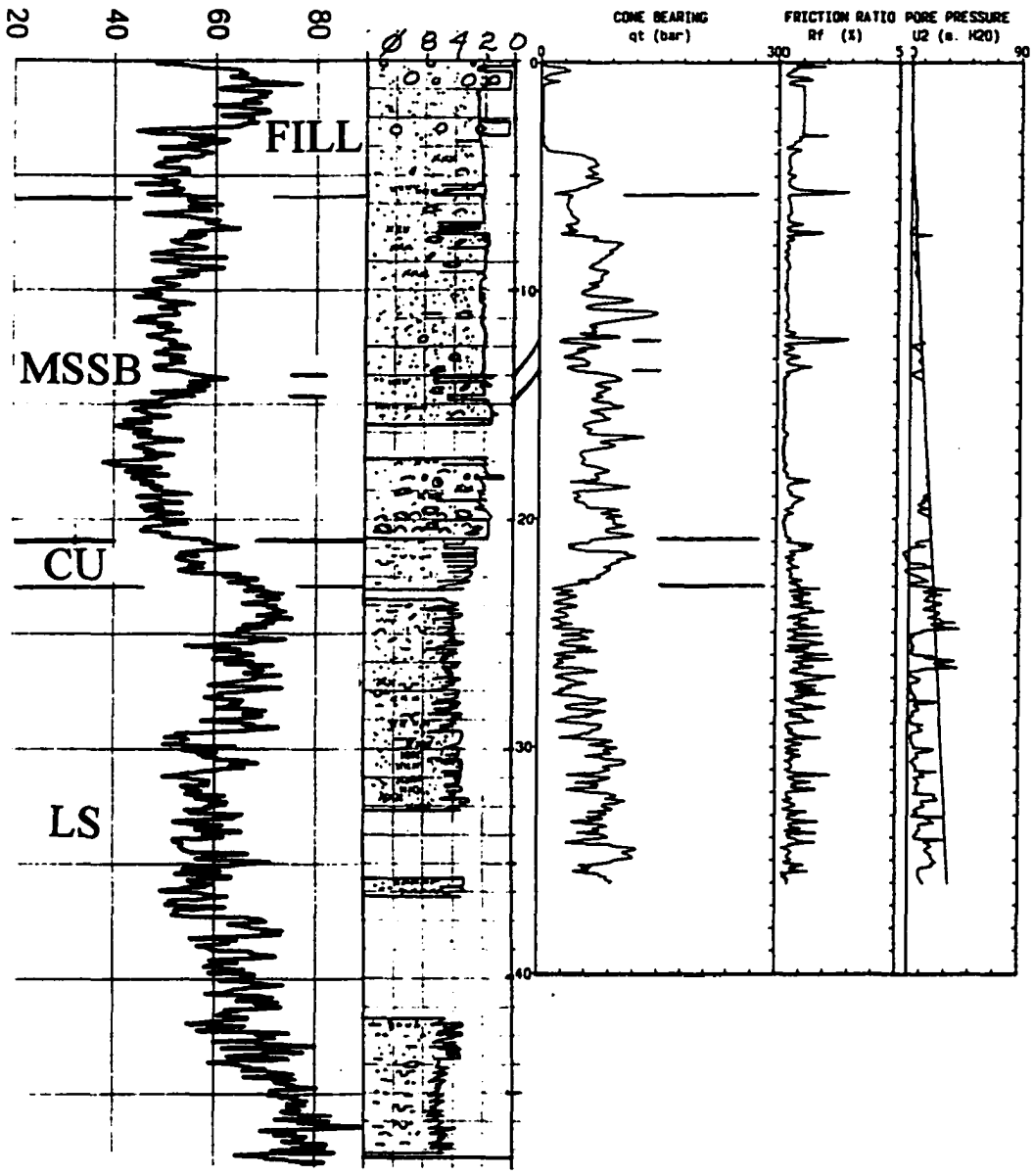

Figure 6-30. Composite log of FD93-5. From left to right; gamma ray log, in counts per second (cps), lithology log; and CPT data (q_t, R_f and U). Silt interbeds in the massive sand facies (shell-bearing subfacies - MSSB) are dipping and occur at different depths in the borehole and CPT (2 m away). The sharp base of MSSB is marked by an abrupt change in excess pore pressure, from strongly negative (U less than hydrostatic) in the thick coarsening upward sand facies (CU) of the foreset to near zero (U near hydrostatic) in MSSB; and that the friction ratio curve is serrate in CU and low and uniform in the MSSB. In core, the sharp base of MSSB is erosional, truncating laminae in the underlying foreset deposits (Figure 6-31). The cone bearing increasing upward sequence in CU corresponds to a sandy coarsening upward sequence, in its lower part. However, grain size peaks near the middle of the sequence, and the continued upward increase in cone bearing reflects increased density (Figure 5-15). This CPT is also shown in Figure 6-3. For facies symbols, see Table 6-1.

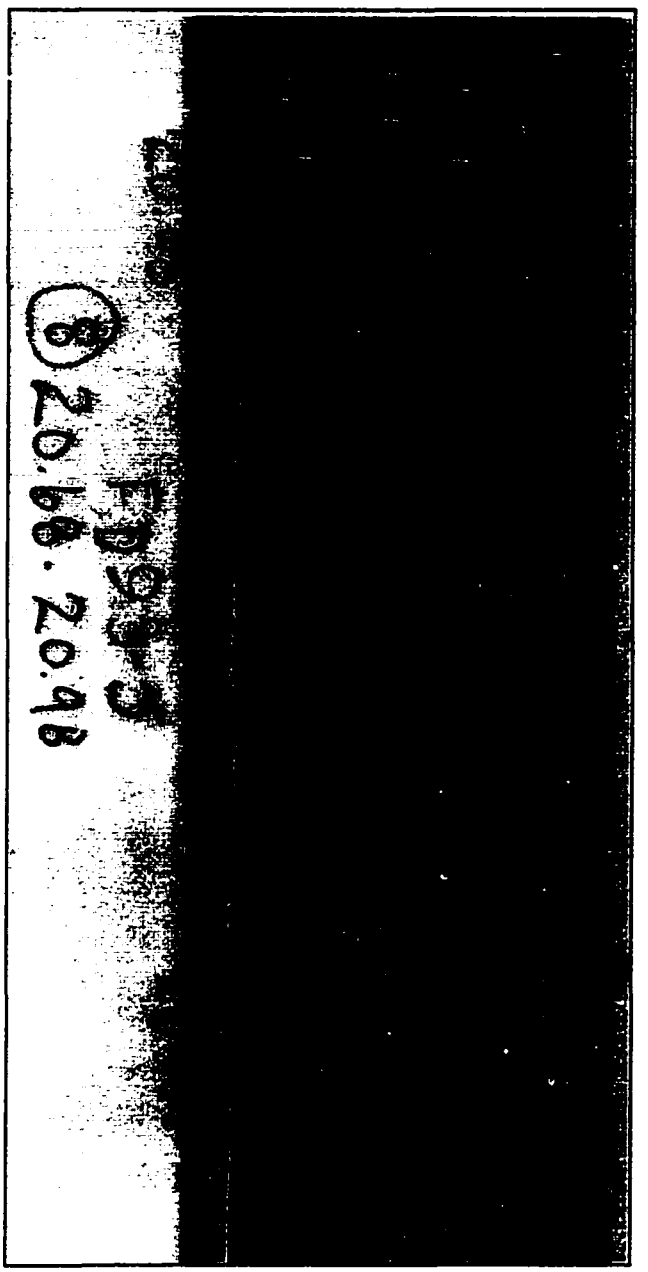

Figure 6-31. Core photograph of the contact between the massive sand facies (shell-bearing subfacies) of the topset and laminated very fine sands and silts of the foreset. Note sharp erosional contact, truncating laminae in the foreset sands and silts, and graded laminae of the foreset. This contact is marked on CPT data by a sharp change from negative dU in the foreset sand and silt, to dU near zero in the massive sand facies (Figure 5-15 and 6-30). FD93-5, CPT depth 20.75 to 21.05 m. Also reproduced in Clague et al. (1998).

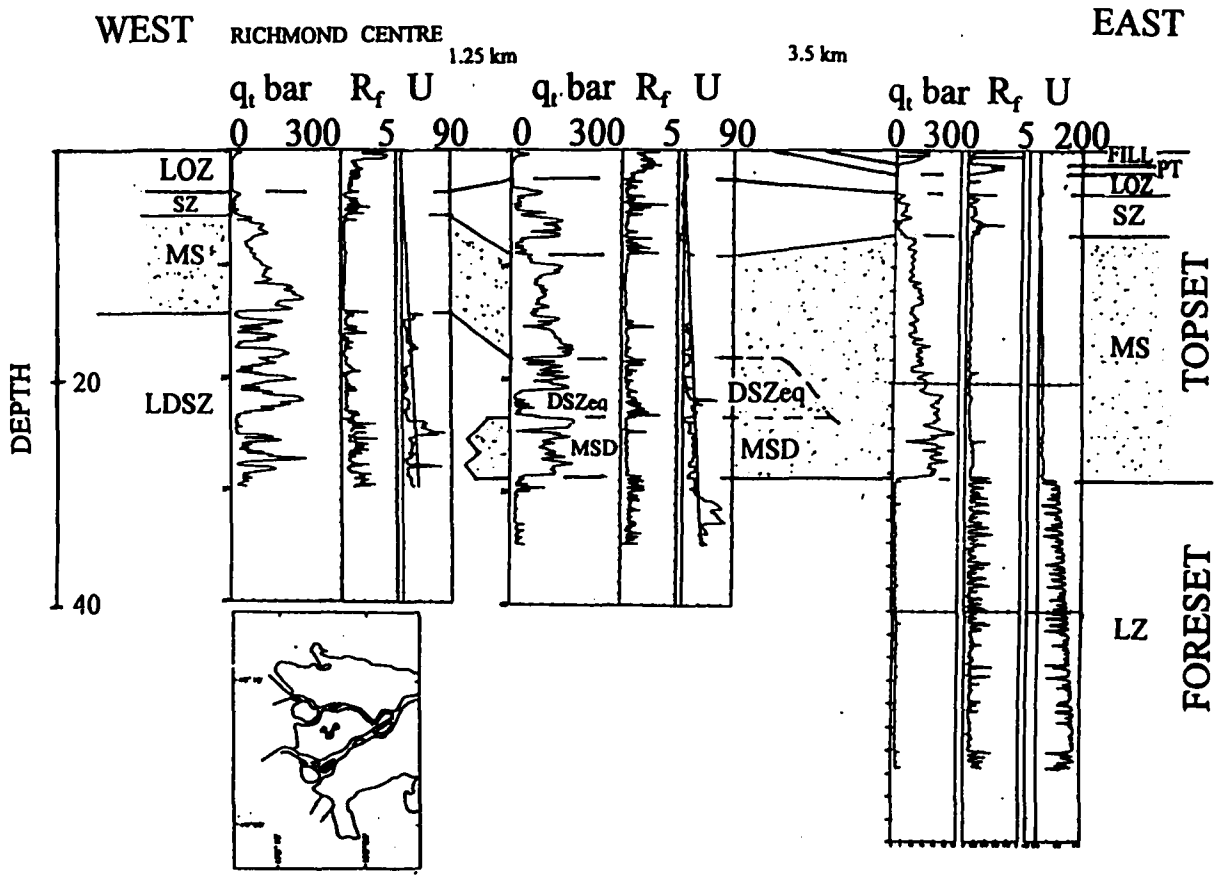

Figure 6-32. East-west CPT cross section in the centre of the delta pain showing the low dipping interbedded sand and silt facies (LDSZ) of the foreset laterally replacing the lower part of the massive sand facies (MS) of the topset to the west. Note the presence of the distal subfacies of the massive sands (MSD), including the distal sand and silt equivalent (DSZeq). Westernmost CPT is also shown in Figure 6-12. For facies symbols, see Table 6-1. R_f in % and U in metres of water.

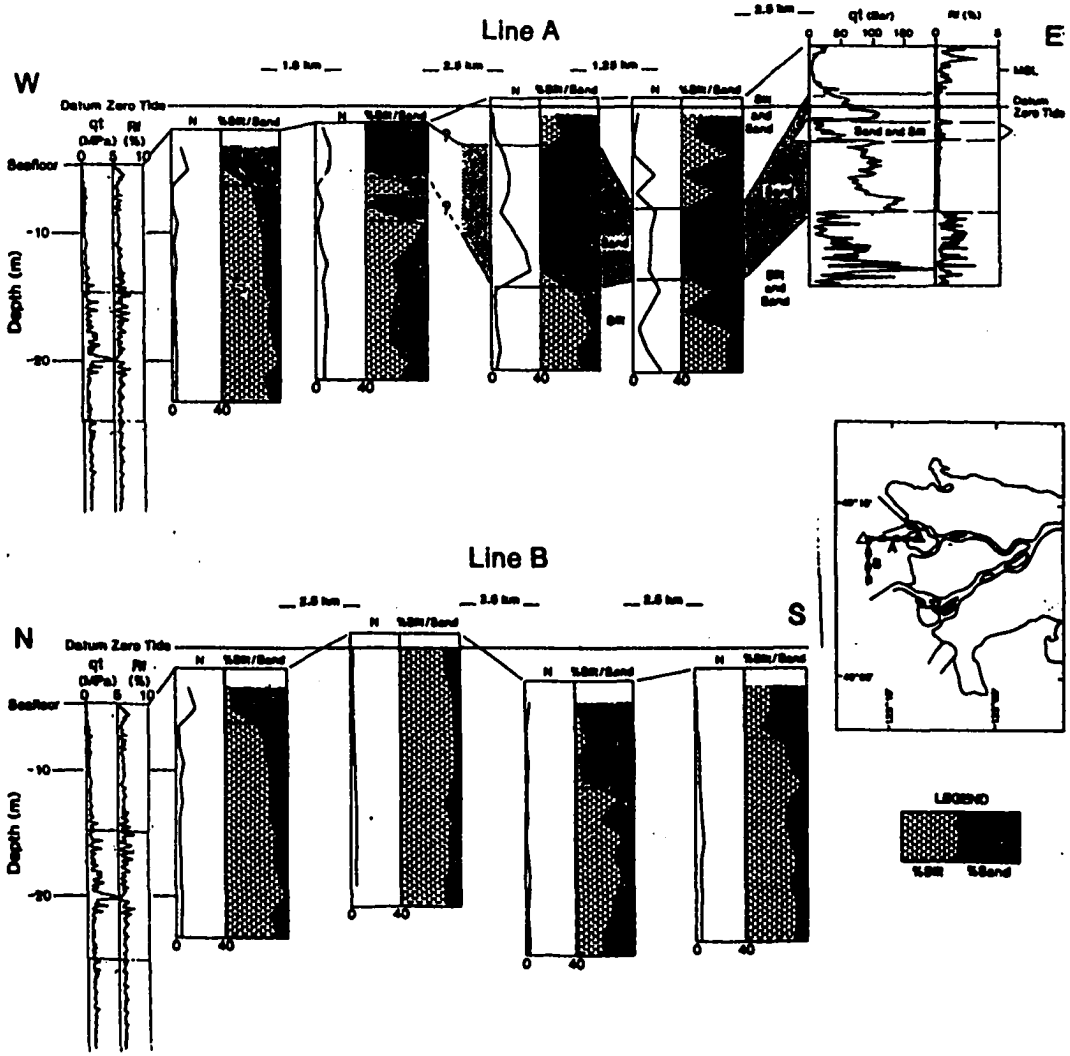

Figure 6-33. CPT and standard penetration test (SPT) cross sections across the tidal flats and subaqueous platform of Sturgeon Bank. Shown at each SPT are the blowcount "N", which is comparable to the CPT cone bearing and the proportion of silt and sand. Note that the massive sand facies of the topset (stippled) can be traced only part of the way across the tidal flats. It is absent on the outer margin of the delta platform (Line B). The CPT on the subaqueous platform is also shown in Figure 6-1; foreset deposits in this CPT are in the laminated silt facies. From Monahan et al. (1993c).

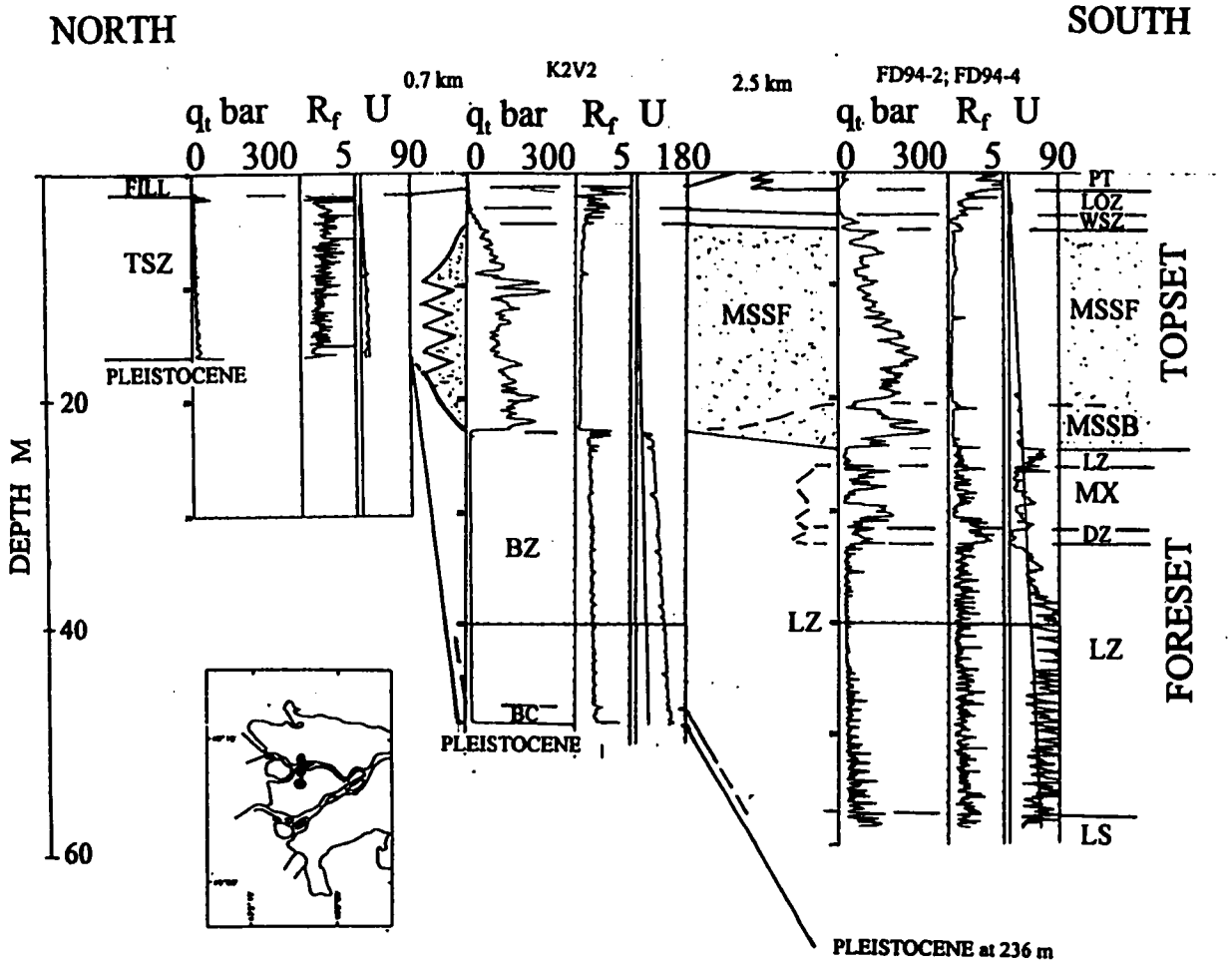

Figure 6-34. North-south CPT cross section from the centre to the northern margin of the delta. Note that the upper foreset is composed primarily of the laminated silt facies (LZ) at boreholes FD94-2 and FD94-4, but it is replaced by the bioturbated silt facies (BZ) along the northern margin of the delta. Note also the interbedded silt and sand in the northernmost CPT, interpreted to be the thick subfacies (TSZ) of the interbedded sand and silt facies. The CPT on the right is also shown in Figure 6-4, and the middle CPT is shown in Figure 6-21. For facies symbols, see Table 6-1. R_f in % and U in metres of water.

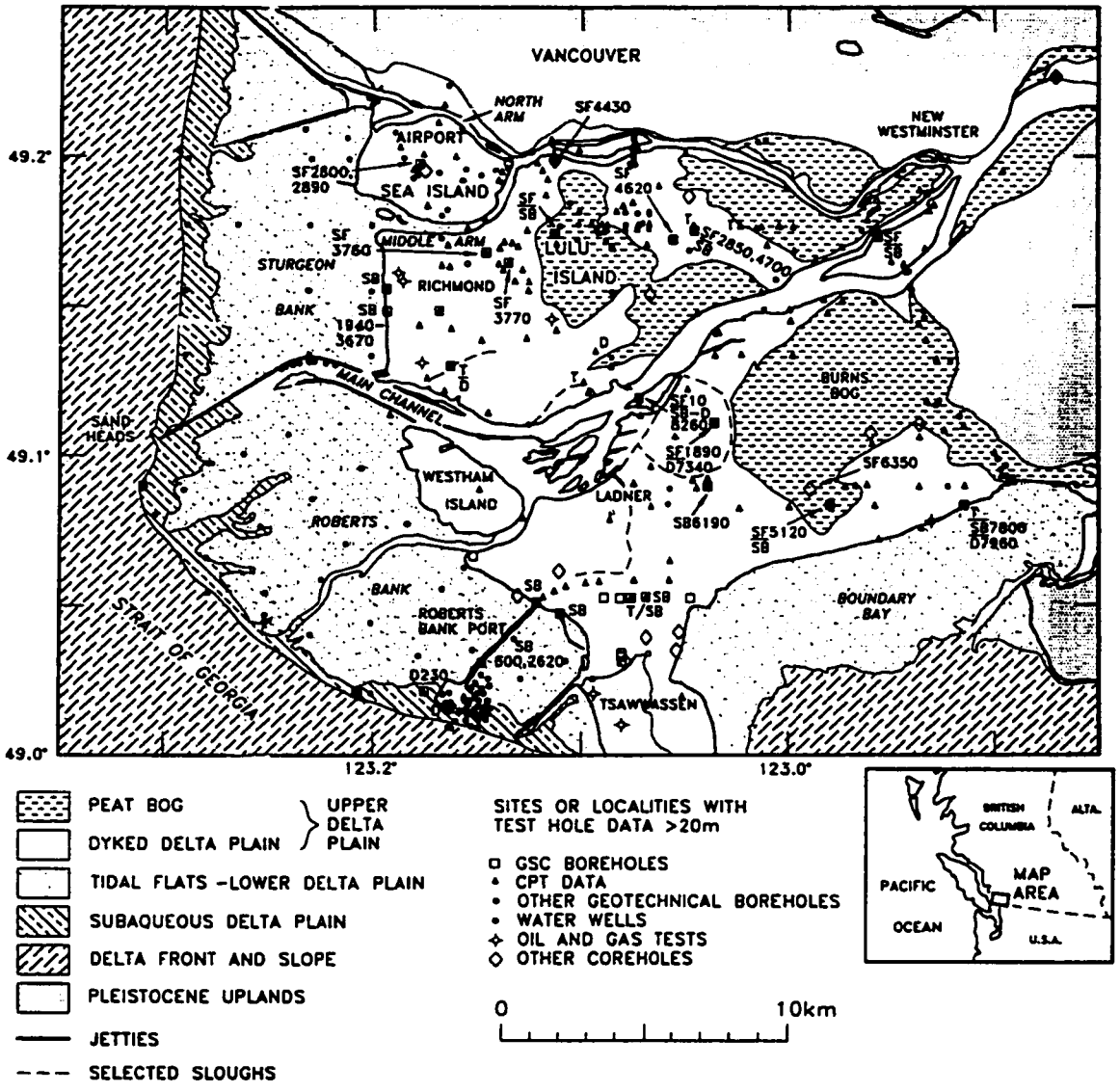

Figure 6-35. Map showing subfacies and ^{14}C dates in the massive sand facies of the topset. See Appendix F for details of ^{14}C dates.

SF - shell-free subfacies

SB - shell-bearing subfacies

D - distal subfacies

T - thick subfacies of the interbedded sand and silt facies

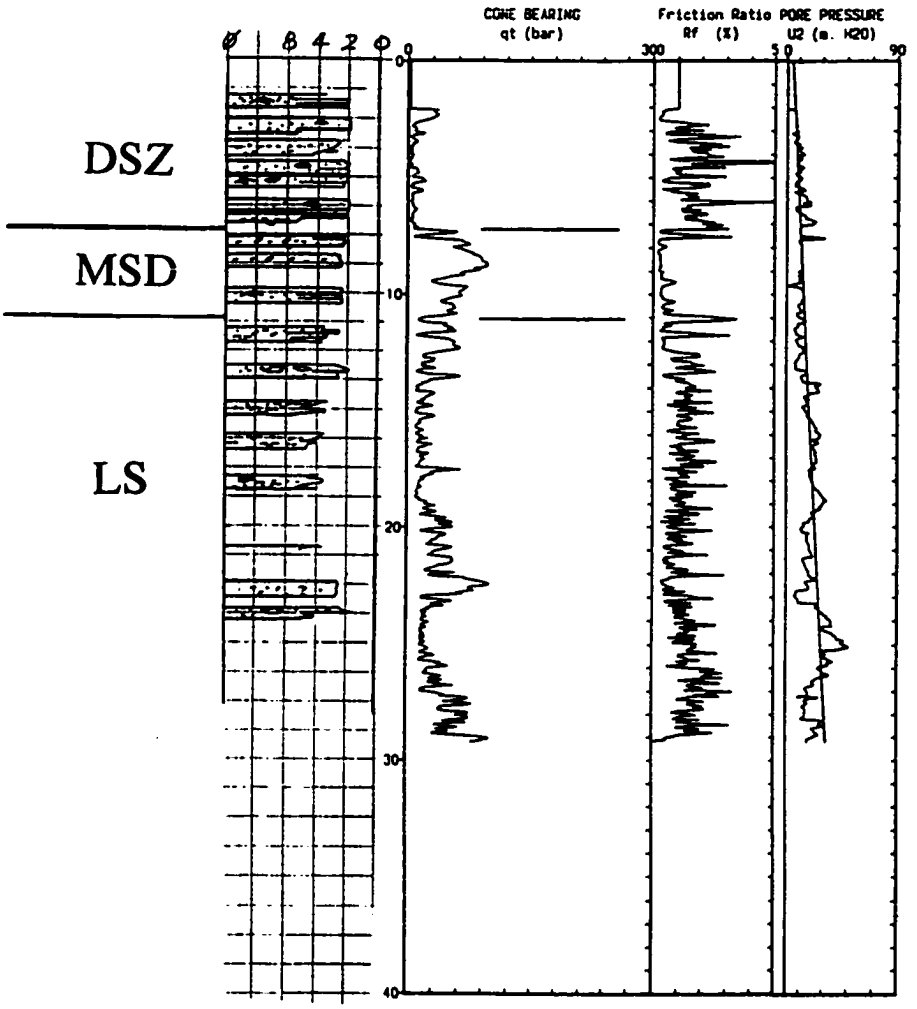

Figure 6-36. Composite log of BHFD93S-1, showing the most distal variant of the distal subfacies of the massive sand facies (MSD). From left to right; lithology log; and CPT data (q_t, R_f and U). Note that the lower pat of MSD has a more serrate friction ratio and lower cone bearing than the upper part. A nearby CPT with resistivity measurements indicates that the upward increasing cone bearing reflects increasing density. For facies symbols, see Table 6-1.

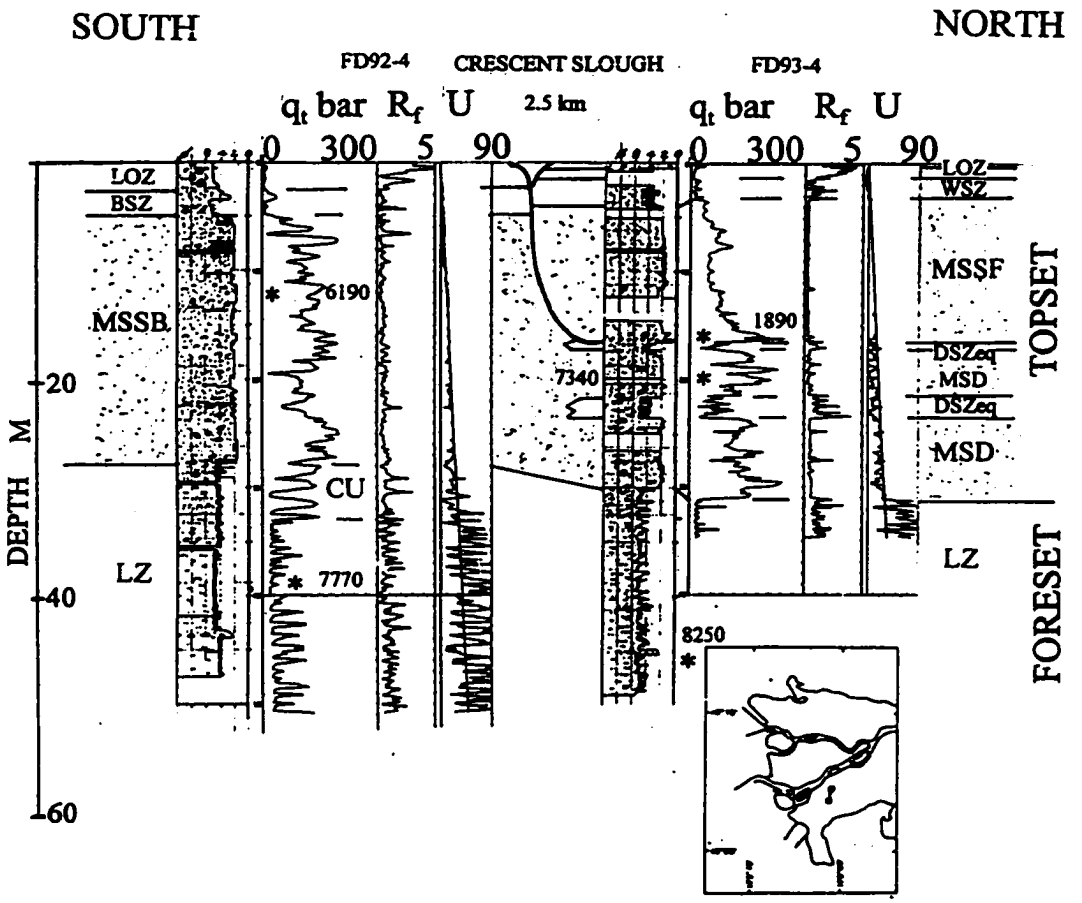

Figure 6-37. North-south CPT cross section across Crescent Slough, an arcuate slough northeast of Ladner (Figure 6-35). Note ^{14}C dates (*; see Appendix F). Note in FD93-4, in the area enclosed by the slough, the upper part of the massive sand facies is the shell-free subfacies (MSSF) and is overlain by the well bedded subfacies of the interbedded sand and silt facies (WSZ). In FD92-4, outside of the area enclosed by the slough, the massive sand facies is in the shell-bearing subfacies (MSSB), is older and has higher cone bearing than the laterally equivalent MSSF in FD93-4, and is overlain by the bioturbated subfacies of the interbedded sand and silt facies (BSZ). Note that the lower part of the massive sand facies in FD93-4 consists of stacked sands of the distal subfacies (MSD) interbedded with the distal sand and silt equivalent (DSZeq). The base of the massive sand facies in FD93-4 is ~1 m shallower than in the CPT, 2 m away (Figure 6-17). FD92-4 is 65 m from the CPT. Note that the thick coarsening upward subfacies occurs in the CPT but is not evident in the borehole. For facies symbols, see Table 6-1. R_f in % and U in metres of water.

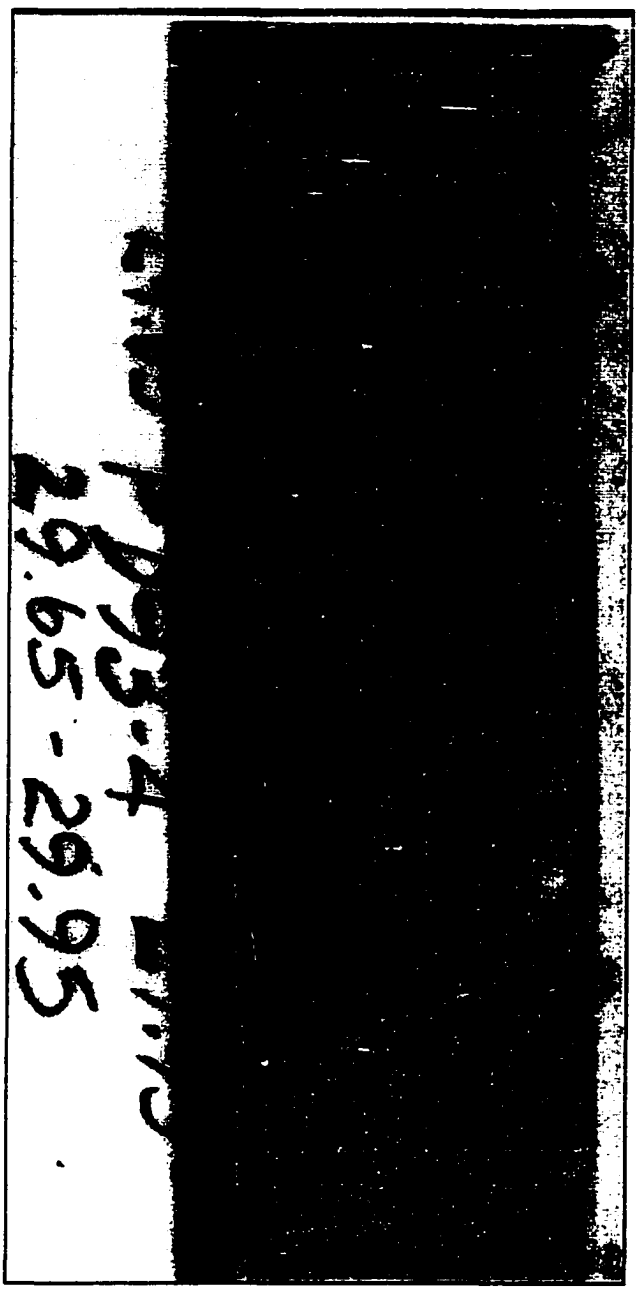

Figure 6-38. Contorted contact of the massive sand facies (distal subfacies) and underlying foreset silts. This contact is ~1 m shallower on the gamma ray log in the borehole than on the CPT, 2 m away (Figure 6-37). Higher markers in this subfacies do not show the same differnces in depth on the gamma ray log and CPT. FD93-4, corrected core depth 29.75 to 30.05 m.

Subfacies of the Massive Sand Facies

Three distinct subfacies can be recognized. The first ("shell-free subfacies") contains no shells and is overlain by the well bedded subfacies of the interbedded sand and silt facies. Silt interbeds in this facies are well bedded and laminated, and include fine to very fine sand laminae. Coarse beds at the base of the decametre-scale fining upward sequences include wood fragments as well as gravel and silt clasts. This subfacies occurs in boreholes on the upper delta plain and in the floodplain upstream of the delta. The second subfacies ("shell-bearing subfacies") contains bivalve shells, commonly whole single valves, and is overlain by either the bioturbated subfacies of the interbedded sand and silt facies or by the shell-free subfacies of the massive sands. Although shells occur at all depths in this subfacies, they are commonly concentrated in clast-rich intervals, particularly near the base (Figure 6-29). Some silt laminae in sands occur as couplets. Although laminated silts like those in the shell-free subfacies also occur in this subfacies, some thin silt interbeds in this subfacies are finer, clayey silts, and lack internal laminae. This subfacies occurs in boreholes in the lower as well as the upper delta plain. Cores are required to distinguish the shell-free and shell-bearing subfacies - they cannot be distinguished on the basis of the CPT data alone. However, the shell-bearing facies can be recognized commonly in geotechnical boreholes, where shells are commonly reported. Generally, the grain size ranges of the shell-free and shell-bearing subfacies are similar. However, coarser sands locally occur in the shell-free subfacies.

In the western part of the upper delta plain, the shell-bearing and shell-free subfacies occur separately (Figure 6-35). However, in thicker developments of this facies in the central and eastern parts of the upper delta plain, the shell-free subfacies commonly overlies the shell-bearing subfacies. Where the subfacies are stacked, the shell-free subfacies is up to 20 m thick, coincides with one or more of the decametre-scale fining upward sequences as described above, and is markedly younger than the shell-bearing subfacies. For example, on at FD94-1 on Deas Island, dates from enclosed organic material in the shell-free and shell-

bearing subfacies are 10±60 (TO- 4374) and 8260±80 (TO-4595) ^{14}C years, respectively (Figure 6-13; Appendix F). As discussed in the prceding chapter, cone bearing in the older deposits is higher for sands of comparable grain size, and dU is more negative, providing a means to distinguish older from younger deposits on CPT data. Elsewhere, the shell-free subfacies is younger than nearby occurrences of the shell-bearing subfacies at comparable depths, based on ^{14}C dates of enclosed materials (Figures 6-35 and 6-36). The shell-free subfacies forms the top of the massive sand in much of northwest Lulu Island. It is present beneath the linear gap in the peat bogs, and extends west beneath parts of the adjacent peat bogs (Figure 6-4), along the North Arm of the Fraser River (Figure 6-21) and across central Richmond (Figure 6-16).

The third subfacies ("distal subfacies") consists of the thin occurrences of the massive sand facies (<6 m) that occur at the outer margins of the tidal flats and subaqueous platform. There, it has been observed in cores and numerous CPTs in the vicinity of Roberts Bank port and is overlain by the distal subfacies of the interbedded sand and silt facies (Figures 6-3 and 6-6). It is shell-bearing, and is in that sense a variant of the shell-bearing subfacies. However, it can be distinguished on CPT data by its lesser thickness. The subfacies consists of 1 or 2 sharp-based fining upward sequences, each indicated on CPT data by upward decreasing dU and increasing and more variable friction ratio. Intervening silt beds are laminated and are locally reverse graded, a feature common in the underlying foreset deposits. In some CPTs in the distal subfacies, cone bearing increases upward, and is associated with increasingly negative dU, indicating upward increasing density rather than grain size[6](Figures 6-4). At its most distal locations, thin silt interbeds occur at the base of the sand: cone bearing is lower, the friction ratio curve changes from uniform to serrate toward the base, and pore pressures are more negative, obscuring the sharp base of the sand on CPT data (Figure 6-36).

6

One of these is a resistivity cone penetration test, and the upward increase in cone bearing can be shown to represent an upward increase in density by an increase in resistivity, according to Archie's Law (Schlumberger, 1989).

In the vicinity of Roberts Bank port, the distal subfacies occurs at elevations of -6 to -15 m (below mean sea level; 3 to 10 m below tide datum). Like the distal subfacies of the interbedded sand and silt facies, it is less than 2000 ^{14}C years old in this part of the delta, and the current depth of this subfacies is similar to the water depths in which they were deposited.

The distal subfacies can also locally be recognized at the base of the massive sand facies in the central and southeastern parts of the upper delta plain (Figures 6-4, 6-13, 6-17, 6-37), where it grades laterally into the shell-bearing facies. In these occurrences, sands of the distal subfacies are directly overlain by a few metres of thin to thick bedded sand and laminated silt. The interbedded sands and silts are similar to the distal subfacies of the interbedded sands and silts, and are designated the "distal sand and silt equivalent" part of the distal massive sands; they include metre-scale coarsening upward sand sequences that grade upward from thin silt beds and are represented by cone bearing increasing upward sequences, and reverse graded laminated silts. The occurrences of the distal subfacies of the massive sand facies in the upper delta plain are between 7340±70 and 8250±100 ^{14}C years old[7], and occur between elevations of -16 and -30 m. Sands of the distal subfacies in this setting have higher cone bearing higher and more negative dU than in younger examples of this subfacies. Furthermore, sand of the distal subfacies in this setting commonly has a sharp top, so that the friction ratio has a blocky shape (Figures 6-17, 6-32 and 6-37). The distal subfacies in this setting may consist of several stacked units of sand and interbedded silt and sand.

In several CPTs where the distal facies of the massive sands overlies silts, cone bearing in the lower metre is about half as much in the sands directly above (Figures 5-29, 6-4, 6-13, 6-17 and 6-37). In one example, the base of the sand in the CPT is about 1 metre deeper than in the borehole (core depth corrected by the gamma ray log), which are within 2 m of

---

7

The age of shells in stacked deposits of the distal subfacies in FD93-4 (Appendix F).

one another (Figure 6-17). The contact in core is contorted and locally overturned (Figure 6-38). These relationships are interpreted to represent a contact deformed and contorted by loading. The low cone bearing at the basal part of the sand is interpreted to reflect the presence of silts nearby at the same elevation due to the loaded contact.

The variant of the distal subfacies in which silt interbeds and a more serrate friction ratio occur toward the base is also preserved on the upper delta plain. In one example[8], it occurs beneath the thick interbedded sand and silt facies (Figures 5-13 and 6-24). This example of the distal massive sands is 2 m thick, coarsens upwards and is capped by a shell- and gravel-rich bed including clasts of silt and sand with calcareous cement.

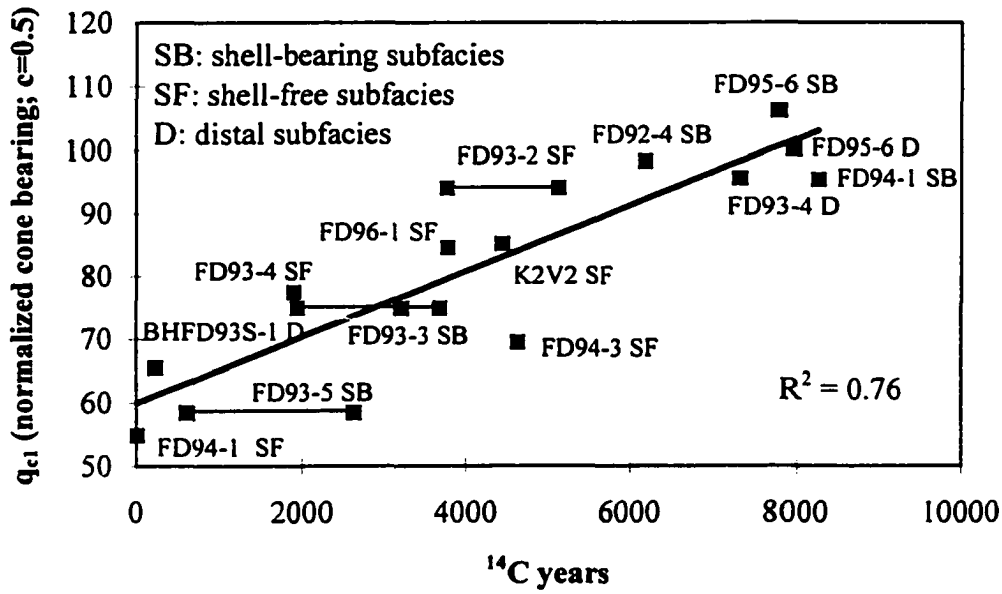

Figure 6- 39. ^{14}C age vs q_{c1} (normalized cone bearing) in the massive sand facies. See Appendix G for details.

8

Unlike all the other examples of the distal subfacies on the upper delta plain, this example is located near the western margin of the upper delta plain.

Relationship of Cone Bearing to Age and Geomorphic Features on the Delta Plain

The increase in cone bearing with age in sands has been discussed in the preceding chapter. This was further investigated by comparing the average normalized cone bearing (q_{c1}) with the ^{14}C age of enclosed organic material in the massive sand facies. This comparison is best made in this facies, because, it is widespread and easily recognizable, and the range of grain sizes is more or less the same in different occurrences. q_{c1} was averaged over either the entire facies, or distinct subunits where they could be discerned. Shell dates were corrected for reservoir age as discussed in Chapter 4. Average q_{c1} varies from 55 to 110 and correlates well with age (R^2=0.76) over a range of 10±60 (TO-4374) and 8260±80 (TO-4595) ^{14}C years (Figure 6-39, Appendices E and F).

Young sands of the massive sand facies with low average cone bearing are particularly common in the vicinity in islands in the Main Channel and on the concave sides of sloughs adjacent to it (Figure 6-35). These sloughs are known or inferred to be underlain by the thick subfacies of the interbedded sands and silts. The youngest dated deposit (10±60 ^{14}C years, TO- 4374), with the lowest average cone bearing observed in the entire dataset (average q_{c1} = 55), is the shell-free subfacies in borehole FD94-1 (Figures 5-18, 5-19 and 6-13). This site is located on Deas Island on the south side of the Main Channel (Figures 2-4).

Another striking field example is provided by comparison of the massive sand in facies either side of Crescent Slough, an arcuate slough south of the Main Channel in the central part of the upper delta plain (Figures 6-35 and 6-37). In borehole FD93-4, within the area enclosed by the slough, the upper 13 m of the massive sand facies is in the shell-free subfacies. The subfacies is dated at 1890+70 (GSC-5804) ^{14}C years by wood from its base and has an average q_{c1} of 77. Similar cone bearing occurs in other CPTs within the area enclosed by the slough. Conversely, in borehole FD92-4, outside of the area enclosed by the slough, the massive sand facies consists entirely of the shell-bearing subfacies. It is older - 6190±70 ^{14}C years based on a shell date - and has higher average q_{c1} - 98. Other CPTs and geotechnical

testholes south of Crescent Slough have similarly high average cone bearing and confirm the presence of the shell-bearing subfacies.

COARSENING UPWARD SAND FACIES

This facies is known from only one CPT located on the east side of Point Roberts peninsula which is marginal to the Fraser delta (Figure 6-40). The facies sequence here is not typical of the Fraser delta, but it is useful to include for comparison with the other deltaic facies. The massive sand facies that characterizes the topset is absent at this site. Overlying normally consolidated silts (Q_t=3 to 5, B_q>0.15) and interbedded sands that resemble foreset deposits elsewhere, is a unit of sand and with minor interbedded silt 4.5 m thick. Sand beds thicken upward and cone bearing in the sand beds increases upwards from 30 to >60 bars. dU is negative in the lower sand beds and near zero at the top of the unit. On the basis of upward increasing cone bearing and dU near zero, sands are interpreted to coarsen upward. Friction ratio values are generally less than 0.5% in sand beds and are higher in thin silt interbeds; peaks greater than 1% occur at sand-silt contacts.

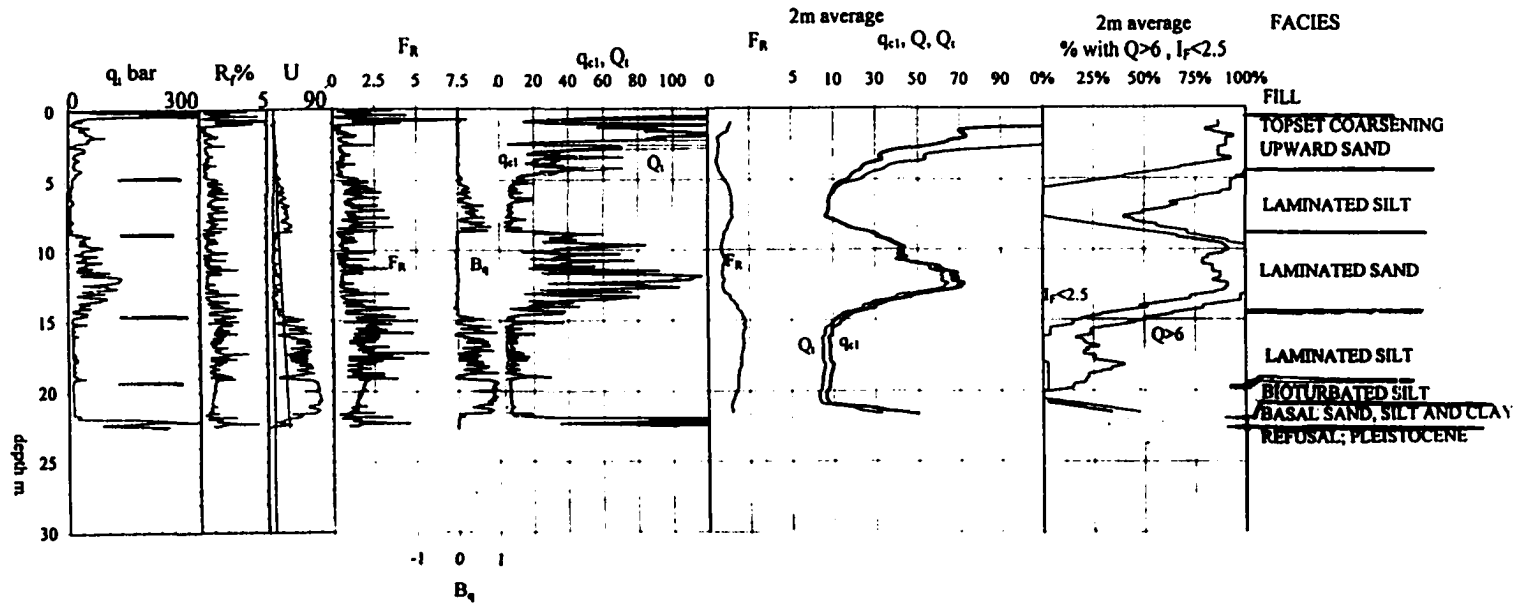

Figure 6-40. Lithology, non-normalized and normalized CPT data from a site on the east side of Point Roberts Peninsula, showing the coarsening upwards and facies of the topset. From left to right: non-normalized data (q_t, R_f and U); normalized data (F_R, B_q, Q_t and q_{c1}); normalized data averaged over 2 m (F_R, Q_t, Q and q_{c1}); and estimates of sand content averaged over 2 m based on Q>6 and I_F<2.5. Note the upward increasing cone bearing (q_t, Q_t, Q and q_{c1}) in the coarsening upward sand facies, interpreted to represent a sandy coarsening upward sequence. Friction ratio (R_f and F_R) is generally low in this facies. Cone bearing minima and friction ratio peaks represent silt interbeds. Although this facies is represented by a single CPT, it contrasts with the thick sharp-based fining upward sands of the massive sand facies.

INTERPRETATION AND DISCUSSION OF THE TOPSET

The massive sand facies of the topset is interpreted to be a complex of distributary channel sand deposits (Monahan et al., 1993a, b, c, 1995, 1997). It has an erosional base, consists of one or more decametre-scale fining upward sequences, and has a gradational top. Sands are fine to medium grained and moderately well sorted, and include silt clasts and other coarse material, commonly concentrated near the bases of fining upward sequences. Planar cross bedding occurs, and silt interbeds are rare and are commonly inclined. These characteristics are typical of channel deposits (Elliott, 1986). In the Fraser delta, the range of grain size found in this facies are most commonly found in distributary channels rather than other environments (Johnston, 1921; Mathews and Shepard, 1962; Clague et al., 1983). Williams and Roberts (1989) have interpreted these deposits to represent "lower tidal flat and subaqueous platform environments, characterized by relatively high energy associated with wave action". However, wave-dominated sandy delta fronts generally *coarsen* upward and delta front sands have a *gradational* and interbedded contact with underlying finer deposits (Reading 1986; Elliott, 1986; Bhattacharya and Walker, 1992). Furthermore, wave energy on the Fraser delta front is relatively low. Most importantly, the massive sand facies is generally *not present* along the modern delta front (Figures 6-1 and 6-33), so that it is formed by processes operating on the delta plain and not at the delta front.

The sand facies may locally include tidal channel deposits in its upper part. However, this facies is not fundamentally a tidal channel facies: modern tidal channels in this delta are a few metres deep, and the thickness of individual fining upward sequences (8 to 20 m) is the same order as the depths of distributary channels (Johnston, 1921; Mathews and Shepard, 1962). Furthermore, the massive sand facies thickens landward from the distal facies in the lower delta plain and similarly, distributary channels of the modern delta (prior to the anthropogenic modifications of this century) deepened in a landward direction (Johnston, 1921). Conversely, tidal channels deepen and their deposits thicken in a seaward direction.

The youngest deposits of the massive sand facies observed in cores and CPTs can be attributed directly to deposition in a distributary channel. These are in the shell-free subfacies in borehole FD94-1 on Deas Island, and form a single fining upward sequence 20 m thick. There, the base of this subfacies is at approximately the same depth as depth of the river channel, and this island formed by the downstream migration of a mid-channel island in historic times (Figures 2-4 and 6-13; Johnston, 1921; North et al., 1979; Monahan et al., 1995).

The presence of metre-scale coarsening upward sequences observed locally in the upper part of the massive sand is not inconsistent with a fluvial origin. Rubin et al. (1998) describe upward coarsening in the upper part of modern fluvial deposits. They attribute this pattern to depletion of finer grain sizes in the river channels during floods, so that sediments deposited on adjacent bars become coarser as a flood progresses. Grain size of suspended sediment in the Fraser River evolves similarly during the course of the spring freshet. The peak in suspended sediment load precedes the peak in fluid flow: suspended silt is transported early in the freshet, and sands are transported preferentially during peak flow when the system is depleted of fines (Kostaschuk and Luternauer, 1989; Kostaschuk et al., 1989, 1992b). Neither is the absence of cross bedding in much of the sand inconsistent with fluvial origin. Kostaschuk (pers. comm. 1995) has observed that many of the sand waves in the Main Channel have lee slopes less than the angle of repose and that flow separation does not occur across them.

The massive sand facies thus records extensive channel migration which has reworked the surface of the delta plain, eroding the original lower tidal flat, subaqueous delta plain and uppermost delta slope deposits, which are preserved on only the outermost parts of the delta plain. Prior to construction of the jetties that now constrain it, the Main Channel migrated extensively where it crossed the modern tidal flats. In particular, a series of downstream-migrating meanders reworked 10 km^2 of the tidal flats between 1896 and 1912 (Figure 2-3; Johnston, 1923; Clague et al., 1983; Luternauer and Finn, 1983). Extensive distributary

channel migration in this setting is interpreted to be due to the interaction of tidal and fluvial processes and the high proportion of sand in the sediment load (Monahan, et al, 1993c). Sediment transport and deposition in the distributary channels is influenced by tidal movement of a salt wedge that intrudes beneath the fresh river water. This salt wedge reaches as far upstream as the head of the delta during low water periods, but in the Main Channel it is restricted to the reach crossing the tidal flats during the freshet, when most sand transport occurs (Milliman, 1980). On a rising tide, the suspended sand load is rapidly deposited in the river channel, as the salt wedge flows upstream beneath the fresh river water, and is resuspended more slowly as the tide falls (Kostaschuk and Luternauer, 1989; Kostaschuk et al., 1989, 1992b). These observations indicate that the cyclic interruption of sand transport and the time lag in sand resuspension reduce the capacity of the river to transport its sand load where it crosses the tidal flats. Prior to jetty construction, the cyclic variations in fluid and sediment discharge would have forced the Main Channel to constantly adjust its dimensions and pattern (e.g. Schumm, 1977), resulting in rapid bank edge erosion, channel migration and deposition of the massive sand facies. Tidal flow reversals occur throughout the delta (Thomson, 1981). Sedimentary structures indicative of tidal flow reversals, including paired silt laminae and mud-draped ripples, occur throughout the massive sand and interbedded sand and silt facies.

Distributary channels in the modern upper delta plain have been more stable than those crossing the tidal flats, but historical records, the presence of sloughs adjacent to the Main Channel and the local presence of sand overlying floodplain silts indicate that some channel migration has occurred (Figure 2-4; Johnston, 1923; North et al; Monahan, et al, 1993a, b, c, 1995). Furthermore, the linear gap in the peat bogs in eastern Lulu Island, which has been interpreted to represent a former distributary crossing the floodplain, demonstrates that major avulsive or channel switching events have occurred (Johnston, 1923; Clague et al., 1983; Monahan et al., 1993c; Hutchinson, 1995), presumably taking shorter routes to the sea as older distributaries became too long. The combination of extensive distributary channel migration in the tidal flats (and to a lesser extent in the upper delta plain), and avulsion or

channel switching in the upper delta plain provide the mechanism for the widespread distribution of distributary channel sand deposits in the topset of the delta (Monahan et al., 1993c, 1997).

The shell-bearing subfacies of the massive sands is interpreted to represent the migration and filling of active distributary channels in a tidal flat environment (Monahan et al., 1993a, b, c). The gradationally overlying bioturbated subfacies of the interbedded sand and silt facies contains bivalve shells and an intertidal foraminiferal fauna (Williams, 1988), and is interpreted to represent tidal flat deposits. A burrowing shrimp and bivalve fauna occurs in the modern tidal flats, and the sediments there are extensively bioturbated (Swinbanks and Luternauer, 1987). Shells were most likely incorporated into the shell-bearing subfacies of the massive sand facies by bank edge erosion of tidal flat deposits as the channels migrated, eroding earlier tidal flat deposits.

The shell-free subfacies of the massive sands is interpreted to represent deposits of active distributary channels in an upper delta plain ("floodplain") environment (Monahan et al., 1993a, b, c). It is overlain by the well-bedded subfacies of the interbedded sand and silt facies, which is interpreted to represent the fill of sloughs and shallow partially abandoned channels and bar top deposits in fresh water environment, where burrowing marine organisms could not survive. Sands interbedded with laminated silts were observed in a trench excavated on a bar top beside an active channel at the head of the delta (Monahan et al., 1993a, c). The shell-free subfacies underlies not only the linear gap in the peat bogs in eastern Lulu Island but also the adjacent peat bogs, indicating that several cycles of upper delta plain distributary channels have been developed in this area.

The thick interbedded sand and silt subfacies is interpreted to represent the fill of partially to fully abandoned channels (Monahan et al., 1995). The interbedding of silts with fine to medium sand with silt clasts indicates highly variable energy conditions. Episodes when current energy was sufficient to transport fine to medium sand and erode silts occurred only

intermittently. Occurrences of this facies commonly lie on the courses of historically mapped arcuate sloughs (North, 1979; Township of Richmond, undated), which represent the final stages of channel abandonment and are abandoned meanders. The 2 to 4 m thick sharp-based fining upward sand sequences that pinch out laterally in this subfacies on one side and merge with the upper part of the massive sand facies on the other are interpreted to represent the last stages of active flow in these channels (Figures 6-25 and 6-26).

The distal subfacies of the massive sand facies is thinner than the other subfacies and represents distal distributary channel sand deposits, formed where the distributary channels shallowed near the delta front (Monahan et al., 1997; Clague et al., 1998). At the most distal expressions of this subfacies, the lower part of the sand is interbedded with silt and the sharp base is obscured on CPT data (Figure 6-36). These deposits are interpreted to represent river mouth bar deposits. Johnston (1921) shows a pronounced middle ground bar at the river mouth at Sand Heads prior to construction of the Steveston Jetty. The deposits interpreted to represent distributary mouth bars are transitional between topset massive sand and the coarsening upward sequences common in the foreset. However, the general absence of seaward dips and the presence of centimetre-scale calcareous cemented clasts that occur in one example (Figures 5-13 and 6-24) indicates that these are bedload deposits associated with the river channel. The cemented clasts are interpreted to have been derived from calcareous concretions that form in the distributary channels (Johnston, 1921; Garrison et al., 1969; Nelson and Lawrence, 1984).

The distal subfacies of the interbedded sand and silt facies is interpreted to represent the infill of partially abandoned distal distributary channels. These deposits include fine to medium sands with silt clasts and mud-draped ripples, similar to the thick interbedded sand and silt facies. Metre-scale coarsening upward sand sequences, similar to those of the foreset also occur in this subfacies.

The distal subfacies of the massive sands is locally preserved at the base of the massive sand

facies in the central and southeastern parts of the upper delta plain because of the rapid rise in sea level that occurred between 8000 and 4500 ^{14}C years ago. Elsewhere, this subfacies has been removed by migration of distributary channels in tidal flat and floodplain environments, which were deeper than the distal channels, and replaced by deposits of the shell-bearing and shell-free subfacies. Similarly, the westward climbing of the base of the massive sand facies and the stacking of the shell-free subfacies over the shell bearing subfacies in the central and eastern parts of the upper delta plain are also the result of rapid sea level rise during this period (Monahan et al., 1995, 1997).

The cone bearing increasing upward sequences that represent upward increases in density occur near the top of the massive sand facies, most commonly in the distal subfacies. The increased density is interpreted to be a result of wave loading during winter storms. A similar origin is proposed for such density increases observed in some foreset sequences, and will be discussed further below.

The thin sand locally preserved at the top of the bioturbated subfacies east of Ladner is interpreted to represent a thin beach sand (Figure 6-19). It locally has a sharp base, indicating that it was deposited during a brief transgressive event, probably related to shifts of the river mouth. However, the bioturbation and interbedding of the sands and silts in the bioturbated sand and silt facies suggests that sediment was supplied to the tidal flats primarily by overflow from distributary channels during tidal cycles during the freshet, and that sediment reworking by waves on the tidal flats was generally minimal. Although the tidal flats north of the Main Channel are exposed to the largest waves (Thomson, undated; 1981) the well developed bedforms occurring there today may be in part a recent phenomenon related to jetty construction.

The coarsening upward sand facies of the topset is interpreted to represent prograding beach and tidal flat deposits: it is interpreted to coarsen upward from foreset deposits, based on CPT data, and occurs in the vicinity of modern beach deposits mapped by Armstrong and

Hicock (1980b). This facies was most likely sourced by longshore drift from erosion of Pleistocene deposits at Point Roberts, and/or adjacent areas of the Fraser delta. This facies may not be representative of the beach deposits mapped by Armstrong and Hicock (1980b) to the north and east on the shores of Boundary Bay. There the shoreline is transgressive (Hutchinson et al., 1995), and thin transgressive beach sands are likely to sharply overlie older delta plain sediments and resemble the thin sand at the top of the bioturbated sands and silts east of Ladner (Figure 6-19).

The laminated and organic silt facies is interpreted to represent deposits of brackish and fresh water marshes, analogous to those of the uppermost tidal flats and the upper delta plain prior to European settlement (Williams and Roberts, 1989). Fine grained suspended sediment was transported to these environments when the river overflowed its banks during seasonal and tidal floods. These sediments were deposited within 2 m of sea level, and the accumulations of this facies exceeding 10 m in thickness were deposited as sea level rose between 8000 and 4500 ^{14}C years ago (Williams and Roberts, 1989). Where this facies is thick, the sediments are normally consolidated, but where it is thin, they appear to be slightly overconsolidated. The slight overconsolidation may be related to a slower rate of deposition and potentially more time for subareal exposure. The more heavily overconsolidated desiccated silts that occur at the top of this facies have only been observed where this facies forms the surface of the upper delta plain, and do not occur where thin silt is overlain by peat. This overconsolidation may be a consequence of recent draining of the delta surface and not a natural phenomenon.

The peat facies represents the raised peat bogs that occur at surface on the older parts the upper delta plain. Peat began to accumulate on those parts of the upper delta plain built above the limits of seasonal and tidal flooding, when the rate of sea level rise had slowed after 5000 ^{14}C years ago (Clague et al., 1983; Williams and Roberts, 1989). In humid climates, peat can accumulate at rates of up to 2 mm/yr, and where relative sea level rise is less than this, raised peat bogs, such as those in the Fraser delta can form (McCabe and

Shanley, 1992). However, at higher rates of sea level rise, peat cannot keep pace with the rate of sea level rise.

Discussion of the Relationship of Cone Bearing to Age and Liquefaction Susceptibility

The correlation of cone bearing to grain size in the massive sand facies is remarkable. The ages of the individual deposits are all determined by ^{14}C dates on transported materials that must be somewhat older than the deposits themselves. Furthermore, cone bearing also correlates with grain size and density (Chapter 5). However, similar ranges of grain size occur in most occurrences of the massive sand facies, and the range of density variations in the Fraser delta sands is low (Chapter 5), particularly in this facies. The relationships of cone bearing in age in the massive sand facies and to the distribution of geomorphic features are potentially significant for earthquake hazard mapping in the Fraser delta. Normalized cone bearing can be directly related to the resistance to liquefaction of sand (Robertson and Campanella, 1985; Seed and De Alba, 1985; Stark and Olson, 1995; Robertson and Fear 1996; Robertson and Wride, 1997, 1998). Consequently, the liquefaction hazard is greatest in areas underlain by the youngest deposits of the massive sand facies, which occur most commonly on the on islands in the Main Channel and on the concave sides of sloughs adjacent to it (Monahan et al., 1996).

The thick interbedded sand and silt subfacies also has low liquefaction resistance, using algorithms provided by Robertson and Fear (1996). The distribution of these sediments on the upper delta plain can be mapped using the distribution of the arcuate sloughs that they generally underlie.

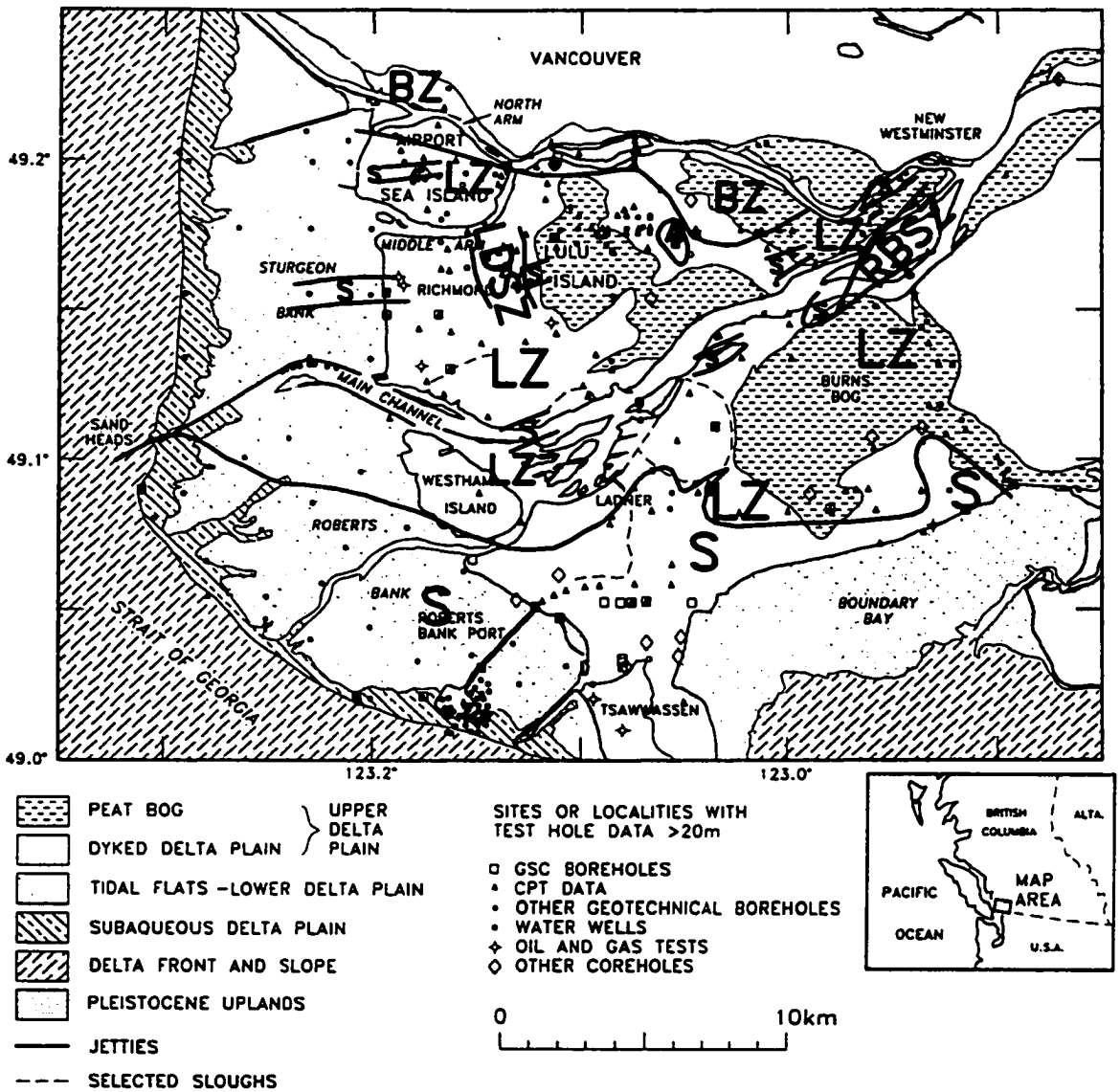

Figure 6-41. Map showing the distribution of principal facies in the upper foreset.

S - primarily sandy facies (laminated sand, mixed sand and sharp-based sand)

LZ - primarily laminated silt facies

LDSZ - low dipping interbedded sand and silt facies

RBSZ - rhythmically bedded sand and silt facies

A - foreset absent

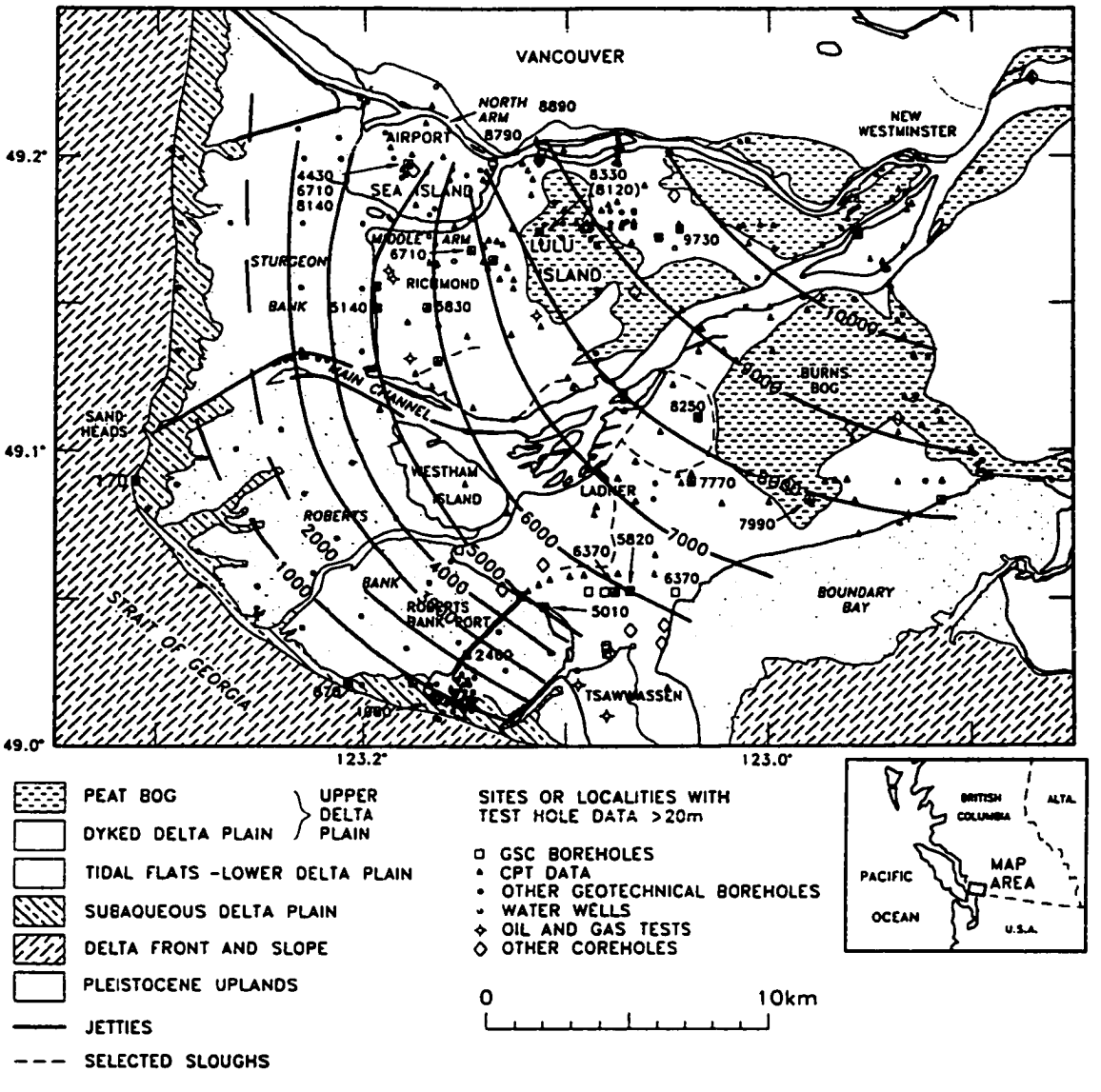

Figure 6-42. Map of ^{14}C dates in upper foreset. Because of the generally steep dips (7°), the contours *approximate* the position of the top of the foreset through time. Only the youngest date in each borehole is shown. These dates are minimum dates, because they were derived from transported material. See Appendix F for more details of ^{14}C dates.

FACIES OF THE FORESET

Several facies can be recognized in the foreset, many of which are intergradational. As described at the beginning of the chapter, CPT data provide a quantitative means to define facies by providing estimates of the relative proportions of silt and sand and of the average grain size. Furthermore, two sedimentological elements are common to several facies and have characteristic signatures on CPT data. These elements provide a basis for interpreting facies that are not well represented in cores. Because of the complexity of the foreset, future work will undoubtedly reveal additional facies variants. The facies and evolution of the foreset is summarized on two maps. The distribution of the principal facies of the upper foreset is shown in Figure 6-41, and, based on ^{14}C dates in the upper foreset, the approximate positions of the delta front through time are shown in Figure 6-42.

FORESET FACIES ELEMENTS

Coarsening Upward Sequences

Metre-scale coarsening-upward sequences are ubiquitous in the foreset, occurring in both silt and sand-dominated facies. They vary from sequences that coarsen upward from clayey to sandy silt, to those that coarsen upward from sandy silt to fine sand (Figures 5-15, 5-25 and 27). Most sequences are 0.5 to 1.5 m thick, although some sand-dominated sequences can be as thick as 4 m. In detail, the upward coarsening is not steady, and the sequences are commonly composed of three or four secondary decimetre-scale coarsening upward sequences. The coarsening-upward sequences are generally composed of thin to medium laminae. Thin to medium sand beds of sand occur at the top of thicker sand-dominated sequences, although these are commonly laminated by sand of varying grain size, and include silt and organic laminae. Coarsening-upward sequences can be generally correlated across a building site on CPT data (Figures 6-4, 6-6 and 6-12).

Complex laminae occur where sands and silts are both present, such as in the lower, silty parts of sand-dominated sequences. These include: both normally and inversely graded laminae, that grade from clayey silt or silt to sandy silt or very fine sand; "double graded" laminae, that are inversely graded at the base and normally graded at the top; and "sandwich sand laminae", a term coined here for very thin laminae of sand sharply bounded by thicker laminae composed of finer sediment (Figure 6-43). The sandwich sand laminae are commonly directly bounded by clayey silts that form the tops and bases of adjacent double graded laminae, in which the coarsest sediment is finer than that of the sandwich sand laminae. In such cases the coarsest sediments, represented by the sandwich sand laminae, are in sharp contact with the finest, represented by the clayey silts of the double graded laminae. Additional complexities observed in core include sandwich sand laminae that alternate in thickness, forming couplets of double graded laminae, and single secondary silt laminae occurring within predominantly normally graded laminae (Figure 6-44). These complex laminae are stacked rhythmically, and in the latter example, 14 complex laminae occur between sand rich peaks of a secondary decimetre-scale coarsening-upward sequence. In other examples, more than 14 complex laminae occur. As will be discussed further below, the laminated sediments of the coarsening upward sequences are interpreted to be tidal rhythmites deposited from suspension.

The CPT expression of the coarsening-upward sequences varies with the grain size. Silt-dominated sequences are represented by dU and B_q decreasing-upward sequences, which may be obscured by rod breaks, particularly in SCPTs (Figures 5-25, 5-27, 6-45 and 6-51). The sequence is not indicated by upward increasing cone bearing, and if sand is present at the top of the sequence, it is expressed as a cone bearing peak. In sequences dominated by very fine sands, sequences are expressed as cone bearing-increasing upward sequences, and to a lesser extent as friction ratio decreasing upward sequences (Figure 6-45). In thick fine sand-dominated sequences, cone bearing increases upward throughout the sequence (Figures 5-15 and 6-46). However, in example shown in the previous chapter, grain size reaches a maximum within the sequence, and the further upward increase in cone bearing is interpreted

to represent an increase in density.

Sharp-Based Sands

Fine to medium sand beds that have sharp bases and grade into overlying finer grained sediments occur in several facies of the foreset. Examples observed in core are up to 5 m, and thicker examples are indicated on CPT data. These sands commonly contain silt clasts and shells (Figure 6-47). In one example, clasts and shells are concentrated in the middle of the unit (Figures 5-18). These deposits are interpreted to be sediment gravity flow deposits, and the thicker examples with shell and clast concentrations above the base may represent several stacked units. In contrast to the coarsening-upward sequences, the sharp-based sand units cannot generally be correlated across a site (Figure 6-4).

The sharp bases and gradational tops of these sequences are generally well expressed on the cone bearing, friction ratio and pore pressure curves (Figures and 5-17 and 5-32). Because these sands are generally coarser, cone bearing is generally higher than in other foreset deposits. dU and B_q vary from near zero to negative. Upward fining is represented in some examples by upward decrease in cone bearing and dU. In the shell and clast concentrations, cone bearing is higher and dU is lower than adjacent parts of the sand unit. Friction ratio is commonly very low and smooth in sharp-based sands thicker than 1 m, reflecting the absence of silt interbeds, but thinner beds have a more serrate character, possibly due to the presence of silt clasts.

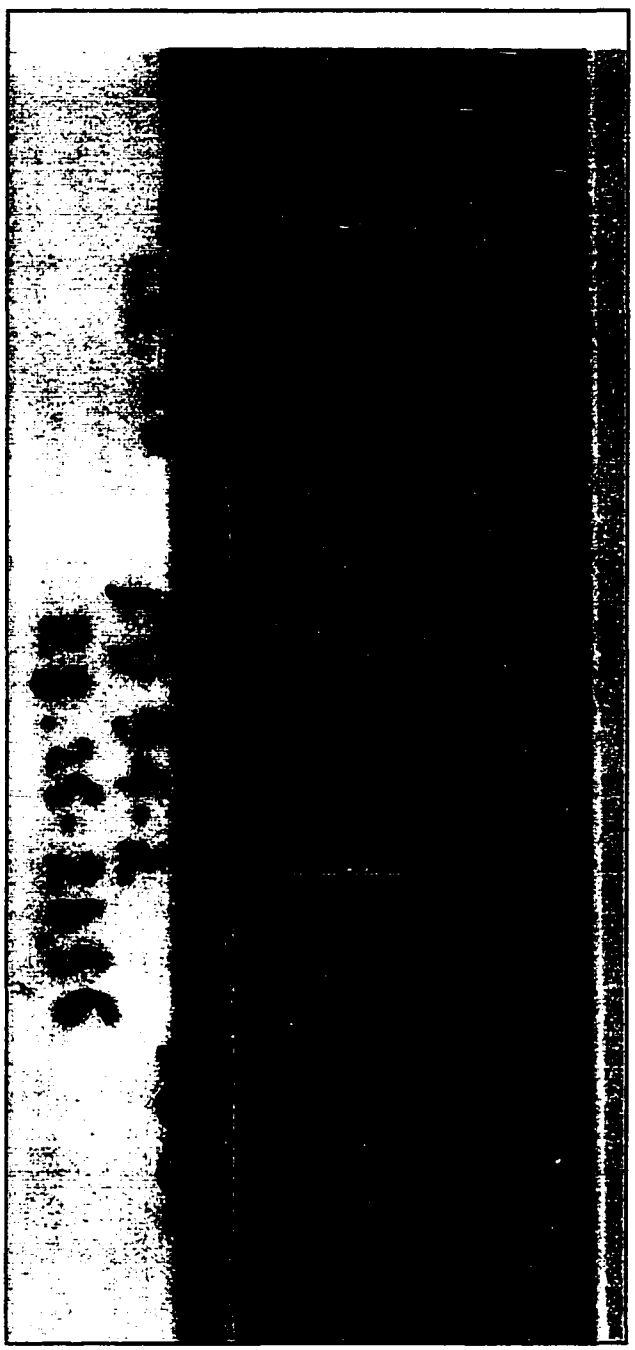

Figure 6-43. Core photograph of laminated silts and sands in the lower part of a coarsening upward sandy sequence in the upper foreset (mixed sand facies). Sediments range from clayey silts (light coloured) to very fine sands (dark coloured). Note cm-scale double graded laminae, which have clayey silt at the top and base and coarser silt in the middle; and mm-scale "sandwich sand laminae", which are in direct contact with clayey silt parts of the double graded laminae and alternate between ~1mm and 3mm in thickness. These rhythmic alternation of sand and silts laminae suggests that these are tidal rhythmites. FD94-2 (same site as FD94-4), CPT depth 28.55 to 28.85. See Figure 6-4.

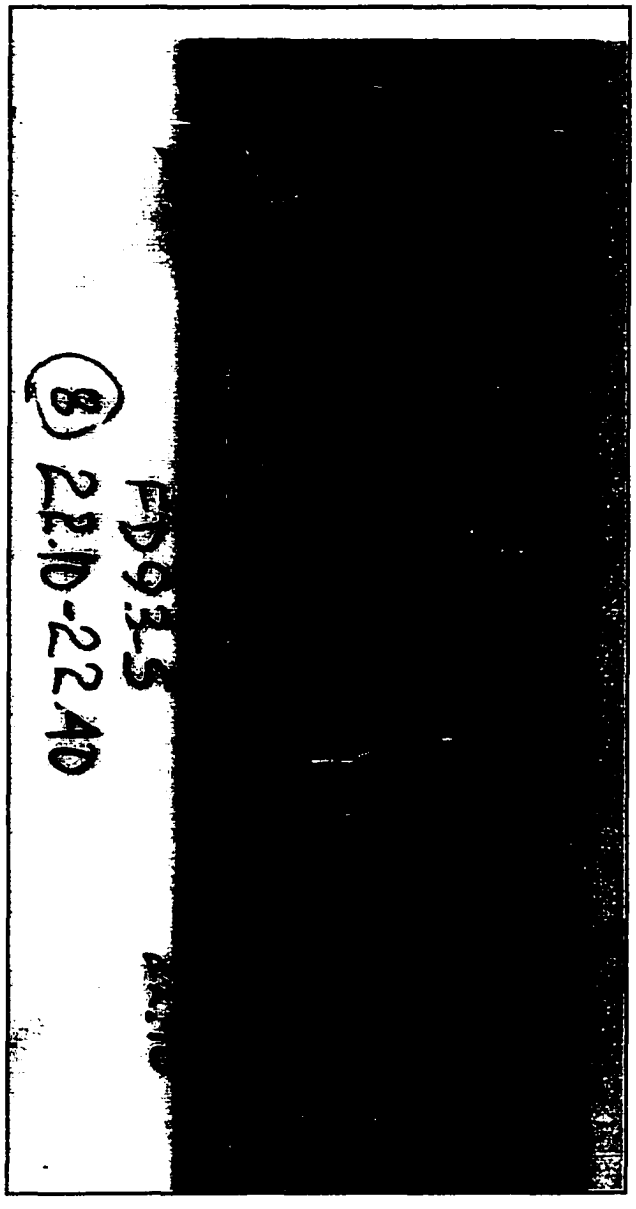

Figure 6-44. Core photograph of laminated fine to very fine sands and silts in the lower part of a coarsening upward sequence in the upper foreset (thick coarsening upward sand facies). The sediments are interpreted to be tidal rhythmites, based on the 14 principal laminae between thin sandy beds at 22.10 and 22.35 m core depth, consistent with a fortnightly spring-neap tidal cycle. The 14 principal laminae form a secondary coarsening upward sequence within the larger sequence (Figure 5-15, between 22.2 and 22.4 CPT depth). Note that the thicker laminae (#8, 11, 12 and 13) are internally laminated, and are interpreted to represent a daily semidiurnal tidal cycle. The sag in the laminae in the middle of the core is deformation due to coring. FD93-5, CPT depth 22.17 to 22.47 m . See also Figure 5-15 and 6-30.

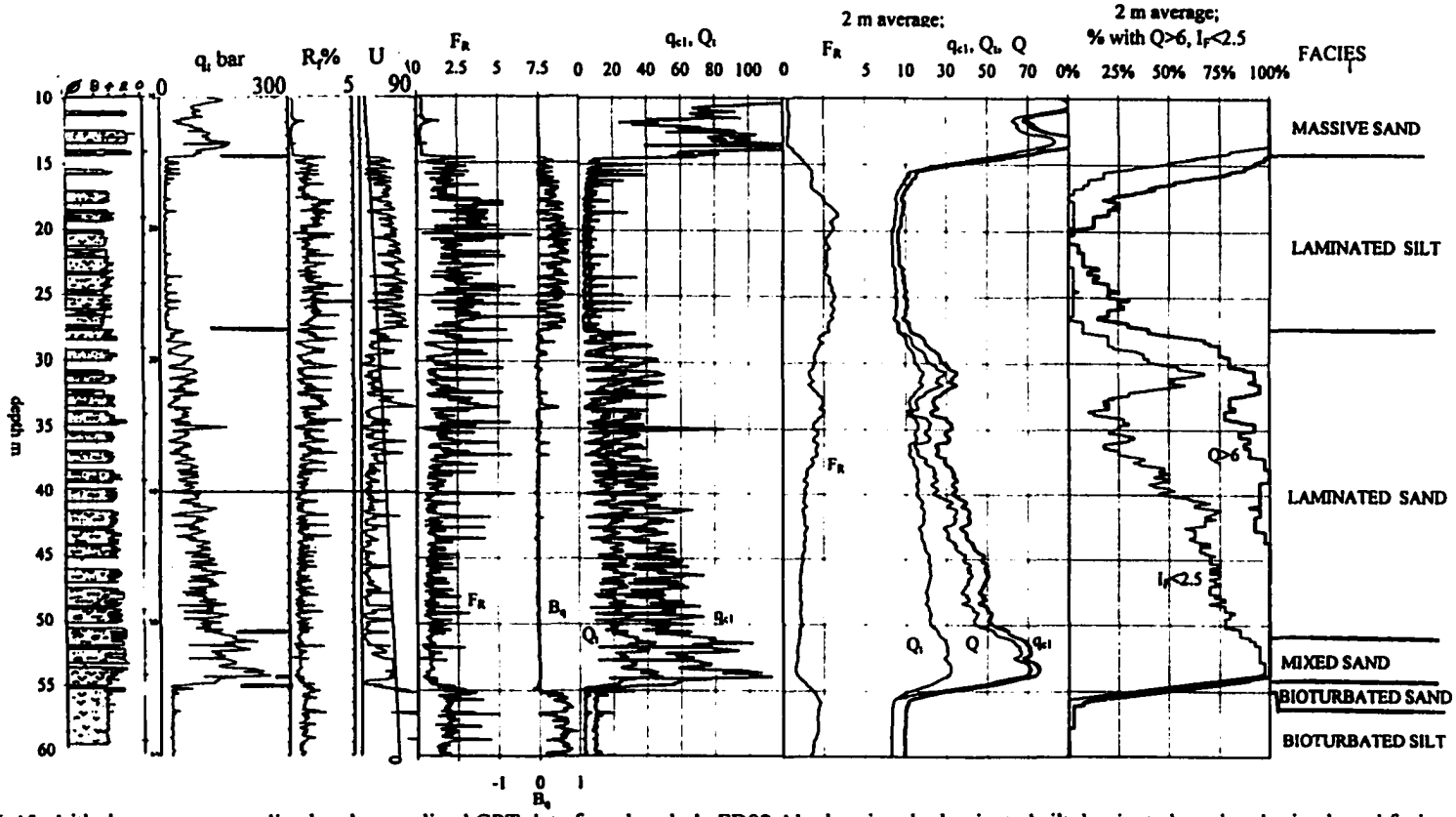

Figure 6-45. Lithology, non-normalized and normalized CPT data from borehole FD92-11, showing the laminated silt, laminated sand and mixed sand facies. From left to right: lithology; non-normalized data (q_t, R_f and U); normalized data (F_R, B_q, Q_t and q_{c1}); normalized data averaged over 2 m (F_R, Q_t, Q and q_{c1}); and estimates of sand content averaged over 2 m based on Q>6 and I_F<2.5. In the laminated silt facies, cone bearing (q_t, Q_t, Q and q_{c1}) is low and may include regularly spaced peaks, excess pore pressure (B_q) is positive, and pore pressure decreasing upward sequences represent metre-scale coarsening upward sequences (Figure 5-25). In the laminated sand facies, coarsening upward sequences are expressed as cone bearing increasing upward sequences, and excess pore pressure is generally negative. In the mixed sand facies, cone bearing is higher and friction ratio (R_f and F_R) lower than the laminated silts and laminated sands. See also Figures 5-8, 5-25, 6-3, 6-8 and 6-48.

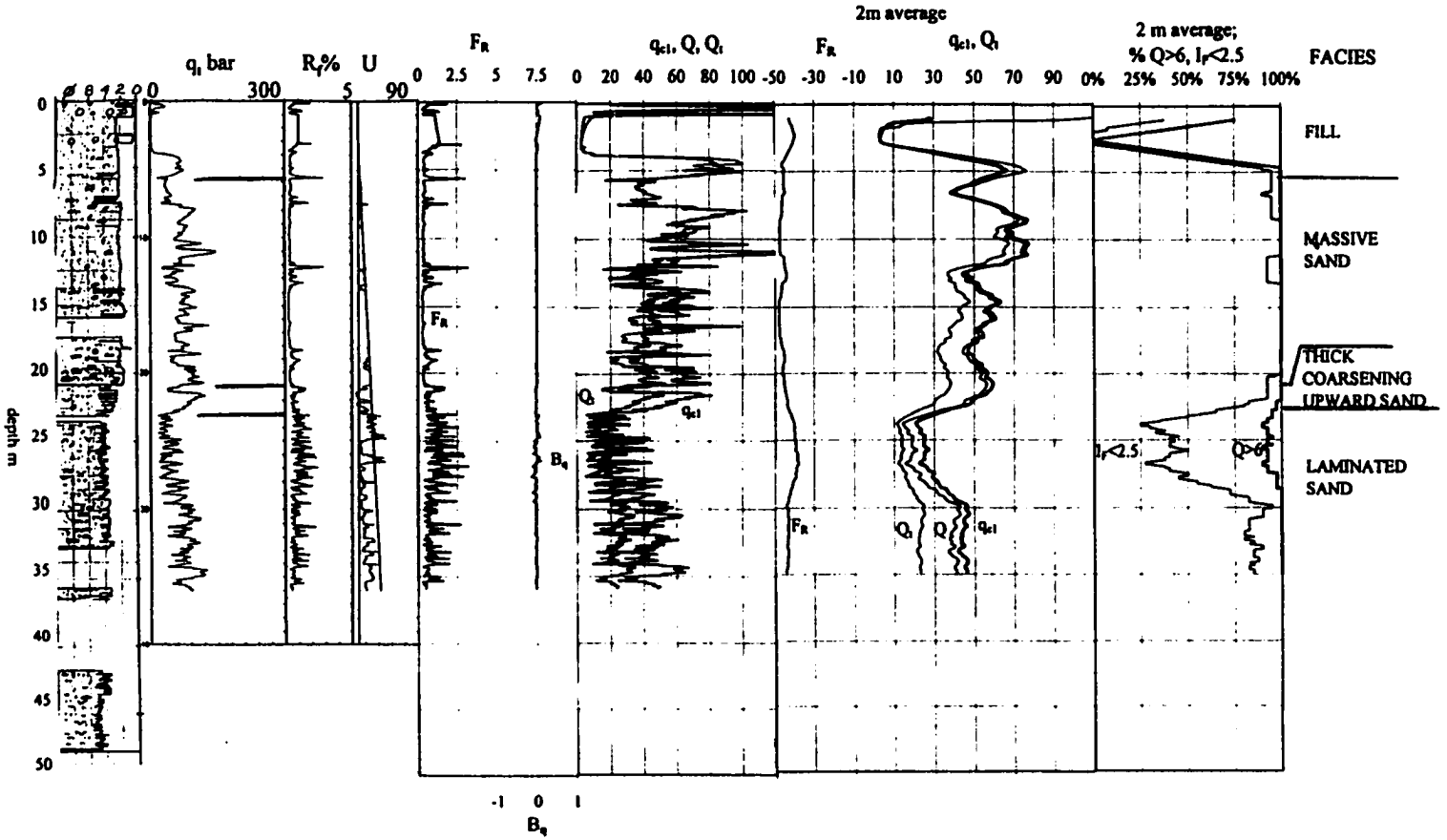

Figure 6-46. Lithology, non-normalized and normalized CPT data from borehole FD93-5, showing the thick coarsening upward sand and the laminated sand facies. From left to right: lithology; non-normalized data (q_t, R_f and U); normalized data (F_R, B_q, Q_t and q_{c1}); normalized data averaged over 2 m (F_R, Q_t, Q and q_{c1}); and estimates of sand content averaged over 2 m based on Q>6 and I_F<2.5. In the thick coarsening upward sand and the laminated sand facies, metre-scale coarsening upward sequences are expressed as cone bearing (q_t, Q_t, Q and q_{c1}) and have negative excess pore pressure (B_q). In the thick coarsening upward sand facies grain size does not increase in the upper part of the sequence shown here, and the continued upward increase in cone bearing reflects increased density (Figures 5-15). This CPT is also shown in Figure 6-3.

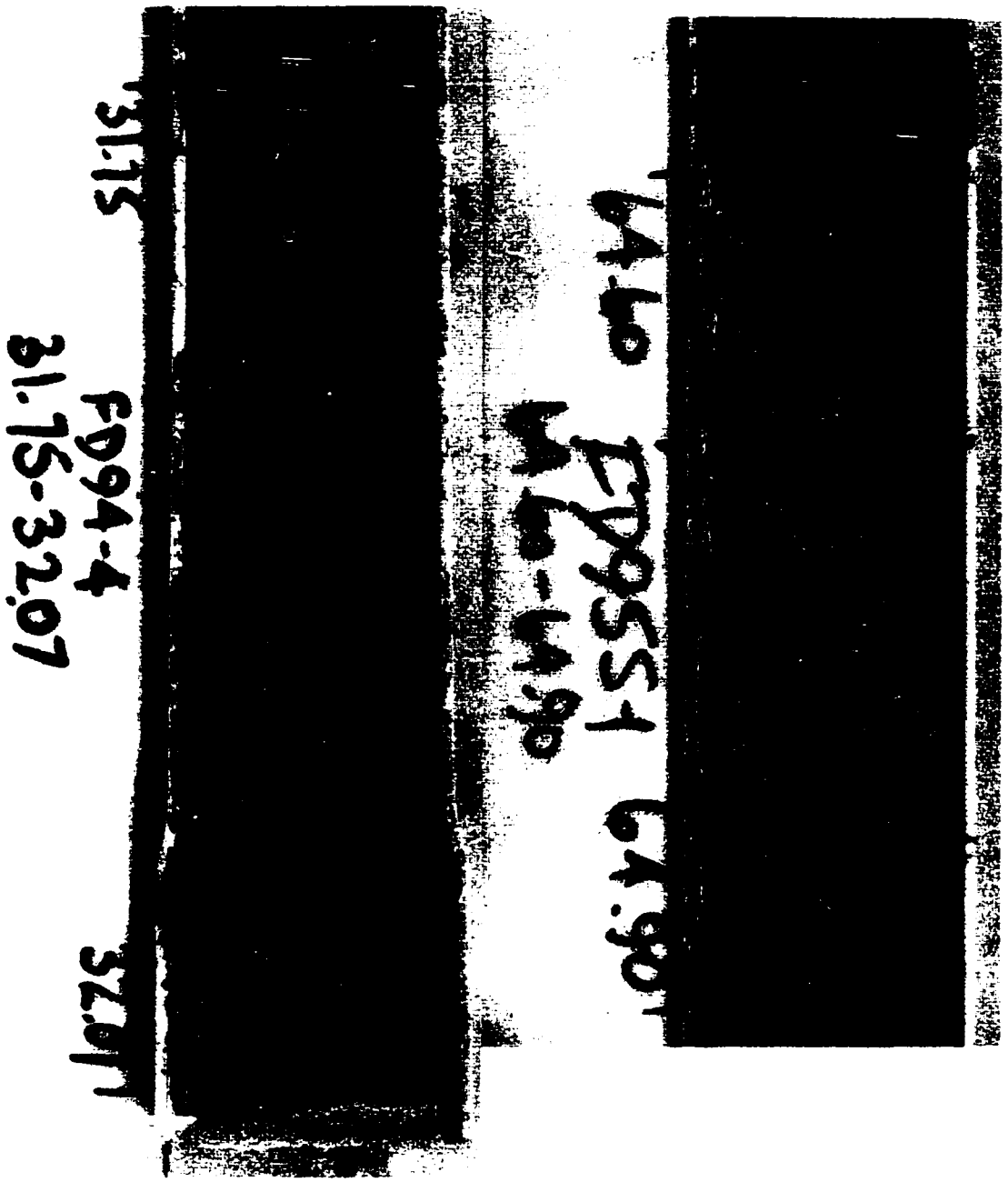

a b

Figure 6-47. Core photographs of sharp-based sands in the foreset; a) base of sharp-based sand in FD94-4, CPT depth 30.452 to 30.74; see Figures 5-32 and 6-4; From Monahan et al. (1997). b) shell- and clast-rich interval in FD95S-1, CPT depth 66.1 to 66.4 m , see Figures 5-17, 6-1 and 6-54. Note similarity between this and the shell- and clast-rich interval in the massive sand facies in Figure 6-29; also reproduced in Clague et al. (1998).

BASAL SAND, SILT AND CLAY FACIES

This facies is defined to include thin intervals of interbedded sand, silt and clay underlying the bioturbated silt facies at the base of the deltaic section (Figures 6-3, 6-21, 6-40 and 6-48). At two sites it includes a distinct silty clay that oxidized to a pink colour, in contrast to light brown in the foreset silts. The clay is a few cm (FD92-11) to 2 m thick (FD96-2; adjacent to K2V2), heavily burrowed, and at one site laminae are offset on fractures. At borehole FD92-11, the clay is gradationally underlain by a metre-scale fining upward sequence of laminated sandy silts and very fine sands, and is overlain by a bioturbated sharp-based sand, from which shell debris provided a date of 9210±70 ^{14}C years (TO-4894; Appendix F).

The CPT expression of this facies is variable, reflecting the mixture of sediments; in FD92-11, low cone bearing peaks represent in the sands and sandy silts, and cone bearing is low in the clay (Q_t=3), indicative of normal consolidation (Figures 6-8 and 6-48; Table 6-2). Friction ratio is high and variable, reflecting the interbedding of sand and finer sediments. Where the clay is thicker at FD96-2, CPT parameters are indistinguishable from those of the overlying bioturbated silt facies: cone bearing is low and uniform (Q_t=2); friction ratio is high (F_R=4); B_q is high (0.8); and I_F is high (3.6; see Figure 6-21).

BIOTURBATED SILT FACIES

This facies is well represented in one borehole logged for this study, where it occupies an interval between depths of 55 and 99 m (FD92-11; Figures 5-8, 6-3, 6-8 and 6-48). The facies consists of olive brown silts grading down to clayey silts. The silts are extensively bioturbated, so that laminae and bedding are poorly preserved. However, some distinct burrows occur: vertical to circular burrows up to 3 cm wide and 4 cm deep with crescentic concave laminae (*Teichichnus?*), as well as vertical, circular, centimetre-scale and finer burrows. Small bivalve shells occur throughout this facies. Coarsening upward sequences from fine to medium silt occur rarely. Locally, non-bioturbated, normally graded laminae

of very fine sand and silt occur, and are organized into thin to medium beds. At this site, the bioturbated silts overlie a thin interval of the basal sand, silt, and clay facies, and is gradationally overlain by a thin interval of the bioturbated sand facies.

On CPT data, this facies is characterized by low, uniform cone bearing that increases linearly with depth. Average Q_t of 3+1 indicated that the silt is normally consolidated (Figures 6-8 and 6-48; Table 6-2; e.g. Lunne et al., 1997). Excess pore pressures are generally positive (B_q= 0.7±0.2), and minima generally represent rod breaks. The friction ratio is high and relatively uniform (R_f =1.3±0.3; F_R=2.2±0.5), but is less variable than in the laminated silt and laminated sand facies because of the general absence of sand interbeds. I_F =3.3, slightly higher than in the laminated silts in this CPT.

The interbeds of laminated very fine sand and silt are represented by medium beds of higher cone bearing (peak q_{c1}= 50)[9] separated by cone bearing minima, and negative dU separated by dU peaks. Friction ratios in this interval are similar but more variable than in the enclosing silts because of the interbedding of sand and silt (F_R=2.0±0.6, with peaks up to 6 at sand silt contacts).

Although this facies is only well represented in one borehole analyzed for this study, it is interpreted to be widespread in the Fraser delta. Silts and clays with a similar CPT expression - low uniform cone bearing, moderate to high and uniform friction ratio, and high B_q, with minima representing rod breaks, and I_F up to 3.6 - occur between the topset massive sand and dense Pleistocene deposits (indicated by refusal on CPT) on the northern margin of the delta (Figures 6-21 and 6-41). The silt is a light grey blue colour and is bioturbated (only a small interval was relogged in the lab). The significance of the blue colour in this area is unknown. Shell material from these silts at one site provided a date of 8890±80 ^{14}C

9

Cone bearing appears to be resolved in these intervals, because the cone bearing is similar to other sand of similar grain size. Bed thickness is 20 cm.

years (TO-4094; Appendix F; FD92-2), coeval with other foreset silts (Figure 6-34). Furthermore, deltaic silts below 100 m in recent deep GSC boreholes are described as weakly stratified to massive clayey silts that are finer with depth and are locally interbedded with sharp-based sand units (Luternauer et al., 1991; Dallimore et al., 1995, 1996), and a thin interval of bioturbated silts occurs at the base of the deltaic section beneath an interval of sharp-based sands at Roberts Bank Port (Figure 6-49). This facies thus occupies the shallow foreset on at least the northern margin of the delta, much of the lower foreset (below ~60 m), and probably most of the bottomset.

LAMINATED SILT FACIES

This facies consists of laminated silt with lesser amounts of very fine sand. These sediments are generally organized into half metre to metre-scale coarsening upward sequences, from clayey silt to sandy silt or very fine sand (Figures 5-26, 5-28, 6-45 and 6-50). Two subfacies can be recognized, based on the presence or absence of sand interbeds at the tops of the coarsening upward sequences. Burrows occur rarely, but become more common with depth. In most cases they occur at the tops of coarsening upward sequences. In sandy intervals, normal, reverse and double graded laminae and sandwich sand laminae are present. Thin laminae of fine woody organic debris occur very rarely. Small bivalve shells occur throughout this facies. The facies is gas rich, and irregular millimetre-scale vessicles commonly form in this facies when cores are brought to the surface. Expansion of the gas in the core is responsible for apparent core recoveries greater than 100%.

Cone bearing is generally low, with Q generally averaging between 5 and 12 (Table 6-2). In silt sections, low cone bearing peaks (Q <6) rise above a baseline of Q=2 to 3 and represent coarser silt beds (Figures 5-26, 5-28, 6-8, 6-45, 6-51 and 6-52). Thin sand beds are represented by higher cone bearing peaks with Q >6 and q_{cl} up to 50. As noted in the previous chapter, sand beds thicker than 10 cm appear to be fully resolved. This facies is

distinguished from sandier facies by having less than 50% with Q>6. The facies boundaries are defined where the 2 m rolling average for these parameters crosses these thresholds). Friction ratio values are high and more variable than in the bioturbated silt facies (typically R_f=1.0±0.6 to 2.0±0.7, and F_R=1.5±1 to 2.5±1), a reflection of interbedding of coarser and finer sediments. As described in the preceding chapter, friction ratio peaks commonly occur at the boundaries of sand beds and at rod breaks. Average I_F generally varies from 2.9±0.3 to 3.3±0.3. However, values up to 3.5 occur in a CPT with anomalously high friction ratio values (F_R=4.6±1.8; Figures 4-5 and 5-21). Excess pore pressures are generally positive (average B_q =0.3). Minima, which may be positive or negative, generally coincide with sandy silt or very fine sand beds.

In this facies, coarsening upward sequences are represented by dU and B_q decreasing-upward sequences (Figures 5-25, 5-27, 6-45, 6-51 and 6-52). However, in the silt subfacies, pore pressure decreasing-upward sequences due to upward coarsening can be obscured by rod breaks, particularly in SCPTs (Figure 5-27). Pore pressure minima due to rod break are exactly 1 m apart and do not coincide with cone bearing peaks. Coarsening upward sequences are not represented by cone bearing increasing upward sequences in this facies. If sand is present at the top of the sequence, it is expressed as a thin cone bearing peak.

Individual beds and sequences can be correlated on CPT data at least several tens of metres in this facies. Apparent dips up to 7° can be observed (Figures 6-4 and 6-5).

Based on its distinct CPT expression - low cone bearing with or without sand peaks, highly variable friction ratio, and generally positive excess pore pressure organized into upward decreasing cycles, this facies can be recognized widely in the upper foreset, particularly in the northern part of the delta (Figure 6-41). It is commonly interbedded with and grades into the laminated sand facies, both vertically and laterally. On the north margin of the delta it is laterally replaced by the bioturbated silt facies (Figure 6-34), which it probably overlies in much of the delta. In the eastern part of the delta it underlies and is laterally equivalent

to the rhythmically interbedded sand and silt facies. In CPTs on the western margin of the subaqueous platform this facies extends to the surface, so that this facies includes subaqueous platform as well as delta slope deposits (Figures 6-1 and 6-33).

LAMINATED SAND FACIES

This facies consists primarily of laminated very fine sand with subordinate amounts of silt, commonly organized into decimeter to metre-scale coarsening upward sequences. This facies varies in composition from thinly to thickly laminated very fine sand, sandy silt and silt, to laminated very fine sand with some thin to medium fine sand beds and scattered silt laminae. Normal, reverse, and double graded laminae and sandwich laminae occur in this facies (Figure 6-43), as well as thin to medium laminae of fine woody organic debris. Some fine to medium grained sharp-based sand units, generally less than a metre thick also occur, sometimes capping coarsening upward sequences. Burrows and small shell fragments occur rarely.

In this facies, coarsening upward sequences are commonly expressed as metre-scale cone bearing increasing upward sequences, and to a lesser extent as friction ratio decreasing upward sequences (Figure 6-45, 6-45, 6-51 and 6-52). Where the silt-dominated lower parts of the sequences are thin, the cone bearing increasing upward sequences are not always well developed and the cone bearing curve has the character of half metre to metre-scale sand beds, separated by thin cone bearing minima, which may not have typical silt values. q_{cl} peaks are commonly between 50 and 70. Average q_{cl} is between 20 ± 10 and 37 ± 15, and average Q is between 14 ± 9 and 30 ± 17 (Table 6-2). This facies is distinguished from the laminated silts by having greater than 50% with Q>6. Friction ratio is generally lower than in the laminated silt facies, although it is highly variable - F_R is generally between 1.1 ± 0.7 and 2.0 ± 1.0, because of the interbedding of sand and silt. Pronounced friction ratio peaks occur at the boundaries of sand beds defined on cone bearing, and friction ratios lows in the

sand units themselves have a serrate character. Average I_F in this facies varies from 2.4 to 2.9±0.4. I_F values are higher than usually recorded in sand because of the high friction ratios generated by the interbedding of sands and silts. Excess pore pressure is generally negative in this facies, with a few peaks greater than zero in the finest intervals. Most sharp-based sands in this facies are thin and cannot be distinguished from other sand beds based on CPT data. However, a 2 m thick sharp-based sand unit shown in Figure 6-53 has a CPT expression typical of such deposits: a sharp base, low uniform friction ratio and upward decreasing cone bearing and excess pore pressure, indicating upward fining.

As in the laminated silt facies, individual beds and coarsening upward sequences can be correlated at least several tens of metres across a site and have apparent dips up to 7° (Figure 6-53). This facies is interbedded with and passes laterally into the mixed sand facies and the laminated silts (Figures 6-4 and 6-6). In CPTs on the seaward margin of the subaqueous platform in the southern part of the delta, this facies extends to the surface (Figures 6-53). Thus, this facies includes subaqueous platform as well as delta slope deposits, like the laminated silts.

MIXED SAND FACIES

This facies is characterized by thin to medium beds of fine sand interbedded with laminated very fine sand and silt (Figures 6-45, 6-41 and 6-52). Fine sands occur in both sharp-based sand units and in the upper parts of metre-scale coarsening upward sequences similar to those in the laminated sand facies. In cores, 25-50% of the facies consists of sharp-based sands. Thin to thick laminae of fine woody debris occur in the laminated sand and silt intervals. Mud-draped ripples are present in some intervals in this facies. In the coarsening upward sequences, normal, reverse and double graded laminae and sandwich sand laminae occur.

This facies is characterized on CPT data by half metre to metre-scale sand units up to 2 m thick with low serrate friction ratios (R_f~1%) and q_{cl} peaks exceeding 50 (Figures 6-45, 6-41 and 6-52; Table 6-2). These units represent individual or stacked sharp-based and coarsening upward sequences. Intervening units vary from thin friction ratio peaks and cone bearing minima, in which values typical of silts are not resolved, to intervals with variable friction ratio and cone bearing like the laminated sand facies. The bases of sharp-based sands and coarsening upward sequences are commonly reflected by sharp and gradual upward increases in cone bearing, respectively. Average friction ratio values are lower than in the laminated sand facies: F_R varies from 0.8±0.4 to 1.5±1.0. Average cone bearing is generally higher than in the laminated sand facies, reflecting higher average grain size. q_{cl} varies from 37±16 to 76±18, and average Q varies from 35±22 to 71±19. I_F varies from 2.0 to 2.4±0.4. Excess pore pressures are generally negative, although dU near zero occurs in some of the thicker sharp-based sands. In such cases the sharp base is indicated by a sharp upward change in dU from negative to near zero, and the upward fining is indicated by a gradual upward decrease in dU (Figure 6-6a).

The mixed sand facies occurs interbedded with other sandy facies of the upper foreset in the southern part of the delta (Figures 6-3 and 6-41). Apparent dips up to 7° occur (Figures 6-4 and 6-6).

SHARP-BASED SAND FACIES

This facies is characterized by thick sharp-based sand units interbedded with laminated sand and silt. It is well represented in only one of the boreholes examined for this study, but intervals with similar expression have been observed on other CPTs (Figures 5-18, 6-3, 6-7 and 6-54). In core, it consists of a 5 m thick sharp-based unit of fine to medium sand with abundant shells and silt clasts, overlying thin to medium beds of fine sand, including both laminated and sharp-based sands, laminated silt, and fine woody organic debris. The sharp-based sands in this facies are coarser than any others observed in the foreset.

This facies is characterized on CPT data by intervals with low, uniform friction ratio (R_f<1%) and excess pore pressures near zero (Figures 5-18, 6-3, 6-7 and 6-54; Table 6-2). The intervals are several metres thick and correspond to thick sharp-based sand units. These intervals comprise more than 50% of the facies. Cone bearing is higher than most other foreset facies, (average q_{c1}=55±10; average Q=50±16) because the sharp-based sands are coarser than other foreset sands. Consistent with this, excess pore pressures are near zero in the sharp-based sands and not as strongly negative as in other foreset sands. Intervals between the sharp-based sand units have higher friction ratio, negative pore pressure, and generally lower cone bearing, similar to the laminated sand facies. However, the highest cone bearing in the cored interval is in a laminated fine sand and is associated with strongly negative excess pore pressure (Figure 5-18). Average dU in this facies in this is -31 to -10 m, average F_R is 0.9±0.5 and average I_F is 2.1±1.

This facies occurs interbedded with other sandy facies in the southern part of the delta (Figures 6-3, 6-6b and 6-41). It also occurs in the northern part of the delta, where a bodies of this facies occupies interval up to 30 m thick at the top of the foreset (Figure 6-7).

At Roberts Bank Port, sharp-based sands that are individually 2 to 4 m thick and are interbedded with bioturbated sands and silts like those of the bioturbated sand facies occur near the base of the deltaic section, overlying a thin interval of bioturbated silts (Figure 6-49). This interval was below the depth of the CPT.

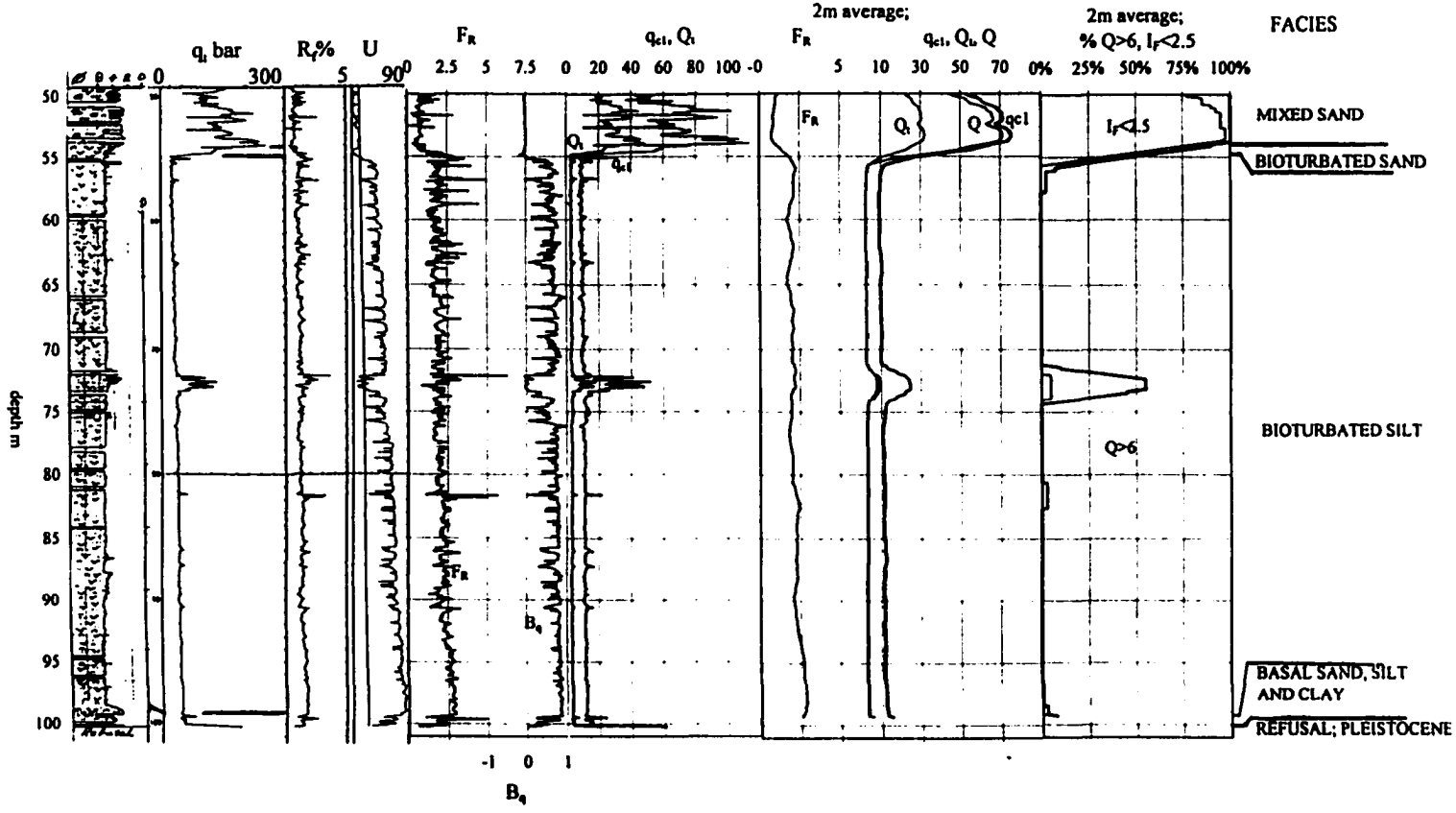

Figure 6-48. Lithology, non-normalized and normalized CPT data from borehole FD92-11, showing the bioturbated and basal sand, silt and clay facies. From left to right: lithology; non-normalized data (q_t, R_f and U); normalized data (F_R, B_q, Q_t and q_{c1}); normalized data averaged over 2 m (F_R, Q_t, Q and q_{c1}); and estimates of sand content averaged over 2 m based on Q>6 and I_F<2.5. Note the low uniform cone bearing (q_t, Q_t, Q and q_{c1}) and positive excess pore pressure (B_q) in the bioturbated silt facies. See also Figures 5-8, 5-25, 6-3, 6-8 and 6-45.

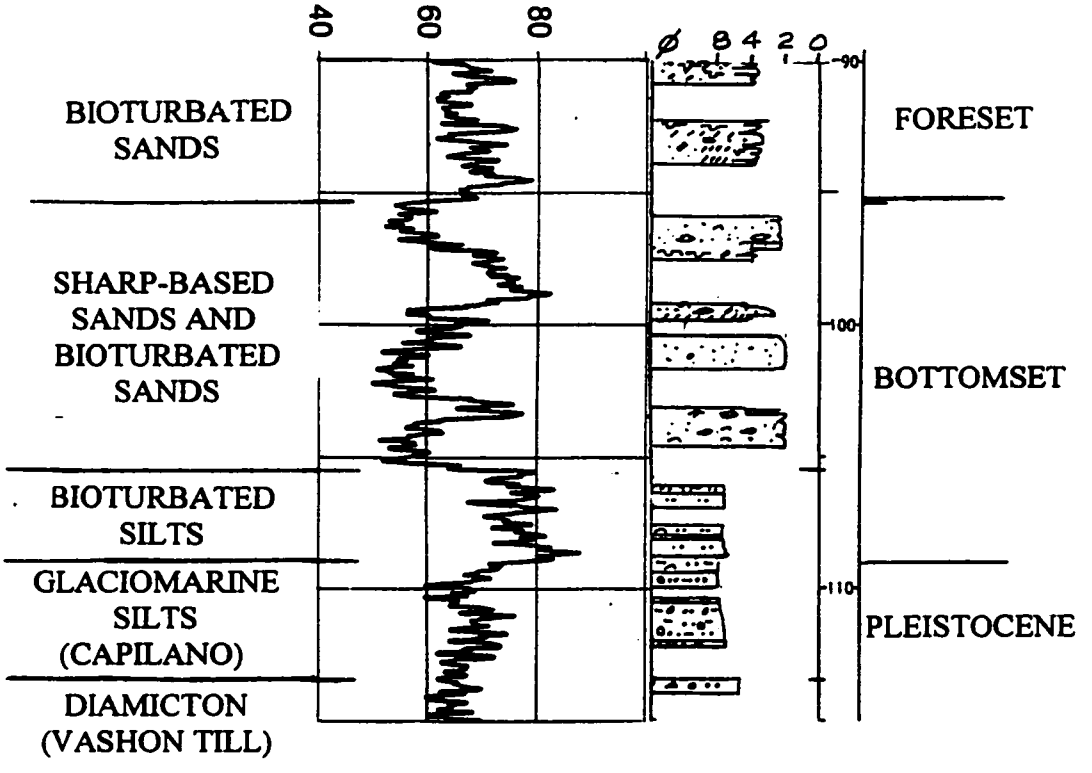

Figure 6-49. FD95S-1 Lithology and gamma ray log at base of deltaic section. From left to right gamma ray log in count per second (CPS). Note the presence of thick sharp-based medium-grained sand beds, interpreted to be sediment gravity flow deposits, overlying bioturbated silts of the bottomset.

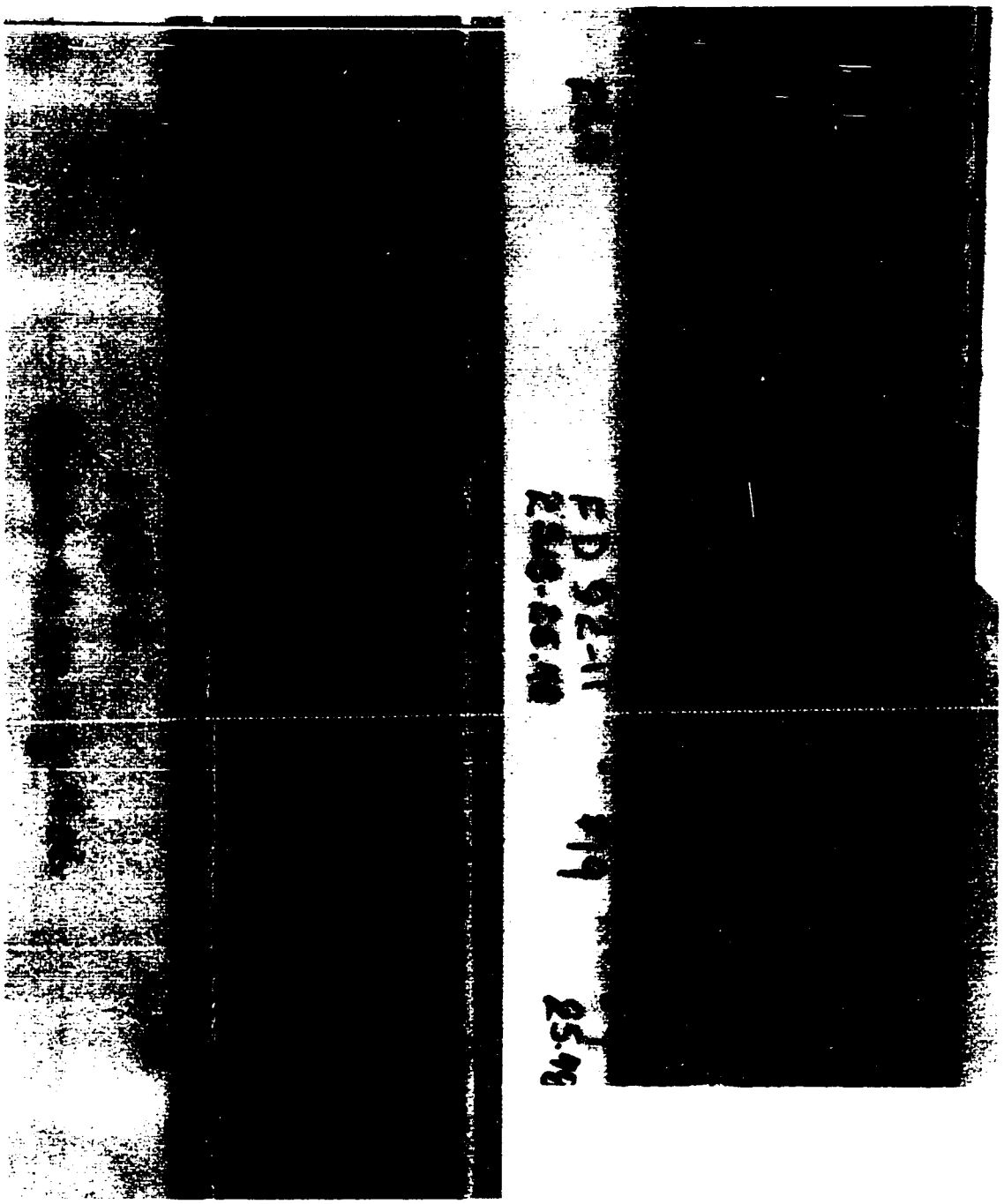

a b

Figure 6-50. Core photographs of laminated silts; a) FD94-4, silt subfacies, CPT depth 40.50 to 40.80 m. Note burrow at 40.70 m core depth (Figure 5-27). From Monahan et al. (1997); b) FD92-11; sandy subfacies, CPT depth 24.10 to 24.40 m. Note reverse grading in sandy laminae at 25.38 m core depth, at top of coarsening upward sequence (Figure 5-25).

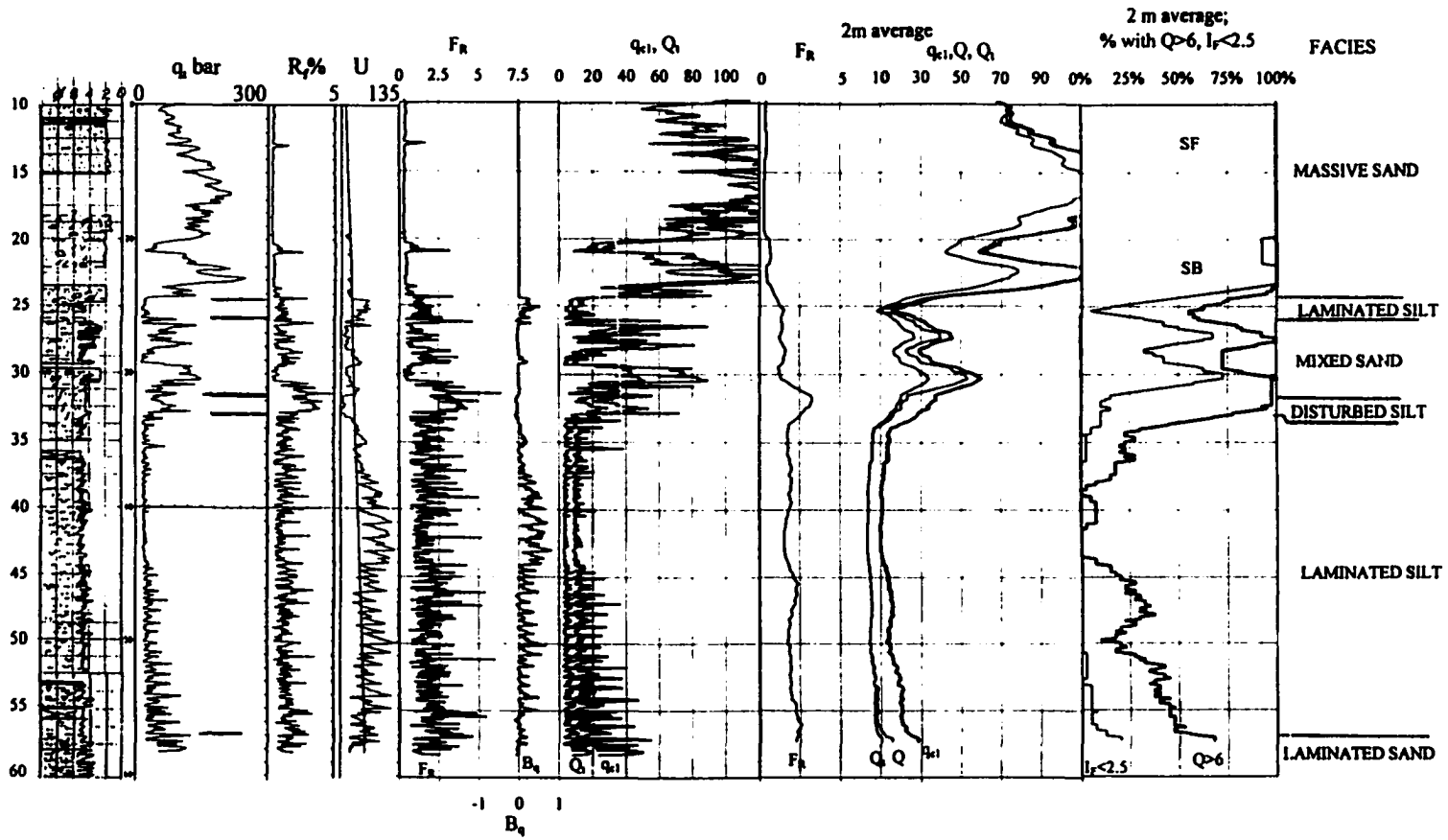

Figure 6-51. Lithology, non-normalized and normalized CPT data from boreholes FD92-2 and FD94-4, showing the disturbed silt and laminated silt facies. From left to right: lithology; non-normalized data (q_t, R_f and U); normalized data (F_R, B_q, Q_t and q_{c1}); normalized data averaged over 2 m (F_R, Q_t, Q and q_{c1}); and estimates of sand content averaged over 2 m based on Q>6 and I_F<2.5. Note the low cone bearing (q_t, Q_t, Q and q_{c1}) in the laminated silt facies; intervals with and without regularly-spaced cone bearing peaks represent sandy and sand-free subfacies respectively. In this facies, B_q is generally positive, and pore pressure decreasing upward sequences represent metre-scale coarsening upward sequences (Figure 5-27). The disturbed silt facies is characterized by moderately high cone bearing, high friction ratio (R_f and F_R), and strongly negative excess pore pressure. This CPT is also shown in Figures 6-4 and 6-34.

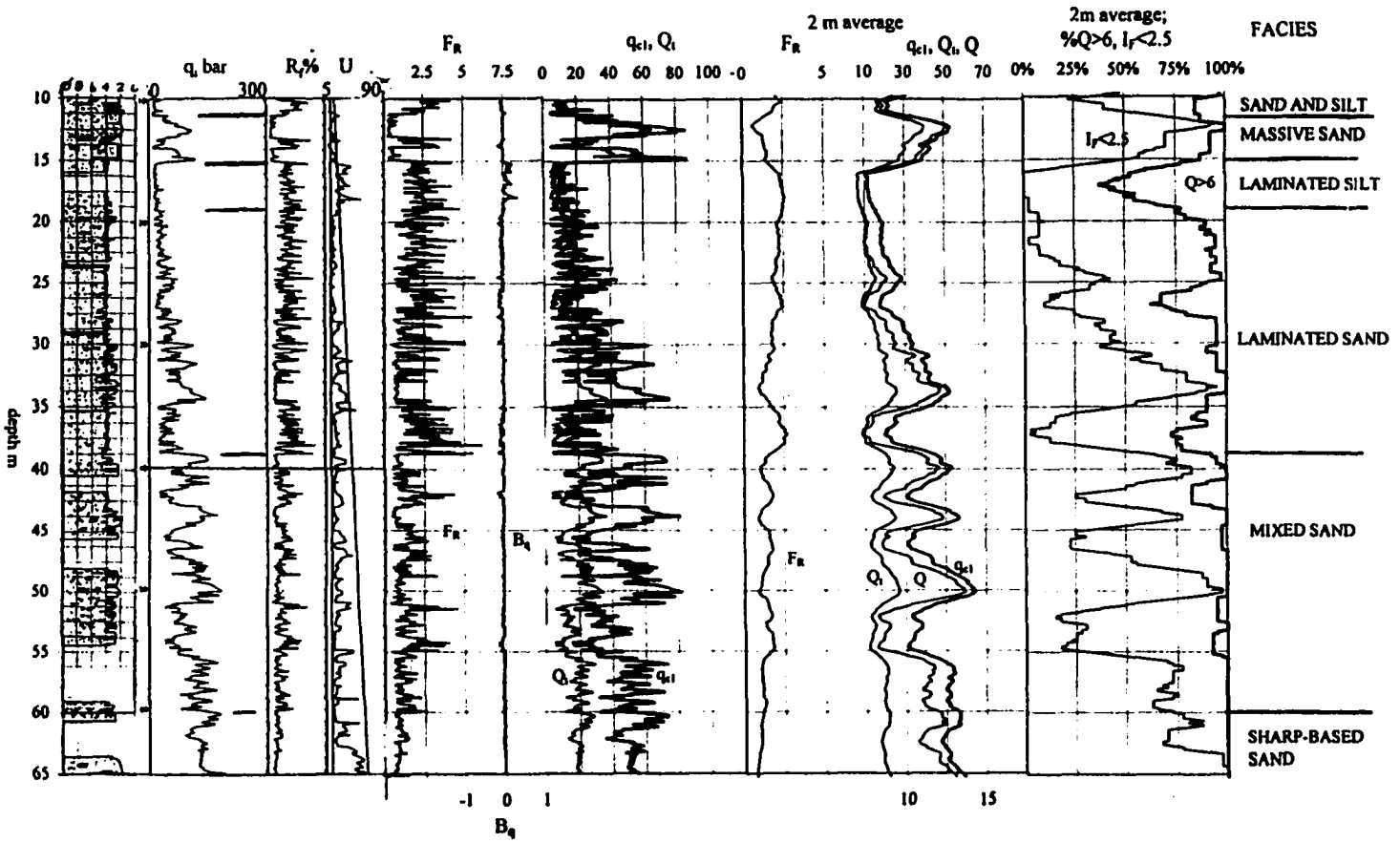

Figure 6-52. Lithology, non-normalized and normalized CPT data from boreholes FD93-1 and FD95S-1, showing the laminated sand and mixed sand facies. From left to right: lithology; non-normalized data (q_t, R_f and U); normalized data (F_R, B_q, Q_t and q_{c1}); normalized data averaged over 2 m (F_R, Q_t, Q and q_{c1}); and estimates of sand content averaged over 2 m based on Q>6 and I_F<2.5. The laminated sand facies is dominated by sandy metre-scale coarsening upward sequences expressed as cone bearing (q_t, Q_t, Q and q_{c1}) increasing upward sequences and with highly variable friction ratio values (R_f and F_R). The mixed sand facies includes packages of sharp-based sands sharp-based sand that have higher cone bearing and lower friction ratio values. This CPT is also shown in Figure 6-3.

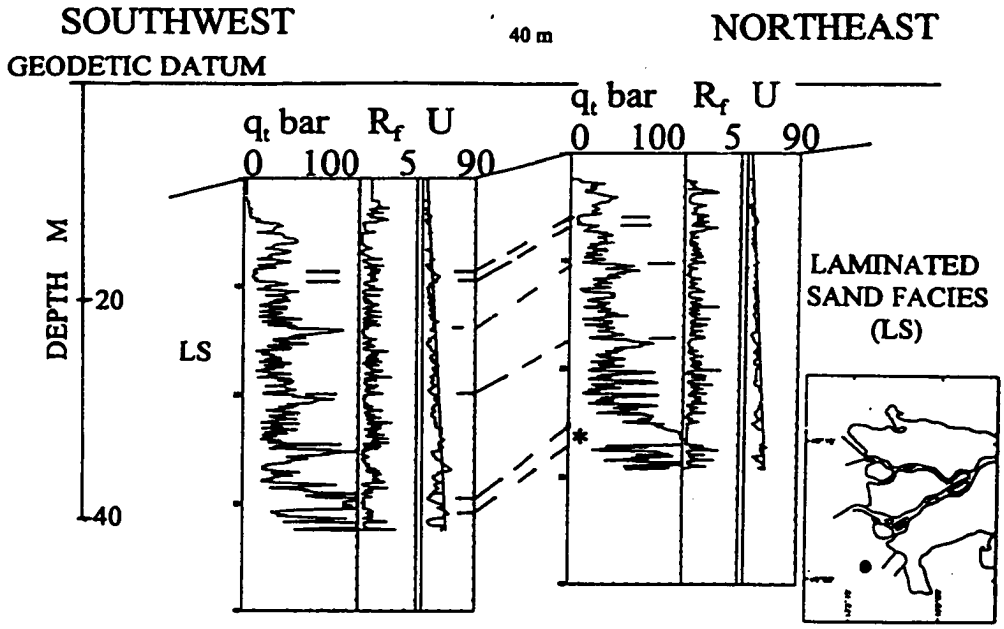

Figure 6-53. CPT cross section on the subaqueous platform of Roberts Bank, showing apparent dips of 6° in foreset strata. These sediments are assigned to the laminated sand facies and consist primarily of metre-scale coarsening upward sequences. Note sharp-based sand (*) interpreted as a sediment gravity flow deposit. For facies symbols, see Table 6-1. R_f in % and U in metres of water.

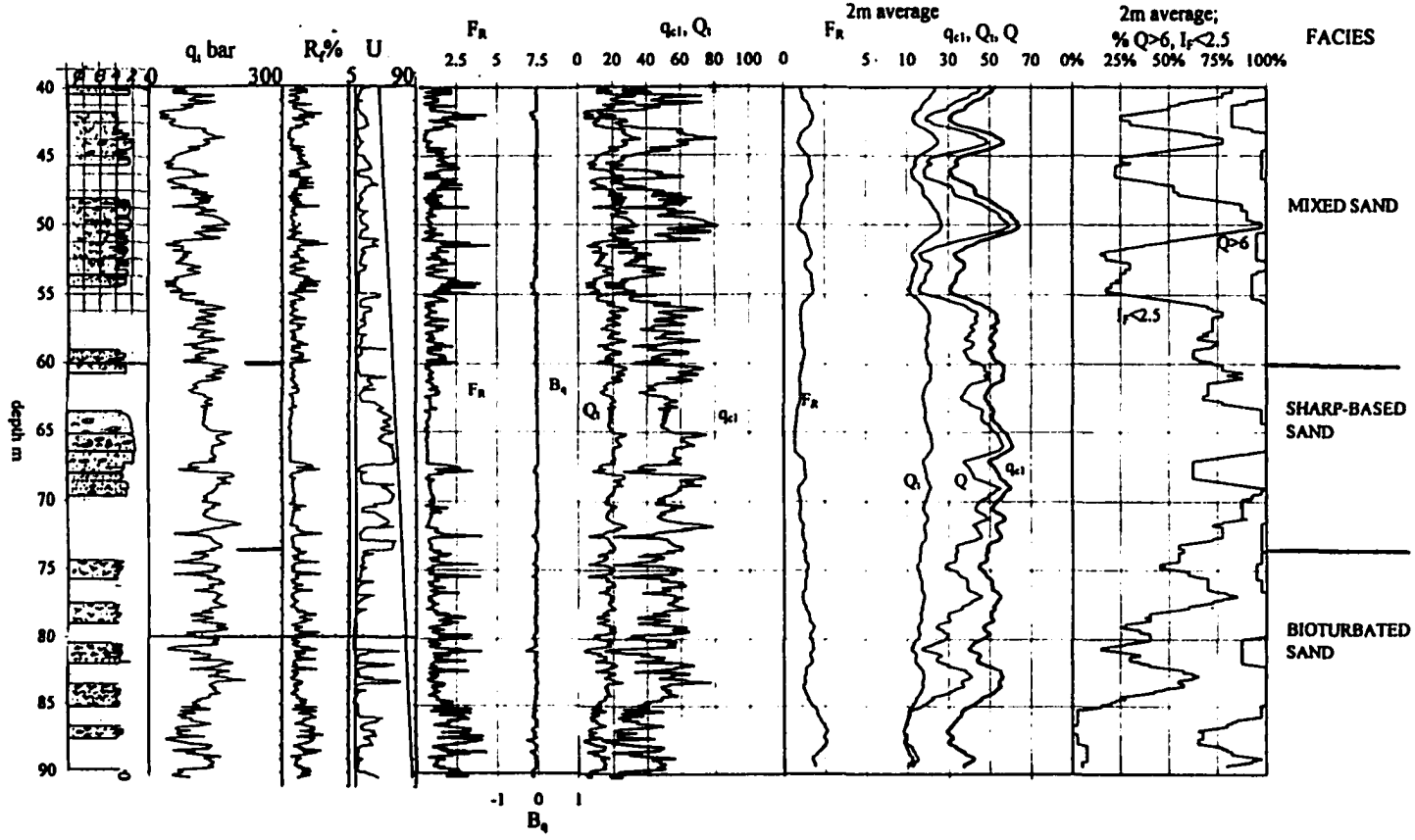

Figure 6-54. Lithology, non-normalized and normalized CPT data from boreholes FD93-1 and FD95S-1, showing the mixed sand, sharp-based sand and bioturbated sand facies. From left to right: lithology; non-normalized data (q_t, R_f and U); normalized data (F_R, B_q, Q_t and q_{c1}); normalized data averaged over 2 m (F_R, Q_t, Q and q_{c1}); and estimates of sand content averaged over 2 m based on Q>6 and I_F<2.5. The sharp-based sand facies is dominated by sharp-based sands interpreted to be gravity flow deposits, with low relatively uniform friction ratio values (R_f and F_R). The bioturbated sand facies has variable cone bearing and friction ratio, and has a CPT expression similar to the mixed sand facies. See also Figure 5-17. This CPT is also shown in Figure 6-3.

BIOTURBATED SAND FACIES

This facies consists of bioturbated sand with amounts of subordinate silt, and generally has a burrow mottled texture, although some discrete centimetre-scale circular burrows occur. Stratification varies from medium laminae to medium beds, and has been partially obscured by burrowing. However, reverse graded silt to sand laminae and ripples draped with mud laminae are locally preserved (Figures 6-3, 6-54 and 6-55). Small patches of fine woody organic debris commonly occur. Some unburrowed intervals are present, and consist of sharply defined thin beds of fine sand with medium to thick laminae of fine woody organic debris, and thin laminae of coarse sand. Metre-scale coarsening upward sequences are not evident in the cores in this facies, although it generally coarsens upward on a decametre-scale. This facies is well developed in only one borehole observed for this study, located on the subaqueous platform adjacent to the sand-wave field on southern Roberts Bank, and occurs between depths of 73 and 95 m. Organic debris in the overlying mixed sand facies provided a date of 1690+60 ^{14}C years (TO-4096; Appendix F).

In CPT data, this facies is characterized by metre-scale high cone bearing sand beds, separated by thin minima in which silt values are not resolved (Figure 6-54; Table 6-2). Average q_{c1} is 44±13 and average Q is 25±19. These beds have a low (R_f<1%) serrate character on the friction ratio curve, and are separated by friction ratio peaks representing sand silt contacts and silt beds. Average F_R is 1.7±0.8. Average I_F is 2.6±0.4, higher than would be anticipated for sands because of high friction ratios associated with the interbedding of sands and silts. As in the laminated sands, excess pore pressures are negative. Although coarsening upward sequences are not evident, the expression of this facies on CPT data resembles that of the mixed sand and laminated facies on CPT data. This facies appears to be a bioturbated equivalent of them.

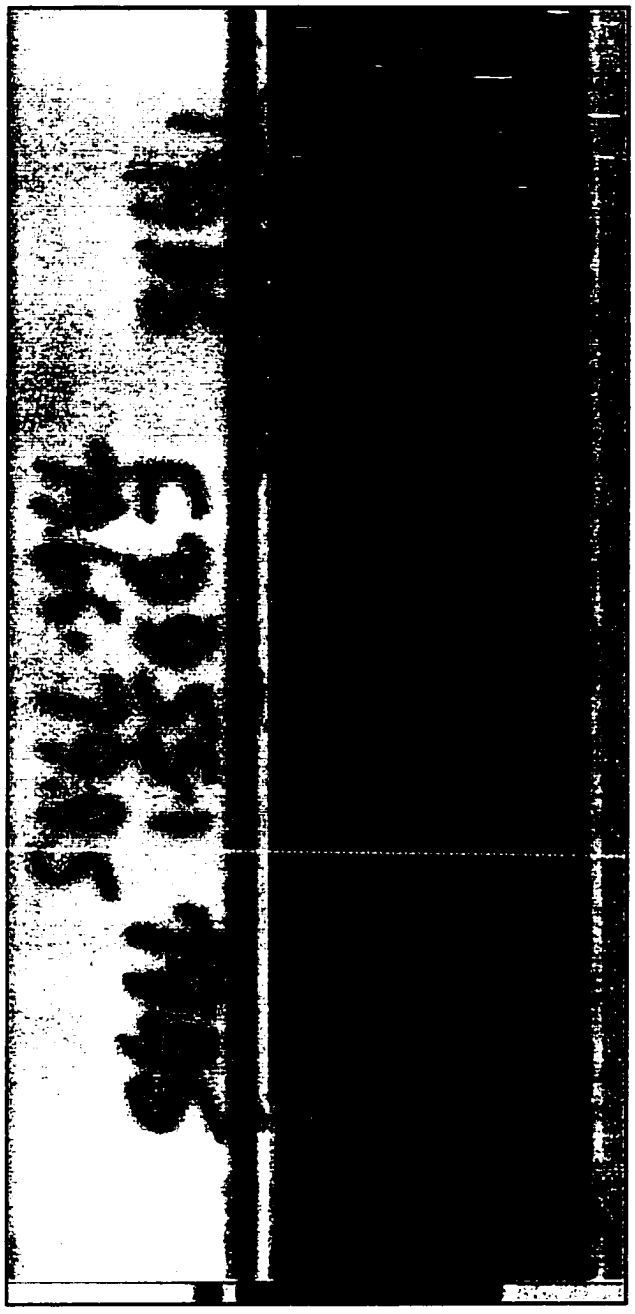

Figure 6-55. Core photograph of the bioturbated sand facies. Note circular burrows, disrupted laminae, and lenticular sand laminae interpreted to be mud-draped ripples. FD95S-1, CPT depth 80.97 to 81.27 m. See Figures 6-1 and 6-54.

THICK COARSENING UPWARD SAND FACIES

This facies consist of one or more stacked coarsening upward sequences dominated by fine sand and more than 1 m thick (Figures 5-15, 6-30 and 6-46). The lower parts of the sequences consist of interbedded and interlaminated very fine sand and silt with normal, reverse and double graded laminae coarsening up to fine sand (Figure 6-44). The upper parts of the sequence consist of thin to medium beds of relatively uniform fine sand with laminae of silt and fine woody organic debris. Little or no upward coarsening occurs in these parts of the sequences. The sequences are sharply bounded at the top.

The coarsening upward sequences are expressed as cone bearing increasing upward sequences with sharp upper boundaries (Figures 5-15, 6-3, 6-30 and 6-46; Table 6-2). However, cone bearing increases upward throughout the sequence, including through the upper part in which little grain size change occurs, peaking at q_{c1} values between 70 and 90. As discussed in the previous chapter, the upward increase in cone bearing that does not coincide with upward coarsening probably indicates upward increase in density. In the coarsening upward sequences, friction ratios are low and have a serrate character, and friction ratio peaks occur at the tops and bases of the sequences. Excess pore pressures are negative, supporting the interpretation of increased density in the upper parts of these sequences. In this facies, q_{c1} averages 50$\pm$25, Q averages 50$\pm$25, R_f averages 0.8$\pm$0.3%, F_R averages 0.9$\pm$0.5, dU averages -10$\pm$10 m and I_F averages 2.2$\pm$0.4.

This facies occur interbedded with the laminated silt facies in the upper part of the foreset. It is commonly overlain by the topset.

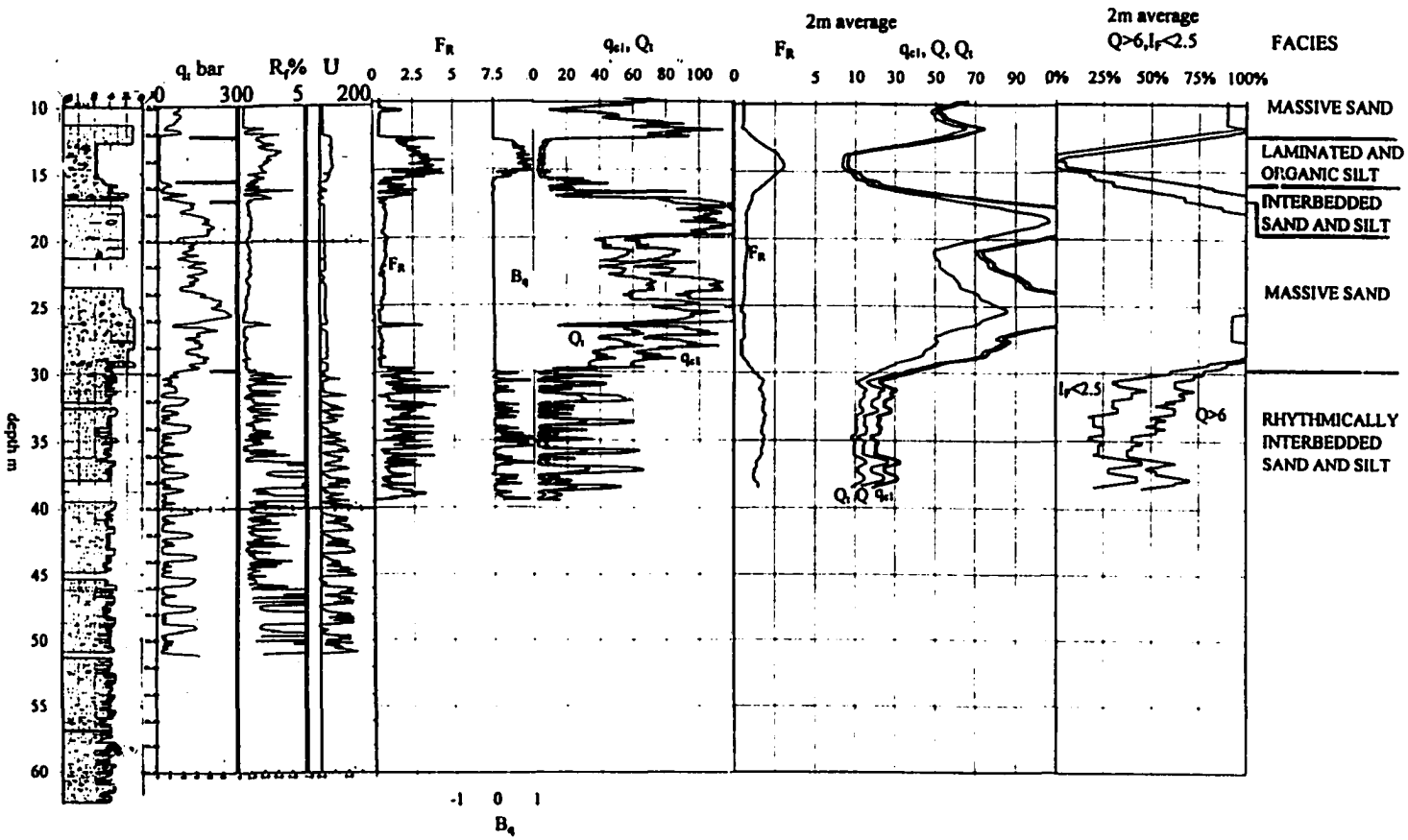

Figure 6-56. Lithology, non-normalized and normalized CPT data from borehole FD92-5, showing the rhythmically interbedded sand and silt facies. From left to right: lithology; non-normalized data (q_t, R_f and U); normalized data (F_R, B_q, Q_t and q_{c1}); normalized data averaged over 2 m (F_R, Q_t, Q and q_{c1}); and estimates of sand content averaged over 2 m based on Q>6 and I_F<2.5. Because digital data were not available for the CPT shown on the left, the normalized data shown are from a different CPT. Note the rhythmic interbedding of medium to thick very fine sand beds, expressed as high cone bearing intervals, with laminated to thinly bedded very fine sand and silt. This borehole and CPT are also shown in Figure 6-10.

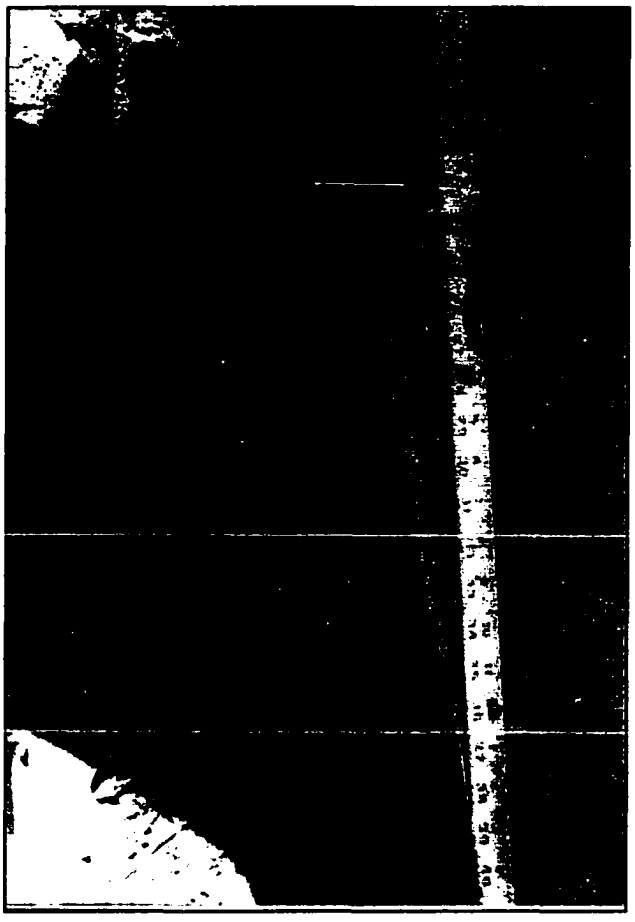

Figure 6-57. Core photograph of the rhythmically interbedded sand and silt facies. Note the laminated silts and very fine sands, and gradational contact with overlying very fine sand bed - silt laminae occur in the lower part of the sand bed. FD92-5, corrected core depth 33.1 to 33.6 m. See Figures 6-10 and 6-56.

RHYTHMICALLY INTERBEDDED SAND AND SILT FACIES

This facies consists of medium to thick beds of clean very fine sand rhythmically interbedded with laminated to thinly bedded very fine sand and silt, and organized into broadly coarsening upward sequences up to 2 m thick (Figure 6-56). It was directly observed in only one borehole examined for this study, but is readily identifiable in several CPTs at the head of the delta (Figures 6-1 and 6-10). The very fine sand beds generally have gradational bases (Figure 6-57); silt laminae occur at their bases and decrease in thickness and abundance upwards. Similar but thinner transitions also occur at the tops of the very fine sand beds. The intervening intervals consist of laminated clayey to sandy silts and very fine sands, commonly organized into decimetre-scale coarsening upward sequences

This facies has a distinct expression on CPT data (Figures 6-1,6-10 and 6-56; Table 6-2). The medium beds of very fine sand are expressed as high cone bearing units in which q_{c1} peaks at 50 to 70, and which are rhythmically repeated every 1 to 2 m. In the intervening sand and silt intervals, thin cone bearing peaks (q_{c1} between 20 and 30) rise above a baseline with Q_t between 2 and 3. Q averages 17±1, and the 2 m continuous average is generally greater than 10. Friction ratio is low in the very fine sand beds (R_f~1), and has a serrate character. In the intervening intervals, friction ratios are higher and peak at sand silt contacts. Overall, R_f averages 1.3±0.7% and F_R averages from 1.6±0.9 to 2.1±1.2. I_F averages 2.9±0.5. Excess pore pressures vary from negative in the very fine sand beds to positive in the intervening intervals. Average excess pore pressures are positive: dU averages 14±35, and B_q 0.17± 0.3.

The coarsening upward sequences are expressed as pore pressure decreasing upward sequences. The coarsening upward sequences are not well expressed on the cone bearing curve, although the gradational bases of the very fine sand beds are commonly expressed thin cone bearing increasing upward intervals.

This facies occurs at the head of the delta, and is well represented in CPTs on Annacis Island and the eastern part of Lulu Island (Figures 6-1, 6-10, 6-41 and 6-42). Thus this facies represents some of the earliest foreset deposits. Wood from the foreset in this area has been dated at 9490+250 (GSC-3919; Williams and Roberts, 1989). Developments of this facies are up to 40 m thick and both overlie and are laterally equivalent to laminated silt facies (Figures 6-1 and 6-10).

LOW DIPPING INTERBEDDED SAND AND SILT FACIES

This facies consist of interbedded fine sands and silts (Figure 6-12, 6-16 and 6-58). The fine sands are generally organized into coarsening upward sequences from less than 1 m to over 4 m in thickness. Silt interlaminae occur in the lower parts of these sequences and diminish in thickness and frequency upward; normal and reverse graded laminae and paired silt laminae occur in these intervals. The upper parts of the thicker sequences are relatively uniform fine sand with faint laminations due to subtle grain size changes. Some sharp-based sands also occur and are between 0.5 and 3 m thick. Laminae of fine woody organic debris also occur in sand. Intervals of stacked coarsening upward sand units are interbedded with intervals of laminated silt up to 3 m thick. Silt dominated units locally include thin sharply bounded sand beds.

Deposits of this facies resemble those of several other facies - the thick coarsening upward sequences, the laminated silts, the laminated sands, and the sharp-based sands - and are distinguished primarily on the basis of CPT data. Correlation of the coarsening upward sequences and the laminated silts intervals across sites using CPT data indicate very low dips compared to other foreset sediments, varying from undetectable to a maximum of 2^{o} (Figure 6-12). Furthermore, dip directions are irregular, varying from south through west to north.

The coarsening upward sequences are well expressed as cone bearing increasing upward

sequences. However, the peak q_{c1} values are generally higher than in other facies - commonly between 100 and 190 (Figure 6-58). Cone bearing increases upwards in the upper parts of thick coarsening upward sequences, although grain size remains more or less constant, as in the thick coarsening upward sand facies. Similarly, the cone bearing increases unaccompanied by grain size increases are interpreted to represent upward increasing density. Excess pore pressures are generally negative in the coarsening upward sequences. Friction ratios are low with a serrate character, and friction ratio maxima occur between the coarsening upward sequences.

The sharp-based sand units have the same expression on CPT data as in the sharp-based sands facies - low uniform friction ratio, excess pore pressures near zero, and relatively high cone bearing . The silt intervals have low cone bearing, with thin cone bearing peaks (q_{c1} up to 50) representing thin sand beds rising above a silt baseline of Q=5. In the silt intervals, friction ratios are low where no sand beds are present, but are generally high where interbedded with thin sands. Excess pore pressures are positive in the silt intervals, with pore pressure minima associated with thin sand beds.

The low dipping interbedded sand and silt facies can be recognized in several sites in the urban core of Richmond (Figure 6-41). It is up to 15 m thick and overlies the laminated silts and underlies the foreset. Based on a ^{14}C date from a twig in the underlying silts in borehole FD93-2 the deposits are less than 6710$\pm$80 ^{14}C years old (TO4143; Appendix F). This facies is laterally replaced to the east by the lower part of the topset massive sand facies, including the parts of the distal subfacies preserved in the central parts of the upper delta plain (Figures 6-1 and 6-32).

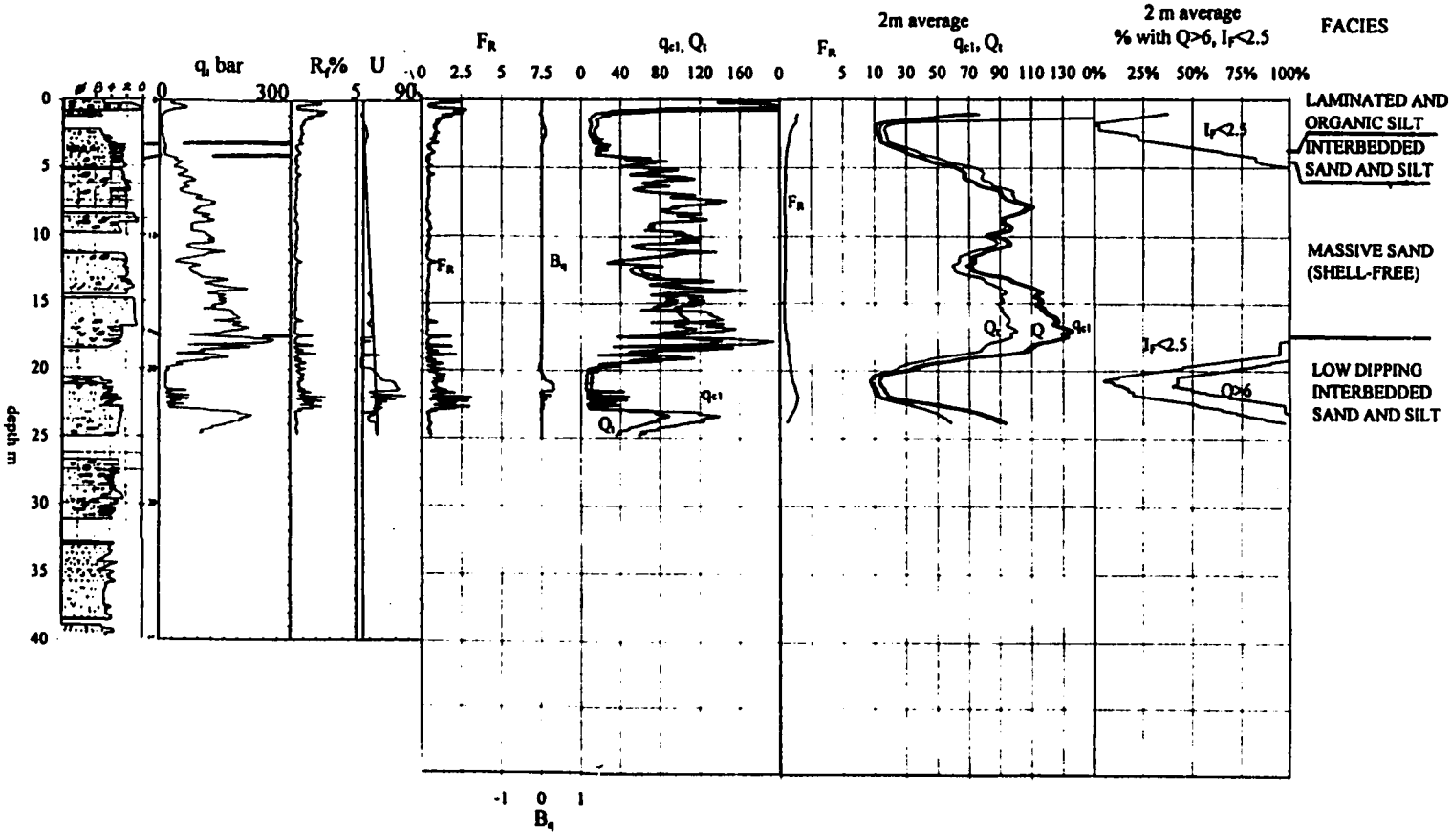

Figure 6-58. Lithology, non-normalized and normalized CPT data from borehole FD93-2, showing the low dipping interbedded sand and silt facies. From left to right: lithology; non-normalized data (q_t, R_f and U); normalized data (F_R, B_q, Q_t and q_{c1}); normalized data averaged over 2 m (F_R, Q_t, Q and q_{c1}); and estimates of sand content averaged over 2 m based on Q>6 and I_F<2.5. Note the high cone bearing (q_t, Q_t, Q and q_{c1}) in the sandy coarsening upward sequences represent by cone bearing increasing upward sequences (q_{c1} up to 190). This facies consists of sands and silts similar to those occurring in several other facies, and is characterized by low dips (Figure 6-12) and high cone bearing. See also Figure 6-16.

DISTURBED SILT FACIES

This facies consists of medium and coarse silt. It generally appears massive, but locally includes large clasts, reoriented decimetre-scale blocks of laminated silt and sand, and deformed laminae. It is interpreted to be a slump deposit (Figure 6-59).

This facies has a distinct expression on CPT data (Figures 5-32 and 6-51). Both cone bearing and friction ratio values are anomalously high. I_F averages 2.5 to 2.7, correctly identifying these deposits as silt. In addition, excess pore pressures are strongly negative (dU = -20 to -30 m, and B_q = -0.04 to -0.07). As discussed in the preceding chapter, these characteristics indicate that this facies is overconsolidated.

This facies was observed in thin intervals in two boreholes in the upper foreset (Figures 6-4 and 6-13. In one case it occurs directly below a sharp-based sand unit.

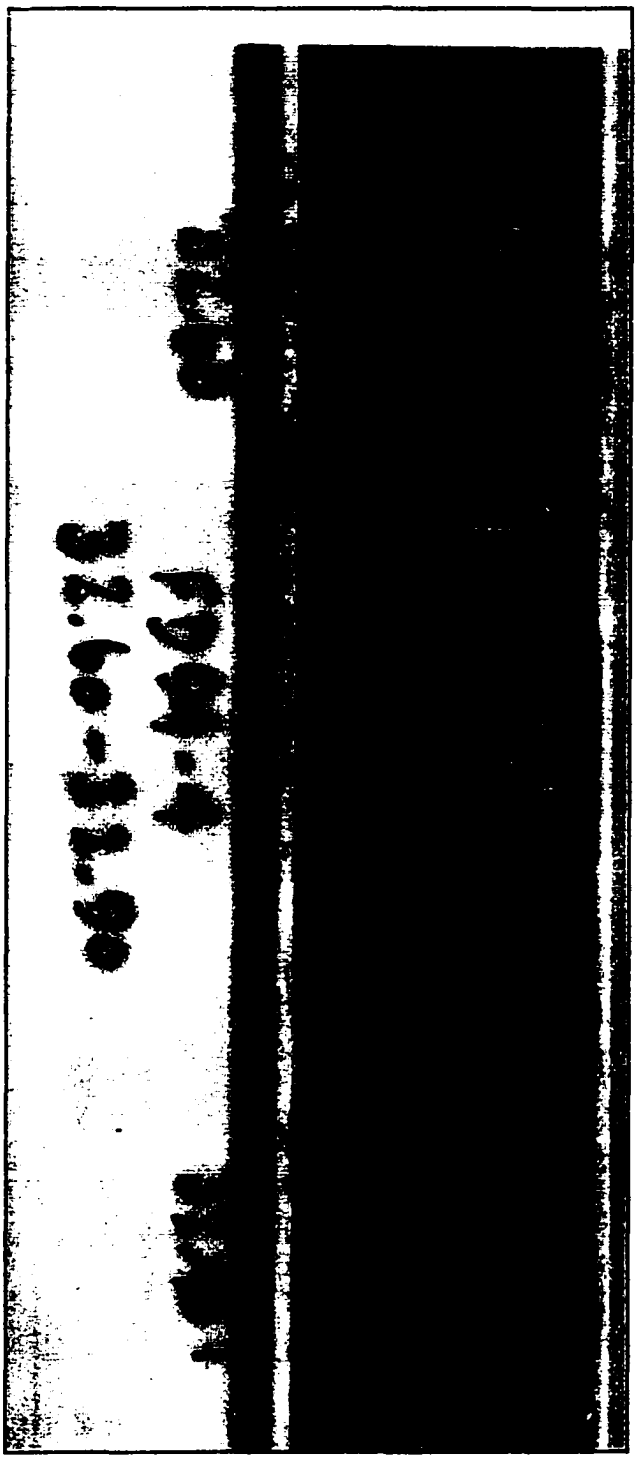

Figure 6-59. Core photograph of the disturbed silt facies in the upper foreset. Note blocks with disturbed bedding in massive appearing matrix. This is interpreted to be slump deposit. FD94-4, CPT depth 31.92 to 32.22 m. See Figures 5-32, 6-4 and 6-51. This borehole was cored using a triple tube retractor core barrel, which did not produce significant core deformation in silts. From Monahan et al. (1997).

FACIES RELATIONSHIPS AND INTERPRETATION OF THE FORESET AND BOTTOMSET

Depositional Processes

Deposition of sand and silt on the delta slope during the spring freshet is currently regulated by tidal and fluvial cycles. At the river mouth, current strength and suspended sediment concentration in the river vary inversely with tidal height (Kostaschuk et al., 1992b). Furthermore, the suspended sand load is rapidly deposited in the river channel on a rising tide, as the salt-wedge intrudes beneath the sediment-laden fresh river water. The sand is resuspended as the tide falls and the salt wedge withdraws from the river channel (Kostaschuk and Luternauer, 1989; Kostaschuk et al., 1989). Consequently, sand is transported past the river mouth only during low tide. Furthermore, sand is rapidly deposited on the delta slope close to the river mouth as the fresh water plume spreads over sea water (Figure 6-60), analogous to the deposition of sand in the river channel when the river water is separated from the river bed by the salt-wedge. The laminated sands and silts of the coarsening upward sequences are thus interpreted to represent suspension deposits derived from the plume.

Direct evidence of tidal processes in the foreset deposits is provided by the complex laminae. The rhythmic interlamination of sand and silt indicates rapid and cyclic changes in the energy and sediment concentration of the sediment-transporting currents, particularly evident in the sandwich sand laminae (Figure 6-43). Furthermore, the 14 principal laminae between sand-rich peaks of the secondary coarsening-upward sequence observed in Figure 6-44 is consistent with the 14 day spring-neap tidal cycle. In the latter example, several laminae contain secondary sandy laminae within them, and are thus interpreted to represent a semi-diurnal tidal cycle. Greater than 14 composite laminae between sand-rich peaks is not inconsistent with a tidal origin, because differentiation between daily and half-daily peaks is not always possible.

Furthermore, the variable grading patterns of the complex laminae can be explained by variation in the mixed semi-diurnal tidal cycle that operates in the Strait of Georgia. Normal grading is interpreted to result from the settling of suspended sediment from the plume during a low tide event, and would form when lower low tide follows higher high tide. However, inverse grading may form when lower low tide follows lesser high tide. Double grading may form when the two high tides are approximately equal, and where associated with the sandwich sand laminae, may represent the interplay of tidal currents on the sea floor with the tidally regulated transport of sand past the river mouth.

In addition, northwest-flowing flood tidal currents along the delta slope are stronger than southeast-flowing ebb tidal currents, and off the southern part of Roberts Bank are strong enough to transport sand-size material at depths of up to 100 m (Figure 6-60; Thomson, 1981; Luternauer, 1978, 1980; Kostaschuk et al., 1995). Consequently, sediments on the modern delta slope generally fine northward, from sands on the southern slope of Roberts Bank to silts on the slope of Sturgeon Bank (Clague et al., 1983, 1991; McLaren and Ren, 1995). Some evidence of winnowing by tidal currents in the foreset is provided by sediment draped ripples that occur locally in the mixed sand and the bioturbated sand facies in the southern part of the delta. The preferential drift of the plume to the north also contributes to the northward fining of foreset sediments.

The metre-scale coarsening-upward sequences of the foreset were recognized in shallow cores on the modern delta slope by B.S. Hart (pers. comm. 1993), who interpreted them to be annual deposits related to variations in fluvial sediment load during the spring freshet. During the spring freshet, the peak in suspended load occurs prior to the peak in river discharge (Kostaschuk and Luternauer, 1989; Kostaschuk et al., 1989, 1992b). Consequently the finer sediments are transported out of the river mouth earlier than the sands, which are most efficiently transported during peak flow. The interpretation that the metre-scale coarsening-upward sequences are annual cycles is consistent with the interpretations presented above that laminated silts and sands of the foreset are tidal rhythmites and that the

secondary coarsening-upward sequences represent fortnightly spring-neap cycles.

The rapid local sedimentation rates implicit in these interpretations are consistent with the narrow range in ^{14}C dates from the foreset in each of the deep GSC boreholes (Figure 2-6; Luternauer et al., 1991; Dallimore et al., 1995, 1996). For example, in FD94-4, five samples from between 31 and 170 m span 800 ^{14}C years (Appendix F; Dallimore et al., 1995)[10].

The sharp-based sands include silt clasts and shell fragments and are interpreted to represent sediment gravity flow deposits. Similar deposits also interpreted as sediment gravity flow deposits have been observed in shallow cores on the delta slope (Evoy et al., 1994). These deposits include sands coarser than found in the laminated sediments were probably derived principally from failures of bed-material load sand accumulations at active distributary mouths (Figure 6-60; Hart et al., 1992; Kostaschuk et al., 1992a). Large failures currently occur at the mouth of the Main Channel (McKenna et al., 1992; Christian et a., 1997a), although the scale of failures may be larger now than in the past because the river is no longer free to migrate and sedimentation is concentrated at the present river mouth (Hart et al., 1992; Monahan et al., 1993c). The disturbed silt facies is interpreted to represent slump deposits, based on the disrupted blocks of sediment and deformed laminae, and provides additional evidence of instability at active distributary mouths. The overconsolidation of these sediments is interpreted to result from shear failure (Terzaghi et al., 1996). The occurrence of sediment gravity flow and slump deposits in modern delta slopes indicates that the fluvial system delivered sediment to the river mouth more rapidly than they could be redistributed by marine processes - sediments accumulate there until they fail.

10

Although the average sedimentation rate of 0.17m/ ^{14}C yr is less than indicated by the coarsening upward sequences, the youngest sample is not the highest in this borehole, nor is the oldest the deepest, so that the samples are reworked and only the order of magnitude of the sedimentation rate can be inferred from these dates.

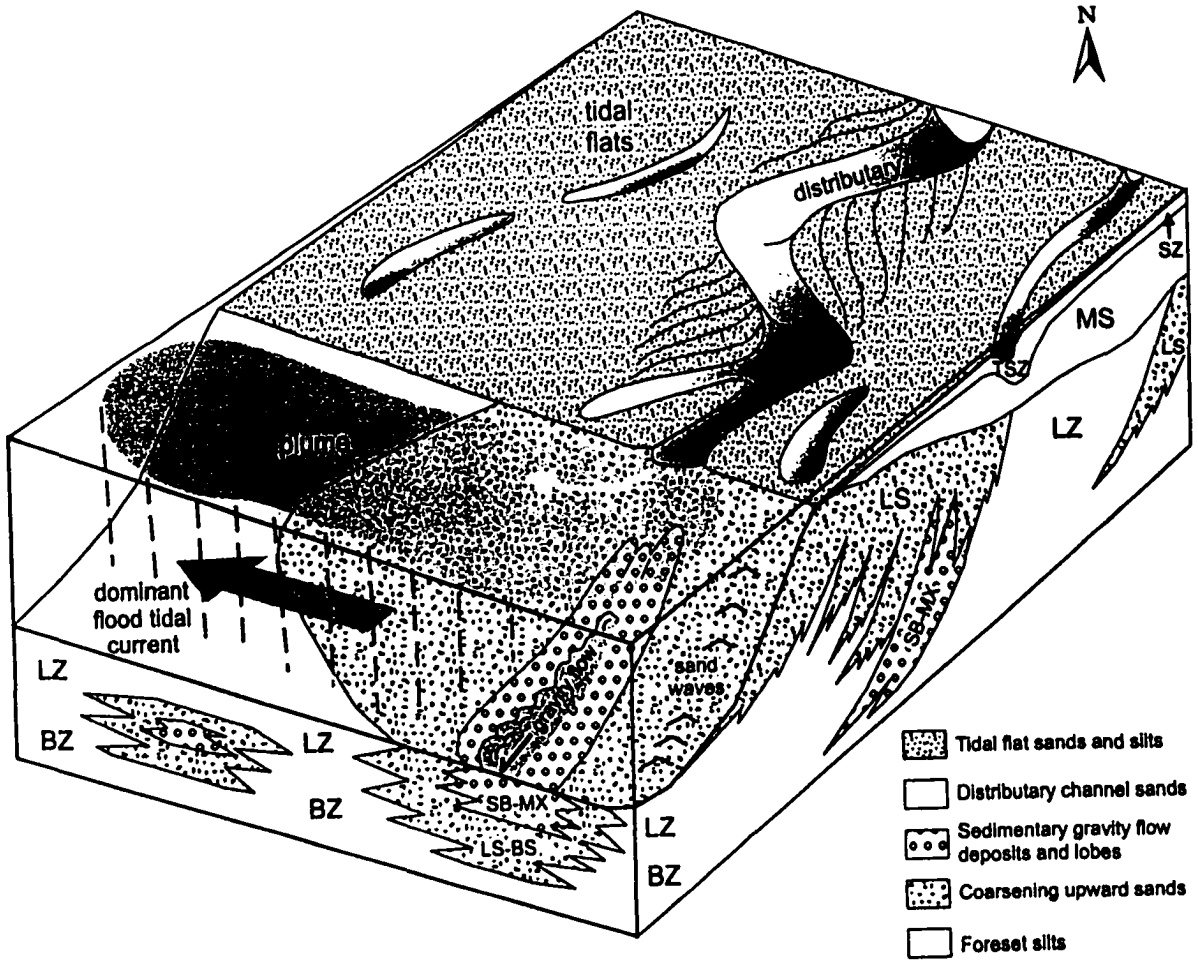

Figure 6-60. Block diagram showing sedimentary processes at the delta front. Suspended sediment in the plume is regulated by tidal and fluvial processes, and the plume drifts preferentially to the north as a result of tidal and coriolis forces. Deposits derived from the plume form laminated coarsening upward sequences that become finer with increasing distance from the river mouth. Gravity flow sands are deposited immediately seaward of active river mouths by failure of river mouth sand accumulations. South of the principal distributary mouth, northward flowing tidal currents rework delta slope deposits, winnowing fines and generating sand waves and other current structures. For facies abbreviations, see Table 6-1

The upward increase cone bearing in upper 1 to 2 m of thick coarsening upward sand sequences commonly corresponds to an upward decrease in excess pore pressure and not to increased grain size, and is interpreted to represent upward increasing density (Figure 5-15). This upward increase in density is interpreted to be the result of wave loading during winter storms, when the sedimentation rate was low. De Mulder and Westerhoff (1985) have attributed the high cone bearing in beach deposits in the Netherlands to the effects of breaking waves. Wave loading is also interpreted to be responsible for similar density increases in other foreset sands, such as the laminated sands and thin sharp-based sands in an interval of the sharp-based sand facies (Figure 5-18). Adjacent thick sharp-based sands do not exhibit high densities, because they were deposited quickly and were protected from months of wave loading by a few metres of sediment.

Wave energy in the Strait of Georgia is generally low (Thomson, undated; 1981) and does not appear to be effective in reworking sediment along the delta slope. Both the laminated silt and laminated sand facies extend up to the lower part of the subaqueous platform.

Facies Relationships and Interpretation

In a general way, the foreset coarsens upwards. The bioturbated silt facies, which forms much of the lower foreset (i.e. below ~60m) as well as the bottomset of the delta, coarsens up from clayey silt to silt (Figure 5-8; Dallimore et al., 1995, 1996) and is overlain by a variety of sandier facies in the upper foreset (~ above 60m; Figure 6-60) . However, the sediments of the foreset generally become finer northward, as a result of the northward sediment drift that still operates today (Figure 6-41). In the southern part of the delta, thick accumulations of sandy facies up to 30 m thick occur interbedded with thinner silts and extend to depths as great as 130 m (Clague et al., 1991; Luternauer et al.,1991), whereas in the northern part of the delta the foreset is predominantly silt.

The bioturbated silt facies is interpreted to represent suspension deposits derived from the

plume of sediment-laden fresh water discharged at the river mouth and deposited mainly on the lower parts of the delta slope (Figure 6-60). The intensity of bioturbation indicates that the rate of deposition was lower than in the overlying, predominantly well bedded facies. Hart et al. (1998) have documented slower sedimentation rates in bioturbated silts on the lower parts of the modern delta slope than in shallower interbedded silts and sands. The graded sand laminae observed in core and the sharp-based sands described elsewhere (Dallimore et al., 1995, 1996) are interpreted to represent gravity flow sands derived from the upper slope and/or delta front.

The bioturbated sand facies occurs in the lower foreset in the southern part of the delta. Based on the disruption of stratification by burrowing organisms and the high sand content, it is interpreted to have been deposited slowly on the lower delta slope where tidal currents limited silt deposition (Figure 6-60). As noted above, some evidence of winnowing tidal currents is provided by mud-draped ripples. Although this facies was observed in only one borehole observed for this study, the deeper parts of the thick sand accumulations in the southern foreset may belong to this or similar facies.

Sharp-based sands also occur near the base of the deltaic section, and are interpreted to represent deposits of sediment gravity flows that bypassed the slope and accumulated at its base and thus constitute bottomset deposits (Figure 2-6; Luternauer et al., 1994; see also Kostaschuk, et al., 1992a; Hart et al., 1992, 1998; Evoy et al., 1994, 1997). In one of the examples observed here, the sharp-based sands overlie a thin interval of the bioturbated silt facies, which is thus also interpreted to be part of the bottomset (Figure 6- 49). In another example, a sharp-based sand is grouped with the basal sand silt and clay facies (Figure 6-48), which probably includes sediment gravity flow deposits elsewhere. The underlying pink oxidizing clays observed at this site and elsewhere are much finer than anything else observed in the delta. They and the underlying sands occupy a similar stratigraphic position similar to the Capilano sediments and, although they are different from the poorly sorted pebbly silts typical of Capilano glaciomarine sediments, could possibly represent a local late

stage facies of them. The presence of offsets along fractures suggests a glacial setting.

The upper foreset is dominated by the laminated silt, laminated sand, mixed sand and sharp-based sand facies. These facies define a continuum from finer to coarser facies, and from those dominated by suspension to those dominated by gravity flow deposits. The grain size continuum is represented by a continuum of CPT parameters, from average Q = $\bar{4}$ to 12 and I_F = 3.3 to 2.9 in the laminated silt facies to Q = 50 and I_F = 2.1 in the sharp-based sand facies. Facies of this continuum grade into one another both vertically and laterally. These facies are complexly interbedded in the southern part of the delta, where thick accumulations of sandy facies are interbedded with the laminated silts (Figure 6-41). However, the upper foreset in the north part of the delta is dominated by the laminated silt facies, and sand-dominated units are highly localized. For example, a 30 m thickness of the sharp-based sand facies occurs in a CPT located 0.8 km north (on depositional strike) of a CPT in which the entire upper foreset is formed by the laminated silt facies (Figure 6-7). The overall northward increase in silt content reflects the northwards sediment drift as a result of tidal currents along the delta front and delta slope (Figure 6-60). In this sense, the deposits assigned to the bioturbated silt facies in upper foreset along the northern margin of the delta represent the finest end member of the facies continuum described above.

Increasing sand content and increasing proportion of gravity flow deposits are also interpreted to reflect increasing proximity to an active distributary mouth (Figure 6-60). On the surface of the delta slope seaward of the mouth of the Main Channel, Hart et al. (1998) has observed that sandy facies pass northward to silts within 0.3 km, the same order of magnitude as the distance between the thick sharp-based sands and the laminated silts described above. Where the sand and silt facies of the foreset are interbedded, they form decametre-scale coarsening and fining upward sequences, which pass from one facies to another, and are interpreted to reflect the changing position of an active distributary mouth. However, in several instances, sharp-based sequences fine upward from the sharp-based or mixed sand facies to the laminated sand and silt facies (Figures 6-3, 6-8 and 6-45). Such

cases may represent in part the fill of valleys incised into the delta slope by large river mouth failures, and comparable to the sea valley off the mouth of the Main Channel (Hart et al., 1992; Christian et al., 1994; Evoy et al., 1994).

The laminated silt and laminated sand facies extend up to the subaqueous platform in the northern part of the modern delta front and thus are transitional into the topset.

Most of the other facies can be interpreted in the context of the depositional patterns described above. The thick coarsening upward sand facies represents the coarsest suspension deposits and thus was probably deposited close to an active distributary mouth.

The rhythmically interbedded sand and silt facies forms a thick body of sediment at the head of the delta. It overlies and passes laterally into the laminated silt facies. As such it represents the earliest sandy facies of the foreset. It does not fit readily into the facies continuum described above: the average silt content is high, based on average Q and I_F, yet sand beds are as thick as those that occur in the mixed sand facies. This pattern is interpreted to represent deposition in a regime where tidal currents capable of transporting suspended were less active than on the modern delta front, so that more silt was deposited near the river mouth. Consistent with this interpretation, the delta front at that time was in a protected embayment between Pleistocene uplands. The thick sand beds of this facies are interpreted to be suspension rather than gravity flow deposits: their bases are gradational with the underlying silts and include silt laminae that decrease in thickness and abundance upward.

The low dipping interbedded sand and silt facies occurs between depths of 15 and 30 m between the laminated silt facies and the topset in the central parts of the upper delta plain. To the east, deposits of this facies pass laterally into the lower part of the massive sand facies of the topset, which is been interpreted as a complex of distributary channel sands. The low and variable dips in this facies indicate that the configuration of the delta front was different when it was deposited than it is today, probably due to the relatively rapid sea level rise that

prevailed between 4500 and 8000 years ago. At that time the subaqueous platform was probably more extensive and occupied larger embayments between distributaries, and provides a likely setting for deposition of this facies. The thicker coarsening upward sequences may represent distributary mouth bar deposits and may grade into the most distal examples of the massive sand facies of the topset (e.g. Figure 6-36). The high cone bearing associated with the coarsening upward sequences in this facies is consistent with a shallow water setting. Deposits in this environment would have been particularly susceptible to wave loading. This facies thus appears to be transitional between the topset and the foreset.

CPT data may explain the character of the bioturbated silts along the northern margin of the delta, where they are a grey blue colour. Although, friction ratios are highly variable, several CPTs have very low friction ratios (R_f>1%) indicating that these clays may be sensitive[11]. Consistent with this interpretation, the electrical conductivity of these deposits is low compared to other foreset silts (100 ms/m), suggesting that they may be leached (Hunter et al., 1994).

SUMMARY AND FACIES MODEL

In summary, the Fraser delta provides a model of a river- and tide-dominated sand-rich delta system. The topset of the delta is dominated by a diachronous and nearly continuous complex of distributary channel sand deposits, represented by the massive sand facies. The sand is overlain by interbedded sands and silts deposited in tidal flat, partially abandoned channel and bar top environments, and is in turn overlain on the upper delta plain by floodplain silts and locally peats.

The massive sand of the topset records extensive channel migration which has reworked the surface of the delta plain, eroding the original lower tidal flat, subaqueous delta plain and

---

[11] For definition, see Appendix A.

uppermost delta slope deposits, which are preserved on only the outermost parts of the delta plain (Figure 6-60). Prior to construction of the jetties that now constrain it, the Main Channel migrated extensively where it crossed the modern tidal flats. Extensive distributary channel migration in the tidal flat setting is interpreted to be due to the interaction of tidal and fluvial processes and the high proportion of sand in the sediment load (Monahan, et al, 1993c). Stratigraphic sequences consisting of the shell-bearing subfacies of the massive sand facies capped by the bioturbated sand and silt subfacies of the interbedded sand and silt facies record channel migration in this environment. Distributary channels in the modern upper delta plain have been more stable than those crossing the tidal flats. However, historical records and geomorphic evidence indicates that major avulsive or channel switching events have occurred (Johnston, 1923; Clague et al., 1983; Monahan et al., 1993c; Hutchinson, 1995), presumably to provide shorter routes to the sea as older distributaries became too long. Sedimentary sequences representing channel migration and/or infilling in an upper delta plain environment are represented by the shell-free subfacies of the massive sand facies overlain by the well bedded subfacies of the interbedded sand and silt facies. The combination of extensive distributary channel migration in the tidal flats and avulsion or channel switching in the upper delta plain provide a mechanism for the widespread distribution of distributary channel sand deposits in the topset of the delta (Monahan et al., 1993c, 1997).

The third dimension of the topset has been controlled by the mid-Holocene rise in sea level. This factor has resulted in the seaward thinning of the topset, the thick accumulations of the laminated and organic silt facies in the eastern parts of the upper delta plain, and the stacking of floodplain distributary channel sands (shell-free subfacies) over tidal flat distributary channel sands (shell-bearing subfacies) of the massive sand and the local preservation of the distal massive sands in the eastern and central parts of the upper delta plain. Furthermore, the accumulation of peat on the upper delta plain did not commence until the rate of sea level rise had fallen below the rate of organic production and those parts of the floodplain were no longer be inundated by seasonal floods.

The foreset is dominated by silt, complexly interlaminated and interbedded with sand on a variety of scales. Sand is most common in the upper foreset and dominates the upper foreset in the southernmost part of the delta (Figure 6-41). There sandy intervals up to 30 m thick are interbedded with thinner silty intervals and extend to depths as great as 130 m (Clague et al., 1991; Luternauer et al.,1991). Further to the north, highly localized sandy intervals up to 30 m thick occur near the top of the foreset (Figure 6-4 and 6-7; Monahan, 1993; Monahan et al., 1997; Luternauer et al., 1994; Clague et al., 1998). The northward fining of the foreset deposits reflects the northward sediment drift resulting from the drift of the plume and tidal currents flowing along the delta slope.

Upper foreset deposits can be broadly subdivided into two sedimentological groups: laminated sediments and sharp-based sands. The laminated sediments vary from dominantly silt to dominantly sand, represent suspension deposits derived from the plume, and were regulated by tidal and fluvial cycles. They are commonly organized into annual metre-scale coarsening upward sequences interpreted to be annual deposits. The sharp-based sands represent sediment gravity flow deposits preferentially derived from failures at active distributary mouths. The two sedimentological groups form several intergradational facies - laminated silts, laminated sands, mixed sands and sharp-based sands. These facies represent a continuum from finer to coarser sediments, from dominantly suspension to dominantly sediment gravity flow deposits, and reflect increasing proximity to active distributary mouths (Figure 6-60). The sandy members of this facies continuum collectively form the upper parts of the sandy intervals described in the preceding paragraph.

The lower foreset and probably much of the bottomset is dominated by bioturbated silts, which are suspension deposits from the plume. However, a bioturbated sand facies occurs in the lower foreset in the southern part of the delta, where tidal currents limit silt deposition. As noted above, some evidence of winnowing tidal currents is provided by mud-draped ripples. The deeper parts of the sand-dominated units in the southern foreset likely belong to this facies. Sandy sediment gravity flow deposits occur locally at the base of the delta

slope.

Relative sea level has had less effect on the foreset than the topset. However, during the period of relatively rapid sea level rise between 8000 and 4500 ^{14}C years ago, the configuration of the delta front and subaqueous platform changed, resulting in deposition of foreset-like sandy and silty sediments on a gently and irregularly dipping shallow water platform analogous to but probably but more extensive than the modern subaqueous platform.

Table 6-2. Summary of CPT Characteristics of Facies (refer to Appendix H for details)

Part 1. Topset

Facies (and abbreviation)	Average Cone Bearing		Average Friction Ratio		Average I_F	Average Pore Pressure		typical CPT expression
	non-normalized q_t, bar	normalized Q	non-normalized R_f %	normalized F_R		non-normalized dU m	normalized B_q	
Peat Facies (PT)	3 to 13 ±1 to 5	4 to 60 ±1 to 20	3 to 6 ±1	3 to 8 ±3	2.5 to 3.2 ±0.1 to 0.9	-3 to 7 ±1 to 5	-0.1 to 0.3 ±0.01 to 0.1	very high friction ratio and low cone bearing
Laminated and Organic Silt Facies (LOZ)	3 to 7 ±1 to 3	2 to 40 ±1 to 40	1 to 3 ±0.5 to 1.5	1 to 4 +0.5 to 1.5	2.7 to 3.3 ±0.1 to 0.4	-5 to 30 ±1 to 10	-0.1 to 0.6 +0.01 to 0.3	low uniform cone bearing, high serrate friction ratio and positive pore pressure. Q<5 where >5m thick, Q>5 where thinner. Where facies occurs at surface, top 1m is desiccated and has higher cone bearing and friction ratio.
Interbedded Sand and Silt Facies (SZ)	10 to 40 ± 1 to 25	7 to 50 ±3 to 50	0.5 to 2.0 +0.5 to 1.0	0.5 to 2.5 ±0.5 to 2.5	2.3 to 3.0 ±0.3	-6 to 2 ±1 to 6	-0.1 to 0.1 +0.01 to 0.1	highly variable cone bearing, moderate and variable friction ratio, negative pore pressure. Distal subfacies has cone bearing increasing (coarsening) upward sequences.
Massive Sand Facies (MS)	70 to 150 ±20 to 50	50 to 100 ±20 to 30	0.3 to 0.7 ±0.1 to 0.5	0.3 to 0.7 ±0.1 to 0.5	1.6 to 2.0 ±0.1 to 0.3	-7 to 0 ±1 to 6	-0.02 to 0.001 ±0.001 to 0.02	high and variable cone bearing, low uniform friction ratio, pore pressures near zero or negative, sharp base and gradational top.
Coarsening Upward Sand Facies of the Topset (CT)	26±15	51±36	0.5±0.3	0.5±0.3	2.1+0.3	-0.5+1.8	-0.001±0.01	based on 1 CPT on east side of Point Roberts. cone bearing variable, peaks increase upward indicating upward coarsening; friction ratio generally low but variable with peaks greater than 1; pore pressure near zero

Table 6-2. Summary of CPT Characteristics of Facies (refer to Appendix H for details)

Part 2. Foreset

Facies (and abbreviation)	Average Cone Bearing		Average Friction Ratio		Average I_F	Average Pore Pressure		typical CPT expression
	non-normalized q_t, bar	normalized Q	non-normalized R_f %	normalized F_R		non-normalized dU m	normalized B_q	
Basal Sand, Silt and Clay Facies (BC)	18 to128 ±1 to 86	2 to 60 ±0.2 to 40	1.2 to 2.1 ±0.4 to 0.8	1.5 to 4 ±0.8	2.3 to 3.7 +0.3	-3 to 140 ±20 to 40	0.03to 0.43 ±0.1	highly variable; interbeds of sand (high cone bearing), silt and clay (low cone bearing)at the base of the deltaic section, clay indistinguishable from bioturbated silts on the basis of CPT data alone
Bioturbated Silt Facies (BZ)	8 to 38 ±1 to 10	2 to 3 ±0.5 to 2	1.1to 1.6 ±0.2 to 0.4	1.3 to 2.8 ±0.3 to 1.3	3.3 to 3.7 ±0.2	40 to 170 ±10 to 60	0.7 to 0.9 ±0.2	low uniform cone bearing, Q<5; moderate to high friction ratio with little variation, high positive pore pressures.
Laminated Silt Facies (LZ)	10 to 45 ±5 to 25	4 to 12 ±2 to 12	1.0 to 1.7 ±0.7	1.5 to 2.5 ±1.0	2.9 to 3.3 +0.3	10 to 45 ±10 to 35	0.1 to 0.5 ±0.2 to 0.4	low variable cone bearing, Q<6 in >50% of interval, thin cone bearing peaks; high variable friction ratio, and generally positive pore pressures with metre-scale pore pressure decreasing upward sequences; apparent dips up to 7^o.
Laminated Sand Facies (LS)	22 to 70 ±15 to 30	15 to 30 ±10 to 20	1.0 to 1.6 ±0.6 to 0.9	1 to 2 ±0.7 to 1.1	2.4 to 2.8 ±0.4	-20 to 0 ±3 to 20	-0.04 to 0.01 ±0.02 to 0.1	metre-scale cone bearing increasing upward sequences, Q>6 in >50% of interval; moderate to high and variable friction ratio, and generally negative pore pressures; apparent dips up to 7^o.

Table 6-2. Summary of CPT Characteristics of Facies (refer to Appendix H for details)
Part 2 (continued). Foreset

Facies (and abbreviation)	Average Cone Bearing		Average Friction Ratio		Average I_F	Average Pore Pressure		typical CPT expression
	non-normalized q_t, bar	normalized Q	non-normalized R_f %	normalized F_R		non-normalized dU m	normalized B_q	
Mixed Sand facies (MX)	60 to 170 ±25 to 40	30 to 70 ±15 to 20	0.8 to 1.3 ±0.3 to 1.0	0.8 to 1.5 ±0.3 to 1.0	2.0 to 2.5 ±0.2 to 0.5	-34 to -5 m ±4 to 17	-0.04 to 0.01 ±0.01 to 0.06	metre-scale intervals with high cone bearing (sharp-based beds as well as cone bearing increasing upward sequences) and low variable friction ratio; intervening intervals with lower cone bearing and high variable friction ratio; pore pressures negative: apparent dips up to 7^o.
Sharp Based Sand Facies (SB)	100 to 150 ±13 to 25	45 to 55 ±15	0.7 to 0.9 ±0.3	0.8 to 1.0 ±0.3 to 0.5	2.1 to 2.2 ±0.2	-30 to -10 ±5 to 20	-0.03 to 0.01 ±0.01 to 0.2	sharp-based intervals several metres thick with low uniform friction ratio, high cone bearing and pore pressure negative or near zero; thinner intervening intervals with lower cone bearing, higher, variable friction ratio and more negative pore pressures.
Bioturbated Sand Facies (BS)	115 to 125 ±36	25 to 43 ±20	1.0 to 1.4 ±0.6	1.1 to 1.7 ±0.8	2.3 to 2.6 ±0.4	-70 to -30 ±15	-0.04 to 0.07 ±0.04	metre-scale high cone bearing intervals with low serrate friction ratio, separated by thinner intervals with low cone bearing and high friction ratio; negative pore pressure.

Table 6-2. Summary of CPT Characteristics of Facies (refer to Appendix H for details)
Part 2 (continued). Foreset

Facies (and abbreviation)	Average Cone Bearing		Average Friction Ratio		Average I_F	Average Pore Pressure		typical CPT expression
	non-normalized q_t, bar	normalized Q	non-normalized R_f %	normalized F_R		non-normalized dU m	normalized B_q	
Thick Coarsening Upward Sand Facies (CU)	75 to 95 ±25 to 45	46 to 50 ±20 to 30	0.7±0.2	0.8±0.3	2.2+0.5	-14 ±7	-0.02±0.01	cone bearing increasing upward sequences (Q higher than in LS), with low variable friction ratios; cone bearing minima and friction ratio peaks at tops and bases of sequences; negative pore pressures.
Rhythmically Interbedded Sand and Silt Facies (RSZ)	44 to 57 ±33 to 45	15 to 17 ±20	1.3 ±0.6	1.6 to 2.1 ±0.9 to 1.2	2.9 to 3.0 ±0.5	13 to 15 ±25 to 47	0.17±0.3	medium beds with Q up to 30 (q_{c1} up to 70), low variable friction ratio and negative pore pressure rhythmically interbedded with intervals of low variable cone bearing (Q 3-20), variable friction ratio and positive pore pressure; characterized by low dips (up to 2^{O}) and high cone bearing peaks (Q and q_{c1} 100 to 190).
Low Dipping Interbedded Sand and Silt Facies (LDSZ)	74 to 91 ±51 to 73	48 to 59 ±38 to 52	0.9 ±0.6	0.9 to 1.1 +0.6 to 0.8	2.3±0.6	-6 to -2 ±13 to 15	0.006 to 0.03 ±0.09	variable: metre-scale cone bearing increasing upward sequences, with low variable friction ratio and negative pore pressure, to low cone bearing intervals with positive pore pressure.
Disturbed Silt Facies (DZ)	66 to 83 ±21 to 49	23 to 32 ±12 to 29	1.3 to 3.0 ±0.7	1.5 to 3.3 ±0.7 to 1.1	2.5 to 2.8 ±0.4	-19 to -25 ±9 to 12	-0.04 ±0.02 to 0.04	moderate cone bearing and high friction ratio, strongly negative pore pressure.

CHAPTER 7

APPLICATION OF CPT DATA TO FACIES ANALYSIS IN THE FRASER DELTA AND OTHER MODERN ENVIRONMENTS

CPT data played a significant role in developing the facies model of the Fraser River delta presented here. Most of the facies identified have distinct expressions on CPT data, so that their distribution could be mapped on the basis of CPT data alone once they had been defined in cores. More importantly however, CPT data provided key criteria for identifying and interpreting several facies, and some of these criteria are readily available on CPT data alone.

Topset

In the topset, each facies has a distinct expression on CPT data: the massive sand facies has low uniform friction ratio (R_f<1%) and high cone bearing (q_t=30-200 bars); the interbedded sand and silt facies has highly variable cone bearing and friction ratio; the laminated and organic silt has low uniform cone bearing (generally less than 10 bars) and higher friction ratio; and the peat facies has the highest friction ratios of any facies in the delta. Furthermore, the decametre-scale sharp-based fining upward sequences formed by the massive sand facies and the gradationally overlying interbedded sand and silt facies have a distinct CPT signature, which provided one of the initial clues in the course of this investigation that the massive sands were distributary channel deposits. This CPT signature corresponds to the "bell-shaped" natural gamma ray log signature, which is typical of channel deposits (Figures 1-1, 4-5, 7-1). In particular, the friction ratio has a "bell-shaped" signature similar to that of the gamma ray log (Monahan et al., 1993a, c; Mwenifumbo, pers. comm. 1992, 1994). Notably the "bell-shaped" signature is generally better expressed on CPTs than on natural gamma ray logs. The natural gamma ray log signal is due to the decay of

individual radiogenic atoms, so that it fluctuates within a uniform deposit and gives the log a "chattered" appearance that does not occur in CPT data. In addition, CPTs generally provide 3 curves, so that grain size sequences inferred on the basis of a single curve can be checked using the others.

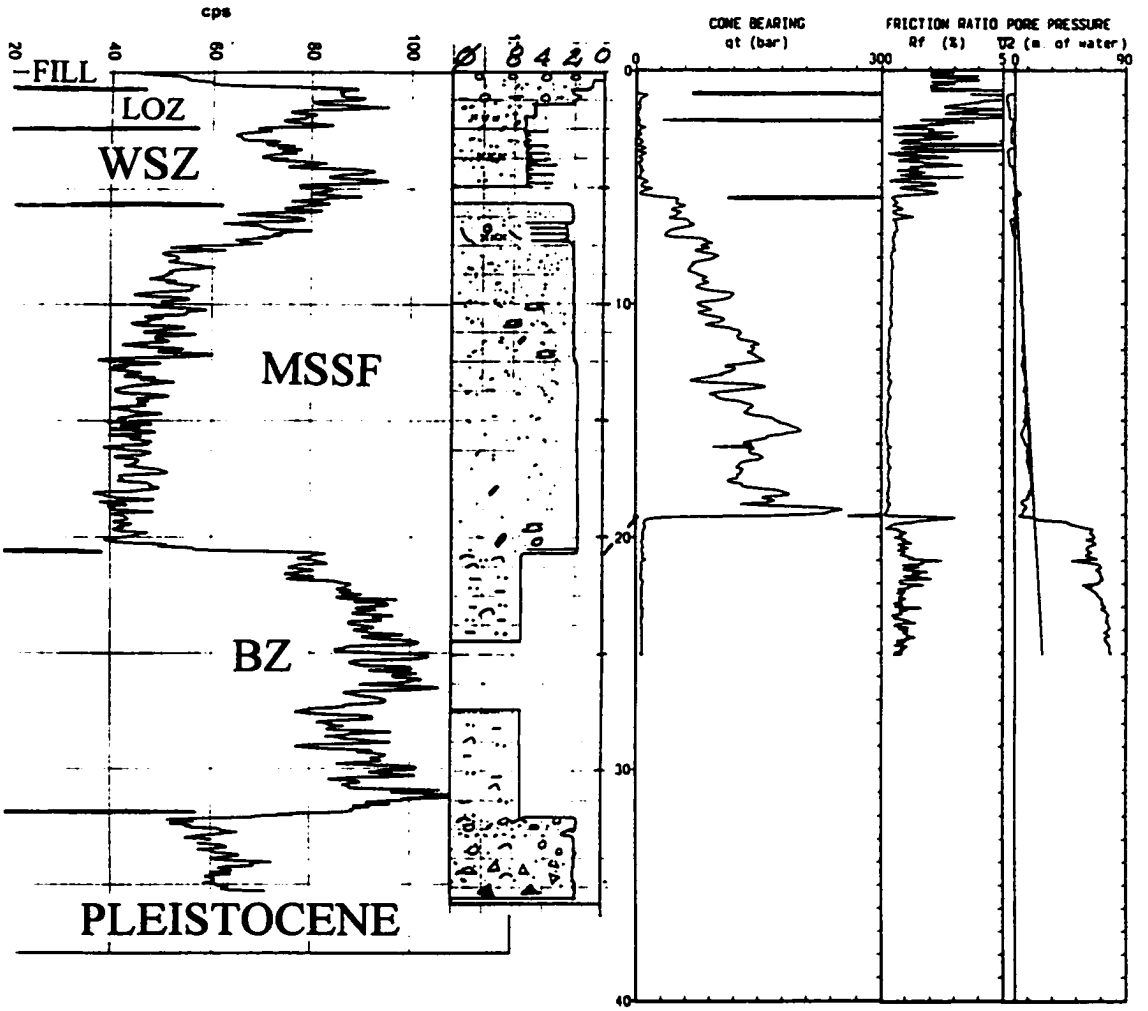

Figure7-1. Composite log of FD92-2. From left to right; gamma ray log, in counts per second (cps), lithology log; and CPT data (q_t, R_f and U). The massive sand facies (MSSF) and interbedded sand and silt facies (WSZ) have a'"bell-shaped" gamma ray log signature, indicating a sharp-based, fining upward sequence typical of channel deposits (see Figure 1-1). Note that the sharp base and upward fining can also be readily identified on CPT data - both the friction ratio and cone bearing curves also display a bell shape. This CPT is ~60 m from the borehole. For facies abbreviations, see Table 6-1.

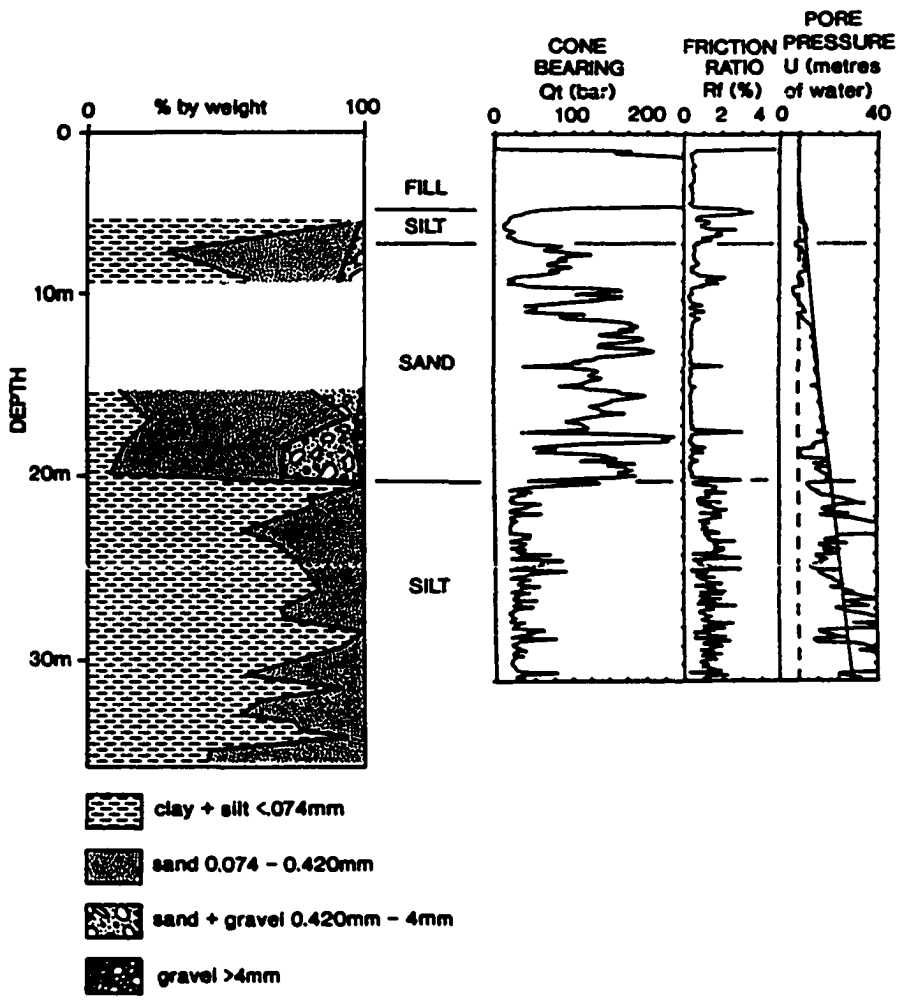

Figure 7-2. Comparison of grain size data from a borehole at the Main Terminal Building, Vancouver International Airport with a nearby CPT. Note that the sharp base, upward fining and gradational top of the topset sand unit (5 to 20 m depth) can be readily identified in the borehole data. Grain size data were derived by sieve analyses of discontinuous samples in the borehole, and were performed by the Ministry of Transport. Figure from Monahan et al. (1993).

The widespread distribution of the "bell-shaped" CPT signature and observations from the continuous cores logged for this study are the basis of the interpretation that the massive sand facies represents a complex of distributary channel sands, and that other environments are not represented. This interpretation, combined with data on channel migration in the tidal

flats (Clague et al., 1983; Luternauer and Finn, 1983) and on the tidal and fluvial processes near the river mouth (Kostaschuk and Luternauer, 1989; Kostaschuk et al., 1989, 1992b), led directly to the depositional model of extensive distributary channel migration in a tidal flat setting due to the interaction of tidal and fluvial processes and the high proportion of sand in the sediment load (Monahan, et al, 1993c). Furthermore, the absence of the "bell-shaped" signature on the seaward margin of the subaqueous platform (also based on geotechnical boreholes; Figures 6-1 and 6-33), demonstrates that the massive sand facies was produced by processes operating on the delta plain and not along the delta front, such as migrating tidal channels or by high wave energy.

The sharp base and upward fining of the massive sand facies is certainly evident in other borehole data (Figure 7-2), and indeed upward fining in this facies was shown by Williams and Roberts (1989, Figure 5). However, the local relief of several metres that occurs at the base of the massive sand facies sand is more convincingly demonstrated using CPTs than other borehole data. Geotechnical boreholes are generally sampled discontinuously, and continuously cored boreholes drilled for scientific purposes generally have problems with depth control (see chapter 4). Consequently, sharp contacts in most boreholes can not be defined more closely than 1 or 2 metres, compared to 10 cm in CPTs. To achieve a similar level of accuracy to CPT data would require a suite of boreholes with gamma ray logs. Such drilling programs have not been conducted in the Fraser delta, whereas there have been hundreds of site investigations with multiple CPTs. Reflection seismic data have locally identified the relief at the base at the sand (Clague et al., 1991; Figure 4), but seismic investigations have generally been designed to resolve deeper horizons and have been restricted to the southern part of the delta (Pullan et al., 1989, 1998). Furthermore, the sharp base of the massive sand facies where it overlies sand in the foreset can be recognized in CPT data, primarily on the basis of the pore pressure curve (Figures 5-15; 6-16 and 6-30), but is exceedingly difficult to identify in most geotechnical boreholes.

Smaller (i.e. metre-scale) fining and coarsening upward sequences in the massive sand facies

are readily apparent in both CPT data and in continuous cores, but could not be identified on the basis of discontinuously samples geotechnical boreholes. However, grain size variability across a site could only be demonstrated using CPT data, because of an insufficient number of continuous cores.

The shell-free and shell-bearing subfacies of the massive sand facies and the bioturbated and the well bedded subfacies of the interbedded sand and silt facies cannot be distinguished using CPT data, but must be identified on the basis of core data. However, average normalized cone bearing increases with age in the massive sand facies, so that the evolution of the topset could be reconstructed using CPT data combined with surficial geomorphic evidence, even though the specific subfacies could not be determined. In an area east of Ladner, a continuous sand bed at the top of the bioturbated sand and silt subfacies can be traced up to a kilometre (Figure 6-19), and has been interpreted as a transgressive beach deposit on the basis of an abrupt base, evident in one continuous core and several CPTs. This bed can be used to define the minimum extent of bioturbated silts and sands in this area. Elsewhere, the continuity of similar beds could potentially be used as an indication that the underlying interbedded silts and sands are the bioturbated subfacies, but so far none have been recognized.

The distal subfacies of the massive sand facies can be identified at the outer margin of the delta and locally at the base of the massive sand facies in the central part of the upper delta plain using CPT data. This subfacies is thinner than the others (<6 m), in some cases the lower part of the friction ratio curve is serrate (Figure 6-36). In addition, half metre- to metre-scale silt to sand coarsening upward sequences can locally recognized in the central part of the upper delta plain.

The thick subfacies of the interbedded sand and silt facies is clearly distinguishable from other subfacies using CPT data on the basis of its thickness and stratigraphic position, laterally replacing the massive sand facies. This subfacies is best defined using CPT data,

because the relative abundance of silt interbedded with sand and the position of geological contacts are defined more repeatably on the friction ratio and cone bearing curves than in discontinuously sampled geotechnical boreholes and continuous cores described by different geologists. CPT data also provided the initial clue that this facies represents the fill of partially abandoned channels, because it fines upward and laterally replaces sands with a "bell-shaped" CPT signature. M. Roberts (pers. comm. 1995; see also Lutēnauer and Moslow, 1991) had recognized this subfacies in cores at a site in the gap in the peat bogs in Lulu Island (Figure 2-2), and interpreted them to represent abandoned channel fill deposits. However, CPT data show that the thick subfacies is interdigitated with the massive sand at this and similar sites (Figure 6-25), clearly demonstrating the complexity of the active and partially abandoned channel fill deposits in the gap in the peat bogs.

The "bell-shaped" CPT signature of the massive sand facies contrasts with that of the upward coarsening sand facies of the topset, which has a gradational interbedded base, coarsens upward and resembles a "funnel-shaped" natural gamma ray log signature typical of prograding beach deposits (Figures 1-1 and 6-40).

The thick accumulations of the laminated and organic silt facies have a CPT signature typical of homogeneous normally consolidated fine grained deposits - low cone bearing increasing linearly with depth, moderate friction ratio and positive excess pore pressure - and could not be distinguished from the bioturbated silt facies of the foreset based on these criteria alone. In the absence of core data, its origin could be inferred from its stratigraphic position, overlying a facies sequence of sands and silts with a "bell-shaped" signature and locally overlain by peat.

Foreset

Similarly, CPT data were critical to the interpretation of the foreset. Seaward dips of these strata are clearly demonstrated by correlating adjacent CPTs, confirming that these are

foreset deposits. Although dipping foreset strata are dramatically documented in reflection seismic data, seismic data are confined to the southern part of the delta because gas in the foreset obscures reflections elsewhere (Clague et al., 1991; Jol, 1988; Jol and Roberts, 1988, 1992; Pullan et al., 1989, 1998). Conversely, CPT data document dips in the foreset throughout the delta. Correlation of decametre-scale sand- and silt-dominated packages in the foreset at Roberts Bank Port using geotechnical boreholes yielded similar dip estimates as CPT-based correlations. However, correlation of metre-scale foreset elements across a site to reveal dips would be difficult even with continuous cores and gamma ray logs, and is only possible to do convincingly using CPT data (Figure 6-6). In thinly interbedded sands and silts, natural gamma ray logs are subject to a statistical "chatter" that masks individual beds and does not occur in CPTs.

Consequently, CPT data alone provide the defining characteristics of the low dipping interbedded sand and silt facies - the low variably-oriented dips, as well as the high cone bearing indicative of wave loading and consistent with a very shallow water environment. These CPT-derived data are the basis of the interpretation that during the period of rapid sea level rise between 8000 and 4500 ^{14}C years ago, the configuration of the subaqueous platform and delta front was different than it is today.

Metre-scale coarsening upward sequences in the upper foreset were identified in continuous cores as well as in CPTs, and confirmed with the suites of grain size analyses shown Chapter 5. However, their occurrence in hundreds of CPTs compared to approximately a dozen continuous cores confirmed that they are a ubiquitous facies element of the foreset. That these strata can be correlated at least several tens of metres is consistent with the interpretation that they represent suspension deposits. The upward increase in density in the thicker sand-dominated sequences, interpreted to represent wave-loading during winter storms, could only have been detected by CPT data. However, widespread coarsening upward sequences can occur in several nearshore marine environments, and cores were necessary to provide the rationale for interpreting them as annual deposits of tidal rhythmites.

The sharp bases, upward fining and gradational tops of the metre-scale sharp-based sands can also be readily identified on CPT data, which provided the initial clue that they represent sediment gravity flow deposits. Sharp-based sand units up to 5 metres thick occur locally, and are distinguished from the massive sand facies of the topset by their stratigraphic position in other foreset deposits and the limited correlation of individual units between CPTs.

CPT data provide both quantitative and qualitative criteria for subdividing a continuum of facies in the upper foreset (Table 6-2). In the laminated silts, average Q is less than 12, I_F is 2.9 to 3.3, and coarsening upward sequences are expressed as pore pressure decreasing upward sequences. In the laminated sands, average Q is 15 to 30, I_F is 2.4 to 2.8, friction ratios are high and variable, and coarsening upward sequences are expressed as cone bearing increasing upward sequences. In the mixed sand facies, average Q is generally 35 to 50, I_F is 2.0 to 2.5, the friction ratio curve is low and serrate, and both sharp-based and coarsening upward sequences occur and are reflected on the cone bearing curve. In the sharp-based sand facies, average Q is 45 to 55, I_F is 2.1 to 2.2, friction ratios are low and uniform, and the facies is dominated by the sharp-based sands. The characteristic grain size and sedimentological features of each of these facies can be identified in continuous cores, but CPT data provide quantitative means for defining them, as well as recognizing their distribution beyond the limited number of continuous cores available.

Similarly, the rhythmically interbedded silt and sand facies can be recognized in both continuous cores and CPTs, but its distribution and relationships to other units can only be determined using CPT data because of the limited number of continuous cores. Geotechnical boreholes have a poor record in this facies. There is an anecdote of a borehole in this facies in which discontinuous samples taken every 1.5 m recovered only very fine sand, giving a completely false impression of the deposits. The disturbed silt facies can also be recognized in both cores and CPTs, but CPT data provide evidence of overconsolidation which would

not be immediately obvious from untested samples.

In contrast to the previously defined foreset facies, the bioturbated sands and silts are not uniquely defined by CPT data. The bioturbated sand facies resembles the laminated sands and the mixed sands on CPT data. It is well known from only one borehole and CPT in the lower foreset, but similar sands probably are widespread in the lower foreset in the southern part of the delta. Further work is required to better define this facies.

The bioturbated silt facies has a CPT signature typical of homogeneous normally consolidated fine grained deposits - low cone bearing increasing linearly with depth, moderate friction ratio and positive excess pore pressure . The CPT characteristics of this facies are not distinct from those other homogeneous normally consolidated fine grained deposits in the delta - the clays of the underlying basal sand silt and clay facies (Figure 6-21), and the laminated and organic silts of the topset. Using CPT data alone, these facies could only be distinguished by their different stratigraphic positions. Similarly, it is unlikely that the bioturbated silt facies could be distinguished from Capilano glaciomarine silts on the basis of CPT data. Although Capilano sediments are not known to have been encountered in any of the CPTs investigated for this study, elsewhere they have CPT characteristics of homogeneous normally consolidated fine grained deposits (Monahan and Levson, 1997; Monahan et al., 1998).

Summary and discussion

CPT data played a crucial role in the development of the facies model of the Fraser delta described here. The facies sequence formed by the massive sand and the interbedded sand and silt facies of the topset has a CPT signature analogous to a "bell-shaped" gamma ray log signature. This signature and its widespread distribution provided the initial indication that the delta plain is underlain by a nearly continuous complex of distributary channel deposits. In the foreset, the coarsening upward sequences and the sharp-based sands, interpreted to be

sediment gravity flow deposits, were readily identified on CPT data. Some of these observations could have been derived from continuously cored and to a lesser extent from geotechnical boreholes. However, acquisition of a volume of continuously boreholes comparable to that of CPTs would have been prohibitively expensive to drill and exceedingly laborious to describe and analyze. CPTs can be performed for a fraction of the cost of coring and most of the data used in this investigation were derived from previous geotechnical investigations and acquired at virtually no cost. Furthermore, the CPT signatures of each facies and their distribution were recognized almost "at a glance", and several characteristics, such as the dips in the foreset, could be convincingly demonstrated on CPT data alone in most of the delta.

However, coring was essential to confirm that the initial inferences based on CPT signatures were valid and to provide data not obtainable from CPTs. For example, data from cores formed the basis of the interpretations that topset sequences represent migration and filling of channels in both tidal flat and upper delta plain settings, and that coarsening upward sequences of the foreset represent annual deposits of tidal rhythmites. CPT data provide repeatable estimates of sediment type, bed boundaries and thicknesses, grain size trends (fining and coarsening upward sequences), bed continuity and dips. Other facies attributes, such as macrofauna and bioturbation cannot be derived from CPT data.

The CPT data provided a suite of signatures that were subsequently evaluated by core. Although locations of several of the continuously cored boreholes examined for this study were chosen for other reasons, eight continuously cored boreholes were located by the author to examine specific CPT signatures, such as the "bell-shaped" signature of the topset, the thick subfacies of the interbedded sand and silt facies, and the inferred coarsening upward sequence of the topset. Once the facies significance of these signatures and the CPT characteristics of each facies were established, the distribution of each facies could be determined on the basis of CPT data

Application of CPT data to other modern environments

A similar approach is thus recommended in the application of CPT data to facies analysis in other modern sedimentary environments dominated by sands and finer sediments. A suite of CPTs should be performed to provide an overall stratigraphic framework, and should be supplemented by CPT and other data from previous geotechnical investigations, if available. At some sites, multiple CPTs should be performed to determine local stratigraphic variability and dips. Continuously cored boreholes should be located to test specific CPT signatures, and widespread CPT signatures should be investigated by several boreholes in order to test for the presence of distinct subfacies defined by criteria other than sediment type, bedding characteristics, grain size trends, or dips. Subsequent to the definition of facies and their expression on CPTs, the facies distribution can be mapped on the basis of existing and newly acquired CPT data and possibly additional coring. A stratigraphic investigation conducted in this way would ultimately involve fewer cored boreholes than an investigation without CPTs. However, the boreholes would be better focussed on defining specific facies and CPT data would provide subsurface information at a much larger number of sites.

CPT data in the Fraser delta demonstrate that channel sands can be characterized by a sharp-based fining upward CPT signature similar to a "bell-shaped" gamma ray log signature (Figure 1-1). A CPT signature similar to the "funnel-shaped" gamma ray log signature can be anticipated in beach and other shoreline deposits characterized by upward coarsening, although cone bearing is likely to be higher than in channel deposits for sands of comparable grain size because of the densifying effect of breaking waves (Pryor, 1973; de Mulder and Westerhoff, 1985). In the Fraser delta, sediment gravity flow deposits also have a distinct sharp-based fining upward CPT signature, on a smaller scale than channel deposits, and is likely to be repeated elsewhere. Other distinct signatures may have only local significance, such as the coarsening upward sequences of the Fraser delta foreset. De Mulder and Westerhoff (1985) have described the CPT characteristics of some facies in a coastal barrier setting in the Netherlands. Caution has to be exercised in the interpretation of homogeneous

normally consolidated silts, which can occur in a variety of environments, and different facies consisting of such sediments cannot be distinguished on the basis of CPT data alone. In the Fraser delta, facies consisting of homogeneous normally consolidated silts occur at opposite ends of the depositional spectrum, the laminated and organic silts of the topset and the bioturbated silts of the lower foreset. On the basis of CPT data alone, these facies could only be distinguished on the basis of stratigraphic position.

CHAPTER 8

CONCLUSIONS

CPT data played a key role in developing the facies model of the Fraser River delta presented here, by providing a large volume of repeatable data in which several distinct and widespread signatures were observed. These signatures could be correlated with specific sedimentary facies, and thus facilitated the determination of facies distributions and relationships with greater precision and detail than the limited number of continuous cores available. Consequently, CPT data are potentially an invaluable tool for stratigraphic investigations of other modern sedimentary environments dominated by sands and finer sediments. These conclusions are discussed in more detail below.

1. CPT data interpretation

Grain size correlates well with CPT parameters in the sediments of the Fraser delta. Cone bearing values are generally insensitive to grain size finer than $5\phi_{50}$, increase gradually with grain size in coarse silts, and increase sharply with grain size in the sand range. Excess pore pressures are near zero in medium sands, negative in the fine sand to coarse silt range, and are commonly positive in sediments finer than $5\phi_{50}$. Friction ratio values are generally low in sands and high in silts. These general correlations are well known (Figure 3-3; Robertson, 1990), and combined with the high resolution of CPT measurements (within 10 cm), permit the recognition of gross lithology, bed thicknesses, sharp and gradational contacts and metre- and decametre-scale coarsening and fining upward sequences.

Coarsening and fining upward sequences in the Fraser delta sediments can be most confidently recognized where sequences include both sands and silts. Sands and silts have

distinct expressions on the cone bearing curve, and 80% of the total variation in cone bearing in these ranges can be explained by grain size variations. Based on cone bearing data alone, coarsening and fining upward sequences can be less confidently determined within the sand range, where only 50% of the variation in cone bearing can be explained by grain size variations. However, excess pore pressures provide a useful check on cone bearing data in sands: where cone bearing increases are related to grain size, excess pore pressures remain near zero; where cone bearing increases reflect increased density, excess pore pressures become increasingly negative. In silts, decimetre to metre-scale coarsening upward sequences are expressed as pore pressure decreasing upward sequences.

Operational factors can also influence CPT data. In SCPTs, pore pressure dissipation at rod breaks in silt can mask and mimic the pore pressure decreasing upward sequences generated by coarsening upward sequences. In pore pressure decreasing upward sequences due to rod breaks, pore pressure minima occur 1 m apart and are associated with friction ratio peaks. Friction ratio measurements are generally consistent within a particular CPT, but may not be repeatable between CPTs, primarily because of the susceptibility of the cone and friction sleeve to wear.

In addition, the following specific conclusions can be made regarding the analysis of CPT data.

- In sands, normalizing cone bearing for effective overburden stress using q_{c1} (cone stress exponent (c)=0.5; equation 9, Chapter 3) produces more consistent results than Q_t (c=1.0; equation 5, Chapter 3). Conversely, Q_t produces more consistent results than q_{c1} in the silt range. These conclusions provide a rational basis for using the parameter Q, in which c is variable, as proposed by Robertson and Wride (1997, 1998).

- In the sands of the Fraser delta analyzed here, approximately half the variation in

normalized cone bearing can be explained by variations in median grain size, and all other factors, including age, density, thin bed effects, and stratigraphic changes and correlation errors between the cores and the CPTs account for the remaining half. This correlation is partly related to the fines content (FC), which does correlate with cone bearing where FC is greater than 10%. However, the correlation of grain size with cone bearing in the sand range is not simply a matter of sorting or fines content: the same grain size to cone bearing trend occurs in clean moderately well sorted sands as in all the sand samples, which include very poorly sorted silty sands. The implications of this conclusion for geotechnical investigations, such as the application of CPT data to the determination of liquefaction susceptibility are not clear, but should be considered in future research.

- In the massive sands in the topset of the delta, average cone bearing increases by a factor of two from deposits that are historic to 8000 ^{14}C years in age. Older sands have more negative excess pore pressures than younger ones. The ageing of sands is probably partly due to particle rearrangement on a microscopic scale, as suggested by Schmertmann (1991), but could also include the densifying effects of periodic earthquakes. Cementation does not appear to be a factor.

- Cone bearing appears to be resolved in beds of very fine sand as thin as 10 cm, where interbedded with silts, and in silt beds as thin as 15 cm where interbedded with sand. Similarly, sharp sand to silt contacts are resolved within 10 cm on the cone bearing curve.

- Friction ratio peaks commonly occur at sand to silt bed boundaries, so that friction ratios in interbedded sands and silts include higher values and are more variable than in silts without sand interbeds. Because I_F is dependent upon friction ratios, average I_F is also anomalously high in interbedded sands and silts.

2. The Fraser delta

The Fraser delta provides a model of a river- and tide-dominated, sand-rich delta system. This model was developed on the basis of a large volume of CPT data and a limited number of continuous cores.

The topset of the delta is dominated by a diachronous, nearly continuous massive sand facies that is interpreted to be a complex of distributary channel deposits. It is generally 8 to 30 m thick, consists one or more decametre-scale sharp-based fining upward sequences, and grades into an overlying interbedded sand and silt facies. Two distinct stratigraphic sequences occur in the massive sands and the interbedded sands and silts. Shell-bearing massive sands are generally overlain by bioturbated interbedded sands and silts; and shell-free massive sands are overlain by well bedded interbedded sands and silts. These stratigraphic sequences are interpreted to represent distributary channel migration and filling in tidal flat and upper delta plain environments respectively. The widespread distribution of the massive sand facies is the result of both extensive distributary channel migration in a tidal flat setting, due to the tidal and fluvial processes and the high proportion of sand in the sediment load, and avulsion or channel switching in the upper delta plain. The interbedded sand and silt facies is overlain on the upper delta plain by floodplain silts, which are locally capped by peats.

The thickness of the topset has been controlled by the mid-Holocene rise in sea level. This has resulted in the seaward thinning of the topset, preservation of thick accumulations of floodplain silts in the eastern parts of the upper delta plain, and the stacking of upper delta plain distributary channel sands over tidal flat distributary channel sands in the eastern and central parts of the upper delta plain.

The foreset is dominated by silt, complexly interlaminated and interbedded with sand on a variety of scales. Deposits of the upper foreset (above ~60m) are primarily laminated

suspension deposits derived from the fresh water plume, in which sediment concentration and calibre were regulated by tidal and fluvial cycles. The laminated sediments vary from dominantly silt to dominantly sand, representing increasing proximity to active river mouths, and are commonly organized into metre-scale coarsening upward sequences interpreted to be annual deposits. Sharp-based sediment gravity flow sand deposits, preferentially derived from failures of sand accumulations at active distributary mouths, also occur in the upper foreset, both interbedded with sandy suspension deposits and in stacked units several metres thick. Superimposed on the pattern of increasing sand content in proximity to active distributary mouths is an overall sediment fining to the north along the delta front, as a result of northward flowing tidal currents and the northward drift of the plume. Consequently, the upper foreset is dominated by sandy sediments in the southernmost part of the delta, but further to the north, sandy deposits are highly localized.

The lower foreset (below ~60m) and much of the bottomset is characterized by bioturbated deposits that accumulated more slowly than the overlying foreset. These are primarily silts, but in the southernmost part of the delta, bioturbated sands are present as a consequence of the northward sediment drift described above. Sandy sediment gravity flow deposits occur locally at the base of the delta slope.

Relative sea level has had less effect on the foreset than the topset. However, during the period of relatively rapid sea level rise between 8000 and 4500 ^{14}C years ago, the configuration of the delta front and subaqueous platform changed, resulting in deposition of foreset-like sandy and silty sediments on a gently and irregularly dipping shallow water platform more extensive than the modern subaqueous platform.

3.Application of CPT data to facies analysis in the Fraser delta

Most of the facies of the Fraser delta have distinct expressions on CPT data. Furthermore,

CPT data provided key criteria for interpreting several facies. For example, the facies sequence formed by the massive sand and the interbedded sand and silt facies of the topset has a CPT signature analogous to a "bell-shaped" gamma ray log signature. This signature provided the initial indication that the delta plain is underlain by distributary channel deposits. The coarsening upward sequences and the sharp-based sandy sediment gravity flow deposits in the foreset were also readily identified using CPT data. Although these facies elements could be recognized in cores, acquisition of a volume of borehole data comparable to that of CPTs to demonstrate their widespread distribution would have been prohibitively expensive to drill and laborious to analyze. Most of the CPT data used in this investigation were acquired at virtually no cost from previous geotechnical investigations, and the CPT signatures of each facies and their distribution could be recognized "at a glance". CPT data also provided a quantitative means of distinguishing several intergradational facies of the foreset. Furthermore, several characteristics, such as the dips in the foreset, could be derived from CPT data alone in most of the delta. The only facies without distinct CPT signatures are those consisting of homogenous, normally consolidated fine grained deposits, which can occur in several environments.

Coring was essential to determine the facies significance of CPT signatures and to provide data not obtainable from CPTs. CPT data provide repeatable estimates of sediment type, bed boundaries and thicknesses, fining and coarsening upward sequences, bed continuity and dips. Other facies attributes, such as macrofauna and sedimentary structures can only be derived from cores.

CPT data are thus potentially an invaluable tool for the facies analysis of modern sedimentary environments which do not include thick gravels or very dense sands. CPT data can provide an overall stratigraphic framework, a suite of signatures that can be tested in subsequent coring programs, and data not readily available from cores, such as dips and consolidation characteristics. Furthermore, CPT data can be acquired at a fraction of the cost of continuous coring, and some data may be available at virtually no cost from earlier

geotechnical investigations. Consequently, CPT data can provide more focus to stratigraphic investigations, as well as subsurface data at a greater number of sites than investigations based on coring programs alone.

REFERENCES

ARMSTRONG, J.E. 1981. Post-Vashon Wisconsin Glaciation, Fraser Lowland, British Columbia. Geological Survey of Canada, Bulletin 322, 34 p.

ARMSTRONG, J.E. 1984. Environmental and Engineering Applications of the Surficial Geology of the Fraser Lowland, British Columbia. Geological Survey of Canada, Paper 83-23, 54p.

ARMSTRONG, J.E. and HICOCK, S.R. 1980a. Surficial Geology, New Westminster, British Columbia. Geological Survey of Canada, Map 1484A.

ARMSTRONG, J.E. and HICOCK, S.R. 1980b. Surficial Geology, Vancouver, British Columbia. Geological Survey of Canada, Map 1486A.

ATKINS, J.E. and McBRIDE, E.F. 1992. Porosity and Packing of Holocene River, Dune, and Beach Sands. The American Association of Petroleum Geologists Bulletin, **76**: 339-355.

BARRIE, J.V. and CURRIE, R. in press. Human impact and sediment distribution, Fraser River delta, Canada. Journal of Coastal Research.

BHATTACHARYA, J.P. and WALKER, R.G. 1992. Deltas. *In* Facies Models - Response to Sea Level Change. *Edited by* R.G. Walker and N.P. James. Geological Association of Canada, pp. 157-177.

BROMS, B.B. and FLODIN, N. 1988. History of soil penetration testing. *In* Penetration Testing 1988, Proceedings of the International Symposium on penetration testing, ISOPT-1, Orlando, Vol. 1. *Edited by* J. de Ruiter, Balkeema, Rotterdam, pp. 157-220.

BYRNE, P.M., 1978. An evaluation of the liquefaction potential of the Fraser Delta. Canadian Geotechnical Journal, **15** ; 32-46.

CAMPANELLA, R.G. 1993. CPTINT 5.0, PiezoCone Penetration Test Interpretation Program for IBM-PC. Department of Civil Engineering, University of British Columbia.

CAMPANELLA, R.G. and ROBERTSON, P.K. 1988. Current status of the piezocone test. *In* Penetration Testing, 1988, Proceedings of the International Symposium on penetration testing, ISOPT-1, Orlando, Vol. 1. *Edited by* J. de Ruiter, Balkeema, Rotterdam, pp. 93-116.

CAMPANELLA, R.G. and WEEMEES, I. 1990. Development and use of an electrical resistivity cone for groundwater contamination studies. Canadian Geotechnical Journal, **27**: 557-567.

CAMPANELLA, R.G., ROBERTSON, P.K., and GILLESPIE, D. 1983. Cone penetration testing in deltaic soils. Canadian Geotechnical Journal, **20**: 23-35.

CANADIAN FOUNDATION ENGINEERING MANUAL. 1992. Third Edition. Canadian Geotechnical Society, Technical Committee on Foundations, 512 p.

CANT, D.J. 1992. Subsurface Facies Analysis. *In* Facies Models - Response to Sea Level Change. *Edited by* R.G. Walker and N.P. James. Geological Association of Canada, pp. 27-45.

CHRISTIAN, H.A., MONAHAN, P.A., and BARRIE, J.V. 1994a. Deep Hole Investigation Adjacent to the BC Hydro Canoe Pass Submarine Cable Terminal, Fraser River Delta, British Columbia. Geological Survey of Canada, Open File Report 2861, 16 p.

CHRISTIAN, H.A., MULDER, T., COURTNEY, R.C., MOSHER, D.C., BARRIE, J.V., CURRIE, R.G., OLYNYK, H.W., and MONAHAN, P.A. 1994b. Slope instability on the Fraser River delta foreslope, Vancouver, British Columbia. *In* Proceedings, 48th Canadian Geotechnical Conference, Halifax, 21-23 September. Canadian Geotechnical Society, pp. 155-165.

CHRISTIAN, H.A., BARRIE, J.V., MACDONALD, R., MONAHAN, P.A., HUNTER, J.A., and LUTERNAUER, J.L. 1995. Slope instability on Roberts Bank, Fraser River delta, Vancouver, British Columbia. *In* Proceedings, 48th Canadian Geotechnical Conference, September 25-27 1995, Vancouver, B.C., Preprint Volume 2. Canadian Geotechnical Society, pp. 937-946.

CHRISTIAN, H.A., WOELLER, D.J., ROBERTSON, P.K., and COURTNEY, R.C. 1997a. Site investigations to evaluate flow liquefaction slides at Sand Heads, Fraser River delta. Canadian Geotechnical Journal, **34**: 384-397.

CHRISTIAN, H.A., MOSHER, D.C., MULDER, T., BARRIE, J.V., and COURTNEY, R.C. 1997b. Geomorphology and potential slope instability on the Fraser River delta foreslope, Vancouver, British Columbia. Canadian Geotechnical Journal, **34**: 432-446.

CHURCH, M., MCLEAN, D.G., KOSTASCHUK, R., MACFARLANE, S., TASSONE, B., and WALTON, D. 1990. Channel stability and management of Lower Fraser River field excursion guide. Water Survey of Canada, Water Resources Branch, Inland

Waters Directorate, Environment Canada. Vancouver, Canada.

CLAGUE, J.J., LUTERNAUER, J.L., and HEBDA, R.J. 1983. Sedimentary environments and postglacial history of the Fraser River delta and lower Fraser Valley, British Columbia. Canadian Journal of Earth Sciences, **20**: 1314-1326.

CLAGUE, J.J., LUTERNAUER, J.L., PULLAN, S.E., and HUNTER J.A. 1991. Postglacial deltaic sediments, southern Fraser River Delta, British Columbia. Canadian Journal of Earth Sciences, **28**: 1386-1393.

CLAGUE, J.J., NAESGAARD, E., and SY, A. 1992. Liquefaction features on the Fraser River delta: evidence for prehistoric earthquakes? Canadian Journal of Earth Sciences, **29**: 1734-1745.

CLAGUE, J.J., NAESGAARD, E., and NELSON, A. 1997. Age and significance of earthquake-induced liquefaction near Vancouver, British Columbia, Canada. Canadian Geotechnical Journal, **34**: 53-62.

CLAGUE, J.J., LUTERNAUER, J.L., MONAHAN, P.A., EDWARDSON, K.A., DALLIMORE, S.R., and HUNTER, J.A. 1998. Quaternary stratigraphy and evolution. *In* Geology and Natural Hazards of the Fraser River delta, British Columbia. *Edited by* J.J. Clague, J.L. Luternauer, and D.C. Mosher. Geological Survey of Canada, Bulletin 525, pp. 57-90.

COLLINSON, J.D. 1986. Alluvial Sediments. *In* Sedimentary environments and facies. Edited by H. G. Reading. Blackwell Scientific Publications, Oxford, pp. 20-62.

CONETEC INVESTIGATIONS Ltd. 1987. Presentation and Interpretation of Seismic Cone Penetration Test Data, 28th Avenue, Delta, British Columbia. Prepared for Energy, Mines & Resources, Geological Survey of Canada, July 28, 1987.

CURRIE, R.G., and MOSHER, D.C. 1996. Swath bathymetric surveys in the Strait of Georgia, British Columbia. *In* Current Research 1996-E. Geological Survey of Canada, pp. 33-40.

DALLIMORE, S.R., EDWARDSON, K.A., HUNTER, J.A., CLAGUE, J.J. and LUTERNAUER, J.L. 1995. Composite geotechnical logs for two deep boreholes in the Fraser River delta, British Columbia. Geological Survey of Canada, Open File 3018.

DALLIMORE, S.R., EDWARDSON, K.A., HUNTER, J.A., MELDRUM, J.L., LUTERNAUER, J.L., and CLAGUE, J.J. 1996. Lithologic, geotechnical and geophysical logs for a deep borehole at Richmond City Hall, British Columbia:

Geological Survey of Canada, Open File Report 3356.

DEVORE, J.L. 1991. Probability and Statistics for Engineering and the Sciences, Third Edition. Brooks/Cole Publishing Company, Pacific Grove, California, 716 p.

ELLIOTT, T. 1986. Deltas. *In* Sedimentary environments and facies. Edited by H. G. Reading. Blackwell Scientific Publications, Oxford, pp. 113-154.

ESLAAMIZAAD and ROBERTSON, P.K. 1996. Seismic cone penetration test to identify cemented sands. *In* 49th Canadian Geotechnical Conference, 23-25 September, St. John's Newfoundland. Canadian Geotechnical Society, pp. 849-858.

EVERARD, J.L. 1995. Characterization of a Hydrocarbon Contaminated Site Using in-Situ Methods. M.A.Sc. Thesis, University of British Columbia, Vancouver, B.C.

EVOY, R.W., MOSLOW, T.F., PATTERSON, R.T., and LUTERNAUER, J.L. 1993. Patterns and variability in sediment accumulation rates, Fraser River delta foreslope, British Columbia, Canada. Geo-Marine Letters, **13**: 212-218.

EVOY, R.W. , MOSLOW, T.F., and LUTERNAUER, J.L. 1994. Origin and variability of the sedimentary facies of the Fraser River delta foreslope, British Columbia. Marine Geology, **118**: 49-60.

FINN, W.D.L. 1988. Liquefaction studies in the Fraser delta. Preliminary Draft Report to the Geological Survey of Canada, October 10, 1988.

FINN, W.D.L., WOELLER, D.J., DAVIES, M.P., LUTERNAUER, J.L., HUNTER, J.A., and PULLAN, S.E. 1989. New approaches for assessing liquefaction potential of the Fraser River Delta, British Columbia. *In* Current Research, Part E. Geological Survey of Canada, Paper 89-1E, pp. 221-231.

FINN, W.D.L., ROBERTSON, P.K., and WOELLER, D.J. 1990. Liquefaction Studies in the Fraser delta. Research Report to Energy, Mines and Resources, Geological Survey of Canada, 24 p.

FRIEDMAN, G.M. and SANDERS, J.E. 1978. Principles of Sedimentology. John Wiley and Sons, New York, 792 p.

GARRISON, R.E., LUTERNAUER, J.L., GRILL, E., MACDONALD, R.D. and MURRAY, J.W. 1969. Early diagenetic cementation of recent sands, Fraser River delta, British Columbia. Sedimentology, **12**: 27-46.

HAMILTON, T.S. 1991, Seismic Stratigraphy of Unconsolidated Sediments in the

Central Strait of Georgia: Hornby Island to Roberts Bank, Geological Survey of Canada, Open File 2350.

HART, B.S. 1993. Large-scale rotational failure on a low angle delta slope: The Foreslope Hills, Fraser Delta, British Columbia, Canada. Geo-Marine Letters, **13**: 219-226.

HART , B.S. and HAMILTON, T.S., 1993, High-resolution acoustic mapping of shallow gas in unconsolidated sediments beneath the strait of Georgia, British Columbia. Geo-Marine Letters, **13**: 49-55.

HART, B.S., PRIOR, D.B., BARRIE, J.V., CURRIE, R.G., and LUTERNAUER, J.L. 1992c. A river mouth submarine channel and failure complex, Fraser delta, Canada. Sedimentary Geology, **81**: 73-87.

HART, B.S., HAMILTON, T.S., BARRIE, J.V., and PRIOR, D.B. 1995. Seismic stratigraphy and sedimentary framework of a deep-water Holocene delta; The Fraser delta, Canada. *In* Geology of Deltas. *Edited by* N. Oti and G. Potsma. A.A. Balkema, Rotterdam, pp. 167-178.

HART, B.S., HAMILTON, T.S., and BARRIE, J.V. 1998. Sedimentation rates and patterns on a deep water delta (Fraser delta, Canada): integration of high-resolution seismic stratigraphy, core lithofacies, and ^{137}Cs fallout stratigraphy. Journal of Sedimentary Research, **68**: 556-568.

HOLLAND, S.S. 1976. Landforms of British Columbia. British Columbia Department of Mines and Petroleum Resources, Bulletin 48, 138 p.

HUNTER, J.A., LUTERNAUER, J.L., ROBERTS, M.C., MONAHAN, P.A. and DOUMA, M. 1994. Borehole Geophysical Logs, Fraser River Delta (92G), British Columbia. Geological Survey of Canada, Open File 2841.

HUNTER, J.A., BURNS, R.A., GOOD. R.L., WANG, Y., and EVANS, M.E. 1995. Borehole magnetic susceptibility measurements in unconsolidated overburden of the Fraser River delta, British Columbia. *In* Current Research 1995-E. Geological Survey of Canada, pp. 77-82.

HUNTER, J.A., BURNS, R.A., GOOD, R.L., and PELLETIER, C. (with contributions by J.R. Britton, H.A. Christian, S.R., Dallimore, M. Douma, J.B. Harris, J.L. Luternauer, P.A. Monahan, K.G. Neave, M.C. Roberts, and D.J. Woeller) 1998. A compilation of shear wave velocities and borehole geophysics logs in unconsolidated overburden of the Fraser River delta. Geological Survey of Canada Open File, 3622.

HUTCHINSON, I., ROBERTS, M.C., and WILLIAMS, H.F.L. 1995. Stratigraphy,

diatom biofacies, and palaeogeomorphology of a mid Holocene distributary channel system, Fraser River delta, British Columbia, Canada. Canadian Journal of Earth Sciences, **32**: 749-757.

ISSMFE TECHNICAL COMMITTEE ON PENETRATION TESTING, 1988. Cone penetration test (CPT): International reference test procedure. *In* Penetration Testing 1988, Proceedings of the International Symposium on penetration testing, ISOPT-1, Orlando, Vol. 1. *Edited by* J. de Ruiter, Balkeema, Rotterdam, pp. 27-51.

ISSMFE, 1989. Appendix A: International reference test for cone penetration test (CPT). *In* Report of the ISSMFE technical Committee on Penetration testing of soils - TC 16, with Reference to test procedures. Swedish Geotechnical Institute, Linköping, Information, 7, pp. 6-16.

JEKEL, J.W.A. 1988. Wear of the friction sleeve and its effect on the measured local friction. *In* Penetration Testing 1988, Proceedings of the International Symposium on penetration testing, ISOPT-1, Orlando. *Edited by* J. de Ruiter, Balkeema, Rotterdam, pp. 805-808.

JOHNSTON, W.A. 1921. Sedimentation of the Fraser River Delta. Geological Survey of Canada, Memoir 125, 46 p.

JOHNSTON, W.A. 1922. The character of the stratification of the sediments in the recent delta of Fraser River, British Columbia, Canada. Journal of Geology, **30**: 115-129.

JOL, H.M. 1988. Seismic stratigraphic analysis of the southwestern Fraser River delta, British Columbia. M.Sc. thesis, Simon Fraser University, Burnaby. B.C., 176 p.

JOL, H.M., and ROBERTS, M.C. 1988. The seismic facies of a delta onlapping an offshore island: Fraser River Delta, British Columbia. *In* Sequences, Stratigraphy, Sedimentology: Surface and Subsurface. *Edited by* D.P. James and D.A. Leckie. Canadian Society of Petroleum Geologists, Memoir 15, pp. 137-142.

JOL, H.M., and ROBERTS, M.C. 1992. The seismic facies of a tidally influenced Holocene delta: Boundary Bay, Fraser River delta, B.C.: Sedimentary Geology, **77**: 173-183.

KAYEN, R.E., MITCHELL, J.K., SEED, R.B., LODGE, A., NISHIO, S., and COUTINHO, R. 1992. Evaluation of SPT-, and CPT-, and shear wave-based methods for liquefaction potential assessment using Loma Prieta data. Proceedings of the Fourth Japan-US Workshop on Earthquake Resistant Design of Lifeline Facilities and Countermeasures for Soil Liquefaction, Technical Report NCEER-94-0019, 1, pp. 177-204.

KONRAD, J.-M. 1997. In situ sand state from CPT: evaluation of a unified approach at two CANLEX sites. Canadian Geotechnical Journal, **34**: 120-130.

KOSTASCHUK, R.A., and LUTERNAUER, J.L. 1989. The Role of the Salt-Wedge in Sediment Resuspension and Deposition: Fraser River Estuary, Canada. Journal of Coastal Research, **5**: 93-101.

KOSTASCHUK, R.A., LUTERNAUER, J.L., and CHURCH, M.A. 1989. Suspended sediment hysteresis in a salt wedge estuary: Fraser River, Canada. Marine Geology, **87**: 273-285.

KOSTASCHUK, R.A., LUTERNAUER, J.L., MCKENNA, G.T., and MOSLOW, T.F. 1992a. Sediment transport in a submarine channel system: Fraser delta, Canada. Journal of Sedimentary petrology, **62**: 273-282.

KOSTASCHUK, R.A., CHURCH, M.A., and LUTERNAUER, J.L. 1992b. Sediment transport over salt-wedge intrusions: Fraser River estuary, Canada. Sedimentology, **39**: 305-317.

KOSTASCHUK, R.A., LUTERNAUER, J.L., BARRIE, J.V., LEBLOND, P.H., AND VON DEICHMANN, L.W. 1995. Sediment transport by tidal currents and implications for slope stability: Fraser River delta, British Columbia. Canadian Journal of Earth Sciences, **32**: 852-859.

KULHAWY, F.H. and MAYNE, P.H. 1990. Manual on estimating soil properties for foundation design. Electric Power Research Institute.

LECLAIR, D.G. 1988. Prediction of embankment performance using in-situ tests. M.A.Sc. thesis, University of British Columbia, Vancouver, B.C.

LEOPOLD, L.B. 1994. A View of the River. Harvard University Press, Cambridge Massachusetts, 298 p.

LIAO, S.S. and WHITMAN, R.V. 1986. Ovberburden correction factors for SPT in sand. Journal of Geotechnical Engineering, **112**: 373-377.

LIST, B.R., and ROBERTSON, P.K. 1995. Canadian Liquefaction Experiment Update - Characterization of sand for static and dynamic liquefaction. *In* Proceedings, 48th Canadian Geotechnical Conference, September 25-27 1995, Vancouver, B.C., Preprint Volume 1. Canadian Geotechnical Society, pp. 49-58.

LUNNE, T., EIDSMOEN, T., GILLESPIE, D., and HOWLAND, J.D. 1986 Laboratory and Field Evaluation of Cone Penetrometers. *In* Use of In Situ Tests in Geotechnical

Engineering, Proceedings of In Situ '86, a Specialty Conference sponsored by the Geotechnical Engineering Division of the American Society of Civil Engineers. *Edited by* S.P. Clemence. American Society of Civil Engineers, Geotechnical Special Publication No.6, pp. 714-729.

LUNNE, T., ROBERTSON, P.K., and POWELL, J.J.M. 1997. Cone Penetration Testing in Geotechnical Practice. Blackie Academic & Professional, London, 312 p.

LUTERNAUER, J.L. 1977. Fraser delta sedimentation, Vancouver, British Columbia. *In* Geological Survey of Canada Paper 77-1A, pp. 65-72.

LUTERNAUER, J.L. 1980. Genesis of Morphologic Features on the Western Delta Front of the Fraser River, British Columbia - Status of Knowledge. *In* The Coastline of Canada. *Edited by* S.B. McCann. Geological Survey of Canada, Paper 80-10, pp. 381-396.

LUTERNAUER, J.L, and FINN, W.D.L. 1983. Stability of the Fraser River Delta Front. Canadian Geotechnical Journal, **20**: 603-616.

LUTERNAUER, J.L. AND MOSLOW, T.F. 1991 (Organizers/Leaders). The sedimentary environments and facies of the Fraser River delta. Canadian Society of Petroleum Geologists Field Trip Guidebook, June 9-14, 1991.

LUTERNAUER, J.L., and MURRAY, J.W. 1973. Sedimentation of the Fraser River Delta. Canadian Journal of Earth Sciences, **10**: 1642-1663.

LUTERNAUER, J.L., CLAGUE, J.J., HAMILTON, T.S., HUNTER, J.A., PULLAN, S.E., and ROBERTS, M.C. 1986. Structure and Stratigraphy of the southwestern Fraser River Delta: a trial shallow seismic profiling and coring survey. *In* Current Research, Part B. Geological Survey of Canada Paper 86-IB, pp. 707-714.

LUTERNAUER, J.L., CLAGUE, J.J., and FEENEY, T.D. 1991, A 367 meter core from south western Fraser River Delta, British Columbia, *in* Current Research, Part E: Geological Survey of Canada, Paper 91-IE, pp. 127-134.

LUTERNAUER, J.L., CLAGUE, J.J., HUNTER, J.A.M., PULLAN, S.E., ROBERTS, M.C., WOELLER, D.J., KOSTASCHUK, R.A., MOSLOW, T.F., MONAHAN, P.A., and HART, B.S. 1993. The Fraser River delta, architecture, geological dynamics and human impact. *In* Deltas of the World. Proceedings of the Eighth Symposium on Coastal and Ocean Management, New Orleans, July 19-23, 1993, pp. 99-113.

LUTERNAUER, J.L., BARRIE, J.V., CHRISTIAN, H.A., CLAGUE, J.J., EVOY, R.W., HART, B.S., HUNTER, J.A., KILEEN, P.G., KOSTASCHUK, R.A., MATHEWES,

R.W., MONAHAN, P.A., MOSLOW, T.F., MWENIFUMBO, C.J., OLYNYK, H.W, PATTERSON, R.T., PULLAN, S.E., ROBERTS, M.C., ROBERTSON, P.K., TARBOTTON, M.R., and WOELLER, D.J. 1994. Fraser River delta: geology, geohazards and human impact. *In* Geology and Geological Hazards of the Vancouver Region, British Columbia. Edited by J.W.H. Monger. Geological Survey of Canada, Bulletin 481, pp. 197-220.

MATHEWS, W.H. and SHEPARD, F.P. 1962. Sedimentation of the Fraser River Delta. Bulletin of the American Association of Petroleum Geologists, **46**: 1416-1463.

MCCABE, P.J. and SHANLEY, K.W. 1992. Organic control on shoreface stacking patterns: Bogged down in the mire. Geology, **20**: 741-744.

MCCAVE, I.N. and SYVITSKY, J.P.M. 1991. Principals and methods of geological particle size analysis. *In* Principles, applications and methods of particle size analysis. Cambridge University Press, Cambridge, England, pp. 3-21

MCKENNA, G.T., LUTERNAUER, J.L., and KOSTASCHUK, R.A. 1992. Large-scale mass wasting events on the Fraser River delta front near Sand Heads, British Columbia. Canadian Geotechnical Journal, 29: 151-156.

MCLAREN, P. and REN, P. 1995. Sediment transport and its environmental implications in the lower Fraser River and Fraser delta. Environment Canada, DOE FRAP 1995-03, 41 p.

MCLEAN, D.G., and TASSONE, B.L., 1991, A Sediment Budget of the Lower Fraser River. *In* Proceedings of the Fifth Federal Interagency Sedimentation Conference, March 18-21, 1991, Las Vegas, Nevada, pp. 2-33 - 2-40

MILLIMAN, J.D. 1980. Sedimentation in the Fraser River and its Estuary, Southwestern British Columbia (Canada). Estuarine and Coastal Marine Science, **10**: 609-633.

MITCHELL, J.K. and HOUSTON, W.N. 1975. Static penetration Testing on the Moon. *In* Proceedings of the European Symposium on Penetration Testing ESOPT, Stockholm, June 5-7, 1974, Volume 2:1 General Reports, Discussions and other activities. National Swedish Building Research, pp. 277-284

MONAHAN, P.A. 1993. Stratigraphy of the Delta Plain. In Trip 2, Marine geological studies of coastal areas: Saanich Inlet to the Fraser River delta. In Applied Quaternary Research, Program with Abstracts and Field Guide, Canadian Quaternary Association Meeting, Victoria, April 18-21, 1993, pp. G35-G40.

MONAHAN, P.A. and LEVSON, V.M. 1997: Earthquake Hazard Assessment in Greater

Victoria, British Columbia: Development of a Shear-Wave Velocity Model for the Quaternary Sediments. *In* Geological Fieldwork 1996. *Edited by* Lefebure, D.V., McMillan, W.J. and McArthur, J.G. British Columbia Geological Survey, Ministry of Employment and Investment, Paper 1997-1, pp. 467-479.

MONAHAN, P.A. and LUTERNAUER, J.L. 1994. Greater Vancouver Geotechnical Database (British Columbia): Richmond Pilot Project. *In* Current Research 1994-E. Geological Survey of Canada, pp. 85-91.

MONAHAN, P.A., LUTERNAUER, J.L. and BARRIE, J.V. 1993a. A delta topset sheet sand and modern sedimentary processes in the Fraser River delta, British Columbia. *In* Current research, part A. Geological Survey of Canada, Paper 93-1A, pp. 263-272.

MONAHAN, P.A., LUTERNAUER, J.L. and BARRIE, J.V. 1993b. Subsurface Mapping of the Fraser River delta: implications for delta front instability. *In* Proceedings of the Fourth Canadian Conference on Marine Geotechnical Engineering, St. John's, June 27-30, 1993, pp. 450-463.

MONAHAN, P.A., LUTERNAUER, J.L. and BARRIE, J.V. 1993c. A delta plain sheet sand in the Fraser River delta, British Columbia, Canada. Quaternary International, **20**: 27-38.

MONAHAN, P.A., LUTERNAUER, J.L. and BARRIE, J.V. 1994. Application of cone penetration test data to facies analysis in the Fraser River delta, British Columbia (abstract). Geological Society of America, Abstracts with Programs, **26**: A253.

MONAHAN, P.A., LUTERNAUER, J.L. and BARRIE, J.V. 1995a. Applying Cone Penetration Test Data to Facies Analysis of the Fraser River Delta, British Columbia: implications for hazard mapping and foundation design (abstract). Geological Association of Canada-Mineralogical Association of Canada, Final Program with Abstracts, **20:** A72.

MONAHAN, P.A., LUTERNAUER, J.L. and BARRIE, J.V. 1995b, The Geology of the CANLEX Phase II Sites in Delta and Richmond, British Columbia. *In* Proceedings, 48th Canadian Geotechnical Conference, September 25-27 1995, Vancouver, B.C., Preprint Volume 1. Canadian Geotechnical Society, pp. 59-68.

MONAHAN, P.A., LUTERNAUER, J.L. and BARRIE, J.V. 1996. Facies analysis for earthquake hazard mapping in the Fraser River delta. *In* Abstracts for the Pan Pacific Hazards '96 Conference and Trade Show, Vancouver, B.C., July 29-August 2, 1996, p. 177.

MONAHAN, P.A., LUTERNAUER, J.L. and BARRIE, J.V. 1997. The Topset and Upper Foreset of the modern Fraser River Delta, British Columbia, Canada. *In* Core Conference, June 5-6, 1997, CSPG-SEPM Joint Convention June 1-6, 1997. *Compiled by* J. Wood and W. Martindale. Canadian Society of Petroleum Geologists, pp. 491-517.

MONAHAN, P.A., LEVSON, V.M., MCQUARRIE, E.J., BEAN, S.M., HENDERSON, P., and SY, A. (1998a): Seismic microzonation mapping in Greater Victoria, British Columbia, Canada. *In*, Geotechnical Earthquake Engineering and Soil Dynamics III. *Edited by* P. Dakoulas, M. Yegian, and R.D. Holtz. American Society of Civil Engineers, Geotechnical Special Publication No. 75, pp. 128-140.

MORAN, K., HILL, P.R., and BLASCO, S.M. 1989. Interpretation of piezocone penetrometer profiles in sediment from the Mackenzie trough, Canadian Beaufort Sea. Journal of Sedimentary Petrology, **59**: 88-97.

MULDER, E.F.J. de 1979. Engineering-geological investigations in the mouth of the Eastern Scheldt (SW Netherlands). Geologie en Mijnbouw, **58**: 471-476.

MULDER. E.F.J. de 1990. Engineering Geology in the Netherlands. *In* Proceedings Six International Congress International Association of Engineering Geology, 6-10 August 1990, Amsterdam, Netherlands. *Edited by* D.G. Price. pp. 3-20.

MULDER, E.F.J. de and BAKKER, J.G. 1989. Construction. *In* Earth Science Mapping for Planning, Development, and Conservation. *Edited by* J. McCall and B. Marker. Graham and Trotman, London, pp. 175-197.

MULDER, E.F.J. de and WESTERHOFF, W.E. 1985. Geology. *In* The Netherlands Commemorative Volume, Eleventh International Conference on Soil Mechanics and Foundation Engineering, San Francisco, 12-18 August 1985. *Edited by* E.H. de Leeuw. The Netherlands Member Society, pp. 19-28.

MWENIFUMBO, C.J., KILLEEN, P.G. and ELLIOT, B. 1994. Downhole logging measurements in the Fraser Delta, British Columbia. *In* Current Research 1994-E. Geological Survey of Canada, pp. 77-94.

NACE, R.L. 1970. World hydrology; status and prospects. In International Association of Hydrologists Special Publication 92, pp. 1-10.

NELSON, C.S. and LAWRENCE, M.F. 1984. Methane-derived high-Mg calcite submarine cement in Holocene nodules from the Fraser Delta, British Columbia, Canada. Sedimentology, **31**: 645-654.

NORTH, M.E.A., DUNN, M.W., and TEVERSHAM, J.M. 1979. Vegetation of the southwestern Fraser Lowland, 1858-1880. Lands Directorate, Environment Canada.

OLSEN, R.S. 1994. Normalization and prediction of geotechnical properties using the cone penetrometer test (CPT). Ph.D. dissertation, University of California, Berkeley, 290 p.

OLSON, S.M. and STARK, T. D. 1998. CPT based liquefaction resistance of sandy soils. *In*, Geotechnical Earthquake Engineering and Soil Dynamics III. *Edited by* P. Dakoulas, M. Yegian, and R.D. Holtz. American Society of Civil Engineers, Geotechnical Special Publication No. 75, pp. 325-333.

PATTERSON, R.T., and CAMERON, B.E.B. 1991. Foraminiferal biofacies succession in the late Quaternary Fraser River delta British Columbia. Journal of Foraminiferal Research, **21**: 228-243.

PATTERSON, R.T., and LUTERNAUER, J.L. 1993. Holocene foraminiferal faunas from cores collected on the Fraser River delta, British Columbia: a paleoecological interpretation. *In* Current Research Part A. Geological Survey of Canada, Paper 93-1A, pp. 245-254.

PHARO, C.H., and BARNES, W.C. 1976. Distribution of surficial sediments of the central and southern Strait of Georgia, British Columbia. Canadian Journal of Earth Sciences, **13**: 684-696.

PRYOR, W.A. 1973. Permeability-Porosity Patterns and Variations in Some Holocene Sand Bodies. The American Association of Petroleum Geologists Bulletin, **57**: 162-189.

PULLAN, S.E., JOL, H.M., GAGNE, R.M., and HUNTER, J.A. 1989. Compilation of high resolution "optimum offset" shallow seismic reflection profiles from the southern Fraser River delta, British Columbia. Geological Survey of Canada, Open File 1992.

PULLAN, S.E., HUNTER, J.A., JOL, H., ROBERTS, M.C., BURNS, R.A. and HARRIS, J.B. 1998. Seismostratigraphic investigations of the southern Fraser River delta. *In* Geology and Natural Hazards of the Fraser River delta, British Columbia. *Edited by* J.J. Clague, J.L. Luternauer and D.C. Mosher. Geological Survey of Canada, Bulletin 525, pp. 91-122.

READING, H.G. 1986. Facies. *In* Sedimentary environments and facies. *Edited by* H. G. Reading. Blackwell Scientific Publications, Oxford, pp. 4-19.

REINECK, H.-E. and SINGH, I.B. 1975. Depositional Sedimentary Environments,

Corrected Reprint of the First Edition. Springer-Verlag, Heidelberg, 439 p.

RIDER, M.H. 1990. Gamma-ray log shape used as a facies indicator: critical analysis of an oversimplified methodology. *In* Geological Applications of wireline Logs. *Edited by* A. Hurst, M.A. Lovell, and A.C. Morton. Geological Society of London Special Publication No. 48, pp. 27-37.

ROBERTSON, P.K. 1990. Soil classification using the cone penetration test. Canadian Geotechnical Journal, **27**: 151-158.

ROBERTSON, P.K. and CAMPANELLA, R.G. 1983a. Interpretation of cone penetration tests. Part I: Sand. Canadian Geotechnical Journal, **20**: 718-733.

ROBERTSON, P.K. and CAMPANELLA, R.G. 1983b. Interpretation of cone penetration tests. Part II: Clay. Canadian Geotechnical Journal, **20**: 734-745.

ROBERTSON, P.K. and CAMPANELLA, R.G. 1985. Liquefaction Potential of Sands Using the CPT. Journal of Geotechnical Engineering, **111**: 384-403.

ROBERTSON, P.K. and CAMPANELLA, R.G. 1986. Guidelines for the use and application of the CPT and CPTU. Soil Mechanics series No. 105, Department of Civil Engineering, The University of British Columbia, 187 p.

ROBERTSON, P.K. and FEAR, C.E. 1996. Soil Liquefaction and its Evaluation based on SPT and CPT. A Symposium on Recent Developments in Seismic Liquefaction Assessment, April 12, 1996, Vancouver, B.C. *Sponsored by* ConeTec Investigations Ltd.

ROBERTSON, P.K. and WRIDE (FEAR), C.E. 1997. Cyclic Liquefaction and its Evaluation based on the SPT and CPT. Final Contribution to the Procedings of the 1996 NCEER Workshop on Evaluation of Liquefaction Resistance, August 1997.

ROBERTSON, P.K. and WRIDE (FEAR), C.E. 1998. Evaluating cyclic liquefaction potential using the cone penetration test. Canadian Geotechnical Journal, **35**: 442-459.

ROBERTSON, P.K., CAMPANELLA, R.G., and WIGHTMAN, A. SPT-CPT Correlations. Journal of Geotechnical Engineering, **109**: 1449-1459.

ROBERTSON, P.K., CAMPANELLA, R.G., GILLESPIE, D., and GREIG, J. 1986. Use of Piezometer Cone Data. *In* Use of In Situ Tests in Geotechnical Engineering, Proceedings of In Situ '86, a Specialty Conference sponsored by the Geotechnical Engineering Division of the American Society of Civil Engineers. *Edited by* S.P.

Clemence. American Society of Civil Engineers, Geotechnical Special Publication No.6, pp. 1263-1280.

ROBERTSON, P.K., WOELLER, D.J. and FINN, W.D.L. 1992a. Seismic cone penetration test for evaluating liquefaction potential under cyclic loading. Canadian Geotechnical Journal, **29**: 686-695.

ROBERTSON, P.K., SULLY, J.P., WOELLER, D.J., LUNNE, T., POWELL, J.J.M. and GILLESPIE, D.G. 1992b. Estimating coefficient of consolidation from piezocone test. Canadian Geotechnical Journal, **29**: 539-550.

ROBERTSON, P.K., WRIDE, (FEAR), C.E., LIST, B.R., ATUKORALA, U., BIGGAR., K.W., BYRNE, P.M., CAMPANELLA, R.G., CATHRO, D.C., CHAN, D.H., CZAJEWSKI, K., FINN, W.D.L., GU, W.H., HAMMAMJI, Y., HOFMANN, B.A., HOWIE, J.A., HUGHES, J., IMRIE, A.S., KONRAD, J.-M., KUPPER, A., LAW, T., LORD, E.R.F., MONAHAN, P.A., MORGENSTERN, N.R.,PHILLIPS, R., PICHE, R., PLEWES, H.D., SCOTT, D., SEGO, D.C., SOBKOWICZ, J., STEWART, R.A., TAN, S., VAID, Y.P., WATTS, B.D., WOELLER, D.J., YOUD, T.L., and ZAVODNI, Z. in preparation. The Canadian Liquefaction Experiment: an Overview. Canadian Geotechnical Journal.

ROBINSON, S.W. and THOMPSON, G. 1980.. Radiocarbon corrections for marine shell dates with application to the Southern Pacific Northwest prehistory. Syesis, **14**: 45-57.

ROGERS, G.C. 1994. Earthquakes in the Vancouver area. *In* Geology and Geological Hazards of the Vancouver Region, British Columbia. *Edited by* J.W.H. Monger. Geological Survey of Canada, Bulletin 481, pp. 221-229.

RUBIN, D.M., NELSON, J.M. and TOPPING, D.J. 1998. Relation of inversely graded deposits to suspended-sediment grain-size evolution during the 1996 flood experiment in Grand Canyon. Geology, **26**: 99-102.

SCHAAP, L.H.J. and ZUIDBERG, H.M. 1982. Mechanical and electrical aspects of the electric cone penetrometer tip. In Proceedings of the Second European Symposium on Penetration Testing, ESOPT-II, Amsterdam 2. Balkeema, Rotterdam, pp. 841-851.

SCHMERTMANN, J.H. 1991. The Mechanical Aging of Soils. Journal of Geotechnical Engineering, **117**: 1288-1330.

SCHOUSTRA, J.J. 1975. Application of Static Cone Penetrometer Tests for Determining Continuity of Stratigraphic Horizons. *In* Proceedings of the European Symposium

on Penetration Testing ESOPT, Stockholm, June 5-7, 1974, Volume 2:1 General Reports, Discussions and other activities. National Swedish Building Research, pp. 150-154.

SCHLUMBERGER 1989. Log Interpretation Principles/Applications. Schlumberger Educational Services, Houston, Texas, 225 p.

SCHUMM, S.A. 1977. The Fluvial System. Wiley Interscience, New York, 338 p.

SEED, H.B. and De ALBA, P. 1986. Use of SPT and CPT Tests for Evaluating the Liquefaction Resistance of Sands. *In* Use of In Situ Tests in Geotechnical Engineering, Proceedings of In Situ '86, a Specialty Conference sponsored by the Geotechnical Engineering Division of the American Society of Civil Engineers. *Edited by* S.P. Clemence. American Society of Civil Engineers, Geotechnical Special Publication No.6, pp. 281-302.

SERRA, O. 1986. Fundamentals of well-log interpretation. 2. The interpretation of logging data. Developments in Petroleum Science, 15B. Elsevier, Amsterdam and Elf-Aquitaine, Pau, 339 p.

SERRA, O and SULPICE, L. 1975. Sedimentological analysis of sand-shale series from well logs. Transactions of the Society of Professional Well Log Analysts 16th Annual Logging Convention, paper W.

SHIBATA, T, and TEPARASKA, W. 1988. Evaluation of Liquefaction Potentials of Soils using Cone Penetration Tests. Soils and Foundations, **28**: 49-60.

SINGA, S., WEEMEES, I., WOELLER, D.J., ROBERTSON, P.K., AND SULLY, J.P. 1997. Gamma logging for geotechnical and environmental applications. Proceedings of the 50th Canadian Geotechnical Conference, Ottawa, Canadian Geotechnical Society.

SOUTHON, J.R., Nelson, D.E. and Vogel, J.S. 1990, A record of past ocean-atmosphere radiocarbon differences from the northeast Pacific. Paleoceanography, **5**: 197-206.

SPIEGEL, M.R. 1996. Schaum's outline of theory and problems of statistics, Second Edition. McGraw-Hill, 516 p.

STARK, T.D. and OLSON, S.M. 1995. Liquefaction Resistance Using CPT and Field Case Histories. Journal of Geotechnical Engineering, **121**: 856-869.

SULLY, J.P. and ECHEZURIA, H.I. 1988. In situ density measurements with a nuclear cone penetrometer. *In* Penetration Testing, 1988, Proceedings of the International

Symposium on penetration testing, ISOPT-1, Orlando, Vol. 1. *Edited by* J. de Ruiter, Balkeema, Rotterdam, pp. 1001-1005.

SWANSON, G.J. 1994. Rotasonic Revisited: Is There a Production Breakthrough in Its Future? Water Well Journal, October, 1994.

SWINBANKS, D.D. and LUTERNAUER, J.L. 1987. Burrow distribution of Thalassinidean shrimp on a Fraser Delta tidal flat, British Columbia. Journal of Paleontology, **61**: 315-332.

SY, A., WIGHTMAN, A., and Hodge, W.E. 1987. A piezometer cone penetration testing system. *In* Proceedings of the 1st Canadian Symposium on Microcomputer Applications to Geotechnique, Oct. 1987, Regina, Saskatchewn, pp. 105-110.

TAYLOR, B.B., LEWIS, J.F., INGERSOLL, R.W. 1993. Comparison of interpreted seismic profiles to geotechnical borehole data at Hibernia. *In* Proceedings of the Fourth Canadian Conference on Marine Geotechnical Engineering, St. John's, June 27-30, 1993, pp. 684-708.

TERZAGHI, K. 1962. Discussion of "Sedimentation of Fraser River delta by W.H. Mathews and F.P. Shepard. Bulletin of the American Association of Petroleum Geologists, **46**: 1438- 1443.

TERZAGHI, K., PECK, R.B. and MESRI, G. 1996. Soil Mechanics in Engineering Practice, Third Edition. John Wiley and Sons, New York, 549 p.

THOMSON, R.E. undated. The estuarine/oceanographic setting of the Fraser River delta front. *In* The sedimentary environments and facies of the Fraser River delta. *Organizers/Leaders* J.L. Luternauer and T.F. Moslow. Canadian Society of Petroleum Geologists Field Trip Guidebook, June 9-14, 1991.

THOMSON, R.E. 1975. Longshore current generation by internal waves in the Strait of Georgia. Canadian Journal of Earth Sciences, **12**: 472-488.

THOMSON, R.E. 1981. Oceanography of the British Columbia Coast. Canadian Special Publication of Fisheries and Oceans 56, 291 p.

TIFFIN, D.L., MURRAY, J.W., MAYERS, I.R., and GARRISON, R.E. 1971. Structure and origin of foreslope hills, Fraser delta, British Columbia. Bulletin of Canadian Petroleum Geology, **19**: 589-600.

TOWNSHIP OF RICHMOND, undated. Sloughs and archaeological sites of Richmond. Map sheet 1.

UNIVERSITY OF BRITISH COLUMBIA, 1995. CANLEX Phase II, Activity 3A, General Site Characterization, Kidd 2 Site, August 1995. Unpublished report by UBC In-Situ Testing Group.

VAN DER GRAAF, H.C. and ZUIDBERG, H.M. 1985. Field Investigations. *In* The Netherlands Commemorative Volume, Eleventh International Conference on Soil Mechanics and Foundation Engineering, San Francisco, 12-18 August 1985. *Edited by* E.H. de Leeuw. The Netherlands Member Society, pp.29-44

VISHER, G.S. 1969. How to distinguish barrier bar and channel sands. World Oil, May 1969: 106-113.

VREUGDENHILL, R., DAVIS, R., and BERRIHILL, J. 1994. Interpretation of cone penetration results in multilayered soils. International Journal for Numerical and Analytical Methods, **18**: 585-599.

WALLIS, D.M. 1979. Ground motions in the Fraser delta due to earthquakes. M.A.Sc. thesis, University of British Columbia, Vancouver, B.C., 199 p.

WATTS, B.D., SEYERS, W.C., and STEWART, R.A. 1992. Liquefaction susceptibility of Greater Vancouver area soils. *In* Geotechnique and Natural Hazards, A symposium sponsored by the Vancouver Geotechnical Society and the Canadian Geotechnical Society, May 6-9, 1992, pp. 145-157.

WENTWORTH C.K. 1922. A scale of grade and class terms for clastic sediments. Journal of Geology, **30**: 377-392.

WILLIAMS, H.F.L. 1988. Sea-level change and delta growth: Fraser Delta, British Columbia. Ph.D. dissertation, Simon Fraser University, Burnaby. B.C., 256 p.

WILLIAMS, H.F.L. and ROBERTS, M.C. 1989. Holocene sea-level change and delta growth: Fraser River Delta, British Columbia. Canadian Journal of Earth Sciences, **26**: 1657-1666.

WILLIAMS, H.F.L. and ROBERTS, M.C. 1990, Two middle Holocene marker beds in vertically accreted floodplain deposits, lower Fraser River, British Columbia: Geographie Physique et Quaternaire, 44: 27-32.

WOELLER, D.J. and ROBERTSON, P.K. 1997. Penetration testing for geoenvironmental site characterization. *In* A short Course on Site Characterization for Environmental and Geotechnical projects, October 1, 1997. *Presented by* J.A. Howie, P. Mayne, P.K. Robertson and D.J. Woeller. ConeTec Investigations Ltd. and Mud Bay Drilling Ltd.

WOELLER, D.J., HUNTER, J.A., and LUTERNAUER, J.L. 1993a. Results of SCPT and SASW Testing of the Fraser River delta sediments, British Columbia (92 G/2,3). Geological Survey of Canada, Open File 2714.

WOELLER, D.J., LUTERNAUER, J.L., and HUNTER, J.M. 1993b. Presentation & Interpretation of Seismic Cone Penetration Test Data, Fraser River delta, British Columbia (92 G/2,3). Geological Survey of Canada, Open File 2715.

WOELLER D.J., HUNTER J.A., and LUTERNAUER J.L., 1994, Results of Seismic Cone Penetration Testing in the Fraser River Delta, February March, 1994: Geological Survey of Canada, Open File 2956.

WOLMAN, M.G., CHURCH, M., NEWBURY, R., LAPOINTE, M., FRENETTE, M., ANDREWS, E.D., LISLE, T.E., BUCHANAN, J.P., SCHUMM, S.A., and WINKLEY, B.R. 1990. The riverscape. *In* Surface water hydrology. Edited by M.G. Wolman and H.C. Riggs. The Geology of North America, volume O-1, Geological Society of America, Boulder, Colorado, pp 281-328.

APPENDIX A

GLOSSARY OF GEOTECHNICAL TERMS AND LIST OF SYMBOLS

GEOTECHNICAL TERMS

Cone stress exponent. The exponent applied to the reciprocal of effective overburden stress used to correct cone bearing measurements for overburden stress. It varies from 0.5 in sands to 1.0 in normally consolidated silts.

Drained penetration. In drained penetration, the force of penetration is taken by the solid phase and is not transferred to the liquid phase.

Effective overburden stress. Overburden stress less hydrostatic (i.e. water) pressure.

Excess pore pressure. The difference between pore pressure measured in a cone penetration test and hydrostatic pore pressure.

Fines content. The silt and clay fraction of geotechnical engineering usage, defined as the fraction finer than 0.074mm (Terzaghi et al., 1996). It differs from the silt and clay fraction of geological usage, which is the fraction finer than 0.062 mm. In Canada, FC is defined as the fraction finer than 0.075mm (Canadian Foundation Engineering Manual, 1992). However, this usage is not followed in the CPT and related literature (e.g. Stark and Olsen, 1995; Robertson et al., in prep.) and is not followed here.

Friction ratio. The ratio of sleeve friction to cone bearing measured in a cone penetration test.

Normally consolidated. Normally consolidated sediments have not been subjected to higher effective overburden stresses in the past.

Moon pool. A "moon pool" is an opening in the deck of a drilling vessel through which the drill string is lowered to the sea floor.

Normalized CPT parameters. CPT parameters corrected for overburden stress.

Overburden stress (vertical). Stress acting in a vertical direction due to the weight of overburden. Overburden stress is the product of unit weight times depth. Unit weight is the product of density times acceleration due to gravity.

Overconsolidated. Overconsolidated sediments are those that have been subjected to higher effective overburden stresses in the past than at present. Glacial loading, removal of overlying deposits, water table fluctuations and desiccation result in overconsolidation.

Sensitive fines. Sensitive fines have a much lower undrained shear strength in their remoulded, or disturbed, state than in their undisturbed state.

Spud barge. A spud barge has vertical poles ("spuds") on either side that can be dropped into the sea floor, so that it maintains its position during drilling. Metal sleeves attached to the barge fit around the spuds so that the vessel can move vertically with the tide.

Undrained penetration. In undrained penetration, the force of penetration is transferred to the liquid rather than the solid phase and results in a pore pressure increase.

LIST OF SYMBOLS

a: cone bearing net area ratio, roughly the ratio of the load cell cross sectional area to the projected area of the cone.

B_q: pore pressure parameter ratio; $B_q = dU/(q_t-\sigma_{vo})$.

c: cone stress exponent.

D_{50}: median grain size in millimetres.

dU: excess pore pressure; $dU = u - u_0$.

FC: fines content.

F_R: normalized friction ratio; $F_R = f_s/(q_t-\sigma_{vo}) \times 100\%$.

f_s: measured sleeve friction.

I_F: normalized soil behaviour type index, based on variable cone stress exponent; see Chapter 3 for explanation.

I_C: normalized soil behaviour type index, based on constant cone stress exponent (c=1.0);

$I_C = [(3.47 - \log Q_t)^2 + (\log F_R + 1.22)^2]^{0.5}$.

Pa: atmospheric pressure.

Q: normalized cone bearing, based on a variable cone stress exponent; see Chapter 3.

q_c: measured cone bearing or tip resistance.

q_t: cone bearing corrected for pore pressure; $q_t = q_c + (1-a)\,u$.

q_{c1}: normalized cone bearing, based on a constant cone stress exponent (c=0.5);

$q_{c1} = (q_c/Pa)(Pa/\sigma'_{vo})^{0.5}$; other methods have been proposed to calculate q_{c1}; see Chapter 3.

Q_t: normalized cone bearing, based on constant cone stress exponent (c=1.0);

$Q_t = (q_t - \sigma_{vo})/\sigma'_{vo}$.

R_f: friction ratio, or ; $R_f = f_s / q_t$.

u: measured pore pressure.

u_0: hydrostatic pore pressure.

U_1, U_2 and U_3: positions for measuring pore pressure in a cone penetrometer; on the cone face immediately above the cone and above the friction sleeve respectively; see Figure 3-1.

σ_{vo}: vertical overburden stress.

σ'_{vo}: effective vertical overburden stress.

ϕ_{50}: median grain size in ϕ units; ϕ is the negative log to base 2 of the grain size in millimetres.

APPENDIX B

COMPOSITE LOGS OF BOREHOLES

At each site, the following data are shown, from left to right; gamma ray log, in counts per second (cps), lithology log; and CPT data (q_t, R_f and U). For facies symbols, see Table 6-1.

LEGEND

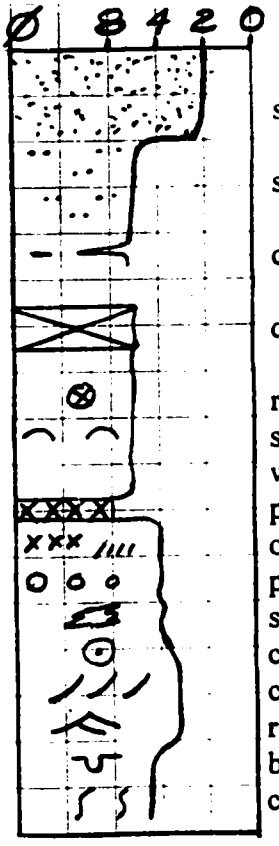

sand
silt
clay
disturbed by coring
rhizoconcretions
shell
wood
peat
organic laminae
pebbles
silt clasts
concretion clasts
cross bedding
ripples
burrows
contorted bedding

* ^{14}C date

FD92-2

Sonic Borehole ~ 60 m from CPT
River dyke, No. 4 Rd. and River Road, Richmond.
UTM: E 491820 N 5449530 (NAD27; Hunter et al., 1994)

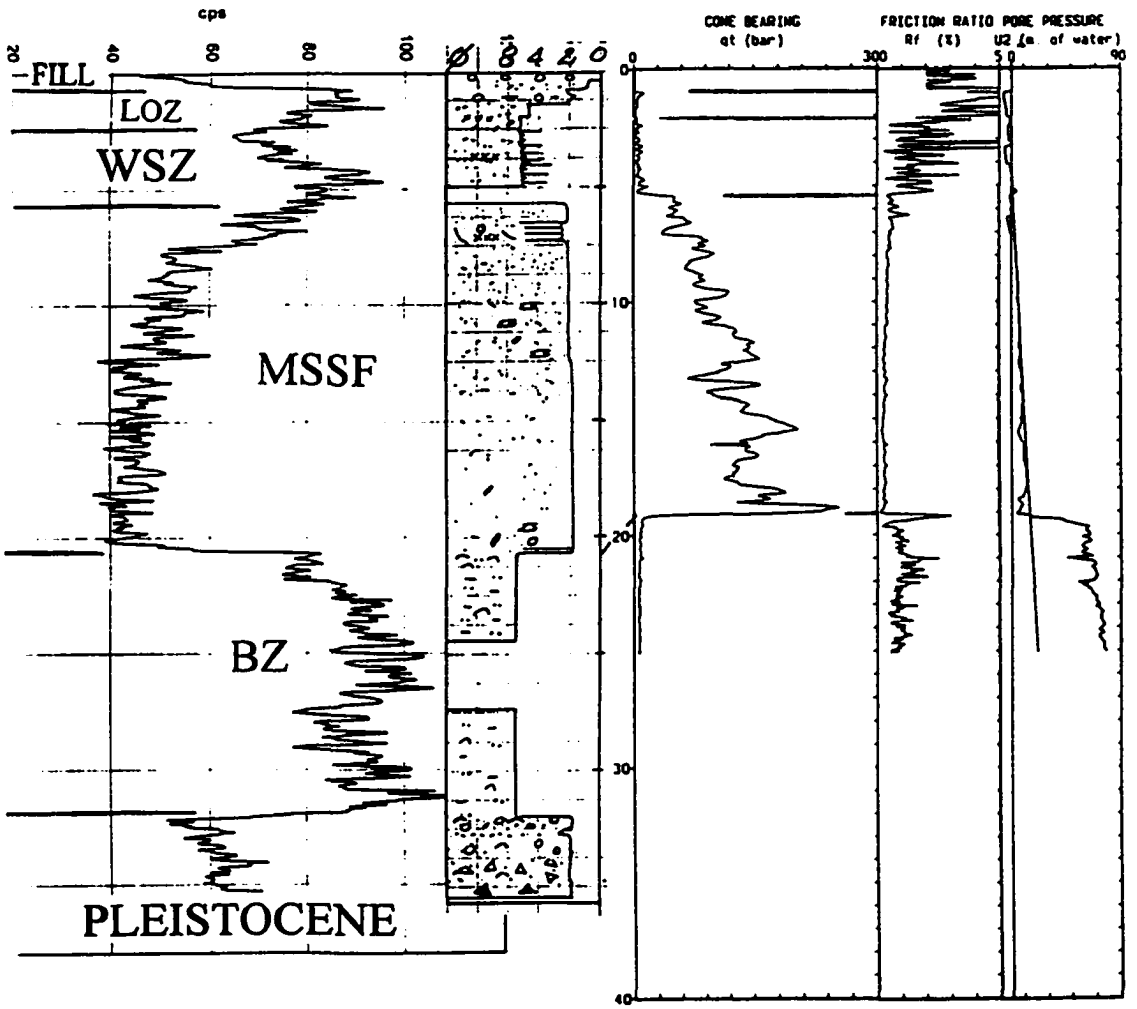

FD92-3

Sonic Borehole
MOT Radio Tower, north of Westminster highway between #6 and #7 Road, Richmond.
UTM: E 495850 N 5446500 (NAD27; Hunter et al., 1994)

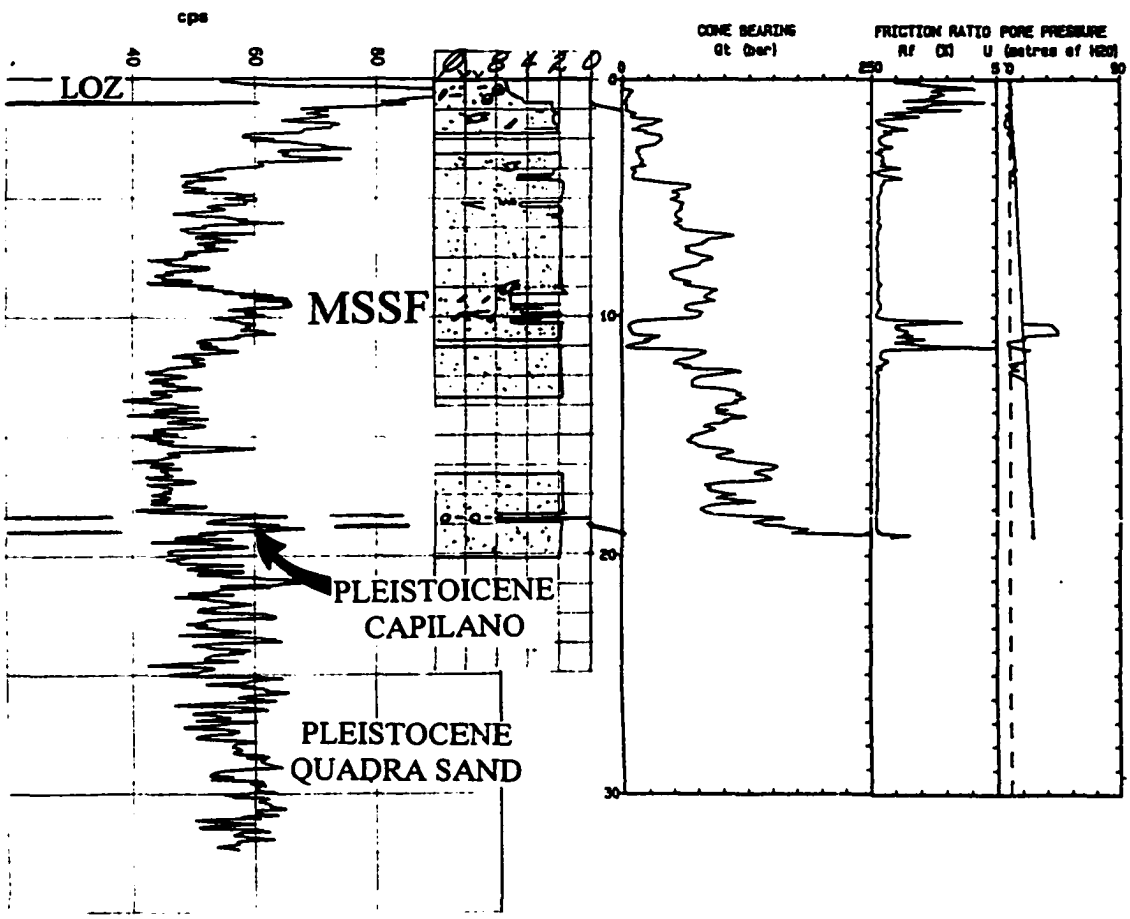

FD92-4

Sonic Borehole ~65 m from CPT
Southeast corner of Arnott Substation, Ladner, Delta
UTM: E 497170 N 5437300 (NAD27; Hunter et al., 1994)

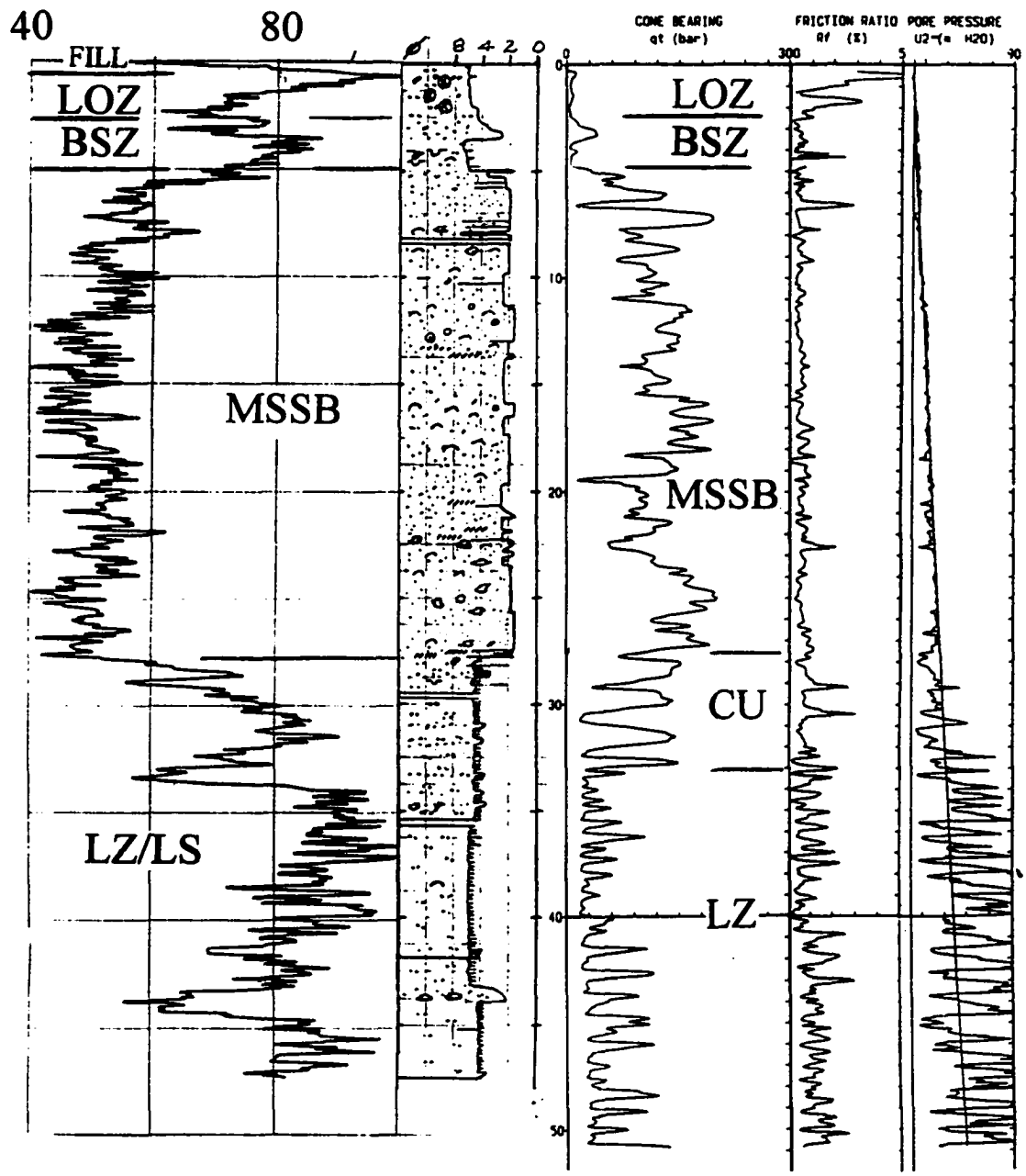

FD92-5

Sonic Borehole ~ 10 m from CPTs

Westbridge Site, northwest shore of Annacis Island, Delta

UTM: E 503250 N 5446600 (NAD27; Hunter et al., 1994)

FD92-5 and CPT 87-C1A

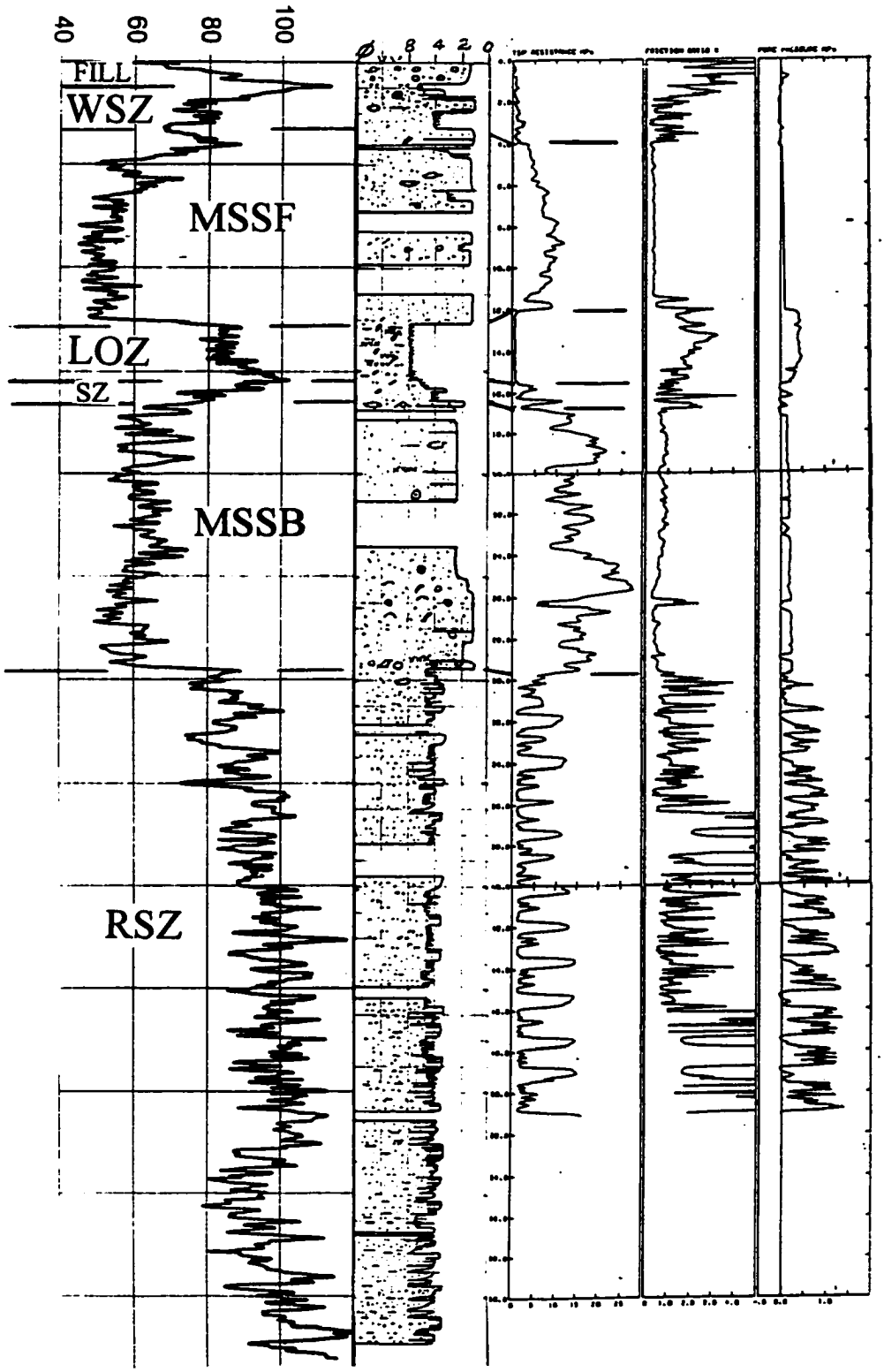

FD92-5 and SCPT 91-3

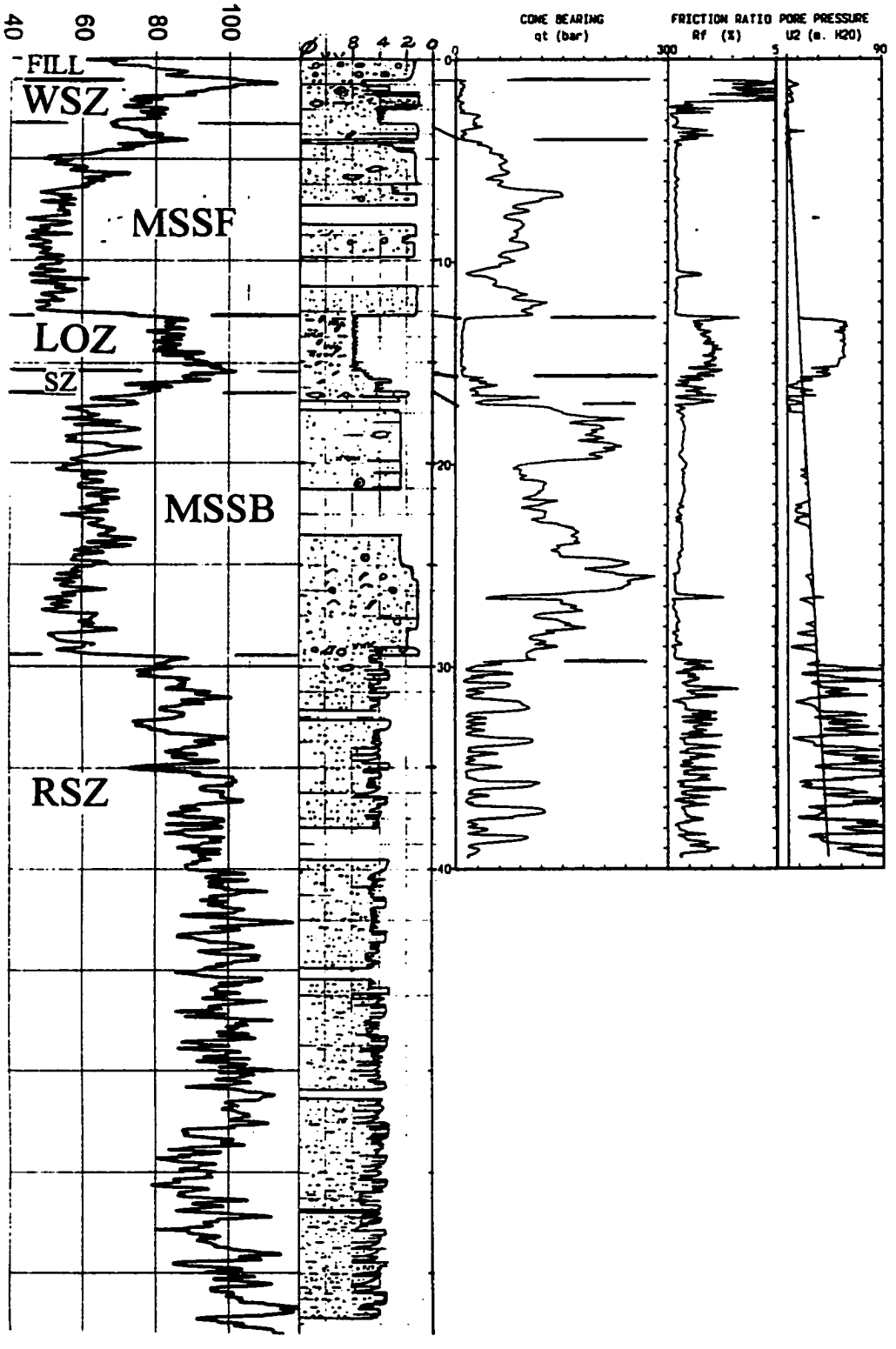

FD92-11

Triple Tube Retractor Borehole 7.7 m from CPT

Canoe Pass Substation, Tsawwassen, Delta

UTM: E 4910960 N 5432978 (NAD27; Hunter et al., 1994)

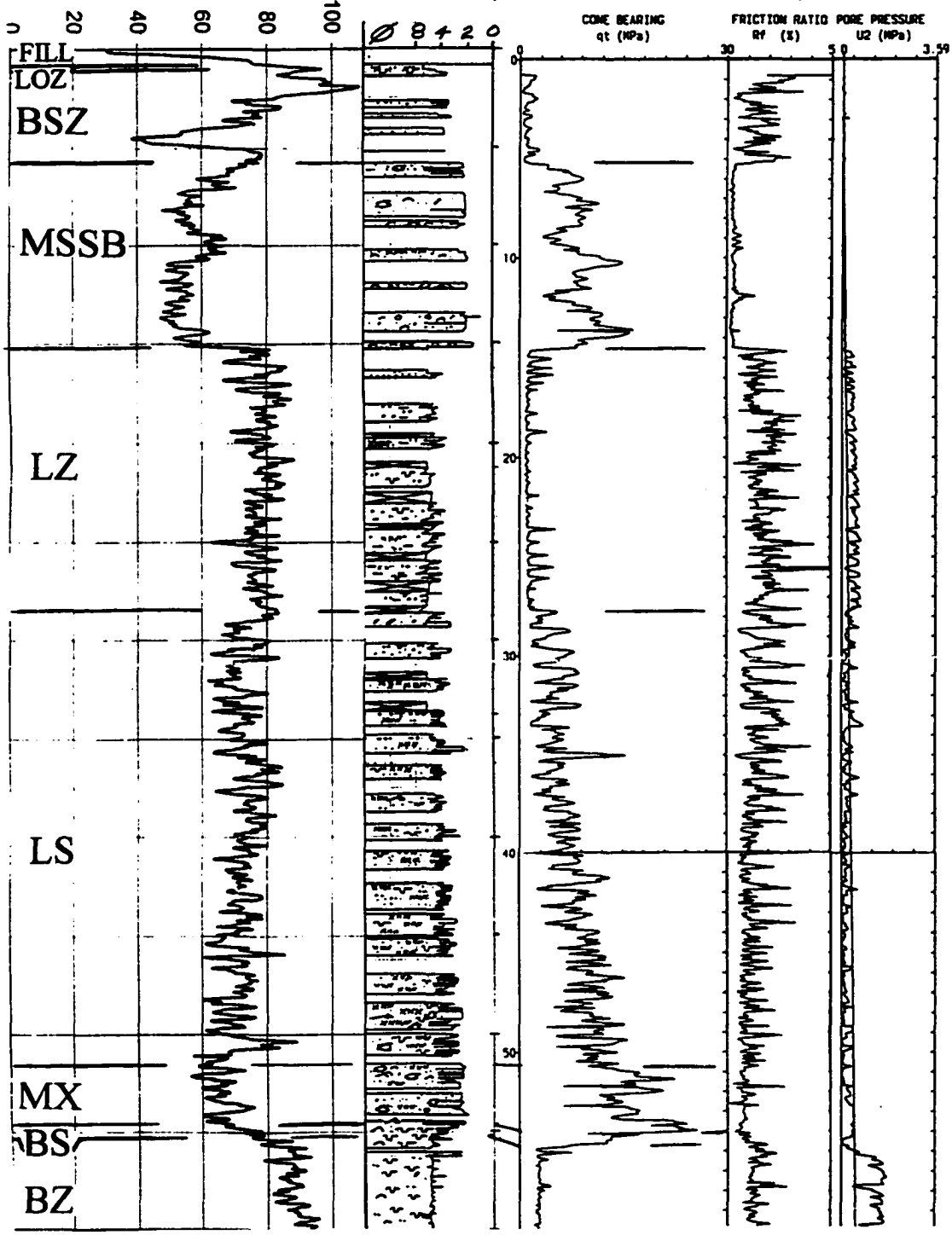

FD92-11 (cont'd)

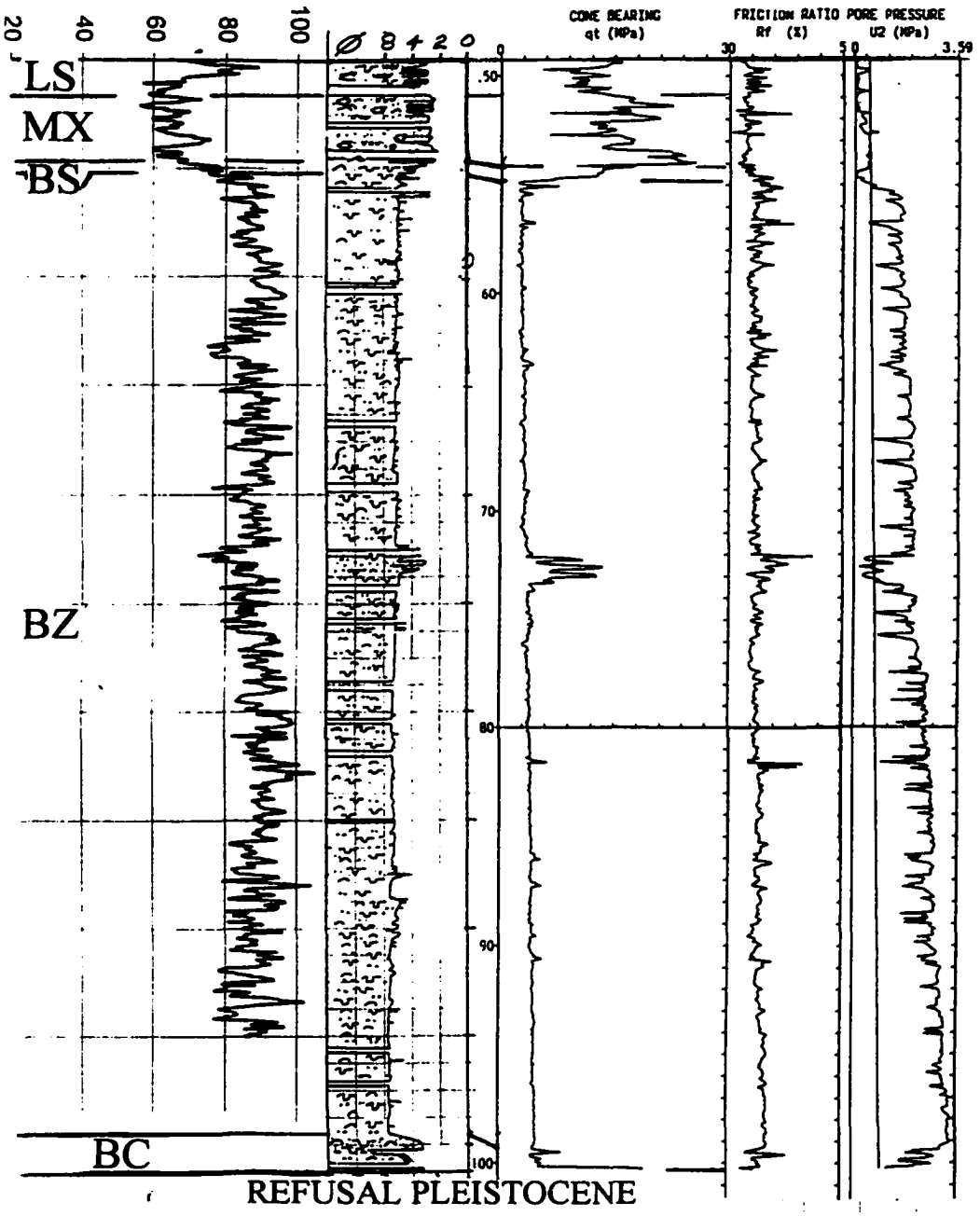

FD93-1

Sonic Borehole; 5 m southeast of CPT and 8.7 m southeast of Borehole FD95S-1
Southwest shoreline of Westshore Terminals site, near dumper pit, Roberts Bank Port, Delta;
UTM: E 487816 N 5429049 (NAD27; Hunter et al., 1994)

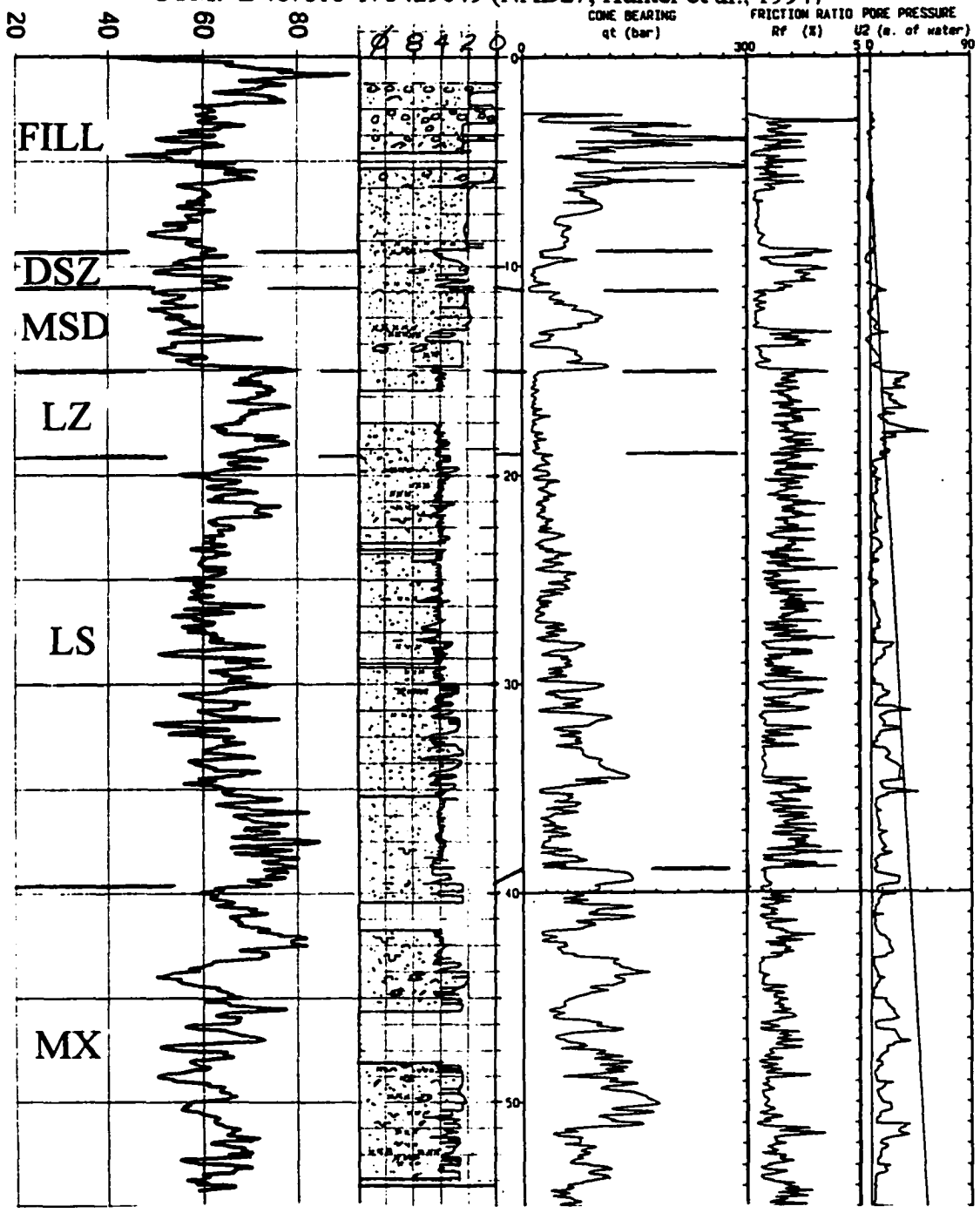

FD93-2

Sonic Borehole <3 m from CPT
North side of Richmond Hospital, Richmond
UTM: E 489381 N 5446142 (NAD27; Hunter et al., 1994)

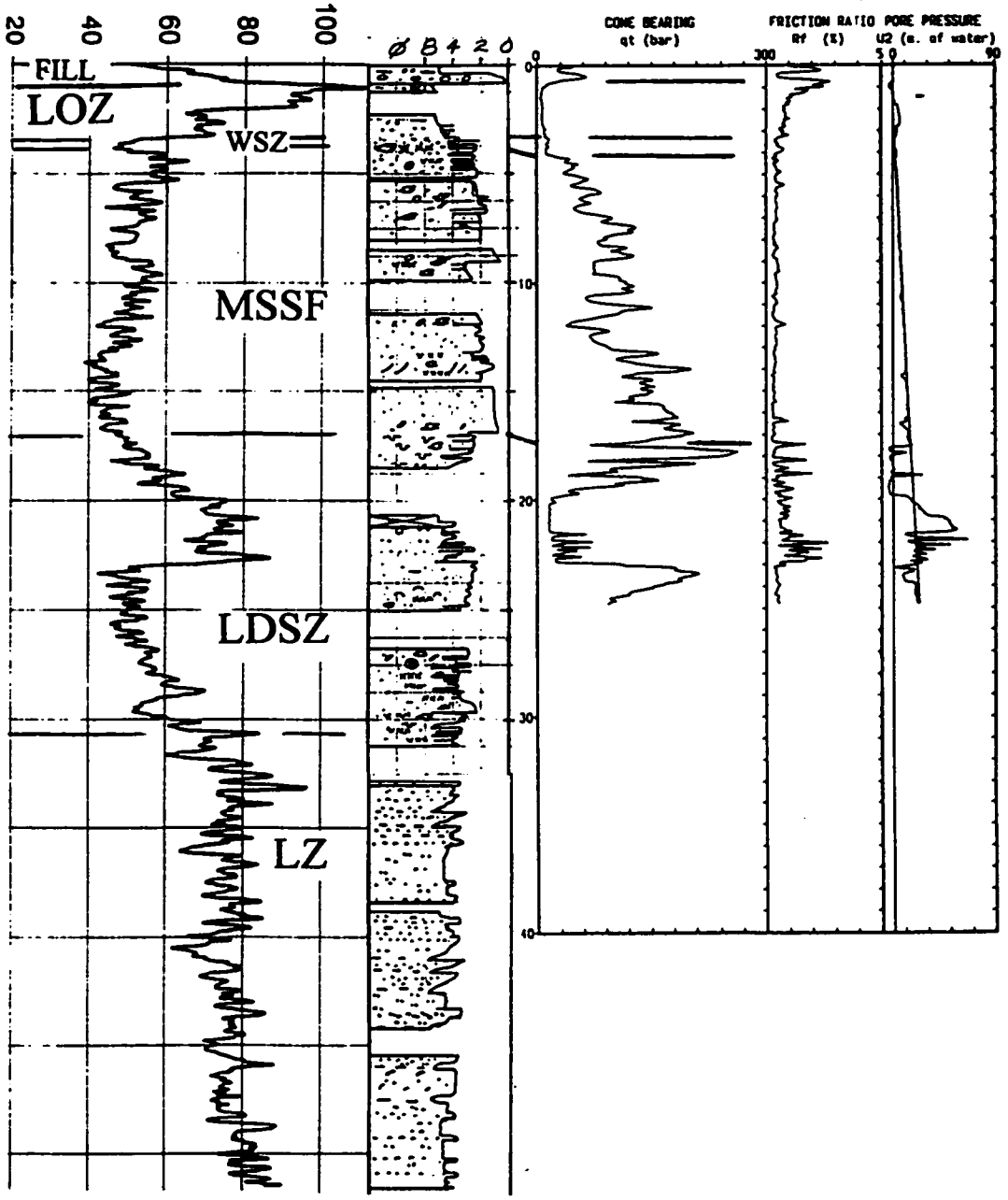

FD93-3

Sonic Borehole <3 m from CPT
Sea Dykes at west end of Francis Road, Richmond
UTM: E 485903 N 5443812 (NAD27; Hunter et al., 1994)

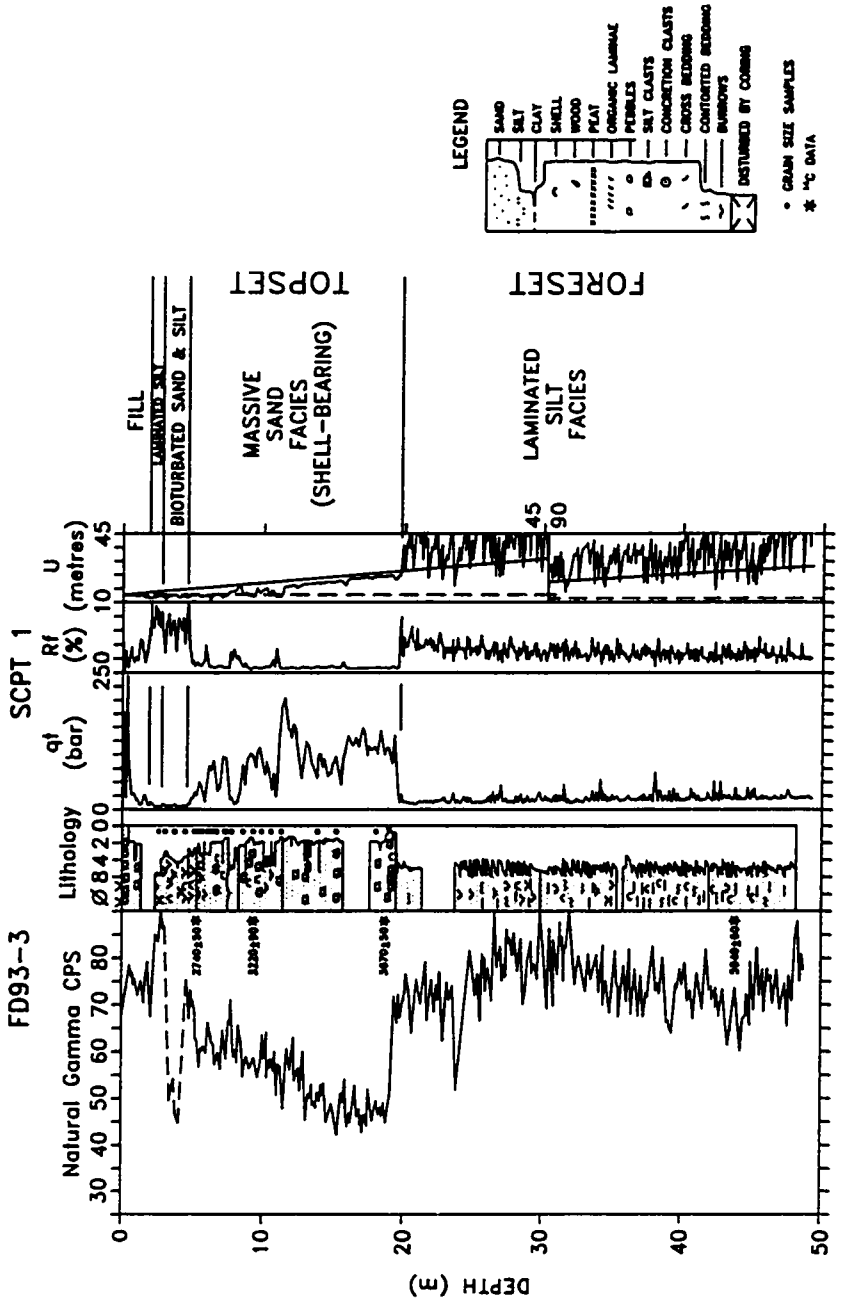

FD93-4

Sonic Borehole <3 m from CPT
Front of Nottingham farm, 60th Ave. and 60th St., Delta
UTM: E 497530 N 5439650 (NAD27; Hunter et al., 1994)

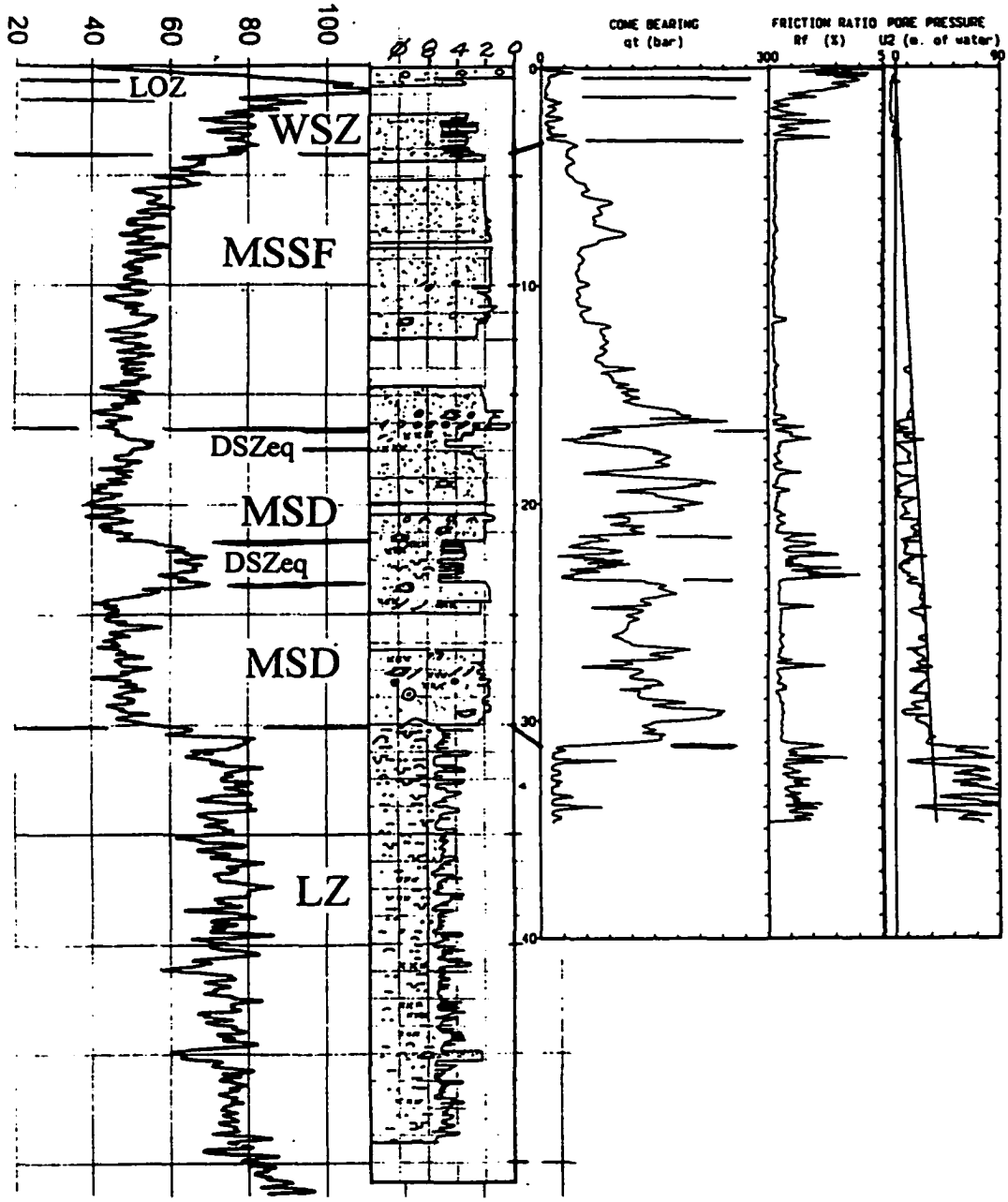

FD93-5

Sonic Borehole 2 m from CPT
Soth side of causeway to Roberts Bank, opposite pole #13-4
UTM: E 489280 N 5430812 (NAD27; Hunter et al., 1994)

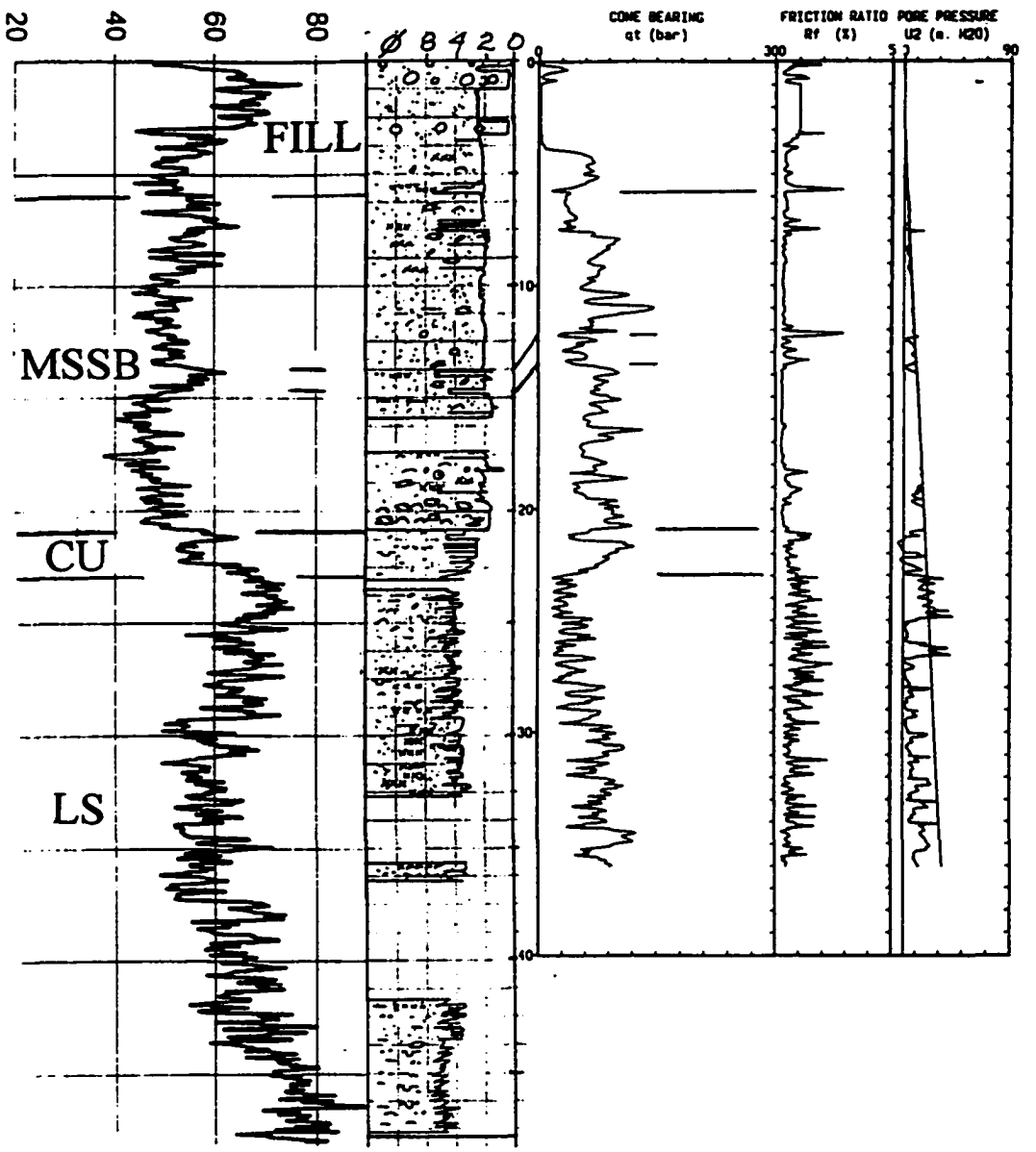

FD94-1

Sonic Borehole 1.5 m from CPT
Northeast of south portal of Massey Tunnel, Deas Island, Delta (CANLEX SITE)
(Monahan et al., 1995b)

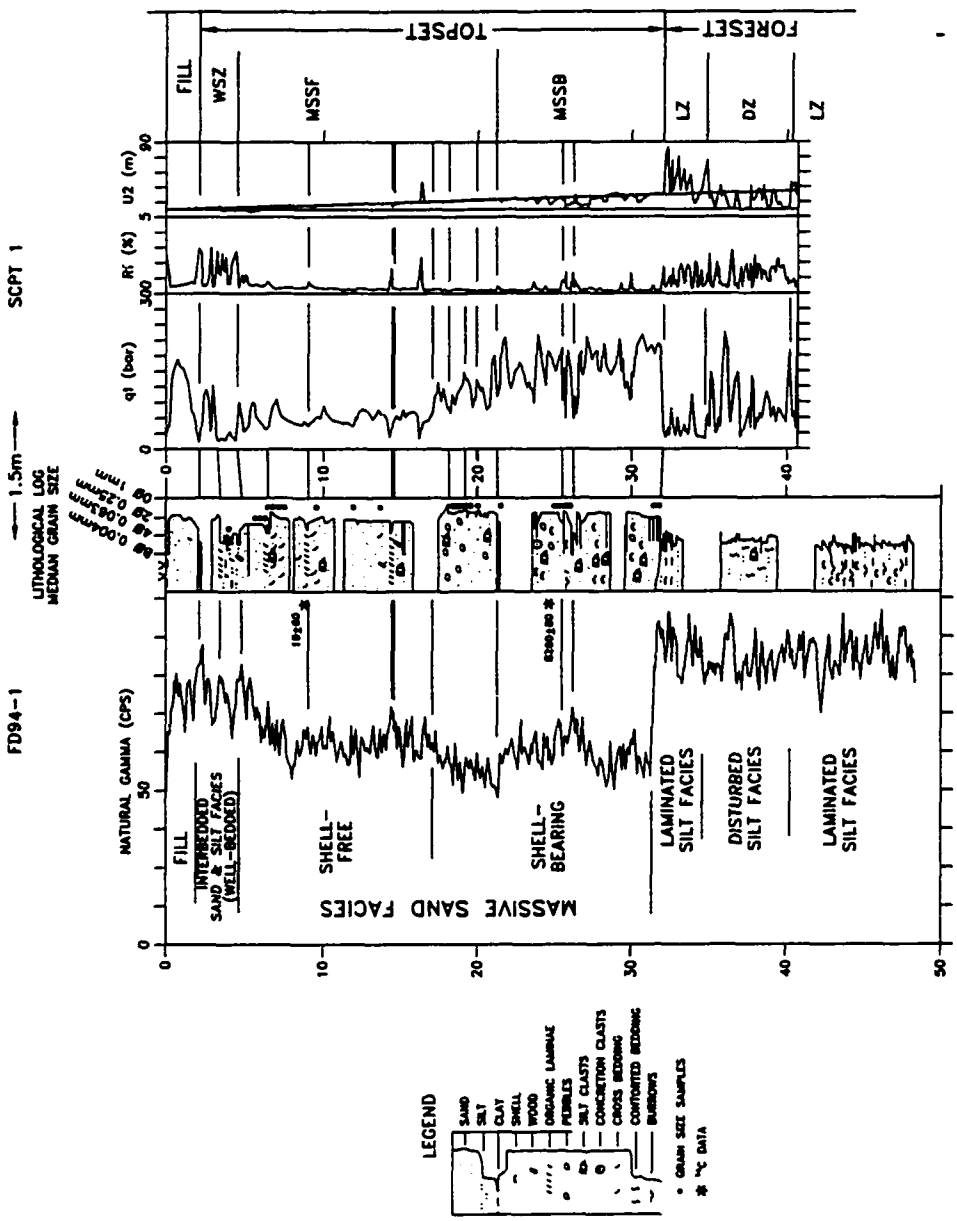

FD94-2

Sonic Borehole 1.5 m from CPT
Coast Guard Radio Tower, West side of No. 4 Rd, south of Alderbridge Way, Richmond
49° 10' 32" N 123° 06' 48" W (Dallimore et al., 1995)

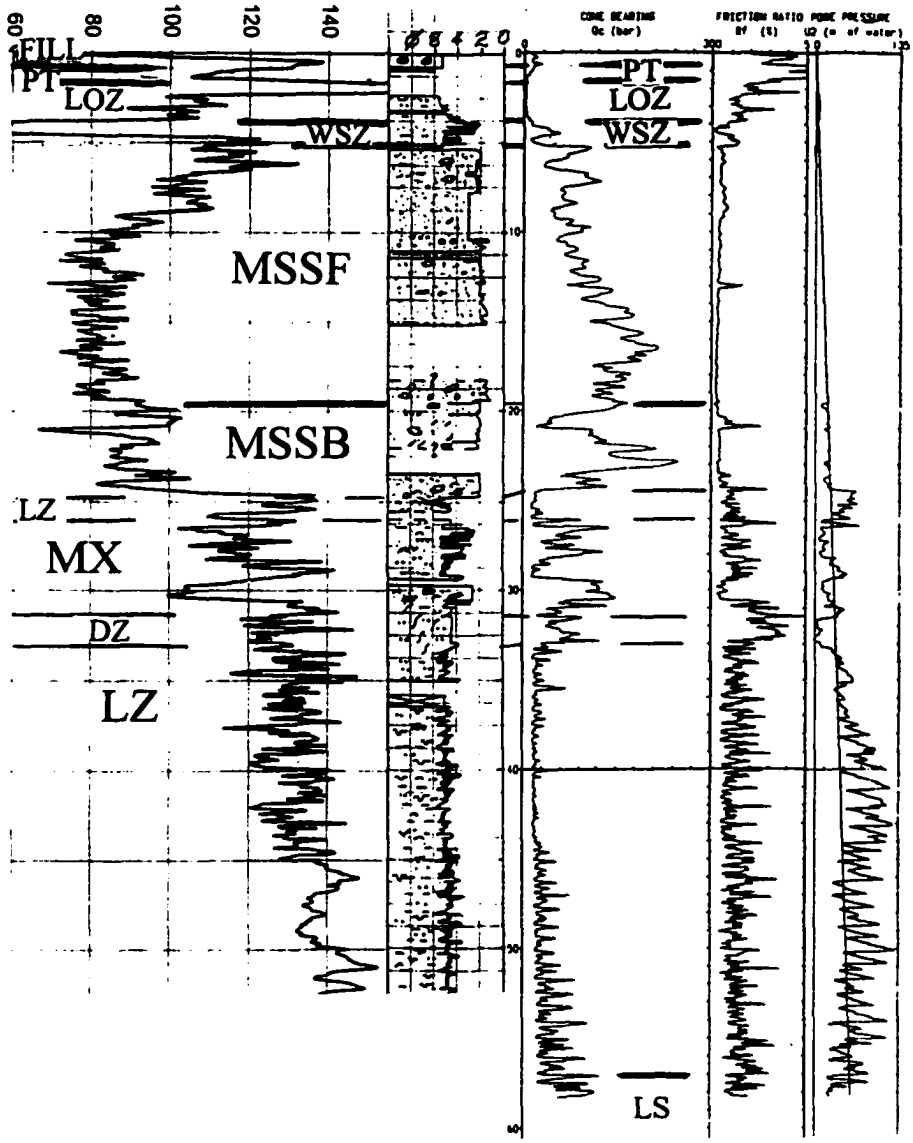

FD94-4

Triple Tube Retractor Borehole
Coast Guard Radio Tower, West side of No. 4 Rd, south of Alderbridge Way, Richmond
49° 10' 32" N 123° 06' 48" W (Dallimore et al., 1995)

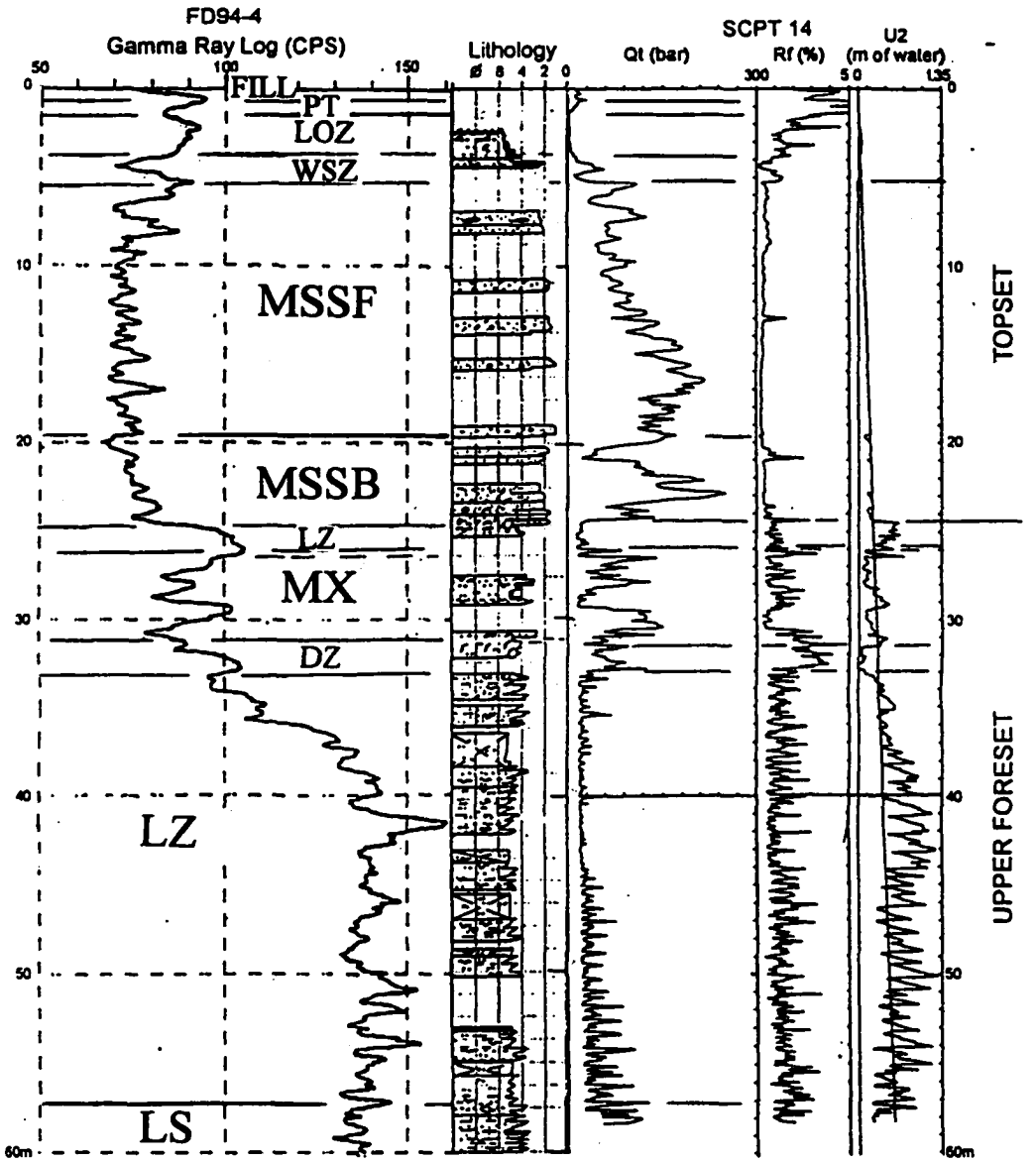

FD94-5

Sonic Borehole <3 m from CPT
Wetstwind Elementary School, Kingfisher Drive, Richmond

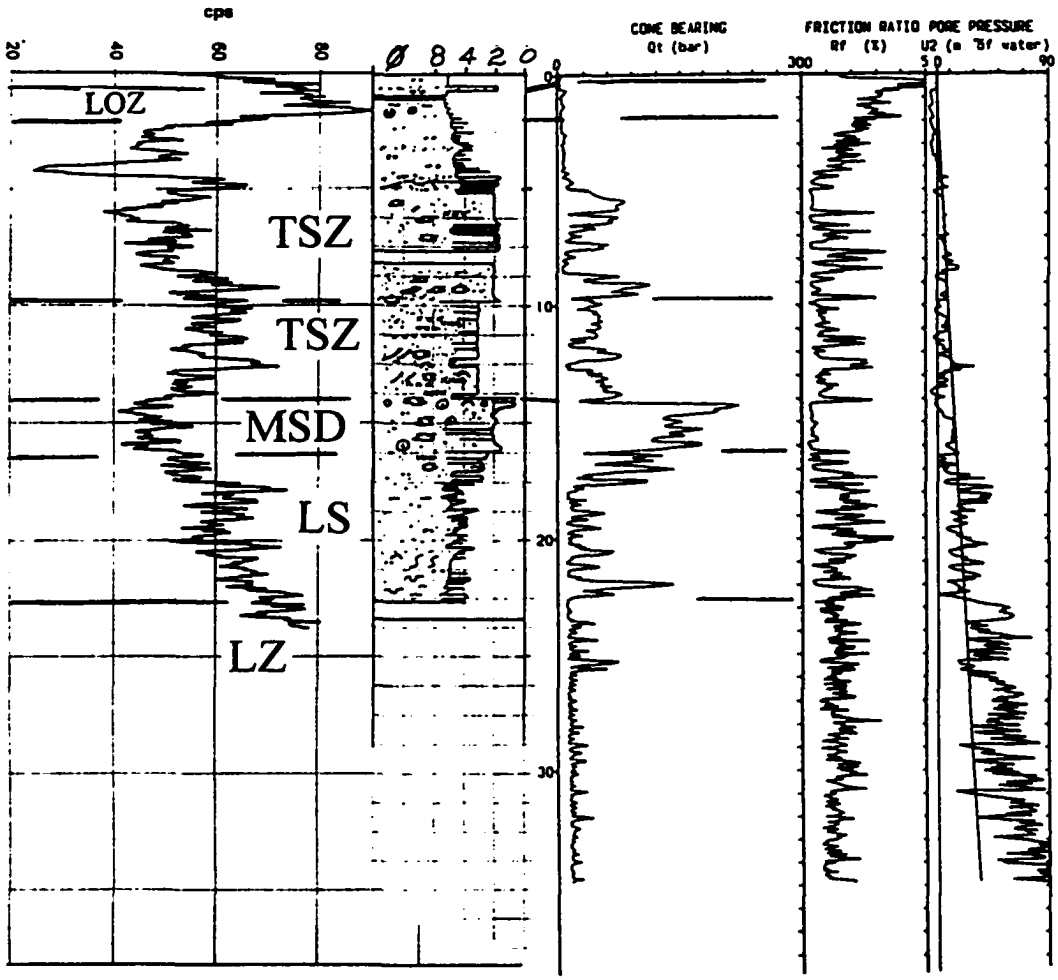

FD94-6

Sonic Borehole <3 m from CPT
BC Rail Tracks and 88th St., Delta

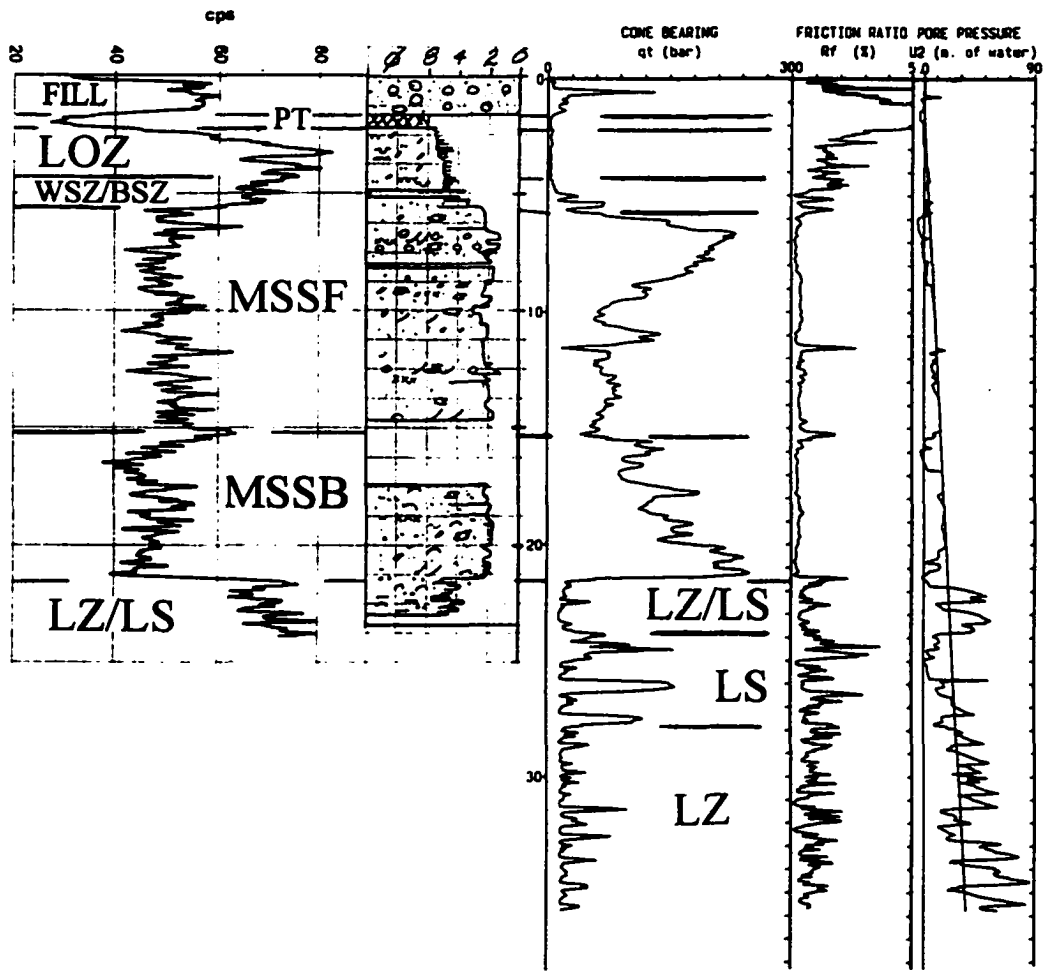

FD95S-1

Triple Tube Retractor Borehole 3.7 m northest of CPT and 8.7 m northeast of FD931
Southwest shoreline of Westshore Terminals site, near dumper pit, Roberts Bank Port, Delta;
UTM: E 487720 N 5429260 (NAD83)

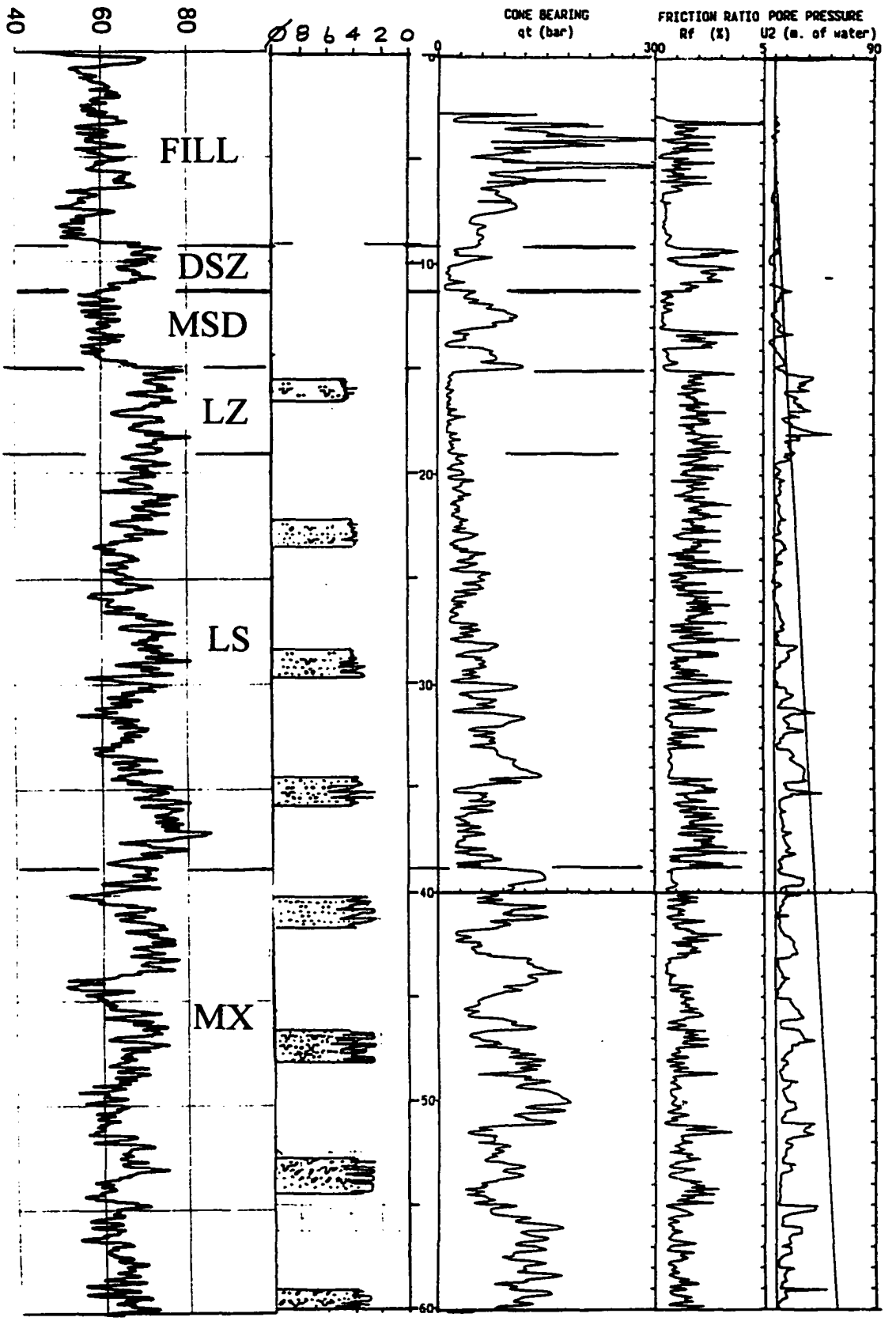
40
60
80
Ø 8 6 4 2 0
CONE BEARING
qt (bar)
0
300
FRICTION RATIO
Rf (%)
PORE PRESSURE
U2 (m. of water)
5
90
FILL
DSZ
MSD
LZ
LS
MX
10
20
30
40
50
60

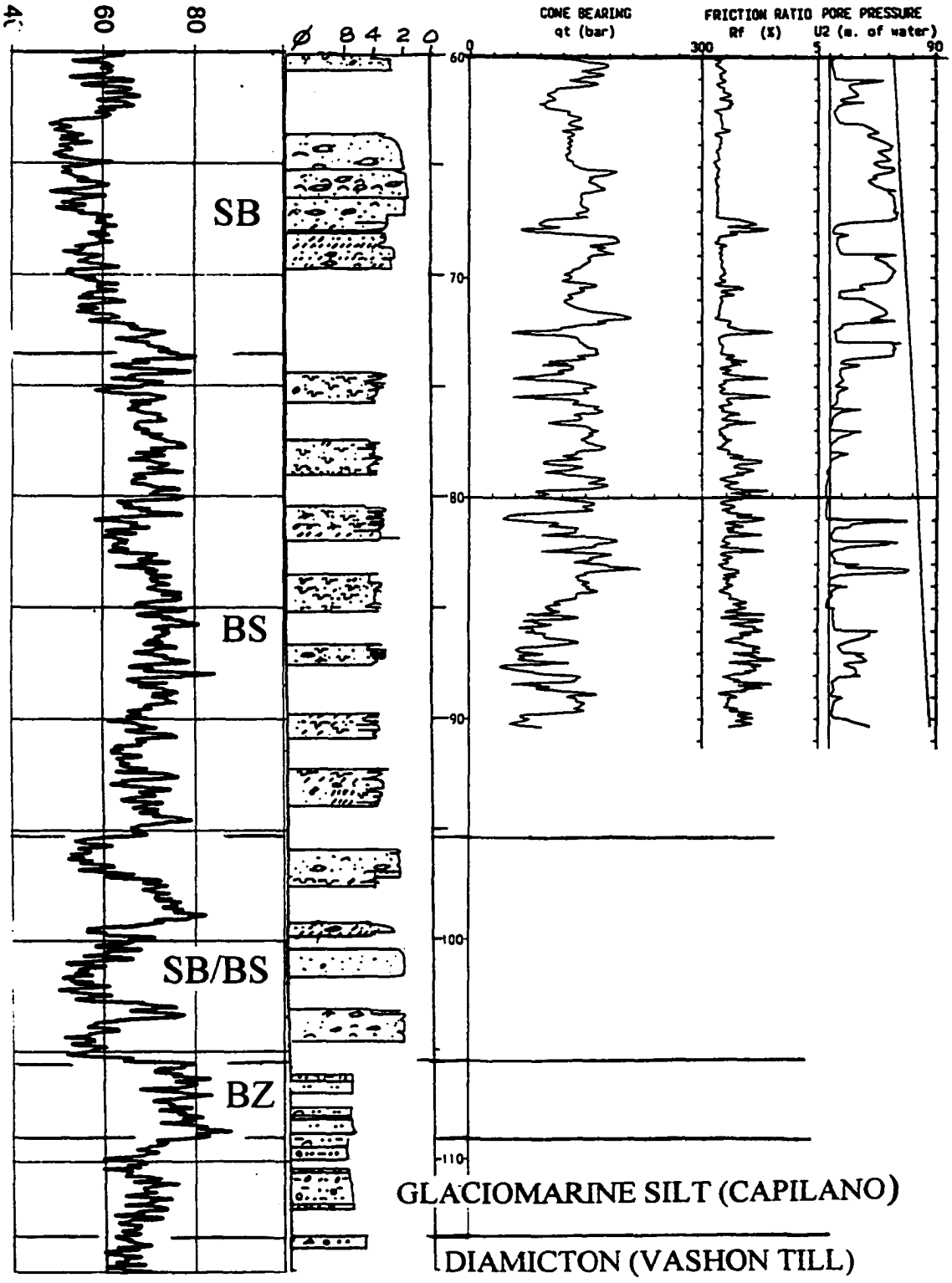
40
60
80
Ø 8 4 2 0
CONE BEARING
qt (bar)
FRICTION RATIO
Rf (%)
PORE PRESSURE
U2 (m. of water)
0
300
5
90
60
70
80
90
100
110
SB
BS
SB/BS
BZ
GLACIOMARINE SILT (CAPILANO)
DIAMICTON (VASHON TILL)

FD95-6

Sonic Borehole <3 m from CPT
Sea dykes at south end of 112th ST, Delta

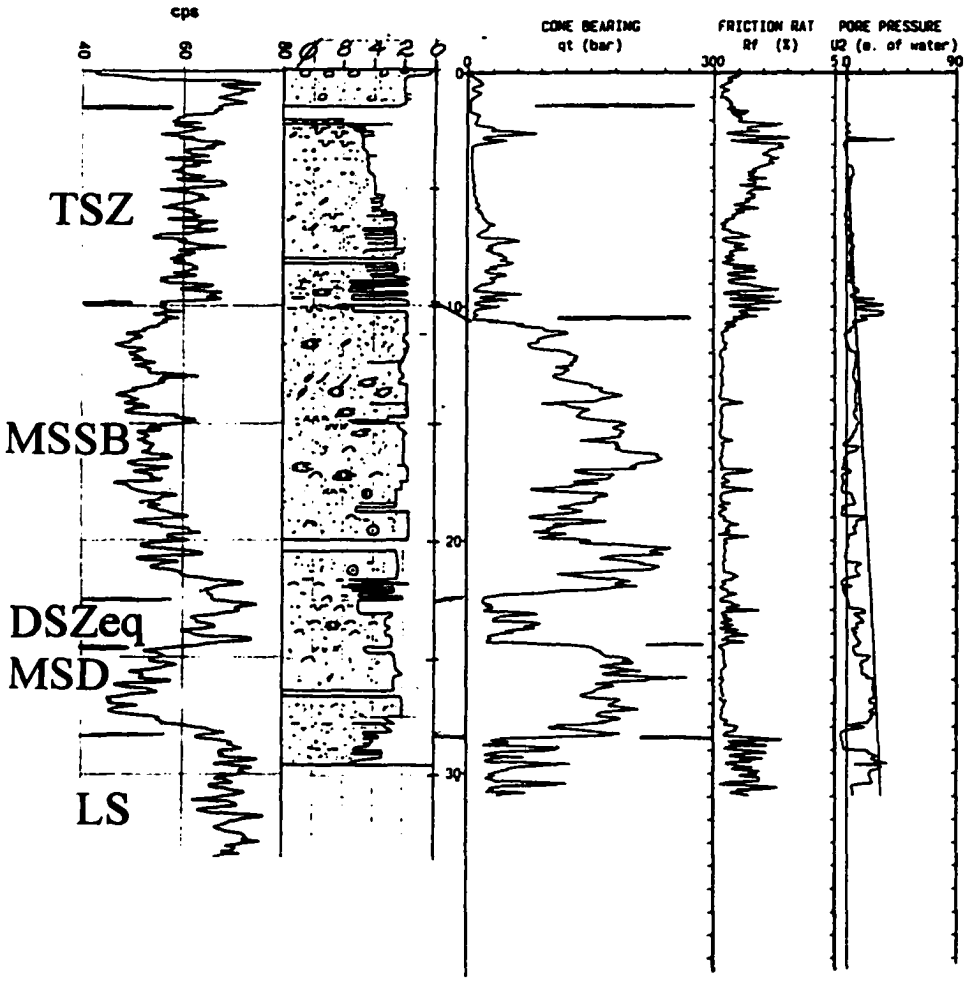

K2V2

Sonic Borehole 4.5m from CPT; 'Southeast side of Kidd 2 Substation, No. 4 Rd. and River Rd., Richmond (CANLEX Site); (Monahan et al, 1995b)

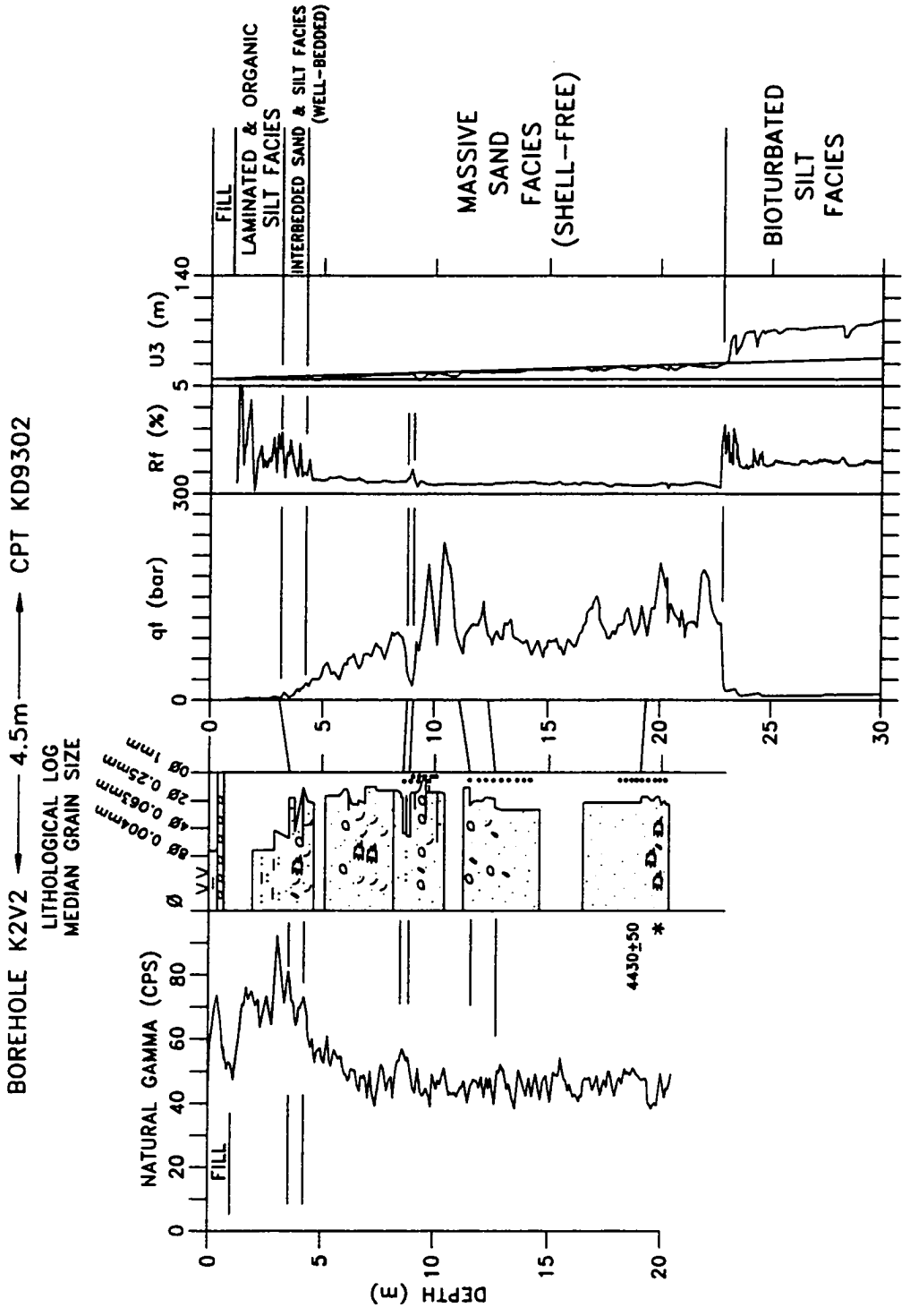

BHFD93S-1

Shelby Tube Sampled Borehole ~65 m from CPT
Roberts Bank, 0.75 km northwest of Roberts Bank Port
49° 1.4819±0.0162 N 123° 10.4752±0.0152 W
CPT location: 49° 1.4651±0.0059 N 123° 10.4284±0.0015 W

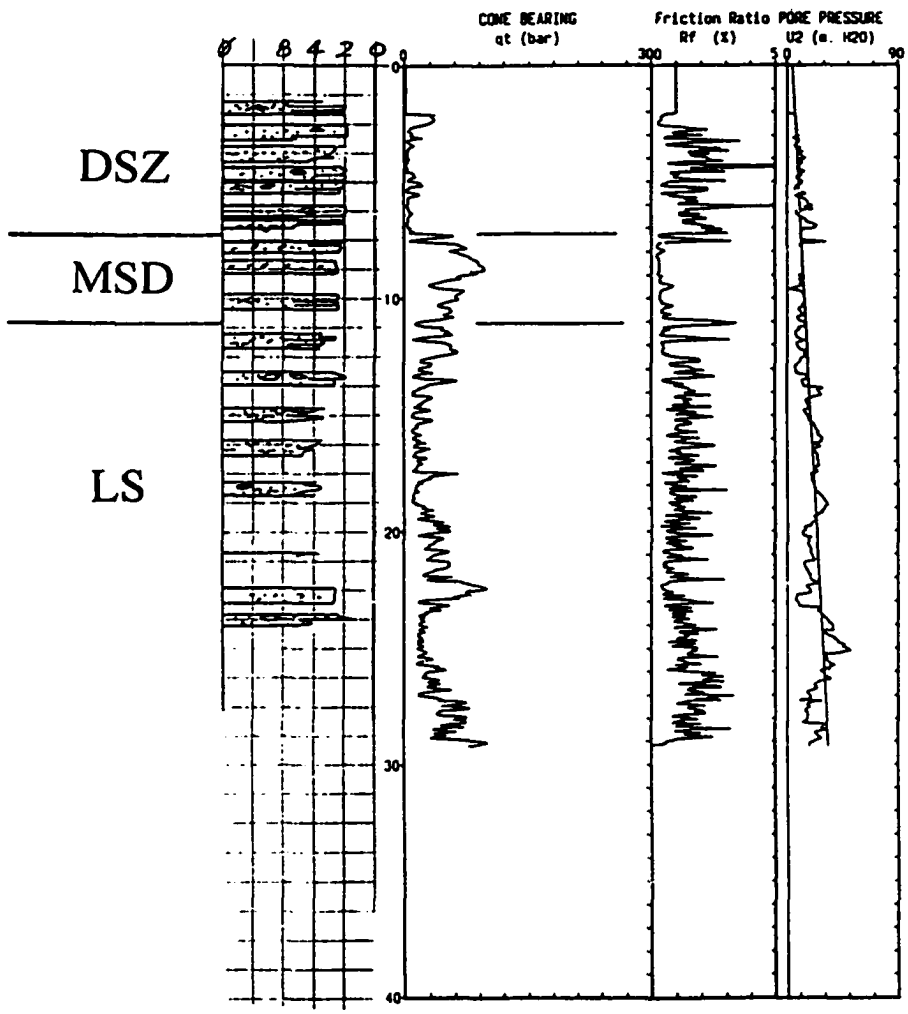

BHFD93S-2

Shelby Tube Sampled Borehole ~55 m from CPT
Sand Heads, south side of Main Channel
49° 5.6649±0.0149 N 123° 18.5419±0.0204 W
CPT location: 49° 5.6958±0.0119 N 123° 18.5470±0.0124 W
(see Figure I-2 for correlation)

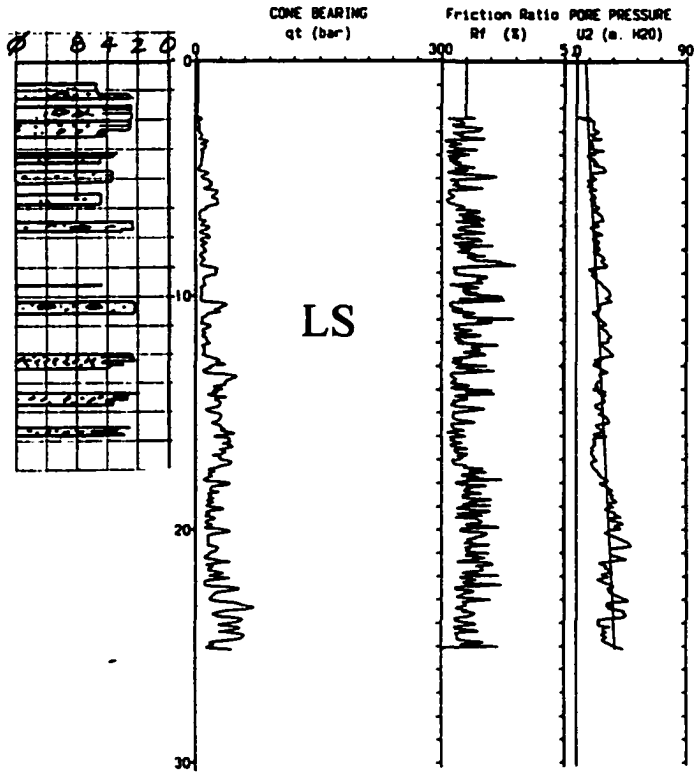

BHFD94S-1

Shelby Tube Sampled Borehole ~120 m from CPT
Roberts Bank, 2.5 km west of Roberts Bank Port
49° 1.4006 N ± 4 m 123° 12.2695 W ± 3 m
CPT location: 49° 1.3481 N ± 11 m 123° 12.3306 W ± 8 m

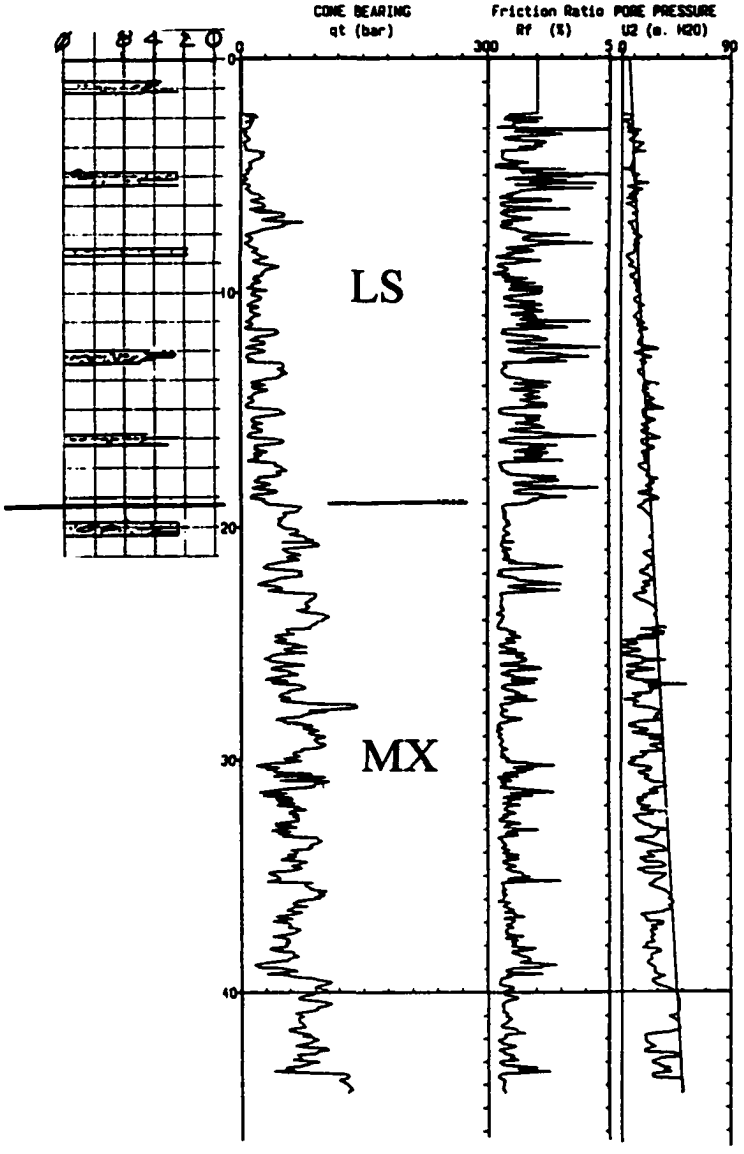

APPENDIX C. GRAIN SIZE SAMPLE DATA

PART 1; PGC LABORATORY (see Table 6-1 for Facies abbreviations)

sample depth m	sample thickness cm	ϕ_{50}	mean ϕ	standard deviation ϕ	gravel %	sand %	Fines Content %	silt & clay %	silt %	clay %	Facies (see Table 6-1)
FD92-11											
2.89	3	5.49	5.73	2.30	0	29.57	76.29	70.43	56.81	13.62	BSZ
2.92	5	3.46	3.97	1.68	0	83.56	28.21	16.44	11.72	4.72	BSZ
3.49	6	3.27	4.01	2.07	0	76.73	31.08	23.27	16.68	6.59	BSZ
4.16	10	3.64	4.54	2.14	0	62.26	45.45	37.74	29.52	8.22	BSZ
5.89	12	2.39	2.85	1.56	0	90.34	10.42	9.66	7.13	2.53	MSSB
6.19	5	2.14	2.22	0.49	0	98.55	1.87	1.45	1.45	0.00	MSSB
7.47	5	2.05	2.30	1.26	0	96.21	4.93	3.80	2.36	1.44	MSSB
10.71	10	1.98	2.26	1.24	0	96.45	4.30	3.55	2.16	1.39	MSSB
14.27	10	2.01	2.32	1.35	0	94.97	6.22	5.03	3.47	1.56	MSSB
15.03	11	1.79	1.78	3.47	21.46	61.68	17.12	16.86	10.28	6.58	MSSB
16.58	4	3.77	4.73	2.33	0	54.67	50.43	45.34	34.66	10.68	LZ
16.64	4	4.82	5.28	2.50	0	39.94	62.60	60.06	45.84	14.22	LZ
18.01	10	5.68	6.27	2.41	0	15.08	87.70	84.92	65.06	19.86	LZ
18.38	5	5.21	5.78	2.53	0	29.94	75.34	70.06	52.36	17.70	LZ
19.71	10	3.88	4.94	2.47	0	51.68	51.80	48.32	35.36	12.96	LZ
21.93	10	5.94	6.49	2.34	0	11.29	90.98	88.71	67.48	21.23	LZ
22.18	10	6.60	7.11	2.34	0	6.44	94.54	93.56	65.07	28.49	LZ
24.55	9	3.53	4.56	2.32	0	61.03	44.31	38.97	28.85	10.12	LZ
24.68	10	6.38	6.86	2.41	0	11.79	90.68	88.21	62.33	25.88	LZ
26.23	7	6.49	6.90	2.47	0	12.63	89.39	87.37	60.08	27.29	LZ
26.61	5	3.68	4.82	2.56	0	55.01	48.34	44.99	32.04	12.95	LZ
29.18	10	5.70	6.26	2.53	0	20.59	81.77	79.41	57.78	21.63	LS
29.44	12	3.35	4.47	2.31	0	64.30	39.12	35.70	25.32	10.38	LS
30.49	3	3.41	4.01	1.84	0	77.76	32.10	22.24	16.23	6.01	LS
34.03	8	5.85	6.45	2.59	0	20.54	83.04	79.46	55.03	24.43	LS
34.13	8	5.77	6.22	2.66	0	27.39	75.78	72.61	49.62	22.99	LS
34.23	9	3.44	4.69	2.51	0	59.81	42.89	40.19	27.21	12.98	LS
36.78	6	4.82	5.50	2.53	0	41.00	66.05	59.00	42.69	16.31	LS
40.88	7	3.68	4.62	2.23	0	59.59	47.59	40.42	31.12	9.30	LS
41.51	7	3.35	4.11	2.00	0	76.23	31.14	23.77	16.88	6.89	LS
45.66	7	2.87	3.37	1.62	0	87.63	13.78	12.37	8.59	3.78	LS
45.76	4	4.91	5.52	2.65	0	41.20	61.96	58.80	41.04	17.76	LS
50.85	5	2.74	3.18	1.58	0	88.83	12.73	11.17	8.01	3.16	LS
53.28	10	2.64	3.00	1.46	0	91.72	9.02	8.28	5.50	2.78	MX
54.80	6	2.77	3.85	2.39	0	75.41	26.92	24.59	15.67	8.92	MX
55.09	7	3.64	4.95	2.73	0	53.20	48.60	46.81	30.62	16.19	BS
55.20	11	5.16	5.70	2.92	0	39.87	61.90	60.13	37.25	22.88	BS
55.52	10	5.94	6.23	2.75	0	28.04	73.78	71.97	46.67	25.30	BS
58.83	10	6.27	6.64	2.69	0	19.78	82.23	80.22	52.26	27.96	BZ
59.06	9	6.64	7.03	2.52	0	10.34	90.83	89.66	58.55	31.11	BZ
62.99	10	5.92	6.34	2.77	0	25.95	76.27	74.05	49.08	24.97	BZ
67.36	4	6.79	7.21	2.55	0	9.36	91.96	90.64	57.45	33.19	BZ
67.42	10	6.36	6.78	2.56	0	13.75	87.81	86.25	57.65	28.60	BZ

APPENDIX C, PART 1 (cont'd). GRAIN SIZE SAMPLE DATA											
sample depth m	sample thickness cm	ϕ_{50}	mean ϕ	standard deviation ϕ	gravel %	sand %	Fines Content %	silt & clay %	silt %	clay %	Facies (see Table 6-1)
FD92-11 (cont'd)											
72.04	10	6.49	6.97	2.56	0	10.75	90.72	89.25	59.43	29.82	BZ
72.29	4	5.79	6.38	2.72	0	26.34	79.11	73.66	47.31	26.35	BZ
73.07	10	3.17	3.79	1.92	0	81.63	25.02	18.37	12.40	5.97	BZ
73.37	1	3.49	4.57	2.27	0	59.82	43.27	40.18	30.33	9.85	BZ
73.77	10	6.11	6.67	2.57	0	14.70	87.49	85.30	58.39	26.91	BZ
76.68	10	6.54	7.11	2.47	0	8.22	92.97	91.78	61.64	30.14	BZ
82.51	10	7.10	7.50	2.55	0	6.44	94.51	93.56	56.20	37.36	BZ
88.47	9	7.16	7.50	2.49	0	5.44	95.34	94.56	57.36	37.20	BZ
88.58	7	7.31	7.62	2.70	0	8.82	93.29	91.18	50.69	40.49	BZ
93.78	10	7.46	7.69	2.78	0	10.51	91.63	89.49	47.22	42.27	BZ
99.28	10	7.78	8.13	2.47	0	2.56	97.78	97.44	51.24	46.20	BZ
99.83	10	3.81	5.51	3.09	0	54.80	51.45	45.20	22.63	22.57	BC
100.14	7	3.57	5.26	3.06	0	60.20	44.79	39.80	18.85	20.95	BC
100.26	5	10.09	9.96	2.48	0	5.42	94.97	94.58	8.44	86.14	BC
24.35	5	6.67	7.16	2.45	0	6.02	94.54	93.98	63.40	30.58	LZ
24.40	5	6.52	7.05	2.41	0	5.89	94.73	94.11	65.30	28.81	LZ
24.45	5	7.14	7.31	2.69	0	13.31	88.02	86.69	49.49	37.20	LZ
24.50	5	3.58	4.81	2.55	0	54.01	47.90	45.99	32.83	13.16	LZ
24.55	5	3.21	4.28	2.31	0	64.30	37.75	35.70	26.60	9.10	LZ
24.60	5	3.95	4.81	2.47	0	50.43	51.87	49.57	37.79	11.78	LZ
24.65	5	5.68	6.35	2.43	0	12.98	88.86	87.02	64.73	22.29	LZ
24.75	5	6.17	6.74	2.31	0	6.97	94.47	93.03	68.07	24.96	LZ
24.80	5	5.73	6.34	2.58	0	17.24	85.10	82.76	60.52	22.24	LZ
24.85	5	5.18	5.70	1.99	0	15.64	87.08	84.36	69.30	15.06	LZ
24.90	5	5.69	6.21	1.95	0	5.93	95.22	94.07	74.87	19.20	LZ
24.95	5	6.34	6.95	2.17	0	2.54	100.00	97.46	71.29	26.17	LZ
25.00	5	5.36	5.77	2.58	0	29.32	72.81	70.68	52.44	18.24	LZ
25.05	5	5.89	6.38	2.43	0	13.72	87.82	86.28	65.41	20.87	LZ
25.15	5	6.51	6.81	2.55	0	14.51	86.93	85.49	57.56	27.93	LZ
25.20	5	6.63	7.01	2.53	0	10.60	90.41	89.40	59.45	29.95	LZ
25.25	5	7.24	7.27	2.93	0	17.72	82.98	82.28	42.60	39.68	LZ
25.30	5	5.84	6.26	2.62	0	21.18	80.13	78.82	56.17	22.65	LZ
25.35	5	5.18	5.61	2.77	0	35.58	65.93	64.42	45.06	19.36	LZ
25.40	5	6.23	6.61	2.73	0	18.08	82.92	81.92	53.79	28.13	LZ
25.45	5	5.96	6.33	2.74	0	21.44	79.82	78.56	53.64	24.92	LZ
FD93-2											
0.90	5	7.22	7.69	2.30	0	2.65	100.00	97.35	61.66	35.69	LOZ
1.00	5	7.22	7.59	2.24	0	2.86	100.00	97.14	61.01	36.13	LOZ
1.10	5	6.79	7.18	2.04	0	3.55	100.00	96.45	69.42	27.03	LOZ
2.30	5	6.75	7.13	2.10	0	4.11	100.00	95.89	69.43	26.46	LOZ
2.40	5	5.74	6.10	2.16	0	15.61	85.46	84.39	68.27	16.12	LOZ
2.50	5	5.76	6.16	2.21	0	14.10	87.29	85.90	68.81	17.09	LOZ
2.60	5	5.75	6.17	2.26	0	13.07	88.35	86.93	69.05	17.88	LOZ
2.70	5	5.59	6.01	2.14	0	13.85	87.43	86.15	70.99	15.16	LOZ

APPENDIX C, PART 1 (cont'd). GRAIN SIZE SAMPLE DATA											
sample depth m	sample thickness cm	ϕ_{50}	mean ϕ	standard deviation ϕ	gravel %	sand %	Fines Content %	silt & clay %	silt %	clay %	Facies (see Table 6-1)
FD93-2 (cont'd)											
2.80	5	5.82	6.24	2.11	0	11.28	89.60	88.72	72.69	16.03	LOZ
2.90	5	5.76	6.14	2.02	0	12.32	88.70	87.68	73.28	14.40	LOZ
3.00	5	4.88	5.23	2.35	0	37.05	64.10	62.95	50.78	12.17	LOZ
3.10	5	5.22	5.53	2.39	0	32.08	69.65	67.92	53.93	13.99	LOZ
3.20	5	4.14	5.01	2.44	0	45.62	56.37	54.38	42.08	12.30	WSZ
3.30	5	3.40	4.42	2.28	0	58.90	43.19	41.10	31.97	9.13	WSZ
3.40	5	3.86	4.58	2.46	0	50.90	50.65	49.10	38.75	10.35	WSZ
3.50	5	3.43	4.36	2.64	0	53.86	47.00	46.14	35.86	10.28	WSZ
3.60	5	2.09	3.17	2.48	0	75.59	25.62	24.41	17.81	6.60	WSZ
3.65	5	4.43	4.57	2.16	0	41.28	59.74	58.72	52.02	6.70	WSZ
3.70	5	3.91	4.71	2.48	0	50.70	51.31	49.30	38.62	10.68	WSZ
3.80	5	2.72	3.96	2.55	0	66.54	35.64	33.46	24.02	9.44	MSSF
3.90	5	2.46	4.04	2.78	0	64.18	36.87	35.82	25.40	10.42	MSSF
3.95	5	2.00	2.09	0.66	0	96.10	3.90	3.90	3.90	0.00	MSSF
4.00	5	2.16	2.56	1.59	0	91.97	8.76	8.03	5.43	2.60	MSSF
4.10	5	2.44	3.53	2.48	0.04	75.95	25.28	24.01	16.19	7.82	MSSF
4.20	5	2.03	2.17	0.80	0	94.87	5.88	5.13	5.13	0.00	MSSF
4.30	5	2.14	2.53	1.49	0	90.20	10.16	9.80	7.82	1.98	MSSF
4.40	5	2.29	3.02	1.95	0	81.19	19.46	18.81	14.86	3.95	MSSF
4.50	5	2.88	4.03	2.49	0	62.22	39.98	37.78	28.65	9.13	MSSF
4.60	5	2.62	3.88	2.49	0	64.72	35.78	35.28	27.36	7.92	MSSF
4.70	5	2.49	2.98	3.27	12.65	56.01	33.30	31.34	23.95	7.39	MSSF
4.80	5	2.36	3.32	2.13	0	77.46	24.14	22.54	17.06	5.48	MSSF
4.90	5	2.13	2.20	0.50	0	98.27	2.13	1.73	1.73	0.00	MSSF
22.22	5	2.56	2.64	0.55	0	97.51	3.67	2.49	2.49	0.00	LDSZ
22.77	5	2.23	2.32	0.51	0	98.01	2.39	1.99	1.99	0.00	LDSZ
24.07	5	2.61	2.89	1.21	0	92.42	8.76	7.58	6.04	1.54	LDSZ
FD93-3											
2.85	5	6.54	6.76	1.78	0	6.37	100.00	93.63			BSZ
3.40	5	2.32	3.09	1.77	0	81.23	20.21	18.77			BSZ
4.05	5	3.93	4.83	2.19	0	51.71	54.76	48.29			BSZ
4.55	5	3.08	3.84	1.95	0	73.55	29.90	26.45			BSZ
5.30	5	2.01	2.21	0.78	0	95.50	5.13	4.50			MSSB
5.33	5	2.24	2.34	0.64	0	97.51	2.49	2.49			MSSB
5.65	5	3.27	3.82	1.51	0	76.95	29.02	23.05			MSSB
6.10	5	2.83	3.06	1.18	0	91.93	10.82	8.07			MSSB
6.41	5	1.96	2.06	0.60	0	98.53	2.08	1.47			MSSB
6.83	5	2.30	2.41	0.53	0	96.99	3.65	3.01			MSSB
7.15	5	1.80	1.85	0.48	0	99.19	0.81	0.81			MSSB
7.85	5	5.66	5.73	2.10	0	26.83	74.52	73.17			MSSB
8.70	5	2.30	2.55	1.14	0	93.81	6.89	6.19			MSSB
9.15	5	1.68	1.74	0.51	0	99.27	0.73	0.73			MSSB
9.80	5	2.08	2.17	0.54	0	97.62	2.38	2.38			MSSB
10.50	5	2.77	2.98	1.03	0	93.24	9.00	6.76			MSSB

APPENDIX C, PART 1 (cont'd). GRAIN SIZE SAMPLE DATA											
sample depth m	sample thickness cm	ϕ_{50}	mean ϕ	standard deviation ϕ	gravel %	sand %	Fines Content %	silt & clay %	silt %	clay %	Facies (see Table 6-1)
FD93-3 (cont'd)											
11.20	5	1.68	1.96	1.23	0.05	95.47	4.48	4.48			MSSB
13.85	5	2.24	2.36	0.53	0	97.37	2.63	2.63			MSSB
15.30	5	1.79	1.86	0.52	0	98.81	1.19	1.19			MSSB
17.60	5	1.96	2.03	0.64	0	97.66	2.34	2.34			MSSB
18.78	5	1.51	1.62	0.98	2.62	92.66	4.72	4.72			MSSB
FD93-5											
20.40	5	1.92	2.06	0.91	0	93.94	6.47	6.06	6.06	0.00	MSSB
20.50	5	1.87	1.97	0.81	0	95.77	4.61	4.23	4.23	0.00	MSSB
20.60	5	1.97	2.03	0.78	0	96.21	4.19	3.79	3.79	0.00	MSSB
20.70	5	2.13	2.16	0.69	0	97.02	3.38	2.98	2.98	0.00	MSSB
20.75	5	3.08	3.85	1.90	0	72.93	29.32	27.07	21.50	5.57	CU
20.80	5	3.00	3.75	1.91	0	74.99	26.92	25.01	19.45	5.56	CU
20.90	5	4.89	5.51	2.63	0	35.72	66.33	64.28	46.26	18.02	CU
21.00	5	4.22	4.85	2.35	0	41.55	60.04	58.45	48.07	10.38	CU
21.10	5	4.49	5.12	2.71	0	43.99	57.08	56.01	40.40	15.61	CU
21.15	5	2.62	3.20	1.18	0	86.87	13.50	13.13	8.72	4.41	CU
21.20	5	2.60	2.94	1.33	0	91.50	9.26	8.50	6.56	1.94	CU
21.30	5	2.68	3.44	1.98	0	79.96	20.70	20.04	15.08	4.96	CU
21.40	5	2.51	2.82	1.34	0	93.08	7.33	6.92	4.80	2.12	CU
21.50	5	2.64	3.02	1.52	0	91.16	9.62	8.84	6.21	2.63	CU
21.60	5	2.62	3.08	1.65	0	89.43	11.34	10.57	7.14	3.43	CU
21.70	5	2.47	2.83	1.38	0	92.01	8.77	7.99	5.69	2.30	CU
21.80	5	2.56	3.04	1.66	0	89.09	13.06	10.91	7.65	3.26	CU
21.90	5	2.45	2.66	0.73	0	93.99	7.96	6.01	6.01	0.00	CU
22.00	5	2.69	3.09	1.43	0	91.06	12.37	8.94	6.45	2.49	CU
22.05	5	3.33	4.11	2.01	0	67.58	36.97	32.42	25.50	6.92	CU
22.10	5	2.92	3.35	1.47	0	87.61	15.71	12.39	9.31	3.08	CU
22.15	5	3.12	3.70	1.78	0	82.13	22.53	17.87	12.43	5.44	CU
22.20	5	3.20	3.79	1.86	0	79.47	26.15	20.53	14.86	5.67	CU
22.25	5	3.63	4.32	1.98	0	61.26	45.61	38.74	31.41	7.33	CU
22.30	5	3.78	4.57	2.21	0	54.15	50.66	45.85	36.68	9.17	CU
22.35	5	2.97	3.58	1.74	0	81.07	22.37	18.93	14.69	4.24	CU
22.40	5	3.40	4.37	2.14	0	60.70	41.77	39.30	31.16	8.14	CU
22.45	5	3.47	4.34	2.13	0	59.88	42.82	40.12	31.98	8.14	CU
22.50	5	4.63	5.25	2.42	0	36.16	66.25	63.84	50.07	13.77	CU
22.55	5	5.58	6.08	2.38	0	17.58	83.88	82.42	62.70	19.72	CU
22.60	5	4.03	4.96	2.69	0	49.56	51.63	50.44	34.77	15.67	CU
22.65	5	2.82	3.51	1.91	0	81.84	19.19	18.16	13.04	5.12	CU
22.70	5	3.23	4.54	2.57	0	62.32	38.97	37.68	24.05	13.63	CU
22.80	5	4.72	5.37	2.49	0	39.22	63.05	60.78	44.98	15.80	CU
FD94-1											
3.45	5	5.91	6.27	1.69	0	3.60	100.00	96.40			WSZ
5.77	5	2.72	2.81	0.47	0	98.27	3.42	1.73			MSSF
6.07	5	2.58	2.64	0.41	0	99.20	1.53	0.80			MSSF

APPENDIX C, PART 1 (cont'd). GRAIN SIZE SAMPLE DATA											
sample depth m	sample thickness cm	ϕ_{50}	mean ϕ	standard deviation ϕ	gravel %	sand %	Fines Content %	silt & clay %	silt %	clay %	Facies (see Table 6-1)
FD94-1 (cont'd)											
6.37	5	3.04	3.34	1.20	0	90.04	15.22	9.96			MSSF
6.67	5	2.27	2.27	0.62	0	98.89	1.76	1.11			MSSF
6.87	5	1.82	1.99	0.74	0	97.82	2.92	2.18			MSSF
7.07	5	2.14	2.22	0.60	0	98.78	2.00	1.22			MSSF
7.27	5	2.15	2.19	0.50	0	99.35	1.59	0.65			MSSF
10.30	5	2.35	2.42	0.50	0	98.60	1.89	1.40			MSSF
12.60	5	2.39	2.44	0.53	0	98.79	2.19	1.21			MSSF
14.15	5	2.60	2.66	0.48	0	98.94	2.81	1.06			MSSF
19.01	5	2.01	1.93	0.58	0.09	99.34	0.57	0.57			MSSF
19.21	5	2.00	1.95	0.60	0.72	98.69	1.24	0.59			MSSF
19.41	5	1.92	1.87	0.64	0.55	98.55	0.90	0.90			MSSF
19.61	5	1.85	1.81	0.68	0.64	98.29	1.07	1.07			MSSF
19.81	5	2.04	2.03	0.52	0.04	99.37	1.27	0.59			MSSF
20.36	5	1.64	1.68	0.64	0	99.32	1.07	0.68			MSSF
21.83	5	2.12	3.00	2.15	0.93	77.16	22.60	21.91			MSSB
25.65	5	1.96	2.04	0.57	0	98.58	1.42	1.42			MSSB
25.75	5	1.95	2.04	0.60	0	98.35	2.38	1.65			MSSB
26.15	5	2.08	2.06	0.57	0	99.27	0.73	0.73			MSSB
26.25	5	1.71	1.84	0.66	0	99.22	0.78	0.78			MSSB
26.35	5	2.45	2.47	0.60	0.02	97.99	2.82	1.99			MSSB
26.45	5	2.38	2.39	0.63	0	97.66	2.34	2.34			MSSB
26.55	5	5.91	6.25	2.23	0	15.20	86.86	84.80			MSSB
32.15	5	1.96	2.16	0.73	0.07	95.68	5.01	4.25			MSSB
32.35	5	2.03	2.39	1.16	0	92.21	8.55	7.79			MSSB
FD94-4											
24.45	5	2.06	2.15	0.68	0	97.22	3.56	2.78	2.78	0.00	MSSB
24.55	5	2.09	2.16	0.60	0	98.49	2.44	1.51	1.51	0.00	MSSB
24.65	5	7.16	7.57	2.30	0	2.27	100.00	97.73	61.53	36.20	MSSB
24.75	5	1.76	1.87	0.68	0	97.07	2.93	2.93	2.93	0.00	MSSB
24.85	5	1.86	1.94	0.56	0	98.36	2.02	1.64	1.64	0.00	MSSB
24.95	5	4.84	5.46	2.47	0	38.81	63.42	61.19	45.11	16.06	LZ
25.05	5	4.06	4.94	2.38	0	48.75	52.95	51.25	39.23	12.02	LZ
25.15	5	3.19	4.46	2.46	0	63.70	37.70	36.30	25.14	11.16	LZ
31.55	5	2.38	2.43	0.63	0.88	96.76	3.20	2.36	2.36	0.00	MX(SB)
31.70	5	2.44	2.52	0.48	0	97.80	2.20	2.20	2.20	0.00	MX(SB)
31.85	5	2.35	2.42	0.54	0	97.56	3.21	2.44	2.44	0.00	MX(SB)
32.00	5	5.43	5.73	2.29	0.05	26.91	75.59	73.04	56.01	17.03	MX(LZ)
32.10	5	6.14	6.43	2.29	0	14.45	87.18	85.55	62.95	22.37	MX(LZ)
32.25	5	4.01	4.59	1.91	0	49.67	56.42	50.33	42.68	7.65	DZ
32.40	5	4.64	4.83	1.64	0	32.30	74.67	67.70	61.88	5.82	DZ
32.55	5	5.25	5.79	2.30	0	23.90	79.83	76.10	57.70	18.43	DZ
32.70	5	5.22	5.63	2.09	0	23.77	80.28	76.23	62.59	13.64	DZ
32.85	5	4.75	5.26	2.21	0	36.92	67.50	63.08	50.07	13.01	DZ
32.90	5	5.12	5.58	2.22	0	28.87	75.30	71.13	56.59	14.54	DZ

APPENDIX C, PART 1 (cont'd). GRAIN SIZE SAMPLE DATA											
sample depth m	sample thickness cm	ϕ_{50}	mean ϕ	standard deviation ϕ	gravel %	sand %	Fines Content %	silt & clay %	silt %	clay %	Facies (see Table 6-1)
FD94-4 (cont'd)											
40.50	5	6.04	6.45	2.19	0	8.88	92.12	91.12	70.58	20.54	LZ
40.55	5	7.01	7.41	2.24	0	2.95	100.00	97.05	64.29	32.76	LZ
40.60	5	6.72	6.95	2.56	0	12.46	88.22	87.54	56.43	31.10	LZ
40.65	5	6.03	6.43	2.48	0	16.94	84.33	83.06	59.39	23.67	LZ
40.70	5	5.56	6.01	2.35	0	18.62	82.70	81.38	64.43	16.95	LZ
40.75	5	5.64	6.14	2.27	0	13.63	87.65	86.37	68.24	18.13	LZ
40.80	5	5.80	6.29	2.17	0	9.02	92.22	90.98	72.31	18.67	LZ
40.85	5	5.91	6.35	2.16	0	8.74	92.24	91.26	72.67	18.59	LZ
40.90	5	5.54	6.02	2.06	0	10.56	91.02	89.44	73.84	15.60	LZ
40.95	5	6.04	6.46	2.13	0	7.87	93.34	92.13	72.28	19.85	LZ
41.00	5	6.51	6.93	2.32	0	6.32	94.48	93.68	66.74	26.94	LZ
41.05	5	7.43	7.77	2.20	0	1.88	100.00	98.12	58.10	40.02	LZ
41.10	5	6.84	7.04	2.63	0	13.63	87.34	86.37	52.76	33.61	LZ
41.15	5	5.02	5.57	2.38	0	28.72	73.82	71.28	56.22	15.06	LZ
41.20	5	5.53	6.00	2.33	0	18.65	82.92	81.35	63.62	17.73	LZ
41.25	5	6.09	6.57	2.39	0	10.75	90.40	89.25	64.99	24.26	LZ
41.30	5	6.36	6.78	2.23	0	6.47	94.29	93.53	69.44	24.09	LZ
41.35	5	6.39	6.86	2.15	0	3.95	100.00	96.05	72.15	23.90	LZ
41.40	5	6.67	7.05	2.28	0	5.30	95.30	94.70	66.89	27.81	LZ
41.45	5	5.60	6.03	2.59	0	25.14	76.17	74.86	54.30	20.56	LZ
41.50	5	6.00	6.47	2.50	0	14.36	86.74	85.64	62.19	23.45	LZ
41.55	5	6.48	6.86	2.29	0	6.47	94.07	93.53	67.44	26.09	LZ
41.60	5	5.96	6.39	2.45	0	14.84	85.97	85.16	63.01	22.15	LZ
41.65	5	5.78	6.29	2.46	0	16.06	85.10	83.94	62.19	21.75	LZ
41.70	5	6.44	6.75	2.35	0	10.42	90.82	89.58	63.36	26.22	LZ
41.75	5	5.62	6.10	2.32	0	16.13	85.32	83.87	64.78	19.09	LZ
41.80	5	6.10	6.53	2.34	0	11.17	90.13	88.83	66.47	22.36	LZ
41.85	5	6.19	6.59	2.14	0	7.38	93.67	92.62	71.37	21.25	LZ
41.90	5	6.33	6.71	2.18	0	6.86	93.88	93.14	69.74	23.40	LZ
41.95	5	7.40	7.73	2.34	0	4.53	100.00	95.47	56.25	39.22	LZ
42.00	5	5.49	5.96	2.46	0	23.33	78.34	76.67	58.66	18.01	LZ
42.05	5	5.56	5.97	2.42	0	22.67	79.26	77.33	59.46	17.87	LZ
FD94-5											
12.00	5	2.93	3.04	0.55	0.18	95.95	7.02	3.87	3.87	0	TSZ?
12.20	5	4.67	5.32	2.47	0	43.05	60.79	56.95	42.05	14.9	TSZ?
12.40	5	5.01	5.57	2.41	0	36.03	67.10	63.97	47.07	16.9	TSZ?
12.60	5	3.18	3.62	1.45	0	84.80	21.31	15.20	11.87	3.33	TSZ?
12.80	5	3.31	3.80	1.47	0	80.79	26.73	19.21	15.24	3.97	TSZ?
13.00	5	3.17	3.31	0.70	0	89.57	16.45	10.43	10.43	0	TSZ?
13.20	5	3.19	3.48	1.23	0	87.05	18.95	12.95	10.96	1.99	TSZ?
13.40	5	2.84	3.06	1.22	0	91.67	10.99	8.33	6.83	1.5	TSZ?
13.55	5	2.88	3.08	1.04	0	93.95	9.50	6.05	4.96	1.09	TSZ?
13.65	5	2.92	3.09	0.76	0	90.27	12.90	9.73	9.73	0	TSZ?
13.75	5	4.26	4.96	2.03	0	45.78	59.94	54.22	45.20	9.02	TSZ?

APPENDIX C, PART 1 (cont'd). GRAIN SIZE SAMPLE DATA											
sample depth m	sample thickness cm	ϕ_{50}	mean ϕ	standard deviation ϕ	gravel %	sand %	Fines Content %	silt & clay %	silt %	clay %	Facies (see Table 6-1)
FD94-5 (cont'd)											
13.85	5	1.05	-0.04	2.87	41.12	54.74	4.47	4.14	3.15	0.99	MSD
13.95	5	2.17	2.17	0.68	0	97.19	3.66	2.81	2.81	0	MSD
14.05	5	1.52	1.41	1.38	6.95	89.36	3.69	3.69	3.69	0	MSD
14.15	5	1.28	0.76	3.08	23.21	68.04	8.75	8.75	5.36	3.39	MSD
14.25	5	1.46	1.53	0.62	0.31	98.44	1.83	1.25	1.25	0	MSD
14.45	5	2.08	2.17	0.53	0	97.73	2.27	2.27	2.27	0	MSD
14.65	5	2.12	2.22	0.60	0.31	97.00	3.49	2.69	2.69	0	MSD
14.85	5	2.13	2.07	1.03	6.21	90.21	4.17	3.58	3.58	0	MSD
15.05	5	2.16	2.23	0.53	0	97.58	2.42	2.42	2.42	0	MSD
15.40	5	2.22	2.30	0.46	0	98.51	2.28	1.49	1.49	0	MSD
15.62	5	2.18	2.22	0.49	0	98.45	1.55	1.55	1.55	0	MSD
15.80	5	1.43	1.60	0.69	0	97.66	3.00	2.34	2.34	0	MSD
16.00	5	1.64	1.74	0.58	0	98.75	1.95	1.25	1.25	0	MSD
16.13	5	5.67	5.96	2.01	0	13.93	88.89	86.07	72.18	13.89	LS
16.30	5	2.47	2.60	0.64	0	96.87	5.55	3.13	3.13	0	LS
FD94-6											
2.80	5	6.19	6.63	2.04	0	3.99	100.00	96.01			LOZ
3.10	5	6.83	7.24	2.10	0	2.04	100.00	97.96			LOZ
3.40	5	6.21	6.47	2.15	0	8.86	92.51	91.14			LOZ
3.70	5	6.62	6.69	2.36	0	10.07	91.23	89.93			LOZ
4.00	5	6.17	6.34	2.22	0	13.01	88.51	86.99			LOZ
4.30	5	5.38	5.69	2.25	0	23.40	78.96	76.60			LOZ
4.60	5	5.22	5.65	2.23	0	23.69	79.85	76.31			LOZ
4.90	5	4.83	5.23	2.10	0	32.58	71.91	67.42			LOZ
6.45	5	2.06	2.10	0.58	0	98.33	2.04	1.67			MSSF
6.65	5	2.15	2.21	0.43	0	98.79	1.60	1.21			MSSF
6.76	4	4.36	4.88	2.01	0	41.54	63.19	58.46			MSSF
6.85	5	2.09	2.09	0.60	0.15	99.13	1.14	0.72			MSSF
7.05	5	1.67	1.86	0.67	0.11	99.35	3.33	0.54			MSSF
7.25	5	1.46	1.51	0.54	0.73	99.04	0.60	0.23			MSSF
7.45	5	2.01	1.99	0.68	0.62	97.33	2.49	2.05			MSSF
7.65	5	1.62	1.50	0.87	4.67	94.85	0.83	0.48			MSSF
7.85	5	2.15	2.21	0.48	0.04	98.92	1.78	1.04			MSSF
8.05	5	2.11	2.15	0.43	0	99.22	1.22	0.78			MSSF
9.05	5	1.80	1.77	0.56	0.53	98.66	0.81	0.81			MSSF
9.25	5	1.82	1.82	0.55	0.65	98.35	1.00	1.00			MSSF
9.45	5	2.09	2.14	0.55	0.06	97.98	1.96	1.96			MSSF
9.65	5	2.13	2.18	0.47	0	98.67	1.69	1.33			MSSF
9.85	5	2.16	2.38	0.85	0	92.50	8.30	7.50			MSSF
10.05	5	2.19	2.28	0.57	0.05	97.44	2.51	2.51			MSSF
10.25	5	1.97	1.98	0.53	0.9	98.43	0.67	0.67			MSSF
10.45	5	2.21	2.29	0.51	0	98.69	1.31	1.31			MSSF
10.65	5	2.70	2.81	0.52	0	96.97	4.47	3.03			MSSF
10.85	5	2.48	2.57	0.47	0	98.10	2.70	1.90			MSSF

APPENDIX C, PART 1 (cont'd). GRAIN SIZE SAMPLE DATA											
sample depth m	sample thickness cm	ϕ_{50}	mean ϕ	standard deviation ϕ	gravel %	sand %	Fines Content %	silt & clay %	silt %	clay %	Facies (see Table 6-1)
FD94-6 (cont'd)											
11.05	5	2.48	2.57	0.40	0	98.79	1.21	1.21			MSSF
11.25	5	2.29	2.35	0.44	0	99.03	1.62	0.97			MSSF
11.45	5	2.37	2.44	0.48	0	98.58	2.21	1.42			MSSF
18.15	5	2.26	2.36	0.59	0	96.67	3.33	3.33			MSSB
18.55	5	2.21	2.27	0.54	0	98.27	2.50	1.73			MSSB
18.95	5	1.93	1.98	0.70	0	97.93	3.34	2.07			MSSB
19.35	5	2.01	2.04	0.44	0	98.98	1.02	1.02			MSSB
19.75	5	1.61	1.70	0.50	0	99.11	0.89	0.89			MSSB
20.15	5	1.86	1.93	0.51	0	98.68	1.32	1.32			MSSB
20.55	5	2.20	2.27	0.48	0	98.64	1.36	1.36			MSSB
20.95	5	1.91	1.95	0.50	0	98.95	1.05	1.05			MSSB
21.25	5	2.18	2.28	0.67	0	96.42	3.58	3.58			MSSB
21.55	5	1.80	1.88	0.60	0	97.88	2.12	2.12			MSSB
21.89	5	2.12	2.33	0.88	0	93.26	8.00	6.74			MSSB
21.94	5	5.60	5.85	2.15	0	19.73	82.24	80.27			LS(LZ)
K2V2											
9.20	5	2.76	3.29	2.03	0	78.21	23.16	21.79			MSSF
9.45	5	1.05	1.15	0.67	0	98.97	1.03	1.03			MSSF
9.60	5	2.27	2.14	1.08	0	95.37	6.07	4.63			MSSF
9.66	5	0.92	1.00	0.62	1.01	98.35	0.64	0.64			MSSF
9.85	5	1.09	1.17	0.61	0.2	98.62	1.18	1.18			MSSF
10.05	5	0.59	0.50	0.64	5.54	93.86	0.60	0.60			MSSF
10.25	5	1.10	1.17	0.57	0.34	99.07	1.00	0.59			MSSF
10.45	5	1.12	1.19	0.57	0	98.72	1.28	1.28			MSSF
10.65	5	1.08	1.22	0.73	0	97.49	2.51	2.51			MSSF
11.65	5	1.79	1.81	0.55	0	98.83	1.54	1.17			MSSF
11.90	5	1.46	1.52	0.54	0.56	98.77	0.67	0.67			MSSF
12.15	5	1.47	1.47	0.85	4.11	94.08	1.81	1.81			MSSF
12.40	5	2.15	2.23	0.57	0	97.95	2.05	2.05			MSSF
12.65	5	2.12	2.19	0.52	0	98.13	1.87	1.87			MSSF
12.90	5	2.17	2.23	0.45	0	98.78	1.22	1.22			MSSF
13.15	5	2.17	2.24	0.46	0	99.00	1.42	1.00			MSSF
13.40	5	2.15	2.21	0.44	0	99.00	1.42	1.00			MSSF
13.65	5	2.20	2.28	0.48	0	98.32	2.14	1.68			MSSF
17.75	5	1.837	1.871	0.475	0.05	98.65	1.3	1.3			MSSF
18.15	5	1.85	1.89	0.4735	0	98.48	1.52	1.52			MSSF
18.55	5	1.84	1.879	0.4607	0	99.21	0.79	0.79			MSSF
18.95	5	1.926	1.981	0.4453	0	99.12	0.88	0.88			MSSF
19.35	5	1.699	1.717	0.3673	0	99.53	0.47	0.47			MSSF
19.55	5	1.84	1.86	0.44	0.16	99.27	1.00	0.57			MSSF
19.75	5	1.61	1.71	0.62	0	97.92	2.08	2.08			MSSF
19.95	5	2.00	2.05	0.45	0	99.07	0.93	0.93			MSSF
20.15	5	1.83	1.86	0.47	0	99.30	0.70	0.70			MSSF

APPENDIX C, PART 1 (cont'd). GRAIN SIZE SAMPLE DATA											
sample depth m	sample thickness cm	ϕ_{50}	mean ϕ	standard deviation ϕ	gravel %	sand %	Fines Content %	silt & clay %	silt %	clay %	Facies (see Table 6-1)
DT13											
21.33	5	0.87	0.83	0.90	5.75	92.70	1.59	1.55			MSSF
21.52	5	1.04	0.96	0.77	3.24	95.62	1.32	1.14			MSSF
21.72	5	1.10	1.06	0.92	4.5	92.97	2.73	2.53			MSSF
21.92	5	1.87	2.10	1.25	2.3	86.98	11.41	10.72			MS
22.12	5	1.87	1.94	0.58	0	97.84	2.20	2.16			MS
22.32	5	1.90	2.02	0.76	0.28	96.22	3.90	3.50			MS
22.52	5	1.82	1.85	0.69	0	98.07	2.29	1.93			MS
22.72	5	1.60	1.71	0.59	0.11	98.42	1.51	1.47			MS
22.98	5	2.14	2.40	1.00	0	90.21	10.89	9.79			MS
FD95S-1											
65.51	5	1.98	2.09	0.60	0	97.94	2.40	2.06			SB
65.86	5	1.98	2.08	0.60	0	98.00	2.04	2.00			SB

APPENDIX C . GRAIN SIZE SAMPLE DATA

PART 2; AGC LABORATORY (see table 6-1 for Facies abbreviations)

sample depth m	sample thickness cm	ϕ_{50}	mean ϕ	standard deviation ϕ	gravel %	sand %	Fines Content %	silt & clay %	silt %	clay %	Facies (see Table 6-1)
FD95S-1											
40.23	5	2.60	2.80	1.13	0	96.37		3.63	2.12	1.50	MX
40.33	5	2.92	4.04	2.46	0	74.64		25.36	15.59	9.77	MX
40.43	5	2.78	3.55	2.02	0	82.46		17.54	11.68	5.86	MX
62.50	5	2.65	3.11	1.77	0	91.06		8.91	4.55	4.36	SB
63.00	5	2.08	2.43	1.70	0	94.72		5.28	2.11	3.16	SB
65.71	5	1.92	2.12	1.20	0.12	96.96		2.91	1.57	1.34	SB
65.86	5	1.95	2.19	1.29	0.17	96.41		3.42	1.88	1.54	SB
66.01	5	2.42	2.58	1.03	0.0	97.19		2.81	1.70	1.11	SB
66.46	5	2.49	2.64	1.00	0.0	96.97		3.03	2.02	1.01	SB
66.86	5	2.36	2.56	1.27	0.06	95.97		3.97	2.34	1.63	SB
67.15	5	2.92	3.60	2.06	0.0	84.66		15.34	8.45	6.89	SB
67.30	5	2.54	2.85	1.42	0.0	93.63		6.37	3.91	2.45	SB
67.75	5	2.72	3.32	1.92	0.01	88.66		11.33	5.44	5.89	SB
67.90	5	2.41	2.61	1.21	0.0	95.97		4.03	2.50	1.53	SB
68.05	5	2.46	2.70	1.30	0.0	95.39		4.61	2.73	1.89	SB
73.44	5	3.67	4.76	2.45	0.0	57.02		42.98	31.49	11.49	BS
79.65	5	3.35	4.35	2.36	0.0	65.77		34.23	24.64	9.59	BS
79.85	5	2.85	3.54	1.95	0.0	82.74		17.26	11.91	5.34	BS
79.95	5	2.72	3.06	1.40	0.0	92.74		7.26	4.80	2.46	BS
80.05	5	2.94	3.39	1.60	0.0	86.43		13.57	10.26	3.30	BS
80.15	5	2.84	3.38	1.77	0.01	87.60		12.39	7.94	4.45	BS
82.45	5	3.60	4.72	2.43	0.0	59.04		40.96	29.42	11.53	BS
82.65	5	3.45	4.53	2.41	0.0	63.73		36.27	25.73	10.54	BS
82.68	5	3.11	4.02	2.21	0.0	75.75		24.25	16.30	7.95	BS
83.22	5	3.49	4.58	2.38	0.0	62.76		37.24	26.37	10.87	BS
83.33	5	3.87	4.99	2.57	0.0	53.02		46.98	33.24	13.74	BS
83.42	5	3.87	5.08	2.69	0.0	52.21		47.79	32.34	15.44	BS
88.515	5	5.09	5.91	2.88	0.0	36.16		63.84	41.28	22.56	BS
88.59	5	2.90	3.49	1.84	0.01	86.06		13.93	9.08	4.85	BS
88.89	5	3.15	4.00	2.14	0.0	77.42		22.58	14.97	7.61	BS

APPENDIX D. GRAIN SIZE TO CPT CORRELATIONS
PART 1; 10 cm^2 cones (see list of symbols)

samples		CPT parameters															
depth m	Facies	ϕ_{50}	depth m	q_c bar	F_s bar	U m H_20	q_t bar	R_f	dU m H_20	σ_{vo} bar	σ'_{vo} bar	q_{c1}	Q_t	Q	F_R	B_q	I_F
FD92-11																	
2.89	BSZ	5.49	2.05	18.56	0.14	0.2	18.57	0.75%	-0.85	0.390	0.286	34.68	63.45	33.96	0.77	-0.0046	2.23
2.92	BSZ	3.46	2.10	19.38	0.12	0.4	19.39	0.62%	-0.69	0.399	0.291	35.92	65.25	35.21	0.63	-0.0036	2.18
3.49	BSZ	3.27	2.80	16.91	0.17	1.3	16.96	1.00%	-0.47	0 532	0.355	28.36	46.21	27.55	1.04	-0.0028	2.38
4.16	BSZ	3.64	3.50	13.20	0.07	-2.1	13.13	0.53%	-4.64	0.665	0.420	20.37	29.69	19.23	0.56	-0.0365	2.39
5.89	MSSB	2.39	5.35	41.45	0.15	1.2	41.49	0.36%	-3.13	1.017	0.590	53.97	68.63	52.71	0.37	-0.0076	1.92
6.19	MSSB	2.14	5.60	69.90	0.17	4.3	70.05	0.24%	-0.32	1.064	0.613	89.30	112.58	88.13	0.25	-0.0005	1.64
7.47	MSSB	2.05	6.90	76.50	0.17	5.6	76.69	0.22%	-0.29	1.311	0.732	89.40	102.95	88.09	0.23	-0.0004	1.63
10.71	MSSB	1.98	9.95	115.27	0.26	8.6	115.56	0.22%	-0.39	1.891	1.013	114.56	112.27	112.97	0.23	-0.0003	1.53
14.27	MSSB	2.01	13.70	159.39	0.30	12.1	159.81	0.19%	-0.57	2.603	1.357	136.82	115.84	134.94	0.19	-0.0004	1.43
15.03	MSSB	1.79	14.50	82.69	0.44	12.7	83.13	0.53%	-0.76	2.755	1.431	69.13	56.18	67.20	0.55	-0.0009	1.90
16.58	LZ	3.77	16.25	32.79	0.26	11.4	33.18	0.78%	-3.83	3.088	1.591	25.99	18.91	23.86	0.86	-0.0125	2.39
16.64	LZ	4.82	16.30	23.09	0.36	13.5	23.55	1.53%	-1.84	3.097	1.596	18.28	12.82	12.82	1.76	-0.0088	2.78
18.01	LZ	5.68	17.50	10.52	0.13	45.2	12.07	1.08%	28.66	3.325	1.706	8.05	5.13	5.13	1.49	0.3215	3.09
18.38	LZ	5.21	17.85	17.94	0.37	20.5	18.64	1.98%	3.64	3.392	1.739	13.61	8.77	8.77	2.43	0.0234	2.99
19.71	LZ	3.88	19.25	16.29	0.29	29.9	17.32	1.67%	11.62	3.658	1.867	11.92	7.31	7.31	2.12	0.0834	3.03
21.93	LZ	5.94	20.95	8.87	0.15	55.8	10.78	1.39%	35.81	3.981	2.023	6.24	3.36	3.36	2.20	0.5163	3.33
22.18	LZ	6.60	21.20	8.04	0.17	63.1	10.21	1.67%	42.90	4.028	2.046	5.62	3.02	3.02	2.75	0.6811	3.42
24.55	LZ	3.53	23.60	51.34	0.44	18.6	51.98	0.85%	-4.05	4.484	2.267	34.10	20.95	31.54	0.93	-0.0084	2.30
24.68	LZ	6.38	23.70	16.29	0.43	22.8	17.07	2.52%	0.13	4.503	2.276	10.80	5.52	5.52	3.42	0.0010	3.24
26.23	LZ	6.49	25.10	11.14	0.24	51.5	12.91	1.86%	27.38	4.769	2.405	7.18	3.38	3.38	2.95	0.3300	3.39
26.61	LZ	3.68	25.45	36.09	0.40	40.1	37.47	1.07%	15.61	4.836	2.437	23.12	13.39	13.39	1.23	0.0469	2.68
29.18	LS	5.70	28.40	13.61	0.56	38.3	14.93	3.75%	10.93	5.396	2.708	8.27	3.52	3.52	5.88	0.1125	3.54
29.44	LS	3.35	28.65	65.78	0.33	15.3	66.31	0.50%	-12.36	5.444	2.731	39.80	22.29	36.83	0.54	-0.0199	2.13
30.49	LS	3.41	29.75	74.44	0.44	6.2	74.65	0.59%	-22.53	5.653	2.832	44.23	24.36	41.00	0.64	-0.0320	2.12
34.03	LS	5.85	33.40	13.40	0.49	79.0	16.11	3.04%	46.60	6.346	3.168	7.53	3.08	3.08	5.02	0.4681	3.55
34.13	LS	5.77	33.50	14.43	0.47	84.8	17.34	2.71%	52.31	6.365	3.177	8.10	3.46	3.46	4.28	0.4675	3.47
34.23	LS	3.44	33.60	71.55	0.58	22.4	72.32	0.80%	-10.17	6.384	3.186	40.09	20.70	36.94	0.88	-0.0151	2.23

APPENDIX D; PART 1 (cont'd). GRAIN SIZE TO CPT CORRELATIONS

samples		CPT parameters															
depth m	Facies	ϕ_{50}	depth m	q_c bar	F_s bar	U m H_20	q_t bar	R_f	dU m H_20	σ_{vo} bar	σ'_{vo} bar	q_{c1}	Q_t	Q	F_R	B_q	I_F
FD92-11 (cont'd)																	
36.78	LS	4.82	35.95	40.62	0.69	17.8	41.23	1.67%	-17.11	6.831	3.402	22.02	10.11	10.11	2.01	-0.0488	2.90
40.88	LS	3.68	39.85	59.18	0.60	7.5	59.44	1.01%	-31.31	7.572	3.760	30.52	13.79	13.79	1.16	-0.0592	2.66
41.51	LS	3.35	40.45	88.87	0.62	18.6	89.51	0.69%	-20.90	7.686	3.815	45.50	21.44	41.89	0.76	-0.0251	2.15
45.66	LS	2.87	44.65	91.35	0.70	3.7	91.48	0.77%	-39.98	8.484	4.201	44.57	19.75	40.49	0.84	-0.0473	2.19
45.76	LS	4.91	44.75	55.47	1.19	18.0	56.09	2.12%	-25.71	8.503	4.211	27.03	11.30	11.30	2.50	-0.0530	2.91
50.85	LS	2.74	50.35	111.97	0.74	7.3	112.22	0.66%	-42.01	9.567	4.725	51.51	21.72	47.22	0.72	-0.0401	2.09
53.28	MX	2.64	53.00	167.64	1.21	49.0	169.32	0.71%	-2.97	10.070	4.969	75.21	32.05	71.44	0.76	-0.0018	1.96
54.80	MX	2.77	54.15	171.76	0.84	49.9	173.48	0.48%	-3.20	10.289	5.074	76.25	32.16	72.44	0.51	-0.0019	1.86
55.09	BS	3.64	54.45	124.34	1.18	4.8	124.50	0.95%	-48.66	10.346	5.102	55.05	22.38	50.54	1.03	-0.0418	2.15
55.20	BS	5.16	54.60	116.92	1.34	3.7	117.05	1.14%	-49.93	10.374	5.116	51.69	20.85	47.16	1.26	-0.0459	2.23
55.52	BS	5.94	54.95	23.92	0.44	49.2	25.61	1.72%	-4.71	10.441	5.148	10.54	2.95	2.95	2.90	-0.0305	3.44
58.83	BZ	6.27	57.60	22.48	0.19	160.9	28.00	0.68%	104.26	10.944	5.392	9.68	3.16	3.16	1.11	0.5995	3.23
59.06	BZ	6.64	57.90	22.48	0.24	153.6	27.75	0.86%	96.72	11.001	5.419	9.66	3.09	3.09	1.43	0.5663	3.28
62.99	BZ	5.92	61.80	18.35	0.18	170.5	24.21	0.74%	109.74	11.742	5.778	7.63	2.16	2.16	1.44	0.8638	3.43
67.36	BZ	6.79	66.15	22.68	0.35	213.1	30.00	1.17%	148.00	12.569	6.177	9.13	2.82	2.82	2.01	0.8330	3.38
67.42	BZ	6.36	66.25	23.71	0.38	214.1	31.06	1.22%	148.82	12.588	6.186	9.53	2.99	2.99	2.06	0.7903	3.36
72.04	BZ	6.49	71.75	28.25	0.41	214.1	35.60	1.15%	143.32	13.633	6.692	10.92	3.28	3.28	1.87	0.6400	3.31
72.29	BZ	5.79	72.00	35.26	0.40	174.9	41.27	0.97%	103.92	13.680	6.715	13.61	4.11	4.11	1.45	0.3696	3.17
73.07	BZ	3.17	72.90	121.86	0.94	33.7	123.02	0.76%	-38.16	13.851	6.798	46.74	16.06	41.87	0.86	-0.0343	2.18
73.37	BZ	3.49	73.15	63.72	1.21	80.0	66.47	1.82%	7.87	13.899	6.821	24.40	7.71	7.71	2.30	0.0147	3.03
73.77	BZ	6.11	73.60	40.62	0.64	145.9	45.63	1.40%	73.27	13.984	6.862	15.51	4.61	4.61	2.02	0.2271	3.19
76.68	BZ	6.54	76.55	25.57	0.32	220.9	33.15	0.97%	145.35	14.545	7.133	9.57	2.61	2.61	1.72	0.7662	3.38
82.51	BZ	7.10	82.30	30.11	0.51	264.9	39.21	1.30%	183.63	15.637	7.661	10.88	3.08	3.08	2.16	0.7643	3.36
88.47	BZ	7.16	86.95	32.58	0.57	260.6	41.53	1.37%	174.60	16.521	8.089	11.46	3.09	3.09	2.28	0.6850	3.37
88.58	BZ	7.31	87.05	32.38	0.49	251.9	41.03	1.19%	165.84	16.540	8.098	11.38	3.02	3.02	2.00	0.6643	3.35
93.78	BZ	7.46	92.35	33.82	0.62	314.3	44.61	1.39%	222.92	17.547	8.585	11.54	3.15	3.15	2.29	0.8080	3.37
99.28	BZ	7.78	98.65	35.88	0.81	336.6	47.44	1.71%	238.95	18.744	9.164	11.85	3.13	3.13	2.82	0.8169	3.41
99.83	BC	3.81	99.20	34.23	0.77	325.0	45.39	1.70%	226.77	18.848	9.215	11.28	2.88	2.88	2.90	0.8382	3.45

APPENDIX D; PART 1 (cont'd). GRAIN SIZE TO CPT CORRELATIONS

samples		CPT parameters															
depth m	Facies	ϕ_{50}	depth m	q_c bar	F_s bar	U m H_20	q_t bar	R_f	dU m H_20	σ_{vo} bar	σ'_{vo} bar	q_{c1}	Q_t	Q	F_R	B_q	I_F
FD92-11 (cont'd)																	
100.14	BC	3.57	99.50	73.41	0.68	250.9	82.02	0.83%	152.37	18.905	9.242	24.15	6.83	6.83	1.08	0.2368	2.92
100.26	BC	10.09	99.60	32.58	1.09	256.2	41.38	2.63%	157.57	18.924	9.251	10.71	2.43	2.43	4.85	0.6885	3.63
24.35	LZ	6.67	23.40	10.31	0.17	52.9	12.13	1.40%	30.51	4.446	2.249	6.88	3.42	3.42	2.21	0.3896	3.33
24.40	LZ	6.52	23.45	8.66	0.13	66.0	10.92	1.19%	43.50	4.456	2.253	5.77	2.87	2.87	2.01	0.6597	3.38
24.45	LZ	7.14	23.50	8.66	0.19	69.6	11.05	1.72%	47.12	4.465	2.258	5.76	2.92	2.92	2.89	0.7020	3.44
24.50	LZ	3.58	23.55	23.51	0.22	52.2	25.30	0.87%	29.64	4.475	2.262	15.63	9.21	9.21	1.06	0.1396	2.80
24.55	LZ	3.21	23.60	51.34	0.44	18.6	51.98	0.85%	-4.05	4.484	2.267	34.10	20.95	31.54	0.93	-0.0084	2.30
24.60	LZ	3.95	23.65	42.27	0.51	14.9	42.78	1.19%	-7.77	4.494	2.272	28.05	16.86	16.86	1.33	-0.0199	2.62
24.65	LZ	5.68	23.70	16.29	0.43	22.8	17.07	2.52%	0.13	4.503	2.276	10.80	5.52	5.52	3.42	0.0010	3.24
24.75	LZ	6.17	23.75	12.58	0.32	41.5	14.00	2.28%	18.74	4.513	2.281	8.33	4.16	4.16	3.37	0.1937	3.34
24.80	LZ	5.73	23.80	11.14	0.25	59.4	13.18	1.90%	36.63	4.522	2.285	7.37	3.79	3.79	2.89	0.4150	3.34
24.85	LZ	5.18	23.85	13.40	0.19	52.4	15.20	1.25%	29.55	4.532	2.290	8.86	4.66	4.66	1.78	0.2717	3.16
24.90	LZ	5.69	23.90	9.90	0.23	62.8	12.06	1.91%	39.89	4.541	2.295	6.54	3.28	3.28	3.06	0.5208	3.41
24.95	LZ	6.34	23.95	11.34	0.18	63.3	13.51	1.33%	40.35	4.551	2.299	7.48	3.90	3.90	2.01	0.4417	3.26
25.00	LZ	5.36	24.00	10.10	0.21	61.2	12.20	1.72%	38.16	4.560	2.304	6.65	3.32	3.32	2.75	0.4900	3.38
25.05	LZ	5.89	24.05	8.45	0.19	68.6	10.81	1.76%	45.55	4.570	2.308	5.56	2.70	2.70	3.05	0.7166	3.48
25.15	LZ	6.51	24.10	9.28	0.17	70.7	11.71	1.45%	47.64	4.579	2.313	6.10	3.08	3.08	2.38	0.6555	3.38
25.20	LZ	6.63	24.15	8.87	0.18	74.2	11.42	1.58%	51.06	4.589	2.317	5.83	2.95	2.95	2.64	0.7334	3.42
25.25	LZ	7.24	24.20	10.52	0.41	73.2	13.03	3.15%	49.99	4.598	2.322	6.90	3.63	3.63	4.86	0.5814	3.48
25.30	LZ	5.84	24.25	26.19	0.57	35.0	27.39	2.08%	11.71	4.608	2.327	17.17	9.79	9.79	2.50	0.0504	2.96
25.35	LZ	5.18	24.30	20.21	0.71	29.9	21.24	3.34%	6.57	4.617	2.331	13.24	7.13	7.13	4.27	0.0388	3.21
25.40	LZ	6.23	24.35	13.20	0.63	54.3	15.07	4.18%	30.98	4.627	2.336	8.64	4.47	4.47	6.04	0.2912	3.46
25.45	LZ	5.96	24.40	11.75	0.43	38.8	13.08	3.29%	15.44	4.636	2.340	7.68	3.61	3.61	5.09	0.1793	3.49
FD93-2																	
0.90	LOZ	7.22	0.90	11.04	0.22	-3.4	10.99	2.00%	-2.32	0.171	0.171	26.70	63.27	26.16	2.03	-0.0210	2.56
1.00	LOZ	7.22	1.00	5.87	0.14	-3.5	5.82	2.41%	-2.48	0.190	0.190	13.47	29.63	19.56	2.49	-0.0432	2.71
1.10	LOZ	6.79	1.10	6.44	0.08	-1.9	6.41	1.25%	-0.95	0.209	0.209	14.09	29.68	20.07	1.29	-0.0150	2.54
2.30	LOZ	6.75	2.40	5.87	0.05	5.8	5.96	0.84%	5.38	0.456	0.417	9.09	13.19	13.19	0.91	0.0960	2.63

APPENDIX D; PART 1 (cont'd). GRAIN SIZE TO CPT CORRELATIONS

samples		CPT parameters															
depth m	Facies	ϕ_{50}	depth m	q_c bar	F_s bar	U m H_20	q_t bar	R_f	dU m H_20	σ_{vo} bar	σ'_{vo} bar	q_{c1}	Q_t	Q	F_R	B_q	I_F
FD93-2 (cont'd)																	
2.40	LOZ	5.74	2.50	6.52	0.05	6.3	6.61	0.76%	5.81	0.475	0.426	9.99	14.41	11.64	0.81	0.0929	2.66
2.50	LOZ	5.76	2.60	6.20	0.05	5.6	6.28	0.80%	4.98	0.494	0.435	9.40	13.30	13.30	0.86	0.0844	2.62
2.60	LOZ	5.75	2.70	7.13	0.05	6.1	7.22	0.69%	5.41	0.513	0.444	10.70	15.09	12.32	0.75	0.0791	2.62
2.70	LOZ	5.59	2.80	7.99	0.06	4.5	8.06	0.74%	3.66	0.532	0.454	11.86	16.59	13.61	0.80	0.0477	2.59
2.80	LOZ	5.82	2.90	10.88	0.06	3.5	10.93	0.55%	2.63	0.551	0.463	15.99	22.44	15.26	0.58	0.0249	2.49
2.90	LOZ	5.76	3.00	7.74	0.06	3.1	7.79	0.77%	2.13	0.570	0.472	11.27	15.29	12.67	0.83	0.0290	2.63
3.00	LOZ	4.88	3.10	10.31	0.07	3.2	10.36	0.68%	2.06	0.589	0.481	14.86	20.30	14.08	0.72	0.0207	2.56
3.10	LOZ	5.22	3.20	9.13	0.09	3.3	9.18	0.98%	2.05	0.608	0.490	13.04	17.48	14.63	1.05	0.0235	2.62
3.20	WSZ	4.14	3.30	12.87	0.07	2.3	12.90	0.54%	0.99	0.627	0.499	18.21	24.58	17.37	0.57	0.0079	2.43
3.30	WSZ	3.40	3.40	14.37	0.06	0.4	14.38	0.42%	-1.01	0.646	0.509	20.15	26.99	19.25	0.44	-0.0072	2.35
3.40	WSZ	3.86	3.50	13.56	0.06	-0.1	13.56	0.44%	-1.57	0.665	0.518	18.84	24.90	17.92	0.47	-0.0119	2.39
3.50	WSZ	3.43	3.60	11.04	0.06	0.9	11.05	0.54%	-0.73	0.684	0.527	15.21	19.67	14.28	0.58	-0.0069	2.52
3.60	WSZ	2.09	3.70	15.15	0.08	0.3	15.16	0.53%	-1.36	0.703	0.536	20.69	26.95	19.74	0.55	-0.0092	2.38
3.65	WSZ	4.43	3.75	11.12	0.07	1.1	11.14	0.63%	-0.69	0.713	0.541	15.12	19.27	14.17	0.67	-0.0065	2.54
3.70	WSZ	3.91	3.80	11.49	0.08	1.9	11.52	0.69%	0.06	0.722	0.545	15.56	19.79	14.62	0.74	0.0005	2.55
3.80	MSSF	2.72	4.10	20.48	0.07	2.8	20.52	0.34%	0.66	0.779	0.573	27.06	34.45	26.08	0.35	0.0033	2.19
3.90	MSSF	2.46	4.20	29.38	0.14	3.6	29.43	0.48%	1.39	0.798	0.582	38.51	49.19	37.53	0.49	0.0048	2.10
3.95	MSSF	2.00	4.25	42.17	0.11	2.1	42.20	0.26%	-0.18	0.808	0.587	55.05	70.54	54.04	0.27	-0.0004	1.85
4.00	MSSF	2.16	4.30	40.95	0.11	0.5	40.96	0.27%	-1.84	0.817	0.591	53.25	67.88	52.20	0.27	-0.0045	1.87
4.10	MSSF	2.44	4.40	34.76	0.18	1.9	34.79	0.52%	-0.51	0.836	0.601	44.85	56.53	43.81	0.53	-0.0015	2.06
4.20	MSSF	2.03	4.50	54.01	0.16	1.8	54.04	0.30%	-0.67	0.855	0.610	69.17	87.22	68.11	0.30	-0.0012	1.78
4.30	MSSF	2.14	4.60	44.61	0.17	2.4	44.65	0.38%	-0.21	0.874	0.619	56.70	70.72	55.64	0.39	-0.0005	1.91
4.40	MSSF	2.29	4.70	45.59	0.20	2.9	45.63	0.44%	0.16	0.893	0.628	57.52	71.23	56.45	0.45	0.0004	1.93
4.50	MSSF	2.88	4.80	40.49	0.18	3.4	40.54	0.44%	0.58	0.912	0.637	50.72	62.18	49.64	0.45	0.0014	1.98
4.60	MSSF	2.62	4.90	33.09	0.22	3.5	33.14	0.66%	0.63	0.931	0.647	41.15	49.82	40.06	0.68	0.0019	2.14
4.70	MSSF	2.49	5.00	47.42	0.20	3.8	47.48	0.42%	0.75	0.950	0.656	58.56	70.95	57.46	0.43	0.0016	1.91
4.80	MSSF	2.36	5.10	56.57	0.23	3.8	56.63	0.41%	0.65	0.969	0.665	69.38	83.71	68.26	0.41	0.0011	1.84
4.90	MSSF	2.13	5.20	67.03	0.27	3.7	67.08	0.40%	0.52	0.988	0.674	81.64	98.05	80.51	0.41	0.0008	1.77

APPENDIX D; PART 1 (cont'd). GRAIN SIZE TO CPT CORRELATIONS

samples		CPT parameters															
depth m	Facies	ϕ_{50}	depth m	q_c bar	F_s bar	U m H_20	q_t bar	R_f	dU m H_20	σ_{vo} bar	σ'_{vo} bar	q_{c1}	Q_t	Q	F_R	B_q	I_F
FD93-2 (cont'd)																	
22.22	LDSZ	2.56	22.60	56.73	0.42	20.8	57.04	0.74%	0.15	4.294	2.273	37.63	23.20	34.98	0.80	0.0003	2.23
22.77	LDSZ	2.23	23.15	183.30	0.52	1.4	183.32	0.28%	-19.73	4.399	2.324	120.25	77.00	117.38	0.29	-0.0108	1.56
24.07	LDSZ	2.61	24.45	109.30	0.55	19.7	109.59	0.50%	-2.77	4.646	2.443	69.93	42.95	67.14	0.52	-0.0026	1.89
FD93-3																	
2.85	BSZ	6.54	2.45	5.05	0.33	-1.7	5.02	6.57%	-1.43	0.466	0.466	7.40	9.79	9.79	7.24	-0.0308	3.24
3.40	BSZ	2.32	3.00	6.71	0.23	-3.3	6.66	3.45%	-3.62	0.570	0.541	9.13	11.27	11.27	3.78	-0.0583	3.01
4.05	BSZ	3.93	3.65	6.23	0.38	0.3	6.23	6.10%	-0.65	0.694	0.600	8.04	9.23	9.23	6.86	-0.0115	3.24
4.55	BSZ	3.08	4.15	7.24	0.40	0.2	7.24	5.52%	-1.25	0.789	0.646	9.01	9.99	9.99	6.20	-0.0190	3.19
5.30	MSSB	2.01	4.90	25.10	0.20	0.1	25.10	0.80%	-2.12	0.931	0.715	29.68	33.80	28.58	0.83	-0.0086	2.31
5.33	MSSB	2.24	5.35	53.51	0.46	-1.3	53.49	0.86%	-3.90	1.017	0.757	61.52	69.36	60.33	0.88	-0.0073	2.05
5.65	MSSB	3.27	5.70	27.14	0.37	0.1	27.14	1.36%	-2.90	1.083	0.789	30.56	33.04	29.34	1.42	-0.0109	2.43
6.10	MSSB	2.83	6.15	77.51	0.65	-3.6	77.46	0.84%	-7.01	1.169	0.830	85.08	91.91	83.73	0.85	-0.0090	1.93
6.41	MSSB	1.96	6.45	71.33	0.43	1.3	71.35	0.60%	-2.47	1.226	0.858	77.02	81.76	75.72	0.61	-0.0035	1.88
6.83	MSSB	2.30	6.80	56.32	0.42	-1.3	56.30	0.75%	-5.35	1.292	0.890	59.71	61.82	58.32	0.76	-0.0095	2.03
7.15	MSSB	1.80	7.15	95.05	0.52	1.4	95.07	0.55%	-2.99	1.359	0.922	98.99	101.65	97.60	0.55	-0.0031	1.77
7.85	MSSB	5.66	7.85	9.68	0.15	6.7	9.78	1.53%	1.56	1.492	0.986	9.75	8.40	8.40	1.81	0.0185	2.94
8.70	MSSB	2.30	8.70	73.56	0.47	2.6	73.60	0.64%	-3.35	1.653	1.064	71.30	67.59	69.73	0.65	-0.0046	1.93
9.15	MSSB	1.68	9.15	100.20	0.57	-0.3	100.20	0.57%	-6.72	1.739	1.106	95.29	89.04	93.63	0.58	-0.0067	1.79
9.80	MSSB	2.08	9.80	78.81	0.63	6.1	78.90	0.80%	-0.94	1.862	1.165	73.00	66.10	71.36	0.82	-0.0012	1.97
10.50	MSSB	2.77	10.55	69.87	0.54	-0.9	69.86	0.77%	-8.75	2.005	1.234	62.89	54.97	61.07	0.80	-0.0127	2.02
11.20	MSSB	1.68	11.25	194.00	1.05	7.4	194.11	0.54%	-1.13	2.138	1.299	170.23	147.81	168.45	0.55	-0.0006	1.57
13.85	MSSB	2.24	13.85	101.20	0.65	11.0	101.36	0.64%	-0.15	2.632	1.538	81.61	64.21	79.62	0.66	-0.0001	1.88
15.30	MSSB	1.79	15.30	73.12	0.76	10.6	73.28	1.04%	-2.01	2.907	1.671	56.57	42.11	54.44	1.08	-0.0028	2.14
17.60	MSSB	1.96	17.65	112.80	0.70	15.0	113.02	0.62%	0.02	3.354	1.887	82.12	58.12	79.84	0.64	0.0000	1.87
18.78	MSSB	1.51	18.85	82.69	0.80	13.1	82.88	0.97%	-3.02	3.582	1.997	58.51	39.71	56.11	1.01	-0.0037	2.11
FD93-5																	
20.40	MSSB	1.92	20.50	84.71	0.30	17.8	84.97	0.35%	0.31	3.895	2.178	57.40	37.22	54.93	0.37	0.0004	1.90
20.50	MSSB	1.87	20.60	97.93	0.36	17.9	98.19	0.37%	0.32	3.914	2.187	66.21	43.10	63.75	0.38	0.0003	1.85

APPENDIX D; PART 1 (cont'd). GRAIN SIZE TO CPT CORRELATIONS

samples		CPT parameters															
depth m	Facies	ϕ_{50}	depth m	q_c bar	F_s bar	U m H_20	q_t bar	R_f	dU m H_20	σ_{vo} bar	σ'_{vo} bar	q_{c1}	Q_t	Q	F_R	B_q	I_F
FD93-5 (cont'd)																	
20.60	MSSB	1.97	20.70	119.62	0.42	17.8	119.88	0.35%	0.13	3.933	2.197	80.71	52.79	78.23	0.36	0.0001	1.76
20.70	MSSB	2.13	20.80	89.43	0.47	17.4	89.69	0.52%	-0.44	3.952	2.206	60.21	38.87	57.73	0.55	-0.0005	1.96
20.75	CU	3.08	20.85	69.08	0.41	17.8	69.34	0.59%	-0.10	3.962	2.210	46.46	29.58	43.98	0.63	-0.0002	2.09
20.80	CU	3.00	20.90	65.21	0.25	8.3	65.33	0.38%	-9.65	3.971	2.215	43.82	27.70	41.23	0.41	-0.0154	2.03
20.90	CU	4.89	21.00	50.81	0.64	6.1	50.90	1.26%	-11.95	3.990	2.224	34.07	21.09	31.45	1.36	-0.0250	2.39
21.00	CU	4.22	21.10	47.51	0.44	13.7	47.71	0.92%	-4.42	4.009	2.233	31.79	19.57	29.24	1.01	-0.0099	2.35
21.10	CU	4.49	21.20	37.67	0.55	1.0	37.69	1.46%	-17.17	4.028	2.243	25.15	15.01	15.01	1.63	-0.0500	2.70
21.15	CU	2.62	21.25	50.32	0.53	0.6	50.33	1.05%	-17.63	4.038	2.247	33.57	20.60	30.88	1.14	-0.0374	2.36
21.20	CU	2.60	21.30	51.54	0.66	0.6	51.55	1.28%	-17.68	4.047	2.252	34.35	21.10	31.66	1.39	-0.0365	2.40
21.30	CU	2.68	21.40	112.54	0.66	-4.8	112.47	0.59%	-23.17	4.066	2.261	74.84	47.95	72.09	0.61	-0.0210	1.90
21.40	CU	2.51	21.50	107.58	0.84	-3.9	107.52	0.78%	-22.35	4.085	2.270	71.40	45.56	68.65	0.81	-0.0212	1.99
21.50	CU	2.64	21.60	120.44	0.41	-2.5	120.40	0.34%	-21.05	4.104	2.279	79.77	51.02	77.03	0.35	-0.0178	1.76
21.60	CU	2.62	21.70	98.26	0.71	-1.9	98.23	0.72%	-20.59	4.123	2.289	64.95	41.12	62.21	0.75	-0.0215	2.00
21.70	CU	2.47	21.80	103.67	0.45	-0.2	103.67	0.43%	-18.96	4.142	2.298	68.39	43.31	65.66	0.45	-0.0187	1.87
21.80	CU	2.56	21.90	90.36	0.52	13.4	90.56	0.57%	-5.52	4.161	2.307	59.49	37.45	56.88	0.60	-0.0063	1.99
21.90	CU	2.45	22.00	85.20	0.65	15.2	85.42	0.76%	-3.83	4.180	2.316	55.98	35.08	53.38	0.80	-0.0046	2.07
22.00	CU	2.69	22.10	91.30	0.47	1.2	91.32	0.51%	-17.90	4.199	2.325	59.87	37.47	57.13	0.54	-0.0202	1.96
22.05	CU	3.33	22.15	89.59	0.36	-3.0	89.55	0.40%	-22.19	4.209	2.330	58.69	36.63	55.91	0.42	-0.0255	1.92
22.10	CU	2.92	22.20	86.58	0.50	-2.9	86.54	0.58%	-22.05	4.218	2.334	56.67	35.26	53.88	0.61	-0.0263	2.01
22.15	CU	3.12	22.25	83.20	0.47	-1.7	83.18	0.57%	-20.90	4.228	2.339	54.40	33.75	51.62	0.60	-0.0260	2.02
22.20	CU	3.20	22.30	82.31	0.46	0.3	82.31	0.56%	-19.01	4.237	2.344	53.77	33.31	51.00	0.59	-0.0239	2.02
22.25	CU	3.63	22.35	76.08	0.50	2.5	76.12	0.66%	-16.81	4.247	2.348	49.65	30.61	46.90	0.70	-0.0229	2.09
22.30	CU	3.78	22.40	71.52	0.43	5.2	71.60	0.60%	-14.24	4.256	2.353	46.63	28.62	43.90	0.64	-0.0207	2.10
22.35	CU	2.97	22.45	77.91	0.39	8.2	78.03	0.50%	-11.24	4.266	2.357	50.74	31.29	48.04	0.53	-0.0149	2.02
22.40	CU	3.40	22.50	74.78	0.40	9.4	74.92	0.53%	-10.07	4.275	2.362	48.66	29.91	45.97	0.57	-0.0140	2.05
22.45	CU	3.47	22.55	67.90	0.47	11.9	68.07	0.69%	-7.67	4.285	2.367	44.14	26.95	41.47	0.74	-0.0118	2.15
22.50	CU	4.63	22.60	57.36	0.61	13.9	57.56	1.06%	-5.68	4.294	2.371	37.25	22.47	34.59	1.15	-0.0105	2.32
22.55	CU	5.58	22.65	50.85	0.49	15.8	51.08	0.96%	-3.81	4.304	2.376	32.99	19.69	30.35	1.05	-0.0080	2.34

APPENDIX D; PART 1 (cont'd). GRAIN SIZE TO CPT CORRELATIONS

samples		CPT parameters															
depth m	Facies	ϕ_{50}	depth m	q_c bar	F_s bar	U m H_20	q_t bar	R_f	dU m H_20	σ_{vo} bar	σ'_{vo} bar	q_{c1}	Q_t	Q	F_R	B_q	I_F
FD93-5 (cont'd)																	
22.60	CU	4.03	22.70	64.73	0.33	6.2	64.82	0.51%	-13.55	4.313	2.380	41.95	25.42	39.22	0.55	-0.0220	2.11
22.65	CU	2.82	22.75	56.22	0.35	-0.2	56.22	0.62%	-19.95	4.323	2.385	36.40	21.76	33.60	0.67	-0.0377	2.21
22.70	CU	3.23	22.80	51.26	0.39	0.4	51.27	0.76%	-19.43	4.332	2.390	33.16	19.64	30.36	0.83	-0.0406	2.29
22.80	CU	4.72	22.90	33.07	0.31	13.2	33.26	0.93%	-6.68	4.351	2.399	21.35	12.05	12.05	1.07	-0.0227	2.70
FD94-1																	
3.45	WSZ	5.91	3.95	10.07	0.23	-1.9	10.04	2.29%	-2.38	0.751	0.706	11.98	13.15	13.15	2.48	-0.0251	2.85
5.77	MSSF	2.72	5.85	50.03	0.25	-1.6	50.01	0.50%	-3.90	1.112	0.881	53.30	55.50	52.09	0.51	-0.0078	1.98
6.07	MSSF	2.58	6.15	37.40	0.22	2.2	37.43	0.59%	-0.46	1.169	0.909	39.24	39.91	38.05	0.61	-0.0012	2.14
6.37	MSSF	3.04	6.45	31.27	0.29	2.6	31.31	0.93%	-0.36	1.226	0.936	32.32	32.14	31.09	0.96	-0.0012	2.32
6.67	MSSF	2.27	6.75	65.44	0.34	3.1	65.49	0.52%	-0.17	1.283	0.964	66.66	66.62	65.40	0.53	-0.0003	1.90
6.87	MSSF	1.82	6.95	87.96	0.30	3.0	88.00	0.34%	-0.50	1.321	0.982	88.76	88.27	87.47	0.35	-0.0006	1.71
7.07	MSSF	2.14	7.15	87.41	0.33	3.6	87.46	0.38%	-0.04	1.359	1.000	87.39	86.07	86.09	0.38	0.0000	1.73
7.27	MSSF	2.15	7.35	63.85	0.24	4.2	63.91	0.38%	0.32	1.397	1.019	63.26	61.36	61.93	0.38	0.0005	1.86
10.30	MSSF	2.35	9.75	55.30	0.24	5.8	55.39	0.43%	-0.46	1.853	1.239	49.67	43.19	48.09	0.45	-0.0008	1.99
12.60	MSSF	2.39	11.95	53.31	0.11	8.1	53.43	0.21%	-0.37	2.271	1.442	44.40	35.49	42.61	0.22	-0.0007	1.92
14.15	MSSF	2.60	13.50	75.39	0.26	9.9	75.54	0.34%	-0.10	2.565	1.584	59.90	46.07	57.98	0.36	-0.0001	1.87
19.01	MSSF	2.01	18.50	90.44	0.30	15.0	90.66	0.33%	0.00	3.515	2.044	63.27	42.65	60.96	0.34	0.0000	1.85
19.21	MSSF	2.00	18.70	103.48	0.35	14.8	103.70	0.34%	-0.40	3.553	2.062	72.07	48.57	69.74	0.35	-0.0004	1.80
19.41	MSSF	1.92	18.90	116.87	0.35	15.2	117.09	0.30%	-0.23	3.591	2.080	81.03	54.56	78.69	0.31	-0.0002	1.73
19.61	MSSF	1.85	19.10	144.04	0.41	15.0	144.26	0.28%	-0.59	3.629	2.099	99.43	67.01	97.08	0.29	-0.0004	1.63
19.81	MSSF	2.04	19.30	133.25	0.38	16.0	133.49	0.28%	0.23	3.667	2.117	91.58	61.32	89.22	0.29	0.0002	1.67
20.355	MSSF	1.64	19.85	131.18	0.34	16.3	131.42	0.26%	-0.01	3.772	2.168	89.10	58.89	86.70	0.27	0.0000	1.66
21.83	MSSB	2.12	21.30	95.61	0.56	16.9	95.86	0.58%	-0.88	4.047	2.301	63.03	39.90	60.53	0.61	-0.0009	1.96
25.65	MSSB	1.96	25.15	178.22	0.45	20.8	178.53	0.25%	-0.89	4.779	2.655	109.38	65.45	106.64	0.26	-0.0005	1.58
25.75	MSSB	1.95	25.25	182.84	0.45	20.3	183.14	0.25%	-1.44	4.798	2.664	112.03	66.95	109.27	0.25	-0.0008	1.56
26.15	MSSB	2.08	25.65	185.44	0.46	6.9	185.54	0.25%	-15.25	4.874	2.701	112.84	66.90	109.94	0.25	-0.0083	1.56
26.25	MSSB	1.71	25.75	178.75	0.50	8.2	178.87	0.28%	-14.04	4.893	2.710	108.59	64.20	105.69	0.29	-0.0079	1.60
26.35	MSSB	2.45	25.85	164.73	0.48	10.5	164.88	0.29%	-11.88	4.912	2.719	99.90	58.84	97.02	0.30	-0.0073	1.64

APPENDIX D; PART 1 (cont'd). GRAIN SIZE TO CPT CORRELATIONS

samples		CPT parameters															
depth m	Facies	ϕ_{50}	depth m	q_c bar	F_s bar	U m H_20	q_t bar	R_f	dU m H_20	σ_{vo} bar	σ'_{vo} bar	q_{c1}	Q_t	Q	F_R	B_q	I_F
FD94-1 (cont'd)																	
26.45	MSSB	2.38	25.95	151.69	0.32	11.7	151.86	0.21%	-10.80	4.931	2.728	91.84	53.86	88.96	0.22	-0.0072	1.62
26.55	MSSB	5.91	26.05	99.21	1.51	9.7	99.35	1.52%	-12.89	4.950	2.737	59.96	34.49	57.06	1.60	-0.0134	2.23
32.15	MSSB	1.96	31.45	195.92	0.52	25.1	196.29	0.26%	-2.87	5.976	3.234	108.95	58.85	105.83	0.27	-0.0015	1.59
32.35	MSSB	2.03	31.65	198.16	0.47	25.6	198.54	0.24%	-2.51	6.014	3.252	109.89	59.20	106.76	0.24	-0.0013	1.56
FD94-4																	
24.45	MSSB	2.06	23.85	127.98	0.54	14.8	128.20	0.42%	-8.64	4.532	2.231	85.68	55.43	82.79	0.44	-0.0069	1.77
24.55	MSSB	2.09	23.95	95.87	0.57	16.6	96.11	0.59%	-6.92	4.551	2.240	64.05	40.87	61.18	0.62	-0.0074	1.97
24.65	MSSB	7.16	24.05	83.50	0.69	20.8	83.81	0.82%	-2.85	4.570	2.249	55.67	35.23	52.83	0.87	-0.0035	2.10
24.75	MSSB	1.76	24.15	121.38	0.47	17.1	121.63	0.39%	-6.63	4.589	2.259	80.77	51.82	77.88	0.40	-0.0056	1.78
24.85	MSSB	1.86	24.25	118.78	1.04	21.0	119.09	0.87%	-2.81	4.608	2.268	78.83	50.48	76.02	0.91	-0.0024	1.98
24.95	LZ	4.84	24.35	31.74	0.93	23.7	32.09	2.90%	-0.30	4.627	2.277	21.03	12.06	12.06	3.39	-0.0011	2.96
25.05	LZ	4.06	24.45	26.08	0.20	47.7	26.78	0.75%	23.65	4.646	2.286	17.25	9.68	9.68	0.90	0.1048	2.75
25.15	LZ	3.19	24.55	19.89	0.18	61.7	20.80	0.87%	37.53	4.665	2.295	13.13	7.03	7.03	1.12	0.2282	2.91
31.55	MX(SB)	2.38	30.25	141.57	0.51	19.3	141.85	0.36%	-10.53	5.748	2.819	84.32	48.28	81.06	0.37	-0.0076	1.75
31.70	MX(SB)	2.44	30.40	146.82	0.64	20.6	147.12	0.44%	-9.41	5.776	2.833	87.23	49.89	83.98	0.45	-0.0065	1.78
31.85	MX(SB)	2.35	30.55	120.41	1.17	21.1	120.72	0.97%	-9.09	5.805	2.847	71.36	40.37	68.11	1.02	-0.0078	2.05
32.00	MX(LZ)	5.43	31.35	37.47	0.88	34.0	37.97	2.32%	3.09	5.957	2.920	21.93	10.96	10.96	2.75	0.0095	2.94
32.10	MX(LZ)	6.14	31.45	24.70	1.23	34.7	25.21	4.88%	3.60	5.976	2.929	14.43	6.57	6.57	6.39	0.0184	3.34
32.25	DZ	4.01	31.60	93.22	2.64	10.6	93.38	2.83%	-20.63	6.004	2.943	54.34	29.69	29.69	3.02	-0.0232	2.62
32.40	DZ	4.64	31.75	45.04	1.31	2.8	45.08	2.91%	-28.54	6.033	2.957	26.19	13.21	13.21	3.35	-0.0717	2.93
32.55	DZ	5.25	31.90	47.04	1.39	4.1	47.10	2.95%	-27.37	6.061	2.971	27.29	13.81	13.81	3.39	-0.0654	2.91
32.70	DZ	5.22	32.05	41.87	1.61	4.9	41.94	3.84%	-26.78	6.090	2.985	24.24	12.01	12.01	4.49	-0.0733	3.04
32.85	DZ	4.75	32.20	61.08	1.96	12.6	61.26	3.20%	-19.25	6.118	2.998	35.27	18.39	18.39	3.55	-0.0342	2.83
32.90	DZ	5.12	32.25	61.20	2.16	9.0	61.33	3.52%	-22.83	6.128	3.003	35.32	18.38	18.38	3.91	-0.0406	2.85
40.50	LZ	6.04	40.40	30.60	0.35	64.5	31.55	1.11%	24.45	7.676	3.752	15.80	6.36	6.36	1.47	0.1005	3.01
40.55	LZ	7.01	40.45	18.23	0.37	65.4	19.19	1.93%	25.37	7.685	3.757	9.41	3.06	3.06	3.22	0.2163	3.45
40.60	LZ	6.72	40.50	18.10	0.14	75.4	19.21	0.73%	35.25	7.695	3.761	9.33	3.06	3.06	1.22	0.3003	3.26
40.65	LZ	6.03	40.55	17.29	0.20	82.9	18.51	1.08%	42.73	7.704	3.766	8.91	2.87	2.87	1.85	0.3879	3.36

APPENDIX D; PART 1 (cont'd). GRAIN SIZE TO CPT CORRELATIONS

samples		CPT parameters															
depth m	Facies	ϕ_{50}	depth m	q_c bar	F_s bar	U m H_20	q_t bar	R_f	dU m H_20	σ_{vo} bar	σ'_{vo} bar	q_{c1}	Q_t	Q	F_R	B_q	I_F
FD94-4 (cont'd)																	
40.70	LZ	5.56	40.60	18.51	0.15	89.4	19.83	0.76%	49.23	7.714	3.770	9.53	3.21	3.21	1.24	0.3987	3.24
40.75	LZ	5.64	40.65	18.06	0.14	89.8	19.38	0.72%	49.51	7.723	3.775	9.30	3.09	3.09	1.20	0.4166	3.25
40.80	LZ	5.80	40.75	19.32	0.14	102.0	20.82	0.67%	61.69	7.742	3.784	9.93	3.46	3.46	1.07	0.4627	3.19
40.85	LZ	5.91	40.80	19.12	0.17	96.6	20.54	0.83%	56.21	7.752	3.789	9.82	3.38	3.38	1.33	0.4311	3.23
40.90	LZ	5.54	40.85	17.78	0.13	105.4	19.33	0.67%	64.97	7.761	3.793	9.13	3.05	3.05	1.12	0.5509	3.24
40.95	LZ	6.04	40.90	17.82	0.11	107.3	19.40	0.57%	66.84	7.771	3.798	9.14	3.06	3.06	0.95	0.5639	3.21
41.00	LZ	6.51	40.95	16.68	0.12	113.0	18.34	0.65%	72.40	7.780	3.803	8.55	2.78	2.78	1.14	0.6725	3.28
41.05	LZ	7.43	41.00	16.92	0.18	117.9	18.65	0.96%	77.27	7.790	3.807	8.67	2.85	2.85	1.66	0.6977	3.34
41.10	LZ	6.84	41.05	19.20	0.26	120.9	20.98	1.24%	80.24	7.799	3.812	9.83	3.46	3.46	1.97	0.5973	3.30
41.15	LZ	5.02	41.10	21.89	0.54	90.4	23.22	1.38%	49.65	7.809	3.816	11.21	4.04	4.04	3.50	0.3161	3.36
41.20	LZ	5.53	41.15	21.24	0.27	92.8	22.61	2.39%	52.06	7.818	3.821	10.87	3.87	3.87	1.83	0.3454	3.24
41.25	LZ	6.09	41.25	17.86	0.12	58.7	18.72	0.64%	17.85	7.837	3.830	9.13	2.84	2.84	1.10	0.1609	3.27
41.30	LZ	6.36	41.30	19.65	0.12	65.0	20.61	0.58%	24.09	7.847	3.835	10.03	3.33	3.33	0.94	0.1852	3.18
41.35	LZ	6.39	41.35	17.70	0.14	71.0	18.74	0.75%	30.04	7.856	3.839	9.03	2.84	2.84	1.29	0.2707	3.30
41.40	LZ	6.67	41.40	17.41	0.19	77.8	18.55	1.02%	36.81	7.866	3.844	8.88	2.78	2.78	1.78	0.3378	3.36
41.45	LZ	5.60	41.45	22.62	0.19	80.1	23.80	0.80%	39.00	7.875	3.848	11.53	4.14	4.14	1.19	0.2403	3.13
41.50	LZ	6.00	41.50	20.46	0.14	83.5	21.69	0.65%	42.44	7.885	3.853	10.42	3.58	3.58	1.01	0.3016	3.16
41.55	LZ	6.48	41.55	17.70	0.10	89.0	19.01	0.53%	47.85	7.894	3.858	9.01	2.88	2.88	0.90	0.4223	3.23
41.60	LZ	5.96	41.60	17.25	0.10	96.5	18.67	0.54%	55.25	7.904	3.862	8.78	2.79	2.79	0.93	0.5035	3.25
41.65	LZ	5.78	41.65	17.09	0.12	102.6	18.60	0.65%	61.33	7.913	3.867	8.69	2.76	2.76	1.12	0.5630	3.28
41.70	LZ	6.44	41.70	16.56	0.17	107.9	18.15	0.94%	66.58	7.923	3.871	8.42	2.64	2.64	1.66	0.6388	3.37
41.75	LZ	5.62	41.80	18.47	0.21	103.9	20.00	1.05%	62.47	7.942	3.881	9.38	3.11	3.11	1.74	0.5083	3.32
41.80	LZ	6.10	41.85	17.90	0.15	109.0	19.50	0.77%	67.52	7.951	3.885	9.08	2.97	2.97	1.30	0.5734	3.28
41.85	LZ	6.19	41.90	21.64	0.13	107.0	23.21	0.56%	65.45	7.961	3.890	10.97	3.92	3.92	0.85	0.4209	3.10
41.90	LZ	6.33	41.95	18.23	0.20	108.7	19.83	1.01%	67.18	7.970	3.894	9.24	3.05	3.05	1.69	0.5557	3.32
41.95	LZ	7.40	42.00	19.04	0.17	116.2	20.75	0.82%	74.60	7.980	3.899	9.64	3.28	3.28	1.33	0.5731	3.25
42.00	LZ	5.49	42.05	23.76	0.19	87.9	25.05	0.76%	46.25	7.989	3.904	12.03	4.37	4.37	1.11	0.2659	3.10
42.05	LZ	5.56	42.10	17.41	0.56	98.6	18.86	2.97%	56.86	7.999	3.908	8.81	2.78	2.78	5.16	0.5136	3.59

APPENDIX D; PART I (cont'd). GRAIN SIZE TO CPT CORRELATIONS

samples		CPT parameters															
depth m	Facies	ϕ_{50}	depth m	q_c bar	F_s bar	U m H_20	q_t bar	R_f	dU m H_20	σ_{vo} bar	σ'_{vo} bar	q_{c1}	Q_t	Q	F_R	B_q	I_F
FD94-5																	
12.00	TSZ?	2.93	12.30	50.21	0.73	10.6	50.37	1.45%	-0.81	2.337	1.219	45.48	39.41	43.51	1.52	-0.0017	2.31
12.20	TSZ?	4.67	12.50	10.42	0.28	12.0	10.60	2.64%	0.41	2.375	1.237	9.37	6.65	6.65	3.41	0.0049	3.17
12.40	TSZ?	5.01	12.70	12.25	0.28	17.5	12.51	2.24%	5.73	2.413	1.255	10.93	8.04	8.04	2.77	0.0557	3.06
12.60	TSZ?	3.18	12.90	54.15	0.38	3.8	54.21	0.70%	-8.23	2.451	1.274	47.98	40.63	45.86	0.73	-0.0156	2.11
12.80	TSZ?	3.31	13.10	60.83	0.42	0.7	60.84	0.69%	-11.46	2.489	1.292	53.51	45.16	51.33	0.72	-0.0193	2.06
13.00	TSZ?	3.17	13.30	56.40	0.35	1.8	56.43	0.62%	-10.60	2.527	1.311	49.27	41.13	47.08	0.65	-0.0193	2.07
13.20	TSZ?	3.19	13.50	55.37	0.65	-1.7	55.35	1.17%	-14.29	2.565	1.329	48.03	39.72	45.78	1.23	-0.0266	2.23
13.40	TSZ?	2.84	13.70	69.99	0.53	-5.6	69.91	0.76%	-18.37	2.603	1.347	60.30	49.95	57.98	0.79	-0.0268	2.04
13.55	TSZ?	2.88	13.85	70.48	0.49	-1.8	70.45	0.70%	-14.70	2.632	1.361	60.41	49.83	58.13	0.72	-0.0213	2.02
13.65	TSZ?	2.92	13.95	60.38	0.53	1.5	60.40	0.88%	-11.53	2.651	1.370	51.58	42.15	49.34	0.92	-0.0196	2.13
13.75	TSZ?	4.26	14.05	25.47	0.71	-1.3	25.45	2.79%	-14.46	2.670	1.379	21.69	16.51	16.51	3.12	-0.0623	2.83
13.85	MSD	1.05	14.30	223.30	0.67	-1.0	223.28	0.30%	-14.44	2.717	1.402	188.56	157.27	186.25	0.30	-0.0064	1.39
13.95	MSD	2.17	14.40	210.30	0.75	0.8	210.31	0.36%	-12.75	2.736	1.412	177.00	147.04	174.71	0.36	-0.0060	1.45
14.05	MSD	1.52	14.50	198.70	0.62	2.5	198.74	0.31%	-11.13	2.755	1.421	166.70	137.93	164.42	0.32	-0.0056	1.45
14.15	MSD	1.28	14.60	191.20	0.77	4.5	191.27	0.40%	-9.21	2.774	1.430	159.89	131.81	157.62	0.41	-0.0048	1.52
14.25	MSD	1.46	14.70	152.00	0.60	4.4	152.06	0.39%	-9.42	2.793	1.439	126.70	103.72	124.43	0.40	-0.0062	1.60
14.45	MSD	2.08	14.90	133.10	0.57	13.3	133.30	0.43%	-0.69	2.831	1.458	110.24	89.51	108.06	0.44	-0.0005	1.67
14.65	MSD	2.12	15.10	138.90	0.75	12.4	139.08	0.54%	-1.84	2.869	1.476	114.33	92.29	112.12	0.55	-0.0013	1.71
14.85	MSD	2.13	15.30	178.90	0.64	15.2	179.12	0.36%	0.77	2.907	1.494	146.35	117.92	144.15	0.36	0.0004	1.53
15.05	MSD	2.16	15.50	137.20	0.59	12.7	137.39	0.43%	-1.91	2.945	1.513	111.55	88.87	109.31	0.44	-0.0014	1.67
15.40	MSD	2.22	15.70	115.40	0.69	12.0	115.58	0.60%	-2.79	2.983	1.531	93.26	73.54	90.99	0.61	-0.0024	1.82
15.62	MSD	2.18	15.80	112.60	0.68	11.5	112.77	0.60%	-3.37	3.002	1.540	90.73	71.26	88.44	0.62	-0.0030	1.83
15.80	MSD	1.43	15.95	177.90	0.38	6.6	178.00	0.21%	-8.41	3.031	1.554	142.70	112.58	140.35	0.22	-0.0047	1.44
16.00	MSD	1.64	16.15	111.50	0.48	11.6	111.67	0.43%	-3.70	3.069	1.572	88.92	69.06	86.61	0.44	-0.0033	1.76
16.13	LS	5.67	16.30	28.27	0.53	17.0	28.52	1.86%	1.60	3.097	1.586	22.45	16.03	16.03	2.08	0.0062	2.74
16.30	LS	2.47	16.45	106.60	0.61	1.7	106.62	0.57%	-2.78	2.007	1.570	85.07	66.62	83.48	0.58	-0.0026	1.84
FD94-6																	
2.80	LOZ	6.19	2.45	3.74	0.08	-1.2	3.72	2.15%	-2.37	0.466	0.353	6.30	9.23	9.23	2.46	-0.0714	2.98
3.10	LOZ	6.83	2.75	5.53	0.13	-1.2	5.51	2.36%	-2.64	0.523	0.380	8.97	13.12	13.12	2.61	-0.0519	2.86

APPENDIX D; PART 1 (cont'd). GRAIN SIZE TO CPT CORRELATIONS

samples		CPT parameters															
depth m	Facies	ϕ_{50}	depth m	q_c bar	F_s bar	U m H_20	q_t bar	R_f	dU m H_20	σ_{vo} bar	σ'_{vo} bar	q_{c1}	Q_t	Q	F_R	B_q	I_F
FD94-6 (cont'd)																	
3.40	LOZ	6.21	3.05	3.21	0.04	0.4	3.22	1.24%	-1.31	0.580	0.408	5.03	6.47	6.47	1.52	-0.0487	3.01
3.70	LOZ	6.62	3.35	3.54	0.05	1.0	3.56	1.41%	-1.03	0.637	0.435	5.36	6.70	6.70	1.71	-0.0346	3.02
4.00	LOZ	6.17	3.65	3.66	0.05	1.5	3.68	1.36%	-0.86	0.694	0.463	5.38	6.45	6.45	1.67	-0.0282	3 03
4.30	LOZ	5.38	3.95	2.65	0.03	3.5	2.70	1.11%	0.83	0.751	0.491	3.78	3.98	3.98	1.54	0.0417	3.20
4.60	LOZ	5.22	4.25	3.34	0.04	4.3	3.40	1.18%	1.30	0.808	0.518	4.64	5.01	5.01	1.54	0.0491	3.11
4.90	LOZ	4.83	4.55	5.98	0.14	2.6	6.02	2.33%	-0.66	0.865	0.546	8.10	9.44	9.44	2.72	-0.0126	2.99
6.45	MSSF	2.06	5.90	87.17	0.22	-3.8	87.11	0.25%	-8.41	1.121	0.670	106.52	128.40	105.08	0.26	-0.0096	1.58
6.65	MSSF	2.15	6.10	151.10	0.57	-5.4	151.02	0.38%	-10.16	1.159	0.688	182.15	217.78	180.66	0.38	-0.0067	1.45
6.76	MSSF	4.36	6.20	146.17	0.57	-5.0	146.10	0.39%	-9.93	1.178	0.697	175.04	207.82	173.54	0.39	-0.0067	1.48
6.85	MSSF	2.09	6.30	157.08	0.46	-4.5	157.01	0.29%	-9.53	1.197	0.707	186.88	220.55	185.38	0.30	-0.0060	1.39
7.05	MSSF	1.67	6.50	213.85	0.45	-4.0	213.79	0.21%	-9.20	1.235	0.725	251.17	293.23	249.66	0.21	-0.0042	1.20
7.25	MSSF	1.46	6.70	224.02	0.61	-2.6	223.98	0.27%	-7.96	1.273	0.743	259.85	299.64	258.33	0.27	-0.0035	1.25
7.45	MSSF	2.01	6.90	218.77	0.30	-1.5	218.75	0.14%	-7.09	1.311	0.762	250.68	285.49	249.15	0.14	-0.0032	1.13
7.65	MSSF	1.62	7.10	206.32	0.34	-1.7	206.29	0.16%	-7.53	1.349	0.780	233.61	262.74	232.05	0.17	-0.0036	1.19
7.85	MSSF	2.15	7.30	204.89	0.38	-1.0	204.87	0.19%	-7.03	1.387	0.798	229.30	254.87	227.73	0.19	-0.0034	1.22
8.05	MSSF	2.11	7.50	198.75	0.46	-1.1	198.73	0.23%	-7.32	1.425	0.817	219.91	241.57	218.32	0.23	-0.0036	1.27
9.05	MSSF	1.80	8.00	176.29	0.41	1.5	176.31	0.23%	-5.24	1.520	0.863	189.80	202.60	188.18	0.23	-0.0029	1.33
9.25	MSSF	1.82	8.20	173.40	0.32	2.0	173.43	0.18%	-4.95	1.558	0.881	184.73	195.06	183.10	0.19	-0.0028	1.30
9.45	MSSF	2.09	8.40	164.77	0.58	1.2	164.79	0.35%	-5.91	1.596	0.899	173.73	181.43	172.07	0.36	-0.0036	1.46
9.65	MSSF	2.13	8.60	141.78	0.60	1.5	141.80	0.42%	-5.80	1.634	0.918	147.99	152.71	146.30	0.43	-0.0041	1.56
9.85	MSSF	2.16	8.80	104.99	0.39	5.4	105.07	0.37%	-2.10	1.672	0.936	108.51	110.44	106.86	0.38	-0.0020	1.65
10.05	MSSF	2.19	9.00	128.06	0.47	6.3	128.15	0.37%	-1.44	1.710	0.955	131.07	132.45	129.41	0.37	-0.0011	1.57
10.25	MSSF	1.97	9.20	123.38	0.45	6.9	123.48	0.36%	-0.98	1.748	0.973	125.08	125.11	123.41	0.37	-0.0008	1.59
10.45	MSSF	2.21	9.40	108.69	0.44	7.3	108.80	0.40%	-0.81	1.786	0.991	109.16	107.94	107.47	0.41	-0.0007	1.66
10.65	MSSF	2.70	10.05	64.42	0.25	8.7	64.55	0.39%	-0.03	1.910	1.051	62.83	59.59	61.10	0.40	0.0000	1.87
10.85	MSSF	2.48	10.25	57.70	0.26	9.0	57.83	0.45%	0.02	1.948	1.070	55.79	52.25	54.04	0.47	0.0000	1.95
11.05	MSSF	2.48	10.45	71.46	0.25	8.9	71.59	0.35%	-0.27	1.986	1.088	68.51	63.98	66.73	0.36	-0.0004	1.82
11.25	MSSF	2.29	10.65	93.43	0.34	8.8	93.56	0.36%	-0.60	2.024	1.106	88.83	82.74	87.03	0.37	-0.0006	1.72

APPENDIX D; PART 1 (cont'd). GRAIN SIZE TO CPT CORRELATIONS

samples		CPT parameters															
depth m	Facies	ϕ_{50}	depth m	q_c bar	F_s bar	U m H_20	q_t bar	R_f	dU m H_20	σ_{vo} bar	σ'_{vo} bar	q_{c1}	Q_t	Q	F_R	B_q	I_F
FD94-6 (cont'd)																	
11.45	MSSF	2.37	10.85	124.40	0.24	9.0	124.53	0.19%	-0.55	2.062	1.125	117.30	108.90	115.48	0.20	-0.0004	1.50
18.15	MSSB	2.26	17.65	171.81	0.43	15.9	172.04	0.25%	-0.45	3.354	1.750	129.89	96.42	127.53	0.25	-0.0003	1.50
18.55	MSSB	2.21	18.05	130.14	0.40	14.4	130.35	0.31%	-2.37	3.430	1.786	97.37	71.05	94.96	0.32	-0.0018	1.66
18.95	MSSB	1.93	18.45	111.50	0.36	16.8	111.75	0.32%	-0.32	3.506	1.823	82.58	59.77	80.17	0.33	-0.0003	1.73
19.35	MSSB	2.01	18.85	143.61	0.47	16.3	143.85	0.33%	-1.29	3.582	1.860	105.30	75.42	102.85	0.34	-0.0009	1.64
19.75	MSSB	1.61	19.25	153.70	0.49	14.6	153.91	0.32%	-3.38	3.658	1.897	111.61	79.22	109.11	0.33	-0.0022	1.61
20.15	MSSB	1.86	19.65	150.73	0.51	16.1	150.97	0.34%	-2.28	3.734	1.933	108.40	76.15	105.89	0.35	-0.0015	1.63
20.55	MSSB	2.20	20.05	200.21	0.47	17.5	200.47	0.23%	-1.23	3.810	1.970	142.64	99.82	140.11	0.24	-0.0006	1.45
20.95	MSSB	1.91	20.45	225.69	0.47	11.7	225.86	0.21%	-7.48	3.886	2.007	159.31	110.61	156.69	0.21	-0.0033	1.39
21.25	MSSB	2.18	20.75	210.92	0.31	1.9	210.95	0.15%	-17.56	3.943	2.034	147.87	101.75	145.13	0.15	-0.0083	1.37
21.55	MSSB	1.80	21.05	227.80	0.61	9.8	227.94	0.27%	-9.92	4.000	2.062	158.64	108.60	155.95	0.27	-0.0043	1.44
21.89	MSSB	2.12	21.35	203.51	0.84	-1.7	203.48	0.41%	-21.77	4.057	2.090	140.78	95.44	137.96	0.42	-0.0107	1.58
21.94	LS(LZ)	5.60	21.45	57.99	1.34	-0.9	57.98	2.31%	-21.02	4.076	2.099	40.03	25.68	25.68	2.49	-0.0383	2.62
K2V2																	
9.20	MSSF	2.76	8.85	25.96	0.29	7.3	26.10	1.12%	0.49	1.682	1.010	25.84	24.19	24.31	1.20	0.0020	2.46
9.45	MSSF	1.05	9.10	88.54	0.30	1.0	88.56	0.34%	-6.07	1.729	1.032	87.14	84.10	85.45	0.34	-0.0069	1.71
9.60	MSSF	2.27	9.25	71.00	0.41	-0.6	70.99	0.58%	-7.84	1.758	1.046	69.41	66.17	67.68	0.59	-0.0111	1.92
9.66	MSSF	0.92	9.31	86.63	0.52	0.9	86.65	0.60%	-6.41	1.769	1.052	84.47	80.70	82.76	0.61	-0.0074	1.85
9.85	MSSF	1.09	9.50	139.36	0.69	5.9	139.48	0.50%	-1.59	1.805	1.069	134.77	128.75	133.14	0.50	-0.0011	1.63
10.05	MSSF	0.59	9.70	198.77	0.89	7.7	198.92	0.44%	-0.03	1.843	1.088	190.59	181.20	188.97	0.45	0.0000	1.48
10.25	MSSF	1.10	9.90	149.09	0.54	5.9	149.21	0.36%	-1.97	1.881	1.106	141.76	133.20	140.09	0.36	-0.0013	1.54
10.45	MSSF	1.12	10.10	95.74	0.43	7.6	95.89	0.45%	-0.51	1.919	1.124	90.29	83.57	88.62	0.46	-0.0005	1.76
10.65	MSSF	1.08	10.30	164.92	0.77	8.3	165.08	0.46%	0.04	1.957	1.143	154.27	142.75	152.60	0.47	0.0000	1.56
11.65	MSSF	1.79	11.43	107.75	0.42	9.5	107.94	0.39%	0.10	2.171	1.246	96.52	84.87	94.75	0.39	0.0001	1.70
11.90	MSSF	1.46	11.78	113.40	0.48	8.1	113.56	0.43%	-1.65	2.237	1.278	100.30	87.08	98.46	0.43	-0.0014	1.71
12.15	MSSF	1.47	12.08	134.32	0.51	9.9	134.51	0.38%	-0.19	2.294	1.306	117.54	101.25	115.70	0.38	-0.0001	1.62
12.40	MSSF	2.15	12.33	92.33	0.44	8.9	92.50	0.47%	-1.43	2.342	1.329	80.09	67.85	78.21	0.48	-0.0016	1.82
12.65	MSSF	2.12	12.58	95.74	0.48	9.6	95.93	0.50%	-0.94	2.389	1.352	82.34	69.19	80.45	0.51	-0.0010	1.82

APPENDIX D; PART 1 (cont'd). GRAIN SIZE TO CPT CORRELATIONS

samples		CPT parameters															
depth m	Facies	ϕ_{50}	depth m	q_c bar	F_s bar	U m H_20	q_t bar	R_f	dU m H_20	σ_{vo} bar	σ'_{vo} bar	q_{c1}	Q_t	Q	F_R	B_q	I_F
K2V2 (cont'd)																	
12.90	MSSF	2.17	12.83	90.21	0.44	10.1	90.41	0.49%	-0.74	2.437	1.375	76.94	63.99	75.03	0.50	-0.0008	1.84
13.15	MSSF	2.17	13.08	117.07	0.56	11.1	117.29	0.48%	0.03	2.484	1.398	99.02	82.13	97.10	0.49	0.0000	1.74
13.40	MSSF	2.15	13.33	118.86	0.60	9.3	119.04	0.50%	-2.04	2.532	1.421	99.72	82.01	97.75	0.51	-0.0017	1.75
13.65	MSSF	2.20	13.58	90.05	0.49	8.1	90.21	0.54%	-3.46	2.579	1.444	74.94	60.70	72.93	0.56	-0.0039	1.87
17.75	MSSF	1.84	17.98	114.26	0.50	15.3	114.56	0.43%	-0.65	3.415	1.848	84.05	60.14	81.76	0.45	-0.0006	1.78
18.15	MSSF	1.85	18.38	134.16	0.54	14.8	134.45	0.40%	-1.62	3.491	1.885	97.72	69.48	95.39	0.41	-0.0012	1.71
18.55	MSSF	1.84	18.78	98.10	0.37	12.7	98.35	0.38%	-4.10	3.567	1.922	70.77	49.32	68.37	0.39	-0.0042	1.83
18.95	MSSF	1.93	19.18	119.79	0.53	15.5	120.09	0.44%	-1.72	3.643	1.958	85.60	59.46	83.21	0.45	-0.0014	1.78
19.35	MSSF	1.70	19.58	137.45	0.66	16.7	137.78	0.48%	-0.88	3.719	1.995	97.31	67.19	94.91	0.49	-0.0006	1.75
19.55	MSSF	1.84	19.78	198.04	0.81	15.2	198.34	0.41%	-2.60	3.757	2.014	139.56	96.64	137.13	0.41	-0.0013	1.57
19.75	MSSF	1.61	19.98	173.95	0.77	12.3	174.19	0.44%	-5.64	3.795	2.032	122.03	83.86	119.54	0.45	-0.0032	1.64
19.95	MSSF	2.00	20.18	153.97	0.58	15.0	154.26	0.38%	-3.19	3.833	2.050	107.53	73.37	105.06	0.39	-0.0021	1.66
20.15	MSSF	1.83	20.38	134.28	0.59	12.2	134.52	0.44%	-6.14	3.871	2.069	93.36	63.16	90.84	0.45	-0.0046	1.75
DT13																	
21.33	MSSF	0.87	21.08	115.80	0.25	18.6	116.16	0.22%	-0.27	4.004	2.153	78.93	52.10	76.45	0.22	-0.0002	1.69
21.52	MSSF	1.04	21.28	137.30	0.24	19.1	137.67	0.17%	0.03	4.042	2.171	93.18	61.55	90.69	0.18	0.0000	1.59
21.72	MSSF	1.10	21.48	130.20	0.24	19.1	130.57	0.18%	-0.18	4.080	2.189	87.99	57.78	85.49	0.19	-0.0001	1.62
21.92	MS	1.87	21.68	96.30	0.20	19.1	96.67	0.21%	-0.38	4.118	2.208	64.81	41.92	62.29	0.22	-0.0004	1.76
22.12	MS	1.87	21.88	146.40	0.20	11.6	146.63	0.14%	-8.08	4.156	2.226	98.12	64.00	95.49	0.14	-0.0056	1.53
22.32	MS	1.90	22.08	188.10	0.45	13.6	188.37	0.24%	-6.28	4.194	2.245	125.55	82.05	122.93	0.24	-0.0033	1.51
22.52	MS	1.82	22.28	177.00	0.34	18.4	177.36	0.19%	-1.68	4.232	2.263	117.66	76.51	115.09	0.20	-0.0009	1.50
22.72	MS	1.60	22.48	210.90	0.43	17.5	211.24	0.20%	-2.78	4.270	2.281	139.63	90.73	137.03	0.21	-0.0013	1.44
22.98	MS	2.14	22.73	131.50	0.18	18.8	131.87	0.14%	-1.73	4.318	2.304	86.63	55.35	84.03	0.14	-0.0013	1.59

APPENDIX D. GRAIN SIZE TO CPT CORRELATIONS
PART 2; 15 cm^2 cone (see list of symbols)

samples		CPT parameters															
depth m	Facies	ϕ_{50}	depth m	q_c bar	F_s bar	U m H_20	q_t bar	R_f	dU m H_20	σ_{vo} bar	σ'_{vo} bar	q_{c1}	Q_t	Q	F_R	B_q	I_F
FD95S-1																	
40.23	MX	2.60	40.75	121.35	0.99	3.7	121.40	0.82%	-32.1	7.743	4.235	58.96	26.84	55.23	0.87	-0.0277	2.08
40.33	MX	2.92	40.85	98.40	1.26	4.3	98.46	1.28%	-31.6	7.762	4.245	47.76	21.37	44.02	1.39	-0.0341	2.28
40.43	MX	2.78	40.95	90.10	0.9	2.1	90.13	1.00%	-33.8	7.781	4.254	43.69	19.36	39.93	1.09	-0.0403	2.25
62.50	SB	2.65	63.45	130.26	1.04	42.2	130.88	0.79%	-16.3	12.056	6.322	51.81	18.80	47.26	0.88	-0.0134	2.14
63.00	SB	2.08	63.95	125.80	0.94	49.4	126.53	0.74%	-9.6	12.151	6.368	49.85	17.96	45.33	0.82	-0.0082	2.14
65.51	SB	1.98	66.90	152.54	0.93	55.3	153.35	0.61%	-6.6	12.711	6.639	59.20	21.19	54.59	0.66	-0.0046	2.02
65.71	SB	1.92	67.10	136.55	0.91	57.6	137.40	0.66%	-4.5	12.749	6.657	52.92	18.72	48.31	0.73	-0.0035	2.09
65.86	SB	1.98	67.25	151.81	0.89	57.6	152.66	0.58%	-4.7	12.778	6.671	58.78	20.97	54.16	0.64	-0.0033	2.02
65.86	SB	1.95	67.25	151.81	0.89	57.6	152.66	0.58%	-4.7	12.778	6.671	58.78	20.97	54.16	0.64	-0.0033	2.02
66.01	SB	2.42	67.50	91.38	1.85	16.1	91.62	2.02%	-46.4	12.825	6.694	35.32	11.77	11.77	2.35	-0.0578	2.88
66.46	SB	2.49	67.95	104.99	1.21	3.4	105.04	1.15%	-59.6	12.911	6.735	40.46	13.68	13.68	1.31	-0.0634	2.69
66.86	SB	2.36	68.25	192.16	1.27	6.7	192.26	0.66%	-56.6	12.968	6.763	73.89	26.51	68.94	0.71	-0.0309	1.95
67.15	SB	2.92	68.55	154.98	1.56	7.2	155.09	1.01%	-56.4	13.025	6.790	59.47	20.92	54.52	1.10	-0.0389	2.14
67.30	SB	2.54	68.70	163.10	1.34	8.1	163.22	0.82%	-55.6	13.053	6.804	62.53	22.07	57.57	0.89	-0.0363	2.07
67.75	SB	2.72	69.15	154.52	1.17	39.3	155.10	0.75%	-24.8	13.139	6.845	59.06	20.74	54.26	0.82	-0.0172	2.07
67.90	SB	2.41	69.30	150.80	1.27	46.6	151.49	0.84%	-17.7	13.167	6.859	57.58	20.17	52.81	0.92	-0.0126	2.11
68.05	SB	2.46	69.45	145.79	1.19	49.9	146.52	0.81%	-14.5	13.196	6.873	55.61	19.40	50.86	0.89	-0.0107	2.12
73.44	BS	3.67	74.60	55.88	1.56	11.3	56.05	2.78%	-58.3	14.174	7.346	20.62	5.70	9.38	3.73	-0.1367	3.25
79.65	BS	3.35	81.00	67.35	1.54	60.3	68.24	2.26%	-15.8	15.390	7.934	23.91	6.66	11.18	2.91	-0.0292	3.14
79.85	BS	2.85	81.20	108.86	1.41	18.3	109.13	1.29%	-58.0	15.428	7.953	38.60	11.78	11.78	1.50	-0.0607	2.78
79.95	BS	2.72	81.30	122.23	1.93	17.6	122.49	1.58%	-58.7	15.447	7.962	43.32	13.44	13.44	1.80	-0.0538	2.77
80.05	BS	2.94	81.40	137.12	1.37	4.3	137.18	1.00%	-72.1	15.466	7.971	48.57	15.27	15.27	1.13	-0.0581	2.62
80.15	BS	2.84	81.50	138.34	1.46	3.8	138.40	1.05%	-72.7	15.485	7.980	48.97	15.40	15.40	1.19	-0.0580	2.62
82.45	BS	3.60	83.80	154.15	1.58	0.8	154.16	1.02%	-78.1	15.922	8.192	53.86	16.88	48.30	1.14	-0.0554	2.20
82.65	BS	3.45	84.00	154.34	1.86	15.9	154.57	1.20%	-63.1	15.960	8.210	53.86	16.88	16.88	1.34	-0.0447	2.62
82.68	BS	3.11	84.05	151.10	1.33	7.7	151.21	0.88%	-71.3	15.970	8.215	52.72	16.46	47.19	0.98	-0.0517	2.17
83.22	BS	3.49	84.55	134.74	1.48	-0.3	134.74	1.10%	-79.9	16.065	8.261	46.88	14.37	14.37	1.25	-0.0660	2.66

APPENDIX D; PART 2 (cont'd). GRAIN SIZE TO CPT CORRELATIONS																	
samples		CPT parameters															
depth m	Facies	ϕ_{50}	depth m	q_c bar	F_s bar	U m H_20	q_t bar	R_f	dU m H_20	σ_{vo} bar	σ'_{vo} bar	q_{c1}	Q_t	Q	F_R	B_q	I_F
FD95S-1 (cont'd)																	
83.33	BS	3.87	84.65	115.76	1.77	-1.9	115.73	1.53%	-81.5	16.084	8.270	40.25	12.05	12.05	1.78	-0.0803	2.80
83.42	BS	3.87	84.75	113.07	2.04	-2.1	113.04	1.80%	-81.8	16.103	8.279	39.30	11.71	11.71	2.10	-0.0828	2.85
88.515	BS	5.09	89.95	66.99	1.45	3.6	67.04	2.16%	-81.3	17.091	8.757	22.64	5.70	9.81	2.90	-0.1597	3.19
88.59	BS	2.90	90.05	73.58	1.19	17.3	73.84	1.61%	-67.7	17.110	8.766	24.85	6.47	11.13	2.10	-0.1171	3.07
88.89	BS	3.15	90.35	93.97	1.05	34.7	94.48	1.11%	-50.6	17.167	8.794	31.69	8.79	8.79	1.36	-0.0643	2.87

Appendix E

Tests of the Variability in CPT Data in Uniform Layers At Five Sites

In order to assess the repeatability of the CPT data in the Fraser delta, data were compared at five sites: Kidd 2 (borehole K2V2), Coast Guard Radio Tower (borehole FD94-4), Hamilton Interchange (eastern Lulu Island; Figure 6-9), Westbridge (across the river form borehole FD92-5) and Deas Island (FD94-1). At each site, data from the same depth intervals were compared to remove the effects of overburden stress on CPT measurements. The mean and standard deviation were computed for the CPT measurements in each these intervals. CPTs compared were operated by ConeTec, UBC, MOTH and Hughes. ConeTec, UBC and Hughes manufacture their own penetrometers. MOTH uses penetrometers manufactured by Hogentogler, and at one site UBC used a Hogentogler penetrometer. CPT parameters compared are cone bearing corrected for water pressure (q_t), friction ratio (R_f), sleeve friction and excess pore pressure (dU).

Kidd 2

At the Kidd 2 site, CPT data were compared in the topset massive sand and the underlying foreset silts. The foreset silts generally lack sand interbeds and are interpreted to be uniform across the site (Figure 6-21; Monahan et al., 1995b, 1997).

Data from 11 CPTs were compared. Of these, one was operated by ConeTec, 5 were operated by UBC and 5 were operated by Hughes. Two of the UBC CPTs used penetrometers manufactured by Hogentogler. Intervals compared in these CPTs were from 12 to 17 m in the topset massive sand, and from 22 to 24 and from 25 to 27 m in the foreset silts. Mean CPT readings were not computed in the silt intervals in all CPTs: in 3 CPTs, sandy interbeds occur in the interval from 22 to 24 m, and 2 CPTs do not reach 27 m. The results are summarized in Tables E1 to E3.

In each CPT, q_t is very uniform in the silt intervals (Table E1; Figure 4-2a); standard deviations are generally less than 1 bar, indicating that the deposit is uniform, at least within each CPT. However, mean q_t in each CPT varies from 6.8 to 11.3 bars, a range of 4.5 bars. The lowest mean q_t is in the CPT operated by ConeTec. The range in mean q_t in the other CPTs is 2.5 bars. The range of mean q_t is similar in the UBC and Hughes CPTs. In the sand interval from 12-17, mean q_t falls into two groups: one ~90 bars that includes all CPTs in the southern part of the site, and the other ~140 bars. These differences reflect the natural variability in the topset massive sand across the site and do not reflect differences between operators. Mean q_t in the entire massive sand shows less variation between CPTs, but more variation within each CPT, and the ranges as defined by 1 standard deviation overlap. No difference between operator can be discerned.

R_f values are more variable than cone bearing (Table E2; Figure 4-2b). In the silt intervals, mean R_f varies from 0.27% to 4.03%. However, the variability within each CPT (i.e. standard deviation) is low, and there is little overlap in the R_f values between CPTs. The variation in mean R_f between CPTs is primarily due to variation in sleeve friction measurements (f_s); mean f_s correlates well with mean R_f (R^2 = 0.98). The lowest mean R_f in these CPTs are in the Hogentogler penetrometers, followed in increasing order by ConeTec, UBC and Hughes. In the sand interval, mean R_f in the UBC and ConeTec CPTs varies between 0.26 and 0.56%. Here too, the standard deviation in each CPT is very low (generally <0.06%), so that there is little overlap in the R_f values between CPTs, and in each CPT the R_f curve is very uniform. However, the variation in R_f in the Hughes CPTs is greater than in the UBC and ConeTec CPTs, so that a less smooth curve is generated.

dU values are consistently greater in the ConeTec and UBC CPTs than in the Hughes CPTs in both the silt and sand intervals (Table E3). In the ConeTec and UBC CPTs, average dU values for the U_2 position are within 1 m of each other in the silt intervals, although the standard deviations are up to 8 m.

Coast Guard Radio Tower

At the Coast Guard Radio Tower site, CPT data from 3 ConeTec CPTs were compared in three intervals of the topset: in the peat facies, which is less than 1 metre thick; in an interval between 2 and 3 m in the organic silt facies, which is interpreted to be uniform across the site; and the topset massive sand, which is approximately 20 m here (Tables E4 to E7; Figure 6-4).

Variation in q_t in the organic silt in each CPT is low (standard deviation = 0.2 to 0.6 bar), indicating that at each CPT it is uniform (Table E4). However, mean q_t in SCPT 14 is 1.5 and 1.7 bars lower than in SCPTs 15 and 16 respectively. Although the massive sand is variable across the site, the variation in mean q_t in the different CPTs is proportionately less than in the organic silt unit, and the range in q_t values (as defined by st andard deviations) in the 3 CPTs overlap. q_t in the peat facies varies considerably both within and between CPTs.

R_f values are consistently highest in SCPT 14 and, with the exception of the organic silt, lowest in SCPT 16 (Table E5). However, in the organic silt, mean sleeve friction values vary only from 0.02 to 0.03 bars, which are near the limits of sleeve friction measurement (0.01 bars; Table E6). The relatively high mean R_f in the organic silt in SCPT 14 (1.3%) is due to the *combination* of high sleeve friction (mean=0.03 bars) and low q_t (mean=2.6 bars) in this interval.

Mean dU values in the organic silt vary from 2.7 to 3.6 m, and standard deviations vary from 0.3 to 0.4 m (Table E7). In the sand unit the variation is similar, from -0.6 to -1.2 m, but the standard deviation is much greater - up to 2.5 m.

Hamilton Interchange

At Hamilton interchange two CPTs directly adjacent to each other were compared (91-9 and 91-9b; CPT 91-9b is shown in Figures 6-1, 6-9 and 6-10). The CPTs were operated by

MOTH and the penetrometers were manufactured by Hogentogler. Three intervals were compared: peat between 5.5 and 7.5 m, organic silt between 10 and 15 m, and the topset massive sand between 19 and 24 m.

Mean q_t is consistently higher in SCPT 91-9, by 2.4 bars in the peat, by 0.6 bars in the organic silt, and by 3 bars in the sand (Table E8). However, the difference is proportionately less in the sand unit, in which the absolute values of q_t are greater.

Mean R_f values are consistently lower in SCPT 91-9 (Table E9), although there is overlap between the CPTs. In the peat interval, the lower R_f in SCPT 91-9 is due to entirely to lower mean cone bearing - the sleeve friction is higher there than in CPT 91-9b (Table E10). In the other intervals, the lower mean R_f is due to both lower sleeve friction as well as higher mean q_t.

Mean dU vary by 0.5 to 2.8 m between the two CPTs in the intervals compared (Table E11).

Westbridge

CPT data were compared in organic silts in two CPTs operated by MOTH at Westbridge (Table E12). Mean q_t varies by 4 bars in these CPTs, whereas standard deviations are 1.0 and 1.5 bars respectively, indicating uniform deposits. Mean sleeve friction values are close, so that the difference in mean R_f values is due to the difference in q_t. dU values are within 1 m of each other.

Deas Island

At the Deas Island CANLEX site, 7 CPTs in the topset massive sand were compared. One CPT was operated by ConeTec, and the remainder were operated by UBC. The objective of this comparison is to see if the ConeTec CPT differs from the UBC CPTs. Although the topset sand is a variable deposit, these CPTs were all located within 9 m of each other. The mean CPT parameters in ConeTec CPT fall within the range of mean CPT parameters

established by the UBC CPTs across the site.

Discussion and Conclusions

The variation in q_t between CPTs in the apparently uniform silts compared here is generally less than 3 bars. Although the sands are more variable than the silts, mean q_t values are similar across the sites studied here. At Hamilton, where two adjacent CPTs were compared, the difference in mean q_t is 3 bars. These observations are consistent with conclusions of Schaap and Zuidberg (1982) and Lunne et al. (1986) that the most significant errors in q_t are due to a zero shift that has a proportionately greater affect in soft normally consolidated silts with low q_t than in other sediments where q_t is higher. All penetrometers evaluated generate similar q_t readings. The low q_t in the ConeTec CPT at Kidd 2 is anomalous compared to other ConeTec CPTs; B_q in this CPT is anomalously high due to the low q_t (Appendix H, part 7).

In contrast, R_f values are less repeatable than cone bearing measurements in both the sands and silts compared here, consistent with conclusions of Lunne et al. (1986) and Robertson (1990). Although R_f values are generally very uniform within the silt or sand interval in each CPT (i.e. low standard deviation), they display much greater variability between CPTs, and there may be little overlap in R_f values in different CPTs. For example, mean R_f can vary in apparently uniform silt from $0.3\pm0.1\%$ to $2.3\pm0.1\%$ in different CPTs performed by the same operator (Figure 4-2b). In peat, mean R_f can vary from 3% to 5.2% in different CPTs in a site. Consequently, data from adjacent CPTs can plot in different soil types on the soil classification chart (Figure 3-3), particularly in silt and organic rich soils intervals where the range in R_f values is high. The variation in R_f values is due largely to variations in sleeve friction measurements, as at Kidd 2 m. Furthermore, sleeve friction measurements in silts are commonly very low, near the limits of resolution. However, R_f variation can also be the result of variation in q_t, such as Coast Guard Radio Tower, Hamilton and Westbridge. On this basis, R_f values in a particular CPT are meaningful relative to other friction ratio measurements in that CPT, and can be used for interpretation qualitatively. However,

caution should be exercised in using R_f values for quantitative analysis at a site.

R_f values and their variability (i.e. standard deviation) are similar the ConeTec, UBC, and Hogentogler penetrometers. Although in the silts at Kidd 2, there is a trend of increasing R_f from Hogentogler through ConeTec to UBC, at Deas Island the UBC and ConeTec penetrometers produce similar R_f values, and the range in mean R_f in peat in the ConeTec and Hogentogler penetrometers is similar. The exception is the Hughes penetrometer, in which the range of R_f values is greater in uniform deposits, This is demonstrated in the topset massive sands at Kidd 2, where the R_f standard deviation is between 0.1% and 0.25% in the Hughes CPTs, but is generally less than 0.06% in the others.

Mean dU in uniform deposits are generally repeatable within 1 m of water for the ConeTec, Hogentogler and UBC cones compared here. However, larger variation is observed in the sands at Hamilton, where two adjacent CPTs were compared. The dU values from the Hughes CPTs compared here are consistently lower than those of the other operators.

Table E1: Mean cone bearing (qt)± 1 standard deviation (bars); Kidd 2

CPT	OPERATOR	sand	sand 12-17 m	silt 22-24 m	silt 25-27 m
4F 92-180	ConeTec	116±44	138±29	6.8±1.0	
KD9301	UBC (HOG)	95±44	91±15		11.6±0.6
k9311	UBC (HOG)	113±44	144±20	10.4±0.4	11.3±0.5
kd9302*	UBC	102±40	93±21		10.1±0.3
KD9308*	UBC	104±33	91±24	8.7±0.4	
K9309	UBC	83±45	87±20	9.8±0.9	10.3±0.5
cpt9301 A	Hughes	113±50	138±25	10.7±0.4	11.0±0.6
cpt9302 B	Hughes	96±39	132±19	11.3±0.8	11.2±0.3
cpt9303 C	Hughes	89±35	83±24	10.7±1.6	11.3±1.5
cpt9304 D	Hughes	115±41	122±26	8.7±0.3	9.4±0.3
cpt9305 E	Hughes	119±45	150±27	10.2±0.3	10.5±1.1

* Pore pressure element in U3 position

Table E2: Mean friction ratio (Rf) ± 1 standard deviation; Kidd 2

CPT	OPERATOR	sand 12-17 m	silt 22-24 m	silt 25-27 m
4F 92-180	ConeTec	0.29±0.05%	0.9±0.3%	
KD9301	UBC (HOG)	0.39±0.06%		0.4±0.1%
k9311	UBC (HOG)	0.26+0.04%	0.5±0.1%	0.3+0.1%
kd9302*	UBC	0.49±0.04%		1.4±0.1%
KD9308*	UBC	0.40±0.05%	1.3±0.1%	
K9309	UBC	0.56±0.14%**	2.3±0.2%	2.3±0.1%
cpt9301 A	Hughes	0.17±0.12%	1.5±0.1%	1.9±0.5%
cpt9302 B	Hughes	0.55±0.25%	3.4±0.6%	3.3±0.3%
cpt9303 C	Hughes	0.51±0.15%	4.0±0.7%	3.0±1.6%
cpt9304 D	Hughes	0.43±0.17%	2.0±0.2%	1.9±0.1%
cpt9305 E	Hughes	0.36±0.10%	2.3+0.6%	2.5±1.3%

* Pore pressure element in U3 position

** silt interbeds contribute to higher mean and standard deviation

Table E3: Mean excess pore pressure (dU) ± 1 standard deviation (m. of water); Kidd 2

CPT	OPERATOR	sand 12-17 m	silt 22-24 m	silt 25-27 m
4F 92-180	ConeTec	-2.6±1.4	51.0±4.9	
KD9301	UBC (HOG)	-0.2±0.3		56.8±8.5
k9311	UBC (HOG)	-0.4±1.6	52.1±2.5	57.4±8.1
kd9302*	UBC	-1.0+1.1		42.9±2.2
KD9308*	UBC	-0.6±0.9	39.0±2.0	
K9309	UBC	-0.8±0.5	48.1±4.3	55.2±6.0
cpt9301 A	Hughes	-9.3±0.8	39.1±6.0	53.7+1.3
cpt9302 B	Hughes	-6.0±1.2	44.4±2.0	49.2±1.8
cpt9303 C	Hughes	-3.3±0.9	34.3±5.9	48.7±6.2
cpt9304 D	Hughes	-2.5±0.9	42.8±2.3	48.7±2.5
cpt9305 E	Hughes	-4.4±1.2	43.6±6.4	52.7±1.1

* Pore pressure element in U3 position

Table E4: Mean cone bearing (qt) ± 1 standard deviation (bars); FD94-4

CPT	OPERATOR	peat	organic silt 2-3m	sand
SCPT 14	ConeTec	10.0+5.1	2.6±0.3*	115±49
SCPT 15	ConeTec	12.6±5.2	4.1±0.6	116±36
SCPT 16	ConeTec	5.5±1.3	4.3±0.2	107±34

*2.3-3.1 m to avoid inclusion of peat beds

Table E5: Mean friction ratio (Rf) ± 1 standard deviation; FD94-4

CPT	OPERATOR	peat	organic silt 2-3m	sand
SCPT 14	ConeTec	5.2±0.8%	1.3±0.9%*	0.42+0.20%
SCPT 15	ConeTec	4.4± 0.8%	0.5±0.1%	0.39±0.11%
SCPT 16	ConeTec	3.0±0.4%	0.8±0.1%	0.23±0.09%

*2.3-3.1 m to avoid inclusion of peat beds

Table E6: Mean sleeve friction (fs) ± 1 standard deviation (bars); FD94-4

CPT	OPERATOR	peat	organic silt 2-3m	sand
SCPT 14	ConeTec	0.50±0.23	0.03±0.01*	
SCPT 15	ConeTec	0.52±0.18	0.02+0.01	
SCPT 16	ConeTec	0.17±0.05	0.03±0.01	

*2.3-3.1 m to avoid inclusion of peat beds

Table E7: Mean excess pore pressure (dU) ± 1 standard deviation (m. of water); FD94-4

CPT	OPERATOR	peat	organic silt 2-3m	sand
SCPT 14	ConeTec	-0.5+0.8	2.7+0.3*	-0.9±2.3
SCPT 15	ConeTec	-0.4±0.9	3.6±0.4	-0.6±0.7
SCPT 16	ConeTec	2.0±1.8	3.2±0.4	-1.2±2.5

*2.3-3.1 m to avoid inclusion of peat beds

Table E8: Mean cone bearing (qt) ± 1 standard deviation; Hamilton

CPT	OPERATOR	peat 5.5 -7.5m	organic silt 10-15m	sand 19-24 m
SCPT 91-9	MOTH	6.2±2.0	5.7±2.0	113±21
CPT 91-9b	MOTH	3.8±0.8	5.1±0.8	110±30

Table E9: Mean friction ratio (Rf) ± 1 standard deviation; Hamilton

CPT	OPERATOR	peat 5.5 -7.5m	organic silt 10-15m	sand 19-24 m
SCPT 91-9	MOTH	4.8+2.6%	1.5+0.8%	0.50+0.08%
CPT 91-9b	MOTH	6.0±1.3%	1.7±0.3%	0.56±0.14%

Table E10: Mean sleeve friction (fs) ± 1 standard deviation Hamilton

CPT	OPERATOR	peat 5.5 -7.5m	organic silt 10-15m	sand 19-24 m
SCPT 91-9	MOTH	0.26±0.05	0.08±0.02	0.57±0.12
CPT 91-9b	MOTH	0.22±0.04	0.09±0.02	0.61±0.20

Table E11: Mean excess pore pressure (dU) ± 1 standard deviation; (m. of water); Hamilton

CPT	OPERATOR	peat 5.5 -7.5m	organic silt 10-15m	sand 19-24 m
SCPT 91-9	MOTH	7.5±2.9	14.7±3.0	-1.2+2.0
CPT 91-9b	MOTH	7.9±1.4	12.9±2.2	-4.0±4.6

Table E12: CPT data: organic silts 11-14 m at Westbridge; mean ± 1 standard deviation

CPT	OPERATOR	qt (bar)	Fs (bar)	Rf	dU (m of water)
SCPT 91-1	MOTH	10.5±1.5	0.10±0.02	0.9±0.2%	18.7±3.0
SCPT 91-2	MOTH	6.5±1.0	0.09±0.02	1.3±0.2%	19.6±3.2

Table E13: CPT data; massive sand 7-14 at Massey Tunnel; mean ± 1 standard deviation

CPT	OPERATOR	qt (bar)	Fs (bar)	Rf	dU (m of water)
SCPT 1 94-11	ConeTec	56±13	0.21±0.06	.39±0.10%	-0.1±0.3
MSSC9401	UBC	61±11	0.26±0.08	.43±0.05%	0.1±0.1
MSSC9402	UBC	58±12	0.21±0.06	.36±0.04%	0±0.1
MSSC9403	UBC	54±9	0.18±0.05	.34±0.11%	0.1±0.2
MSSC9404	UBC	52±10	0.18±0.07	.34±0.10%	-0.1±0.3
MSSC9405	UBC	53±10	0.23±0.06	.43±0.07%	0±0.2
MSSC9406	UBC	53±9	0.18±0.04	.35±0.04%	0.1±0.8

APPENDIX F. RADIOCARBON DATES
PART 1; SAMPLES FROM BOREHOLES LOGGED FOR THIS STUDY

borehole	Laboratory and sample #*	collector **	nominal depth m	corrected depth m	material	age uncorrected ^{14}C years	±2 σ	age correction ^{14}C years	corrected age ^{14}C years	facies ****
FD92-2A	TO-4094	PAM	20.8	20.8	bivalve	9690	80	-800	8890	BZ
FD92-4	TO-4098	PAM	12.2	12.2	bivalve	6990	70	-800	6190	MSSB
	TO-4095	PAM	38.5	38.5	bivalve	8570	70	-800	7770	LZ
FD92-11	TO-4097	PAM	85.3	85.3	bivalve	6540	170	-800	5740	BZ
	TO-4894	PAM	100.1	100.1	bivalve	10010	70	-800	9210	BC
FD93-1	TO-3977	JJC	19.9	19.9	leaf	1060	80	0	1060	LS
	TO-3978	JJC	21.0	21.0	wood	1120	50	0	1120	LS
	TO-4096	JJC	53.5	53.1	wood	1690	60	0	1690	MX
FD93-2	GSC-5790	JJC	7.6	7.6	wood	3740	90	20	3760	MSSF
	GSC-5792	JJC	16.7	16.7	wood	5110	100	10	5120	MSSF
	TO-4142	JJC	29.0	29.0	wood, needles	7600	70	0	7600	LDSZ
	GSC-5802	JJC	42.6	42.6	wood	8290	110	-70	8220	LZ
	TO-4143	JJC	46.2	46.2	twig	6710	80	0	6710	LZ
FD93-3	TO-4148	JJC	5.0	4.8	bivalve	2740	50	-800	1940	MSSB
	GSC-5785	JJC	8.9	8.8	wood	3220	90	-20	3200	MSSB
	TO-4149	JJC	18.4***	18.3	wood	3670	50	0	3670	MSSB
	TO-4150	JJC	44.2	43.6	bivalve	5940	60	-800	5140	LZ
FD93-4	GSC-5804	JJC	16.3	16.6	wood	1900	70	-10	1890	MSSF
	TO-4215	JJC	21.1	20	bivalve	8140	70	-800	7340	MSD
	TO-4216	JJC	46.7	45.8	bivalve	9050	100	-800	8250	LZ
FD93-5	TO-4281	JLL	8.7	8.2	twig	600	60	0	600	MSSB
	TO-4217	JLL	15.5	15.5	bivalve	3420	60	-800	2620	MSSB
	TO-4218	JLL	38.4	35.8	twigs	2460	50	0	2460	LS
BHFD93S-1	TO-4371	PAM	10.4	10.4	twig	230	50	0	230	MSD
	TO-4370	PAM	23.7	23.7	bivalve	1670	50	-800	870	LS
BHFD93S-2	TO-4372	PAM	16	16.0	twig w bark	170	70	0	170	LS
FD94-1	TO-4374	PAM	9.6	9.1	twig	10	60	0	10	MSSF
	TO-4595	PAM	25.5	24.9	bivalve	9060	80	-800	8260	MSSB
FD94-4	TO-4465	JJC	31.9	31.1	bivalve	9130	80	-800	8330	MX (SB)

APPENDIX F; PART 1 (cont'd). RADIOCARBON DATES										
borehole	Laboratory and sample #*	collector **	nominal depth m	corrected depth m	material	age uncorrected ^{14}C years	±2 σ	age correction ^{14}C years	corrected age ^{14}C years	facies
FD94-4	TO-4466	JJC	118.7	118.7	bivalve	8920	80	-800	8120	BZ?
	TO-4467	JJC	142.5	142.5	bivalve	9710	100	-800	8910	BZ?
	TO-4468	JJC	158.4	158.4	gastropod	9520	90	-800	8720	BZ?
	TO-4469	JJC	170.6	170.6	bivalve	9540	90	-800	8740	BZ?
	TO-4470	JJC	235.2	235.2	bivalve	10870	100	-800	10070	BZ?
FD94-6	TO-4895	PAM	7.5	7.2	twig	5120	60	0	5120	MSSF
	TO-4896	PAM	22.1	21.6	bivalve	8790	70	-800	7990	LZ
K2V2	TO-4897	PAM	20.2***	20.2	twig	4430	50	0	4430	MSSF
FD95-6	TO-5418	JLL	19.4	19.1	bivalve	8600	70	-800	7800	MSSB
	TO-5419	JLL	23.9	23.7	bivalve	8760	70	-800	7960	MSD

*Laboratory: TO- Isotrace Laboratory, University of Toronto; GSC - Geological Survey of Canada

** collectors: PAM - P.A. Monahan; JLL- J.L. Luternauer; JJC- J.J. Clague

*** these nominal depths reflect partial correction for excess sand; other nominal depths are unadjusted field depths (as are the depths of the grain size samples reported in Appendices C and D).

**** see Table 6-1 for facies abbreviations

APPENDIX F. RADIOCARBON DATES
PART 2; SAMPLES FROM OTHER BOREHOLES

borehole	Laboratory and sample # *	depth m	material	age uncorrected ^{14}C years	+2 σ	age correction ^{14}C years	corrected age ^{14}C years	Facies ****	Reference
FD86-1	TO-870	7	shell	3950	50	-800	3150	SZ	Clague et al., 1991
FD86-2	TO-576	31	wood	6710	90	0	6710	FSS	Clague et al., 1991
	TO-577	46	wood	6370	90	0	6370	FSZ	Clague et al., 1991
FD86-5	TO-583	31	wood	5280	70	0	5280	FSS	Clague et al., 1991
	TO-583a	31	shell	5810	80	-800	5010	FSS	Clague et al., 1991
FD86-6	TO-588	18	wood	6380	70	0	6380	FSS?	Clague et al., 1991
FD87-1	TO-777	40	wood	5820	60	0	5820	SB	Clague et al., 1991
	TO-778	66	shell	6870	60	-800	6070	FSS	Clague et al., 1991
	TO-779	99	wood	6250	80	0	6250	FSZ	Clague et al., 1991
	TO-780	143	wood	7470	60	0	7470	BZ?	Clague et al., 1991
	TO-781	158	shell	8720	70	-800	7920	BZ?	Clague et al., 1991
	TO-782	168	shell	9560	70	-800	8760	BZ?	Clague et al., 1991
	TO-783	171	shell	9820	70	-800	9020	BZ?	Clague et al., 1991
	TO-784	179	shell	10360	80	-800	9560	BC?	Clague et al., 1991
	TO-1095	184	shell	12330	90	-800	11530	CAP	Clague et al., 1991
	TO-785	201	wood	37460	660	0	37460		Luternauer et al., 1991
	TO-	219	wood	46840	880	0	46840		Luternauer et al., 1991
	TO-786	223	wood	26880	200	0	26880		Luternauer et al., 1991
	TO-787	247	wood	33490	270	0	33490		Luternauer et al., 1991
	TO-788	267	wood	24460	160	0	24460		Luternauer et al., 1991
FD90-1	TO-2749	35	shell	9590	70	-800	8790	BZ?	Patterson et al., 1993
FD90-2	TO-2748	19	shell	6630	60	-800	5830	LZ?	Patterson et al., 1993
	TO-2747	35	wood	6400	80	0	6400	LZ	Patterson et al., 1993
FD91-1	TO-2756	7.2(6.4**)	twigs	2860	50	0	2860	MSSF	Patterson et al., 1993
	TO-2757	8.2(7.4**)	twig	2980	50	0	2980	MSSF	Patterson et al., 1993
	TO-2758	14.4(15.8**)	wood	4610	50	0	4610	LS	Patterson et al., 1993
	TO-2759	14.9(16.3**)	twigs	4430	50	0	4430	LS	Patterson et al., 1993
	TO-2754	22.1	bivalve	8940	100	-800	8140	MX-SB	Patterson et al., 1993
	TO-2755	22.8	bivalve	7870	90	-800	7070	MX-SB	Patterson et al., 1993

APPENDIX F; PART 2 (cont'd). RADIOCARBON DATES									
borehole	Laboratory and sample #*	depth m	material	age uncorrected ^{14}C years	+2 σ	age correction ^{14}C years	corrected age ^{14}C years	Facies ****	Reference
	TO-2750	25.0	bryophyte frag	6380	60	0	6380	MX-SB	Patterson et al., 1993
	TO-2751	26.5	bivalve	7510	60	-800	6710	MX-SB	Patterson et al., 1993
	TO-2752	28.9	bivalve	8620	700	-800	7820	MX-SB	Patterson et al., 1993
FD91-2	TO-2760	3.6	twigs	2740	50	0	2740	MSSF	Patterson et al., 1993
	TO-2761	5.3	bryophyte	2850	50	0	2850	MSSF	Patterson et al., 1993
	TO-2762	9.5	twigs	3940	50	0	3940	MSSF	Patterson et al., 1993
	TO-2763	26.3	twig	4700	50	0	4700	MSSF	Patterson et al., 1993
	TO-3307	44.1	bivalve	10530	90	-800	9730	LZ-BZ	Patterson et al., 1993
FD94-3	TO-4461	15.4	wood	4620	70	0	4620	MSSF	Dallimore et al, 1995
FD96-1	Beta-93808	13	wood	3770	60	0	3770	MSSF	Dallimore et al, 1996
D41	GSC4275	2.3***	wood	1840	160	0	1840	MSSB	Williams and Roberts, 1989
D60	TO-409	1.2***	wood	2080	110	0	2080	SZ	Williams and Roberts, 1989
D59	TO-408	3.2***	wood	2490	60	0	2490	MS	Williams and Roberts, 1989
D44	TO-407	1.8***	wood	4090	60	0	4090	SZ	Williams and Roberts, 1989
D23	GSC4194	1.2***	peat	4410	70	0	4410	PT	Williams and Roberts, 1989
	GSC4238	3.6***	org detritus	5500	70	0	5500	LOZ	Williams and Roberts, 1989
	GSC4255	11.7***	org detritus	7960	140	0	7960	LOZ	Williams and Roberts, 1989
D-52	S-2872	3.8***	peat	6025	105	0	6025	LOZ	Williams and Roberts, 1989
93-32	Beta-70576	2	peat	4140	60	0	4140	SZ-TSZ	Hutchinson et al., 1995
93-32	Beta-70575	3	*Scirpus* achenes	4360	50	0	4360	SZ-TSZ	Hutchinson et al., 1996
93-17	Beta-67404	3	wood	5190	120	0	5190	LOZ?	Hutchinson et al., 1997
DC-6	TO-122	5	wood	6350	70	0	6350	MSSF	Hutchinson et al., 1998
apex of delt	GSC3919	55	wood	9490	250	0	9490	FS	Williams and Roberts, 1989

* Laboratory: 'TO- Isotrace Laboratory, University of Toronto; GSC - Geological Survey of Canada; S - Simon Fraser University.

** corrected depths

*** elevation below sea level

**** FSS - Foreset sand; FSZ- Foreset silts; CAP - Capliano sediments; for other abbreviations see Table 6-1.

APPENDIX G: AVERAGE NORMALIZED CONE BEARING AND AGE OF MASSIVE SAND FACIES (FIGURE 6-39)

For details on CPTs and ^{14}C dates, see Table 4-2 and Appendix F respectively

Borehole	Subfacies	corrected age ^{14}C years	CPT	interval m	average q_{c1}
FD92-4	MSSB	6190±70	CPT 9309	4.85-27.35	98
FD93-2	MSSF	3760±90	CPT-1 93-109	4.1-17.4	94
	MSSF	5120±100		4.1-17.4	94
FD93-3	MSSB	1940±50	SCPT-1 93-140	4.7-19.2	75
	MSSB	3200±90		4.7-19.2	75
	MSSB	3670±50		4.7-19.2	75
FD93-4	MSSB	1890±70	SCPT-13 93-102	3.3-16.45	77
	MSD*	7340±70		17.2-21.4 23.55-31.05	96
FD93-5	MSSB	600±60	SCPT-13 94-112	5.8-20.8	58
	MSSB	2620±60		5.8-20.9	58
BHFD93S-1	MSD	230±50	SCPT-6 93-175	7.25-10.9	66
FD94-1	MSSF	10±60	SCPT-1 94-112	4.7-21.2	55
	MSSB	8260±80		21.25-31.8	95
FD94-3	MSSF	4620±70	SCPT-17 94-112	5.15-18.7	70
FD95-6	MSSB	7800±70	SCPT-10 94-112	10.6-22.25	106
	MSD*	7960±70		24.45-28.45	100
FD96-1	MSSB	3770±60	CPT-3 93-190	10-15.95	85
K2V2	MSSB	4430±50		4.47-44.63	85

* excluding interbedded sand and silt intervals equivalent to DSZ

APPENDIX H. CPT PARAMETERS BY FACIES FOR SELECTED CPTS

Part 1. Peat Facies (PT)

CPT	Borehole	thickness m	qt bar	Q_t	Q	R_f %	F_R	I_F	dU m	B_q	Comments
SCPT 14 94-112 **	FD94-2 FD94-4	0.8	10±5	82±54	51±21	5.2±0.8	5.4±0.9	2.7±0.2	-0.5±0.8	-0.007±0.01	
SCPT 15 94-112**		1	13±5	129±52	56±16	4.4±0.8	4.4±0.8	2.5±0.1	-0.4±0.8	-0.005±0.009	47 m south of SCPT 14
SCPT 16 94-112**		0.7	5±1	47±19	29±9	3.0±0.4	3.1±1.4	2.7±0.9	2.0±1.8	0.04±0.04	28 m west of SCPT 14
SCPT 7 94-112**	FD94-6	0.45	3±0.5	9 ± 1	9±1	5.8±1.1	6.5±1.3	3.2+0.1	-2.5±0.9	-0.10±0.03	
CPT 91-9b ***	91-10 84-760***	3.9	5±2	4±3	4±3	5.5±1.2	8.0±2.8	3.6±0.3	7.2±5.1	0.28±0.10	Hamilton Interchange
SCPT 91-2 ***	87-4 91-1***	1.85	4±1	10±5	10±5	3.9±1.2	4.4±1.4	3.1±0.2	4.9±2.9	0.15±0.09	Westbridge, north side of Annacis Channel; silt interbedded with peat

**Woeller et al., 1994

***British Columbia Ministry of Transportation and Highways boreholes

APPENDIX H. CPT PARAMETERS BY FACIES FOR SELECTED CPTS

Part 2. Laminated and Organic Silt Facies (LOZ)

CPT	Borehole	thickness m	qt bar	Q_t	Q	R_f %	F_R	I_F	dU m	B_q	Comments
overlain by peat and other deposits											
SCPT 14 94-112 **	FD94-2 FD94-4	2.4 m	3±27	10±4	9±3	1.8±.8	2.2±1	3.0±0.1	1.6±1.1	0.07±0.05	
SCPT 15 94-112**		1.8	5±1	19±11	13±6	0.9±0.6	1.0±0.6	2.7±0.1	2.5±1.7	0.07±0.05	47 m south of SCPT 14
SCPT 7 94-112**		2.3	5±0.6	16±5	12+2	0.84±0.3	0.92±0.3	2.7±0.5	3.7±0.9	0.09 ±0.02	28 m west of SCPT 14
SCPT 7 94-112**	FD94-6	2.15	4±0.8	8±3	8+3	1.7±0.7	2.1±0.8	3.0±0.1	-1.0±1.2	-0.027±0.007	
CPT 91-9b ***	91-10 84-760***	9.0	5±1	2±0.5	2±0.5	2.9±0.3	3.2±1	3.6±0.1	14±4	0.52±0.15	Hamilton Interchange
SCPT 91-2 ***	87-4 91-1***	12.1	5±2	4±1	4±1	1.6±0.6	2.4±0.7	3.3+0.1	13±6	0.36±0.14	Westbridge north side; across Annacis channel from FD92-5
facies at surface or beneath anthropogenic fill											
CPT 4F 92-180	FD92-2	1.1	4±3	16±18	14±13	4.2±1.3	5.0±2.0	3.1±0.4			above water table
CPT 9309	FD92-4	2.25	7±2	39±43	21±17	2.1±1.6	2.2±1.6	2.7±0.2	1.8±0.6	0.05±0.01	all LOZ; dU and B_q below water table only
		0.45	9±2	109±45	50±18	4.5+1.1	4.5+1.1	2.6±0.1			desiccated silt
		1.8	5±1	19±10	14±6	1.5±0.9	1.5±0.9	2.7±0.2	1.8±0.6	0.05±0.01	non- desiccated silt; dU and B_q below water table only

APPENDIX H. CPT PARAMETERS BY FACIES FOR SELECTED CPTS

Part 2 (cont'd). Laminated and Organic Silt Facies (LOZ)

CPT	Borehole	thickness m	qt bar	Q_t	Q	R_f %	F_R	I_F	dU m	B_q	Comments
SCPT 91-3	FD92-5	2.9	9±3	5±3	5±3	1.9±0.4	2.8±0.8	3.3±0.2	34±11	0.62±0.25	Westbridge, south side; overlain by sand (MSSF)
CPT 1 93-109	FD93-2	2.5	7±2	22±15	15±5	1.1±0.5	1.1±0.5	2.6±0.1	4.0±1.5	0.06±0.03	all LOZ; dU and B_q below water table only
		0.55	8±3	40±24	22±7	1.9±0.5	2.0±0.5	2.6±0.1			desiccated silt
		1.95	6.9±1.7	16±2	13±1	0.84±0.1	0.9±0.1	2.6±0.04	4.0±1.5	0.06±0.03	non-desiccated silt; dU and B_q below water table only
SCPT 1 89-140	FD93-3	1.05	6.3±2.4	14±8	14±8	6.9±1.0	7.5±1.1	3.2±0.2	-1.1±0.6	-0.02±0.01	Friction ratio anomalously high throughout
SCPT 13 93-102*	FD93-4	0.75	7.4±2.2	62±28	36±15	3.0±0.7	3.1±0.7	2.6±0.1	-4.2±0.8	-0.06±0.03	
CPT 2 91-101	FD94-5	1.30	6±2	30±17	25±10	3.1±0.5	3.2±0.6	2.7±0.1	-5.2±1.0	-0.11±0.3	
KD9302	K2V2	2.05	4±1	11±3	11±2	2.2±1.3	2.4±1.4	2.9±0.1			pore pressure measured in U3 position;
KD9308		1.75	6±2	22±18	14±6	0.8±0.4	0.9±0.4	2.6±0.1			85 m north of K2V2; all LOZ; pore pressure measured in U_3 position
		0.275	9±4	56±27	24±10	1.4±0.7	1.4±0.7	2.5±0.1			desiccated silt

APPENDIX H. CPT PARAMETERS BY FACIES FOR SELECTED CPTS

Part 2 (cont'd). Laminated and Organic Silt Facies (LOZ)

CPT	Borehole	thickness m	qt bar	Q_t	Q	R_f %	F_R	I_F	dU m	B_q	Comments
KD9308		1.475	5±1	16±2	12±2	0.8±0.3	0.8±0.3	2.6±0.1			non-desiccated silt
SCPT 1 96-114		1.55	6±1	18±3	17±2	3.3±0.7	3.5±0.7	2.8±0.1	4.1±0.7	0.07±0.02	near Horseshoe Slough
SCPT 2 96-114			5±2	10±6	10±6	6.6±3.3	8.1±4.9	3.3±0.4	-0.3±1.6	0.0002+0.8	Horseshoe Slough
CPT 5 91-188		3.1	5+2	25±34	17±14	1.5±1.0	1.6±1.0	2.7±0.1	-2.3±0.7	-0.06±0.02	Downtown Richmond; all LOZ; dU and B_q below water table only
		0.6	8±3	77±52	40±21	3.0±1.3	3.1±1.3	2.6±0.1			desiccated silt
		2.5	4±1	13±4	12±3	1.1±0.4	1.3+0.4	2.7±0.1	-2.3±0.7	-0.06±0.02	non-desiccated silt

**Woeller et al., 1994

***British Columbia Ministry of Transportation and Highways boreholes

APPENDIX H. CPT PARAMETERS BY FACIES FOR SELECTED CPTS

Part 3.Interbedded Sand and Silt Facies (SZ)

CPT	Borehole	thickness m	q_t bar	q_{c1}	Q_t	Q	R_f	F_R %	I_F	dU m	B_q	Comments
burrowed sand and silt subfacies (BSZ)												
CPT 9309	FD92-4	2.3	16±12	22±17	31±25	23±17	0.4±0.3	0.4±0.4	2.4±0.3	1.2±0.9	0.01 ±0.01	
CPT 92-1	FD92-11	4.6	12±6	20±12	35±29	22±11	1.6±1.1	1.7±1.2	2.6±0.3	-0.8±2.5	-0.01 ±0.04	
SCPT 7 94-112**	FD93-3	1.8	6.2±2	8±3	8.9±3	9±3	5.0±1.7	5.8±2.2	3.2±0.2	-2.2±1.2	-0.04 ±0.03	Friction ratio anaomalously high throughout
SCPT 91-2 ***	87-4 91-1***	0.9	14±3	10±3	6±2	7±3	1.0±0.4	1.3±0.6	3.0±0.2	8.9±4.7	0.09 ±0.06	Westbridge north side; across Annacis channel from FD92-5; not seen in core; BSZ?
CPT 91-9b ***	91-10 84-760***	0.65	41±16	29±11	20±8	26±13	0.8±0.4	0.9±0.5	2.4±0.4	-3.4±7.6	0.005±0.06	Hamilton Interchange; not seen in core; BSZ?
spet 9401		0.65	19±12	55±38	162±124	62±35	2.4±2.0	2.4±2.0	2.3±0.4	-0.4±1.7	-0.001±0.02	subfacies undefined; overlies coarsening upward topset sand facies
well bedded sand and silt subfacies (WSZ)												
CPT4F 92-180	FD92-2	3.25	6±4	7±4	8±5	8±4	1.8±1.2	2.4±2.4	3.1±0.4	-2.4+2.4	-0.05±0.07	dU and Bq below water table only; WSZ
SCPT 91-3 ***	FD92-5	1.9	16±10	24±15	36±23	24±15	0.8±0.6	0.8±0.7	2.4±0.3	-0.9±2.9	-0.005±0.04	'Westbridge, south side; upper interval WSZ
		1.4	40±24	31±18	22±14	26±20	1.2±0.6	1.3±0.6	2.5±0.3	-2.7±9.3	-0.002 ±0.04	lower interval; WSZ? underlying sand includes some MSSB

APPENDIX H. CPT PARAMETERS BY FACIES FOR SELECTED CPTS

Part 3 (cont'd).Interbedded Sand and Silt Facies (SZ)

CPT	Borehole	thickness m	q_t bar	q_{c1}	Q_t	Q	R_f	F_R %	I_F	dU m	B_q	Comments
CPT 1 93-109	FD93-2	0.8	13±2	17±2	23±4	16±3	0.54±0.1	0.6±0.1	2.5±0.5	-0.2±1.0	-0.002±0.008	WSZ
SCPT 13 93-102*	FD93-4	2.1	13±7	27±14	53±30	28±13	0.92±0.7	1.0±0.8	2.3+0.3	-4.7±1.9	-0.04 ±0.03	WSZ
SCPT-1 94-112**	FD94-1	2.7	37±35	50±50	67±70	48±50	1.5±0.8	1.5±0.8	2.3±0.4	0.1±2.4	0.001 ±0.02	WSZ
SCPT 14 94-112 **	FD94-2 FD94-4	1.4	26±14	39±21	56±31	38±21	0.75±0.4	0.8±0.4	2.2±0.3	-2.6±1.3	-0.01 ±0.005	WSZ
SCPT 15 94-112**		2.45 m	13±8	23±12	28±17	21±10	1.1±0.6	1.2±0.7	2.5±0.3	0.1±3.0	0.01 ±0.04	47 m south of SCPT 14
SCPT 16 94-112**		2.15 m	32±15	46±20	66±27	45±20	0.42±0.39	0.4±0.41	2.0±0.2	-5.5±2.1	-0.02± 0.01	28 m west of SCPT 14
SCPT 7 94-112**	FD94-6	1.4	43±35	35±28	41±34	33±26	1.0±0.7	1.1±0.8	2.4±0.4	-2.0±1.9	-0.01 ±0.02	includes burrowed silt interval WSZ+BSZ
KD9302	K2V2	1.35	17±7	23±10	30±12	24±9	1.3±0.5	1.4±0.6	2.5±0.2			WSZ; pore pressure measured in U3 position
SCPT1 97-108		1.45	14±5	17±6	19±7	18±6	1.2±0.8	1.3±0.8	2.6±0.2	3.0±4.7	0.025±0.46	Annacis Island
CPT 5 91-188			13+7	19±11	26±17	19±10	1.0±0.6	1.1±0.8	2.5±0.3	-4.8±1.1	-0.05±0.03	downtown Richmond; WSZ, based on nearby drill sites
Thick interbedded sand and silt subfacies (TSZ)												
CPT-2 91-101	FD94-5	12.3	35±26	37±27	39±30	37±25	1.2±0.7	1.3±0.9	2.4±0.4	-3.7±5.2	-0.02±0.05	all TSZ
		7.7	29±28	35±32	41±36	36±30	1.2±0.8	1.3±1.0	2.4±0.5	-2.0±3.5	-0.02±0.06	upper interval, shell free

APPENDIX H. CPT PARAMETERS BY FACIES FOR SELECTED CPTS

Part 3 (cont'd).Interbedded Sand and Silt Facies (SZ)

CPT	Borehole	thickness m	q_t bar	q_{ct}	Q_t	Q	R_f	F_R %	I_F	dU m	B_q	Comments
		4.6	44±17	41±15	36±14	38±16	1.1±0.7	1.3±0.8	2.3±0.3	-6.5±6.2	-0.01±0.03	lower interval, shell-bearing
SCPT 10 94-112**	FD95-6	8.35	21±16	21±18	21±24	20±18	1.3±0.7	1.5±0.8	2.7±0.4	2.0±5.9	0.03±0.07	shell-bearing
SCPT 2 96-114		19.3	22±12	20±13	17±15	17±13	2.1±1.3	2.7±2.5	2.8±0.4	-2.6±4.2	-0.008±0.06	probably shell free
KD9308		5.975	24±21	30±28	37±38	30±27	1.0±0.5	1.1±0.6	2.4±0.4			85 m north of K2V2; pore pressure measured in U3 position; probably shell free
Distal sand and silt subfacies (DSZ)												
SCPT 1 95-109	FD93-1	2.00	25±16	21±14	16±12	17±14	2.1±0.9	2.4±1.0	2.8±0.4	-5.0±3.5	-0.024±0.3	
SCPT 6 93-175	BHFD93S-1	5.15	9±8	16±18	26±41	15±18	1.6±1.0	2.4±2.3	2.8±0.5	2.2±3.6	0.08±0.14	
CPT325 92 197		2.4	55+21	47±17	39±15	45±18	0.9±0.7	0.9±0.7	2.2±0.3	-4.2±3.1	-0.007±0.007	Roberts Bank Port
CPT95-5 95-170		4.65	25±23	23±20	19±18	21±20	1.0±0.9	1.9±2.6	2.8±0.8	-3.7±1.4	-0.11+0.19	Roberts Bank Port

*Woeller et al., 1993

**Woeller et al., 1994

***British Columbia Ministry of Transportation and Highways boreholes

Part 4. Coarsening Upward Sand Facies of the Topset (CT)

CPT	Borehole	thickness m	q_t bar	q_{c1}	Q_t	Q	$R_{f\%}$	F_R	I_F	dU m	B_q	Comments
spet 9401		3.675	26±15	51±36	101±85	51±36	0.5±0.3	0.5±0.3	2.1±0.3	-0.5±1.8	-0.001±0.01	east side of Point Roberts; facies observed in this CPT only

APPENDIX H. CPT PARAMETERS BY FACIES FOR SELECTED CPTS

Part 5. Massive Sand Facies (MS)

CPT	Borehole	thickness m	qt bar	qc1	Q	R_f %	F_R	I_F	dU m	B_q	Comments
CPT4F 92-180	FD92-2	19.1	116±44	94±28	92±28	0.4±0.1	0.4±0.1	1.7±0.2	-2.3+2.2	-0.002±0.003	MSSF
CPT 9309	FD92-4	22.55	123+40	98±32	96+33	0.5±0.3	0.6+0.3	1.8±0.2	-0.9+2.6	-0.0008±0.003	MSSB
SCPT 91-3 ***	FD92-5	8.7	76±27	80±29	79+29	0.4±0.2	0.4±0.2	1.8±0.2	-0.3±0.7	-0.0006 ±0.002	Westbridge, south side; upper sand; MSSF
SCPT 7		12.75	154+48	102±34	100+34	0.6±0.3	0.6±0.3	1.8±0.2	-3.0+4.7	-0.002 ±0.004	lower sand; MSSB
SCPT 91-2 ***	87-4 91-1***	11.35	85±61	57±44	54±45	1.0±0.6	1.2±0.9	2.3±0.6	1.1±11	0.04±0.1	Westbridge north side; across Annacis channel from FD92-5;equivalent to lower sand in FD92-5; includes silt and sand interbeds
CPT 92-1	FD92-11	9.35	84±29	84±26	82±25	0.31±0.1	0.32±0.	1.7±0.2	-0.8±0.6	-0.001 ±0.002	MSSE
SCPT 1 95-109	FD93-1	4.8	64±29	49±22	47+22	0.9+0.8	1.0±0.9	2.2±0.4	-4.8±4.0	-0.01±0.03	MSD all; 15 cm^2 cone
		3.95	74±23	57±17	55±18	0.6±0.4	0.6±0.4	2.0±0.2	-4.4+3.0	-0.01±0.03	MSD sand only
		0.85	28±12	22±9	17±10	2.1±0.8	2.4±1.0	2.8±0.3	-6.7±5.8	-0.04 ±0.05	MSD silt and sand interbed
CPT 1 93-109	FD93-2	13.35	104±43	94±30	92±30	0.4±0.1	0.4±0.1	1.7±0.2	-0.7±1.3	0.0005 ±0.001	MSSF
SCPT-1 89-140	FD93-3	14.6	89±43	75±33	73±33	0.9±0.5	0.9±0.5	2.0±0.3	-1.9±2.5	-0.003 ±0.007	MSSB
SCPT 13 93-102*	FD93-4	13.2	77±38	77±27	76±27	0.3±0.1	0.3±0.1	1.7±0.1	-0.5+2.0	-0.0003 ±0.002	MSSF
	FD93-4	14.6	129±46	86±31	83±32	0.7±0.5	0.7±0.6	1.9±0.3	-7.6±6.2	-0.008 ±0.01	all MSD
	FD93-4	11.8	143±36	96±26	93±26	0.5±0.2	0.6±0.3	1.8±0.2	-7.0±6.1	-0.005 ±0.005	MSD, sand only
	FD93-4	2.8	67±25	48±18	43±21	1.4±0.7	1.6±1.0	2.3±0.3	-10.4±6.1	-0.019±0.015	MSD, DSZeq only

APPENDIX H. CPT PARAMETERS BY FACIES FOR SELECTED CPTS

Part 5 (cont'd). Massive Sand Facies (MS)

CPT	Borehole	thickness m	qt bar	qc1	Q	R_f %	F_R	I_F	dU m	B_q	Comments
SCPT 13 94-112**	FD93-5	15.5	71±24	58±19	57±19	0.4±0.3	0.5±0.3	1.9±0.2	-0.9±2.1	-0.001 ±0.004	MSSB
SCPT 1 94-112**	FD94-1	16.6	68±29	55±19	53±19	0.4±0.2	0.4±0.3	2.0±0.2	-0.4±2.0	-0.001 ±0.006	MSSF
		10.55	159±37	95±21	92±22	0.3±0.2	0.4±0.2	1.7±0.2	-5.4±5.0	-0.004 ±0.004	MSSB
SCPT 14 94-112**	FD94-2 FD94-4	19.1	115±49	98±34	85±33	0.4±0.2	0.4±0.3	1.7±0.2	-0.9+2.3	-0.001 ±0.003	all MS
		14.25	111+46	101+32	99+32	0.4+0.2	0.4+0.2	1.7+0.2	-0.6+1.9	-0.001 +0.003	MSSF
		4.85	125+56	87+38	84+38	0.5+0.4	0.6+0.5	1.8+0.3	-1.9+3.2	0.001 +0.003	MSSB
SCPT 15 94-112**		19.05	116±36	99±29	97±29	0.4±0.1	0.4±0.1	1.7±0.1	-0.6±0.07	-0.0005±0.002	47 m south of SCPT 14
SCPT 16 94-112**		18.7	107±34	91±26	89±26	0.2±0.1	0.2±0.1	1.6±0.2	-1.2±2.5	-0.0001 +0.001	28 m west of SCPT 14
CPT 2 91-101	FD94-5	2.05	153+32	126±28	124±28	0.5±0.2	0.5±0.2	1.6±0.1	-5.4±4.7	-0.003±0.03	MSD
SCPT 7 94-112**	FD94-6	15.6	125±54	111±55	109±55	0.4±0.3	0.4±0.3	1.7±0.3	-4.4±5.1	-0.003±0.004	all MS; MSSF densified by trains
		9.45	110±53	113±66	111+66	0.4±0.2	0.4±0.3	1.7±0.3	-3.0±3.3	-0.002±0.002	MSSF; densified by trains
		6.15	147+48	108+32	106+32	0.3+0.2	0.3+0.3	1.6+0.2	-6.5+6.5	-0.005+0.006	MSSB
SCPT 10 94-112**	FD95-6	11.7	148±45	106±30	104±30	0.5±0.2	0.5±0.2	1.7+0.2	-8.6±6.5	-0.006 ±0.005	upper sand MSSB
		6.2	126±66	75±39	71±40	0.5±0.2	0.5±0.3	2.0+0.5	-9.5±7.4	-0.02 ±0.03	MSD all
		2.15	43±23	27±14	21±16	0.6±0.3	0.8±0.4	2.5+0.4	-12.4±4.4	-0.05 ±0.03	MSD, DSZeq only
		4.05	169±29	100±18	97±18	0.4±0.2	0.4±0.2	1.7±0.1	-8.0±8.2	-0.005 ±0.006	MSD sand only
KD9302	K2V2	18.2	102±40	85±30	83±30	0.5±0.1	0.5±0.1	1.8±0.1			MSSF; pore pressure measured in U5 position

APPENDIX H. CPT PARAMETERS BY FACIES FOR SELECTED CPTS

Part 5 (cont'd). Massive Sand Facies (MS)

CPT	Borehole	thickness m	qt bar	qc1	Q	R_f %	F_R	I_F	dU m	B_q	Comments
KD9301		18.75	95±44	79±32	77±32	0.4±0.1	0.4±0.2	1.8±0.2	-0.6±1.1	-0.001±0.003	2 m south of KD9302
KD9308		10.83	104±33	87±25	85±25	0.4±0.2	0.4±0.2	1.8±0.1			85 m north of K2V2; pore pressure measured in U3 position
SCPT-6 93-175	BHFD93S-1	3.7	60±20	66±23	63±23	0.5±0.4	0.5±0.6	1.9±0.3	-1.2±3.9	0.001 ±0.03	MSD
CPT 91-9b ***	91-10 84-760***	12.3	125±38	79±23	76±23	0.6±0.2	0.6±0.2	1.9±0.2	-2.8±4.1	-0.002 ±0.003	Hamilton Interchange
SCPT-1 97-108		28.75	117±43	81±26	78±29	0.5±0.2	0.5±0.3	1.9±0.2	-1.4±2.9	-0.001 ±0.005	Annacis Island
SCPT 1 96-114		19.6	70±30	61±17	60±17	0.6±0.2	0.6±0.2	2.0±0.2	-0.3±0.5	-0.0003 ±0.002	near Horseshoe Slough
SCPT 2 96-114		3.5	99±18	63±11	61±11	0.7±0.3	0.7±0.4	2.0±0.1	-1.8±2.7	-0.002±0.003	Horseshoe Slough, beneath TSZ
CPT5 91-188		9.3	89±49	88±40	85±35	0.4±0.3	0.4±0.3	1.8±0.3	-1.2±1.9	-0.005±0.02	MSSF (based on nearby sites)
CPT 325 92-197		3.9	106±38	83±30	80±31	0.6±0.6	0.7±0.7	1.9±0.4	-1.8±2.5	-0.003 ±0.008	MSD
CPT 95-5 95-170		2.5	107±21	89±17	87±17	0.3±0.1	0.3±0.1	1.7±0.1	-1.5±1.4	-0.001 ±0.001	MSD

*Woeller et al., 1993

**Woeller et al., 1994

APPENDIX H. CPT PARAMETERS BY FACIES FOR SELECTED CPTS

Part 6. Basal Sand, Siltand Clay Facies (MS)

CPT	Borehole	thickness m	q_t bar	q_{c1}	Q_t	Q	R_f %	F_R	I_F	dU m	B_q	Comments
CPT 92-1	FD92-11	0.7	53±10	15±3	4±1	4±1	1.5±0.5	2.3±0.9	3.3±0.2	140±46	0.43±0.2	sequence of silt and sand,overlain by pink oxidizing clay, and sharp-based sand, at depth of 100m (immediately above refusal)
KD9302	K2V2 (FD96-2)	1.65	18±1	7±0.4	2±0.2	2±0.2	2.1±0.4	4.1±0.7	3.7±0.03			pore pressure measured in U3 position; in FD96-2, pink oxidizing clay overlain by sandy silt at depth of 45m (immediately above refusal)
spet9401		1.05	128±86	88±60	59±41	78±61	1.2±0.8	1.4±0.9	2.3+0.4	-2.6±17.2	0.03±0.06	east side of Point Roberts; interbedded sands and silts inferred from CPT profile at depth of 22 m (immediately above refusal)

APPENDIX H. CPT PARAMETERS BY FACIES FOR SELECTED CPTS

Part 7. Bioturbated Silt Facies (BZ)

CPT	Borehole	thickness m	q_t bar	Q_t	Q	R_f %	F_R	I_F	dU m	B_q	Comments
CPT 92-1	FD92-11	44.55	38±11	3±1	3±2	1.3±0.3	2.2±0.5	3.3±0.1	149±61	0.65±0.2	all BZ
		43.35	37±7	3±0.5	3±0.5	1.3±0.3	2.2±0.5	3.4±0.1	153±56	0.67±0.2	silt intervals only
		1.2	86±28	11±4	10±3	1.6±0.4	2.0±0.6	2.9±0.3	-6±30	0.005±0.05	interval of graded sands
CPT 4F 92-180	FD92-2	6	8±4	2±2	2±2	1.0±0.5	2.8±2.2	3.7±0.3	47±11	1.90±1.44	
KD9302	(K2V2)	24.04	13±3	2±1	2±1	1.6±0.2	3.2±0.5	3.6±0.1			pore pressure measured in U3 position; facies not penetrated in K2V2
KD9301		5.875	12±3	3±1	3±2	0.8±0.9	1.3±1.3	3.3±0.1	53±13	0.77±0.22	2 m south of KD9302
KD9308		4.95	10±4	3±2	3±2	1.1±0.4	2.0±0.8	3.4±0.2			85 m north of K2V2;pore pressure measured in U3 position
SCPT-1 97-108		8.35	35±3	2±0.4	2±0.4	0.5±0.2	1.0±0.3	3.4±0.1	170±34	0.93±0.22	Annacis Island
spet 9401		2.45	10±1	3±0.4	3±0.4	1.0±0.2	1.6±0.4	3.3±0.1	44±9	0.75±0.19	BZ

APPENDIX H. CPT PARAMETERS BY FACIES FOR SELECTED CPTS

Part 8. Laminated Silt Facies (LZ)

CPT	Borehole	thickness m	q_t bar	Q_t	Q	R_f %	F_R	I_F	dU m	B_q	Comments
CPT9309	FD92-4	17.9	42+26	8±6	12±14	1.1±0.6	1.5±0.9	2.9±0.45	14±25	0.11±0.16	borderline with laminated sands
CPT 92-1	FD92-11	13.15	15+8	6±5	6±6	1.7±0.7	2.7±1.2	3.2±0.3	25±15	0.35±0.2	
SCPT-1 95-109	FD95S-1 FD93-1	3.95	17±5	7±2	7±2	2.0±0.5	2.5+0.7	3.1±0.1	7.4±9	0.06±0.07	15 cm^2 cone
SCPT 7 94-112**	FD93-3	30	9±4	3±2	4±2	2.7±0.8	4.6±1.8	3.5±0.3	24±21	0.29±0.25	friction ratio anaomalously high
SCPT 13 93-102*	FD93-4	3.7	24±15	6±5	7±8	1.3±0.6	1.9±0.9	3.2±0.3	29±21	0.27±0.22	
SCPT 1 94-112**	FD94-1	3.2	38+22	9±6	12±13	1.1±0.6	1.4±0.7	2.9±0.3	15±20	0.07±0.12	borderline with laminated sands
SCPT 14 94-112**	FD94-2 FD94-4	24.1	30±15	5±3	5±5	1.3±0.6	2.0±0.9	3.2±0.3	21±24	0.15±0.18	
SCPT 15 94-112**		39.1	32±17	6±4	7±8	1.3±0.6	1.8+1.0	3.1±0.3	47±33	0.30±0.2	47 m south of SCPT 14
SCPT 16 94-112**		17	27±11	5±3	6±5	0.8±0.3	1.2±0.5	3.1±0.2	41±26	0.27±0.19	28 m west of SCPT 14; upper and lower intervals combined
		4.15	21±9	7±4	7±5	0.8±0.5	1.0±0.6	2.9±0.2	27±14	0.21±0.14	upper interval
		13.85	28±11	5±3	5±5	0.8±0.4	1.1±0.5	3.1±0.2	43±27	0.28±0.20	lower interval
CPT 2 91-101	FD94-5	12.45	18±9	5±4	5±5	1.4±0.5	2.1±0.7	3.2±0.2	27±19	0.29±0.22	
SCPT 7 94-112**	FD94-6	7.95+	26±14	7±5	8±8	0.8±0.5	1.2±0.6	3.0±0.3	11±17	0.09±0.13	
SCPT 91-2 ***	87-4 91-1***	27.75	30±19	5±4	6±6	1.2±0.6	1.8±0.9	3.2±0.3	32±26	0.32±0.29	Westbridge north side; across Annacis channel from FD92-5
CPT 91-9b ***	91-10 84-760***	29.95	27±18	4±4	5±7	1.0±0.6	1.7±0.9	3.3±0.3	43±34	0.44±0.35	Hamilton Interchange
SCPT 1 96-114		15.7	22±13	6±6	7±8	1.7±0.6	2.5±1.0	3.2±0.3	30±22	0.29±0.25	near Horseshoe Slough

APPENDIX H. CPT PARAMETERS BY FACIES FOR SELECTED CPTS

Part 8 (cont'd). Laminated Silt Facies (LZ)

CPT	Borehole	thickness m	q_t bar	Q_t	Q	R_f %	F_R	I_F	dU m	B_q	Comments
SCPT 2 96-114		6.95	15±10	3±4	4±5	1.3±0.06	2.4±1.3	3.4±0.3	27±16	0.47±0.38	Horseshoe Slough
SCPT-1 97-108		14.4	48±30	4±4	6±9	1.1±0.5	1.8±0.9	3.3±0.3	75+77	0.48±0.42	Annacis Island
spet 9401		3.9	7±2	8±4	8+3	1.1±0.4	1.4±0.6	2.9±0.2	9.8±5.7	0.23±0.18	east side of Point Roberts; upper interval
		4.475	12+6	6+4	6+5	1.4+0.5	2.1+0.8	3.2+0.2	20+15	0.32+0.26	lower interval
CPT 325 92-197		1.15	31±8	5±2	5±2	1.7±0.6	2.5±0.9	3.2+0.2	-25±6	-0.13±0.06	Roberts Bank Port
CPT 95-5 95-170		5.75	15±8	4±4	5±5	1.2±0.5	2.1±1.1	3.3±0.3	7.2±7.6	0.12±0.15	Roberts Bank Port; upper interval
		2.25	19+8	4+3	4+3	1.3+0.5	2.2+1.1	3.3+0.3	0.1+6.2	0.004+0.07	lower interval

*Woeller et al., 1993

**Woeller et al., 1994

***British Columbia Ministry of Transportation and Highways boreholes

APPENDIX H. CPT PARAMETERS BY FACIES FOR SELECTED CPTS

Part 9. Laminated Sand Facies (LS)

CPT	Borehole	thickness m	q_t bar	q_{c1}	Q_t	Q	R_f %	F_R	I_F	dU m	B_q	Comments
CPT 92-1	FD92-11	23.05	72±32	37±15	17±7	28±18	1.3±0.7	1.6±1.0	2.5±0.4	-19±18	-0.02±0.06	
SCPT 1 95-109	FD95S-1 FD93-1	19.85	51±28	28±14	14±7	20±16	1.6±0.8	2.0±1.0	2.7±0.4	-16±7	-0.05±0.04	15 cm^2 cone
SCPT-13 94-112**	FD93-5	12.9	63±27	36±14	19±8	30±17	0.8±0.4	1.0±0.6	2.4±0.4	-15±10	-0.03±0.03	
SCPT 7 94-112**	FD94-2 FD94-4	1.25	79±31	34±14	13±6	21±17	1.4±0.6	1.8±0.8	2.7±0.4	-21±20	-0.02±0.07	
SCPT 16 94-112**		2.95	54±30	32±18	17±11	26±20	0.9±0.5	1.1±0.7	2.5±0.5	-2±13	0.01±0.05	28 m west of SCPT 14
CPT-2 91-101	FD94-5	6.2	42±36	31±27	21±21	27±28	1.5±0.8	1.9±1.1	2.7±0.5	0.2+10.4	0.02±0.07	
SCPT 7 94-112**	FD94-6	6.4	47±39	30±25	17±15	24±26	1.0±0.6	1.1±0.8	2.6±0.4	-3.2+16	0.01±0.1	upper part borderline with LZ
SCPT 10 94-112**	FD95-6	2.5	50+30	28±17	14±10	20±19	1.3±0.6	1.6±0.8	2.7±0.4	-13±11	-0.04±0.04	
SCPT 6 93-175	BHFD93S-1	18.3	33±20	24±14	16±11	19±15	1.3±0.6	1.6±0.9	2.7±0.4	-2.7±8	0.002±0.05	
SCPT 4 93-175	BHFD93S-2	22.7	20±13	18±10	15±10	15±10	1.0±0.5	1.4±0.9	2.7±0.4	0.6±6.1	0.04±0.09	5.05m borderline with LZ
CPT 2 94-180	BHFD94S-1	16.65	22±14	22±14	22±18	20±14	1.5±0.9	2.0±2.0	2.6±0.6	-0.9±4.0	0.01±0.09	120m southwest of BHFD94S-1
SCPT 7 93-175		26.9	39+25	33±15	28±17	29±16	0.9±0.6	1.1±0.8	2.4±0.4	-4.5±4.9	-0.01±0.02	200m south of BHFD94S-1
CPT 325 92-197		6.2	33±14	22±10	14±7	15±11	2.1±0.9	2.5±1.2	2.8±0.3	-10.0±2.6	0.04±0.02	Roberts Bank Port; upper interval
		5.3	62±23	32±12	15±6	21±15	1.5±0.5	1.7±0.7	2.7±0.4	-19±6	-0.04±0.03	lower interval

APPENDIX H. CPT PARAMETERS BY FACIES FOR SELECTED CPTS

Part 9 (cont'd). Laminated Sand Facies (LS)

CPT	Borehole	thickness m	q_t bar	q_{c1}	Q_t	Q	R_f %	F_R	I_F	dU m	B_q	Comments
CPT 95-5 95-170		2.5	43±20	30+14	19±10	26±16	1.0±0.7	1.2±1.0	2.5±0.4	-8.2±2.0	-0.03+0.02	Roberts Bank Port; upper interval
CPT 95-5 95-170		2.75	45±21	27±12	14±7	20±15	1.2±0.7	1.5±1.1	2.6±0.4	-8.3±5.9	-0.02±0.03	lower interval
spet 9401		5.925	53±29	50±27	45±25	48±27	1.0±0.6	1.0±0.7	2.2±0.3	-7.9±4.2	-0.02±0.2	east side of Point Roberts

Part 10. Mixed Sand Facies (MX)

CPT	Borehole	thickness m	q_t bar	q_{c1}	Q_t	Q	R_f %	F_R	I_F	dU m	B_q	Comments
CPT 92-1	FD92-11	3.4	169+40	76+18	32+8	71+19	0.8+0.3	0.8+0.4	2.0+0.2	-21+17	-0.01+0.01	
SCPT 1 95-109	FD93-1 FD95S-1	21.2	102±37	45±16	18±7	35±22	1.1±0.5	1.3±0.7	2.4±0.4	-34±10	-0.04±0.03	15 cm^2 cone
SCPT 1 94-112**	FD94-2 FD94-4		71±41	43±25	25±15	37±27	1.3+0.7	1.5±1.0	2.5±0.5	-5.6±13	0.008±0.06	
CPT 2 94-180	BHFD94S-1	25.35	69±24	41±13	22±9	35±16	0.9±0.5	1.0±0.6	2.1±0.4	-11.0±9.6	-0.02±0.02	
CPT 325 92-197		6.55	61±26	37±16	21±11	32±19	1.2±0.6	1.4±0.8	2.5±0.4	-8.5±4.8	-0.02±0.01	Roberts Bank Port; upper
		6.15	101+23	48+11	21+6	41+17	1.1+0.3	1.2+0.4	2.3+0.3	-20.4+8.1	-0.02+0.02	lower interval
CPT 95-5 95-170		3.5	65±19	49±14	36±11	47±14	0.5±0.3	0.5±0.3	2.0±0.2	-5.1±3.7	-0.009±0.007	Roberts Bank Port

**Woeller et al., 1994

APPENDIX H. CPT PARAMETERS BY FACIES FOR SELECTED CPTS

Part 11. Sharp-Based Sand Facies (SB)

CPT	Borehole	thickness m	q_t bar	q_{c1}	Q_t	Q	R_f %	F_R	I_F	dU m	B_q	Comments
SCPT 1 95-109	FD95S-1	14.45	141±26	55±10	19±4	46±16	0.9±0.4	1.0±0.5	2.2±0.3	-31±19	-0.03±0.21	15 cm^2 cone
CPT 325 92-197		6.4	101±13	55±7	29±4	52±8	0.7±0.2	0.8±0.2	2.1±0.1	-8.7±4.8	-0.009±0.005	

Part 12. Bioturbated Sand Facies (BS)

CPT	Borehole	thickness m	q_t bar	q_{c1}	Q_t	Q	R_f %	F_R	I_F	dU m	B_q	Comments
CPT 92-1	FD92-11	0.75	114±36	50+16	20+7	43±21	1.0+0.4	1.1+0.5	2.3+0.4	-32±18	-0.04+0.02	
SCPT 1 95-109	FD95S-1	21.8	125±35	44±13	14±5	25±19	1.4±0.6	1.7±0.8	2.6±0.4	-68±14	-0.07±0.04	15 cm^2 cone

Part 13. Thick Coarsening Upward Sand Facies (CU)

CPT	Borehole	thickness m	q_t bar	q_{c1}	Q_t	Q	R_f %	F_R	I_F	dU m	B_q	Comments
CPT9309	FD92-4	5.55	94+44	55+26	30+15	50+28	0.9+0.4	1.0+0.6	2.2+0.5	-7.1+11.3	-0.002+0.04	
SCPT 13 94-112**	FD93-5	2.15	75±26	49±17	31±11	46±19	0.7±0.2	0.8±0.3	2.2+0.3	-14±7	-0.02±0.01	

Part 14. Rhythmically Interbedded Sand and Silt Facies (RSZ)

CPT	Borehole	thickness m	q_t bar	q_{c1}	Q_t	Q	R_f %	F_R	I_F	dU m	B_q	Comments
SCPT 91-3 ***	FD92-5	19.75	44±33	24±18	11±10	17±19	1.2±0.6	1.6+0.9	2.9±0.5	15±25	0.18±0.26	Westbridge south side, Annacis Island
SCPT 1 97-108		37.9	57±45	24±19	9±8	15±20	1.4±0.7	2.1±1.2	3.0±0.5	13±47	0.16±0.3	Annacis Island

**Woeller et al., 1994

***British Columbia Ministry of Transportation and Highways boreholes

APPENDIX H. CPT PARAMETERS BY FACIES FOR SELECTED CPTS

Part 15. Low Dipping Interbedded Sand and Silt Facies (LDSZ)

CPT	Borehole	thickness m	q_t bar	q_{c1}	Q_t	Q	R_f %	F_R	I_F	dU m	B_q	Comments
CPT-1 93-109	FD93-2	7.4	91±73	63±51	42±37	59±52	0.8±0.5	0.9±0.6	2.3±0.6	-2.5+15.7	0.03±0.09	
CPT 5 91-188		15.7	74±51	52±37	35+27	48±38	0.9±0.6	1.1±0.8	2.3±0.6	-5.7±12.9	0.006±0.08	Downtown Richmond

Part 16. Disturbed Silt Facies (DZ)

CPT	Borehole	thickness m	q_t bar	q_{c1}	Q_t	Q	R_f %	F_R	I_F	dU m	B_q	Comments
SCPT 1 94-112**	FD94-1	5.35	83±49	42±25	20±13	32±29	1.3±0.6	1.5±0.7	2.5±0.4	-19±12	-0.04±0.04	
SCPT 14 94-112**	FD94-2 FD94-4	1.45	66±21	38±12	20±7	23±12	3.0±0.8	3.3±1.1	2.8±0.3	-25±9	-0.04±0.02	

**Woeller et al., 1994

APPENDIX I

COMPARISON WITH OTHER SEDIMENTOLOGICAL INVESTIGATIONS

TOPSET

Williams and Roberts (1989) recognized the four principal facies of the topset defined here. However, they interpreted the massive sand facies (their unit 1) as a tidal flat and subaqueous platform deposit, as noted in Chapter 6, and they did not recognize the typical channel characteristics of this facies. Furthermore, they interpreted the interbedded sands and silts (their unit 2) as tidal flat deposits, not recognizing that subfacies occur and that sediments deposited in an upper delta plain environment are also represented in this facies.

Hutchinson et al. (1995) mapped an abandoned distributary channel system in the southeast part of the delta. Their study was based on 32 coreholes (maximum depth shown ~10 m), supplemented by 390 other boreholes, including CPTs. On the basis of lithologies and diatom assemblages recovered from their cores, they identified distributary channel sands, tidal flat sands and silts, overbank silts, and peat bog deposits. Their distributary channel sands have a fresh water flora, and coincide with the shell-free subfacies of the massive sand facies (upper delta plain distributary channels) of this study (Monahan et al., 1993a, b, c). The overbank silt and peat bog deposits coincide with the laminated and organic silt and peat facies of this study respectively, and their tidal flat deposits appear to coincide with the shell-bearing subfacies of the massive sands and the bioturbated sands and silts.

Except where defined by their own cores or thick accumulations of overbank silts, the boundaries of the upper delta plain distributary system they described, and its evolution, are speculative (Figure I-1). They did not recognize that sands with a distinct channel signature are ubiquitous *beneath* tidal flat deposits (the shell-bearing subfacies and the bioturbated subfacies of this study, respectively; Figure 6-19 ; Monahan et al., 1993a, b, c), so that the

presence of a channel sand signature alone is insufficient to determine the presence of an upper delta plain distributary channel system. On their cross section B-B' (Figure I-1), they show the top of channel sands stepping down to the west, where they are overlain by the Mazama Tephra (ca. 6800 ^{14}C years BP)[1]. Furthermore, if the channel sands underlying the tephra are in the shell-bearing subfacies, as is certainly possible from the thickness of overbank silts, then the tephra provides a maximum rather than a minimum age for the initiation of the upper delta plain channel system, as proposed by them. They recognized the stacking of channel deposits due to sea level rise, but they did not recognize that this includes stacking of shell-free over shell-bearing subfacies (Figures 6-4, 6-13, 6-37 and I-2), because their own cores, from which they recovered a diagnostic fresh water flora, are shallow. Thus, the maximum depth of this channel system and the amount of vertical aggradation that occurred in it is probably less than they propose, and the lower parts of stacked channel deposits may be part of earlier systems that extend beneath tidal flat deposits and beyond the limits of their distributary system. Furthermore, the example of stacked channels in Figure I-2 is in one of their interchannel areas. In this part of their study area, channels were defined where sand occurs in boreholes at depths of less than 2.5 m, compared to depths of up to 3 to 6 m in interchannel areas[2]. The reverse could be true for a channel incised into tidal flat sands and silts. Clearly, the borehole data are inadequate to define systems at the level of detail presented.

Where a channel sand CPT signature occurs beyond the limits of their system, it is interpreted as a tidal channel deposit. Although the presence of shells in offsetting geotechnical boreholes confirms a tidal flat setting, the sand is typical of the massive sand facies, and its thickness of 8 m is consistent with depths of distributary channels.

---

[1] Their paper does not make it clear whether the western margin of the channel system is defined here or not.

[2] These boreholes are less generally less than 5 m deep, and all are less than 10 m.

The base of the channel sand is picked in one of the CPTs shown by them at the base of a sandy coarsening upward sequence, which is typical of foreset deposits (Figure I-3). The base of the sand is better picked 2 m higher.

FORESET

Christian et al. (1997a) presented CPT and borehole data from a site at the mouth of the Main Channel at Sand Heads. The site is located immediately landward of a large gulley incised into the upper foreset and interpreted to have been formed by one or more large scale failures at the river mouth. Sediments at this site were interpreted by these authors to represent the fill of a similar gulley, possibly related to the river mouth in 1912, when it was located nearby.

The deposits at this site are herein assigned to the laminated sand facies, organized into decametre-scale sandier and siltier packages and dipping seaward at 7^{O} (Figure I-4). A twig from a depth of 16 m in a discontinuously cored borehole (FD93S-2) was dated at 170+70 ^{14}C years (TO-4372; Appendix F). Christian et al., (1992a) correlated two gravity flow deposits observed in this borehole with two coarsening upward sequences at the same depth in the closest CPT. However, the borehole is more than 50 metres the CPT in an updip direction, and a better correlation would be with sands in a sandier package 5 m lower that is close to meeting the criteria for the mixed sand facies, which commonly consists of 25 to 50% gravity flow deposits. More importantly, the sediments here are typical of the delta foreset, contrary to statements by Christian et al. There is nothing about them to indicate rapid deposition of sands and silts in a gulley at a river mouth, which would probably filled largely by bed material load that could not accumulate as a river mouth bar. The mixed or sharp-based sand facies would make better candidates for such a gulley fill. Furthermore, no evidence is presented to indicate that such a gulley actually existed when the river mouth was at this point in 1912. The steep headscarp (15^{O}) of the present gulley seaward of this site suggests that it is a recent erosional feature and not a partially filled failure dating from 1912.

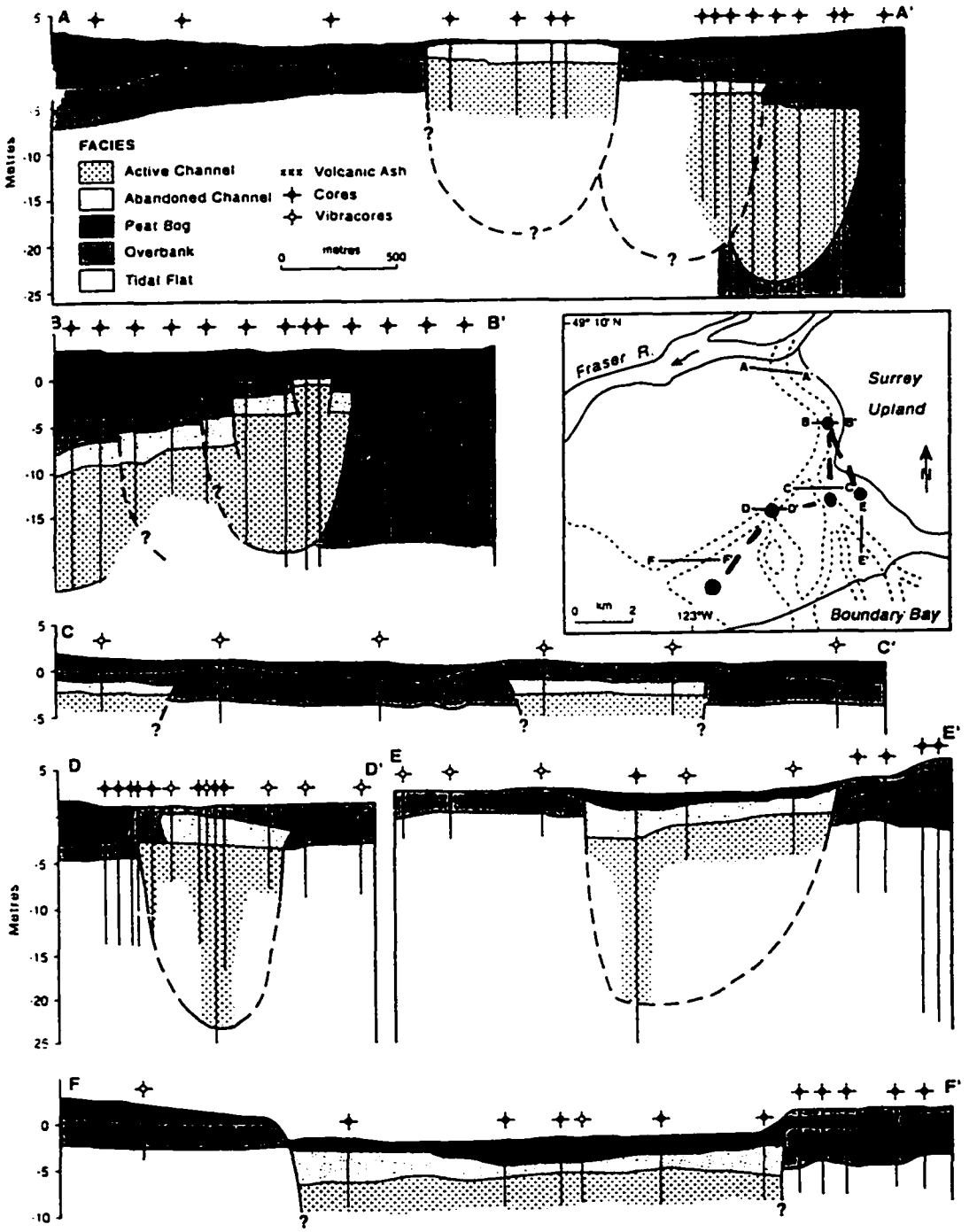

Figure 1-1. The distribution of the distributary channel system defined by Hutchinson et al. (1995) and accompanying cross sections, modified from their Figure 4. The line of the cross section shown in Figure 1-2 is added to the map. Note that the western limit of their channel system is undefined in cross sections A-A' and B-B'. In the western cores in B-B', volcanic ash (Mazama Tephra) is present in the lower part of the overbank facies. Note also that their vibracores are less than 10 m deep. CPTs with channel sand signatures are present both inside and outside of the limits of their channel system (Figure 1-2).

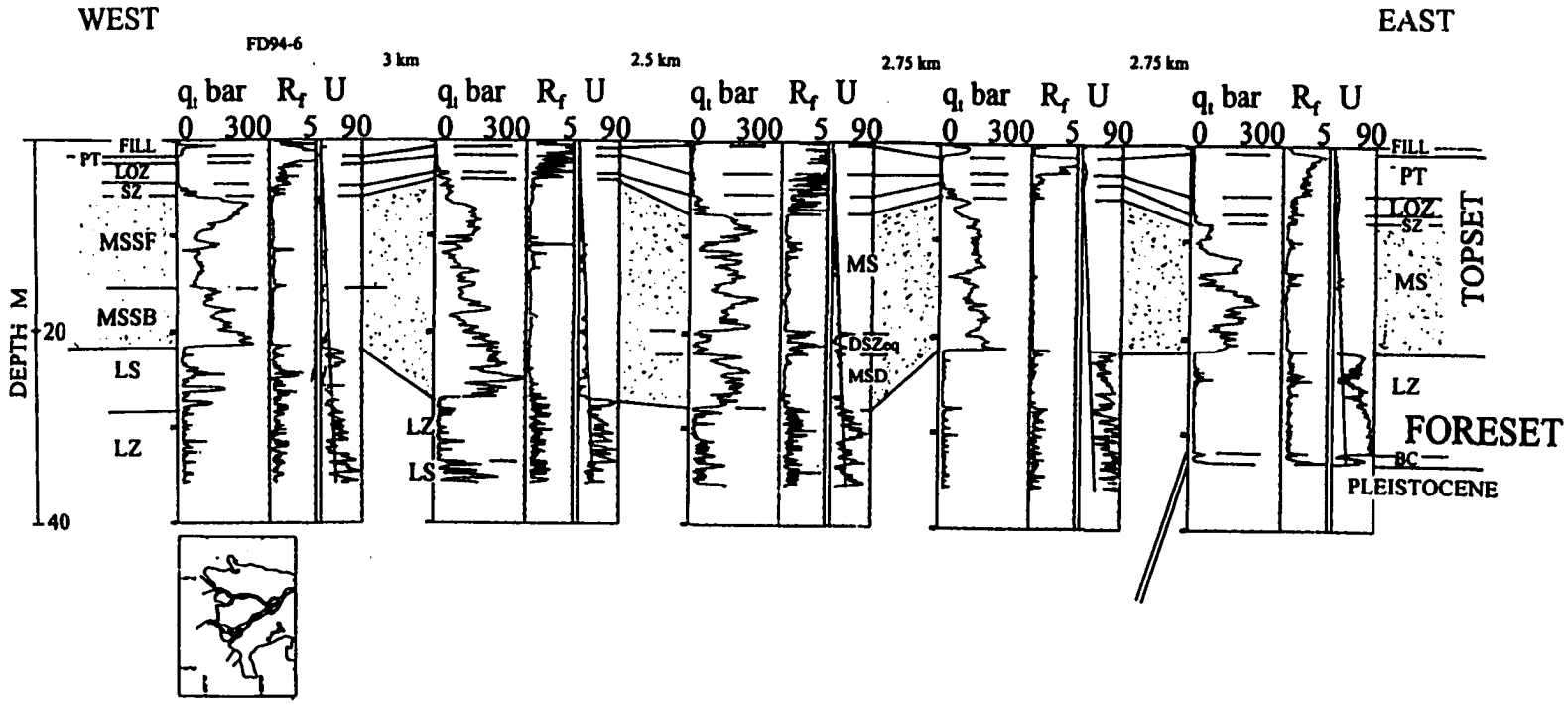

Figure I-2. CPT cross section in the southeast part of the delta showing the presence of the massive sand facies of the topset (MS) consisting of multiple sharp-based fining upward sequences both inside and outside the channel system mapped by Hutchinson et al. (1995; the 3 middle CPTs are within the limits of their channel system; see Figure I-1). Note that MS includes the shall-free (MSSF) and shell-bearing subfacies (MSSB) at FD94-6 (westernmost CPT), and that the distal subfacies and the distal sand and silt equivalent (DSZeq are preserved in the lower part of MS in the middle CPT). For facies symbols, see Table 6-1. R_f in % and U in metres of water.

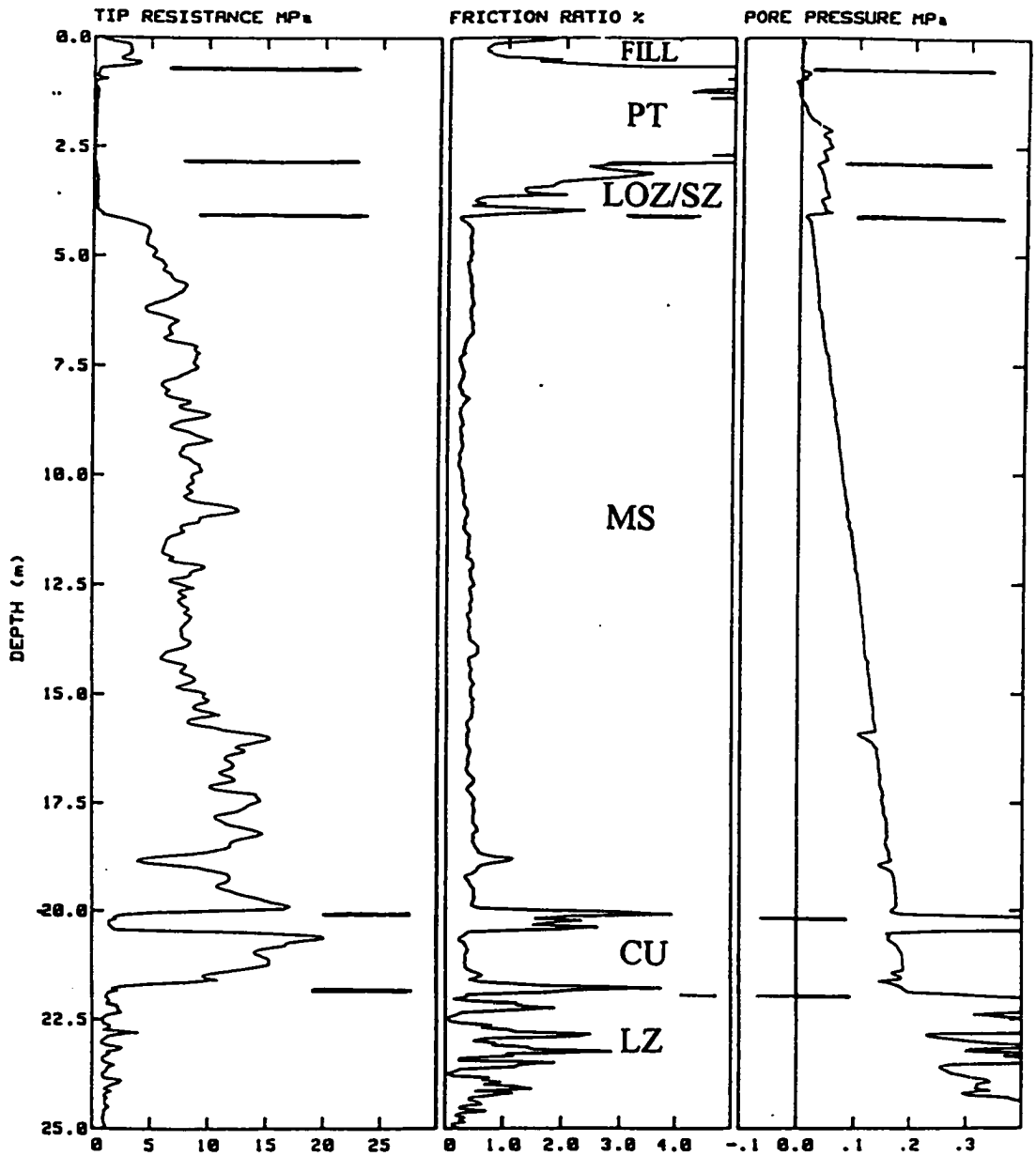

Figure I-3. CPT shown in Figure 2d in Hutchinson et al. (1995). The base of the massive sand facies (MS) is better picked at 20 m, rather than 22 m as picked by Hutchinson et al. (1995). The sand between 20 and 22 m is finer coarsens upward and is better assigned to the thick coarsening upward sand facies of the foreset (CU). For facies symbols, see Table 6-1.

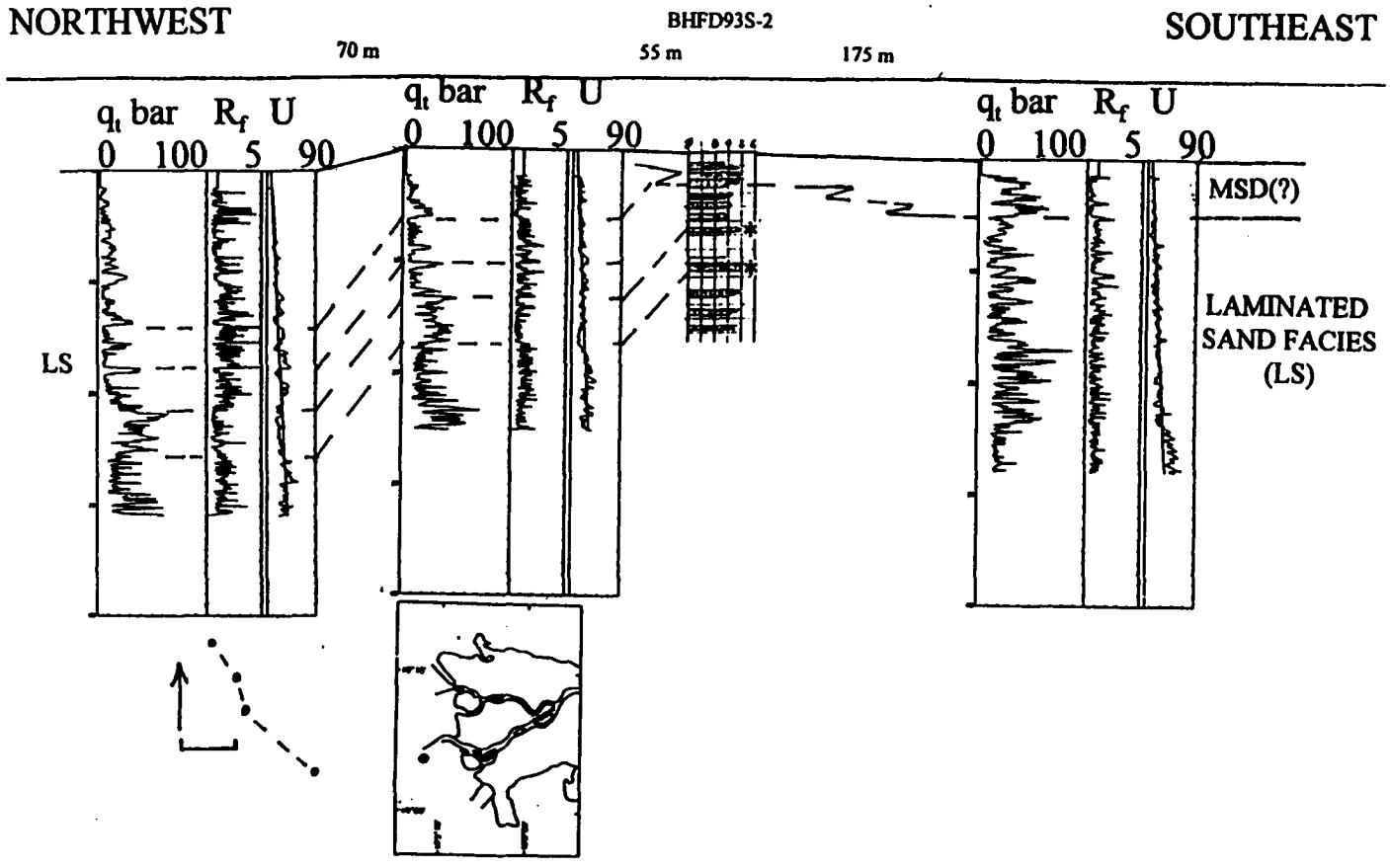

Figure I-4. CPT cross section at Sand Heads, showing apparent dips of 7° in foreset deposits. Fine to medium sand gravity flow deposits in BHFD93S-2 (*) are better correlated with the sandier interval between 13 and 17 m in the CPT to the northwest, than with the sand beds at 8 and 10 m as shown by Christian et al. (1997). The sandy interval at the top of BHFD93S-2 and the southeasternmost CPT is tentatively interpreted to represent a distal expression of the distal subfacies of the massive sand facies of the topset (MSD). For facies symbols, see Table 6-1. R_f in % and U in metres of water.